Designing Structurally Adaptable Multi-mode Products Using Emerging Constrained Layer Pneumatic System Technologies

by

Koray Benli

A dissertation submitted in partial fulfillment
of the requirements for the degree of
Doctor of Philosophy
(Design Science)
in the University of Michigan
2023

Doctoral Committee:

Professor Diann E. Brei, Co-Chair
Associate Research Scientist Jonathan E. Luntz, Co-Chair
Professor Brent Gillespie
Professor Richard Gonzalez
Wonhee M. Kim, General Motors Company

Koray Benli

bkoray@umich.edu

ORCID iD: 0000-0002-6175-5584

To my parents

Acknowledgements

First and foremost, I would like to express my deepest gratitude to my co-advisors, Diann Brei and Jonathan Luntz, for their unwavering support, guidance, and encouragement throughout my research journey. Their expertise, patience, and invaluable insights have been instrumental in shaping my academic growth. I have learned so much from Diann and Jon and this dissertation's completion would not have been possible without their efforts. I am immensely grateful to my committee members, Richard Gonzalez, Brent Gillespie, and Wonhee Kim, for their invaluable feedback and constructive suggestions. Their rigorous critiques and dedication have inspired me and significantly improved this dissertation's quality.

My heartfelt thanks go to the ISD Design Science at the University of Michigan for providing a supportive, stimulating, and multidisciplinary research environment. I appreciate the staff's assistance and patience with my continuous paperwork demands as an international student.

I owe immense gratitude to my fellow researchers and lab mates, Ellen Kim, Tiantian Li, Jesse Velleu, Laura Giner Muñoz, Clover Thebolt, and Tizoc Cruz-Gonzalez, for their exceptional support, intellectual discussions, and friendship that made this journey more enjoyable and fulfilling. I would also like to extend special thanks to our industry collaborators, Paul Alexander, Nancy Johnson, and Paul Krajewski, for their valuable contributions to this research and their collaborative spirit. I was also very lucky to have an opportunity to work with many great undergraduate and master’s students as a member of Smart Materials and Structures Design Lab.

I am grateful to the Turkish Fulbright Association and General Motors Research & Development for their financial support and for offering an industry perspective, which enabled me to broaden my research scope and make substantial progress in my dissertation.

Finally, I express my profound appreciation to my family and friends for their unwavering love, support, and understanding. To my parents, Gülten and Hikmet, thank you for instilling in me a love for learning and perseverance. To my partner, Alice, your patience, encouragement, emotional support, and belief in my abilities have been my greatest source of strength.

Table of Contents

List of Tables

List of Figures

Abstract

In our designed environment, we interact with a wide variety of products, ranging from simple to complex, each offering different sets of functionalities to meet dynamically changing user needs. Most conventionally designed products offer a stationary set of functions, unable to dynamically address users' changing context-specific diverse array of needs. Multi-mode non-reconfigurable and modularly reconfigurable products enable multiple sets of functionalities (i.e., modes) but inevitably become bulkier, heavier, and more complex to use with increasing functionality and modality. However, a novel genre of products - *structurally adaptable multi-mode products* - presents significant potential to cater more efficiently to changing needs by offering multiple sets of functionalities by transforming their structural configurations on demand through multiple operation states in different modes. To enable these transformations, this dissertation identifies and develops a novel pneumatically activated architecture, *constrained layer pneumatic systems*, as a promising technological platform. These systems provide customizable, lightweight, space-saving, and cost-effective solutions to design multi-mode products. Constrained layer pneumatic systems produce numerous functionalities, such as complex three-dimensional actuation motions, structural property changes, and sensing capabilities, through their hierarchically arranged architectural components (e.g., cells) that are constrained internally and/or externally. Pneumatic affordances and fundamental behaviors are classified, linking subcellular features to system architecture, functionality, and operation. This approach aids in describing and understanding these systems and offers building blocks for designing structurally adaptable multi-mode products tailored to specific user-product interaction contexts. A comprehensive *hierarchical functional architectural decomposition approach* is presented to enable a detailed understanding of product system hierarchy. This approach allows designers to systematically capture the relationships among architectural, functional, operational, and performance system aspects through the architectural and functional hierarchies comprising cell, ensemble, unit, assembly, and system levels. This facilitates various analysis, synthesis, and re-synthesis design methods, enabling

incremental improvements, replacements, and speculative designs of structurally adaptable multi-mode products based on existing ones. Ten distinct goal-oriented design strategies are formulated and grouped under redesign, incremental innovation, and radical innovation categories, providing a systematic approach to re-synthesize structurally adaptable multi-mode product concepts. To demonstrate an effective way of systematically exploring a hierarchically organized broad architectural design space, a specific type of a constrained layer pneumatic system, *internally tiled pneumatic textiles*, is selected as an architectural case study. Three consecutive studies comprising a tile architectural study, a design coupling study, and an architectural feature variations study, provide an understanding of the hierarchical architectural structure, functionality and operation, and the interdependent relationship between architectural and parametric design, as well as the performance of the competing functionalities. This provides a basis to conduct a parametric design case study focusing on the design of a specific structurally adaptable multi-mode product, *the moldable active cargo blanket*, with tailored multi-modal performance attributes. A predictive empirical model is developed and validated based on a half-factorial design-of-experiments, capturing the trading-off performances of the functionalities provided by moldable active cargo blanket, enabling an algebraic tailoring method for selecting tile geometry design variables to achieve intended design outcomes. The method is demonstrated by tailoring the performance of three different cargo blankets for various contexts, with their performances experimentally validated against design goals. This design science foundation fosters a diverse range of rich user-product interaction opportunities by addressing users' varied needs through a new generation of multi-mode products offering functional adaptability via their adaptive structures.

Chapter 1. Introduction

We live in a designed environment teeming with countless types of products, each possessing unique physical characteristics affording a specific set of functionalities. Most products we interact with daily are designed to provide a stationary set of functions, using either non-reconfigurable or reconfigurable structural components. By actively adapting a product's structural components, it becomes possible to transform its overall form and, consequently, the functionalities it provides. However, inducing such transformation requires developing intrinsically safe, affordable, and compact ways of inducing physical transformations that are distributed through the structure of a product in a lightweight manner without introducing excessive complexity to the design of the product system. The goal of this research was to develop the design science foundation enabling a systematic early-stage design space exploration for emergent pneumatic technologies that provides a basis for the design of structurally adaptable multi-mode products providing changing functionalities affording distinct physical interactions with users.

This chapter establishes the need and opportunity for designing structurally adaptable multi-mode products and introduces an emergent approach, constrained layer pneumatic systems, which serves as a technological basis to meet the need. Related research issues are discussed leading to goals and objectives to establish the foundation for this hierarchically structured emergent technology.

1.1. Need for Multi-modality

In our daily lives, we use products with varying levels of complexity and functionalities to meet a diverse array of needs. These products may result from a relatively simple combination of structural components, such as a table providing a stable, flat surface for various activities such as eating, working, writing, placing objects, or displaying items, or a hammer designed to deliver forceful impacts to objects, typically for driving nails into materials like wood. Alternatively, they may be extremely complex, like automobiles or airplanes, which facilitate transportation for people and their belongings from one location to another.

Regardless of a product's complexity, there is always a two-way interaction between the product and its environment, which encompasses other products, natural entities, and us as users. Roozenburg and Eekels define products as artifacts that people perceive, produce, transact, and use due to their properties and corresponding functions [1]. Ulrich further clarifies the term *function* as what a product does, as opposed to its physical characteristics [2]. Following these definitions, a physical product can be considered a system that offers bidirectional interaction possibilities with its environment. This system comprises:

- an *architecture*, which embodies the knowledge of its specifically arranged structural components,
- and an associated set of *functionalities*, actualized through a specific set of operational states that govern the behavior of the product's structural components.

Many products that surround us are typically designed to offer a stationary set of functions. The architecture of these products can range from simple to complex, such as a basic wooden chair or a sophisticated office task chair. A basic wooden chair consists of structural components that remain unchanged during use, providing a surface for users to sit on. Its intended functionality, determined by the designer, remains consistent throughout the user-product interaction cycle. In contrast, an office task chair features a variety of mechanisms and actuators that offer adjustability to users. Although its architecture includes adaptable structural components (e.g., a pneumatic actuator), the set of functions provided by an office task chair remains stationary. Users can adjust the height of the seating surface, tilt it, and modify the reclining mechanism's stiffness; however, these adjustments do not alter the fundamental nature of the resulting set of functions.

As delineated by Merriam-Webster, a mode constitutes "a particular functioning arrangement or condition" [3]. In this context, products affording a stationary set of functions can be categorized as single-mode products. These products facilitate the fulfillment of specific needs or objectives for users. However, the specific needs or objectives may diverge among users or evolve for an individual user, contingent upon the inherent characteristics of the task being executed or the dynamic contextual factors in the user's environment.

This diversity engenders a demand for acquiring, using, and storing a multitude of products, each tailored to perform a designated task throughout their product life cycles. The conventional approach for addressing this demand encompasses the development and manufacturing of an ever-increasing number of tools and devices specifically designed to offer either a solitary, stationary

function or a set of closely related functions. Consequently, users need to possess a collection of products, each fulfilling a particular need at a given time.

A more advanced approach to addressing the same demand involves designing a product of which architectural configuration affords multiple modes as needed. Catering to diverse needs with a multi-mode product is advantageous in terms of user satisfaction on numerous levels. Users can execute various sequential tasks necessitating distinct functionalities by employing a single multi-mode product rather than multiple single-mode products. When not in use, storing a multi-mode product proves more space-efficient than accommodating an assortment of single-mode products. Using multi-mode products also potentially conserves time, as users can transition between functions more expeditiously compared to employing different single-mode products consecutively or concurrently. For instance, a basic wooden chair and a stepladder both exemplify the single-mode product category, offering stationary sets of functions (Figure 1, left). In contrast, their multi-mode counterpart, a folding chair-ladder, is capable of delivering the same range of functions by permitting two distinct configurations of its structural components at a given moment (Figure 1, right).

Figure 1. A set of single-mode products vs a multi-mode product. Basic wooden chair, stepladder, and their multi-mode counterpart providing a combined set of functionalities on demand.

A wide range of products has been organized within a unified design space, based on two dimensions, to further illustrate the advantages and disadvantages of targeting single or multi-modality (Figure 2). The first dimension, encompassing general *architectural approaches*, classifies how a product's structural components enable various architectural configuration strategies during its use. This dimension includes products furnished with non-reconfigurable, modular, and adaptable structural components. The second dimension, referred to as *function*

changeability, differentiates between products offering a stationary set of functions and those providing a changing set of functions.

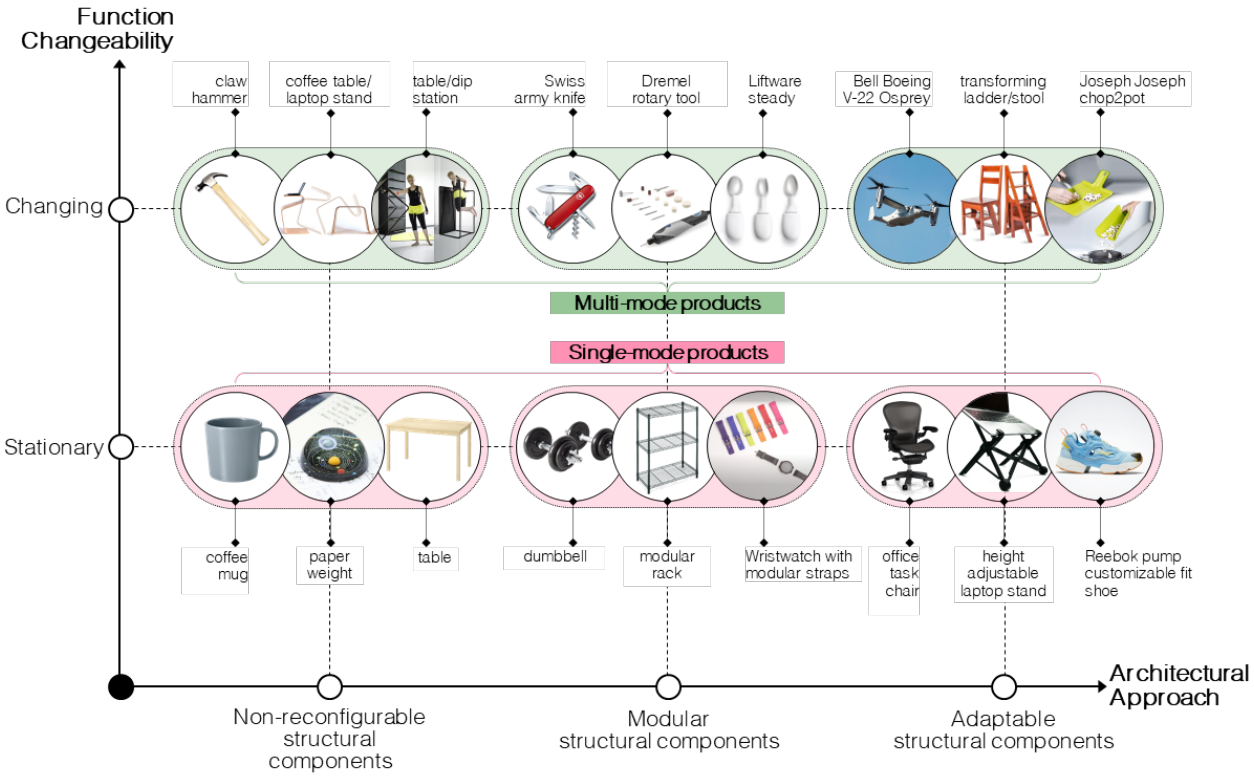

Figure 2. Single-mode and multi-mode product design space classification based on function changeability and architectural approach. The first dimension of the design space, *architectural approaches*, classifies how a product's structural components enable various architectural configuration strategies during its use, including products furnished with non-reconfigurable, modular, and adaptable structural components. The second dimension, *function changeability*, differentiates between products offering a stationary set of functions and those providing a changing set of functions.

As illustrated in Figure 2, there is a direct mapping between product modality and function changeability. It is crucial to distinguish between multi-mode products, capable of providing multiple sets of functions, and multifunctional products. Single-mode products can offer a single primary function or multiple related functions either simultaneously or sequentially. For instance, a mug for containing liquid and a dumbbell with adjustable weight are single-mode products with one primary function each. An office task chair, however, is a multifunctional product with adaptable structural components, but remains single-mode. None of the intended functions provided by these products undergoes a drastic change over time; they remain stationary.

In contrast, multi-mode products are inherently multifunctional, offering distinct functions or sets of functions in various modes. As the product transitions between modes, the provided

functions change accordingly. Examples include the claw hammer, which combines hammering and nail-pulling functions (Figure 2, top left); the Swiss army knife, which features multiple tools like blades and screwdrivers (Figure 2, top middle), screwdrivers, and can openers; and power tool sets that share a common platform and allow for interchangeable modules (Figure 2, top middle). These multi-mode products offer increased functionality but face constraints in terms of size, complexity, and manual effort required to switch modes. Each added function requires a new structural component, and users typically need to manually modify components (e.g., by manually deploying and stowing them) or reorient the product to transition between modes. This design approach offers versatility but may have limitations in accommodating a growing number of functions. As opposed to multi-mode products relying on non-reconfigurable and modular structural components, there is a third category of multi-mode products employing adaptable structural components (Figure 2, top right). For instance, the Chop2Pot Board is a structurally adaptable multi-mode product with a simple folding design, enabling users to seamlessly switch between modes. In its initial mode, it offers a flat surface for chopping ingredients, while in its second mode, it transforms into a chute upon squeezing the handle, forming a funnel-like shape that facilitates the effortless transfer of chopped food into a pot or pan without spillage.

In addition to these conventional product design examples, researchers have been developing innovative multi-mode products employing various actuation technologies to transform the structural components in response to indirect user input or environmental stimuli. This offers significant benefits for users, as all potential functionalities are embedded within the product's architecture and can be activated without manual effort, such as reorienting the entire product or swapping one structural component for another. Researchers in fields such as transportation design engineering, aerospace, and human-computer interaction have used emerging actuation technologies with the potential to enable the development of multi-mode products using adaptable structural components. Some examples include an electromechanically actuated vehicle wheel that transitions from a round form to a triangular track for adapting to varying terrains [4], a variable-geometry chevron designed to minimize jet engine noise during take-off and landing while maintaining maximum thrust at cruise altitude by changing its structural configuration on demand [5], and a reconfigurable user interface that can physically transform for use as a mobile phone, remote control, wristwatch, or game controller [6] (Figure 3).

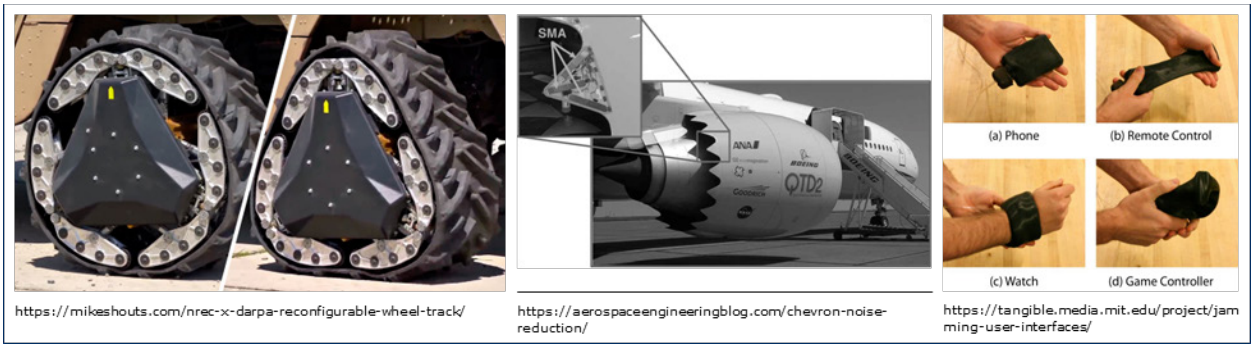

Figure 3. Structurally adaptable multi-mode products examples. An electromechanically actuated vehicle wheel that transitions from a round form to a triangular track for adapting to varying terrains (left) [4], a variable-geometry chevron designed to minimize jet engine noise during take-off and landing while maintaining maximum thrust at cruise altitude by changing its structural configuration on demand (middle) [5], and a reconfigurable user interface that can physically transform for use as a mobile phone, remote control, wristwatch, or game controller (right) [6]

As technological advancements and novelties in the current actuator state of the art lay the groundwork for creating structurally adaptable multi-mode products capable of transforming on demand to deliver distinct functionalities across different modes, it is essential to establish a systematic design basis to support the early-stage design process for this innovative category of multi-mode products.

1.2. Design Methodologies and Approaches Enabling Design of Structurally Adaptable Multi-mode Products

The advantages offered by structurally adaptable multi-mode products are many; however, the design process of these products is more complex compared to their single-mode counterparts due to the highly coupled performances of different sets of functions that are provided in different modes. This coupling stems from the fact that these radical multi-mode products are making use of some of the same structural components in different ways to cause function changes in different modes. Ulrich and Seering alternatively explains this phenomenon as function sharing, which enables the implementation of multiple functions by a single structural component [7]. There is an increase in technology and design complexity as well as performance coupling as we move from products using non-reconfigurable structural components to products using adaptable ones. Similarly, there is an extra layer of complexity introduced to the design process as we move from products providing stationary functions to products providing changing ones (Figure 4). This results in making the design process of structurally adaptable multi-mode products the most challenging due to the increased overall complexity. Since one structural component provides different functions by undergoing a physical transformation, there is an unavoidable coupling

between the performances of these resulting functions, which introduces various technological and design tradeoffs to the design process, especially during the early stages of product development.

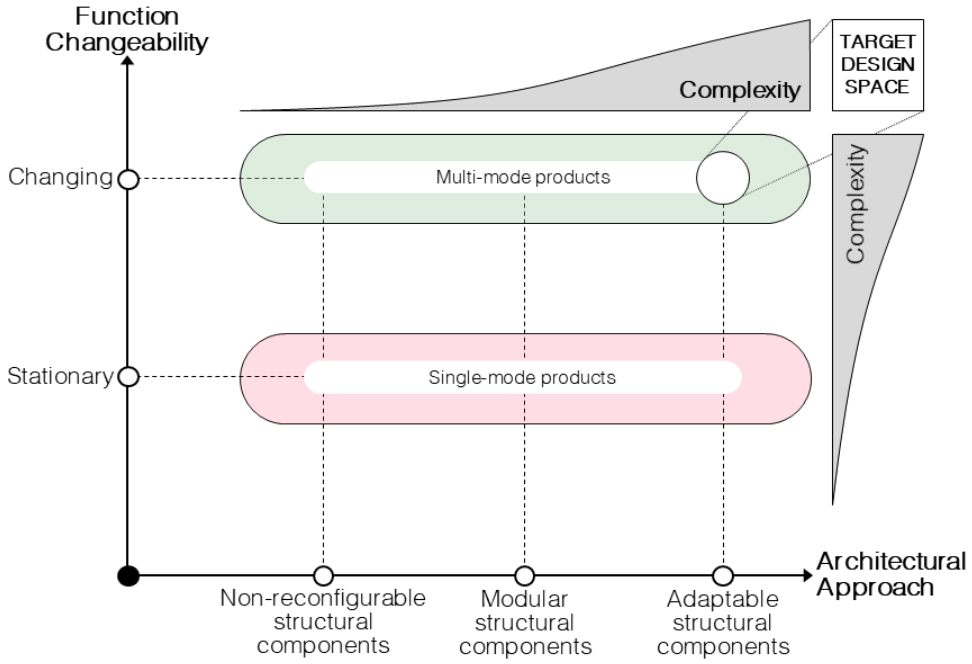

Figure 4. Technology and design complexity, and performance coupling in the design space. There is an increase in technology and design complexity as well as performance coupling as we move from products using non-reconfigurable structural components to products using adaptable ones. Similarly, there is an extra layer of complexity introduced to the design process as we move from products providing stationary functions to products providing changing functions.

The well-established design methodologies often do not address these trade-offs; however, the recently developed design approaches such as the shape-changing interface design, adaptable design, and multimodal product design can potentially be extended to the design of structurally adaptable multi-mode products. The following two sections summarize a set of hallmark systematic design approaches first, and then introduce the more recent ones.

1.2.1. Hallmark Systematic Design Approaches

There are many well-established design research methodologies linking various methods and approaches together to provide support for the systematic execution of product design process in various fields [8]–[14]. These existing approaches are not mutually exclusive, often overlapping with each other by including the following in one form or another: a need identification and analysis stage, a conceptual design stage, and a design detailing stage [15]. For example, Pahl and Beitz's book "*Engineering Design: A Systematic Approach*", provides fundamental guidance for

the product design process by integrating many facets related to the development of technical systems [9]. The interrelationships in technical systems are classified as functional, working, constructional, and system interrelationships. The conversion of energy, materials, and signals provides a basis for the development of functional interrelationships, where an overall function is broken down into its sub-functions. The working interrelationships are established in the working structure, detailing the working principles of a technical system relying on the physical effects and material characteristics. The constructional interrelationships further concretize the working structure into a construction structure, which encompasses the details of components, assemblies, machines and their interconnections in a technical system. A final class of interrelationships, the system interrelationship, examines the technical system in terms of the effects it provides to and receives from users and other artefacts in a larger system.

The ongoing research efforts in literature built on the interrelationships in technical systems [16]–[21] have predominantly focused on the design of all but the structurally adaptable multi-mode product clusters. Liu argues that existing design approaches do not treat products with multiple modes or changes in physical configuration as a major consideration [22]. Although, most of the well-established design methodologies are geared towards the design of products with stationary functions or products equipped with non-reconfigurable structural components, there are widely recognized approaches enabling the design of multi-mode products using modular structural components such as modular design, product family and product platform design (Figure 5).

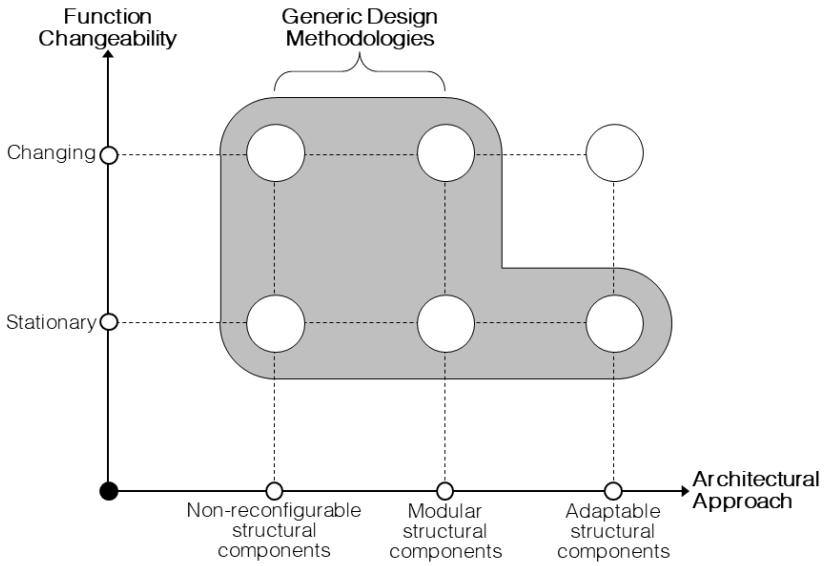

Figure 5. Hallmark systematic design approaches superimposed on the design space. Most of the well-established design methodologies are geared towards the design of products with stationary functions or products equipped with non-reconfigurable structural components. There are also widely recognized approaches, such as modular design, product family and product platform design, enabling the design of multi-mode products using modular structural components. These design approaches often do not treat structurally adaptable multi-mode products as a major consideration.

Modular systems allow function changeability based on a combination of fixed individual parts and assemblies of a product. Gu, Hashemian, and Sosale define modular products as the output of modular design approach, which encompasses the development of product architecture that is made of physically detachable and interchangeable components [23]. Ulrich, Eppinger, and Yang refers to modularity as the most important characteristic of a product's architecture [24]. Ulrich makes a distinction between two main types of product architectures: *a modular architecture*, where there is a one-to-one mapping between the functional elements constituting functional interrelationships and the physical components constituting structural interrelationships, and *an integral architecture*, where the mapping between the functional elements and the physical components is complex and intertwined [2]. By using a modular design approach, a particular product can be transformed into another product, presenting a new functionality. Apart from generic examples such as cars, furniture, and computers, modular sunglasses allowing users to mix and match different components of the frame for customization, and Sensel Morph, which is a tablet-sized pressure sensor with swappable tactile interface overlays enabling users to switch between different tasks such as typing or music making exemplify some of the benefits of modularity as a design approach. The advantages of modular design include ease of reconfiguration, ease of product updating, increased product variety, ease of design, testing, and

maintenance due to the decoupled product functions [25]. However, the challenge relies in successful decoupling of the components regarding their function and form, which makes the resulting modular products relatively heavier, bulkier, and more complex than their counterparts that are based on integral architectures.

Product platform and product family design approaches are directly relevant to modular design approach. A product platform is defined as *"a set of common components, modules, or parts from which a stream of derivative products can be efficiently created and launched"* [26] (p.7). Siddique and Simpson argue that a product family is a derivative product generated by using a common product platform, targeting various market niches [27]. Although developing product platforms and generating product families provide numerous benefits to the manufacturer such as reducing manufacturing costs and broadening their portfolio by increasing the product variety, these design approaches do not directly contribute to the design of multi-mode products using structurally adaptable components.

1.2.2. Recent Design Approaches

Numerous examples of artifact-oriented design can be found in recent literature, each employing distinct approaches and enumerating the benefits of creating multi-mode products including non-reconfigurable and modular as well as structurally adaptable architectures. With the progression of technology as a driver, researchers have been striving to develop approaches for multi-mode product design across various fields. Three primary, often interrelated, areas of interest have emerged: *shape-changing interface design, adaptable design approach,* and *the multi-modal product design paradigm*. These approaches each has addressed the portion of the previously illustrated design space onto which they are superimposed in Figure 6.

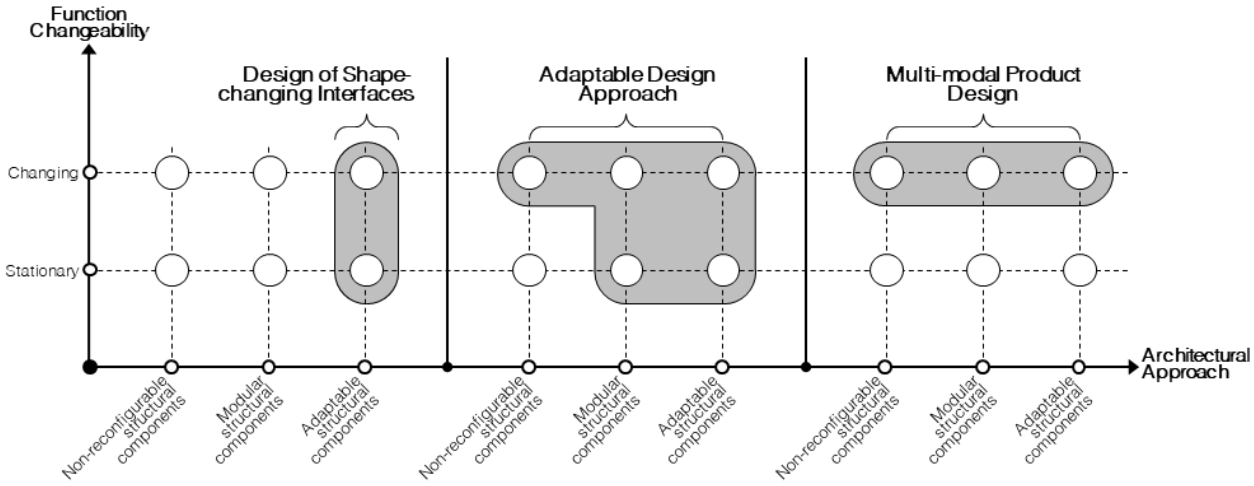

Figure 6. Recent design approaches relevant to the design of structurally adaptable multi-mode products. With the progression of technology as a driver, researchers have been striving to develop approaches for multi-mode product design across various fields. Three primary, often interrelated, areas of interest, *shape-changing interface design, adaptable design approach,* and *the multi-modal product design paradigm,* are superimposed on the design space.

1.2.2.1. Design of Shape Changing Interfaces

Ishii and Ullmer emphasize that the richness of human senses and capabilities, developed through extensive interaction with the physical world, has not been fully addressed by graphical user interfaces due to the absence of tactile feedback [28]. To bridge the gap between the *world of bits and atoms*, they introduced the concept of *tangible bits*. Tangible bits aim to provide dynamic physical affordances and engage multiple senses, facilitating multimodal human-world interactions. Consequently, the field of human-computer interaction has extensively investigated shape-changing interfaces over the past few decades. These interfaces enable rich sensorial experiences through physicalized information by equipping surfaces and structures with diverse actuation methods [29]. Poupyrev, Nashida, and Okabe suggest that dynamically changing the physical properties of user interface elements could expand the design vocabulary of tangible user interfaces [30]. Enhancing the control over interface properties such as shape, texture, position, and motion speed would greatly improve the building blocks for user-product interaction design. They also note that advancements in actuators, microprocessors, and smart materials have reached a maturity level that facilitates the design of shape-changing interfaces.

Rasmussen et al. contend that the literature on shape-changing interface design research primarily consists of point designs, with a focus on technical advancements but lacking a systematic design approach [31]. Alexander et al. enumerate the advantages of shape-changing interfaces, such as providing adaptive affordances, augmenting users, simulating objects,

communicating information, and enabling hedonic and symbolic purposes [32]. Nevertheless, technological (e.g., prototyping toolkits, technology miniaturization, energy consumption, safety), design (e.g., development of design tools and methods, designing for temporality), behavioral (e.g., understanding user experience, theory development), and societal (e.g., policy and ethics, sustainability, and environmental impact) challenges hinder the full realization of these benefits. Moreover, Coelho and Zigelbaum assert that "*there is still much to be done to make physical form equally mutable and controllable*" compared to graphical user interfaces [33] (p.161). Designing such multi-mode systems and applications necessitates a combination of expertise from diverse fields, including engineering, robotics, psychology, design, and architecture.

Examples of using adaptable structural components in the context of shape-changing interface design span various applications (Figure 7): mobile device interfaces offering haptic feedback [34], [35], 2.5D actuated shape displays for tactile data representation [36], and tangible interactions [6], [37], as well as stiffness changing buttons, knobs, and sliders serving as input components for devices [38], [39]. The broad spectrum of technological approaches demonstrated in these examples' design processes can be harnessed for the systematic design of user-interactive structurally adaptable multi-mode products.

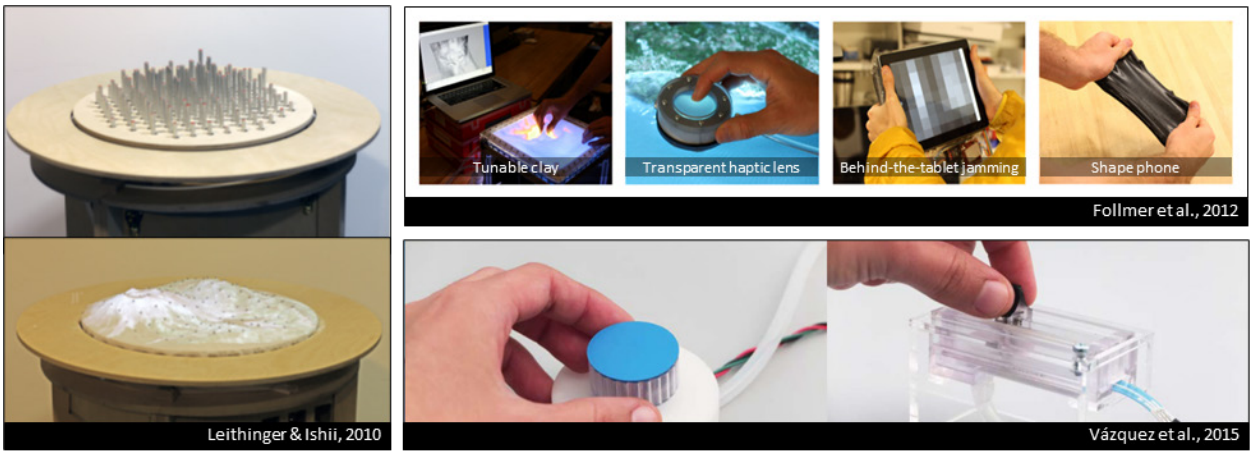

Figure 7. Shape-changing interface design examples. A 2.5D actuated shape display for tactile data representation [36], vacuum-driven malleable user interfaces enabling new forms of interactions and expressiveness through computationally controlled shapes and displays [6], and a set of pneumatically operated stiffness changing rotary knob and slider serving as input components for interactive devices [38] (bottom right).

1.2.2.2. Adaptable Design Approach

The adaptable design approach proposes two types of adaptabilities: design adaptability and product adaptability [40]. Design adaptability allows manufacturers to modify a product's design

to create similar variations, primarily benefiting the manufacturer rather than the user. Conversely, product adaptability extends a product's intended utility into new operational modes.

Gu, Hashemian, and Nee differentiate between specific and general adaptability [41]. Specific adaptability refers to a product or its design accommodating foreseeable future applications during concept inception. General adaptability, however, addresses the unknown future applications of a product. The goal of general adaptability is to maximize adaptability by designing a product's architecture in a segregated manner, allowing local modifications to functional and structural interrelationships without impacting overall function or form. This is consistent with the modular design approach, which seeks to minimize dependencies between functional and structural subsystems.

Gu, Xue, and Chen introduce a methodology for general adaptable product design, including methods for *modeling rationalized functions, modular architecture-based modeling, adaptable interface modeling,* and *adaptable design evaluation* [42]. The modeling methods of rationalized functions involve decomposing the overall function into sub-functions, employing tree-based, network-based, or AND-OR graph function modeling (Figure 8). Modular architecture-based modeling methods parallel those for modeling rationalized functions. Adaptable interface modeling methods are based on Ulrich's classification of interfaces in the modular design approach: slots, buses, and sectionals [2]. Adaptable interfaces should consider physical relations in design solutions and functional relations in design requirements. Adaptable design evaluation methods identify the best design candidates for manufacturing by comparing product adaptation efforts to new product development.

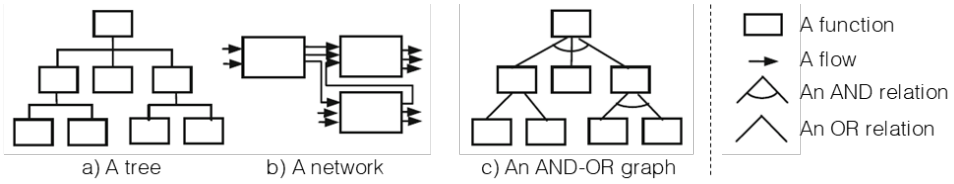

Figure 8. Methods for rationalized function modelling (adapted from Gu, Xue and Chen [42]). The modeling methods of rationalized functions involve decomposing the overall function into sub-functions, employing (a) tree-based, (b) network-based, or (c) AND-OR graph function modeling description.

Examples of adaptable products include the 2003 Ford Freestyle FX concept car [43], which can transform from an SUV into a pickup truck on demand; Boon Bender kitchen utensils [44], which can be bent and repositioned to accommodate any grip, helping children transition to regular utensils; and Liftware Steady [45], featuring an electronic stabilizing handle with a set of

interchangeable spoon and fork components to assist those with hand tremors (Figure 9). While adaptable products offer numerous advantages, such as user, environmental, and economic benefits, achieving the desired product adaptability often requires function independence, which is not the case for user-interacting structurally adaptable multi-mode products due to their integrated architecture.

Figure 9. Adaptable design examples. Adaptable design examples are the 2003 Ford Freestyle FX concept car [43], which can transform from an SUV into a pickup truck on demand; Boon Bender kitchen utensils [44], which can be bent and repositioned to accommodate any grip, helping children transition to regular utensils; and Liftware Steady [45], featuring an electronic stabilizing handle with a set of interchangeable spoon and fork components to assist those with hand tremors.

1.2.2.3. Multi-modal Product Design

Modality, defined as a product's ability to operate in multiple modes [22], forms the foundation for multi-modal product concepts which build on multi-mode integration, which is one of the four primary sharing-in-design categories identified by Chakrabarti [46]. The other three categories include function sharing, structure redundancy, and structure sharing (Figure 10). Unlike products in these three categories, Chakrabarti's multi-modal products change their structural configuration in each mode, activating only a selection of functions and technologies.

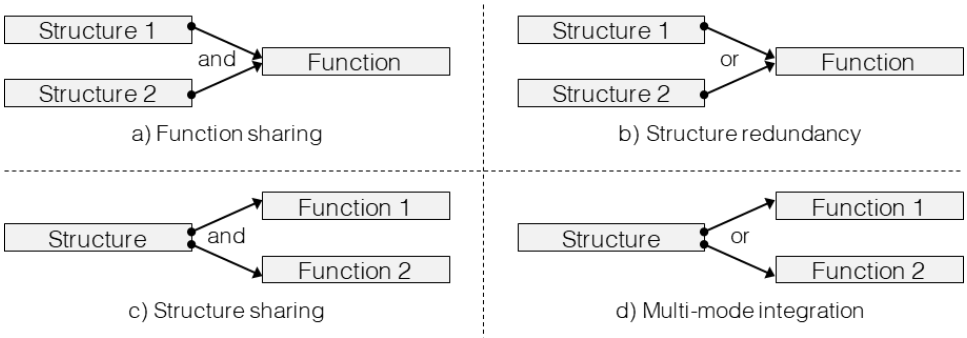

Figure 10. Main categories of sharing in design . The four primary sharing-in-design categories identified by Chakrabarti [46] are (a) function sharing, (b) structure redundancy, (c) structure sharing, and (d) multi-mode integration. The multi-modal product design approach has been built on the multi-mode integration category.

Liu et al. developed a systematic approach for conceptual design [47] and product architecture design [48] of multi-modal mechatronic applications, encompassing function multiplication and technology multiplication based on the function-technology-mode paradigm. Function multiplication refers to a product's ability to switch between modes and provide different functions, such as a washing machine that offers both washing and drying cycles and an electronic wristwatch that can switch between watch mode and sports mode based on the same technology. On the other hand, technology multiplication involves using different technologies in various modes for producing same function, exemplified by hybrid cars powered by both an internal combustion engine and an electric motor (Figure 11).

Figure 11. Multi-modal mechatronic design examples. Function-technology-mode paradigm introduced by Liu et al. is shown on the left [47]. Forerunner® 920XT wristwatch (middle) [49] exemplifying function multiplication, and Hyundai Elentra hybrid car (right) [50] exemplifying technology multiplication.

To facilitate the conceptual design of multi-modal products, Liu [22] proposed merging and clustering methods. For product architecture design, they introduced a design structure matrix that evaluates multi-modal product concept complexity by examining interactions between structural modules in different modes. Two techniques, functional multi-modal capturing and technological multi-modal capturing, allow designers to explore potential mappings of multiple functions to structural modules and analyze the need for distinct technological solutions per mode. The multi-modal design approach is mainly intended to contribute to the generic design process of mechatronic products. The application of this approach is demonstrated through the analysis and design of products such as solar-powered sensor-automated lighting systems, a sports watch providing a time mode and an exercise mode, pasta mixing and extruding machines, and robotic applications with swimming and climbing capabilities. It provides techniques for investigating the impact of multiple modes on the relationship between functions and physical modules. A

significant finding in multi-modal product design research is the positive correlation between increasing product modality and its robustness, usability, and resource effectiveness.

Despite the growing number of multi-mode product concepts emerging in various fields such as human-computer interaction, mechanical engineering, aerospace engineering, architecture, medical, and robotics, showcasing diverse levels of shape-changing interface design, adaptable design, and multimodal product design approaches, their design processes remain largely abstract and generic. Compared to the design process for multi-mode products using non-reconfigurable and modular structural components, designing multi-mode products with adaptable structural components presents a greater level of complexity. This is due to the numerous trade-offs introduced by the required structural configuration changes in each mode, which impact architectural, functional, operational, and performance aspects of the product system. Moreover, multi-mode products with adaptable structural components necessarily have highly-integrated structures with strong couplings that can neither be modularized nor be compartmentalized as a collection of coupled interacting components such as a mechatronic system. Taking full advantage of multi-mode products with structurally adaptable components requires a technology which provides complex array of multi-mode functionalities with simple yet structurally adaptable fully integrated architectures along with design methodologies that can handle the full level of integration specific to the trade-offs introduced by that specific technological approach.

1.3. Technological Approaches Enabling Design of Structurally Adaptable Multi-mode Products

Actuation is the process of transforming energy into a motive force, and a device that can carry out this process is known as an actuator [51]. A broad array of technological advancements in current state-of-the-art actuation technologies has inspired the development of numerous point-designs, which can be classified as structurally adaptable multi-mode product concepts. Current technological approaches encompass the use of conventional electromechanical component-based actuators, smart material-based actuators, and pneumatically activated actuation systems. The latter have been gaining popularity in the variety of fields including engineering, soft robotics, human-computer interaction design, and responsive architectures for the last two decades, providing a foundation for developing an emerging technological platform, *constrained layer pneumatic systems*. These systems as a part of this emerging technological platform can produce

a wide spectrum of distributed, complex, and three-dimensional actuation motions in a space-saving, lightweight, inexpensive, and intrinsically safe manner. By using a diverse range of easily accessible materials and fabrication processes, they lend themselves to the design and fabrication of inherently adaptable structural components affording distinct functionalities, showing great potential for facilitating the design of structurally adaptable multi-mode products.

1.3.1. Current Technological Approaches

Current technological approaches enabling the design of structurally adaptable multi-mode products can be classified into three broad categories. These are *electro-mechanically activated component-based approach, smart materials approach,* and *pneumatically activated systems approach*.

The electro-mechanically activated component-based approach category consists of applications employing conventional electromagnetic (e.g., electric motors) or fluid-powered (i.e., hydraulic or pneumatic) actuators to generate motive forces to physically transform the structural components forming the system, enabling the design of structurally adaptable multi-mode products. Greco et al. classified electromagnetic actuators using electric motors into DC and AC motors, with DC motors being categorized as either self-excited or separately-excited, and AC motors being divided into synchronous, induction, and linear types [52]. Fluid power actuators are categorized into two types, linear and rotary, which differ in their output motion; linear actuators include single-acting, double-acting, telescopic, and tandem cylinders, while rotary actuators comprise rotary vane and rack-pinion actuators.

Electromechanical actuators, despite being widely adopted for their ability to deliver precise positional accuracy while maintaining a balance between stress, strain, and speed, are associated with potential drawbacks. These drawbacks include their relatively larger size and increased overall weight, which can limit their use in applications where space and weight are critical factors, as well as the potential for generating noise due to the presence of multiple components.

Figure 12. Structurally adaptable multi-mode application examples using conventional electro-mechanically activated component-based approach. Examples include a tangible user interface element that can switch between a rotational knob and a linear slider on demand (top left) [53], the tilt-rotor mechanism of the V-22 Osprey, which allows for vertical takeoff and landing like a helicopter while also enabling high-speed, high-altitude forward flight like an airplane (bottom left) [54]; the reconfigurable wheel-track, which functions as either a wheel or a triangular track in separate modes to achieve high speeds on roads or traverse diverse off-road terrains (right) [4].

Some examples (Figure 12) that demonstrate the use of a conventional electro-mechanically activated component-based approach for designing multi-modal products include the reconfigurable wheel-track, which functions as either a wheel or a triangular track in separate modes to achieve high speeds on roads or traverse diverse off-road terrains [4]; the tilt-rotor mechanism of the V-22 Osprey, which allows for vertical takeoff and landing like a helicopter while also enabling high-speed, high-altitude forward flight like an airplane [54]; a tangible user interface element that can switch between a rotational knob and a linear slider on demand [53], and a sonic barrier for traffic noise mitigation that employs an origami-inspired mechanism to convert linear actuation motion, enabling different lattice topology configurations to selectively attenuate targeted frequency bandwidths [55].

In the context of designing structurally adaptable multi-mode products, it is frequently necessary to employ distributed actuation across the product's structure to achieve intricate, typically three-dimensional, structural transformations. This distributed approach to generating sophisticated three-dimensional transformations can be accomplished using electromechanical actuators in one of two ways: either by utilizing multiple sets of actuators for point actuation (e.g., through linear or rotary actuators) or by pairing point actuation with an auxiliary mechanism that converts linear or rotary motion into a three-dimensional driving force. However, both alternatives

often present packaging challenges and render the device architecture and the overall design process more complex.

The smart materials approach comprises applications that use smart structures at the microscopic or mesoscopic level, such as shape memory alloys, shape memory polymers, electro-active polymers, dielectric actuators, magnetorheological fluids, and hydrogels. These materials possess the unique ability to change their physical properties (e.g., stiffness) in response to an external stimulus (e.g., heat). According to Spillman, Sirkis, and Gardiner, smart structures are non-biological physical structures that have a clear purpose, a means of achieving that purpose, and a biological pattern of functioning [56]. Smart materials have been promoted as a fundamental technology, providing functionalities including self-sensing, self-healing, self-actuating, self-diagnostic, and shape changing, which support the development of a diverse range of novel products, each possessing unique capabilities [57].

Based on the specific smart material employed, the external stimulus needed to activate the system differs, allowing for the use of electricity, heat, humidity, pressure, or magnetic field changes as inputs to produce outputs such as surface deformation, actuation, color/opacity transitions, or various shape memory effects. These physical transformations take place across the entire volume of the smart material. Some examples demonstrating the use of smart materials in designing multi-modal products include shape-morphing, wind-responsive facade systems utilizing shape memory polymer and alloy composites with embedded heating wires [58]; a reconfigurable amphibious robot capable of walking on land and swimming in water, employing SMA-activated system components in different modes [59]; a smart sleeping mask using thermoresponsive hydrogel to alternate between a cool-and-transparent mode and a warm-and-opaque mode [60]; and a variable geometry chevron capable of switching between two modes on demand, reducing jet engine noise or increasing fuel efficiency during cruising [5] (Figure 13).

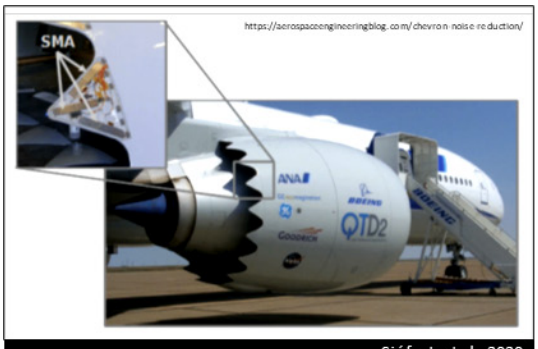

Siéfert et al., 2020

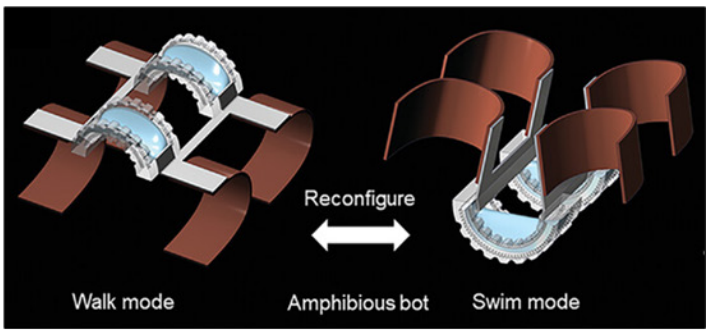

Patel et al., 2022

Figure 13. Structurally adaptable multi-mode application examples using smart materials approach. Examples include a variable geometry chevron capable of switching between two modes on demand to reduce jet engine noise or increase fuel efficiency during cruising (left) [5] and a soft amphibious bot that can reconfigure between walking and swimming modes using embedded SMA wires (on right) [59].

While smart materials inherently offer distributed actuation motions, unlike their electromechanical component-based counterparts, they present drawbacks due to the trade-off between generating substantial strains and producing significant forces [61]. This trade-off has been effectively addressed by introducing various types of smart material actuation device architectures [62], such as spool packaging of SMA wires [63], SMA wire ratchet actuator designs [64], and active knits composed of SMA wires that enable simultaneous multi-dimensional complex strains and substantial forces [65]. However, designing multi-mode products with structurally adaptive components using architected smart materials can be relatively expensive and necessitate complex design and fabrication processes, demanding expert engineering knowledge and a steep learning curve.

The final category of technological approaches, *pneumatically activated systems*, comprises applications which use custom-shaped, airtight bladders and positive-negative fluid pressure to create distributed motive forces that induce physical transformations. Examples of this technology range from miniature soft robots to expandable architectural structures [66]–[72] (Figure 14).

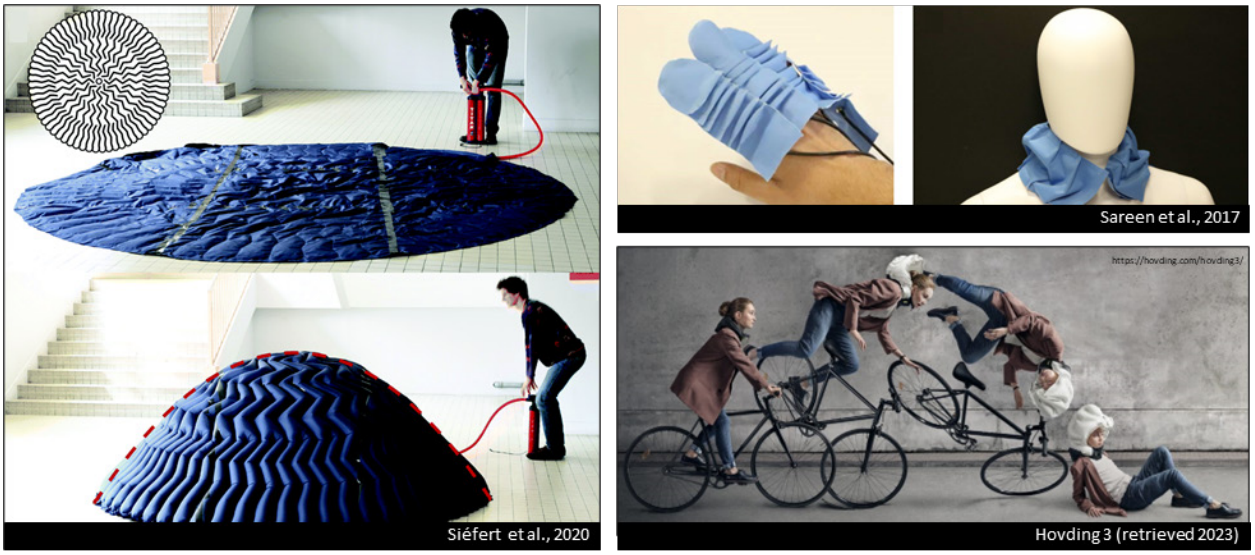

Figure 14. Structurally adaptable multi-mode application examples using pneumatically activated systems approach. Examples include an expandable architectural structure that can transition between thin and flat configuration to dome-shaped configuration (left) [71], pneumatically activated orthopedic devices such as single joint articulation soft exoskeleton for hands and an inflatable neck support (top right) [68], and the Hövding helmet, which is worn around the neck like a collar and deploys less than a second using pneumatic activation when an accident occurs (bottom right) [72].

Pneumatically activated systems offer several advantages, including soft and inherently safe interactions, cost-effective and less complicated fabrication processes, and enhanced packaging capabilities due to their lightweight, stowable-deployable designs. However, when compared to electromechanically activated component-based alternatives, these systems may lack position accuracy and robustness. Additionally, unlike smart materials-based systems, the types of external stimuli necessary for operating the system are limited to fluid pressure (e.g., differential air pressure). Despite these limitations, the future development of pneumatically activated systems remains highly promising as new materials, fabrication techniques [73]–[75], predictive models [76], [77], and design methods [78] continue to emerge in the field. This progress could potentially overcome current drawbacks and render the adoption of pneumatically activated systems increasingly favorable for generating repeatable physical transformations that enable the design of user interacting structurally adaptable multi-mode products.

1.3.2. Emerging Technological Approach: Constrained Layer Pneumatic Systems

Pneumatically activated systems employ a diverse range of architectural approaches, influencing their form and function. Often, the design of these systems is conducted in an ad hoc manner, as they tend to have a free-form structure. A novel type pneumatically activated systems, known as *constrained layer pneumatic systems*, demonstrates significant potential for establishing a systematic design approach due to its hierarchical organized nature. These systems allow for the creation of user-interactive, highly customizable, lightweight, space-saving, and low-cost pneumatically activatable multi-mode products with embedded, repeatable physical transformation capabilities, due to their unique hierarchical architecture and operation principles.

Constrained layer pneumatic systems comprise architectural components (i.e., *cells, ensembles, units, and (sub)assemblies*) consisting of multiple thin, flat, airtight bladder layers that enclose inflatable or vacuumable air cavities. These components are arranged hierarchically, and individually or mutually constrained both internally or externally to provide opportunities for the design of structurally adaptable multi-mode products accommodating architectural and functional transformation capabilities. The fundamental architecture of a constrained layer pneumatic system is made of one or multiple cells containing airtight skin layers enclosing an inflatable air cavity, an extrinsic pneumatic connection, and internal and/or external constraints (Figure 15). Pressure control within the layered structure is achieved through a pneumatic connection port. Based on

pressure variations and cell design, cells produce basic functions which can be combined for higher-level functionalities, such as myriad actuation motions, structural property changes, and sensing capabilities.

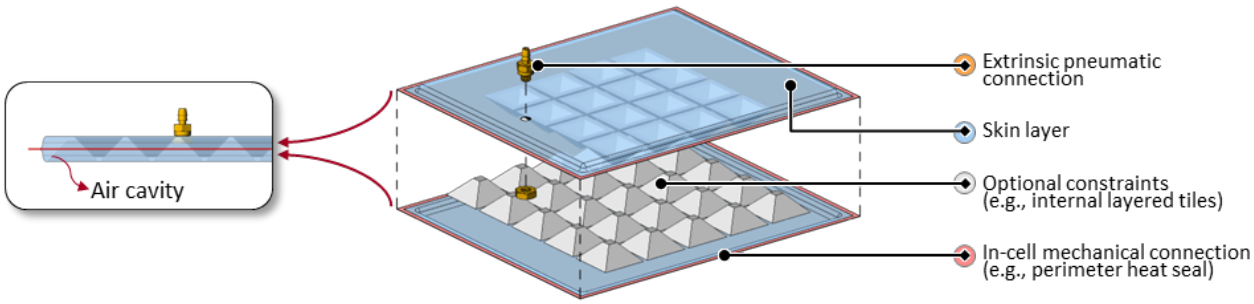

Figure 15. An example generic architecture of the constrained layer pneumatic systems. The architecture of the constrained layer pneumatic systems is composed of airtight skin layers that share a mechanical connection to form an airtight bladder, an extrinsic pneumatic connection to control the pressure level inside the bladder, and a set of optional internal and/or external constraints that affects the physical behavior system exhibits when pneumatically activated.

As a part of a constrained layer pneumatic system, individual cells can be mechanically and pneumatically connected, vertically or horizontally, forming ensembles. Ensembles combine cells' basic functions to create amplified or extended compound functions. For example, a vertically-stacked ensemble aggregates individual angular motions for a large-scale angular expansion. Hierarchical aggregation of the architectural form in constrained layer pneumatic systems coincides with the aggregation of their functional capabilities. Diverse ensembles can be combined to form units with emergent compound functions. Units can then be combined into assemblies, generating higher-level compound functions. These assemblies can function as sub-assemblies within higher-level structures, ultimately constituting a multifunctional constrained layer pneumatic system. enabling the design of various structurally adaptable multi-mode product applications.

Structurally adaptable multi-mode products employing constrained layer pneumatic systems can switch between various operational states, offering users a range of technology capabilities through different interaction modes. Transitioning between these states necessitates pneumatic affordance operations to manipulate air pressure level inside the system relative to atmospheric pressure. These operations fall into four categories based on whether they actively or passively increase or decrease the system's pressure level. Pneumatic affordances include: 1) *get inflated*, achieved using electric or manual devices such as air compressors, diaphragm pumps, hand pumps,

or bellows to actively increase pressure, or through on-demand chemical reactions; 2) *vacuum*, using similar devices to actively decrease pressure; 3) *let air in*, passively directing atmospheric air into vacuumed air cavities using pneumatic valves; and 4) *exhaust air*, passively releasing air from inflated cavities to the atmosphere. The first two affordances create higher or lower pressure air cavities, while the latter two balance pressure differences between the system and atmosphere. Switching between operation states results in activating different sets of functionalities that constrained layer pneumatic systems can produce.

1.4. Research Issues

Constrained layer pneumatic systems show great potential as a technological approach enabling the design of user-interacting structurally adaptable multi-mode products, meeting varying user needs by providing multiple primary functions in different modes. However, there is no design foundation established for the systematic development of structurally adaptable multi-mode products, rendering the holistic early-stage design approach enabling the balance design among the system aspects, such as architecture, functionality, operation, and performance, inaccessible. To realize and evaluate the potential of this novel technological design paradigm, four research issues need to be addressed.

1.4.1. Describe

To effectively use constrained layer pneumatic systems to systematically design structurally adaptable multi-mode products, a formal language enabling the comprehensive **description** of constrained layer pneumatic systems needs to be established. The architectural, functional, operational, and performance components of the system must be detailed to provide a foundation for in-depth **exploration** and **design** by **relating** the structured arrangement of the often-trading-off system aspects.

The architecture of constrained layer pneumatic systems contains the embodied knowledge of its particularly arranged structural components. Currently, there is no unified terminology for describing architectural components of constrained layer pneumatic systems. A description of the overall architecture with a hierarchical classification structure is essential to identify and detail the wide spectrum of architectural components that are available in the design space from the lowest-level of complexity (e.g., sub-cellular level) to the highest-level (e.g., system level). This enables

cataloging differently architected architectural components which can be employed to synthesize new multi-mode product concepts.

The hierarchical nature of the architecture of constrained layer pneumatic systems is reflected in its hierarchical functionality. A structurally adaptable multi-mode product provides a technology capability comprising multiple sub-capabilities corresponding to different modes. Each one of these technology sub-capabilities are fully or partially afforded by the functionalities that are composed by using the emergent functional components embedded in constrained layer pneumatic systems, corresponding to the hierarchically organized architectural components. Therefore, a description of the constrained layer pneumatic systems functionality of which classification structure overlaps with the architectural hierarchy where the lower-level constituent functional components compose the higher-level compound functional components bears an equal importance.

The functionality of a functional component as a part of a constrained layer pneumatic system is activated through a pneumatic operation. To provide an understanding of the system's manner of functioning, the constituents of an operation state need to be described and detailed in the multi-mode context. This enables selectively putting the multiple set of functionalities provided by system's structure governed by its architectural components in simultaneous or sequential use.
To characterize a system's ability to perform a specific functionality that is activated through a specific set of pneumatic operations, it is important to understand and describe how the performance of these functionalities are produced through the architecture, functionality, and operation of the hierarchical system. Decomposing the system's functional performance to its lowest-level constituents aid the extraction and identification of performance metrics. The definition and description of specific performance metrics related to the multi state operation is essential for enabling the quantitative analysis of the multi-modal system performance.

1.4.2. Explore

A comprehensive description of the components of constrained layer pneumatic system aspects provides a basis for generating an array of different architectural components affording unique functionalities. The architectural and functional variation that is achievable in the novel design space of constrained layer pneumatic systems must be hierarchically explored to catalog a range of diverse architectural components and the associated fundamental behaviors lending themselves

to the emerging functionalities. To demonstrate the fundamental behaviors displayed by structural components with varying architectures, it is crucial to explore transferable and novel fabrication techniques that can be employed for their embodiment. Exploring different ways of aggregating a set of same, similar, or dissimilar lowest-level architectural components to form higher-levels architectural components needs to be addressed as a part of the exploration process. This overlaps with the exploration of how to form higher-level functionalities as a combination of the lower-level ones, ultimately resulting in providing technology capabilities at the highest-level. Operational aspects, such as the applicability or degree of sequentially or simultaneously inflating or vacuuming a particular structural component as a part of the multi-mode product system, are dependent on the architectural approach governing the organization of the structural system components; therefore, needs to be considered during the exploration process. The exploration of how to obtain same or similar functionalities using alternative architectural and/or operational approaches is also crucial for providing flexibility for the synthesis of structurally adaptable multi-mode products.

1.4.3. Relate

The aspects of constrained layer pneumatic systems, such as architectural, functional, operational, and performance, are interdependent and influence each other in numerous ways. For example, changing the architectural design of a particular structural component affects the way it interfaces with the remaining structural components forming the structure of the entire constrained layer pneumatic system as a part of a multi-mode product. Furthermore, changing the architectural design often affects the nature or the extent of the functionality that is provided as a part of the overall system as well as having an impact on how it operates and how well it performs. The highly hierarchical architectural organization of constrained layer pneumatic systems coincides with the hierarchy of produced functions. This provides an opportunity for capturing the inherent relationship between architectural and functional hierarchies, exposing the operational and performance aspects of the overall multi-mode product system. Changing the design of architectural features and specific design parameter values may affect the remaining system aspects (e.g., performance); therefore, the relationship among these system aspects needs to be established to enable informed design decisions.

1.4.4. Design

The early-stage design of user-interacting structurally adaptable multi-mode applications employing constrained layer pneumatic systems at a conceptual level requires an iterative approach comprising synthesis, analysis, and re-synthesis.

Synthesis is a process of combining parts to compose a whole, which corresponds to the multi-mode product system at the highest-level of the hierarchy. Systematic description and the design space exploration of the emergent constrained layer pneumatic systems, which produces a range of diverse architectural and functional components that are interrelated, enables synthesis by providing building blocks for the composition of multi-mode product concepts.

Analysis is a detailed examination of a complex system to understand its nature or to determine its essential features by decomposing the whole into its constituents. To aid the decomposition process, a systematic approach must be developed for gaining understanding and providing insights into the architecture, functionality, operation, and performance of the multi-mode systems. The decomposition should provide a direct view into the hierarchical structure of the coupled components of system aspects, which enables the analysis of the interdependencies among these components, motivating the re-synthesis of the system being designed.

Re-synthesis is a process of modifying the already-synthesized system for generating alternative and novel designs. To initiate a re-synthesis, a set of design goals, objectives, modifications, and an associated tradeoffs (if applicable) must be identified as a part of the design analysis. A designer must answer the following four questions: 1) ***why*** the design change is being made, 2) ***what*** design change is being made, 3) ***how*** the design change is being made, 4) ***why-not*** make the design change. To systematize and guide the re-synthesis as a process of achieving a design objective by actualizing a design modification to attain a design goal while allowing a design tradeoff, design strategies must be formulated by leveraging the hierarchical nature of the constrained layer pneumatic systems.

This early-stage design approach should facilitate the systematic understanding of the interrelated architectural, functional, operational, and performance breakdown of constrained layer pneumatic systems, enabling designers to iteratively synthesize, analyze, and re-synthesize multi-mode product concepts. In addition, the early-stage design approach should enable transitioning to the embodiment design stage by providing a basis for relating the effects of architectural and parametric design variations to the quantifiable performance aspects of structurally adaptable multi-mode product concept prototypes.

1.5. Research Goal and Objectives

The goal of this research is to develop the design science foundation enabling a systematic early-stage design space exploration for emerging constrained layer pneumatic system technologies that provides a basis for the design of structurally adaptable multi-mode products providing multiple functionalities affording physical interaction with users. Three research objectives are crucial to meeting this goal.

1. **Technological Foundation for Emerging Constrained Layer Pneumatic Systems (CLPS).** Develop a technological foundation for constrained layer pneumatic systems, capturing the breadth of structurally adaptable basic architectural and corresponding functional components that provide elemental building blocks for exploring, designing, and implementing multi-mode product concepts enabling users to access a variety of technology capabilities across different operation states and interaction modes.
2. **Design Supported by Hierarchical Functional Architectural Decomposition.** Establish a formal hierarchical analytical design description that provides a direct view into the hierarchical structure of a system's interrelated form and function, which supports goal-oriented re-synthesis of user-interacting structurally adaptable multi-mode products employing constrained layer pneumatic systems at a conceptual level.
3. **Architectural and Parametric Design for Multi-modal Performance.** Build an understanding of how to explore and relate conceptual architectural variations and parametric design variations within a particular category of constrained layer pneumatic systems, internally tiled pneumatic textiles, to the quantifiable performance of a structurally adaptable multi-mode product, enabling negotiation between performance metrics to obtain intended design outcomes.

It is necessary to address all these objectives to realize constrained layer pneumatic systems as an enabler for the systematic design of numerous user-interacting structurally adaptable multi-mode products, providing different technology capabilities to users in different operational states.

1.6. Research Approach

To meet the goals of this research and establish the design science base for designing structurally adaptable multi-mode products using constrained layer pneumatic systems, the

research objectives are addressed through three primary tasks: 1) defining and detailing constrained layer pneumatic systems architecture, operation, behavior, and fabrication, 2) developing a hierarchical functional architectural decomposition approach for supporting the synthesis, analysis, and re-synthesis of structurally adaptable multi-mode product concepts, and 3) demonstrating an approach for the exploration and architectural and parametric design for tailored multi-modal performance.

1.6.1. Technological Foundation for Constrained Layer Pneumatic Systems

Constrained layer pneumatic systems is an emerging technology that provides distributed physical transformation capabilities, enabling the development of adaptable structural components that are lightweight, compactly packaged, inexpensive to build, and intrinsically safe to interact with. However, currently there is no technological foundation for understanding, documenting, and communicating the basic constituents of such systems, hindering the design and evaluation of potential multi-mode products using this technology.

Recent efforts have been made to organize the constituent components of constrained layer pneumatic systems with the development of technological platforms and modular toolkits aiding in their design and fabrication [73], [79]–[83]. Researchers have introduced various pneumatically activated shape-changing and reconfigurable interfaces [6], [84], [85]; soft robots and structures [59], [66]–[68]; and tangible user interfaces [39], [86], [87] through alternative fabrication techniques and material libraries. These tools aim to facilitate creative exploration in the field of shape-changing interface design by providing basic building blocks that enable various structural transformations. Although these approaches identify some of the useful structural transformation abilities (e.g., bending, expanding, and sensing) that can be accomplished in a specific architectural subclass and how they are related in terms of form, operation, function, and performance, most of them have a major drawback of not having a systematic arrangement for describing a broader range of interrelated components that potentially make up a complete multi-mode product using pneumatic systems. This hinders the understanding of the interplay between system's architectural, operational, functional, and performance aspects, resulting in a production of a vast range of specific point-design prototypes in the literature without a robust logical basis. To address this limitation and enable the systematic design and assessment of structurally adaptable multi-mode products using emerging constrained layer pneumatic systems, it is essential to develop a formal

language that describes the generic architecture, operation, and behavior of these systems in conjunction with detailing the fabrication techniques and materials necessary for implementation.

To facilitate an in-depth understanding, documentation, and communication of the basic constituents of constrained layer pneumatic systems that are hierarchical in nature, the architecture of constrained layer pneumatic systems is described and detailed systematically by classifying the subcellular features of the lowest-level functional architectural component, *cell*, into skin, connectivity, and constraint categories, with each category further divided into subcategories to fully define the organization of cell's structure. Pneumatic affordances, which activate the cell's functionality through its imposed structure, are categorized into four types based on their ability to actively or passively increase or decrease the pressure level inside the system. The operation of these affordances triggers fundamental behaviors that are categorized into four types as well based on their ability to expand or contract the air cavity in the cell's structure in-plane or out of plane. The characteristics of subcellular features are then related to the corresponding fundamental behaviors through a set of pneumatic affordance operations, resulting in a comprehensive understanding of the system's architectural, functional, and operational aspects. This provides a basis to analyze the system's performance. Potential fabrication techniques and material systems are categorized into three different approaches: adhering existing skin layers, fusing existing skin layers, and producing already-fused skin layers. Alternative ways of fabricating a proto-cell (i.e., the simplest possible cell) are enumerated, enabling the embodiment of structurally adaptable multi-mode products in the later stages of the design process. Systematic architectural modifications to the subcellular feature characteristics of a fundamental proto-cell are related to the corresponding fundamental behaviors and emergent cell functions through a set of multi-state pneumatic affordance operations. This results in the enumeration of a sampling of the range of diverse cell alternatives that serve as building blocks for composing higher-level constrained layer pneumatic systems (e.g. ensembles, units, assemblies). The design of a variety of structurally adaptable multi-mode product concepts are described, building upon the enumerated building blocks forming different constrained layer pneumatic systems, demonstrating a range of technology capabilities tailored to specific contexts.

Chapter 2 will provide a comprehensive description of constrained layer inflatable systems' lowest-level architectural organization, pneumatic affordance operations, fundamental behaviors,

and a catalog of emergent cell functions, along with five multi-mode product concepts presented in detail.

1.6.2. Design Supported by Hierarchical Functional Architectural Decomposition

For designing structurally adaptable multi-mode products employing constrained layer pneumatic systems, an integrated hierarchical characterization scheme needs to be established first. This scheme should allow designers to systematically capture the relationships among architectural, functional, operational, and performance system aspects, facilitating iterative synthesis and analysis of structurally adaptable multi-mode product concepts during the early-stage product design process.

Existing research in literature investigating the interrelationships in technical systems has mainly concentrated on the product clusters excluding the structurally adaptable multi-mode ones [22]. Although several systematic approaches, such as function structures and functional decomposition [16], [19], [20] [9]; product architecture [2]; and modular design methodologies [23], [25], have been proposed to guide the development of generic product systems by often segregating the analysis of product form and function, they can still serve as valuable starting points for the development of an integrated characterization scheme. This scheme would be specifically aimed at designing multi-mode products using constrained layer pneumatic systems, which serves as an ideal technological platform for capturing the inherent and cyclic relationship between architectural and functional organization forming the overall product system. The functional and architectural variety afforded by constrained layer pneumatic systems is organized in a hierarchical manner, where basic functions produced by basic architectural components combine in compound architectural components to produce higher-level compound functions, and ultimately technology capabilities of a system.

In Chapter 3 of this document, an integrated hierarchical characterization scheme called *hierarchical functional architectural decomposition* is introduced. This scheme describes the product system hierarchy in detail to support various analysis and synthesis design methods and enables incremental improvements, replacements, and speculative designs based on existing ones. A block diagrammatic technique to analyze and visualize the coupled functional and architectural relationship within and between the hierarchical levels is developed to establish hierarchical functional architectural decomposition. This provides a direct view into the system's multi-mode

operation by describing the architectural and functional hierarchies comprising cell, ensemble, unit, assembly, and system levels and detailing and classifying architectural and functional components into three groups based on their constituent and/or constitutive roles in composing the overall product system with its corresponding technology (sub)capabilities at the system level. To demonstrate the implementation of the hierarchical functional architectural decomposition in context, the approach is applied to a specific structurally adaptable multi-mode product, namely the mobile phone restraint mat. The proposed approach inter-relates the architectural and functional components at each level, starting from the cell level up to the ensemble, unit, assembly, and system levels. This provides a comprehensive view of the system hierarchy, including its multi-mode operation and sequencing, and enables the extraction of generalized structural features of the decomposition. Additionally, the diagramming conventions and pneumatic operating states and sequences are concretized to ensure a consistent and transferable iterative analysis, synthesis, and re-synthesis of multi-mode products using constrained layer pneumatic product systems. For the re-synthesis of already-synthesized multi-mode product concepts, ten distinct design strategies are formulated and grouped under three design strategy direction categories, *re-design, incremental innovation,* and *radical innovation*. These re-synthesis strategies encompass different combinations of design objectives (*what*), design goals (*why*), design modifications (*how*), and associated tradeoffs (*why-not*), where the design objective of each strategy is achievable by actualizing a design modification to attain a design goal while allowing a design tradeoff for the re-synthesis of an existing multi-mode product using a constrained layer pneumatic product system. The usefulness of the ten proposed design strategies in guiding the re-synthesis process towards re-design, incremental innovation, and radical innovation is demonstrated by using a set of already-synthesized multi-mode products (which are described in Chapter 2) that employ constrained layer pneumatic systems as starting points, resulting in the generation of early-stage conceptual design alternatives that achieve the intended design outcome.

The complete details of the design process supported by hierarchical functional architectural decomposition approach will be provided in Chapter 3.

1.6.3. Architectural and Parametric Design for Multi-modal Performance

Constrained layer pneumatic systems are a promising technological approach producing unique technology capabilities such as locally tailorable distributed complex actuation motions,

changes in structural properties, and different means of sensing. To demonstrate the implementation of these technology capabilities in structurally adaptable multi-mode applications, a systematic design approach is developed by focusing on a particular architectural variation of constrained layer pneumatic systems, the internally tiled pneumatic textiles, which are equipped with the capability of physically transforming from soft to rigid states enabling moldability on demand.

Internally tiled pneumatic textiles are based on layers of rigid tiles arrayed in regular patterns within an airtight bladder, enabling the overall stiffness to be controlled as a function of vacuum pressure applied. The architecture of these pneumatic textiles is described, detailed, and categorized into three types of tile architectural classes based on the approaches providing a defined spatial order among the adjacent tiles inside a bladder. Due to the ability of adjacent tiles to move relative to each other, these pneumatic textiles provide a thin profile surface that can be molded into arbitrary complex geometries. The multiple operation states for the internally tiled pneumatic textiles are emerged as draping, shaping, and rigidizing states in relation with the envisioned interaction scenarios with users, supported by the cell level operation states and emergent cell functions as described in Chapter 2. In draping state, the pneumatic textile can be draped over arbitrary objects at atmospheric pressure. In shaping state, it can be manually shaped into various configurations to accommodate target forms as the vacuum pressure is introduced to the airtight bladder. In rigidizing state, it can be fully rigidized as the vacuum pressure reaches a practically available maximum. In line with the multiple operation states, the overall technology capability, moldability, is decomposed into sub-capabilities, drapability, shapability, and rigidizability, the constituents of which are fully captured by using hierarchical functional architectural decomposition approach described in Chapter 3, interrelating architectural components to the functional ones from the lowest- to the highest-levels in the system hierarchy. This enables characterization of the system's moldability performance by considering the architectural, functional, and operational system aspects, providing a basis for a holistic design process.

To quantify the overall moldability performance concerning functional, operational, and architectural aspects, a set of empirical metrics and procedures is developed, enabling the characterization of five dimensionless performance metrics (i.e., draping angle, conformability, setability, flexural rigidity, post yield elasticity) to quantify the performance of the lower-level

functions contributing to the performance of the higher-level technology (sub)capabilities (drapability, shapability, and rigidizability). A hierarchical series of three experimental studies to develop an in-depth understanding of how tile architectural class/subclass and corresponding architectural feature variations affect the performance of internally tiled pneumatic textiles is conducted. These experimental studies include analyzing comparative performances across three tile architectural classes, analyzing design couplings within the bladder-attached tiles architectural class using correlation matrices, and evaluating comparative performances among different pneumatic textiles equipped with equilateral triangle tiles representing the bladder-attached non-connected tiles subclass based on tile layer overlap and intermediate layer layup architectural feature variations. A predictive algebraic design approach using controlled experimental parametric studies is developed and validated, enabling an empirical fit to describe the relationship between sub-cellular feature characteristics (i.e., tile size, gap, and height) of a particular type of internally tiled pneumatic textiles and the metrics which quantify the performance of higher-level technology (sub)capabilities. This enables the design of structurally adaptable multi-mode products with tailored technology sub-capability performance by facilitating the balance among engineering performance metrics. The predictive algebraic design approach is employed for designing a particular structurally adaptable multi-mode product, *moldable active cargo blanket,* which provides moldability with various tailorable performance-balancing aspects. The moldability performance of three different active cargo blankets each suited to different target use contexts are tailored by using this approach, and the performances of the resulting designs are experimentally validated against their intended design goals.

While the specific results will be presented in the context of internally tiled pneumatic textiles in Chapter 4, the design techniques and specific analysis apply equally well to other constrained layer pneumatic system architectures providing complex array of trading-off functionalities through multiple operation states.

1.7. Outcomes and Contributions

The development of a design science foundation for facilitating systematic early-stage exploration of the emerging constrained layer pneumatic system technologies provides a basis for designing structurally adaptable multi-mode products that offer multiple functionalities affording physical interactions with users. Furthermore, this foundation holds the potential to be extended to

various non-pneumatically operated technological approaches capable of delivering complex, three-dimensional, and distributed actuation motions throughout a product's structure.

Multi-mode products have been used for centuries, offering users multiple sets of functionalities across different interaction modes. These modes are made possible through non-reconfigurable, modular, or adaptable structural configurations dictated by their architecture. While the majority of these products have traditionally been operated manually by users due to their non-reconfigurable or modular configurations, recent advancements in pneumatically activated system technologies pave the way for embedded methods of on-demand structural transformations, enabling seamless switching between modes. The ability to seamlessly switch between modes allows for the design of a new genre of products across various fields, including transportation, aerospace, architecture, robotics, biomedical, and consumer devices. These innovative products aim to address users' context-specific, changing needs by offering multiple primary sets of functionalities through their multiple operation states tailored to different situations. A novel type of pneumatically activated system, *constrained layer pneumatic systems*, has been identified as a promising technological platform to enable on-demand structural transformations. These systems facilitate complex three-dimensional actuation motions distributed throughout a product's structure in a highly customizable, lightweight, space-saving, and cost-effective manner. However, several challenges must be addressed to implement constrained layer pneumatic systems in the design of user-interacting, structurally adaptable multi-mode products. This research lays the foundation for the design science of early-stage structurally adaptable multi-mode products, capitalizing on the rich design space unveiled by this emerging and versatile technological approach.

Constrained layer pneumatic systems produce a plethora of functionalities, such as various actuation motions, structural property changes, and sensing capabilities, through their hierarchically arranged architectural components that are individually or mutually constrained internally or externally. To explore the breadth of achievable functionalities afforded by the constrained layer pneumatic system architecture, a hierarchical classification scheme is established, describing five levels of system hierarchy comprising cell, ensemble, unit, assembly, and system levels. A formal language is developed to systematically describe and detail the basic constituents of constrained layer pneumatic systems architecture, operation, and corresponding functionalities at the cell level, providing a basis for a bottom-up in-depth understanding of the

relationships among the system's architectural, functional, operational, and performance components at the higher-levels of the system hierarchy. The most basic architectural components, *cells*, residing at the cell level are detailed and classified into their subcellular features, fully defining the organization of cell's structure, aiding the unification of the documentation, communication, and exploration of this emerging technological design space, which facilitates the production of a sampling of the range of diverse cell alternatives and corresponding emergent functionalities that serve as building blocks for composing higher-level constrained layer pneumatic systems (e.g. ensembles, units, assemblies) producing a multi-mode product application at the highest-level (i.e., system level) providing technology (sub)capabilities.

An integrated hierarchical characterization scheme, *hierarchical functional architectural decomposition approach*, and a unified terminology is established to describe constrained layer pneumatic system components and hierarchy in detail to facilitate analysis and synthesis design methods for developing structurally adaptable multi-mode products and to enable incremental improvements, replacements, and speculative designs based on existing ones. A block diagrammatic technique is developed to analyze and visualize the coupled functional and architectural relationship as well as describing the system's operational aspects within and between the hierarchical levels, promoting collaboration across different disciplines by facilitating a consistent and transferable iterative analysis, synthesis, and re-synthesis of structurally adaptable multi-mode products using constrained layer pneumatic product systems. Ten distinct design strategies for re-synthesizing multi-mode product concepts are formulated, categorized under re-design, incremental innovation, and radical innovation, encompassing various combinations of design objectives, goals, modifications, and tradeoffs, enabling the achievement of each strategy's objective through specific design modifications attaining a design goal while allowing for tradeoffs in the re-synthesis process using constrained layer pneumatic product systems. The formulated design strategies aid designers in generating goal-oriented alternative designs as well as creating novel ones. The combination of formulated design strategies, hierarchical functional architectural decomposition, and the emerging constrained layer pneumatic systems technology serves as a basis facilitating a holistic design approach through which the interrelated architectural, functional, operational, and performance system aspects can be systematically captured throughout the early-stage product design process. Moreover, the same design approach can be adapted to incorporate

diverse technological approaches that are inherently hierarchical in respect to their architecture and functionality.

A design case study, comprising a series of architectural and parametric design studies, demonstrates an effective way of systematically exploring a hierarchically organized broad architectural design space and quantitatively modelling the relationship between parametric design variables and multi-modal performance. This approach is showcased through facilitating the design of a specific structurally adaptable multi-mode product, *moldable active cargo blanket*, with tailored multi-modal performance attributes. The architecture of the moldable active cargo blanket is based on a specific type of constrained layer pneumatic system, *internally tiled pneumatic textiles*, providing three primary technology sub-capabilities: *drapability, shapability,* and *rigidizability*, which altogether produce the technology capability, *moldability*. The architecture of the pneumatic textiles is categorized into various architectural classes and sub-classes, the selection of which affects the types of architectural features available for the design detailing. The approach employed in conducting the series of architectural design studies is targeted towards exploring the layers of the architectural hierarchy including analyzing performance across tile architectural classes, investigating design couplings within a tile architectural subclass, and assessing the effects of architectural feature variations. The results obtained through this approach inform the process identifying the detailed design variables that can be parametrized. The parametric design study forms a basis for developing a predictive algebraic design approach enabling an empirical fit to describe the relationship between detailed design variables (i.e., specific values for a subcellular feature characteristic) and the metrics which quantify the performance of higher-level technology sub-capabilities. These metrics are identified by relating the cell level operation states and emergent cell functions, which are coupled with the hierarchical functional architectural decomposition approach, to the performance of each technology (sub)capability. This exploits the relationship between technical performance from a technological point of view to the context-specific product use performance from a user-interaction point of view to enable direct empirical measurements that have implications on the product use. In addition to enabling the design of moldable active cargo blankets with tailored moldability performances, the procedures used in these architectural and parametric design studies can be adopted to investigate other types of constrained layer pneumatic system architectures to facilitate the detailed design of other context-specific multi-mode product applications.

The diverse architectures and corresponding functionalities offered by emerging constrained layer pneumatic systems can be harnessed to create a new generation of single or multi-mode products with non-reconfigurable, modular, and/or structurally adaptable architectures. In addition to facilitating the systematic early-stage design of user-interacting single or multi-mode products, the range of building blocks provided can be utilized to develop various soft actuators capable of generating complex, three-dimensional, structurally distributed, and potentially graded miniature to large-scale actuation motions. By expanding the catalog of building blocks, creative cross-pollination among researchers and designers from different fields will be encouraged, setting the stage for future design applications yet to emerge. In addition to important technological advancements, this research provides the design science foundation facilitating a systematic early-stage design space exploration for emerging constrained layer pneumatic system technologies, enabling the design of structurally adaptable multi-mode products providing multiple sets of context-specific functionalities.

This research's contribution extends beyond the design of structurally adaptable multi-mode products using constrained layer pneumatic systems. The hierarchical functional architectural decomposition approach can be broadened to offer a comprehensive perspective on the relationships among architectural, functional, operational, and performance aspects of any product system with hierarchically organized system components. The systematic design process for creating structurally adaptable multi-mode products can be adapted to thoroughly explore the hierarchically organized architectural design spaces provided by electro-mechanical component-based and smart-materials-based technological approaches. This design science foundation fosters a diverse range of inclusive and equitable user-product interaction opportunities by addressing users' varied needs through a new generation of products that offer functional adaptability via their adaptive structures, targeting to provide more by consuming less.

Chapter 2. Technological Foundation for Emerging Constrained Layer Pneumatic Systems

Pneumatically activated devices have been proven useful in various fields due to the technology capabilities they provide such as distributed actuation, changes in structural properties, and distributed sensing. In the medical field, capabilities such as moldability, repositioning, variable stiffness, and actuation have been used across applications including medical casts [88], wheelchairs [89], rehabilitation, [90], and muscle actuators [91]. The aerospace, civil engineering, and architecture fields have developed lightweight deployable systems such as antennas [92], [93] and space structures [94], as well as temporary flood control dams [95], rapidly deployable bridges [96], [97], emergency shelters [69], and inflatable facades [98]. In the automotive field, pneumatic systems capable of morphing and texturization have been explored for developing external aerodynamic surfaces [99], designing driver information and alert systems [86], [100], and building lightweight, portable, and load-bearing mobility devices such as scooters and wheelchairs that can be deployed on demand [101]. The human computer interaction field has demonstrated pneumatically activated devices for interactive displays with flexible [39], [87], malleable [6], and reconfigurable, controllable stiffness controls on pressure-sensitive touch surfaces [84], [86]. Finally, the recently established field of soft robotics has been producing ever-growing numbers of artifact-oriented design examples. These examples adopted and further developed the existing fabrication techniques to demonstrate the capabilities such as locomotion [102], crawling and jumping [59], climbing [66], [103], growing [67], and reconfigurability [102] that can be used to develop assistive devices [104], [105], search and rescue systems [106], [107], and end-effectors employing soft grippers [108]–[111]. These pneumatically activated systems enable the design of structurally adaptable multi-mode products with a wide range of functionalities, using a vast variety of architectural approaches. However, the design of these generally free-form systems is typically done in an ad hoc manner. This makes it difficult to describe their system aspects systematically and consistently across different examples, especially in distinct fields, which in

turn hinders in-depth understanding, analysis, and synthesis of the interplay among their architectural components, their operation, and resulting functionalities and performance.

An emergent technological approach, *constrained layer pneumatic systems*, represents a new architectural class of pneumatically activated systems. They are formed from many flat layers of thin airtight bladders arranged hierarchically, and constrained both internally and externally, either individually or mutually. By leveraging the hierarchical organization of system aspects and corresponding components in constrained layer pneumatic systems, it becomes possible to systematically describe, communicate, and understand their designs in a way that is at least as expressive as existing pneumatically activated systems.

Recently, there has been an effort to establish such hierarchical organization by attempting to provide a technological basis and modular toolkits for aiding the design and fabrication of constrained layer pneumatic systems. Yao et al. [79] developed a technological platform for designing pneumatically activated shape-changing interfaces. This platform addresses the fabrication of the layered structures of soft composite materials that provide shape changing primitives such as curving, curling, vertical and horizontal expansion, and texturization when inflated. Similarly, design and fabrication pipelines comprising software simulation to predict the resulting shape-change based on pneumatically activated bending mechanisms, and alternative fabrication techniques and material libraries are introduced [73], [80]. Researchers have also developed pneumatically operated physical toolkits to simplify the design and fabrication of soft robots and structures and shape-changing tangible user interfaces. Youn and Shtarbanov proposed a collection of origami-inspired modular building blocks that can be effortlessly combined by designers to rapidly create various soft robotic structures capable of providing intricate and dynamic physical behaviors such as contracting, twisting, and folding [81]. Kim et al. [82] introduced a set of basic building blocks that facilitate various structural transformations. These transformations include changes in length, area, volume, and porosity, to promote creative exploration in the field of shape-changing interface design. Similarly, Webb et al. developed a toolkit consisting of primitive components that focus on various aspects of shape-changing structures, including 3D forms, types of movements, textures, pressure levels, and membrane materials, which can be combined to create a diverse range of functionalities for self-inflating structures [112], [83].

While these approaches each enumerate the functionalities (e.g., bending, expanding, sensing) that can be achieved within a particular architectural sub-class, relating the form, operation, function, and performance within that class, a significant limitation of most of these technological approaches is the lack of systematic organization regarding the components that constitute the overall pneumatic systems. In the current state of art, the architectural details of the structures, potential fabrication techniques and material alternatives, pneumatic operation variables, and the resulting structural transformation archetypes are grouped in a non-hierarchical arrangement without a comprehensive discussion of their interrelations and mutual influence on one another. This limits the coherent description and communication of a broader range of system configurations, consequently hindering the in-depth understanding of the interplay between the architectural, operational, and functional components of such systems. This results in promoting the production of a vast range of specific point-design prototypes in the literature without a robust logical basis. Additionally, the absence of a widely accepted and comprehensive terminology and language for describing, communicating, and comprehending the design of pneumatically activated systems has limited the potential collaboration among researchers across disciplines, thereby impeding the systematic exploration and accumulation of knowledge. To explore the multi-mode product design space enabled by the constrained layer pneumatic system and to interrelate the architectural, functional, operational, and performance aspects of such product systems, it is necessary to have a coherent description of the system components that aids in communicating a broader range of system configurations.

The goal of this chapter is to develop a technological foundation for constrained layer pneumatic systems, capturing the breadth of structurally adaptable basic architectural and corresponding functional components that provide elemental components for designing and implementing multi-mode product concepts enabling users to access a variety of technology capabilities across different operation states and interaction modes. To reach this goal, the objectives are listed as:

- developing a grammar and visual language for the description and communication of the architectural design, operation, and functionality of the lowest-level components (i.e., cells) that make up constrained layer pneumatic systems,
- exploring techniques and material systems which are applicable for the scalable fabrication of the structurally adaptable basic architectural components,

- providing an exploration of the relationship among the subcellular features of the basic architectural components, the fundamental behaviors they exhibit in each operation state, and the corresponding emergent functions,
- demonstrating the complexity and range of structurally adaptable multi-mode product concepts achievable within the design space afforded by constrained layer pneumatic systems to provide context-specific technology capabilities.

This chapter enables an understanding, documentation, and communication of the basic constituents of constrained layer pneumatic systems, which are hierarchical in nature. The architecture of constrained layer pneumatic systems is systematically described and detailed by classifying the subcellular features of the lowest-level functional architectural component, *cell*, into skin, connectivity, and constraint categories, with each category further divided into subcategories to fully define the cell's structure. Pneumatic affordances, which activate the cell's functionality through its imposed structure, are categorized into four types based on whether they actively or passively increase or decrease the pressure level inside the system. The fundamental behaviors triggered by these operations are also categorized into four types based on expanding or contracting the air cavity in cell's structure in-plane or out of plane. The characteristics of subcellular features are then related to the corresponding fundamental behaviors through a set of pneumatic affordance operations, resulting in a comprehensive understanding of the system's architectural, functional, and operational aspects, providing a basis to analyze the system's performance. A range of potential fabrication techniques and material systems are explored and categorized under three fabrication approach categories, 1) adhering existing skin layers, 2) fusing existing skin layers, and 3) producing already-fused skin layers. Any of these fabrication approaches can be employed to form a permanent in-cell mechanical connection between the skin layers to produce a proto-cell, enabling the embodiment of structurally adaptable multi-mode products. Systematically modifying the characteristics of the subcellular features of a fundamental proto-cell enables relating the architectural modifications to the corresponding fundamental behaviors and emergent cell functions in relation to a set of multi-state pneumatic affordance operations. Such systematic modification results in the enumeration of a wide range of architecturally diverse, operationally adaptable, and functionally instrumental cell alternatives with tailorable performance, which serve as building blocks for the composition of higher-level multi-mode product systems. A variety of structurally adaptable multi-mode product concepts that

are built upon the enumerated basic architectural and functional components as building blocks forming different constrained layer pneumatic systems are described. This demonstrates that providing a range of technology capabilities tailored to specific contexts is achievable using constrained layer pneumatic systems.

2.1. Constrained Layer Pneumatic Systems

The constrained layer pneumatic systems technology enables the design of highly customizable, lightweight, space saving, and low-cost user interacting multi-mode products. These products are composed of multiple thin flat airtight bladder layers which encapsulate inflatable or vacuumable air cavities, the pneumatic activation of which are constrained both internally and/or externally to produce various combinations of fundamental behaviors affording an array of emergent functionalities. These pneumatic systems are arranged in layered hierarchical architectures that correspond to a hierarchy of functionalities. When these higher-level hierarchical systems are exposed to a relative pressure change, they exhibit various technology capabilities such as deploying and stowing, stiffness changing, texturization, actuation, etc., which build on the emergent lower-level functionalities.

A generic architecture, basic architectural components (i.e., cells), and the characteristics of the constituent (i.e., sub-cellular) features that distinguish these basic architectural components from one another which together enable the composition of higher-level constrained layer pneumatic system architectures are detailed. A set of pneumatic affordance operations as well as the fundamental behavior couplings that are activated by these operations are enumerated, which provides a basis for producing emergent cell functions.

2.1.1. Constrained Layer Pneumatic Architecture

The basic architecture of a constrained layer pneumatic system (Figure 16) is composed of one or multiple *cells* made of 1) airtight skin layers that encapsulate an inflatable/vacuumable air cavity, 2) an extrinsic pneumatic connection, and 3) internal and/or external constraints. The top and bottom layups, which contain skin layers and constraints if any, of a cell are stacked and permanently sealed to enclose the air cavity. A vacuum port vertically attached to one of these skin layers, or laterally sandwiched between both, allows control over pressure inside the layered structure. Based on the pressure level variations in a cell and the architectural design of a cell, the

cell produces *basic functions* (i.e., emergent cell functions), which can be combined to provide higher-level functionalities such as different modes of actuations (e.g., linear actuation, bending, twisting), changes in structural properties (e.g., rigidity and extensibility), and sensing capabilities (e.g., contact pressure, proprioception, or environmental conditions). The architectural design of a cell, particularly the constraints, both internal (e.g., rigid tiles, tethers) and external (e.g., inter-component and/or external structural connections), afford the basic functions it produces through its pneumatic affordance operations as the pressure level changes.

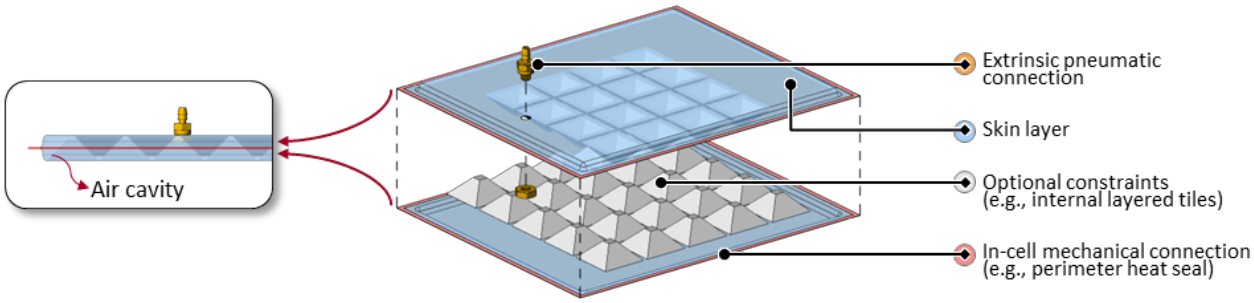

Figure 16. An example generic architecture of the constrained layer pneumatic systems. The architecture of the constrained layer pneumatic systems is composed of airtight skin layers that share a mechanical connection to form an airtight bladder, an extrinsic pneumatic connection to control the pressure level inside the bladder, and a set of optional internal and/or external constraints that affects the physical behavior system exhibits when pneumatically activated.

An individual cell can be mechanically and pneumatically connected to a multiplicity of identical, modified, or brand-new cells in a stacked (vertical) or in-plane (horizontal) fashion, generating various forms of *ensembles*. Because an ensemble is typically formed from an array of cells of the same type, an ensemble often combines the basic functions of the cells that constitute them to create *compound functions* (i.e., functions composed of simpler, lower-level functions) which are generally amplified or extended versions of the basic functions. For example, an ensemble comprising a vertical stack of cells, each of which can expand with a small degree of angular motion, aggregates the individual angular motions into a combined large scale aggregate angular expansion, combining the effects of the individual cells. Thus, the hierarchical aggregation of the architectural form of a constrained layer pneumatic system often coincides with the aggregation of its functional capabilities.

Differently generated ensembles can be combined in myriad ways to produce *units*. Since the compound functions of the ensembles that make up a unit can be vastly different, new emergent *compound functions* can be produced. For example, an ensemble producing aggregate angular expansion can be combined with another ensemble producing aggregate linear expansion to

produce a unit that can deploy from a flat surface and push an object. These units can be combined to form an *assembly* of units, which further creates higher-level compound functions (e.g., two opposing pushes in an assembly create a squeeze). This differs from a unit in that a unit is necessarily formed of ensembles of cells whereas assemblies are generally formed from units rather than e3nsembles directly, and therefore are more complex in form and functionality. In general, assemblies can themselves act as sub-assemblies in a higher-level assembly and eventually constitute the design of a particular, potentially multifunctional, constrained layer pneumatic *system* that produces one or more *technology capabilities* to enable a multi-mode product application.

Detailing the characteristics of the subcellular features of basic architectural components provides a basis to understand the relationship between the composition of the variety of basic (i.e., cell) and compound (e.g., ensemble) architectural components and the corresponding basic and compound functionalities.

2.1.2. Characteristics of Sub-cellular Features of Basic Architectural Components

Cell is the lowest level architectural component but itself has a complex arrangement of a logical set of sub-cellular features the characteristics of which give rise to the emergent cell functions that act as constituent basic functions at the cell level as a part of the hierarchical system. Unlike architectural components that reside within cell-or-above levels in the architectural hierarchy, the sub-cellular features are organized logically rather than being organized with respect to the physicality of their constituents. Such logical organization enumerates three sub-cellular feature categories: 1) *skin,* which describes the characteristics of skin layers, 2) *connectivity*, which describes the rules of connectivity affording the construction of a cell and other higher-level architectural components, and 3) *constraints*, which describes the details of physical restrictions imposed on a cell, contributing to the physical behavior it displays.

2.1.2.1. Skin

There are three major aspects comprising the characteristics of a skin layer: *skin type*, *skin thickness*, and *skin uniformity*. Skin type classifies the potential materials that can be used as skin layers based on two levels of physical extensibility (extensible - inextensible) and three levels of physical flexibility (low-medium-high). For example, a bare sheet of thermoplastic polyurethane (TPU) would be classified as an extensible material with high flexibility, whereas a relatively thick

polypropylene sheet would be classified as inextensible material with low flexibility. Skin thickness applies to the top and bottom skin layers, indicating whether a prospective cell is architecturally symmetric or not. Skin uniformity specifies whether the constituents of a cell layup are uniform or non-uniform (i.e., changing cross-section thickness) transversally.

2.1.2.2. Connectivity

The rules of connectivity that affords cell construction are grouped under four sub-categories: *in-cell mechanical connection, inter-component mechanical connection, inter-component pneumatic connection,* and *extrinsic pneumatic connection*. The in-cell mechanical connection describes the permanent bonding between top and bottom skin layers, forming an enclosed cell or a cell with a designated opening or openings around its perimeter. The inter-component mechanical connection describes how adjacent components (e.g., cells, ensembles) can be permanently bonded together to form a higher-level component (e.g., ensemble, unit). Inter-component pneumatic connection describes the back-and-forth air flow direction between cells or higher-level components as the pressure inside the layered structure changes in relation to atmospheric pressure. The extrinsic pneumatic connection details the way and the location of a pneumatic fitting attached to one of the skin layers or between skin layers to enable air flowing in and out of the corresponding cell.

2.1.2.3. Constraints

There are two main sub-categories of constraints: *internal constraints* and *external constraints*. Internal constraints include volumetric, layered, and tendon-like constraints. Using particles such as glass beads or coffee beans encapsulated in a cell to produce a controllable stiffness change as a function of vacuum pressure or accommodating materials such as sponge or strands of twisted fibers to control the air flow velocity are examples of internal volumetric constraints. Replacing the bulky particles filling a cell with thin uniform sheets such as paper or textile that are layered on top of each other or using one or multiple layers of non-uniform yet regularly arrayed basic or architected tile patterns are examples of internal layered constraints. Accommodating strings or cables attached between skin layers to restrain the inflation of a cell is an example of internal tendon-like constraints, which can be in a discrete or distributed form. External constraints can be surface, boundary, or tendon-like constraints. In the case of using a constrained layer pneumatic system as an actuator, at least one of the cells needs to be attached to a surface that acts as an

external surface constraint. External boundary constraints can be used to restrain a cell around its perimeter or a portion of its perimeter to facilitate a designated physical behavior such as limiting the out of plane translational expansion or allowing out-of-plane curling around a fixed axis. External tendon-like constraints are equivalent to the internal tendons but situated outside a cell with strings or cables attached to the exterior surface of at least one of the skin layers.

2.1.2.4. Sub-cellular Grammar

The characteristics of sub-cellular features together determine the function(s) that a cell provides at the cell level in the architectural hierarchy. The description of the relationship between the sub-cellular features and the corresponding characteristics requires its own grammatical structure which is demonstrated in a tabulated form (Figure 17-bottom) and is accompanied by a corresponding three-dimensional (isometric) illustration showing the exploded view of the constituent features that afford the construction of one of the system cells (Figure 17-top). This sub-cellular grammar uses a color-coding scheme where:

- light blue areas indicate the skin layers (top and bottom),
- red lines (or in some cases areas) indicate the mechanical connection between these skin layers which provide a permanent seal,
- green lines (or in some cases areas) indicate the prospective (in this case off-centered) mechanical connection between the top skin layer of this cell and the bottom skin layer of the adjacent cell or component (which is not shown in the figure),
- the black and white dotted area surrounded by the green border indicates the prospective pneumatic connection to the adjacent cell or component (which is not shown in the figure),
- orange represents the extrinsic pneumatic connection (e.g., vertically attached barbed pneumatic fitting),
- and the various shades of gray indicate internal constraints (e.g., internally attached tiles) and external constraints (e.g., flat rigid base surface).

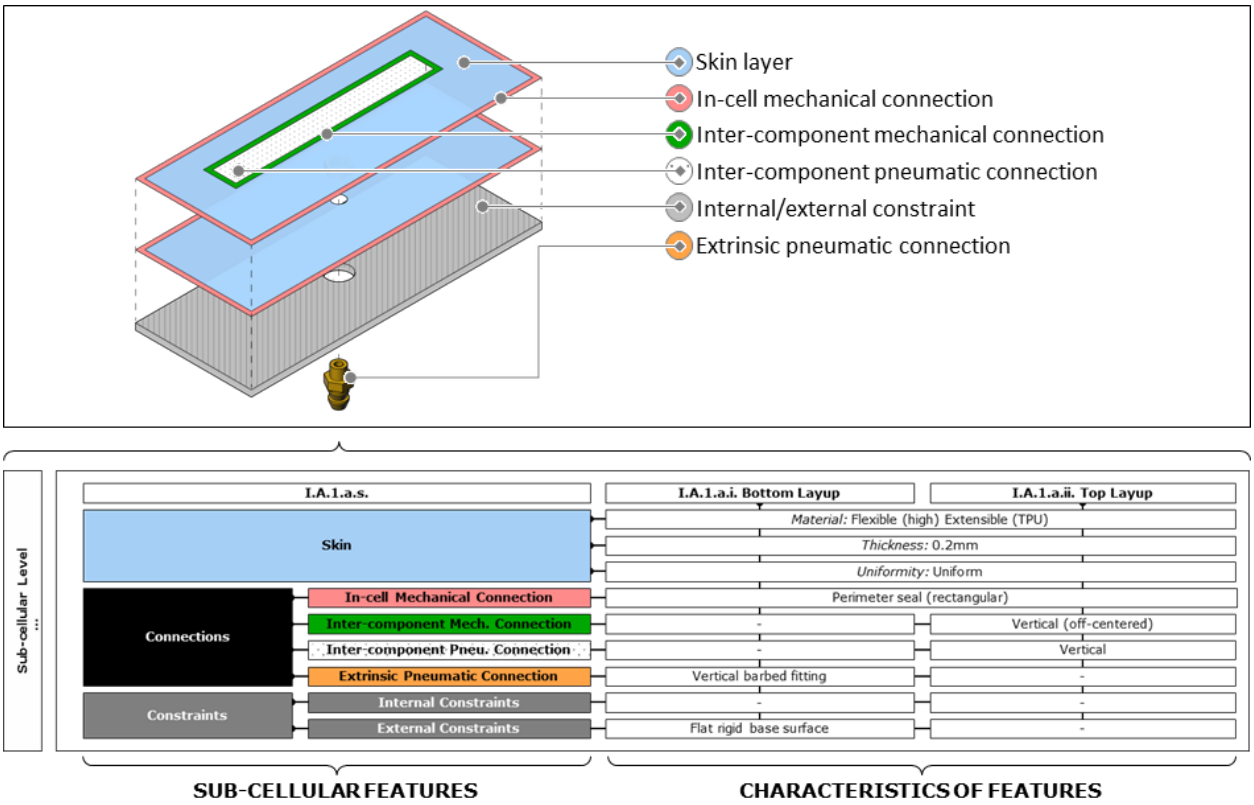

Figure 17. The sub-cellular feature characteristics of an example cell. Three sub-cellular feature categories are listed as: *skin*, *connectivity*, and *constraints*. There are three major aspects comprising the characteristics of a skin layer: *skin type, skin thickness, and skin uniformity*. The rules of connectivity that affords cell construction are grouped under four sub-categories: *in-cell mechanical connection, inter-component mechanical connection, inter-component pneumatic connection,* and *extrinsic pneumatic connection*, and there are two main sub-categories of constraints: *internal constraints* and *external constraints*. The characteristics of these features determine the function(s) that a cell provides at the cell level in the hierarchy.

2.1.3. Pneumatic Affordance Operation

Structurally adaptable multi-mode products that utilize constrained layer pneumatic systems are capable of switching between different operation states. By changing the operation state of the system, users are provided with a range of high-level functionalities that can be accessed through different interaction modes. To switch between operation states, the cells within the system require a set of pneumatic affordance operations that enable the manipulation of air pressure inside the system in relation to atmospheric pressure. These operations can be categorized into four main categories based on whether they actively or passively increase or decrease the pressure level inside the system (Table 1).

Table 1. Pneumatic affordance operations available in constrained layer pneumatic systems

	Active	**Passive**
Increasing (in relation to atmosphere)	Get Inflated	Let air in
Decreasing (in relation to atmosphere)	Vacuum	Exhaust air

These pneumatic affordances are 1) *get inflated*, which can be electrically or manually operated using variety of air compressors, diaphragm pumps, hand pumps, or bellows to actively drive the flow of air into the airtight system to increase the relative pressure level, or to increase the amount of pressure inside the airtight system using chemical reaction [112] on demand, 2) *vacuum*, which can be electrically or manually operated using variety of air compressors, diaphragm pumps, hand pumps, or bellows to actively drive the flow of air out from the airtight system to decrease the relative pressure level, 3) *let air in*, which can be achieved by using an extrinsic pneumatic connection such as a pneumatic valve to passively direct the flow of air from atmosphere to the already-vacuumed air cavities in the airtight system, and 4) *exhaust air*, which can be achieved by using an extrinsic pneumatic connection to passively direct the flow of air from the already-inflated air cavities in the airtight system to the atmosphere.

While the operation of the first two types of pneumatic affordances, get inflated and vacuum, create relatively higher and lower pressure air cavities in the system, respectively, the operation of the last two types, let air in and exhaust air, level the pressure differences between the air cavities in the system and atmosphere. As a result of these operations, cells exhibit a variety of fundamental behavior couplings.

2.1.4. Fundamental Behaviors of Basic Architectural Components

The basic architectural components, or cells, are capable of undergoing elemental structural transformations through the activation of fundamental behaviors that are triggered by the pneumatic affordance operations. These fundamental behaviors can be categorized into four types: expanding (E) or contracting (C) the extent of the air cavity in the system in-plane (I) or out of plane (O) when activated. The access to these fundamental behaviors is determined by the sub-cellular feature characteristics of a cell.

Moreover, depending on the characteristics of the skin, connectivity, and constraints, these fundamental behaviors can be activated in a coupled manner or independently. To illustrate how the relationship between pneumatic affordance operations and fundamental behavior activation

depends on cell feature characteristics, Figure 18 presents four scenarios where a set of selectively alternated feature characteristics within the same basic architectural component are used.

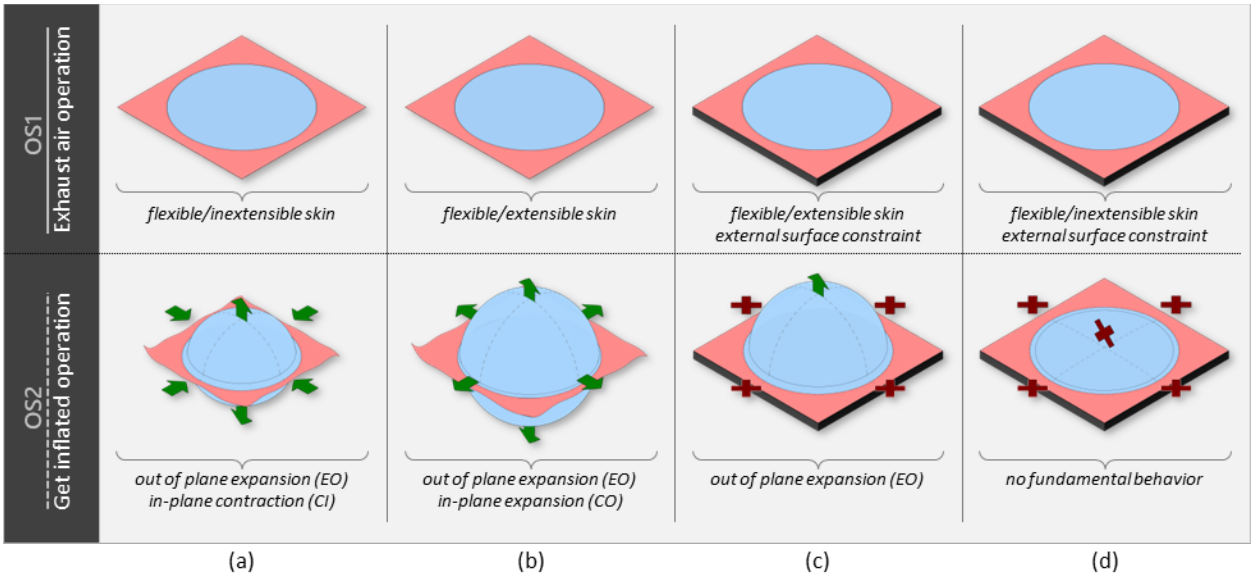

Figure 18. Four different scenarios demonstrating the effects of subcellular feature characteristics on the resulting fundamental behaviors. The fundamental behaviors can be categorized into four types: expanding (E) or contracting (C) the extent of the air cavity in the system in-plane (I) or out of plane (O) when activated. The access to these fundamental behaviors is determined by the sub-cellular feature characteristics of a cell.

For example, a basic architectural component of which skin is made of a highly flexible but inextensible material (e.g., TPU coated 210D nylon) can be activated by the get inflated pneumatic affordance operation to exert out of plane expansion (EO) behavior with a coupled in-plane contraction (CO) behavior, which are both taking place simultaneously (Figure 18a). By changing the skin material of this same basic architectural component with a highly flexible and extensible material (e.g., silicone rubber with a durometer of 15-30 on Shore 00 hardness scale), it is possible to exert coupled out of plane (EO) and in-plane (EI) expansion behaviors unlike the previous example (Figure 18b). Introducing a rigid surface to which the boundary area encircling the air cavity of the same basic architectural component is permanently attached breaks the coupling between out of plane and in-plane behaviors. In the case of using a highly flexible and extensible material, the same pneumatic affordance operation only activates out of plane expansion (EO) with no in-plane expansion (EI) observed (Figure 18c), and in the case of using a highly flexible and inextensible material, neither out of plane expansion (EO) nor in-plane contraction (CI) is accessible due to the skin inextensibility and the external constraint limiting these behaviors (Figure 18d).

To create a range of functional possibilities for a cell, one can experiment with the inherent characteristics of its skin, connectivity, and constraint features. By exploring the different combinations of these feature characteristics, a tailored set of fundamental behaviors can be produced, forming the basis for exploring the potential design space of the emergent cell functions.

2.2. Fabrication Approaches for Basic Architectural Components

Constrained layer pneumatic systems are hierarchically structured and composed of a set of lower-level compound architectural components each of which is made of a set of lowest-level basic architectural components: *cells*. The constituents of a generic cell are airtight skin layers that encapsulate an inflatable or vacuumable air cavity, an extrinsic pneumatic connection, and an optional set of internal and/or external constraints. Therefore, fabricating a cell and aggregating a multiplicity of such cells to form higher-level components afford the assembly of a system. Since constrained layer pneumatic systems can be complex and take myriad forms, applicable alternative fabrication methods are presented in the context of embodiment of a simplest proto-cell (i.e., the simplest possible cell) as an elemental system component.

For the fabrication of similar pneumatic systems that are made of multiple thin, flat, and typically flexible layers of sheets, a wide variety of approaches, methods, and techniques has been demonstrated in the literature. These include molding elastomers using custom-designed molds [113]–[115], employing adhesives to form chemical bonding between layers of plastics [86], [92], [116], using conventional heat-sealing tools such as heat-sealing irons, rollers and heat guns, linear impulse sealers [117]–[119], or hot-air and hot-wedge welding tools, hot-plate [74], [120], RF, and ultrasonic welding [121] using custom-designed dies. In addition to conventional heat-sealing techniques, researchers demonstrated the potentially scalable use of numerically controlled automated tools such as CNC machines [73], [122], laser cutters [123], and various types of 3D printers [78], [124] to fabricate a broad range of constrained layer pneumatic systems.

Within the context of fabricating constrained layer pneumatic systems, independent of the selection of which fabrication technique to apply, at least two of the cell constituents need to exist for the embodiment of a proto-cell. These are two skin layers that are stacked on top of each other and a set of extrinsic pneumatic connection components that are attached to at least one of these skin layers (Figure 19).

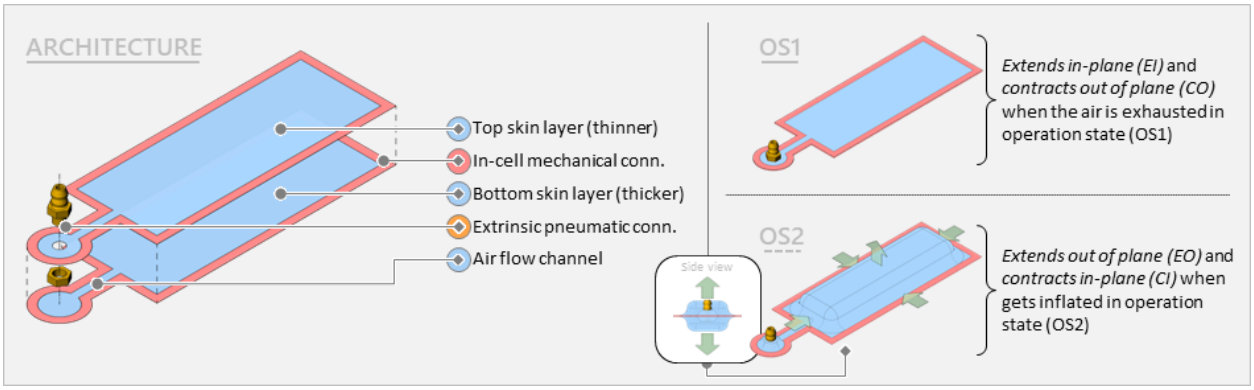

Figure 19. Proto-cell architecture (left) and operation (right). The architecture of a proto-cell contains two skin layers that are stacked on top of each other and a set of extrinsic pneumatic connection components (left). The proto-cell extends in-plane (EI) and contracts out of plane (CO) when the air is exhausted from the system in the first operation state (OS1), and it extends out of plane (EO) and contracts in-plane (CI) when it gets inflated in the second operation state (OS2) (right).

The stacked top and bottom skin layers of a proto-cell require an in-cell mechanical connection, which provides permanent bonding and forms an enclosed air cavity that can be inflated or vacuumed on demand using an extrinsic pneumatic connection. This extrinsic pneumatic connection can be made of various types of pneumatic attachment systems such as barbed or push-to-connect tube fittings, enabling the control of pressure level inside the airtight system using a combination of a wide variety of pumps, manifolds, valves, regulators, gauges, and tubing that are commercially available. The pneumatic fittings can be grouped under two categories based on their spatial organization in relation to the cell skin layers: 1) *fittings on-skin layer* (Figure 20 a and b), which are *vertically* attached to top or bottom skin layer either by using threaded compression systems (e.g., barbed threaded fitting and a nut) or by using one of the chemical/mechanical bonding approaches (e.g., various adhesives, RF/ultrasonic welding, heat pressing), 2) *fittings between-skin layers* (Figure 20c), which are *horizontally* placed between the top and bottom skin layers and attached to both of them using chemical/mechanical bonding approaches.

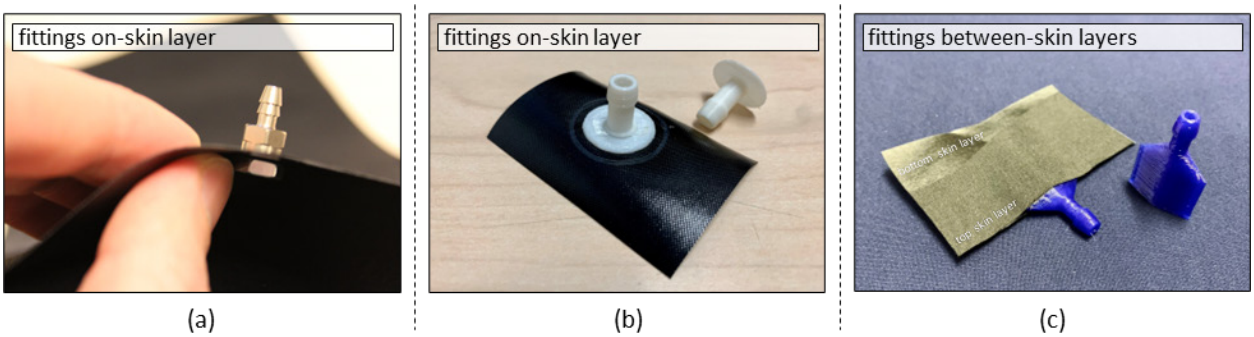

Figure 20. Pneumatic fitting categories. (a) A barbed threaded fitting and a nut and (b) a 3D printed custom fitting that are both vertically attached to the top skin layer are fittings on-skin layer category examples. (c) Another 3D

printed custom fitting that is horizontally placed between the top and bottom cell skin layers is an example for fittings between-skin layers category.

The methods and techniques that can be employed to form a permanent in-cell mechanical connection between two opposing skin layers to fabricate a cell can be grouped under three main categories: 1) *adhering existing skin layers, 2) fusing existing skin layers,* and 3) *producing already-fused skin layers*.

2.2.1. Adhering Existing Skin Layers

One of the most common and obvious approaches to form a permanent mechanical connection between the two existing skin layers within a cell is adhering them using various types of adhesives and adhering methods.

Adhesives are categorized based on their mode of bonding, which can be divided into two groups, reactive and non-reactive adhesives. Reactive adhesives (e.g., two-part adhesives such as epoxy or acrylic, one-part adhesives such as silicone or cyanoacrylate) harden through a chemical reaction, while non-reactive adhesives (e.g., emulsion adhesives, hot melt glue) do not undergo a chemical reaction to solidify. The process of adhering involves employing different applicators that are designed to apply adhesives based on the type of adhesive and the size of the surface it will be applied to. The adhesive can be applied to one or both of the materials to be bonded. The materials are lined up and pressure is applied to help the bond stick and remove any air bubbles. Adhesives can be manually or automatically applied using brushes, rollers, films, pellets, spray guns, or applicator guns. Choosing the right adhesive for a bonding process can be difficult. Several factors need to be considered, including chemical compatibility with both the materials being bonded, adhesive strength, flexibility, resistance to solvents and temperature, setting time, viscosity, and surface roughness of the contact area. While there are many options for bonding rigid parts together, the options for bonding soft parts are limited. The connection between the two parts of a bonded assembly should not be too stiff, but it must provide enough adhesion [125]. Adhesion between two elastic solid bodies occurs when mechanical force or work can be transmitted from one body to the other across an interface where close contact exists. The interface is perpendicular to the stress direction in case of pure tension, and parallel to the stress direction in case of pure shear. The transfer of force or work can occur in tension, shear, or a combination of both [126].

The researchers developed a range of relevant applications using various adhering techniques that can inform the fabrication of constrained layer pneumatic systems. Lachenmeier and Murai designed stowable and deployable high-performance balloons [116] and Chandra et al. developed an inflatable spherical membrane antenna system that can be adapted to different small satellite sizes, providing high gain and high bandwidth communication capabilities [92]. The gore units (i.e., specifically shaped individual sections) of these balloons and membrane systems were made of clear, aluminized, and thin Mylar layers which were adhered to form an inflatable sphere using a double-sided acrylic-based adhesive transfer tape (3M™ Adhesive Transfer Tape 966). Ilievski et al., built a starfish-like soft grippers, which are made of overlapping PDMS (i.e., polydimethylsiloxane) and Ecoflex (i.e., siloxane) parent layers. A thin layer of uncured prepolymer, made of the same material as the parent layers, is manually applied to serve as a permanent adhesive, connecting the parent layers [108]. In the field of soft robotics, same adhesion method using different materials has been employed to fabricate various applications such as a multi-mode glove with adjustable stiffness for hand rehabilitation, soft robotic grippers for biological sample collection in deep reefs, and rotary actuators using pneumatically driven elastomeric structures [127], [109], [128]. Similarly, Konishi, Kawai, and Cusin [129] created a thin and flexible end-effector using arrays of micro balloon actuators that are controlled by air pressure. These miniaturized actuators, measuring only 16x16mm, were made from silicone rubber and polyimide films that were bonded together using silicone rubber-based adhesive. In human-computer interaction field, Hudson demonstrated a potential use of pneumatically activated multi-mode tactile displays in the context of automobile dashboards, kiosks, and ATMs. The tactile displays consist of multiple layers of latex that are adhered together by using double-sided adhesive layers that are laser-cut to specific shapes [39]. Russomanno, Xu, O'Modhrain, and Gillespie used tailored PDMS layers, rather than latex, that were adhered to each other in the fabrication of a keypad interface capable of delivering programmable touch responses [86]. Yao et al. developed a range of shape-changing primitives (e.g., curving, curling, vertical expansion, texturizing) for the design of soft composite interfaces. These multi-mode primitives were fabricated by using uncured silicone layer as well to ensure adhesion among multiple structural and sensing layers [79]. Niiyama et al. developed a new family of portable and inflatable mobility devices, consisting of inflatable frames, wheels, and steering mechanisms made from mass-manufactured drop-stitch fabric. The fabric, made of two layers of PVC woven together with

thousands of yarns, is cut to specific shapes and then clear PVC film side walls are adhered to the edges of the cut fabric [101].

The fabrication steps of a proto-cell, which comprises two skin layers, two masking layers for the adhesive application, and a pneumatic fitting, using an adhering technique are outlined in Figure 21 as follows:

a. The design of the proto-cell layers is created in software (e.g. Rhinoceros), including the details of the masking layer pattern.
b. A large vinyl coated polyester fabric sheet is cut into two identical skin layers manually or using numerically controlled tools (e.g. CNC plotter).
c. Two masking layers, which can be made of virtually any material, are cut from a roll of painter's tape.
d. Masking layers are concentrically placed on the top and bottom skin layer separately.
e. Both skin layers are cleaned using rubbing alcohol and vinyl cement adhesive (e.g., HH-66, RH Adhesives, USA) is applied to the unmasked perimeters of both skin layers using a brush (a roller can be used for larger areas).
f. After waiting 2 to 5 minutes, the masking layers are peeled off from the skin layers.
g. A barbed pneumatic fitting is attached to one of the skin layers around the designated area with a hex nut through a 1/8-inch punched hole before two adhesive applied surfaces are pressed together.
h. The fabrication of the proto-cell is completed after 24 hours of curing time.

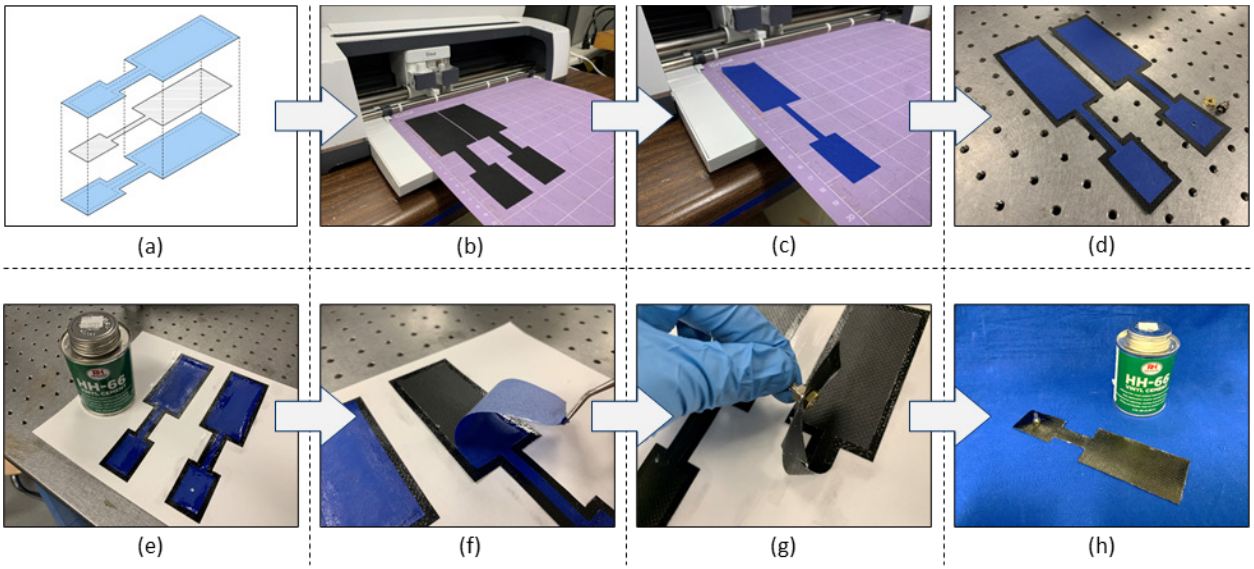

Figure 21. An example fabrication process of a proto-cell using adhering approach. (update) (a) The top and bottom skin layers of the proto-cell and the masking layer are designed in Rhinoceros. (b) A vinyl coated polyester fabric sheet is cut into two identical skin layers using Cricut Maker, a desktop CNC cutting machine. (c) Masking layers are cut from a roll of painter's tape using the same technique. (d) Masking layers are concentrically placed on the top and bottom skin layer separately. (e) Vinyl cement adhesive (e.g., HH-66, RH Adhesives, USA) is applied to the unmasked perimeters of both skin layers using a brush. (f) After waiting 2 to 5 minutes, the masking layers are peeled off from the skin layers. (g) A barbed pneumatic fitting is attached to top skin layer around the designated area with a hex nut through a 1/8-inch punched hole before two adhesive applied surfaces are pressed together. (h) The fabrication of the proto-cell is completed after 24 hours of curing time.

Using adhesives to form a permanent mechanical connection between the two skin layers has certain advantages over other fabrication techniques (e.g., heat-sealing, 3D printing). These advantages include the ability to reliably bond different materials, efficient distribution of stress across a joint, and design flexibility [130]. However, there are also some disadvantages, including decreased stability at high temperatures, a potential requirement of surface pre-treatment to attain a long service life, and difficulty in decomposing the final product into its constituents which potentially may disrupt the recyclability of the primary materials [131].

2.2.2. Fusing Existing Skin Layers

The second approach for forming a permanent mechanical connection between two skin layers within a cell is fusing mass-produced thermoplastic sheet material layers. This is done by applying a combination of heat and pressure for a specific amount of time, either directly or indirectly.

The process of fusing, or heat-sealing, involves applying energy to the thermoplastic material to elevate its temperature to a melting temperature. To successfully form a permanent seal, pressure is necessary to bring two overlapping thermoplastic material layers into close contact for molecular diffusion, and time is needed to allow the heat transfer and molecular motion to occur that results

in molecular entanglements, creating a bond between the two surfaces. This bond is strengthened by the recrystallization of certain segments after cooling down, resulting in a strong seal. The way that heat and pressure are applied to the seal area is what differentiates the various sealing methods [132].

The methods for achieving this can be grouped into four categories: *1) manual heat-sealing, 2) numerically controlled heat-sealing, 3) pre-patterned heat-sealing,* and *4) masked heat-sealing*.

2.2.2.1. Manual Heat-sealing

The manual heat-sealing method involves the use of tools such as heat-sealing irons, heat-sealing rollers, heat guns, linear impulse sealers, or hot-air and hot-wedge welding tools by an operator, to fuse similar or identical thermoplastic sheet materials into a single layer (Figure 22).

The most basic tools for heat-sealing are manually operated heat-sealing irons, heat-sealing rollers, and heat guns, all of which are hand-held tools providing constant heat with a thermostatically controlled temperature maintenance system. The heated flat metal surface (or foot) of most heat-sealing irons is coated or covered with a non-stick surface (e.g. PTFE coated fiberglass sheet), allowing the iron to glide over stacked thermoplastic sheet material layers without causing any permanent surface deformations. The heat-sealing roller employs a metal wheel, which can be rolled over overlapping thermoplastic sheet material layers, resulting in forming a permanently seal between these layers. Some models allow simultaneous cutting during the heat-sealing process. While the feet of heat-sealing irons are made of a flat surface varying in size (~1mm to 100m width) and shape (e.g., pointy vs round tip), the rotating wheels of heat-sealing rollers mostly vary in texture with a limited range of width options (~5 to 10 mm width). Manually operated hand-held heat-sealing tools also include heat guns. Heat guns use an electrically heated component to generate hot air at the desired temperature and have an electric fan that moves the hot air through a metal nozzle. Heat guns can be fitted with various nozzle attachments to direct and concentrate hot air on the desired area. A roller can be used to apply pressure and fuse overlapping layers of thermoplastic material. Manually operated hand-held heat-sealing tools provide flexibility in initial design stages by allowing sealing in both straight and curvilinear paths. However, operating these tools requires a high level of skill, and manual operation makes it challenging to achieve precise control over the duration and pressure applied, which affects process repeatability. Commonly fabricated constrained layer pneumatic systems

using manually operated heat-sealing tools include personal flotation devices, do-it-yourself rafts, sleeping mattresses, dry suits, and drybags.

Figure 22. An example set of manual heat-sealing tools. The manual heat-sealing tools include heat guns (a), linear impulse sealers (b), heat-sealing irons (c-top), and heat-sealing rollers (c-bottom).

Another common tool for manual heat-sealing is a linear impulse sealer, which provides more precise control over the temperature and duration. The most common version of the linear impulse sealers, the table-top impulse sealer, has a sealing jaw, which contains a heating element made of Nichrome (an alloy of nickel and chromium) covered with a non-stick PTFE fiberglass release surface layer, and a hand or foot-operated counter jaw containing a resilient synthetic rubber. Two layers of thermoplastic sheet materials (e.g., polyethylene) are placed between these two jaws. When the counter jaw is pressed against the sealing one, electrical current passing through the heating element is converted into heat that causes the contacting sheet materials to reach glass transition state and to permanently fuse one another under pressure. The resulting temperature and heating duration can usually be adjusted using the interface controls, however the amount of pressure applied varies from one user to another. There are industrial linear impulse sealers that provide precise control over sealing temperature, duration, and pressure applied by employing actuators. Researchers have used linear impulse sealers in the fabrication of a range of constrained layer pneumatic systems. These systems include pleated soft actuators capable of generating a variety of bending motions [117], surfaces that can change their stiffness on demand upon deployment and stowing using multi-layered inflatable structures [118], soft grippers that can securely grasp objects or wrap around various structures [119], and pneumatically activated robotic arm equipped with inflatable sleeves for impact absorption and potential embedded sensing capabilities [133].

Unlike the heat-sealing irons-rollers-guns, and basic linear impulse sealers, the hot-air and hot-wedge welding tools provide precise control on all sealing parameters (temperature, duration, and pressure) to fuse layers of thermoplastic sheet materials. The hot air welding process contains compressing and blowing air through electrical heat elements and injecting that heated air at the precise welding location through a nozzle between thermoplastic layers, which are being fed through a stationary sealing location (i.e., like a sewing machine) using fixed rollers. The hot wedge welding process replaces the heated air blowing system with a metal wedge of which temperature and location can be precisely controlled. During both processes, each thermoplastic layer is pulled toward the welding location using rollers, which apply constant pressure to the glass transitioning layers, resulting in forming a permanent seal. While the hot air welding tool allows straight or curvilinear seal paths, the sealing is mostly limited to straight or large radius paths using the hot wedge welding tool. The use of hot-air and hot-wedge welding tools is widespread in the fabrication of various inflatable structures and equipment. These tools are commonly utilized in the production of white-water rafts, inflatable tents, bouncy castles, airplane evacuation slides, military attack boats, and inflatable drop-stitched paddle boards. Additionally, researchers have leveraged these tools to create large-scale inflatable robotic arms [134].

The generic fabrication steps of a proto-cell, which is made of two layers of thermoplastic sheet material and a pneumatic fitting, using a linear impulse sealing technique are shown in Figure 23:

a. A large thermoplastic sheet is cut in two identically sized skin layers manually or by employing numerically controlled tools (e.g., using scissor or laser cutter).

b. A barbed pneumatic fitting is attached to one of these skin layers near one of the edges with a rubber washer and a hex nut through a 1/8-inch punched hole.

c. And all edges of two overlapping skin layers are heat sealed using one of the manual-heat sealing tools (e.g., a linear impulse sealer), (d) producing a pneumatically operable airtight proto-cell.

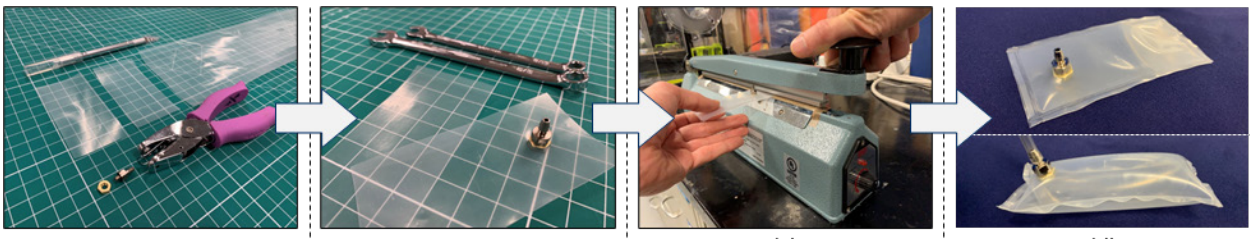

Figure 23. An example fabrication process of a proto-cell using a linear impulse sealing technique. (a) A large thermoplastic sheet is cut in two identically sized skin layers manually. (b) A barbed pneumatic fitting is attached to top skin layer near one of the edges with a rubber washer and a hex nut through a 1/8-inch punched hole. (c) All edges of two overlapping skin layers are heat sealed using linear impulse sealer, (d) producing a pneumatically operable airtight proto-cell.

Fusing existing skin layers by employing manual-heat sealing method enables prototyping new designs quickly using widely available materials without requiring any custom preparation such as tooling (e.g. fabricating custom dies) or material treatment (e.g. applying surface treatment, degassing). In general, as the level of control over the fusing parameters increases, the flexibility regarding the seal shape decreases. For example, while any seal shape - including combinations of curvilinear perimeter seals with a set of arbitrarily located inner spot seals - is achievable using the simplest heat-sealing iron with a narrow foot, it is not possible to fabricate a similarly complex seal shape using linear impulse sealers or hot-wedge welding tools. Although combinations of operations with different manual tools are viable.

2.2.2.2. Numerically Controlled Heat-sealing

A numerical control allows the automated operation of machining tools such as CNC routers, laser cutters/welders, and 3D printers by following a set of programmed instructions (e.g., G-codes) that are generated using specific computer-aided design (CAD) and manufacturing (CAM) software. Such machining tools, which are originally designed for enabling automated subtractive or additive manufacturing, have recently been adapted to be employed in the fabrication of layered pneumatic systems.

By retrofitting a CNC router's cutting tool with a soldering iron of which temperature can be adjusted, Niiyama et. al. developed a numerically controlled heat-sealing machine that can draw sealing lines on two overlapping polyethylene layers [122]. These thermoplastic layers are attached to the router workspace (~12"x12") and are covered with a PTFE fiberglass sheet protecting against scorching. The two-dimensional seal pattern is designed in computer software and turned into G-codes, which precisely informs the movement of the soldering iron in-plane, resulting in fabricating an airtight pouch.

Ou et. al. built on the same approach by introducing a ball transfer and a knife module each of which can be attached to the tip of the heating head (i.e., retrofitted soldering iron) with a dampening mechanism, enabling a smoother heat-sealing and precise cutting capabilities [73]. They increased the size of router workspace from ~12"x12" to 36"x36", which allows the

fabrication of larger scale layered pneumatic systems. They also demonstrated that it is possible to incrementally stack multiple layers (note: demonstrated three layers in total) of thermoplastic materials and only heat-seal the desired pattern on the top-most two layers at a time by tuning the heat-sealing parameters (i.e., temperature, pressure applied, and sealing speed).

At the Smart Materials and Structures Design Laboratory (SMSDL), we have created a large-scale heated roller-ball sealer, built on a 4'x4' CNC router bed (Figure 24). This enables us to fabricate large-sized constrained layer pneumatic systems that can withstand pressures of up to 20 psi. To characterize the sealing process, we conducted an initial study on the effects of temperature, sealing speed, and downward force for various materials on the quality of the seal. Sareen et. al. further improved the numerically controlled heat-sealing technique by developing a custom CNC platform with a mechanism that enables simultaneous feeding of two heat-sealable fabric layers from a spool using rollers, pinching the top layer to form a mountain-like structure that creates a difference in length between the two layers, and then performing two-dimensional heat-sealing before exiting the heat-sealed inflatable structure [68]. These large-scale structures can bend once inflated due to the difference in length in top and bottom skin layers.

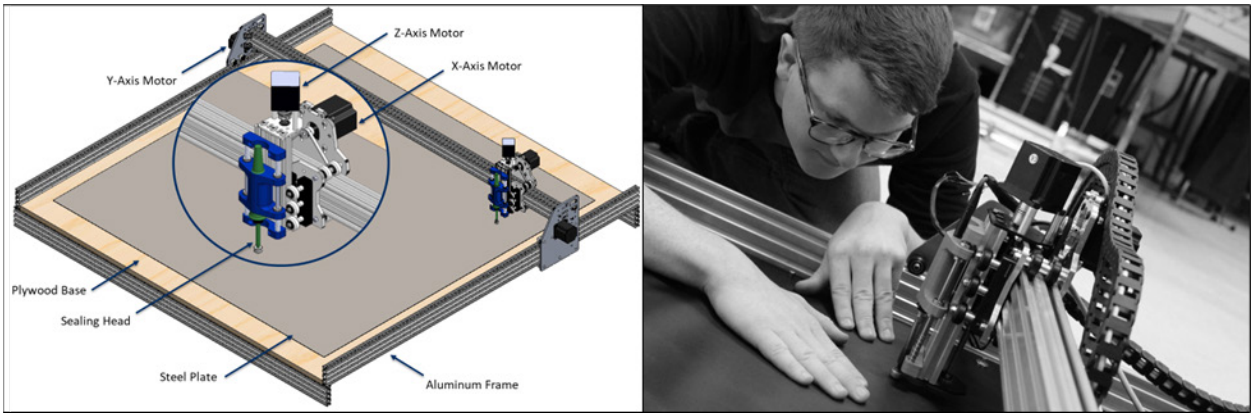

Figure 24. 4'x4' CNC router bed for heat-sealing. The schematic of a large-scale heated roller-ball sealer, built on a 4'x4' CNC router bed in Smart Materials and Structures Design Laboratory (SMSDL) (on the left), and a mechanical engineering graduate student, Jack Teener, conducting an initial study on identifying heat-sealing parameters (on the right).

Researchers created various constrained layer pneumatic products using CNC heat-sealing machines, including an arm rehabilitation device that mimics forearm muscle movements [135], stiffness and shape-changing surfaces [71], reconfigurable pneumatic actuators [136], and biking gloves with textural direction indicators [73]. The gradual reduction in manual intervention in the fabrication process of layered pneumatic systems using these techniques indicates the potential for fully automated industrial manufacturing to be achieved.

Unlike the retrofitted use of CNC routers for heat-sealing, various types of laser sources and beam-delivery systems have been in use for laser welding of rigid plastic parts with complex 3D shapes (e.g., car taillights) and plastic films (e.g. intravenous solution bags). An overview on types of lasers, materials, processes, and quality for the laser welding of thermoplastics is well documented [137]. The heat-sealing process parameters - temperature, time, and pressure - can be controlled by adjusting the laser power, laser spot size, irradiation time, the presence of laser-absorber materials, and clamping load. By tuning these parameters, Jones [123] demonstrated the use of continuous seam heat-sealing method using diode-laser system mounted above a two-axis CNC gantry system for fabricating an inflatable multi-chambered neck brace that is made of two layers of thermoplastic polyester elastomer sheets and a pneumatic fitting. This application provides high level of neck support (e.g., useful while the patient is travelling) when inflated to higher pressure levels; and it provides greater mobility (e.g., useful while the patient is stationery and eating) when the pressure is reduced. The desired shape of the seal can be easily updated without requiring any change to the fabrication system, supporting customized designs for different user needs (e.g., due to anthropometric differences), therefore provides fast and flexible fabrication process.

Multiple hobbyists [138] and enthusiasts as a part of makerspaces [139] have also demonstrated the laser-welding of everyday thermoplastics such as low density polyethylene films with different thicknesses by defocusing laser beam of a commonly used CO2 laser cutting machine to fabricate constrained layered pneumatic systems. Defocusing reduces the amount of energy applied to the surface area, resulting in melting the layers and fusing them to form a permanent seal. As an additional step, the same defocused laser beam was demonstrated to be used to cut the excess material around the perimeter of the layered pneumatic system by increasing the laser power.

Another technique for applying numerically controlled heat-sealing method contains employing fused deposition modelling (FDM) 3D printers without requiring any structural modifications to the components of these commercially available platforms. As a part of the research conducted in the Smart Materials and Structures Design Laboratory (SMSDL), we introduced the idea of heat-stitching using completely unmodified low-end FDM 3D printer by repurposing its built-in hot end, which is originally designed for heating, melting, and extruding a filament material layer by layer through a conical nozzle on a 3D printer bed (i.e., a workspace

usually made of a glass or metal sheet) (Figure 25). This enables the fabrication of complex seal shapes. Instead of melting and extruding filament using the hot end, the temperature-controlled nozzle is driven in a hopping motion like a sewing machine to march along a pre-designed seal path on the 3D printer bed, which is covered with two overlapping layers of TPU coated fabric (Figure 25a). As the heated nozzle touches the top fabric layer, the heat transfer melts the TPU coating on both layers and heat-stitches them, therefore forming a fusion between these layers. The quality of the resulting seal depends on the tuning of the heat-stitching parameters, which are the temperature of the nozzle, the distance between each stitch, the duration of contact with the fabric layers, and the pressure applied to the surface during stitching. The nozzle's hopping motion pattern is governed by a Gcode file. To generate a hopping motion pattern, we developed a specific software (i.e., dxf2gcode) that converts a DXF file, which is a data file format designed for sharing drawing data universally across CAD applications, to a Gcode file format (Figure 25b). By using this technique, we were able to prototype a cargo restraint surface with variable friction properties (Figure 25c and d), enabling easier loading or secure transit [78], as well as a pneumatically operated anti-carsickness device that can be fully integrated into a vehicle's interior trim [124]. Since FDM 3D printers are vastly adopted by small businesses, educational institutions, and individual end-users, the overall heat-stitching process affords a very low-cost-to-employ and flexible technique for the fabrication of constrained layer pneumatic systems without modifying the means of fabrication at all.

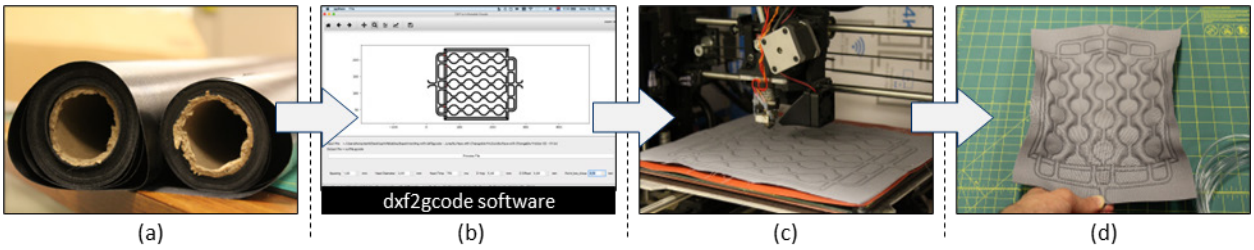

Figure 25. A fabrication process of a specific multi-mode product concept, variable friction cargo surface [78], using heat-stitching technique. (a) Off-the-shelf TPU coated nylon or manually TPU infused cotton fabric can be used for heat-stitching. (b) A hopping motion pattern is generated using a specific software, dxf2gcode, which converts a DXF file to a Gcode file format. (c) A multi-mode cargo restraint surface with variable friction properties is heat-stitched using a stock FDM 3D printer, Lulzbot TAZ 4. (d) The heat-stitched pneumatically operable prototype is inflated using air pressure.

Fusing existing skin layers by employing a numerically controlled heat-sealing method enables fabrication of constrained layer pneumatic systems requiring complex seal patterns. While employing CNC routers for heat-sealing requires modification to the system components (e.g.,

replacing the cutting tool with a soldering iron), employing laser cutters/welders or especially FDM 3D printers does not require any such modifications. All three of the heat-sealing parameters, temperature, time, and pressure, can be numerically controlled by using these tools, facilitating a repeatable fabrication process.

2.2.2.3. Pre-patterned Heat-sealing

A pre-patterned heat-sealing method employs the traditional use of heat presses with custom-built dies, radiofrequency (RF) welding tools with specific tooling, and ultrasonic welding tools with custom-built horn and fixtures that can be applicable for the fabrication of constrained layer pneumatic systems. Each one of these components, which are usually made of metal (e.g., titanium, aluminum, copper), requires to be designed and machined for every different seal shape.

A commonly used heat press machine consists of two main parts: 1) a bottom platen on which thermoplastic sheet material layers and the custom-built die are placed and 2) a temperature controlled top platen which can be pressed down on the layup on the bottom one. The top platen, which can be manually, semi-automatically, or automatically operated, directly applies heat and pressure to the layers to be heat sealed through the custom-built die for a preset time. This results in melting only the targeted locations on the material layers and heat-sealing complex seal patterns in detail. Several researchers demonstrated the use of such dies for the fabrication of constrained layer pneumatic systems in the context of actuator design, designing shape-changing packaging and haptic gloves, and exploration of modular soft robot assemblies [73], [81], [122].

Both RF and ultrasonic welding relies on indirectly generating heat and directly applying pressure on overlapping sheets of materials or volumetric rigid parts in contact for a certain amount of time to fuse these components. RF welding method uses high frequency electromagnetic energy to temporarily cause internal molecular friction in materials, which results in the generation of heat enabling a permanent seal with the help of the pressure applied during the process with fast cycle times. A typical RF welding machine consists of an RF generator and a control unit, a press unit, an RF enclosure, a workpiece handling mechanism, and tooling (i.e., electrode) [140]. The tooling is the pre-patterned component, which needs to be designed and machined for every different seal shape, that is pressed onto the material layers, producing the permanent seal. To be applicable for the RF welding method, a material must be able to produce dipolar polarization under the effect of a rapidly alternating electric field (e.g., TPU, PVC, PET). This introduces material selection limitations. Inflatable life jackets, airbeds, inflatable wheelchair cushions, blood bags, and dialysis

fluid warmer bags are among the commonly manufactured constrained layer pneumatic systems using RF welding method in industry.

Ultrasonic welding method employs ultrasonic energy at high frequencies (i.e., 20-40 kHz) to generate low amplitude mechanical vibrations. These vibrations are directly applied to the overlapping material layers or volumetric rigid parts, resulting in generating heat, which causes materials to melt and form a permanent seal or weld after cooling. A typical ultrasonic welding machine mainly consists of a high-voltage generator, a transducer to convert the voltage to the mechanical vibrations, a booster to amplify the vibrations, and a welding horn (i.e., sonotrode) that transfers the mechanical vibrations to the materials to be fused [140]. The limitations regarding the large seals/joints (e.g., seal area should be smaller than 10”x12”) and the form of the welding horn (e.g., horn shape should be as symmetric and balanced as possible) introduce restrictions for the applications of this technique for the fabrication of constrained layer pneumatic systems. Although ultrasonic welding is mostly used for welding rigid parts, the technology is applicable for the welding of softer plastics and fabrics. An extension of this technique based on the same working principle is the ultrasonic sewing, which employs a roller that can be designed with different embossed patterns. The roller, which gets activated by the vibrating horn as the multiple layers of compatible non-woven fabric or sheet material layers are being fed through the system, permanently seals or simultaneously-seals-and-cuts the multiple layers. Sealed food pouches, blister packs, driver and passenger airbags, medical garments, and medical masks are among the commonly manufactured items using ultrasonic welding and ultrasonic sewing techniques in industry. Additionally, researchers have employed ultrasonic welding tools to create fabric-based actuator modules, enabling the development of soft pneumatic structures with high payload-to-weight ratio [121].

Fusing existing skin layers by employing a pre-patterned heat-sealing method enables fabrication of constrained layer pneumatic systems requiring complex and reliable seal patterns with a very fast fabrication cycle times (e.g., 0.1-1 sec/per job with ultrasonic welding technique). Employing the associated techniques yield repeatable results since all of the main heat-sealing parameters can be numerically controlled. Moreover, especially RF and ultrasonic welding techniques are preferred for the fabrication of devices in healthcare industry due to their contaminant-free nature with long-lasting welds [140]. However, the material and tooling costs of fabricating and the effort for designing and new heat-sealing dies, tooling, and horns (i.e.,

sonotrode) with fixtures that are required to align parts and keep them stationary make employing the pre-patterned heat-sealing method relatively disadvantageous especially for the early stages of the design process through which the targeted form of the product is in a constant state of flux.

2.2.2.4. Masked Heat-sealing

A masked heat-sealing method contains employing an easy-to-customize and fast-to-fabricate masking layer for selectively covering the regions of the overlapping skin layers, resulting in only allowing the non-masked regions to be permanently sealed upon the direct or indirect application of heat and pressure for a certain period. All the tools that afford the application of manual, numerically controlled, and pre-patterned heat-sealing methods can be used to employ masked heat-sealing method to produce complex and precise seals without requiring any specific tooling or preparation. Researchers have also employed a convection oven to bond the clamped skin and masking layers in a single step operation, producing complex constrained layer pneumatic systems [74], [141].

The design of masking layers can be done using any software capable of creating 2D vector shapes, such as Inkscape, Adobe Illustrator, or Rhinoceros. The design can then be cut from a stock sheet material using manual tools, like a utility knife or scissors, or automatic tools, such as a cutting plotter or laser cutter. A wide range of thin and cost-effective materials, including copier paper, biodegradable water-soluble paper, glassine paper, silicone-coated baking sheets, polypropylene sheets, polyethylene sheets, various fabrics, or Kapton (polyamide) tapes, can be used as masking layers in the fabrication process.

When selecting a masking layer material, it's essential to consider the properties of the skin layers it will overlap. The compatibility between the masking and skin layer materials, the thickness of the masking material, its architectural properties (e.g., for fabrics), and its melting temperature (for thermoplastics) all impact the quality of the heat-sealing process and the resulting seal. For example, using different grades of the same thermoplastic material (e.g., low and high-density polyethylene) for the masking and skin layers can result in a permanent seal covering the entire surface of the masking layer, which is not ideal. If the masking layer is thicker than the combined skin layers, the skin layers may not fuse properly, causing a weak seal that may delaminate and leak. Using knitted or woven fabrics as a masking layer can also cause unintended sealing, as the fabric's porosity can cause the skin layers to bond through the masked areas.

When using thermoplastics for both the masking layer and skin layers, it is important to ensure that the melting temperature of the material used for the masking layer is higher than that used for the skin layers. This prevents the masking layer from deforming and causing distortion in the masking pattern or misalignment between the masking and skin layers during the heat-sealing process. In instances where the masking layer is composed of a non-thermoplastic material, such as copier paper, and the skin layers are composed of a thermoplastic material, such as TPU, the heat-sealing process may result in the fusion of the masking layer with the skin layers. To address this, the resulting cell can be inflated to relatively higher-pressure levels (e.g., 15-20 psi) using a pneumatic fitting, which can delaminate the top and bottom skin layers from the masking layer. An alternative solution to address this issue is to employ two overlapping identical masking layers instead of one. This strategy ensures that the top layup, which includes the top skin layer and top masking layer, remains separate from the bottom layup, which includes the bottom skin layer and bottom masking layer, before and after the heat-sealing process in the masked areas. Alternatively, using a biodegradable and water-soluble masking layer, such as biodegradable paper, can eliminate any potential interference with the functionality of the cell and improve user interaction by eliminating undesirable crunching noise. Simply submerging the resulting cell in water will dissolve the masking layer, resulting in a clean, residual-free cell.

The fabrication steps of a proto-cell, which comprises two skin layers, a masking layer, and a pneumatic fitting, using the masked heat-sealing method with a heat press machine, are outlined in Figure 26 as follows:

a. The design of the proto-cell layers is created in software (e.g., Rhinoceros), including the details of the masking layer pattern.

b. The large thermoplastic sheet (e.g., TPU coated nylon) is cut into two identical skin layers manually or using numerically controlled tools (e.g., a desktop CNC plotter).

c. The masking layer is cut from either a non-thermoplastic (e.g., glassine paper) or thermoplastic sheet material with a higher melting temperature (e.g., PP).

d. The layup, consisting of the bottom skin layer, masking layer with an extension, and top skin layer, is placed on the bottom platen of the heat press machine and covered with a PTFE fiberglass sheet before being heat-pressed.

e. After cooling, the extension of the masking layer is removed, providing access to the inner area of the proto-cell through the designated edge.

f. A barbed pneumatic fitting is attached to one of the skin layers around the designated area with a hex nut through a 1/8-inch punched hole.

g. The remaining edge is sealed using a heat press machine or manual heat-sealing tool such as a hand iron or linear impulse sealer, (h) completing the fabrication of the proto-cell.

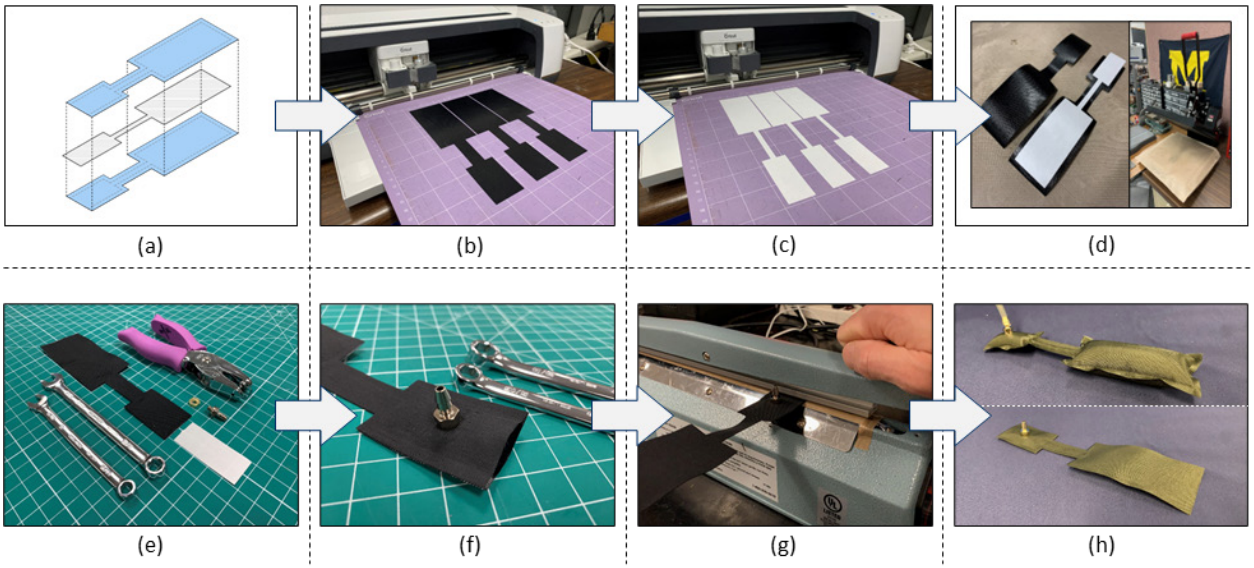

Figure 26. An example fabrication process of a proto-cell using masked heat-sealing method. (a) The design of the proto-cell layers is created in Rhinoceros, including the details of the masking layer pattern. (b) The large thermoplastic sheet (e.g., TPU coated nylon) is cut into two identical skin layers using a desktop CNC plotter. (c) The masking layer is cut from a non-thermoplastic material such as glassine paper. (d) The layup, consisting of the bottom skin layer, masking layer with an extension, and top skin layer, is placed on the bottom platen of the heat press machine and covered with a PTFE fiberglass sheet before being heat-pressed. (e) After cooling, the extension of the masking layer is removed, providing access to the inner area of the proto-cell through the designated edge. (f) A barbed pneumatic fitting is attached to the top skin layer around the designated area with a hex nut through a 1/8-inch punched hole. (g) The remaining edge is sealed using a heat press machine or manual heat-sealing tool such as a hand iron or linear impulse sealer, (h) completing the fabrication of the proto-cell.

Researchers have used masked heat-sealing method to fabricate constrained layer pneumatic systems to develop a range of applications offering a wide range of potential benefits. These applications include shape-shifting clothing [120], repositionable and conformable inflatable stents for endovascular treatments [142], soft or soft-rigid hybrid robotic arms and robots capable of rolling and crawling [74], user-interactive inflatable devices with posable functionality and deploying and stowing capabilities [75], a thin-profiled and direction-controllable distributed heating ventilation and air conditioning system [143], a low-profile ratiometric pressure regulator

[144] and a mobile phone restraint mat that can position and orient a phone on a wireless charger [78].

Fusing existing skin layers by employing a masked heat-sealing method offers versatility in terms of fabrication tools and materials. This method can be carried out using a variety of tools such as manual heat-sealing tools, heat press, convection oven, or an RF welding machine. The process is repeatable as the three heat-sealing parameters (i.e., temperature, time, and pressure) can be precisely controlled. Additionally, this method is cost-effective and easy to implement, as there is no need for custom preparation such as tooling (e.g., machining custom dies and fixtures) or material treatment (e.g., wetting). This makes the masked heat-sealing method ideal for rapid prototyping during the early stages of the constrained layer pneumatic systems design process, where the desired form of the product is still evolving.

2.2.3. Producing Already-fused Skin Layers

The third and final approach for forming a permanent mechanical connection between the two skin layers within a cell is fusing the layers through production. This can be achieved through molding and using additive manufacturing methods.

2.2.3.1. Molding

A mold is a hollowed-out solid block which is used to hold and shape a liquid or pliable material as it hardens into a solid form via chemical reaction or cooling. The solid form takes on the shape of the mold, producing a cast or final product. Molding can be performed using a wide range of raw materials including metals (for which the process is referred to as die-casting), glass, elastomers, and most commonly, thermoplastic and thermosetting polymers. The material used for making a mold can be either rigid, such as aluminum, plaster, or plastic resin, or flexible, such as rubber. The casting material (i.e., what the final product will be made of) and the complexity of the final product (e.g., presence of undercuts) inform the choice of mold material. Several types of molding techniques are used in mass production of industrial products, including compression molding, injection molding, blow molding, rotomolding, spin casting, and lamination.

Researchers, especially in engineering, soft robotics, and human-computer interaction communities, adapted some of these industrial molding techniques to fabricate a wide range of constrained layer pneumatic systems with homogenously distributed monolithic seams, which minimizes the potential risk of having skin layers separated and leakage. A large majority of these

systems are built employing catalyzed polymers, like silicone rubbers, by combining two components before molding.

The most widely used molding technique that facilitates the creation of internal air cavities is multi-step molding. This technique enables the incorporation of cores or removable inserts and masking layers as well as various functional components, such as internal and external constraints (e.g., inextensible fabric) [79], fibers [91], interlocking composite layers [145], sensing elements (e.g., flexible strain sensors [146]), and different types of actuators [115], into the molding process, in addition to the skin layers. The upper skin layer can be molded on top of the partially cured bottom skin layer, leading to a homogeneous fusion of both layers around the defined sealing shape. An alternative technique involves using the same or different molds to create individual skin layers, which are then joined together using an uncatalyzed layer of the same material [147], [90]. This results in a less homogenous seal and may lead to leakage or separation of the layers (see adhering existing skin layers section). Yang and Druga used the multi-step silicone molding technique to create an innovative, air-powered inflatable construction kit, known as Legoons [114]. This kit is designed to be compatible with traditional Lego bricks, allowing children between the ages of 6 and 12 to build characters and structures that can be animated by pumping air. Shitake et al. applied a similar technique, but substituted silicone with gelatin, to fabricate soft pneumatic actuators for the design of edible robotics [148].

A straightforward way of incorporating cores with primitive geometries, such as cylindrical bars [113] or interconnected beads [79], into the multi-step molding process is to suspend them using designated attachment points within the mold during the molding process. Once the molded material cures or cools down, these cores can be easily extracted. The use of cores made of soluble or phase-changing materials (e.g., paraffin) has been demonstrated as an effective method for fabricating pneumatic systems with complex 3D internal air cavity structures in the context of developing a bioinspired soft pump imitating heart-like chamber squeezing [149], a pleated unidirectional gripper [150], and a soft hydraulic robotic fish [150].

An alternative technique, which is analogue to masked heat-sealing, for creating internal air cavities includes using flat masking layers instead of 3D cores. These masking layers can define internal flat cavities that can expand when air or fluid is introduced into the airtight system. Yao et al. [79] used masking layers made of perforated extensible fabric to create a variety of tangible user interfaces that can change their forms and textures based on the internal pressure applied.

Kow, Culmer, and Alazmani [151] developed a customized film applicator platform that enables the fabrication of millimeter-scale soft actuators made of thin silicone layers with integrated masks and/or strain-limiting layers. The asymmetrical layering of the strain-limiting layer and the integration of the masks determine the bending motion of these flat actuators, opening up the possibility for a range of potential uses in areas such as biomedical technology and search and rescue operations. Kow used the multi-step masked molding/lamination technique not only for the creation of thin and soft actuators but also for the fabrication of a soft sensor with adjustable rigidity and a soft, flat robot with the ability to perform gait-like movement [152]. Rocha, Tomico, Markopoulos, and Tetteroo used a combination of masking layers [153] and chemical embroidery [154] as means to integrate silicone-based inflatables into garments. They explored the programmable nature of machine embroidery to create a locally tailored lace-like substrate. This substrate was created on a water-soluble film and was produced by dissolving the film in water. During the silicone molding process, they used a water-soluble masking layer to keep the substrate separate, resulting in the creation of inflatable cavities embedded within the final composite garment.

The fabrication steps of a proto-cell, which comprises two skin layers, two masking layers, and a pneumatic fitting using the multi-step molding technique, are outlined in Figure 27 as follows:

a. The bottom and top skin layers and their mold are designed in software (e.g., Rhinoceros), including the details of the masking layer pattern.
b. Two identical masking layers are cut into shape using a desktop plotter cutter (e.g., Cricut Maker, USA) using a copier paper.
c. The mold is 3D printed using an FDM 3D printing machine using PLA and pre-polymer silicone (e.g., Mold Star™ 15 SLOW, Smooth-On Inc., USA) mixture is prepared.
d. After mixing, the mixture is poured into the mold to form a silicone sheet of 2.5 mm, which is left in the mold for overmolding the top skin layer in later stages.
e. Two overlapping masking layers are placed on the partially cured bottom skin (note: full cure time is 4 hours for this specific pre-polymer silicone mixture) with a thin mandrel placed in-between extending outside of the mold structure.

f. Another batch of pre-polymer silicone mixture is poured into the mold, encapsulating the masking layers and mandrel, and chemically forming a bond around the unmasked perimeter once the curing is complete.

g. The thin mandrel is removed from the system, and a barbed pneumatic fitting is horizontally attached between the skin layers, (h) producing a pneumatically operable proto-cell.

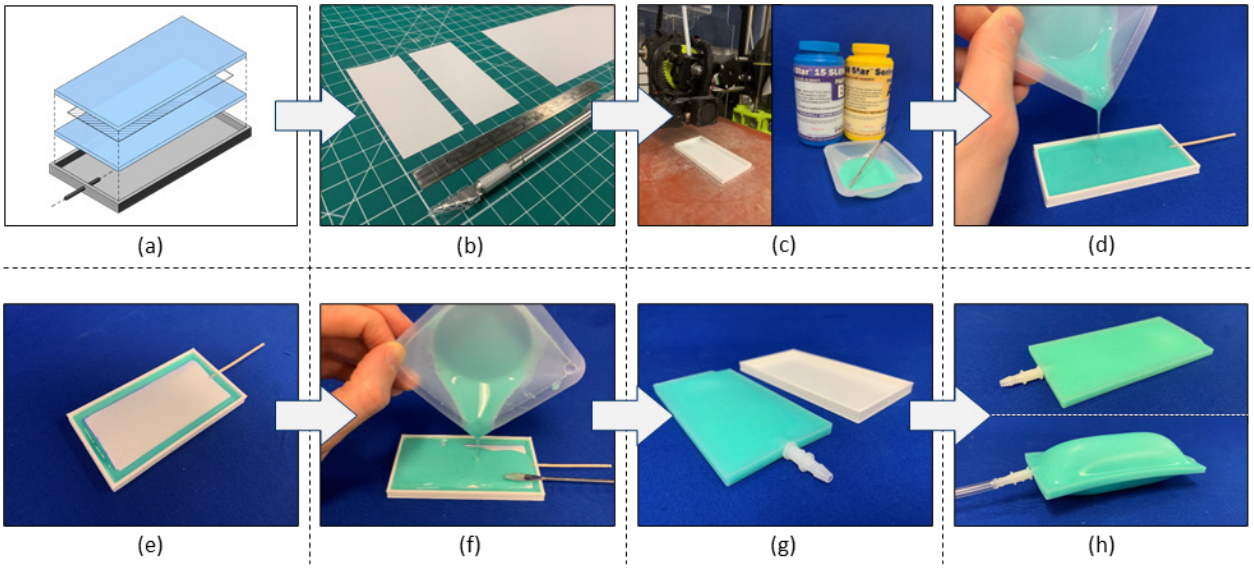

Figure 27. An example fabrication process of a proto-cell using the multi-step molding technique. (a) The bottom and top skin layers and their mold are designed in software (e.g., Rhinoceros), including the details of the masking layer pattern. (b) Two identical masking layers are cut into shape using a Cricut Maker desktop plotter cutter using a copier paper. (c) The mold is 3D printed using an FDM 3D printing machine using PLA and pre-polymer silicone (e.g., Mold Star™ 15 SLOW, Smooth-On Inc., USA) mixture is prepared. (d) The pre-polymer silicone mixture is poured into the mold to form a silicone sheet of 2.5 mm, which is left in the mold for overmolding the top skin layer in later stages. (e) Two overlapping masking layers are placed on the partially cured bottom skin with a thin mandrel placed in-between extending outside of the mold structure. (f) Another batch of pre-polymer silicone mixture is poured into the mold, encapsulating the masking layers and mandrel, and chemically forming a bond around the unmasked perimeter once the curing is complete. (g) The thin mandrel is removed from the system, and a barbed pneumatic fitting is horizontally attached between the skin layers, (h) producing a pneumatically operable proto-cell.

Molding techniques enable the production of constrained layer pneumatic systems with reliably formed seal patterns. The use of already-fused skin layers provides homogeneity, while mold design and fabrication add complexity to the process but allow for finer details and better tolerance control. While manual intervention may be necessary for prototyping or small-batch production, the process is scalable and can be automated for industrial settings.

2.2.3.2. Additive Manufacturing

Additive manufacturing (AM) involves combining materials to create objects from 3D model data. The process usually involves adding material layer by layer, as opposed to subtractive methods of manufacturing. It is also known as 3D printing, rapid prototyping (RP), freeform fabrication (FF), layer manufacturing, among other names [155]. The 2009 ASTM Standard categorizes additive manufacturing processes into seven categories, which include: material extrusion, vat polymerization, material jetting, binder jetting, sheet lamination, powder bed fusion, and directed energy deposition [156]. The last one of these categories is typically used for the additive manufacturing of metal parts made of materials including aluminum, copper, titanium, stainless steel, tool steel, copper, nickel alloys, and several steel alloys. Each group of additive manufacturing processes has unique methods of operation, production properties, and compatible material types. These attributes have an impact on the cost, quality, color, and size of the produced parts, thus affecting design choices [157]. Advancements in additive manufacturing technology, especially in 3D printing using FDM (i.e., fused-deposition modeling) approach, have made it more affordable and capable, leading to increased adoption not only in industrial settings, but also in academia and makerspaces by research groups and hobbyists. These advancements have enabled the production of complex geometries that were previously difficult or impossible to achieve with traditional manufacturing methods [158].

Researchers have shown the adoption and innovative application of various AM processes in the context of fabricating constrained layer pneumatic systems. A large majority of these systems are built employing vat polymerization, material jetting, and material extrusion processes using a variety of photosensitive thermoset polymer resins, uncatalyzed silicone, and thermoplastic powders or filaments.

The vat photopolymerization process involves a liquid photopolymer resin held in a shallow vat, in which geometries and features are fabricated through selective photo-initiated crosslinking of the resin using mask projection in the ultraviolet spectrum. The layer-by-layer fabrication process used in this method results in the production of the final solid object in an upside-down orientation, allowing for the creation of intricate shapes with undercuts and internal cavities [159].

As part of the vat polymerization process, Peele et al. developed a digital mask projection stereolithography technique and utilized it to produce an antagonistic system of artificial muscle [160]. The muscle is fabricated using a commercially available photosensitive polymer resin (Spot-

E resin, Spot-A Materials, Inc.) and is consisted of four pneumatically actuatable air chambers, each operating independently, serving as a building block for producing arbitrarily complex soft machines. Patel et al. developed a bespoke elastomer resin for vat polymerization that can be stretched up to 1100% after curing [161]. In comparison to commercially available photosensitive polymer resins, including Carbon EPU 40, Stratasys TangoPlus, Formlab Flexible, and Spot-A Elastic, with the highest reported elongation at break of 170-220%, they demonstrated significantly improved performance. By using digital light processing (DLP) based stereolithography (SLA) technique, they fabricated pneumatically controlled soft grippers. Yan and Peng modified an off-the-shelf SLA 3D printer (Elegoo Mars LCD) as an inexpensive and efficient way of prototyping hydraulic devices through SLA 3D printing [162]. The process utilizes flexible photosensitive resin (F39/F69, Resione) and customized panel supports for the submerged fabrication of sealed 3D structures that encapsulate uncured resin. The produced structures can be hydraulically actuated with the help of the enclosed uncured resin, providing bending, straightening, extending, and curling motions. By using these controllable motions as a building block, they demonstrated a range of product concepts including a robotic gripper that can be controlled from 3.3-meter distance, a posable lamp, and a shape-changing mobile phone stand.

The material jetting (MJ) AM process involves the selective deposition of photopolymer material and/or wax as droplets, which form thin layers on the build platform. The droplets are cured by UV light of a specific wavelength. After each layer is cured, the build platform is lowered and new material is jetted onto the previous layer, and this process is repeated until a full-scale part is built. To allow the fabrication of parts with cavities and overhang areas, support structures made of wax are used, and these structures are removed from the part using methods such as heating and high-pressure water jetting [163].

Researchers used a material jetting process to fabricate highly integrated linear [164] and rotary [165] bellows actuators, both of which were employed in the development of a vacuum-operated multi-material lightweight robotic gripper [166]. This process enables the use of both rigid and flexible materials in a single step fabrication operation. Husker [167] also employed the material jetting process to create an inflatable acoustic metamaterial structure made of an auxetic pattern. This unique structure can be inflated and deflated to alter its geometry and stiffness, resulting in affecting the acoustic noise attenuation when used as a part of a headphone design. Matsuura et al. introduced a method called "Blow-up Print" to fabricate a compressed 3D silicone structure using

material jetting and restore its original shape by inflation [168]. By fabricating the targeted shape in a compressed state to reduce the overall volume, the printing time and consumption of support material were reduced. Alternatively, Schlatter et al. used the same fabrication process to create soft and flat structures, such as a flexible peristaltic pump and a compliant slug drive inspired by the locomotion of slugs, comprising stretchable elastomer parts, multilevel fluidic channels, and compliant electrodes [169]. The material jetted flat structures are transformed into fully functional 3D soft machines by inflating the embedded thin elastomer channels.

The material extrusion is one of the most common additive manufacturing processes, which is also referred as 3D printing, in which material is selectively dispensed through a nozzle or orifice on a substrate [156]. The initial patent by Crump emphasizes that any material can be employed in this process, provided that the extruded material can properly sticks to the preceding layer once it has solidified [170]. This includes self-hardening waxes, thermoplastic resins, molten metals, two-part epoxies, foaming plastics, and glass. The most used 3D printing technology is fused deposition modelling (FDM), which involves extruding a heated thermoplastic filament through a nozzle and depositing it layer by layer. The filament softens and flows onto a plate or previously deposited material before solidifying and bonding to the substrate. Most parts require support structures, and the accuracy of the z-axis is partially determined by the nozzle's height above the previous layer [171].

By using FDM 3D printers and flexible thermoplastic polyurethane filaments, researchers have developed pneumatically operated bending and twisting actuators, which were used in the design of soft grippers [172], [173], wearable assistive hand and wrist exoskeletons [105], and posture correcting cushion and active porosity window blind [82]. Han et al. have developed an innovative technique for 3D printing airtight monolithic structures that consist of an inflatable membrane (i.e., skin layer) and internal tethers. These tethers, which can be tailored length-wise, enable the fabrication of angled skin layers as well as parallel ones. By using this technique, they have demonstrated the feasibility of fabricating compactly stowable tablet stands and flip-flops that can be inflated and rigidized for use [174].

Apart from the use of FDM 3D printers, researchers have been developing material extrusion technologies that enable depositing various types of silicone polymers. The commercially available flexible materials that can be used by material jetting technique (e.g., SLA and polyjet materials) have an elongation yield of about 240%, which is lower compared to silicones of similar

hardness that have an elongation yield of 340%. However, 3D printable silicones with lower hardness are capable of achieving deformations of up to 1000% [175]. The emergence of new functionalities can be enabled by using silicone 3D printing techniques to design constrained layer pneumatic systems that can expand tenfold.

By using silicone 3D printing techniques, researchers have fabricated traditional pneu-net and tentacle-like actuators, the latter of which comprise four independently inflatable channels [176]. Hajash et al. developed a rapid liquid printing (RLP) process where uncured liquid silicone polymer is deposited into a bath of water-based gel using a robotic arm or a gantry CNC system [177]. Sparrman et al. employed RLP to fabricate an entirely soft robotic arm consisting of three linear actuators and three bending actuators integrated in one multi-chambered design made of same material [175], and a range of shape-changing products for everyday life including lamps and vases that can be stored in a deflated state for more efficient shipping logistics and can be inflated to be used [178]. The use of a variety of materials in a single silicone 3D printing process has also been implemented, enabling the fabrication of flexible strain sensors composed of silicone and conductive ink, as well as a pneumatically driven artificial muscle made of two distinct types of silicone with different stiffness characteristics [179], [180].

Most of the pneumatic systems fabricated using FDM or silicone 3D printing techniques in the current state of art are designed with three-dimensional air cavities that increase in volume as positive pressure is applied, resulting in a range of actuation motions. Alternatively, to minimize overall structure volume during fabrication and when not in use, pneumatic systems can be designed as thin and flat structures comprising skin layers and zero-volume air cavities. Alexander et al. developed a masked fabrication technique for multi-layered thin inflatable devices, creating internal air cavities shaped by the use of thin and flat masks during 3D printing [181]. This technique achieves the same actuation motion as bulky air cavities without incorporating them into the structure.

The fabrication steps of a proto-cell, which comprises two skin layers, a masking layer, and a pneumatic fitting using the masked 3D printing technique, are outlined in Figure 28 as follows:

a. The bottom and top skin layers, and the mask to be placed in-between are designed in software (e.g. Rhinoceros), and exported as stereolithography (stl) and drawing exchange format (dxf) files, respectively.

b. Separate gcode files are generated for bottom and top skin layers using their respective stl files in a 3D printer slicer software (e.g., Lulzbot Cura 3.6.37).

c. The masking layer is cut into shape using a desktop plotter cutter (Cricut Maker, USA) using a copier paper or silicone coated baking sheet.

d. The bottom skin layer with a 1 mm thickness is 3D printed on a printing substrate.

e. Once the printing task is complete, the mask is placed on the fabricated bottom skin layer and secured using thin double-sided tape or PVA glue stick.

f. The gcode file for the top skin layer contains a specific set of code lines that redefines the zero point on the Z axis, forcing the 3D printer's nozzle to begin depositing material right above the already-fabricated bottom skin layer. These lines are:

   - G1 Z1.0; which is the targeted z-offset since the bottom skin layer has 1 mm thickness,
   - G92 Z0; which defines z-offset as absolute zero,
   - G1 Z15; which moves the nozzle up 15 mm before print starts.

g. The top skin layer fuses to the bottom one only around the non-masked areas (perimeter in this case), producing an airtight thin and flat constrained layer pneumatic system.

h. The 3D printed proto-cell is removed from the printing substrate before laterally attaching a barbed pneumatic fitting.

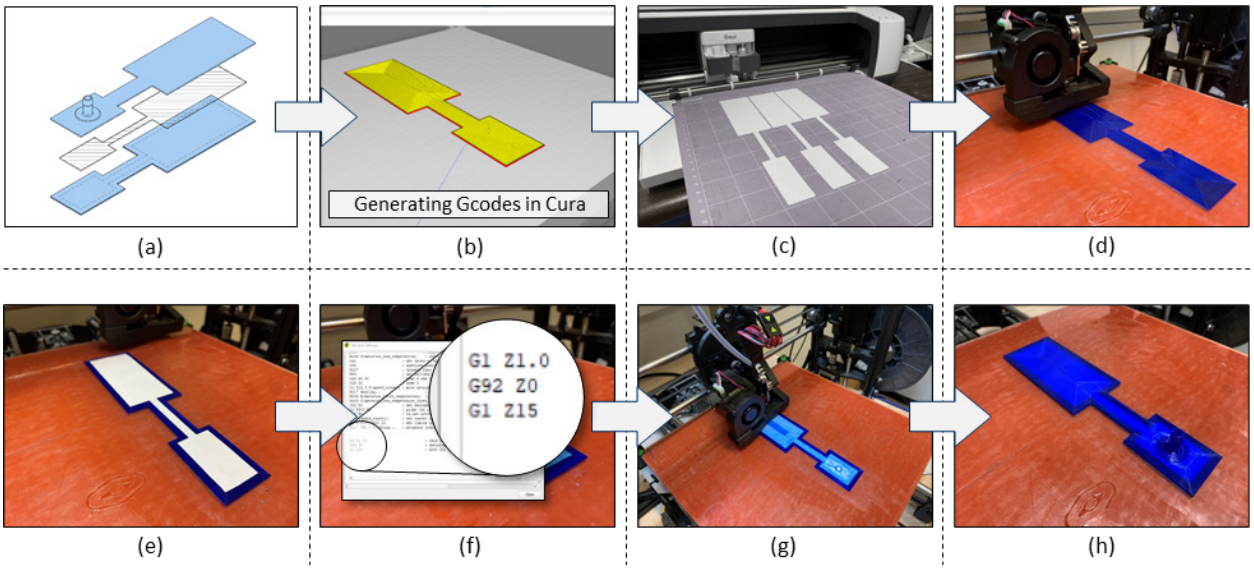

Figure 28. An example fabrication process of a proto-cell using the masked 3D printing technique. (a) The bottom and top skin layers, and the mask to be placed in-between are designed in Rhinoceros and exported as stereolithography (stl) and drawing exchange format (dxf) files, respectively. (b) Separate gcode files are generated for bottom and top skin layers using their respective stl files in a 3D printer slicer software, Lulzbot Cura 3.6.37. (c)

The masking layer is cut into shape using a Cricut Maker desktop plotter cutter using a copier paper. (d) The bottom skin layer with a 1 mm thickness is 3D printed on a printing substrate. (e) Once the printing task is complete, the mask is placed on the fabricated bottom skin layer and secured using thin double-sided tape. (f) The gcode file for the top skin layer contains a specific set of code lines that redefines the zero point on the Z axis, forcing the 3D printer's nozzle to begin depositing material right above the already-fabricated bottom skin layer. (g) The top skin layer fuses to the bottom one only around the non-masked areas (perimeter in this case). (h) This produces an airtight, thin, and flat proto-cell prototype.

Additive manufacturing offers several advantages over conventional manufacturing (CM) processes, including reduced production time, decreased need for human intervention, lower costs for expensive materials, and improved cost-competitiveness and structural integrity through the production of unified structures with arbitrary shapes [155]. While manual intervention may be required for prototyping or small-batch production, additive manufacturing processes are scalable and can be automated for industrial settings, making them suitable for the fabrication of constrained layer pneumatic systems, similar to molding techniques.

2.2.4. The Selection of a Fabrication Approach

The selection of an appropriate fabrication approach and method is significantly influenced by factors such as the materials employed, scalability, and cycle rate (i.e., prototyping versus production). Additionally, the chosen method impacts design flexibility, the degree of control over fabrication process variables (e.g., heat, time, pressure for heat-sealing), and the potential complexity of the system structure, especially when constructing multilayered systems. It is crucial for designers to consider these factors to determine the most suitable fabrication technique for their specific applications given the resources (e.g., fabrication tools, materials, time) available. The table below (Table 2) provides an overview of the advantages and disadvantages associated with each fabrication approach and method for creating constrained layer pneumatic system prototypes. By examining these factors, designers can make informed decisions on the most appropriate fabrication method for their projects. Furthermore, understanding the intricacies of various fabrication approaches can enable the development of innovative solutions to overcome potential limitations and facilitate the realization of more complex and efficient constrained layer pneumatic systems.

Table 2. Advantages and disadvantages of fabrication approaches and associated methods for the fabrication of constrained layer pneumatic systems

	Fabrication Approaches for Constrained Layer Pneumatic Systems						
	Adhering Existing Skin Layers	Fusing Existing Skin Layers				Producing Already-fused Skin Layers	
		Manual Heat-sealing	Numerically Controlled Heat-sealing	Pre-patterned Heat-sealing	Masked Heat-sealing	Molding	Additive Manuf.
Design flexibility	High	High	High	Low (strict design requirements for RF and ultrasonic welding)	High	Low (new mold design is required for different applications)	High
Initial investment cost	Low	Low to medium	Medium to high	High	Low to medium	Medium	Medium to high
Ongoing tooling/process cost	Medium	Low	Low	High	Low	High	Medium to high
Control over process variables	Good	Poor	Excellent	Excellent	Excellent	Excellent	Excellent
Fabrication cycle	Very slow (mins to hours)	Slow (mins)	Slow (mins)	Very fast (msec to sec)	Medium (sec to mins)	Very slow (mins to hours)	Very slow (mins to hours
Fabrication scalability	High	Low	Low	High	High	High	Low
Multilayering	Applicable (highly flexible)	NA (applicable in special cases)	Applicable (limited)	Applicable (limited)	Applicable (highly flexible)	Applicable (highly flexible)	Applicable
Material applicability	Thermoplastics, thermosets	Thermoplastics	Thermoplastics	Thermoplastics	Thermoplastics	Thermoplastics, thermosets	Thermoplastics, thermosets
Use of non-alike skin layers	Applicable	NA	NA	Applicable (RF and ultrasonic welding)	NA	NA	NA
Miscellaneous advantages (+) / disadvantages (-)	- ageing - surface preparation/heat activation may be required - potential health and safety hazard	+ no additional materials required other than skin layers - requires dexterous manual labor	+ no additional materials required other than skin layers	+ no additional materials required other than skin layers + ultrasonic welding can be used to seal thermosets	+ negligible masking material cost - mask alignment is required	+ molds can be reused - surface preparation, degassing, and heat-curing may be required	NA

2.3. Emergent Cell Functions as a part of Constrained Layer Pneumatic Systems

Pneumatic affordance operations activate fundamental behaviors that are usually coupled (e.g., expand out-of-plane (EO) and contract in-plane (CI)). By constraining these coupled fundamental behaviors based on the sub-cellular feature characteristics of a particular cell in its respective operation state (e.g., push operation state), it is possible to produce a particular set of emergent cell functions (e.g., push) (Figure 29). The emergence of a cell function requires switching from an arbitrary initial operation state to a next operation state. These operation states are usually cyclic in nature and require separate pneumatic affordance operations activating relevant set of fundamental behaviors.

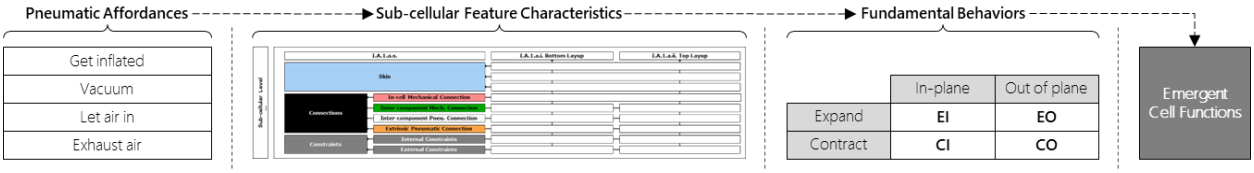

Figure 29. Emergence of cell functions as a part of constrained layer pneumatic systems. Pneumatic affordance operations activate fundamental behaviors that are usually coupled (e.g., expand out-of-plane (EO) and contract in-plane (CI)). By constraining these coupled fundamental behaviors based on the sub-cellular feature characteristics of a particular cell in its respective operation state (e.g., push operation state), it is possible to produce a particular set of emergent cell functions (e.g., push).

A generic operation state transition diagram describing a cell, *C*, with two cyclic operation states, *OS1* and *OS2*, each of which is providing a set of emergent cell functions, *ECF1* and *ECF2*, is shown in Figure 30. To initiate switching from *OS1* to *OS2*, the pneumatic affordance operation, *PAO12*, simultaneously activates a set (either one or two) of coupled fundamental behaviors, *FB12*. Each operation state comprises a transition sub-state and an end sub-state. The transition sub-state (*TS*) corresponds to when a cell begins undergoing a structural transformation (e.g., pushing due to increasing cell pressure) as a response to the relative pressure level change in the system. The end sub-state (*ES*) corresponds to when the targeted structural transformation (e.g., being pushed) is completely achieved as the pressure level in the system reaches the intended extent (note: the extent of the intended pressure level may be changed on the fly to adjust the performance of the behavior). The set of coupled fundamental behaviors, *FB12*, is constrained based on the characteristics of the subcellular features of this particular cell, *C*, therefore are forcing *C* to carry out a designated structural transformation in transition sub-state, *TS2*. Once this structural transformation is executed, *C* accomplishes providing the set of emergent cell functions, *ECF2*, in the end sub-state, *ES2*, of this operation state, *OS2*. Switching from *OS2* to *OS1* is initiated by a separate pneumatic affordance operation, *PAO21*, activating a different set of coupled fundamental behaviors, *FB21*, which are constrained based on the same characteristics of the subcellular features of the cell, *C*, activating the transition and end sub-states, *TS1* and *ES1*, of the first operation state, *OS1*, which eventually generates the respective set of emergent cell functions, *ECF1*.

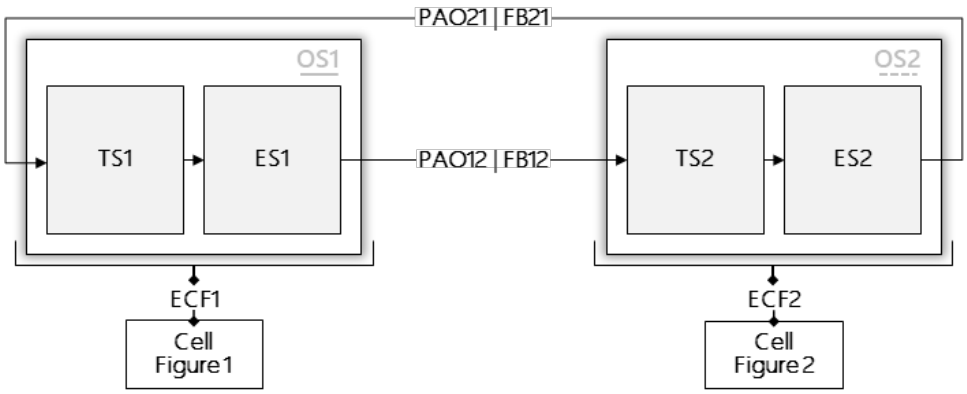

Figure 30. Generic operation state transition diagram. A generic operation state transition diagram describing a cell, *C*, with two cyclic operation states, *OS1* and *OS2*, each of which comprises transition (e.g., TS1) and end sub-states (e.g., ES1), and each of which provides a set of emergent cell functions, *ECF1* and *ECF2,* respectively.

It is important to note that the performance of an emergent cell function (e.g., performance of *push*) in each operation state can be analyzed as a combined performances of transition and end sub-state functions (e.g., *pushing* and *being pushed*). For example, the effects of the temporal aspects (e.g., the time it takes for a cell that is *pushing*) and aesthetic factors (e.g., the structural transformation or the movement of a cell that is *pushing*) on the experience of a user who physically interacts (e.g., having tactile interaction, simply observing the transformation) with a constrained layer pneumatic system (which is made of cells that are *pushing*) in a particular design context can be analyzed. To capture the rich interaction potentialities between a constrained layer pneumatic system and a user, a complex array of design of experiments involving human subjects needs to be conducted, which is beyond the scope of this dissertation. Throughout the dissertation, the engineering performances of the emergent cell functions (e.g., *push*) will be characterized and quantified by focusing on the end sub-state function as the targeted structural transformation is completely achieved in a particular operation state.

Since the design of the characteristics of subcellular features is open-ended and can be arranged in numerous different ways, it is possible to generate an ever-growing catalogue of emergent cell functions in the constrained layer pneumatic system context. To introduce how an array of emergent cell functions can be generated by incrementally changing the sub-cellular feature characteristics, a simple proto-cell, which was used to demonstrate the applicable fabrication approaches in Section 3, will be used as a starting point, providing the emergent cell functions, *flatten* and *push*.

The architecture of the cell that provides emergent cell functions, *flatten* and *push*, once activated in its respective operation states (OS1 and OS2) are shown in Figure 31. Its architecture

contains top and bottom skin layers, which are mechanically connected, and a set of extrinsic pneumatic connection made of a low-pressure barbed pneumatic fitting that is vertically attached to the bottom skin layer (Figure 31, left). This extrinsic pneumatic connection enables controlling the pressure level inside the encapsulated air cavity through the air flow channel, producing the *flatten* emergent cell function by operating the pneumatic affordance, exhaust air, and producing the *push* emergent cell function by operating the pneumatic affordance, get inflated (Figure 31, right).

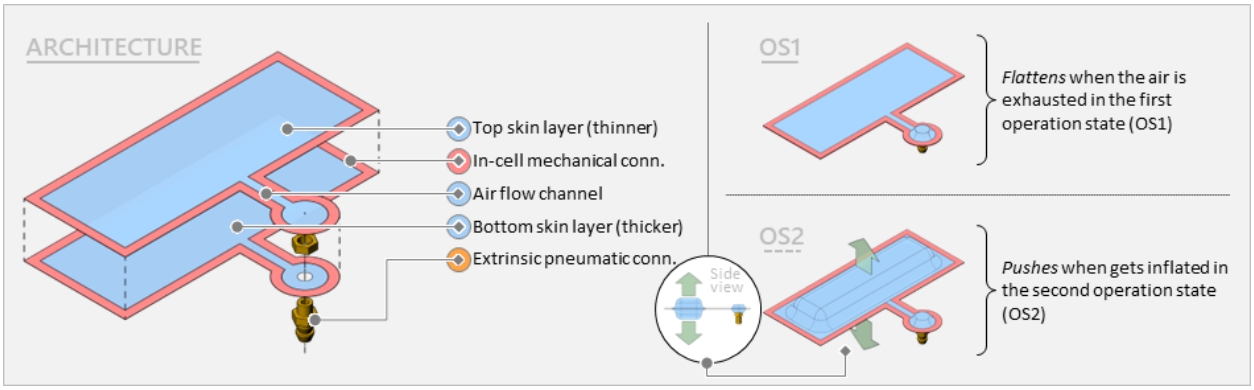

Figure 31. Architecture and operation states of the cell providing *flatten/push* emergent cell functions. The architecture of a cell providing *flatten/push* emergent cell functions contains two skin layers that are stacked on top of each other and a set of extrinsic pneumatic connection components (left). The *flatten* and *push* emergent cell functions are activated in operation states, OS1 and OS2, using exhaust air and get inflated operations, respectively (right).

The cyclic *flatten*/*push* operation state transition diagram is described in Figure 32. To switch from the first operation state (OS1) to the second one (OS2), the operation of the pneumatic affordance, get inflated, activates the coupled fundamental behaviors, expand out of plane and contract in-plane (EO+CI), which simultaneously contribute to the structural transformation that the cell undergoes in its respective operation state denoted as OS2 comprising transition sub-state, *pushing*, and end sub-state, *pushed*. Likewise, to switch from the second operation state (OS2) to the first one (OS1), the operation of the pneumatic affordance, exhaust air, activates the coupled fundamental behaviors, expand in-plane and contract out of plane (EI+CO), which simultaneously contribute to the structural transformation that the cell undergoes in its respective operation state denoted as OS1 comprising transition state, *flattening*, and end state, *flattened*.

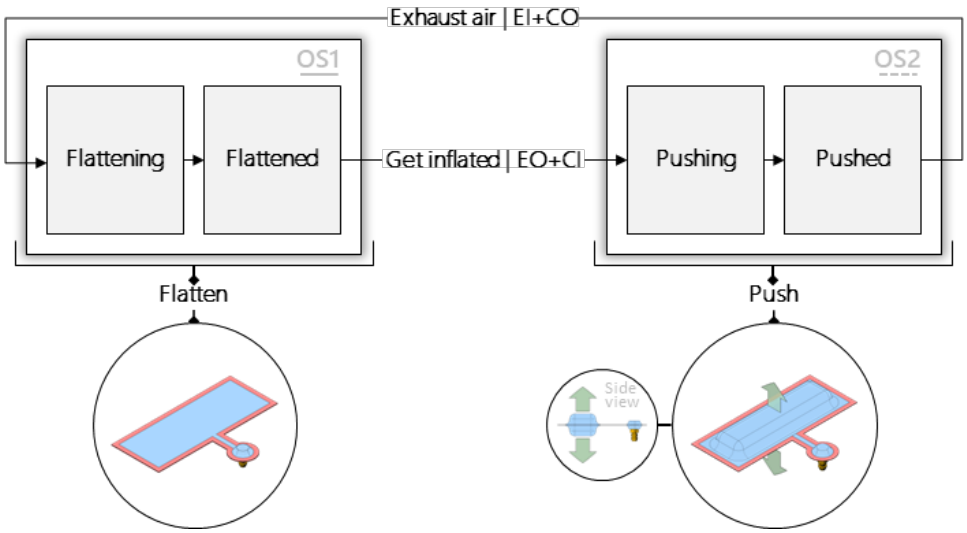

Figure 32. *Flatten/push* operation state transition diagram. The *flatten* operation state denoted as OS1 comprises transition state, *flattening*, and end state, *flattened,* and the *push* operation state denoted as OS2 comprises transition state, *pushing*, and end state, *pushed.*

The sub-cellular feature characteristics of this cell is tabulated (Figure 33), detailing the characteristics of the bottom and top layups in three main feature categories that are shown on the left: *skin*, *connections*, and *constraints*. Both skin layers of this cell are made of flexible (high) and inextensible TPU coated 70 denier nylon fabric (0.17mm thickness) with a uniform cross-section. This results in granting a symmetric architecture. The transversally elongated convex perimeter seal characterizes the in-cell mechanical connection sub-cellular feature of this cell. Since this cell exists in isolation without requiring any adjacent cell to provide a higher-level function, the characteristics describing the inter-component mechanical and pneumatic connections are left blank. The vertical barbed fitting is attached to the bottom skin, therefore only listed under the bottom layup column. The cell is free of any constraints, therefore the characteristics describing the internal and external constraints are left blank as well.

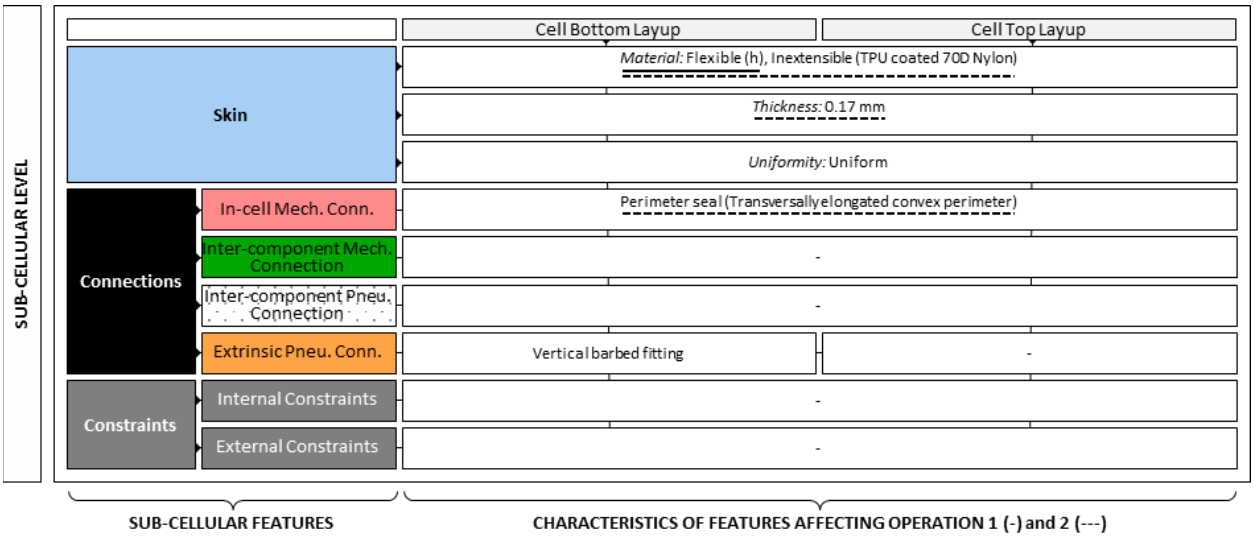

Figure 33. The sub-cellular feature characteristics contributing to *flatten/push* emergent cell functions. The characteristics of the bottom and top layups of the cell providing *flatten/push* emergent cell functions are detailed in three main feature categories, skin, connections, and constraints. The characteristics that primarily contribute to the set of emergent cell functions, *flatten* and *push*, are underlined using solid (-) and dashed (---) lines, respectively.

The characteristics that primarily contribute to the set of emergent cell functions, *flatten* and *push*, are underlined using solid (-) and dashed (---) lines, respectively. Based on this, the material flexibility (h) for bottom and top layups are the only primary contributing characteristics for the generation of the emergent cell function, *flatten*. For example, instead of using flexible and inextensible material, using flexible but extensible material would not have affected the nature of the *flatten* emergent cell function when the vacuum is applied. However, for generating the emergent cell function, *push*, the material flexibility (h), the material inextensibility, and the symmetry granted by the same skin layer material thickness are all contributing characteristics. Changing the parameters associated with these characteristics would affect the nature of the resulting *push* emergent cell function. Introducing sub-cellular features of which characteristics are currently left blank for this particular cell may change the resulting emergent cell function as well.

It is possible to produce new emergent cell functions by changing the characteristics of the existing features of and/or introducing new features to the proto-cell described earlier and by activating same or different sets of fundamental behaviors through same or different pneumatic affordance operations. Figure 34 lists ten sets of emergent cell functions that can be obtained either by modifying the existing skin and/or connection feature characteristics of the generic cell or by importing new features such as internal and/or external constraints. For the sake of simplicity, the set of pneumatic affordance operations and fundamental behavior couplings required for

generating these emergent cell functions are not shown in Figure 34. These specific aspects will be described later in the relevant sub-sections detailing the generation of each set of emergent cell functions listed. It is important to note that there can be multiple ways to produce same set of emergent cell functions. For example, *extend* and *pull* emergent cell functions can be obtained by introducing an external (e.g., boundary) constraint to the proto-cell's architecture (as listed in the Figure 34) as well as employing a specially designed internal constraint (e.g., 90° corrugated flexible V-frame sheet). The wide-range of emergent cell functions and their on-demand recurrent activation obtained by operating a relevant pneumatic affordance provide a basis for the emergence of a new design space.

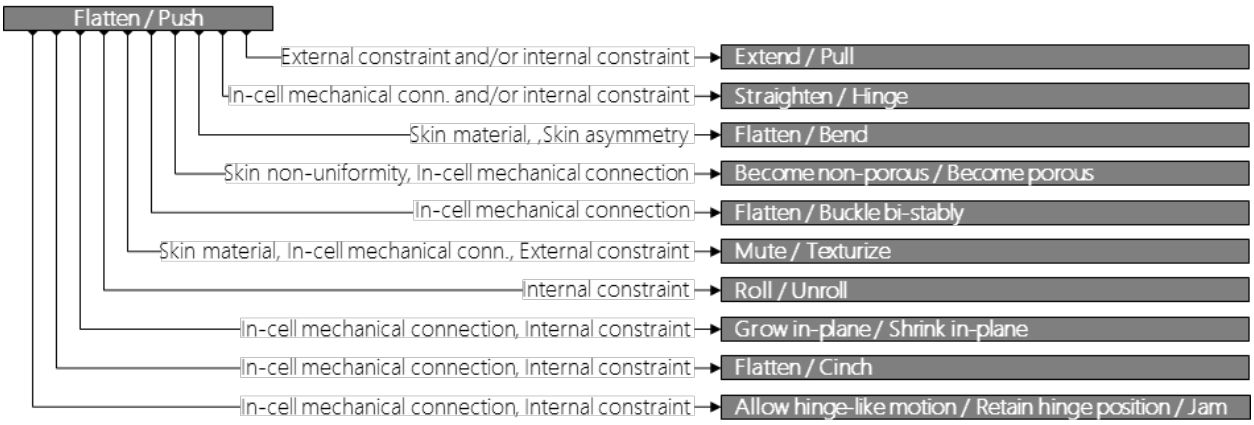

Figure 34. Using an existing cell as a basis to generate new sets of emergent cell functions. Ten sets of emergent cell functions that can be obtained either by modifying the existing skin and/or connection feature characteristics of the generic cell or by importing new features such as internal and/or external constraints.

By employing these emergent cell functions provided by cells (i.e., the lower-level functionalities provided by the basic architectural components), it is possible to attain a range of high-level functionalities, e.g., technology sub-capabilities, as these cells are combined to form higher-level architectural components as a part of a constrained layer pneumatic system. This enables synthesis and re-synthesis of highly customizable, lightweight, space saving, and low-cost user interacting multi-mode products employing constrained layer pneumatic systems in myriad ways.

A list of emergent cell functions, which are produced by constraining the fundamental behavior couplings in its respective operation state based on the sub-cellular feature characteristics of the lowest-level architectural components (i.e., cells), is catalogued. Such a catalogue provides a basis for the composition of higher-level constrained layer pneumatic systems that afford higher-level functionalities (e.g., technology sub-capabilities), enabling the design of user-interacting multi-

mode products. To demonstrate the breadth of the design space of multi-mode products employing constrained layer pneumatic systems, five different multi-mode product concepts are introduced.

2.3.1. Extend/Pull

The architecture and sub-cellular feature characteristics of the modified cell that provides *extend* and *pull* emergent cell functions in the first and second operation states, respectively, are almost identical to the architecture and sub-cellular feature characteristics of the simplest proto-cell providing *flatten* and *push* emergent cell functions except for the introduction of an external boundary constraint (Figure 35-bottom, highlighted in yellow). This constraint enables re-purposing of the in-plane contraction fundamental behavior that is coupled to the out of plane expansion fundamental behavior and generates *extend* and *pull* emergent cell functions.

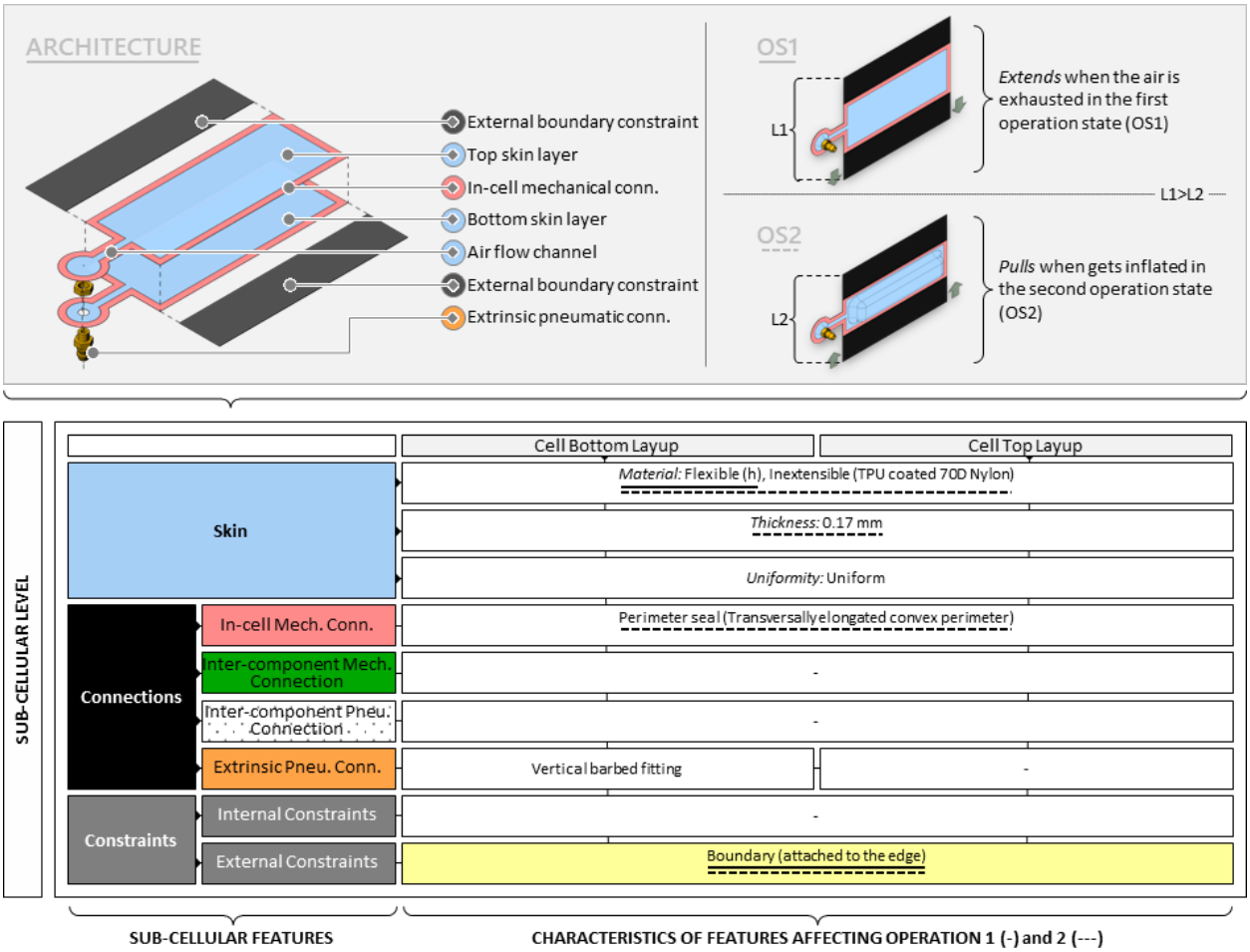

Figure 35. Cell architecture, operation states, and the modified sub-cellular feature characteristics of the cell providing *extend/pull* emergent cell functions. The architecture of a cell providing *extend/pull* emergent cell functions contains two skin layers that are stacked on top of each other, a set of extrinsic pneumatic connection components, and a set of external boundary constraints (top left). The *extend* and *pull* emergent cell functions are activated in operation states, OS1 and OS2, using exhaust air and get inflated operations, respectively (top right). The

characteristics that primarily contribute to the set of emergent cell functions, *extend* and *pull*, are underlined using solid (-) and dashed (---) lines, respectively. The architecture and the modified sub-cellular feature characteristics of the cell that provides *extend* and *pull* emergent cell functions in the first and second operation states, respectively, are almost identical to the architecture and sub-cellular feature characteristics of the simplest proto-cell providing *flatten* and *push* emergent cell functions except for the introduction of an external boundary constraint (bottom, highlighted in yellow).

This modified cell is suspended in an upright position as one of its longer edges is fixed to a rigid component to lift a weight that is attached to the other longer edge using straps and grommets as illustrated in Figure 35 (top right). The cyclic *extend/pull* operation state transition diagram of this modified cell is described in Figure 36. Once it gets inflated to switch from its first operation state (OS1) to the second operation state (OS2) activating the same fundamental behavior coupling (EO+CI) as the proto-cell, the in-plane contraction is being employed to enable the *pull* emergent cell function due to the external boundary constraint. To switch from the second operation state to the first one, the exhaust air operation activates the same fundamental behavior coupling (EI+CO) as the proto-cell, which makes the modified cell relax due to the in-plane expansion, therefore enabling the *extend* emergent cell function.

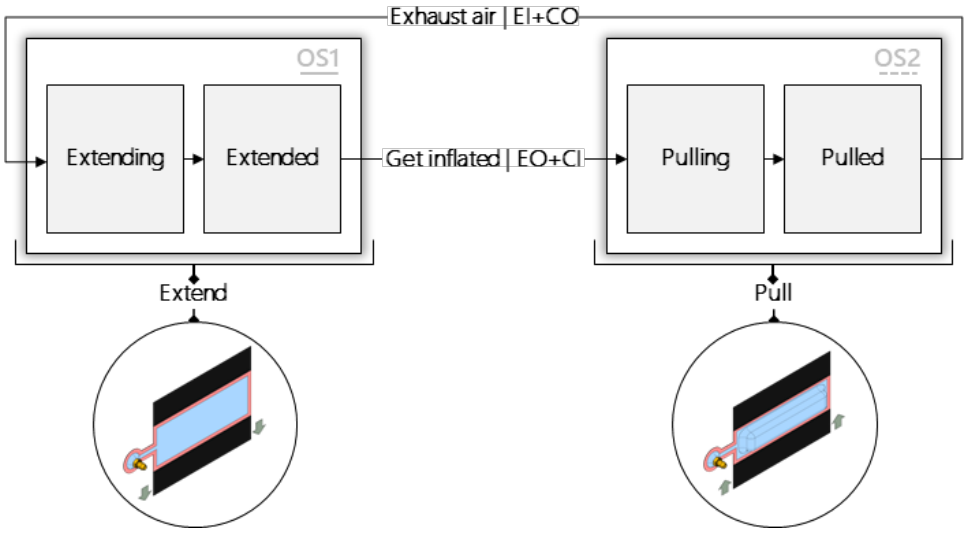

Figure 36. *Extend/pull* operation state transition diagram of the modified cell. The *extend* operation state denoted as OS1 requires an exhaust air in operation and comprises transition state, *extending*, and end state, *extended.* The *pull* operation state denoted as OS2 requires a get inflated operation and comprises transition state, *pulling*, and end state, *pulled*.

The extent of the pulling action can be increased by further modification of this already-modified cell. Introducing an internal constraint, which is made of a 90° corrugated flexible V-frame sheet, divides the air cavity in the modified cell into three major compartments (Figure 37). Instead of using the *get inflated* operation, this further modified cell uses the *vacuum* operation to shrink these three major compartments, which results in temporary folding of the flexible V-frame

sheet almost to a planar formation, creating a version of the *pull* emergent cell function with an enhanced stroke.

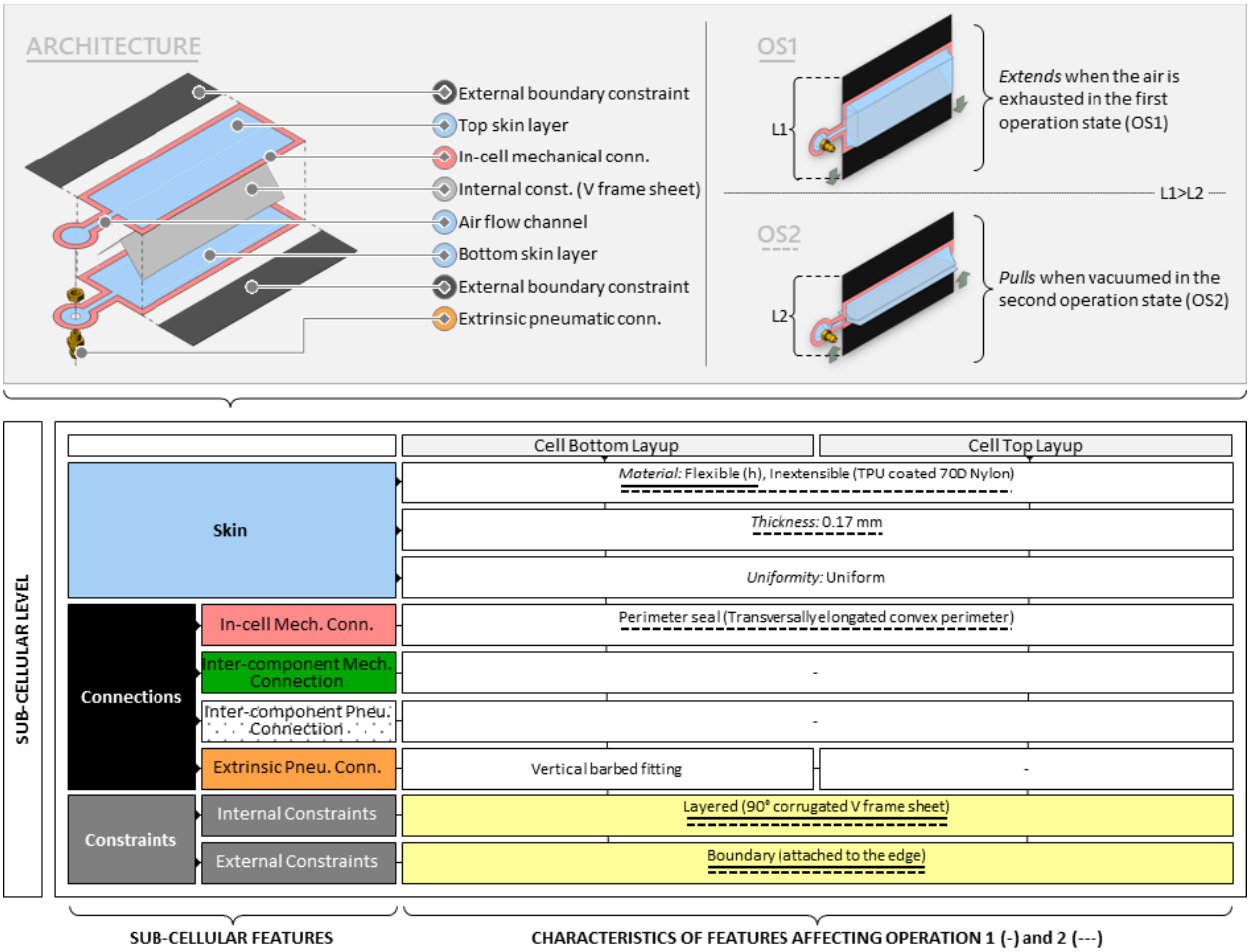

Figure 37. Cell architecture, operation states, and the further modified sub-cellular feature characteristics of the alternative cell providing *extend/pull* emergent cell functions. The architecture of a cell providing *extend/pull* emergent cell functions contains two skin layers that are stacked on top of each other, a set of extrinsic pneumatic connection components, a set of external boundary constraints, and an internal constraint, which is made of a 90° corrugated flexible V-frame sheet, dividing the air cavity in the modified cell into three major compartments (top left). The *extend* and *pull* emergent cell functions are activated in operation states, OS1 and OS2, using exhaust air and vacuum operations, respectively (top right). The characteristics that primarily contribute to the set of emergent cell functions, *extend* and *pull*, are underlined using solid (-) and dashed (---) lines, respectively. The architecture and the further modified sub-cellular feature characteristics of the cell that provides *extend* and *pull* emergent cell functions in the first and second operation states, respectively, are almost identical to the architecture and sub-cellular feature characteristics of the simplest proto-cell providing *flatten* and *push* emergent cell functions except for the introduction of an external boundary constraint and an internal constraint (bottom, highlighted in yellow).

The cyclic *extend/pull* operation state transition diagram of this further modified cell is described in Figure 38. Once it gets vacuumed to switch from the first operation state (OS1) to the second operation state (OS2), which activates a different fundamental behavior coupling (CI+CO) from the proto-cell, the in-plane and out of plane contractions simultaneously generate the *pull*

emergent cell function. To switch back from the second operation state to the first one, the let air in operation activates another fundamental behavior coupling (EI+EO). The in-plane and out of plane expansions generate the *extend* cell function.

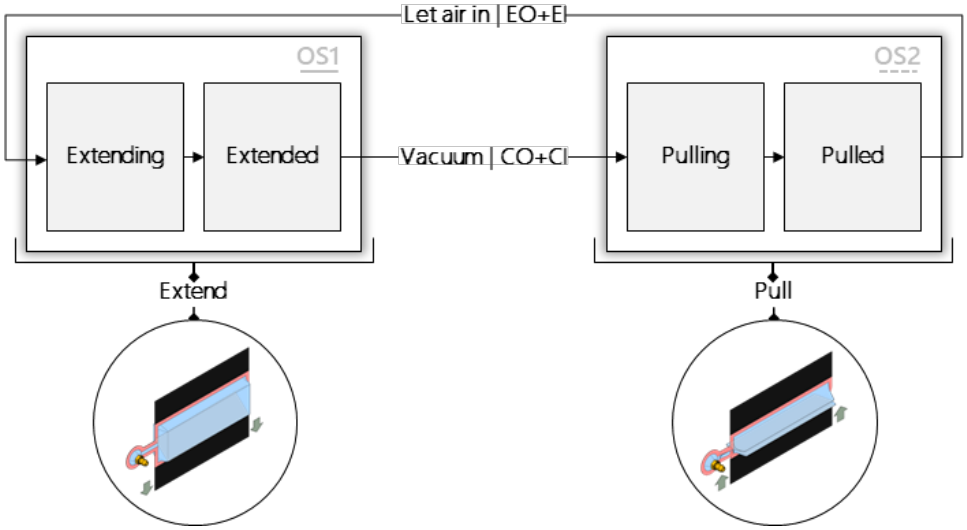

Figure 38. Extend/pull operation state transition diagram of the further-modified cell. The *extend* operation state denoted as OS1 requires a let air in operation and comprises transition state, *extending*, and end state, *extended.* The *pull* operation state denoted as OS2 requires a vacuum operation and comprises transition state, *pulling*, and end state, *pulled*.

2.3.2. Straighten/Hinge

The architecture and sub-cellular feature characteristics of the modified cell that provides *straighten* and *hinge* emergent cell functions in the first and second operation states, respectively, are almost identical to the architecture and sub-cellular feature characteristics of the proto-cell providing *flatten* and *push* emergent cell functions except for the modified in-cell mechanical connection, which contains two parts: 1) a transversely elongated convex perimeter seal (same as the proto-cell's) and 2) a 45° rotated concentric square inner seal (Figure 39). This inner seal divides the inflatable air cavity into two main pneumatically connected compartments. Simultaneous inflation of these compartments activates out of plane expansion and in-plane contraction fundamental behaviors, the latter of which generates a tensile force that pulls the cell perimeter inward in-plane. Since the cell is symmetrically made of inextensible skin material and the inner seal transversally creates a natural bending location, the cell arbitrarily hinges upward or downward. The hinging direction can be controlled by modifying the material flexibility and/or thickness of one of the cell skin layers. Ou et al. documents the relationship between the geometric parameters of the inner seal shape (line, ellipse, and diamond) and the resulting degree of hinging

behavior as well as providing a digital tool to design and simulate the physical transformation of the hinging cells [73].

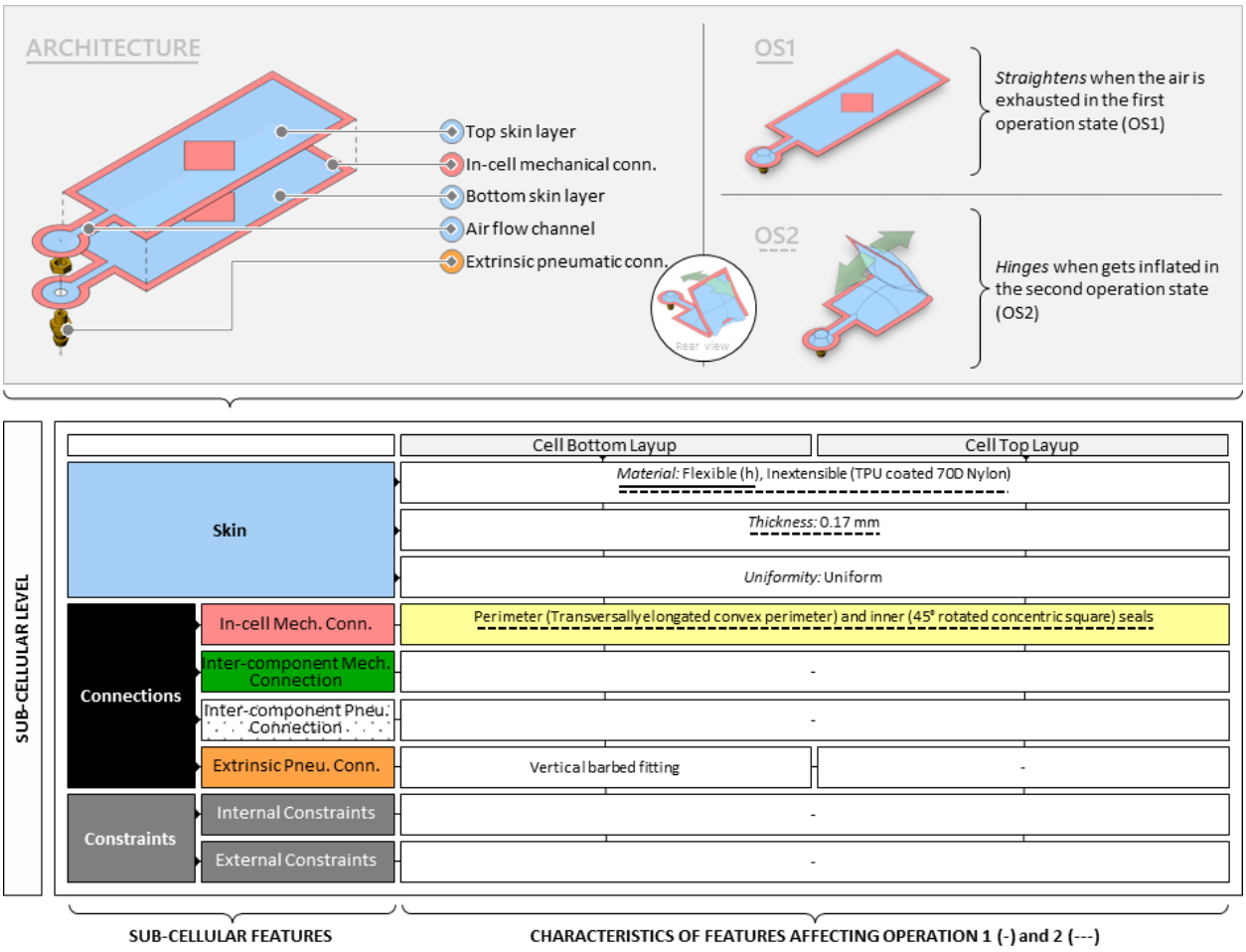

Figure 39. Cell architecture, operation states, and the modified sub-cellular feature characteristics of the cell providing *straighten/hinge* emergent cell functions. The architecture of a cell providing *straighten/hinge* emergent cell functions contains two skin layers that are stacked on top of each other and a set of extrinsic pneumatic connection components (top left). The *straighten* and *hinge* emergent cell functions are activated in operation states, OS1 and OS2, using exhaust air and get inflated operations, respectively (top right). The characteristics that primarily contribute to the set of emergent cell functions, *straighten* and *hinge*, are underlined using solid (-) and dashed (---) lines, respectively. The architecture and the modified sub-cellular feature characteristics of the cell that provides *straighten* and *hinge* emergent cell functions in the first and second operation states, respectively, are almost identical to the architecture and sub-cellular feature characteristics of the simplest proto-cell providing *flatten* and *push* emergent cell functions except for the modified in-cell mechanical connection, which contains two parts: 1) a transversely elongated convex perimeter seal (same as the proto-cell's) and 2) a 45° rotated concentric square inner seal (bottom, highlighted in yellow).

The cyclic operation state transition diagram of this modified cell is described in Figure 40. Once it gets inflated to switch from its first operation state (OS1) to the second operation state (OS2) activating the same fundamental behavior coupling (EO+CI) as the proto-cell, the in-plane contraction and out of plane expansion are producing the *hinge* emergent cell function due to the modified in-cell mechanical connection. To switch from the second operation state to the first one,

the exhaust air operation activates the same fundamental behavior coupling (EI+CO) as the proto-cell, which makes the modified cell *straightened*.

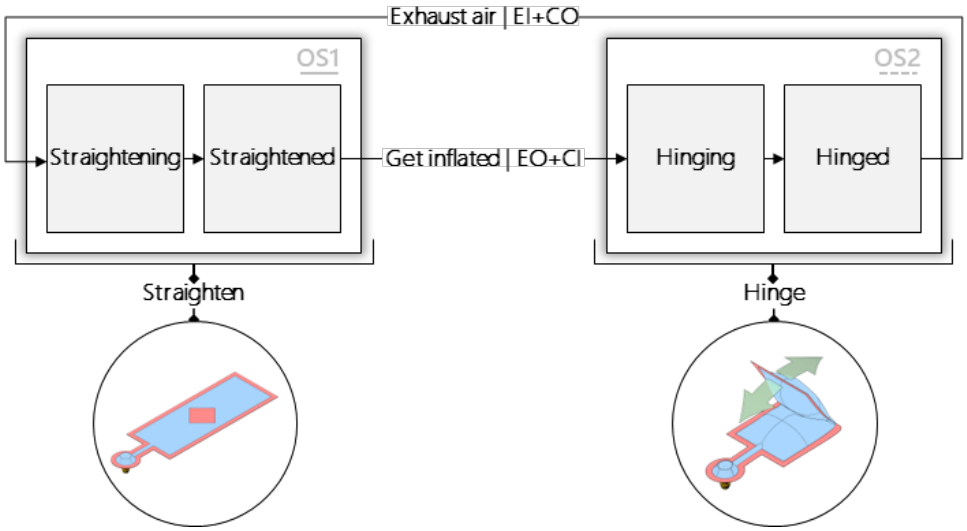

Figure 40. *Straighten/Hinge* operation state transition diagram of the modified cell. The *straighten* operation state denoted as OS1 requires an exhaust air operation and comprises transition state, *straightening*, and end state, *straightened.* The *hinge* operation state denoted as OS2 requires a get inflated operation and comprises transition state, *hinging*, and end state, *hinged*.

An alternative approach for providing the same set of emergent cell functions, *straighten* and *hinge*, is employing an internal constraint. This constraint is made of two asymmetrical T-shaped tiles that are mirrored around the center line of this alternatively modified cell. The bottom-most and the top-most surfaces of these tiles are mechanically connected to the inner surfaces of the skin layers forming a vacuumable cavity consisting of three major compartments that are pneumatically connected along with a foldable hinge line on the bottom skin layer (Figure 41). Instead of using the get inflated operation, this alternatively modified cell uses the vacuum operation to make these three major compartments shrink, which causes the top skin layer to pull the two tile protrusions together, folding the alternatively modified cell along the hinge line. Li et al. introduced and explored a curling air surface architecture based on ensembles of hinged T-shaped tiles, providing higher-level straightening and aggregated hinging (i.e., curling) functionalities [77]. The relationship between internal tile geometry design variables and the resulting curling performance is analytically modelled and validated through a structurally adaptable multi-mode design case study, morphing windshield cowling.

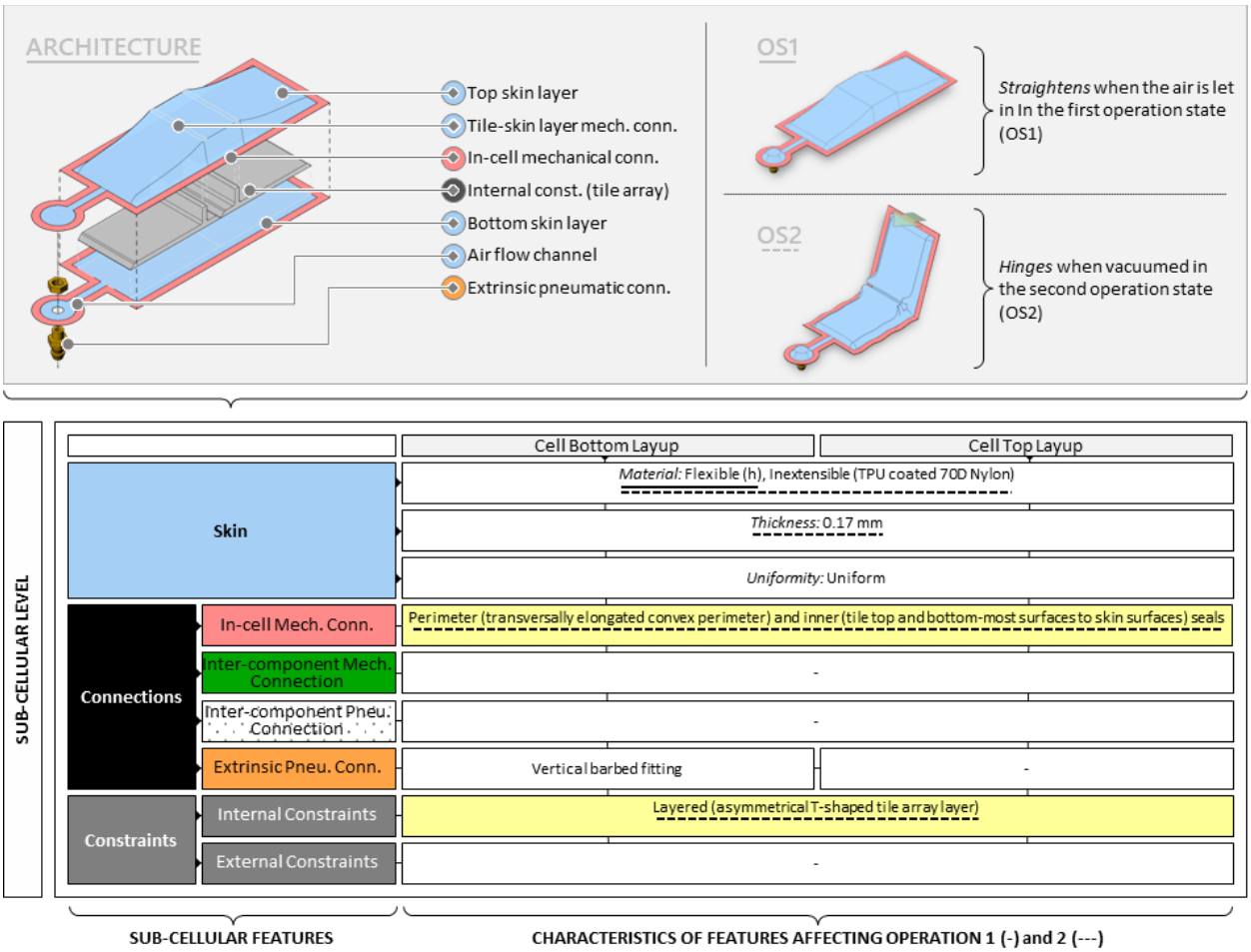

Figure 41. Cell architecture, operation states, and the further-modified sub-cellular feature characteristics of the alternative cell providing *straighten/hinge* emergent cell functions. The architecture of this alternative cell providing the same *straighten/hinge* emergent cell functions contains two skin layers that are stacked on top of each other, a set of extrinsic pneumatic connection components, and a set of internal constraints, which is made of asymmetrical T-shaped tiles (top left). The *straighten* and *hinge* emergent cell functions are activated in operation states, OS1 and OS2, using let air in and vacuum operations, respectively (top right). The characteristics that primarily contribute to the set of emergent cell functions, *straighten* and *hinge*, are underlined using solid (-) and dashed (---) lines, respectively. The architecture and the further modified sub-cellular feature characteristics of this cell are almost identical to the architecture and sub-cellular feature characteristics of the simplest proto-cell providing *flatten* and *push* emergent cell functions except for the introduction of an internal tile constraint and the modified in-cell mechanical connection (bottom, highlighted in yellow). The bottom-most and the top-most surfaces of these tiles are mechanically connected to the inner surfaces of the skin layers forming a vacuumable cavity consisting of three major compartments that are pneumatically connected along with a foldable hinge line on the bottom skin layer.

The cyclic *straighten-hinge* operation state transition diagram of this further modified cell is described in Figure 42. Once it gets vacuumed to switch from the first operation state (OS1) to the second operation state (OS2), which activates a different fundamental behavior coupling (CI+CO) from the proto-cell, the in-plane and out of plane contractions are simultaneously generating the *hinge* emergent cell function. To switch from the second operation state to the first one, let air in

operation activates another fundamental behavior coupling (EI+EO). The in-plane and out of plane expansions generate the *straighten* cell function.

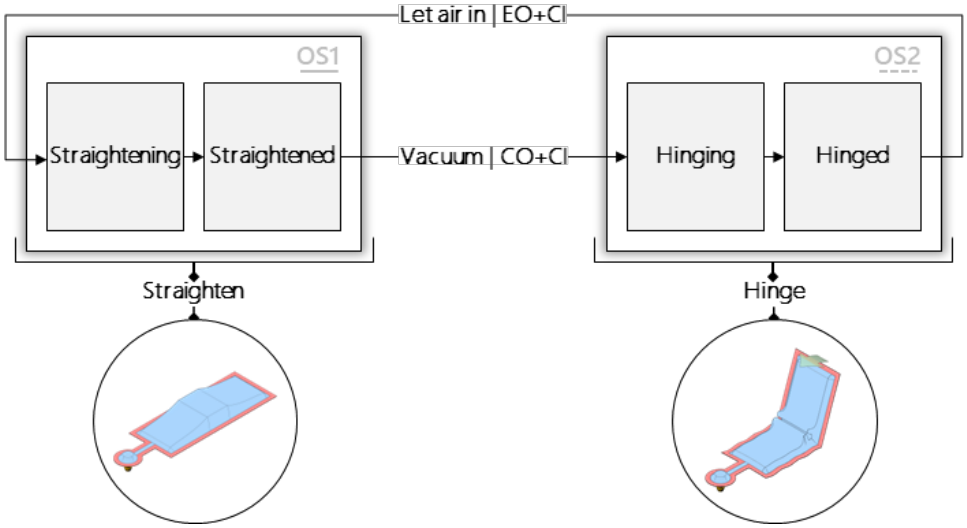

Figure 42. *Straighten/hinge* operation state transition diagram of the further-modified cell. The *straighten* operation state denoted as OS1 requires a let air in operation and comprises transition state, *straightening*, and end state, *straightened.* The *hinge* operation state denoted as OS2 requires a vacuum operation and comprises transition state, *hinging*, and end state, *hinged*.

2.3.3. Flatten/Bend

The architecture and sub-cellular feature characteristics of the modified cell that provides *flatten* and *bend* emergent cell functions in the first and second operation states, respectively, are almost identical to the architecture and sub-cellular feature characteristics of the proto-cell except for the modification made to the skin thickness of the bottom skin layer of the latter, therefore affecting its material flexibility (Figure 43). The symmetrical architecture of the proto-cell is disrupted by changing the bottom skin layer thickness from 0.17mm to 0.53mm. Although the same material (TPU coated nylon) is used, the resulting bottom layer is less flexible than the top layer due to the increase in denier (from 70D to 420D), which consequently increases the overall thickness. Expanding on this fundamental architectural approach, Alexander et al. showcased potential architectural variations that laid the foundation for the development of diverse structurally adaptable multi-mode design applications. Examples include an active seatback pocket that opens and closes on demand by utilizing aggregated bending functionality, as well as an active gill system that offers distributed and embedded methods for controlling heating, ventilation, and air conditioning in vehicles. These innovative solutions demonstrate the versatility of the architectural approach and its potential to revolutionize various aspects of product design and user experience [181].

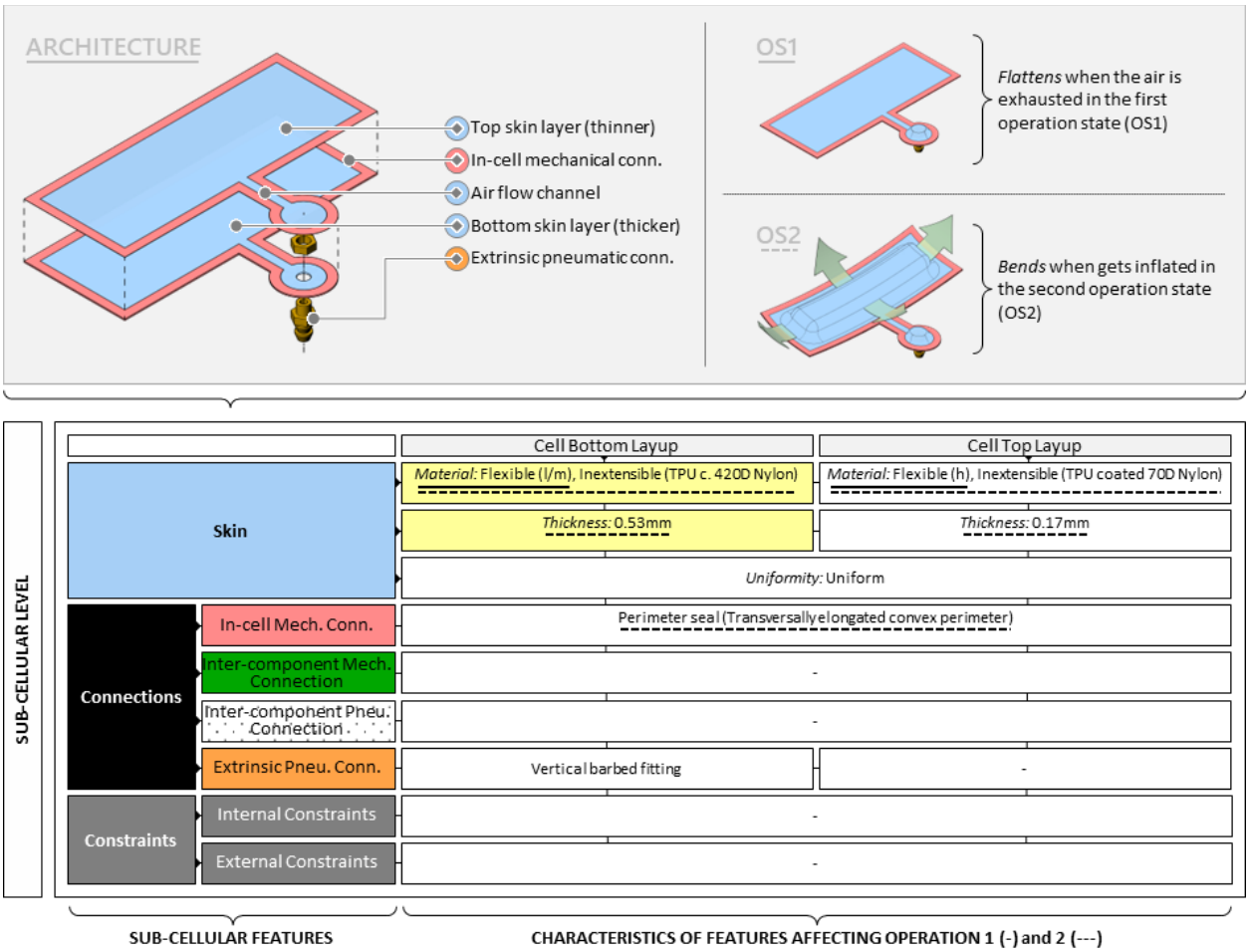

Figure 43. Cell architecture, operation states, and the modified sub-cellular feature characteristics of the cell providing *flatten/bend* emergent cell functions. The architecture of a cell providing *flatten/bend* emergent cell functions contains two skin layers with different thicknesses that are stacked on top of each other and a set of extrinsic pneumatic connection components (top left). The *flatten* and *bend* emergent cell functions are activated in operation states, OS1 and OS2, using vacuum air and get inflated operations, respectively (top right). The characteristics that primarily contribute to the set of emergent cell functions, *flatten* and *bend*, are underlined using solid (-) and dashed (---) lines, respectively. The architecture and the modified sub-cellular feature characteristics of this cell are almost identical to the architecture and sub-cellular feature characteristics of the simplest proto-cell providing *flatten* and *push* emergent cell functions except for the modified skin thickness of the bottom skin layer, which affects its material flexibility and results in generating *bend* emergent cell function (bottom, highlighted in yellow).

The cyclic *flatten/bend* operation state transition diagram of this modified cell is described in Figure 44. Once it gets inflated to switch from its first operation state (OS1) to the second operation state (OS2) activating the same fundamental behavior coupling (EO+CI) as the proto-cell, the top skin layer of this modified cell expands out of plane more than its bottom skin layer can do due to the material thickness and flexibility differences. This generates a net moment that forces the slab of permanently bonded top and bottom skin layers surrounding the inflated air cavity to bend upward (Figure 44, bottom right), enabling generating the *bend* emergent cell function. To switch from the second operation state to the first one, the exhaust air operation activates the same

fundamental behavior coupling (EI+CO) as the proto-cell, which makes the modified cell *flattened*.

Changing the parameters associated with the characteristics affecting the skin material thickness therefore flexibility would influence the nature of the resulting *bend* emergent cell function (e.g., the extent of bending would change at the same pressure level inside the airtight system). It is important to note that the material flexibility could have been changed simply by using different material than TPU coated nylon fabric (e.g., PVC or PP sheet) while keeping the thickness same for both skin layers. This would have resulted in providing the same set of emergent cell functions.

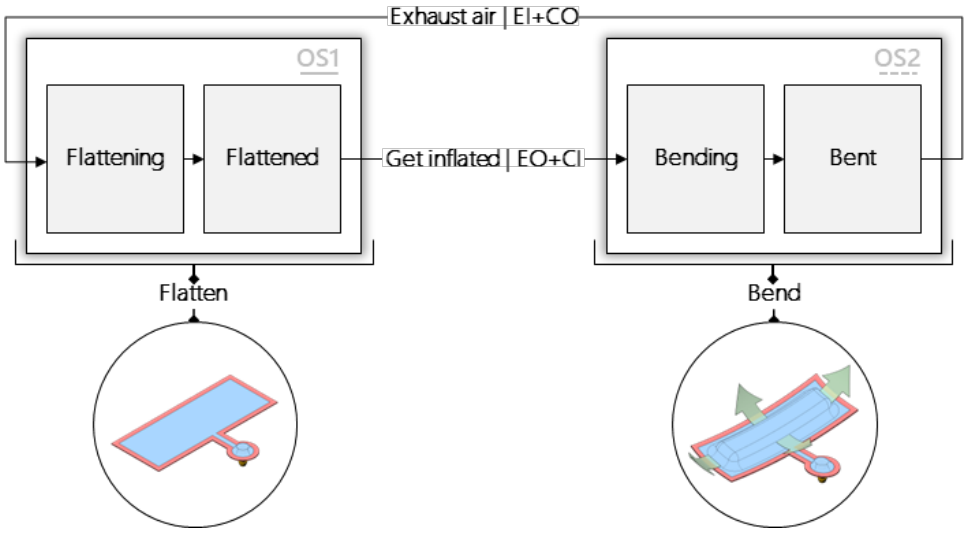

Figure 44. *Flatten/bend* operation state transition diagram of the modified cell. The *flatten* operation state denoted as OS1 requires an exhaust air operation and comprises transition state, *flattening*, and end state, *flattened.* The *bend* operation state denoted as OS2 requires a get inflated operation and comprises transition state, *bending*, and end state, *bent.*

2.3.4. Become non-porous/Become porous

Disrupting the non-uniformity by cutting out a slit through the skin layers along the longitudinal axis and having an inner seal surrounding this slit are the essential changes in the sub-cellular feature characteristics of this modified cell that provides the *become non-porous* and *become porous* emergent cell functions when compared to the proto-cell (Figure 45). The modified cell remains flat and seemingly non-porous (e.g., impervious to light, blocking air flow to a degree) from the top view under atmospheric pressure. The slit and the surrounding perimeter seal form a somewhat compressed oval shaped inflatable cavity. The inflation of this cavity activates the out of plane expansion (EO) and in-plane contraction (CI) fundamental behavior coupling, which

generates a distributed force affecting the inner surface of the air cavity. This morphs the modified cell into a torus-like shape, which results in pulling the perimeter around the slit outward and creating a visible opening.

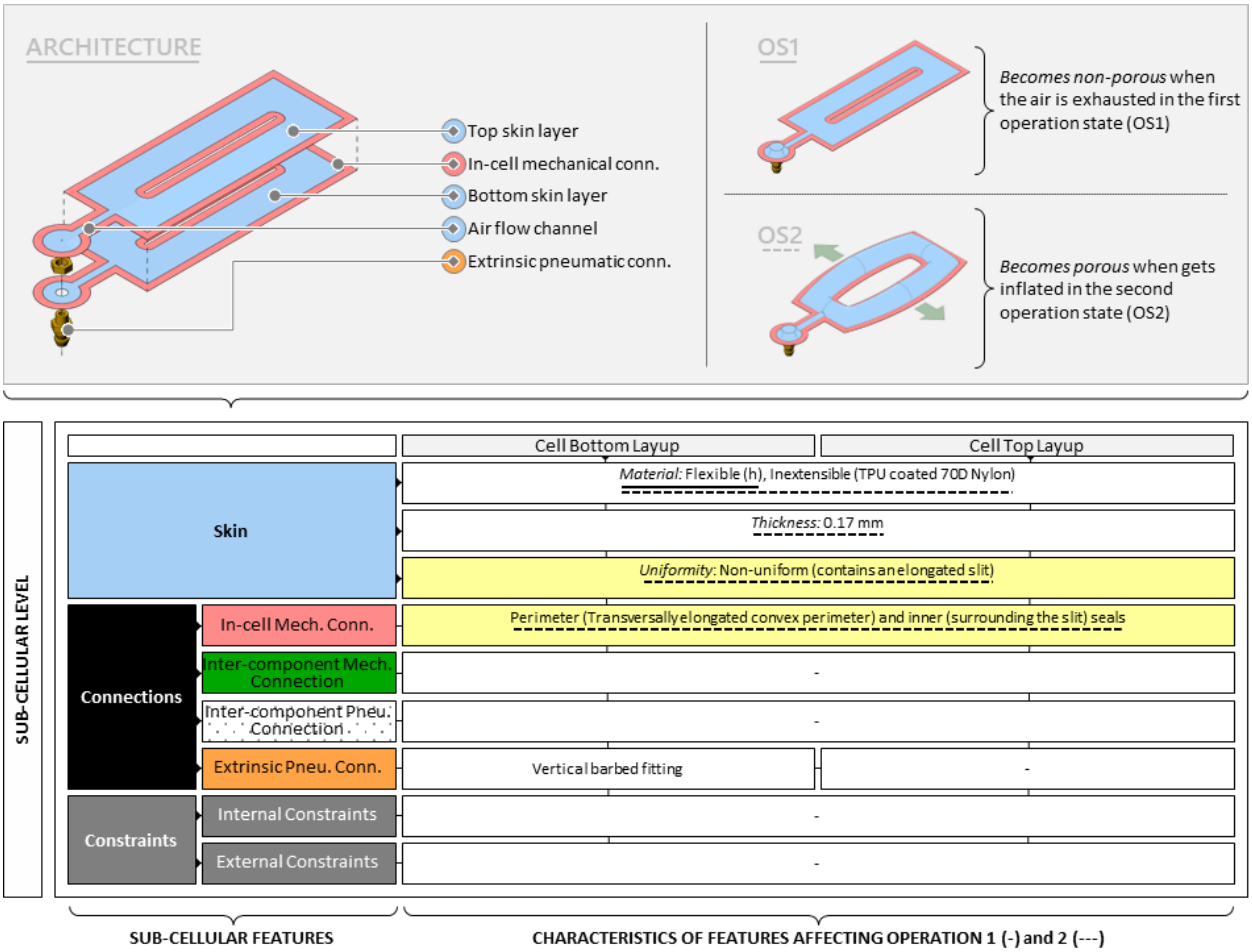

Figure 45. Cell architecture, operation states, and the modified sub-cellular feature characteristics of the cell providing *become non-porous/become porous* emergent cell functions. The architecture of a cell providing *become non-porous/become porous* emergent cell functions contains two skin layers that are stacked on top of each other and a set of extrinsic pneumatic connection components (top left). The *become non-porous* and *become porous* emergent cell functions are activated in operation states, OS1 and OS2, using exhaust air and get inflated operations, respectively (top right). The characteristics that primarily contribute to the set of emergent cell functions, *become non-porous* and *become porous*, are underlined using solid (-) and dashed (---) lines, respectively. The architecture and the modified sub-cellular feature characteristics of this cell are similar to the architecture and sub-cellular feature characteristics of the simplest proto-cell providing *flatten* and *push* emergent cell functions except for the modified skin uniformity and in-cell mechanical connection, which affect the way the cell expands once inflated and forcing it to *become porous* (bottom, highlighted in yellow).

The cyclic operation state transition diagram of this modified cell is described in Figure 46. Once it gets inflated to switch from its first operation state (OS1) to the second operation state (OS2) activating the same fundamental behavior coupling (EO+CI) as the proto-cell, the in-plane contraction and out of plane expansion are being employed to produce the *become porous*

emergent cell function afforded by the skin non-uniformity caused by the slit and the modified in-cell mechanical connection. To switch from the second operation state to the first one, exhaust air operation activates the same fundamental behavior coupling (EI+CO) as the proto-cell, which generates the *become non-porous* emergent cell function.

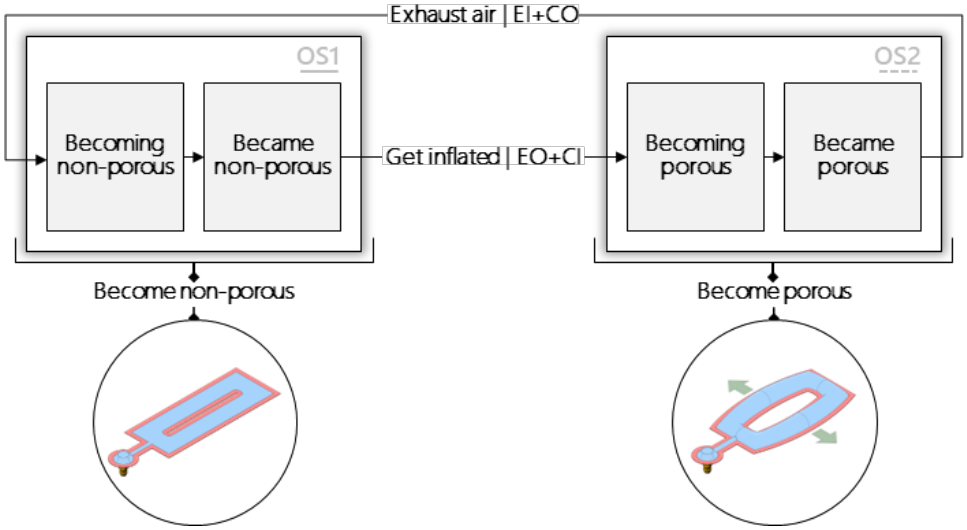

Figure 46. *Become non-porous/become porous* operation state transition diagram of the modified cell. The *become non-porous* operation state denoted as OS1 requires an exhaust air operation and comprises transition state, *becoming non-porous*, and end state, *became non-porous.* The *become porous* operation state denoted as OS2 requires a get inflated operation and comprises transition state, *becoming porous*, and end state, *became porous*.

2.3.5. Flatten/Buckle bi-stably

Replacing the transversally elongated convex perimeter seal with an irregular concave perimeter seal and cutting out corner portions of the skin layers to form a circular segment as demonstrated in Figure 47 (top left) are the essential changes in the sub-cellular feature characteristics of this modified cell that provides the *flatten* and *buckle bi-stably* emergent cell functions when compared to the proto-cell. The modified cell remains flat under atmospheric pressure. The inflation of the "C" shaped cavity activates the out of plane expansion (EO) and in-plane contraction (CI) fundamental behavior coupling, which constricts the modified cell. This constriction actuates the heat-sealed inner circular segment arbitrarily upward or downward due to the symmetric cell architecture, forming a bi-stably buckling protruded surface. This buckled surface can be manually pushed up or down. The force required to push the buckled surface correlates with the pressure level applied to the airtight system, therefore is easily tailorable for different design applications.

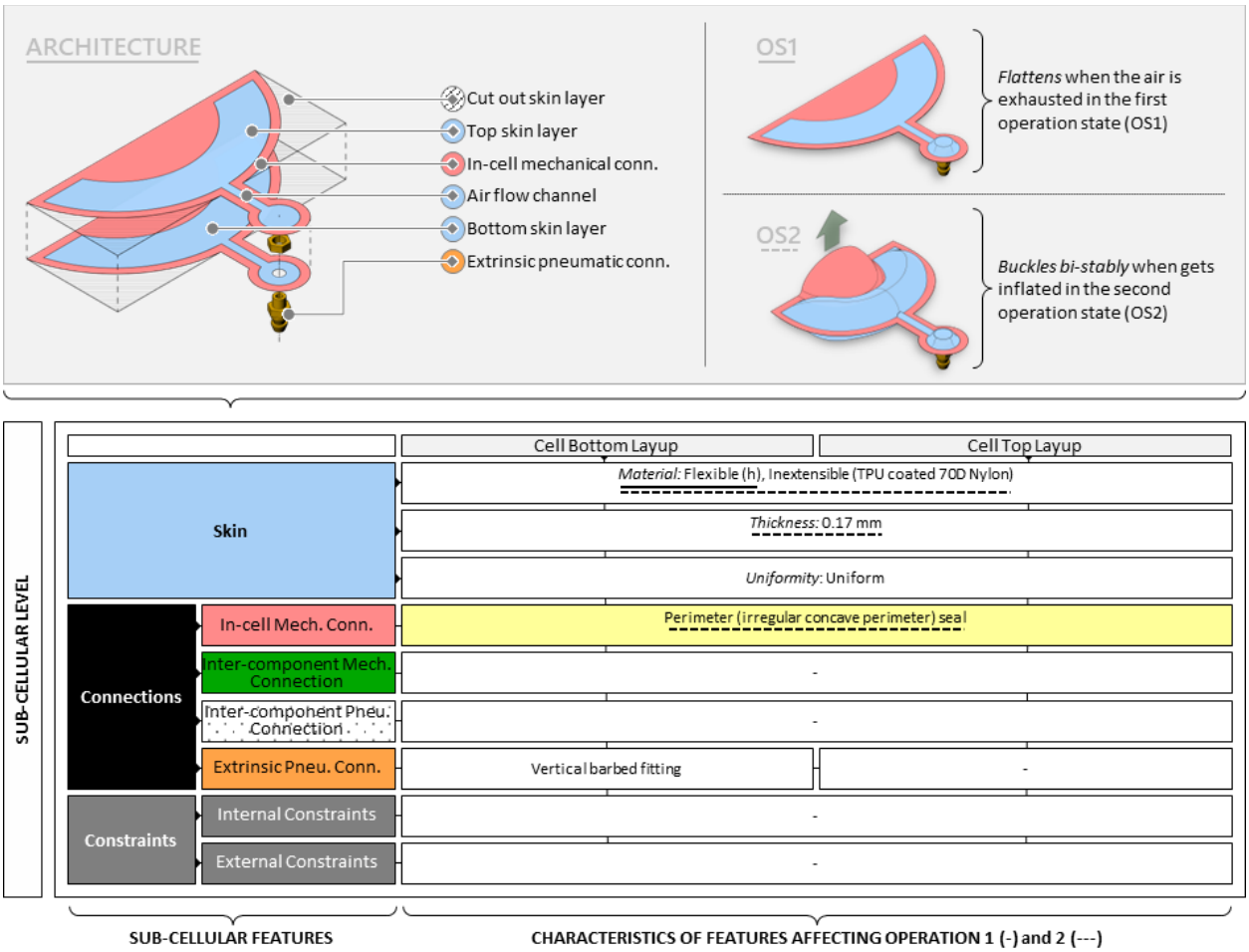

Figure 47. Cell architecture, operation states, and the modified sub-cellular feature characteristics of the cell providing *flatten/buckle bi-stably* emergent cell functions. The architecture of a cell providing *flatten/buckle bi-stably* emergent cell functions contains two skin layers that are stacked on top of each other and a set of extrinsic pneumatic connection components (top left). The *flatten* and *buckle bi-stably* emergent cell functions are activated in operation states, OS1 and OS2, using exhaust air and get inflated operations, respectively (top right). The characteristics that primarily contribute to the set of emergent cell functions, *flatten* and *buckle bi-stably*, are underlined using solid (-) and dashed (---) lines, respectively. The architecture and the modified sub-cellular feature characteristics of this cell are similar to the architecture and sub-cellular feature characteristics of the simplest proto-cell providing *flatten* and *push* emergent cell functions except for the modified in-cell mechanical connection, which affect the way the expansion of the "C" shaped air cavity in the second operation state and forcing the cell to *buckle bi-stably* (bottom, highlighted in yellow).

The cyclic operation state transition diagram of this modified cell is described in Figure 48. Once it gets inflated to switch from its first operation state (OS1) to the second operation state (OS2) activating the same fundamental behavior coupling (EO+CI) as the proto-cell, the in-plane contraction and out of plane expansion are being employed to produce the *buckle bi-stably* emergent cell function due to the change in in-cell mechanical connection characteristic. To switch from the second operation state to the first one, the exhaust air operation activates the same

fundamental behavior coupling (EI+CO) as the proto-cell, which generates the *flatten* emergent cell function.

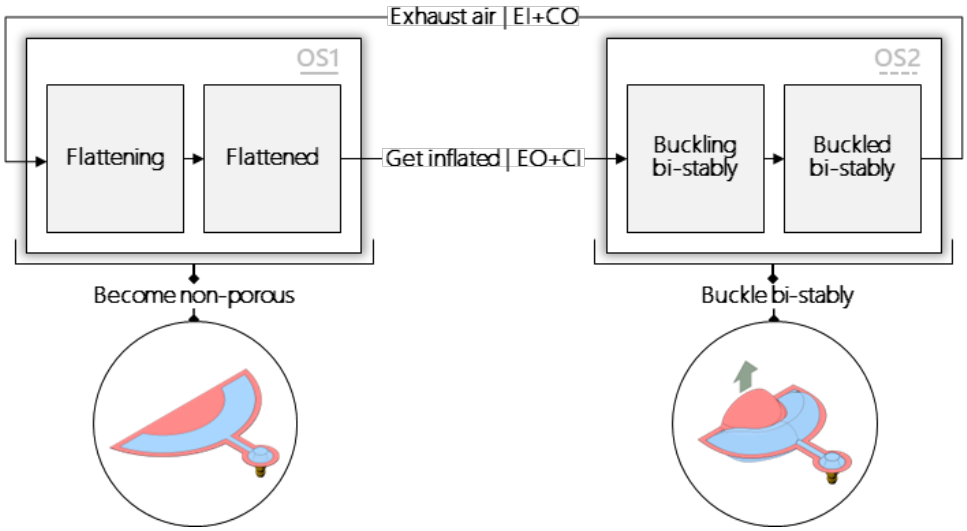

Figure 48. *Flatten/buckle bi-stably* operation state transition diagram of the modified cell. The *flatten* operation state denoted as OS1 requires an exhaust air operation and comprises transition state, *flattening*, and end state, *flattened.* The *buckle bi-stably* operation state denoted as OS2 requires a get inflated operation and comprises transition state, *buckling bi-stably*, and end state, *buckled bi-stably*.

2.3.6. Mute/Texturize

Changing the skin material type, the shape of the in-cell mechanical connection, and introducing an external surface constraint to which the bottom skin layer of the modified cell permanently attached are the essential differences in the sub-cellular feature characteristics of this modified cell that provides the *mute* and *flatten* emergent cell functions when compared to the proto-cell (Figure 49). Unlike the proto-cell, the modified cell is made of flexible (h) and extensible bare TPU sheet (0.2 mm). Due to the extensibility this material provides, the air cavity will be expanding not only out of plane but also in-plane (EO+EI) when the modified cell is inflated. The bottom skin layer of the modified cell is permanently attached to a flat rigid external surface constraint around the region surrounding the air cavity, therefore is limiting the in-plane expansion while allowing the out of plane expansion without imposing any restriction. This produces the *texturize* emergent cell function (array of simple bumps in this case). When the modified cell is deflated, the emerging texturization disappears and visually blends in with the remaining portion of the modified cell's top skin layer, rendering it visually *muted*.

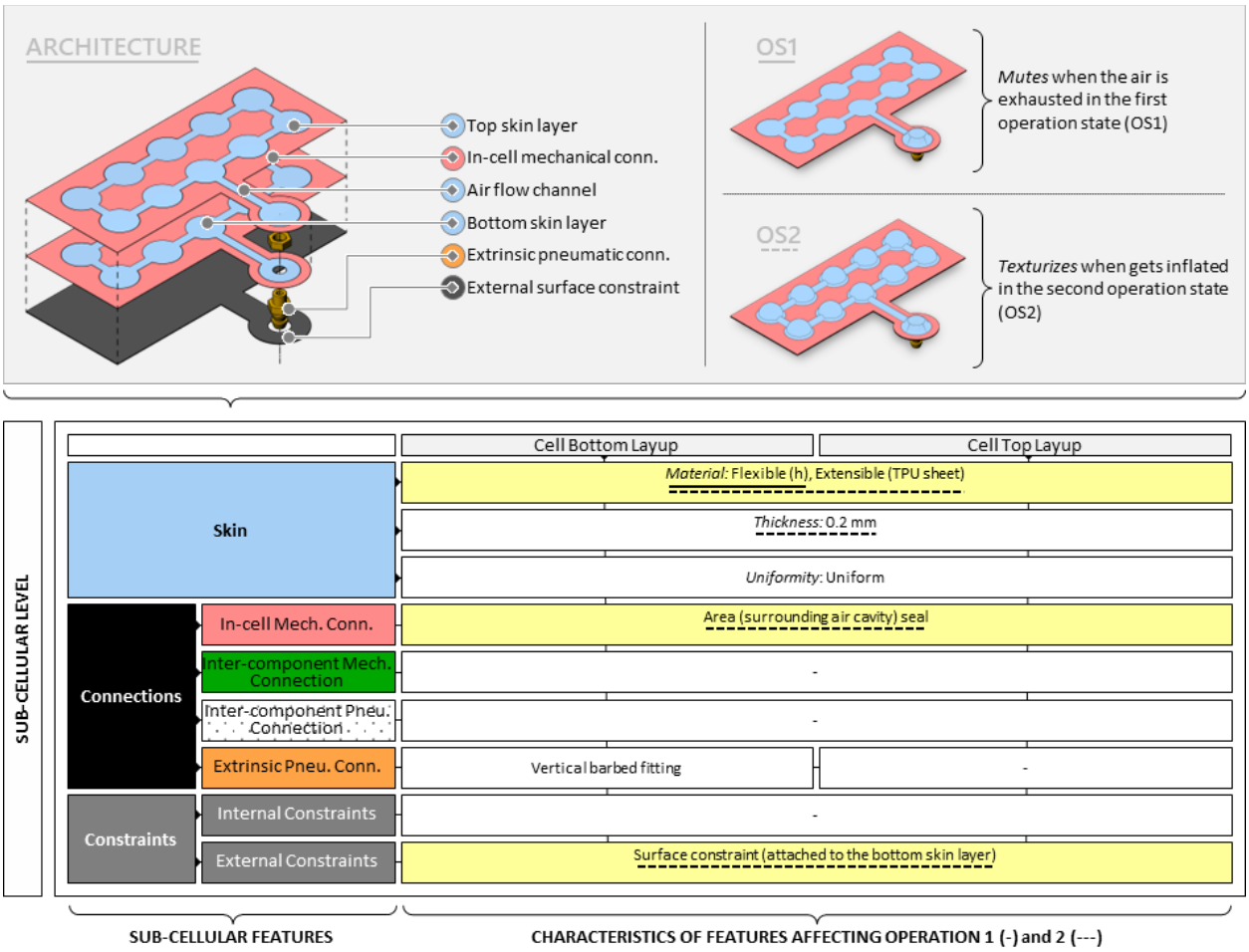

Figure 49. Cell architecture, operation states, and the modified sub-cellular feature characteristics of the cell providing *mute/texturize* emergent cell functions. The architecture of a cell providing *mute/texturize* emergent cell functions contains two skin layers that are stacked on top of each other, a set of extrinsic pneumatic connection components, and an external surface constraint (top left). The *mute* and *texturize* emergent cell functions are activated in operation states, OS1 and OS2, using exhaust air and get inflated operations, respectively (top right). The characteristics that primarily contribute to the set of emergent cell functions, *mute* and *texturize*, are underlined using solid (-) and dashed (---) lines, respectively. The architecture and the modified sub-cellular feature characteristics of this cell are somewhat similar to the architecture and sub-cellular feature characteristics of the simplest proto-cell providing *flatten* and *push* emergent cell functions except for the modified skin material characteristics, in-cell mechanical connection, and the introduction of an external surface constraint to the system, all of which contribute to the resulting surface texturization (bottom, highlighted in yellow).

The cyclic operation state transition diagram of this modified cell is described in Figure 50. Once it gets inflated to switch from its first operation state (OS1) to the second operation state (OS2) activating only one fundamental behavior (EO) differently from the proto-cell, the out of plane expansion produces the *texturize* emergent cell function. To switch from the second operation state to the first one, the exhaust air operation activates the out of plane contraction (CO), which produces the *mute* emergent cell function.

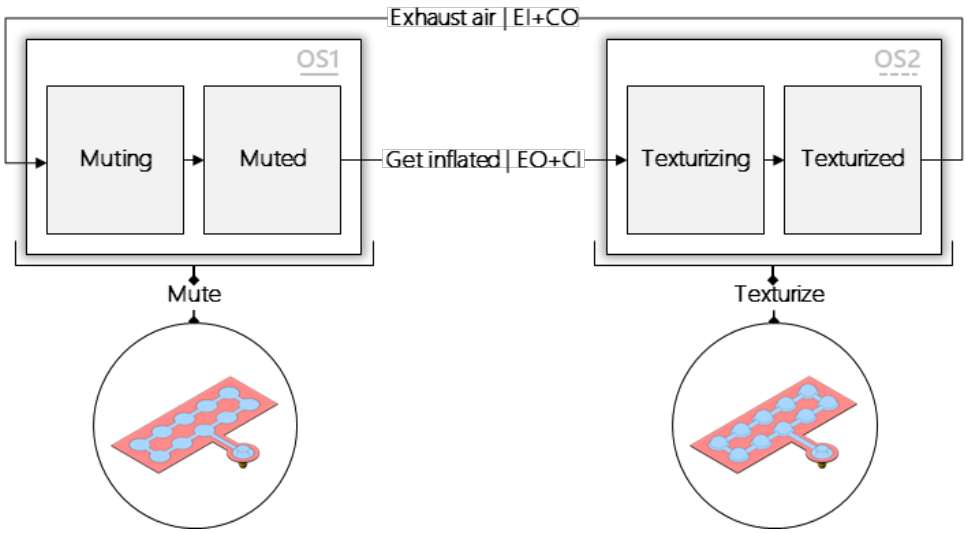

Figure 50. *Mute/texturize* operation state transition diagram of the modified cell. The *mute* operation state denoted as OS1 requires an exhaust air operation and comprises transition state, *muting*, and end state, *muted.* The *texturize* operation state denoted as OS2 requires a get inflated operation and comprises transition state, *texturizing*, and end state, *texturized*.

2.3.7. Roll/Unroll

Introducing a layered internal constraint, which is made of a tempered spring steel plate designed to return to its original rolled form under no stress, is the essential change in the sub-cellular feature characteristics of this modified cell that provides the *roll* and *unroll* emergent cell functions when compared to the proto-cell (Figure 51). The modified cell rolls into its original form under atmospheric pressure due to the shape-memory of the layered internal constraint. The inflation of the air cavity activates the out of plane expansion (EO) and in-plane contraction (CI) fundamental behavior coupling, which forces the initially flat air cavity to morph into a tubular shape, therefore *unrolls* the spring steel and the encapsulating modified cell. Suzuki et al. employed a comparable architectural approach that builds on rolling and unrolling functionalities to develop a series of modular inflatable linear actuators as building blocks [182]. They demonstrated the practical application of these building blocks by creating prototypes of room-scale shape-changing interfaces, showcasing the potential for innovative and interactive design solutions in various contexts [183].

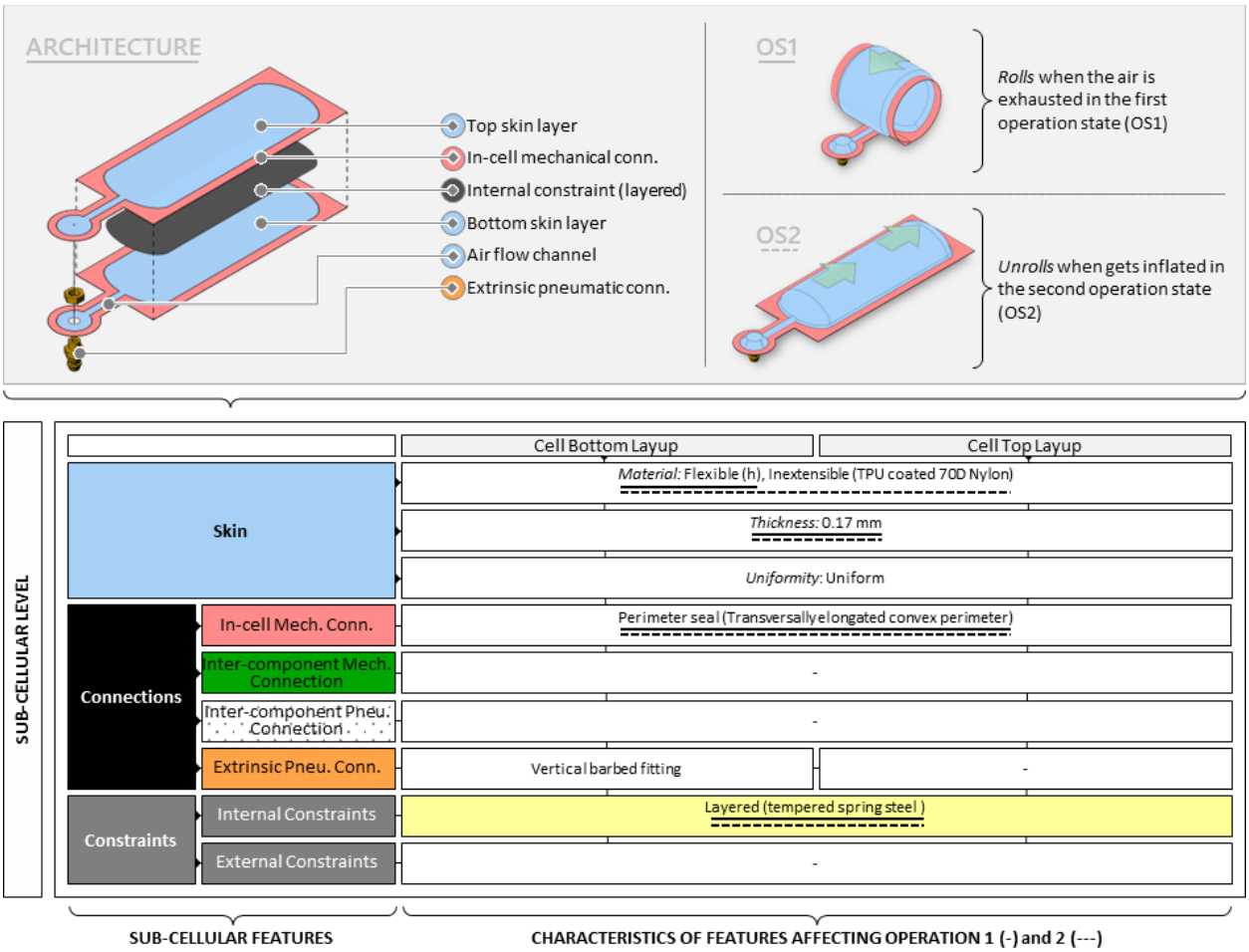

Figure 51. Cell architecture, operation states, and the modified sub-cellular feature characteristics of the cell providing *roll/unroll* emergent cell functions. The architecture of a cell providing *roll/unroll* emergent cell functions contains two skin layers that are stacked on top of each other, a set of extrinsic pneumatic connection components, and a layered internal constraint (tempered spring steel) (top left). The *roll* and *unroll* emergent cell functions are activated in operation states, OS1 and OS2, using exhaust air and get inflated operations, respectively (top right). The characteristics that primarily contribute to the set of emergent cell functions, *roll* and *unroll*, are underlined using solid (-) and dashed (---) lines, respectively. The architecture and the modified sub-cellular feature characteristics of this cell are almost identical to the architecture and sub-cellular feature characteristics of the simplest proto-cell providing *flatten* and *push* emergent cell functions except for the introduction of a layered internal constraint to the system, which contribute to the resulting rolling and unrolling behavior due to the shape memory of the tempered spring steel (bottom, highlighted in yellow).

The cyclic operation state transition diagram of this modified cell is described in Figure 52. Once it gets inflated to switch from its first operation state (OS1) to the second operation state (OS2) activating the same fundamental behavior coupling (EO+CI) as the proto-cell, the in-plane contraction and out of plane expansion produce *unroll* emergent cell function due to the layered internal constraint. To switch from the second operation state to the first one, the exhaust air operation activates the same fundamental behavior coupling (EI+CO) as the proto-cell, producing the *roll* emergent cell function.

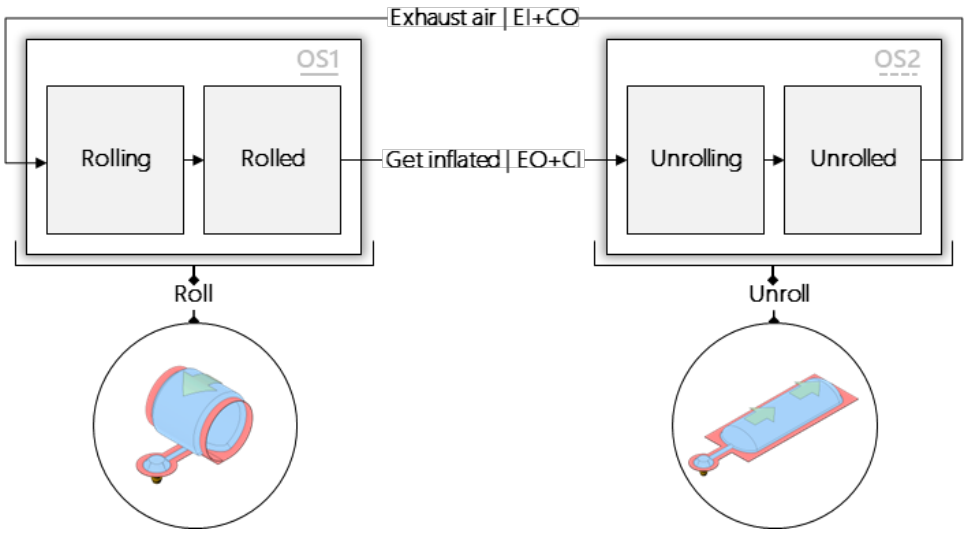

Figure 52. *Roll/unroll* operation state transition diagram of the modified cell. The *roll* operation state denoted as OS1 requires an exhaust air operation and comprises transition state, *rolling*, and end state, *rolled.* The *unroll* operation state denoted as OS2 requires a get inflated operation and comprises transition state, *unrolling*, and end state, *unrolled*.

2.3.8. Grow in-plane/Shrink in-plane

Introducing another type of layered internal constraint, an architected tile array, which is made of symmetrical tiles, and permanently attaching the top and bottom surfaces of these tiles to the TPU coated inner cell skin layers are the essential changes in the sub-cellular feature characteristics of this modified cell that provides the *grow in-plane* and *shrink in-plane* emergent cell functions when compared to the proto-cell (Figure 53). Each tile forming the internal constraint is made of an extruded curve that has rotational symmetry the order of which is 2 and the angle of rotation is 120°. Permanently attaching the top and bottom surfaces of these tiles to the cell skin layers creates a complex air cavity that can be vacuumable. Under atmospheric pressure, these tiles allow relative motion that enables the modified cell to behave like a piece of fabric and to be conformable into a variety of free-form shapes. When vacuum is applied, the cell skin layers are being pulled inward, which forces the adjacent tiles to move closer to each other, producing the *shrink in-plane* emergent cell function. Letting the air in the already shrunk modified cell makes it *grow in-plane*.

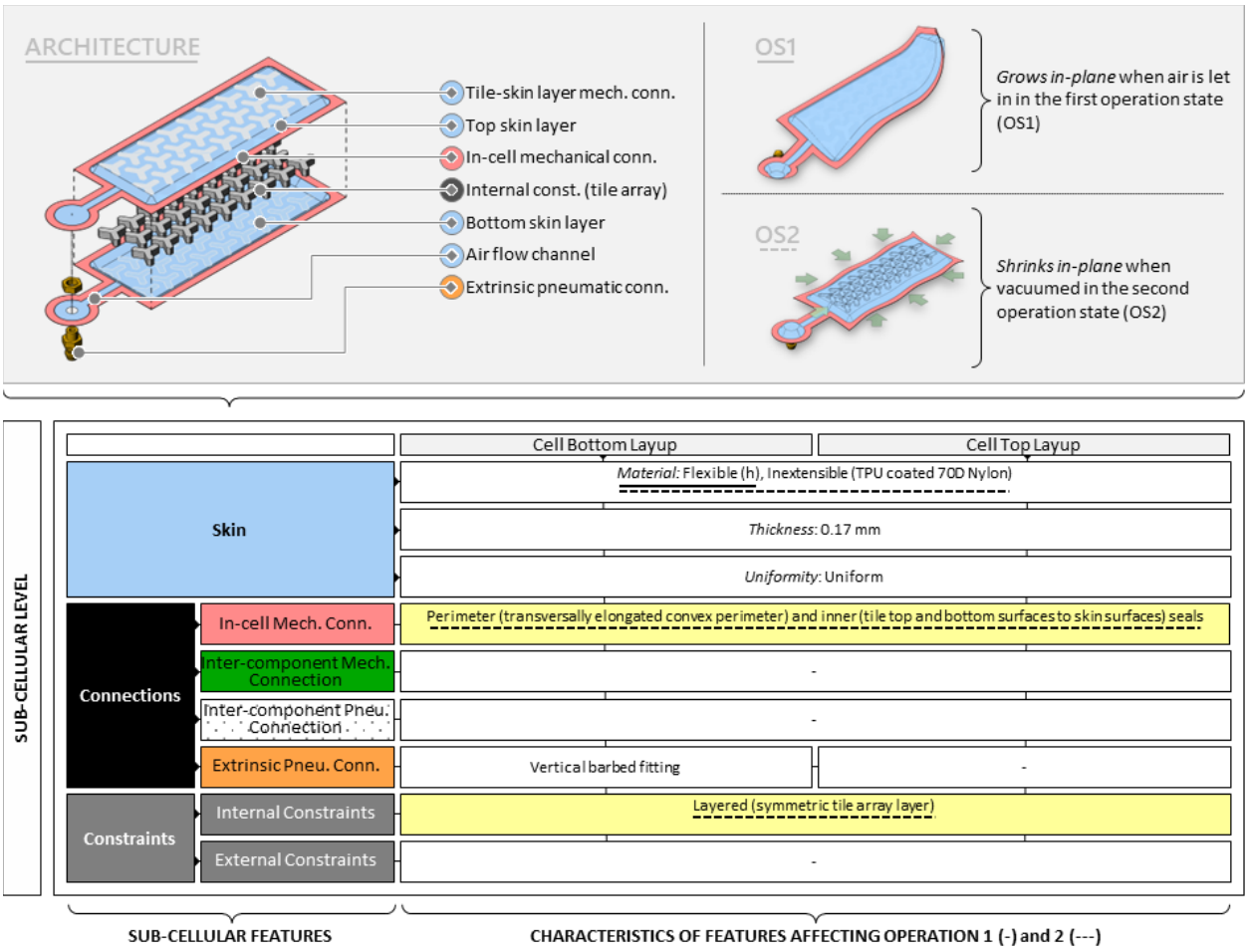

Figure 53 Cell architecture, operation states, and the modified sub-cellular feature characteristics of the cell providing *grow in-plane/shrink in-plane* emergent cell functions. The architecture of a cell providing *grow in-plane /shrink in-plane* emergent cell functions contains two skin layers that are stacked on top of each other, a set of extrinsic pneumatic connection components, and a layered internal constraint made of symmetric tile array layer (top left). The *grow in-plane motion* and *shrink in-plane* emergent cell functions are activated in operation states, OS1 and OS2, using let air in and vacuum operations, respectively (top right). The characteristics that primarily contribute to the set of emergent cell functions, *grow in-plane* and *shrink in-plane*, are underlined using solid (-) and dashed (---) lines, respectively. The architecture and the modified sub-cellular feature characteristics of this cell are similar to the architecture and sub-cellular feature characteristics of the simplest proto-cell providing *flatten* and *push* emergent cell functions except for the introduction of a symmetric tile array layer of which top and bottom surfaces are permanently connected to the inner skin surfaces. This creates a complex array of connected air cavities throughout the cell's structure, resulting in generating *shrink in-plane* emergent cell function (bottom, highlighted in yellow).

The cyclic operation state transition diagram of this modified cell is described in Figure 54. Once it gets vacuumed to switch from its first operation state (OS1) to the second operation state (OS2) activating a different fundamental behavior coupling (CO+CI) from the proto-cell, the out of plane and in-plane contractions produce the *shrink in-plane* emergent cell function due to the internal tile constraint. To switch from the second operation state to the first one, the let air in operation activates another fundamental behavior coupling (EO+EI). The out of plane and in-plane expansions produce the *grow in-plane* emergent cell function.

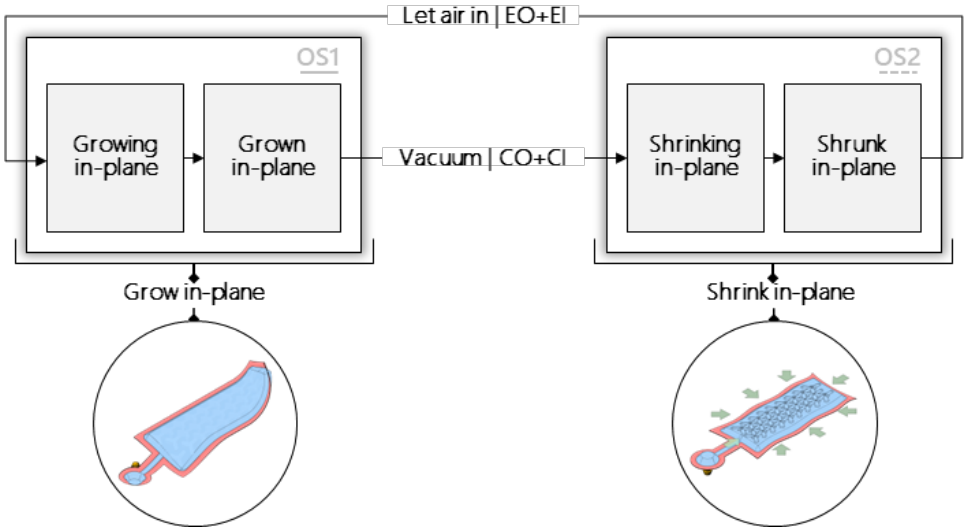

Figure 54. *Grow in-plane/shrink in-plane* operation state transition diagram of the modified cell. The *grow in-plane* operation state denoted as OS1 requires an exhaust air operation and comprises transition state, *growing in-plane*, and end state, *grown in-plane.* The *shrink in-plane* operation state denoted as OS2 requires a get inflated operation and comprises transition state, *shrinking in-plane*, and end state, *shrunk in-plane*.

2.3.9. Flatten/Cinch

A further modified version of the architected tile array layer producing *grow in-plane* and *shrink in-plane* emergent cell functions, which is differently made of asymmetrical tiles this time, and permanently attaching the top and bottom surfaces of these asymmetrical tiles to the TPU coated inner cell skin layers are the essential changes in the sub-cellular feature characteristics of this modified cell that provides the *flatten* and *cinch* emergent cell functions when compared to the proto-cell (Figure 55). Each tile is identically made of an extruded curve that has rotational symmetry the order of which is 2 and the angle of rotation is 120°. However, the top half of each tile is narrower than the bottom half, which makes the gap among the adjacent tiles larger for the top half of the tiles than the gap among the bottom ones when the tile array is formed. Permanently attaching these tiles to the cell skin layers creates an even more complex air cavity. Under atmospheric pressure, these tiles also allow relative motion that enables the modified cell to behave like a piece of fabric and be conformable into a variety of free-form shapes. When vacuum is applied, the cell skin layers are pulled inward, which forces the adjacent tiles to move closer to each other as well. Since the gap among the top half of the tiles is larger than the bottom ones, the bottom halves act as multiaxial hinge lines as the top halves kept being pulled inward, which makes the modified cell *cinch*. Letting the air in the cinched modified cell makes it *flatten*.

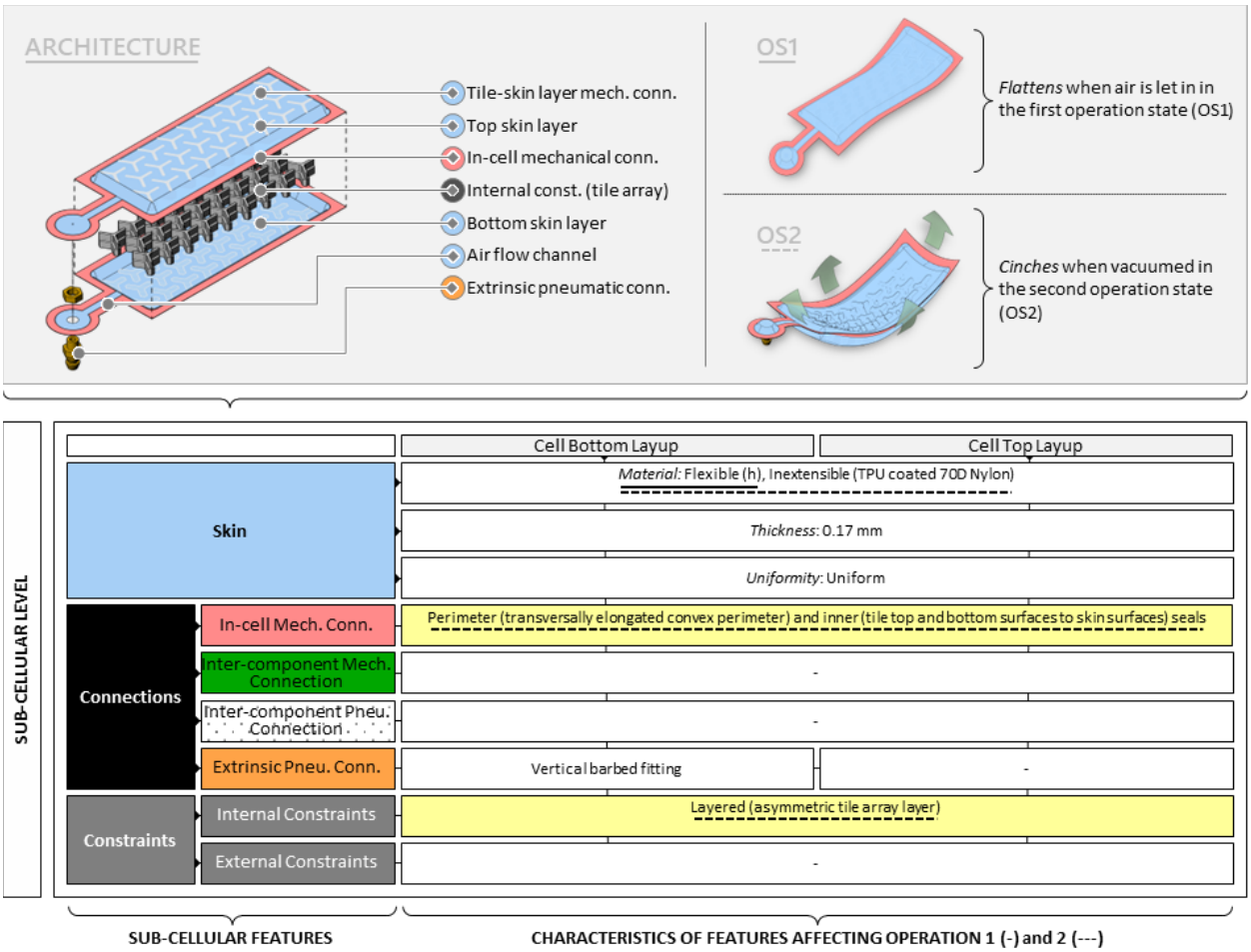

Figure 55. Cell architecture, operation states, and the modified sub-cellular feature characteristics of the cell providing *flatten/cinch* emergent cell functions. The architecture of a cell providing *flatten/cinch* emergent cell functions contains two skin layers that are stacked on top of each other, a set of extrinsic pneumatic connection components, and a layered internal constraint made of asymmetric tile array layer this time (top left). The *flatten* and *cinch* emergent cell functions are activated in operation states, OS1 and OS2, using let air in and vacuum operations, respectively (top right). The characteristics that primarily contribute to the set of emergent cell functions, *flatten* and *cinch*, are underlined using solid (-) and dashed (---) lines, respectively. The architecture and the modified sub-cellular feature characteristics of this cell are similar to the architecture and sub-cellular feature characteristics of the simplest proto-cell providing *flatten* and *push* emergent cell functions except for the introduction of an asymmetric tile array layer of which top and bottom surfaces are permanently connected to the inner skin surfaces. This creates a complex array of connected but asymmetrically shaped (top vs bottom sections) air cavities throughout the cell's structure, resulting in generating *cinch* emergent cell function in the second operation state (bottom, highlighted in yellow).

The cyclic operation state transition diagram of this modified cell is described in Figure 56. Once it gets vacuumed to switch from its first operation state (OS1) to the second operation state (OS2) activating a different fundamental behavior coupling (CO+CI) from the proto-cell, the out of plane and in-plane contractions produce the *cinch* emergent cell function due to the asymmetrical internal tile constraint. To switch from the second operation state to the first one, the let air in operation activates another fundamental behavior coupling (EO+EI). The out of plane

and in-plane expansions produce the *flatten* emergent cell function as the cinched tiles are moving away from each other to their neutral locations.

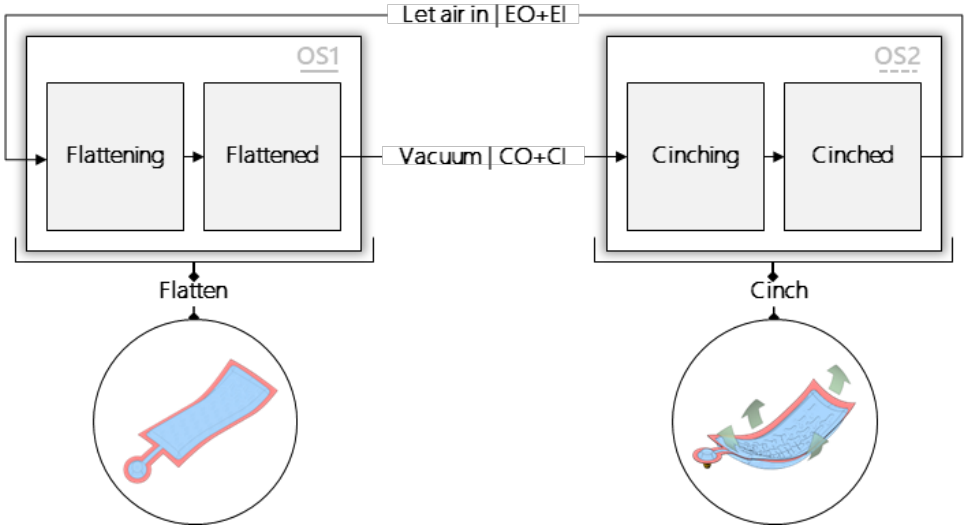

Figure 56. *Flatten/cinch* operation state transition diagram of the modified cell. The *flatten* operation state denoted as OS1 requires an exhaust air operation and comprises transition state, *flattening*, and end state, *flattened.* The *cinch* operation state denoted as OS2 requires a get inflated operation and comprises transition state, *cinching*, and end state, *cinched.*

2.3.10. Allow hinge-like motion/Retain hinge position/Jam

Using a set of extruded equilateral triangle tiles to form two separate tile array layers and separately and permanently attaching each one of these tile array layers to top and bottom cell skin layers are the essential changes in the sub-cellular feature characteristics of this modified cell that provides the *allow hinge-like motion, retain hinge position, and jam* emergent cell functions when compared to the proto-cell (Figure 57, top). The cell skin and the gap among adjacent tiles forming the tile array layer enable the individual tiles to shift, allowing them to have a *hinge-like motion* relative to each other under atmospheric pressure. This makes the modified cell drapable like a fabric, enabling the accommodation of a wide variety of target object topography to a degree by bending to the target form under the modified cell's own weight (Figure 57, middle - OS1). When a partial vacuum pressure is applied to this modified cell, the opposing tiles and the adjacent tiles begin jamming against each other, restricting relative motion of the tile array layers, therefore *retaining the hinge positions* (Figure 57, middle - OS2). Vacuuming most of the air out from the modified cell makes the opposing tiles *jam* against each other, which minimizes the relative shifting or folding along the gap lines among the individual tiles, enhancing the overall stiffness of the modified cell (Figure 57, middle - OS3).

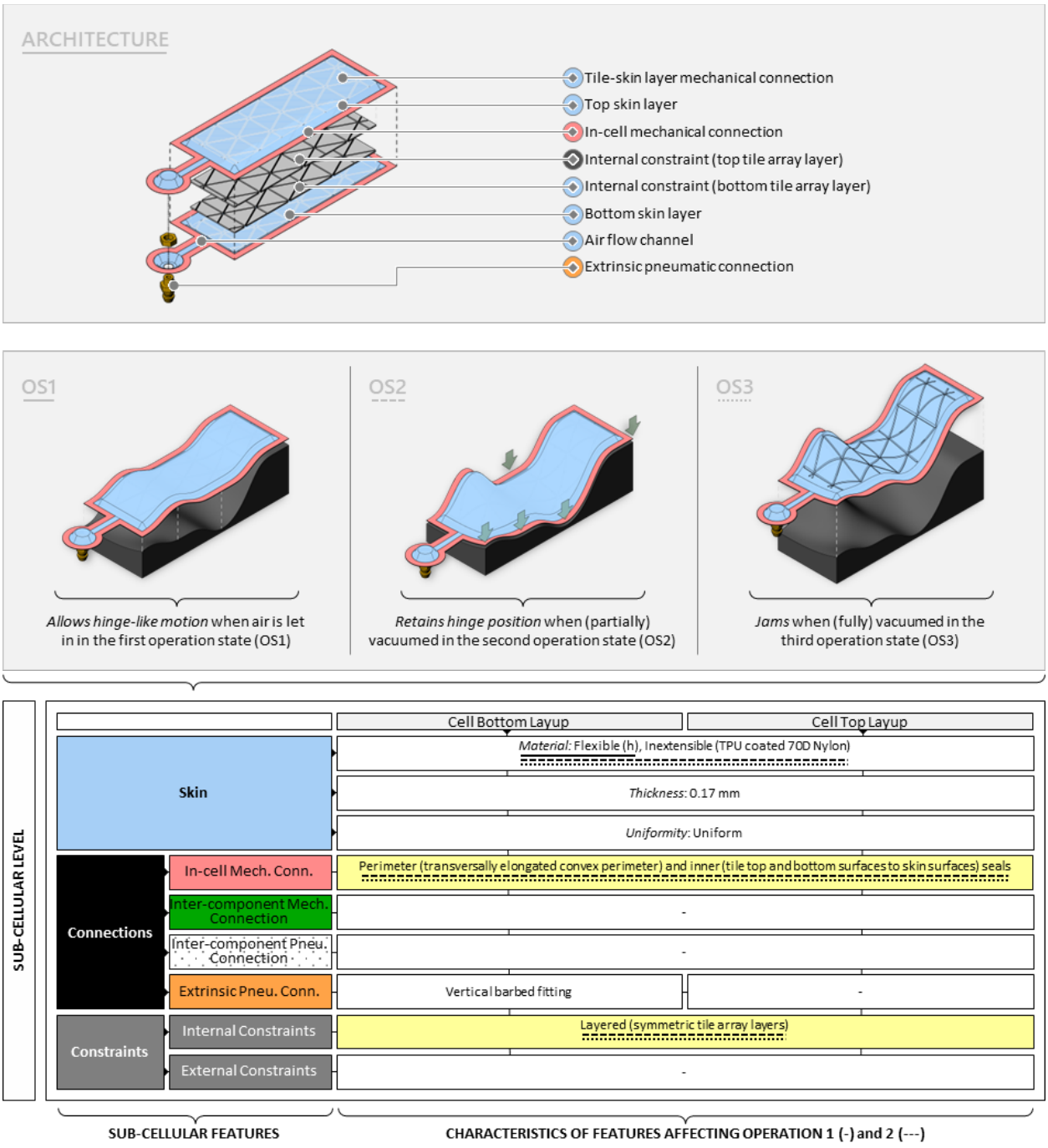

Figure 57. Cell architecture, operation states, and the modified sub-cellular feature characteristics of the cell providing *allow hinge-like motion/retain hinge position/jam* emergent cell functions. The architecture of a cell providing *allow hinge-like motion/retain hinge position/jam* emergent cell functions contains two skin layers that are stacked on top of each other, a set of extrinsic pneumatic connection components, and a layered internal constraint made of two overlapping tile array layers this time (top). The *allow hinge-like motion, retain hinge position,* and *jam* emergent cell functions are activated in operation states, OS1, OS2, and OS3, using let air in, partial vacuum, and full vacuum operations, respectively (middle). The characteristics that primarily contribute to the set of emergent cell functions, *allow hinge-like motion, retain hinge position,* and *jam*, are underlined using solid (-), dashed (---), and dotted (…) lines, respectively. The architecture and the modified sub-cellular feature characteristics of this cell are similar to the architecture and sub-cellular feature characteristics of the simplest proto-cell providing *flatten* and *push* emergent cell functions except for the introduction of two overlapping tile array layers, which are separately and

permanently attached to the inner surfaces of the top and bottom skin layers. Due to the gap among adjacent tiles, the modified cell allows hinge-like motion under atmospheric pressure and retains hinge positions as the air is gradually vacuumed from the system before jamming occurs in the third operation state (bottom, highlighted in yellow).

Differently from the proto-cell and previously introduced modified cell examples, the operation transition diagram of this modified cell is tripartite (Figure 58). As demonstrated in the diagram, the transition among these three operation states (OS1, OS2, and OS3) can be sequenced in four main alternative ways. These are:

- OS1 > OS2 > OS1
- OS1 > OS2 > OS3 > OS1
- OS1 > OS2 > OS3 > OS2 > OS1
- OS1 > OS2 > OS3 > OS2 > OS3 > OS1

Once the modified cell is partially vacuumed to switch from its first operation state (OS1) to the second operation state (OS2) activating a different fundamental behavior coupling (CO+CI) from the proto-cell, the out of plane and in-plane contraction produces the *retain hinge position* emergent cell function because the opposing and adjacent tiles restrict each other's relative motion. It is possible to switch back to the first operation state (OS1) from the second operation state (OS2) by letting the air out from the airtight system. This activates a different fundamental behavior coupling, out of plane and in-plane expansion (EO+EI), which produces the *allow-hinge-like motion* emergent function. However, to switch from the second operation state (OS2) to the third operation state (OS3), the partially vacuumed modified cell needs to be fully vacuumed, which activates the same fundamental behavior coupling, out of plane and in-plane contraction (CO+CI), resulting in *jamming* the opposing and adjacent tiles against each other, rigidizing the entire structure. It is possible to switch to the first (OS1) or second (OS2) operation states from the third operation state (OS3) by letting the air out fully or partially, respectively. The ability to provide alternative operation state transition sequences enables selective activation of emergent cell functions in different orders, which can be leveraged for the design of multi-functional systems.

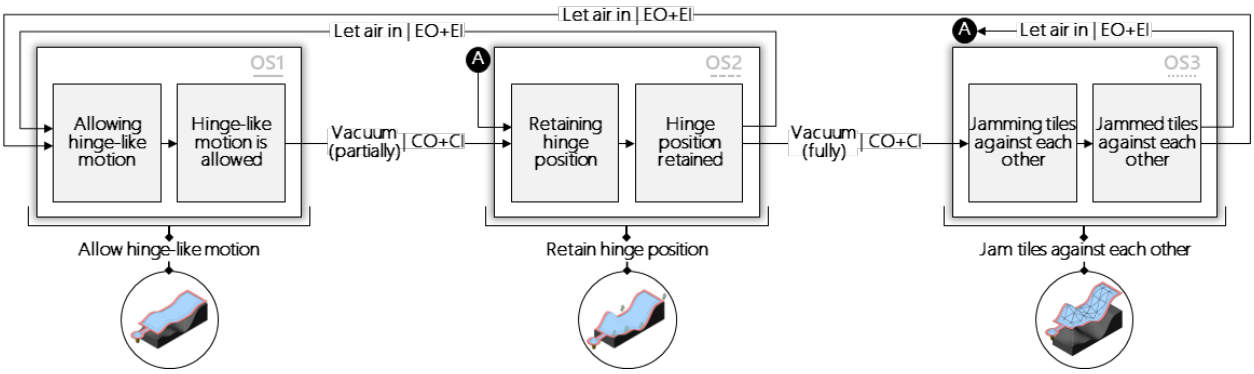

Figure 58. Allow hinge-like motion/retain hinge position/jam operation state transition diagram of the modified cell. The *allow hinge-like motion* operation state denoted as OS1 requires an exhaust air operation and comprises transition state, *allowing hinge-like motion*, and end state, *allowed hinge-like motion.* The *retain hinge position* operation state denoted as OS2 requires a partial vacuum operation and comprises transition state, *retaining hinge position*, and end state, *hinge position retained.* The *jam tiles against each other* operation state denoted as OS3 requires a full vacuum operation and comprises transition state, *jamming tiles against each other,* and end state, *jammed tiles against each other.* Differently from the proto-cell and previously introduced modified cell examples, the operation transition diagram of this modified cell is tripartite, allowing alternative operating sequences (e.g., OS1 > OS2 > OS1 or OS1 > OS2 > OS3 > OS2 > OS1).

2.4. Multi-mode Product Concepts Using Constrained Layer Pneumatic Systems

Structurally adaptable multi-mode products employing constrained layer pneumatic systems are made of basic architectural components (i.e., cells) providing lower-level functionalities (i.e., emergent cell functions) that are combined in numerous ways to compose higher-level architectural components (e.g., ensembles, units) providing higher-level functionalities (e.g., ensemble functions, unit functions). These higher-level functionalities eventually are combined to produce a set of context-specific technology sub-capabilities that can be activated in the user-device system's relevant interaction mode on demand.

To illustrate the variety of cells, ensembles, units, assemblies, and systems and the corresponding basic functions, different types of compound functions, and technology sub-capabilities that constrained layer pneumatic systems can produce, five multi-mode product system examples are given:

1. a deployable mobile phone restraint mat which employs a hierarchy of two assemblies of two units, each unit comprising two ensembles of cells to position and orient a phone on a wireless charger,
2. a re-configurable office space divider which is made up of a single horizontal ensemble of internally tiled cells to be shaped into a variety of partitioning configurations including being stowed compactly in a rolled form,

3. a variable friction cargo mat made up of two interdigitated sets of horizontal ensembles to change friction properties to selectively allow (for loading) or restrict (for transit) sliding of objects,
4. a morphing windshield cowling which employs a hierarchy of a unit of linear combination of ensembles, each ensemble comprising a set of compound cells made up of two unique basic cells to open and cover the gap between a car hood and a windshield on demand for using the wipers, and
5. an active rear seat pocket equipped with a single horizontal ensemble of a set of inflatable cells with asymmetrical cross sections to morph into a target 3D shape for providing easy one-handed access to the storage compartment.

2.4.1. Example Product Concept 1: The Mobile Phone Restraint Mat

The mobile phone restraint mat automatically positions and orients a cell phone over an inductive charger using an embedded constrained layer pneumatic system providing deploying, lifting, squeezing, and stowing functionalities. The system's architecture consists of two separate orthogonally oriented deployable and stowable assemblies attached to a charging mat. The assemblies have the abilities of lifting and squeezing the mobile phone and thereby can accomplish the task of moving and aligning it on the pad using a sequence of these abilities (Figure 59).

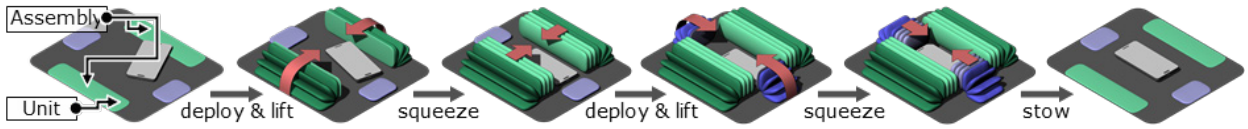

Figure 59. **The operation of the mobile phone restraint mat.** Architectural components of the mobile phone restraint mat sequentially orient a cell phone in an appropriate position on the charging pad by activating a sequence of the provided technology sub-capabilities: deploying & lifting, squeezing, and stowing.

As a part of the mobile phone restraint mat system (Figure 60a), each one of the orthogonal assemblies (Figure 60b) is made of opposing, pneumatically interconnected units, and each of these is made of two vertical cell ensembles that are stacked on top of each other (Figure 60c). These units deploy and stow in sequence and provide the angular deployment and linear pushing functionalities (where two units pushing together creates a higher-level functionality, squeeze). Two vertical ensembles form each of these units, the first of which (Figure 60d) attaches to the

base mat and primarily produces aggregate angular expansion and contraction while the second attaches to the first and primarily provides aggregate linear expansion and contraction. Each cell within one of these ensembles (e.g., I.A.1.a., Figure 60e), is customized to form the vertical cell ensemble (e.g., I.A.1.) by providing specific basic functions such as attachment to the base and to the next cell in addition to angular expansion.

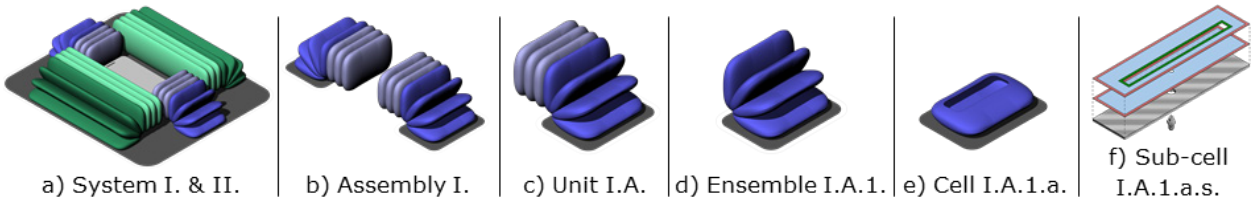

Figure 60. An exemplary partial architectural decomposition of the mobile phone restraint mat. The mobile phone restraint mat's architecture is made of two orthogonal assemblies each of which contains two units. Each unit is composed of two vertically aggregated vertical ensembles made of a set of individual cells. The sub-cellular features visually detail how the components of a cell are brought together to form a cell.

The sub-cellular architecture of an individual cell consists of top and bottom skin layers encapsulating an inflatable air cavity in between, and a set of extrinsic pneumatic connection components attached to the bottom skin layer through a hole through the external surface constraint to which the bottom skin layer is permanently bonded. The bottom skin layer of the next adjacent cell is mechanically connected to the top skin layer of the previous cell in the ensemble around the opening highlighted with green (Figure 61c). The resulting mobile phone restraint mat provides an effortless way to position a wide range of mobile phones over a wireless charger while stowing flush to the surface when not in use.

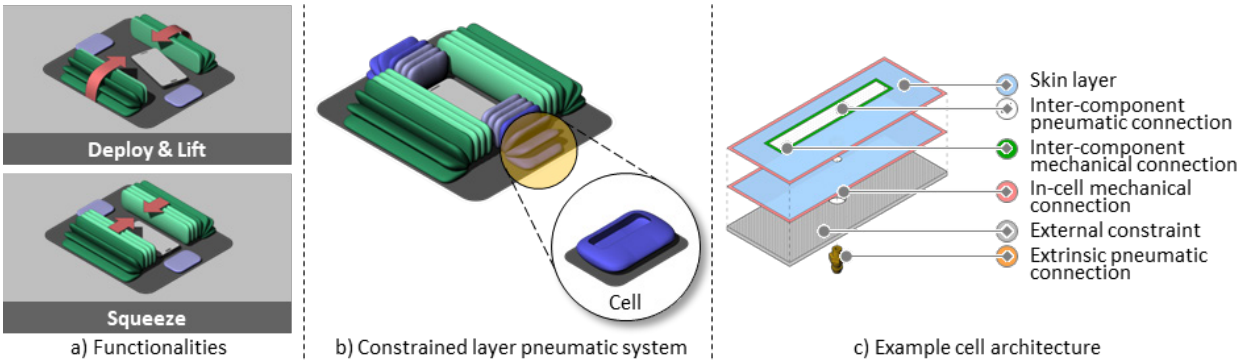

Figure 61. The mobile phone restraint mat product system. a) The orthogonally oriented assemblies provide deploying, lifting, squeezing, and stowing functionalities to orient a cell phone in an appropriate position on the charging pad. b) An example cell that composes a vertical ensemble is shown as a part of the product system. c) The sub-cellular features of this example cell are visually communicated using an isometric exploded view.

2.4.2. Example Product Concept 2: Re-configurable Office Space Divider

The second example application using constrained layer pneumatic system is a re-configurable office space divider that enables customized partitioning in open office or work-from-home settings. It provides thin-profile surface that can be rolled to be stowed compactly, posed into various simple configurations, and rigidized to keep those target partition configurations (Figure 62a). Its architecture is made up of horizontally assembled variations of cells equipped with internal rigid tile constraints. Each cell comprises a set of flat, thin, slender, and rigid opposing tiles sandwiched between airtight bladder layups (Figure 62c). Normally, the opposing tiles allow relative motion: sliding and rotating out of plane. When a vacuum is applied between the bladder layers, the tiles jam against each other, constraining their relative position. When arrayed as a horizontal ensemble, which also forms a single unit making up the assembly and the entire system (Figure 62b), the relative motion compounds a capability of being re-configured including being bent and/or rolled, and the freezing in place compounds setting the target configuration and rigidizing capabilities. This system can also enable applications such as easy-to-operate tonneau cover for pick-up trucks or retractable and rigidizable pool covers that can help maintaining the water temperature and cleanliness and reduce the water evaporation by minimizing the exposure to direct sunlight.

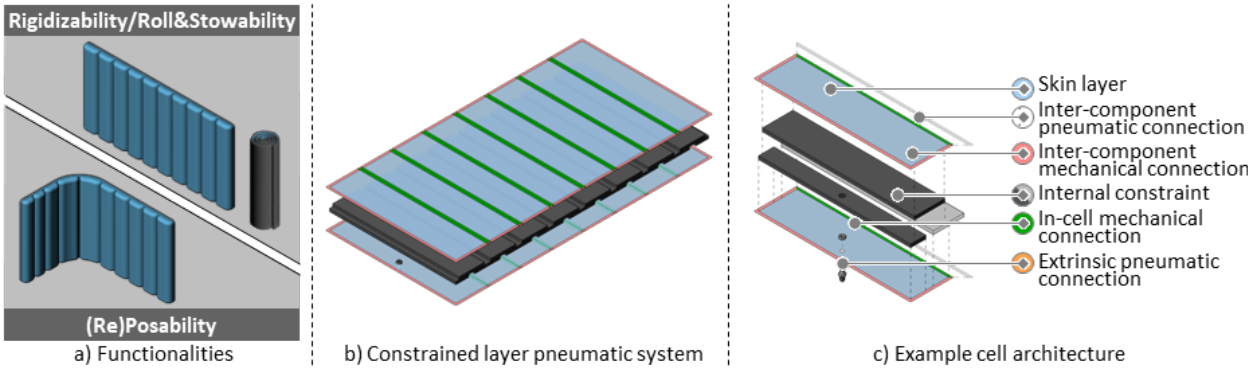

Figure 62. The re-configurable office space divider product system. a) This example system enables customized partitioning in an open office or work-from-home settings by providing rigidizability, roll-and-stowability, and (re)posability functionalities to its users. b) A horizontal ensemble composes the architecture of the product system. c) The sub-cellular features of an example cell composing this horizontal ensemble are visually communicated using an isometric exploded view.

2.4.3. Example Product Concept 3: Variable Friction Cargo Mat

The third example application using a constrained layer pneumatic system is a variable friction cargo mat, which is capable of changing its surface properties between high and low friction states (Figure 63a) and is made up of two interdigitated units (Figure 63b). The low friction unit is a horizontal combination of a number of horizontal ensembles (rows) of circular cells (Figure 63c),

each of which has the basic function of expanding out of plane. Together, the cells in the low friction unit (each made of a low friction material) can support the weight of an object and provide a low friction surface when inflated. Similarly, the angular shaped cells making up the horizontal ensembles of the high friction unit have a rubberized coating and have the capability of lifting the object and providing a high friction surface when inflated. These two units form an interdigitated assembly, which makes up the entire system providing the variable friction capability. The variable friction cargo mat can be used on the floor of a storage compartment of a vehicle, allowing easy loading of items in the low friction mode, while helping to hold them in place during transport in the high friction mode.

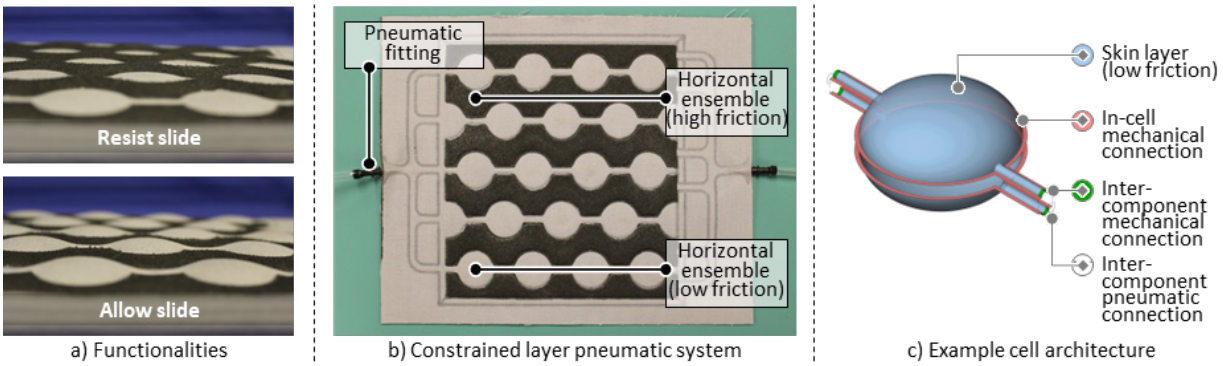

a) Functionalities b) Constrained layer pneumatic system c) Example cell architecture

Figure 63. The variable friction cargo mat product system. a) This example system changes the surface friction properties on demand, enabling easy loading of items in the low friction mode, while helping to hold them in place during transport in the high friction mode. b) Its overall architecture consists of two interdigitated units, each of which is made of a set of horizontal ensembles. c) The sub-cellular features of an example cell composing one of these horizontal ensembles are visually communicated using an isometric exploded view.

2.4.4. Example Product Concept 4: Morphing Windshield Cowling

A fourth example application using constrained layer pneumatic system is morphing windshield cowling that covers the gap between the car hood and windshield improving aerodynamics and aesthetics, and automatically curls up out of the way when the wipers are working (Figure 64a). Its architecture comprises a unit and a cell ensemble, which is made up of two main types of variations of basic cells that can be pneumatically controlled independently. The first type of basic cell, which enables the curling motion due to the upward moment generated when a vacuum is applied, is equipped with upside down T-shaped rigid tiles that are permanently attached to the inner bladder skins forming an airtight bladder. The second one is made up of bladder skins forming an inflatable cavity, which is selectively positioned under the hinge lines between each set of adjacent tiles at the higher level in the system, generating a downward moment that enables the flattening function to securely cover the gap between car hood and windshield

when the wipers are not in use. These two types of basic cells are vertically stacked to form a compound cell (Figure 64c), variations of which is used to create a horizontal ensemble that provides compound functions of curling, rigidly holding the curled shape, and straightening. A linear array of the multiplicity of these cell ensembles forms a single unit making up the assembly and the entire system (Figure 64b, left), providing flattening and curling higher-level functionalities that enable on demand operation of the morphing windshield cowling.

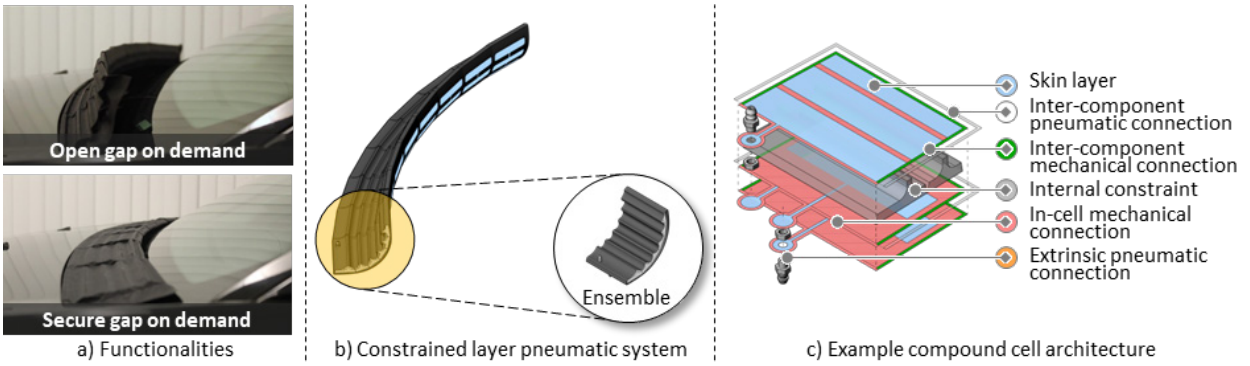

Figure 64. The morphing windshield cowling product system. a) This example system secures the gap between the car hood and windshield improving aerodynamics and aesthetics, and automatically curls up out of the way when the wipers are working. b) Its overall architecture is composed of an array of horizontal ensembles made of compound cells. b) The sub-cellular features of an example compound cell are visually communicated using an isometric exploded view.

2.4.5. Example Product Concept 5: Active Rear Seat Pocket

The fifth and last application example using constrained layer pneumatic system is active rear seat pocket. Storing personal belongings using rear seat storage compartments during transportation is often frustrating for the passengers. The current examples do not provide easy access for storing a wide variety of items or for interacting with the items (e.g., retrieving the item) that are already stored. The active rear seat pocket, employing a constrained layer pneumatic system, can deploy and stow on demand, providing a relatively easier one-handed access to and clearer view of the storage compartment, which potentially improve the overall passenger experience during transportation (Figure 65a).

The active rear seat pocket architecture is made up of a linear array of inflatable cells that are mechanically bonded to a surface of relatively stiff but bendable plastic sheet, forming a horizontal ensemble. This ensemble is attached to the inner surface of a rear seat pocket flatwise and attached to the plastic enclosure of the rear seat edgewise using a set of sliders (Figure 65b). When the cells are inflated, they induce out of plane expansion and in-plane contraction simultaneously,

producing a moment that bends the plastic sheet outwards, resulting in deploying the pocket for the user interaction (Figure 65c). As air is deflated, the moment decreases. This allows the system reverse back to its flattened state due to the synergistic effect of the elastic recovery force generated by the stiff plastic sheet and the lateral pulling forces provided by the springs, securely retaining the stored items.

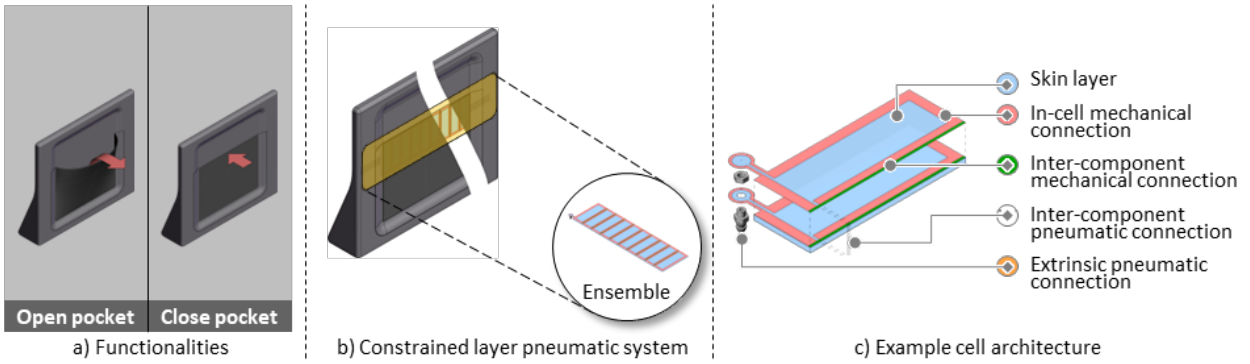

a) Functionalities b) Constrained layer pneumatic system c) Example cell architecture

Figure 65. The active rear seat pocket product system. a) This example product system can deploy and stow on demand, providing a relatively easier one-handed access to and clearer view of the storage compartment. b) Its overall architecture is composed of a horizontal ensemble. c) The sub-cellular features of an example cell forming this ensemble are visually communicated using an isometric exploded view.

2.5. Conclusion

This chapter introduces hierarchically organized constrained layer pneumatic systems, which comprise multiple airtight skin layers that create interconnected inflatable or vacuumable air cavities, pneumatic ports that enable control over the relative pressure inside the system, and internal and/or external constraints that restrain the form and contribute to the corresponding functionalities provided by the system when pneumatically activated.

A five-level architectural hierarchy, which comprises *system, assembly, unit, ensemble,* and *cell levels,* is introduced to communicate the emergent complexity of the system's structural organization from cell to system level. The cell, characterized as the most basic component in the architectural hierarchy of constrained layer pneumatic systems, not only delivers the lowest-level functionalities but also consists of a complex arrangement of sub-cellular features. In contrast to architectural components found at the cell level or higher, sub-cellular features are logically organized rather than based on the physical properties of their constituents. This logical organization is divided into three main sub-cellular feature categories: 1) *skin* that describe the characteristics of skin layers, 2) *connectivity* that describes the manner in which the cell itself is constructed as well as how it can be arranged into the hierarchy of architectural components, and

3) *constraints*, which describe the physical restrictions placed on a cell to influence its exhibited physical behavior.

Pneumatic affordances, responsible for enabling the functionality of the cell through its structure imposed by the cell architecture, are classified into four groups depending on their capacity to actively or passively raise or lower the system's internal pressure: *get inflated, vacuum, let air in,* and *exhaust air*. The operation of the pneumatic affordances activates fundamental cell behaviors, which are also divided into four categories based on their ability to expand or contract the air cavity within the cell's structure, either in-plane or out-of-plane. The characteristics of subcellular features are subsequently related to the respective fundamental behaviors that give rise to the emergent cell functions via a series of pneumatic affordance operations. An operation state diagram, complemented by a graphical representation of the corresponding cell architecture along with a tabulation of its subcellular feature characteristics, is introduced, describing the relationship between different pneumatic affordance operations and corresponding emergent cell functions in each operation state. This results in a comprehensive understanding of the cell's architectural, functional, and operational aspects, laying the groundwork for investigating the possibilities of this innovative architectural scheme. The language formulated to describe the cell and its sub-cellular constituents establishes a consistent foundation for exploring and discussing a range of cell architectures and their associated emergent cell functions.

The exploration and classification of potential fabrication techniques and material systems into three main categories (i.e., *adhering existing skin layers, fusing existing skin layers,* and *producing already-fused skin layers*) based on ways of mechanically connecting cell skin layers to one another provide a practical basis for the embodiment of the cells. This enables the experimental survey of emergent cell functions exhibited across various operation states. By categorically combining various subcellular feature characteristics, an array of architecturally diverse, operationally adaptable, and functionally instrumental cell alternatives is enumerated as building blocks. These building blocks are cataloged, offering a selection of emergent cell function pairings, such as *extend/pull, straighten/hinge, flatten/bend, become non-porous/become porous, flatten/buckle bi-stably, mute/texturize, roll/unroll, grow in-plane/shrink in-plane, flatten/cinch,* and *allow hinge-like motion/retain hinge position/jam*. The practical application of these building blocks in the context of early-stage design of structurally adaptable multi-mode products is demonstrated through five distinct design concepts, each offering unique technology capabilities

for user interaction in context-specific settings, highlighting how cell level components combined hierarchically to produce the system.

The comprehensive description of the interrelated architectural, functional, and operational aspects of constrained layer pneumatic systems at the cell level provides a firm basis for the exploration of architectural variations, enabling a more profound understanding of emergent cell functions. This basis also serves as a foundation for the systematic description, communication, synthesis, analysis, and re-synthesis of higher-level architectural and functional relationships, enabling the design and implementation of structurally adaptable multi-mode product concepts. Such a comprehensive systematic approach not only potentially encourages interdisciplinary collaboration among researchers but also fosters the systematic growth of knowledge in this multidisciplinary field.

Chapter 3. Design Supported by Hierarchical Functional Architectural Decomposition Approach

Constrained layer pneumatic systems offer a diverse range of functionalities such as different modes of actuation, changes in structural properties, and sensing capabilities that can be achieved through various architectural designs. The technological foundation provided by constrained layer pneumatic systems enable the design of structurally adaptable multi-mode products the design space of which is relying on the functional and architectural variety. This functional and architectural variety is structured in a hierarchical manner, where basic functions produced by basic architectural components combine in ensembles and subassembly units to produce higher level aggregate and compound functions, and ultimately technology capabilities of a system which enable a user-interfacing multi-mode application.

A comprehensive description of this hierarchical structure creates the opportunity to enable systematic exploration and design by relating the structured arrangement of the architectural components embedded in a constrained layer pneumatic system to the corresponding structured set of functional components. Such relation between the architectural and functional components enables modifications in the system's hierarchy. This affords alternative design concept generations. The debate on defining the relation between form and function is an age-old question that can be retraced to Sullivan's (1896) dictum "form ever follows function". Instead of spending effort towards unravelling the causality between form and function, the highly structured nature of constrained layer pneumatic systems allows for the coexistence of form and function, which are almost perfectly overlapping in a hierarchical manner.

This chapter introduces an integrated hierarchical characterization scheme: *hierarchical functional architectural decomposition*, geared towards supporting various analysis and synthesis design methods. These methods enable incremental improvements to existing designs, replacements for existing designs, and speculative designs that are based on the existing ones as a starting point. It relies on the coherence between the architectural and functional hierarchy inherent

in constrained layer pneumatic systems. By mapping architectural components to the corresponding functions, compound functions can be directly produced from the aggregation of compound architectural components, where basic functions of cells combine to form aggregate functions in ensembles of cells. Ensembles combine to produce more complex compound functions within a unit, and units combine in assemblies to form a complete system providing technology capabilities to enable applications.

The general architecture detailing the fundamental components of a basic constrained layer pneumatic system is presented in Chapter 2.1.1. Five multi-mode product concepts using constrained layer pneumatic systems are demonstrated in Chapter 2.4, enumerating a wide range of technology capabilities.

In this chapter, the grammar describing the different types of functional and architectural components is introduced, enabling the formation of the hierarchical relationship among these components as a part of the decomposition. The characterization scheme and a set of structural rules are formulated with the purpose of standardizing the hierarchical functional architectural decomposition process the implementation of which is detailed and communicated through a mobile phone restraint mat design example. This scheme provides a direct view into the hierarchical structure of a system's form and function geared toward enabling iterative analysis, synthesis, and re-synthesis at a conceptual level. The design strategies are developed to systematize the use of the hierarchical functional architectural decomposition approach for re-synthesis. These strategies enable the identification of the design goals that motivate the re-synthesis, the design objectives that are to be achieved while implementing the defined goals, the design modifications that actualize these design goals, and the potential design tradeoffs that emerge as a result of the design modifications. A set of re-synthesis examples demonstrate the implementation of these design strategies, showcasing a systematic approach for generating variations of existing systems during the early-stage product design process. The types of performance couplings are described, and the implications of re-synthesizing existing systems' hierarchies are discussed and evaluated in the context of potential performance couplings. The hierarchical functional architectural decomposition approach provides a direct view into the system hierarchy at the conceptual design stage, enabling re-design, incremental innovation, and radical innovation of constrained layer pneumatic product systems by enhancing the systematic re-synthesis process.

3.1. Hierarchical Functional Architectural Decomposition Approach

The goal of the hierarchical functional architectural decomposition is to provide a basis for the iterative analysis, synthesis, and re-synthesis of the relation between the hierarchical architectural form of a design and the corresponding hierarchical functionalities. It allows the decomposition of a constrained layer pneumatic product system to the lowest level where the lowest level functionalities, namely constituent basic functions, are provided by the smallest architected set of components, namely cells. It also enables synthesis at higher levels, where the constituent basic functions (e.g., angular expansion) can be combined to produce constitutive compound functions (e.g., aggregate angular expansion). Thus, functionalities combine as functional components in a functional hierarchy that aligns with the hierarchy of the architectural components, where the basic architectural components (i.e., cell) can be combined to produce compound architectural components (e.g., ensemble). Performing functional and simultaneous architectural synthesis at each level in the hierarchy eventually leads to a formation of a product system providing a set of highest-level functionalities, namely technology (sub)capabilities, at the system level.

Due to their highly structured architectural formation, constrained layer pneumatic systems provide an ideal context for the development of the hierarchical functional architectural decomposition which aims to aid exploration of design alternatives by analysis, synthesis, and re-synthesis of the decomposition. To systematize this exploration, a grammar to navigate through the functional and architectural hierarchies is developed, which enables detailing the levels forming the functional architectural decomposition hierarchy by following a set of structural rules.

First (2.1.), a grammar describing different types of functional and architectural components along with the visual language to signify and communicate the hierarchical relationships among these components as a part of the decomposition is introduced. A set of principles governed by architectural and functional grammars is detailed, formalizing the representation, use, and operational formation of architectural and functional components at each level of the hierarchy.

Second (2.2.), the levels forming the functional architectural decomposition hierarchy is detailed through an example. There are four main levels forming a product system at the *system level*, which is the fifth and the highest level in the functional architectural decomposition hierarchy. These four main levels are: 1) *cell level*, describing the architectural details of a cell, which includes the description of its sub-cellular features and their characteristics, and the corresponding basic functions, 2) *ensemble level*, describing the ways a set of cells is assembled

to form a cell ensemble providing ensemble level compound functions, 3) *unit level*, describing how cell ensembles are brought together to form a unit providing unit level compound functions and 4) *assembly level(s)* describing how multiple units (or sub-assemblies) come together to produce assembly level compound functions affording a constrained layer pneumatic system with a certain set of technology capabilities at the system level. A bottom-up approach used in the context of the mobile phone restraint mat example to describe the architectural and functional hierarchy through the levels along with a brief discussion of how the functional architectural decomposition supports design analysis, synthesis, and re-synthesis in addition to the introduction of diagramming conventions and pneumatic operating states and sequences.

Third (2.3.), a set of structural rules, as well as a generic hierarchical decomposition template, is formulated with the purpose of standardizing the decomposition process across future constrained layer pneumatic product systems.

3.1.1. Functional and Architectural Hierarchies

Forming a representation of the system components and their relationships requires a set of principles. The application of these principles can benefit from a consistent method of visualization, enabling the collective understanding and communication of the systematic use of the hierarchical functional architectural decomposition approach as a tool for analyzing, synthesizing, and re-synthesizing different constrained layer pneumatic product systems. A grammar provides a basis for the consistent implementation of the hierarchical functional architectural decomposition approach by systematizing the composition and representation of the fundamental functional and architectural components at each level in the system hierarchy.

The system hierarchy consists of five levels, which are cell, ensemble, unit, assembly, and system levels (Figure 66, left). For each level in the hierarchy, there is a set of corresponding architectural and functional components forming the interrelated architectural and functional hierarchies.

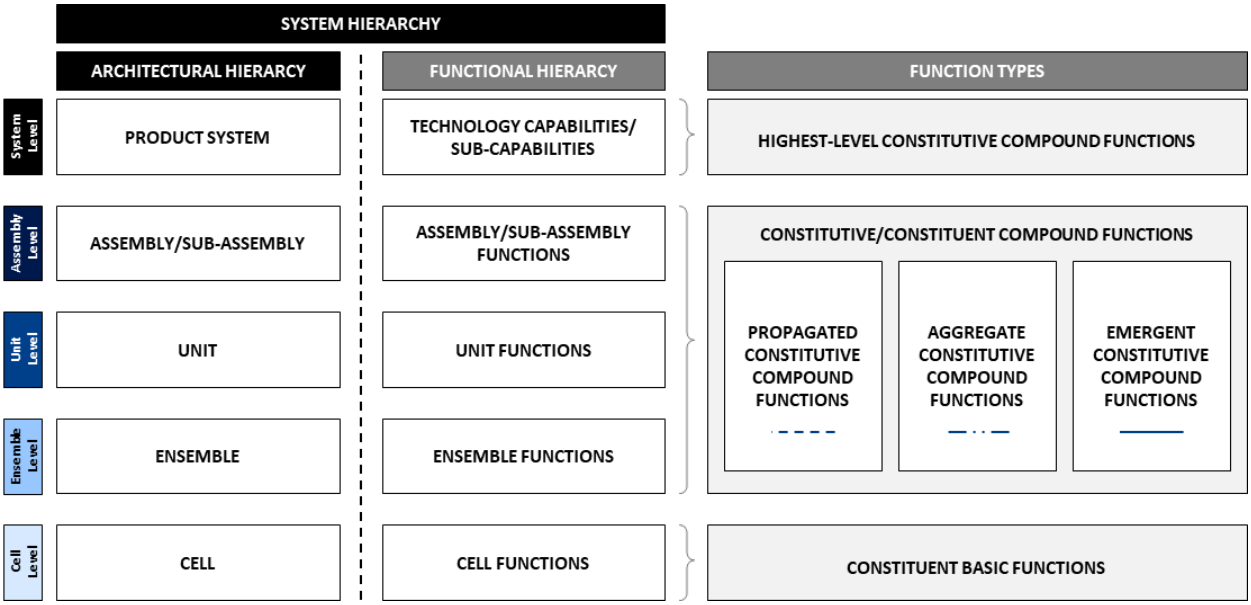

Figure 66. A product system hierarchy. The hierarchy of a multi-mode constrained layer pneumatic product system comprises five levels of functional and architectural hierarchies (left). Three main function types listed as constituent basic functions, constituent/constitutive compound functions, and the highest-level constitutive compound functions (right).

The architectural hierarchy is built from the architectural components that exist at each level as a part of the system hierarchy, forming a product system at the highest level. The constituents of architectural hierarchy are *cells, ensembles, units*, *assemblies/sub-assemblies,* and *product system*. Each component within each level is made up of one or more architectural components from next lower level. When multiple architectural components are combined at one level to form a compound architectural component at the next level up in the constrained layer pneumatic product systems, this can be done horizontally (i.e., in parallel) or vertically (i.e., in series).

The functional hierarchy is built from the functional components that exist at each level as a part of the system hierarchy, affording technology capabilities at the highest level in the system. The constituents of functional hierarchy are *cell functions, ensemble functions, unit functions, assembly/sub-assembly functions,* and *technology capabilities/sub-capabilities*. Each component within each level is made up of one or more functional components from next lower level. A set of functional components are combined at one level to form a higher-level functional component at the next level up in the constrained layer pneumatic product systems. The functional components forming the functional hierarchy are categorized into three groups based on their constituent and/or constitutive role in the hierarchy (Figure 66, right). The constituent basic functions only exist at the cell level and must have a constituent role, generating constitutive functional components at

the ensemble level. The constituent/constitutive compound functions exist at the ensemble, unit, and assembly levels, and have constituent and constitutive roles simultaneously by generating higher-level constitutive functional components and by being generated by lower-level constituent functional components. Three constitutive compound function types are identified as *propagated, aggregated, and emergent constitutive compound functions* based on the distinctive contributory characteristics of their constituent functional components. The highest-level constitutive compound functions (e.g., technology capabilities/sub-capabilities) exist at the system level of the functional hierarchy and are the products of constituent functional components from the assembly level.

Together these two hierarchies describe the system hierarchy forming a basis for the hierarchical functional architectural decomposition approach. The descriptions of the architectural and functional hierarchies are formalized through the architectural and functional grammars.

3.1.1.1. Architectural Grammar

The architectural grammar governs the use of architectural components in the architectural hierarchy. Architectural components at each level, except the system level, in the hierarchy can act as *constituent architectural components* that can be combined to form higher level *constitutive architectural components*, further combination of which forms the product system at the highest level. Figure 67 illustrates an exemplary partial architectural decomposition of the mobile phone restraint mat of which architectural components are combined at each level from the cell level up to the system level. The construction of the lowest level architectural component (i.e., cell) in the architectural hierarchy requires its own grammatical structure describing the relationship between its sub-cellular features and their characteristics.

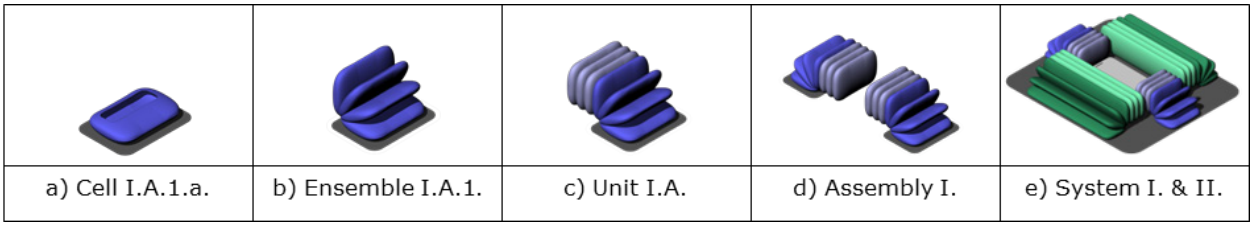

Figure 67. An exemplary partial architectural decomposition of the mobile phone restraint mat. The architectural components that correspond to each level in the architectural hierarchy of the mobile phone restraint mat are shown ranging from the lowest (cell) level (a) up to the highest (system) level (e).

The details regarding the sub-cellular features and their corresponding characteristics that afford a cell formation, and the hierarchical formation of a product system using (compound) cells,

ensembles, units, and (sub) assemblies according to an architectural hierarchy are described in the following sub-sections.

3.1.1.1.1. Cell Description

Cell is the lowest level architectural component but itself has a complex arrangement of a logical set of sub-cellular features the characteristics of which give rise to the constituent basic functions at the cell level. Unlike architectural components that reside within cell-or-above levels in the architectural hierarchy, the sub-cellular features are organized logically rather than being organized with respect to the physicality of their constituents. Such logical organization enumerates three sub-cellular feature categories: 1) *skin,* which describes the characteristics of skin layers, 2) *connectivity*, which describes the rules of connectivity affording the construction of a cell and other higher level architectural components, and 3) *constraints*, which describes the details of physical restrictions imposed on a cell, contributing to the physical behavior it displays.

There are three major aspects comprising the characteristics of a skin layer: *skin type*, *skin thickness*, and *skin uniformity*. Skin type classifies the potential materials that can be used as skin layers based on two levels of physical extensibility (extensible - inextensible) and three levels of physical flexibility (low-medium-high). For example, a bare sheet of thermoplastic polyurethane (TPU) would be classified as an extensible material with high flexibility, whereas a relatively thick polypropylene sheet would be classified as inextensible material with low flexibility. Skin thickness applies to the top and bottom skin layers, indicating whether a prospective cell is architecturally symmetric or not. Skin uniformity specifies whether the constituents of a cell layup are uniform or non-uniform (i.e., changing cross-section thickness) transversally.

The rules of connectivity that affords cell construction are grouped under four sub-categories: *in-cell mechanical connection, inter-component mechanical connection, inter-component pneumatic connection,* and *extrinsic pneumatic connection*. The in-cell mechanical connection describes the permanent bonding between top and bottom skin layers, forming an enclosed cell or a cell with a designated opening or openings around its perimeter. The inter-component mechanical connection describes how adjacent components (e.g., cells, ensembles) can be permanently bonded together to form a higher-level component (e.g., ensemble, unit). Inter-component pneumatic connection describes the back-and-forth air flow direction between cells or higher-level components as the pressure inside the layered structure changes in relation to atmospheric pressure. The extrinsic pneumatic connection details the way and the location of a

pneumatic fitting attached to one of the skin layers or between skin layers to enable air flowing in and out of the corresponding cell.

There are two main sub-categories of constraints: *internal constraints* and *external constraints*. Internal constraints include volumetric, layered, and tendon-like constraints. Using particles such as glass beads or coffee beans encapsulated in a cell to produce a controllable stiffness change as a function of vacuum pressure or accommodating materials such as sponge or strands of twisted fibers to control the air flow velocity are examples of internal volumetric constraints. Replacing the bulky particles filling a cell with thin uniform sheets such as paper or textile that are layered on top of each other or using one or multiple layers of non-uniform yet regularly arrayed basic or architected tile patterns are examples of internal layered constraints. Accommodating strings or cables attached between skin layers to restrain the inflation of a cell is an example of internal tendon-like constraints, which can be in a discrete or distributed form. External constraints can be surface, boundary, or tendon-like constraints. In the case of using a constrained layer pneumatic system as an actuator, at least one of the cells needs to be attached to a surface that acts as an external surface constraint. External boundary constraints can be used to restrain a cell around its perimeter or a portion of its perimeter to facilitate a designated physical behavior such as limiting the out of plane translational expansion or allowing out-of-plane curling around a fixed axis. External tendon-like constraints are equivalent to the internal tendons but situated outside a cell with strings or cables attached to the exterior surface of at least one of the skin layers.

The characteristics of these features together determine the function(s) that a cell provides at the cell level in the architectural hierarchy. The description of the relationship between the sub-cellular features and the corresponding characteristics requires its own grammatical structure which is demonstrated in a tabulated form (Figure 68-bottom) and is accompanied by a corresponding three-dimensional (isometric) illustration showing the exploded view of the constituent features that afford the construction of one of the system cells (Figure 68-top). This sub-cellular grammar uses a color-coding scheme where:

- light blue areas indicate the skin layers (top and bottom),
- red lines (or in some cases areas) indicate the mechanical connection between these skin layers which provide a permanent seal,

- green lines (or in some cases areas) indicate the prospective (in this case off-centered) mechanical connection between the top skin layer of this cell and the bottom skin layer of the adjacent cell or component (which is not shown in the figure),
- the black and white dotted area surrounded by the green border indicates the prospective pneumatic connection to the adjacent cell or component (which is not shown in the figure),
- orange represents the extrinsic pneumatic connection (e.g., vertically attached barbed pneumatic fitting),
- and the various shades of gray indicate internal constraints (e.g., internally attached tiles) and external constraints (e.g., flat rigid base surface).

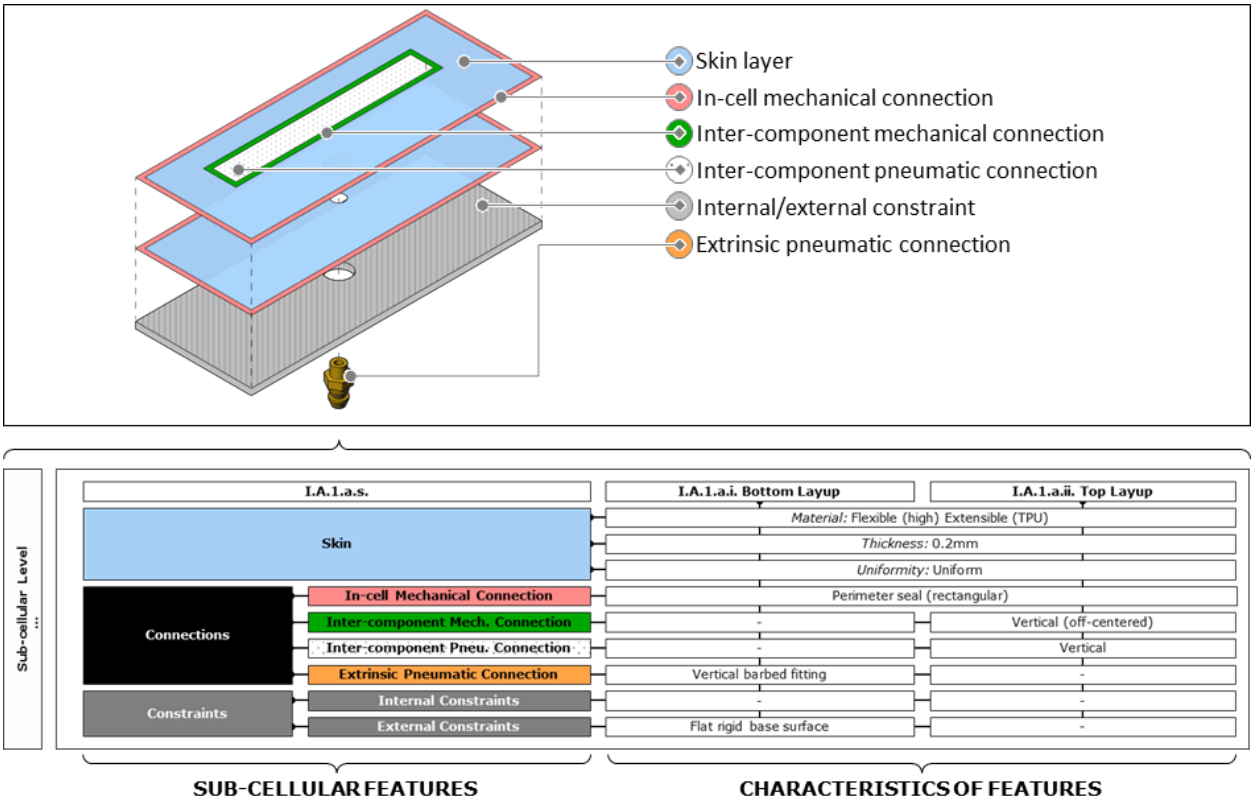

Figure 68. The sub-cellular feature characteristics of an example cell. The sub-cellular feature categories are listed as: *skin*, *connectivity*, and *constraints*. There are three major aspects comprising the characteristics of a skin layer: *skin type, skin thickness, and skin uniformity*. The rules of connectivity that affords cell construction are grouped under four sub-categories: *in-cell mechanical connection, inter-component mechanical connection, inter-component pneumatic connection,* and *extrinsic pneumatic connection*, and there are two main sub-categories of constraints: *internal constraints* and *external constraints*. The characteristics of these features determine the function(s) that a cell provides at the cell level in the hierarchy.

3.1.1.1.2. Architectural Hierarchy

The product system is assembled hierarchically using (compound) cells, ensembles, units, and (sub) assemblies according to a grammar describing how they are connected to each other. Two architecturally different cells can be combined by sharing at least one sub-cellular feature (e.g., a skin layer or an external constraint) to produce a *compound cell* which combines and potentially extends their respective functionalities. Note that the mobile phone charger mat example does not make use of a compound cell.

A set of one or more essentially identical cells (whether compound or not) can be combined in parallel or in series to form an *ensemble*. Cells in a parallel combination share at least one layer (whether skin or external constraint) across all cells in the ensemble forming mechanical and pneumatic connections among cells, and the result is referred to as a *horizontal ensemble*. Likewise, cells in a series combination combine with the topmost layer of one cell attached mechanically and pneumatically to the bottommost layer of the next cell in the ensemble, and the result is referred to as a *vertical ensemble*. It is necessarily the case that the end cells in a horizontal ensemble and the topmost and the bottommost cells in the vertical ensemble have slight structural differences to afford mechanical and pneumatic attachment to other architectural components. All the cells in an ensemble must be pneumatically connected to each other such that they activate together. Generally, the functionality of an ensemble is similar to the functionality of a cell but amplified due to the cells acting in concert thus referred to as aggregated functionality.

A set of essentially identical or different ensembles can be combined horizontally or vertically to form a unit. Horizontally combined ensembles are mechanically connected through at least one layer and may or may not be pneumatically connected. Any pneumatic connection can be through the shared layers or externally (e.g., using tubing). Vertically combined ensembles must be connected mechanically by attaching the topmost layer of one ensemble mechanically but not necessarily pneumatically to the bottommost layer of the next ensemble. It is generally convenient to make a direct pneumatic connection through the upper/lower attachment, but external pneumatic connection is also possible. If a unit is composed of ensembles with shared pneumatic connection, then all the ensembles within the unit activate together, otherwise they can be controlled independently/sequentially on demand.

An assembly is formed from a set of units in the same way that a unit is formed from a set of ensembles. An assembly differs from a unit in that a unit can only be constructed from a set of

ensembles and therefore an assembly can have significantly more complex structure. In addition, an assembly can include external components such as enclosures and brackets which serve as external constraint to the layers to which they attach. A set of assemblies can act as sub-assemblies to form a higher-level set of assemblies, combination of which produces the product system at the highest level in the architectural hierarchy.

In many cases, an architectural component in one layer is made of just a single component from the layer below. For example, an ensemble can be composed from a single cell, but still must be represented as an ensemble to be integrated into the hierarchy. This *propagation* of the architectural components can occur at any level and upwards through multiple levels in the architectural hierarchy. However, because the design context changes upwards through the system hierarchy, the functionality afforded by the propagated architectural component may change.

A product system can be decomposed into its constituent architectural components in alternative ways indicating that there is no unique hierarchical functional architectural decomposition for any given product system. The decision on how to organize the architectural components forming a product system depends heavily on how to organize the relationship among the functional components. The distinction between what makes a particular unit a unit but not an assembly depends on the design context in which the relationship among the functional components takes form.

The relationships among architectural components form a rooted tree graph structure where the product system is the root of the tree and the cells are the leaves. The cells themselves have sub-cellular features that are contained within each leaf. While this tree structure describes the architectural hierarchy, the functional hierarchy has additional structure within the architectural tree.

3.1.1.2. Functional Grammar

Each architectural component affords a set of functions, each of which can be referred to as a functional component. These functional components combine through the system hierarchy to form a functional hierarchy. The functional grammar governs the use of functional components to form the functional hierarchy. The functional components can act as constituent basic or compound functions to form constitutive compound functions at the next higher level as a part of the hierarchy, the further combination of which forms the highest-level constitutive compound functions (i.e., technology capabilities/sub-capabilities) at the system level. In the functional

hierarchical grammar, a functional component is signified by a box object (i.e., functional component box), which is associated with a specific architectural component, which has the following eight features (Figure 69, left):

- a textual description of the constituent function located in the box (e.g., function 1),
- a constituent function identification number, which is unique within its level in the hierarchy, located on the bottom left corner of the box (e.g., 1),
- one or more compound connectors located along the top edge of the constituent function box, each displaying a target constitutive function identification number (e.g., 2) from the layer above (with the exception of the single functional component at the highest (i.e., system technology capability) level which has no compound connector),
- optional operating sequence identification letter (e.g., a), which alphabetically denotes when a particular constituent function is required to be activated as a step within an operation sequence that activates a higher-level constitutive function,
- a compositional line connecting each compound connector of the constituent function to a constituent connector of the corresponding target constitutive function,
- one or more constituent connectors along the bottom edge of the constituent function box (with the exception of functional components in the lowest (i.e., cell) level which have no constituent connector),
- optional connectivity connectors and lines connecting two compatible functional components (e.g., *attach to next ensemble*), which are provided by two adjacent/relevant architectural components, detailing the mechanical and pneumatic connectivity among the adjacent/relevant architectural components at the same hierarchical level (e.g., two adjacent cells at cell level or two relevant ensembles at ensemble level), and
- coloring of connectors and lines corresponding to their type: compositional lines and connectors are blue, and connectivity lines and connectors are orange.

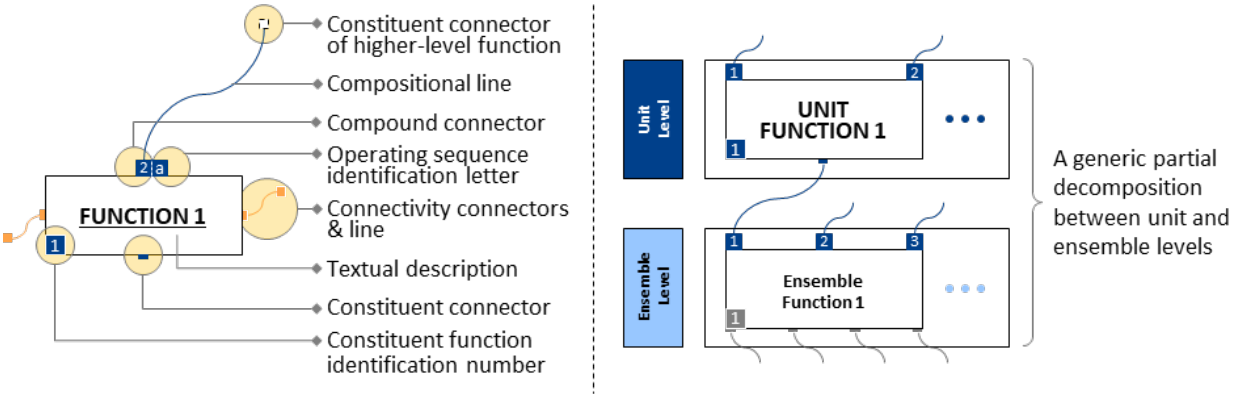

Figure 69. A generic functional component and an exemplary generic partial decomposition. The features of a generic functional component are highlighted on the left, and a generic partial decomposition between unit and ensemble levels is shown as an example on the right.

The textual description font size, and the connector and constituent function identification number colors are adapted to represent the level to which a functional component belongs. A set of compositional lines with different line types are used to indicate the function type of a functional component. A generic partial decomposition between ensemble and unit levels is exemplified in Figure 69 (right), where *ensemble function 1* is a constituent compound function at the ensemble level forming a *unit function 1*, which is a singly emergent constitutive compound function at the unit level. The details regarding two types of constituent functional components (basic and compound), and three types of constitutive functional components (propagated, aggregated, and emergent) are introduced in the following sub-sections.

3.1.1.2.1. Constituent Functional Components

Constituent functional components act as essential components of a larger construction in the functional hierarchy, composing higher-level functions when singly propagated or combined with other constituent functional components.

The lowest level in the hierarchy, the cell level, accommodates the first type of constituent functional components. These are the constituent basic functions, which are directly related to the physical behaviors each cell exhibits once pneumatically activated, such as expand and allow hinge-like motion. As shown in Figure 70a, cell function a can contribute to the construction of a set of n constitutive functional components at the ensemble level, where n is a positive integer. A large number of constitutive functional components stemming from a single constituent functional component may indicate performance couplings among higher-level functions.

A constitutive functional component at the ensemble level or above itself acts as a higher-level constituent functional component to form constitutive functional components at the unit level or above. These functional components are of the second constituent functional components type: constituent compound functions. As shown in Figure 70b, ensemble function a can be constituted by a set of n constituent basic functions at the ensemble level. Ensemble function a also plays a role as a constituent compound function that contributes to the construction of a set of m constitutive compound functions at the unit level in the hierarchy in this generic example.

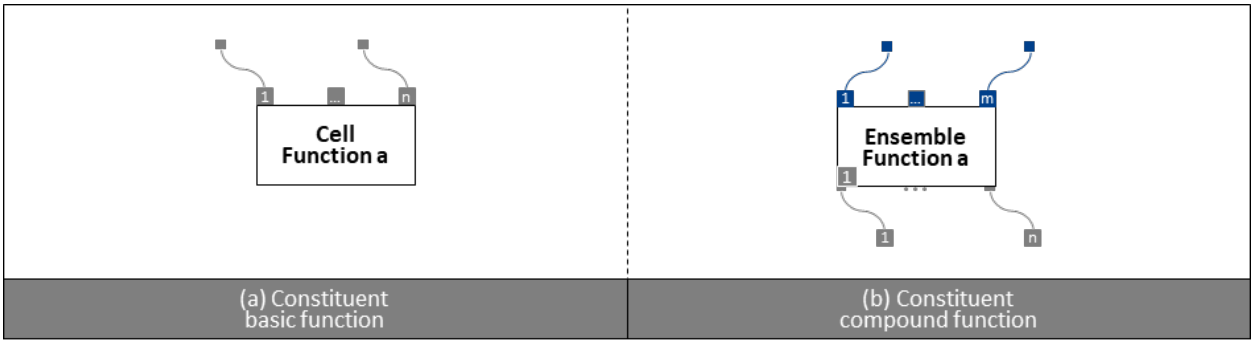

Figure 70. Representations of generic constituent basic (a) and compound (b) functions. a) *Cell function a* represents constituent basic functions at the cell level, which are directly related to the physical behaviors each cell exhibits once pneumatically activated. b) *Ensemble function a* represents constituent compound functions, which act as higher-level constituent functional components to form constitutive functional components at the unit level or above.

These constituent compound functions compose higher-level functionalities upwards through the system hierarchy, ultimately composing the technology sub-capabilities within the system level affording the composition of the single technology capability also within the system level.

3.1.1.2.2. Constitutive Functional Components

Constitutive functional components are combinations of a set of constituent functional components, and therefore are always compound functions by definition (i.e., *constitutive compound functions*). There are three constitutive compound function types: *propagated constitutive compound functions, aggregated constitutive compound functions,* and *emergent constitutive compound functions*.

A propagated constitutive compound function is made up of a single constituent basic or compound function, which propagates to the next level in the hierarchy without changing function afforded. A dashed compositional line connecting the constituent and compound connectors indicates that the resulting constitutive compound function has the quality of being propagated (Figure 71a).

An aggregated constitutive compound function is made up of two or more identical constituent basic or compound functions, resulting with providing an amplified version of the same lower-level functionality at the higher-level. This typically occurs when cells combine into an ensemble. A dashed and dotted compositional line connecting the constituent and compound connectors signifies that the resulting constitutive compound function is being aggregated (Figure 71b).

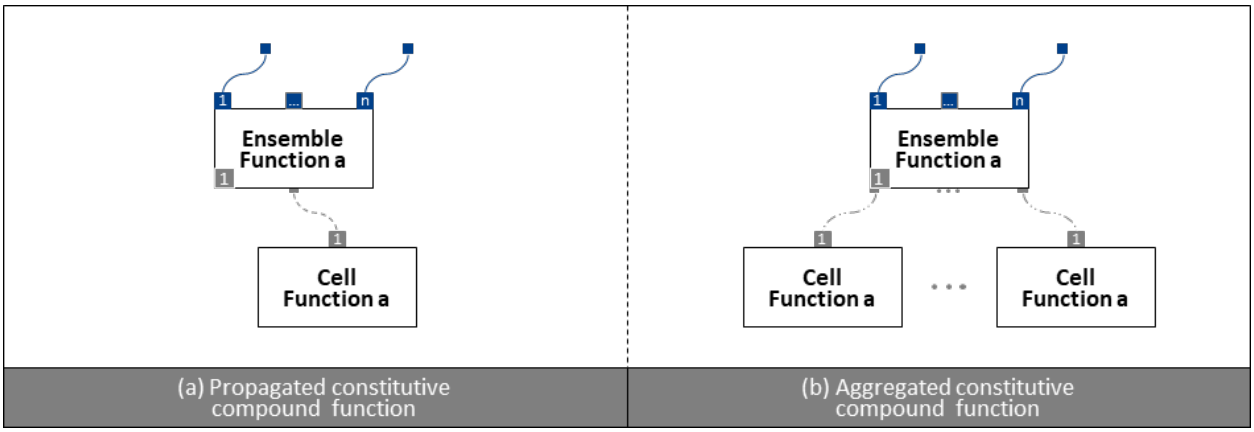

Figure 71. Representations of generic propagated (a) and aggregated (b) constitutive compound functions. a) *Cell function a* is propagated (shown with a dashed line) to the next level in the hierarchy without changing function afforded, generating *ensemble function a*, which is a generic propagated constitutive compound function. b) Multiplicity of *cell function a* is combined into (shown with a dash-dot-dotted line) an amplified version of the same lower-level functionality at the higher-level, generating a *ensemble function a*, which is a generic aggregated constitutive compound function.

An emergent constitutive compound function can be made up of a single constituent basic or compound function, or of a set of homogeneous or heterogeneous constituent basic or compound functions all of which creating a new function through the compounding process. Figure 72 shows three different generic ways of producing an emergent constitutive compound function: 1) by using a single constituent basic or compound function, where the change in design context induces a change in the nature of the functionality, generating a singly emergent constitutive compound function (Figure 72a), 2) by using a set of identical constituent basic or compound functions generating a homogenously emergent constitutive compound function (Figure 72b), providing a higher-level functionality fundamentally different in nature from the lower-level functionality, and 3) by using a set of different constituent basic or compound functions generating a heterogeneously emergent constitutive compound function (Figure 72c).

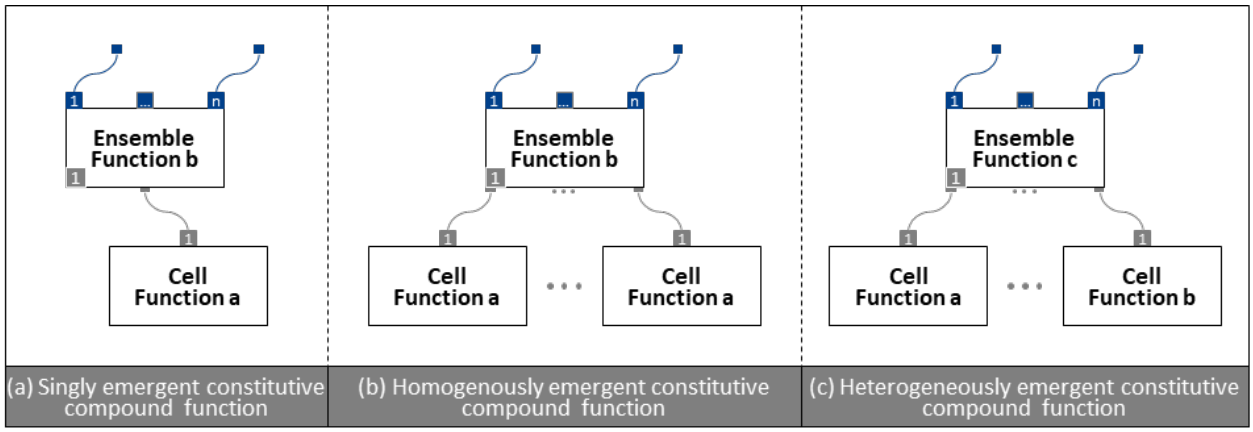

Figure 72. Representations of generic singly (a), homogenously (b), and heterogeneously (c) emergent constitutive compound functions. a) *Cell function a* singly generates an emergent constitutive compound function, *ensemble function b*, which provides a different functionality than its constituent. b) Multiplicity of *cell function a* is homogenously combined into an emergent constitutive compound function, *ensemble function b*. c) A setoff different cell functions (e.g., *cell function a, cell function b*) is heterogeneously combined into an emergent constitutive compound function, *ensemble function c*.

These constitutive compound functions are composed from the lower-level functional components, ultimately arising from the cell functions. While this hierarchy describes which lower-level functions contribute to the higher-level functions, it does not describe the order, if any, each of these functions needs to be activated to activate the higher-level function.

3.1.1.2.3. Operational Formation of Constitutive Functions

The operational formation of constitutive functional components can be achieved in three ways depending on the operational interaction among its constituent functional components: *simultaneous operation*, (cyclic) *sequential operation,* and *separate operation*.

Simultaneous operation of constituent functional components takes place as two or more constituent functional components are concurrently activated through their respective pneumatic affordance operations (e.g., let air in, vacuum air), simultaneously activating the constitutive functional component that they compose. In Figure 73a, the simultaneous operation of a set of generic assembly functions, *B*, *C,* and *D*, is demonstrated, producing a generic technology sub-capability, *A*.

Sequential operation of constituent functional components takes place as two or more constituent functional components are consecutively activated through their respective pneumatic affordance operations (e.g., let air in, vacuum air), sequentially contributing to the activation of the constitutive functional component that they compose. In Figure 73b, the sequential operation

of a set of generic assembly functions, *B*, *C*, and D, is demonstrated, producing a generic technology sub-capability, *A*. In some cases, an operation sequence is cyclic, where the last step and the first step in the sequence correspond to the same constituent functional component. In Figure 73c, the cyclic sequential operation of a set of generic assembly functions, *B*, *C,* and *D*, where *B* is activated as the first and last step in the cycle (as indicated by two operating sequence identification letters, *a* and *d*), is demonstrated, producing a generic technology sub-capability, *A*.

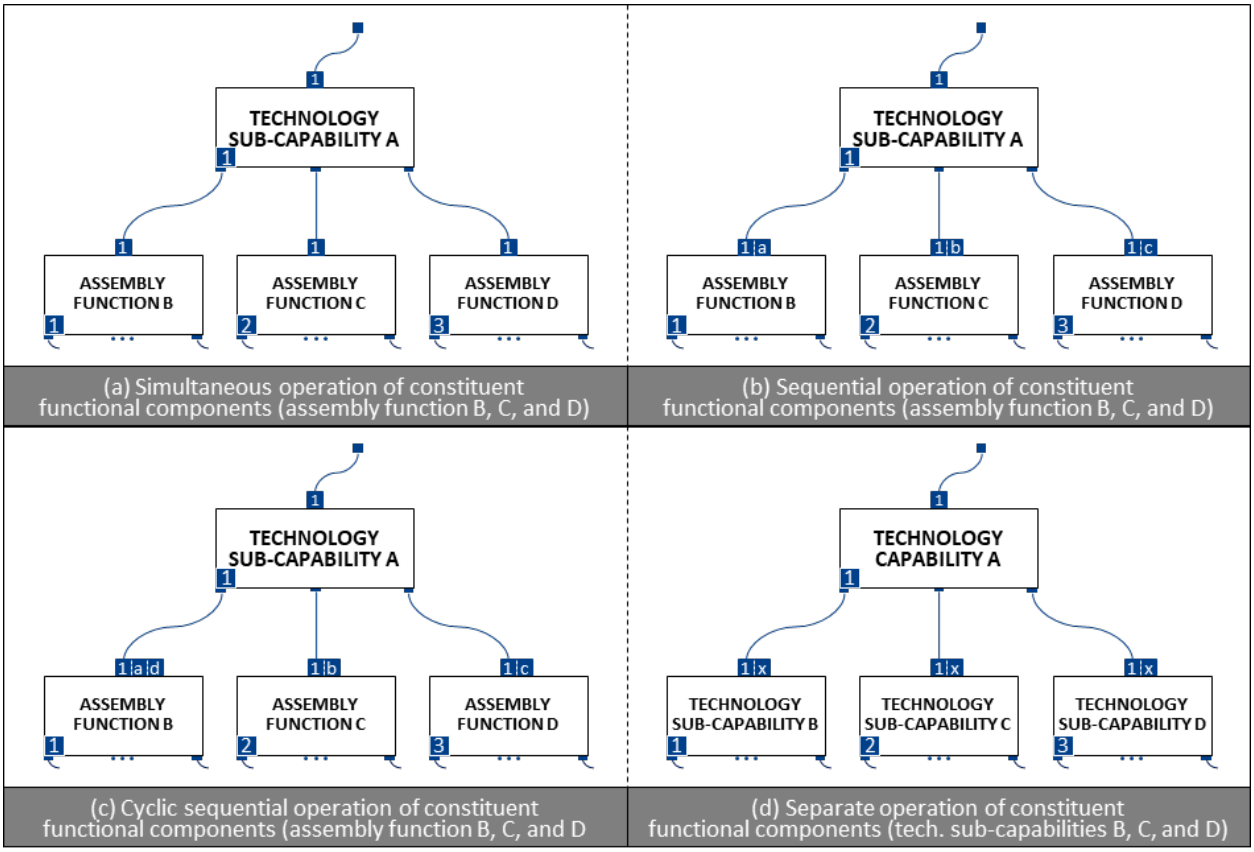

Figure 73. Operational formation of constitutive functions. a) Simultaneous operation of a generic constituent functional component, *technology sub-capability a*, is achieved by the concurrent activation of generic *assembly functions B, C*, and *D*. b) Sequential operation of a generic constituent functional component, *technology sub-capability a*, is achieved by the consecutive activation of generic *assembly functions B, C*, and *D* as indicated by the operating sequence identification letters, *a, b,* and *c*. c) Cyclic sequential operation takes place where the last step (*d*) and the first step (*a*) in the sequence correspond to the same constituent functional component. d) Separate operation of a generic constituent function, *technology sub-capability a,* is achieved by individual activation of generic *assembly functions B, C*, and *D* in arbitrary order as indicated by the operating sequence identification letters, *x.*

Separate operation of constituent functional components takes place as two or more constituent functional components are individually activated in arbitrary order typically controlled by the user or by other external factors through their respective pneumatic affordance operations (e.g., let air in, vacuum air), together creating the constitutive functional component they compose. In Figure 73d, the separate operation of a set of generic technology sub-capabilities, *B*, *C*, and *D*, is

demonstrated, producing a generic technology capability, *A*. The operating sequence identification letters, *x*, indicates that there is no definitive order for the operational formation of the technology capability, *A*.

3.1.1.3. Diagramming Conventions

The hierarchical functional architectural decomposition of a product system simultaneously communicates the hierarchical relationships among the architectural and functional components that compose the system by using a set of diagramming conventions, visually describing what constitutes a system and how it operates. As a part of this diagram, each hierarchical level (e.g., assembly level), both architecturally and functionally, is represented with a horizontal band within the confines of which the corresponding architectural and functional components are detailed. These bands are labelled and arranged on top of each other on the leftmost end of the diagram as a single column in a hierarchically descending order starting with the system level on top and ending with the cell level on the bottom.

Each band (e.g., ensemble level) contains a set of architectural component boxes that are labelled in outline form (e.g., I.A.1., I.A.2.), where the label corresponds to a particular architectural component. Each of these architectural component boxes contains a figure that illustrates the corresponding architectural component as an isometric drawing following the color-coding scheme that is used to visualize the sub-cellular features of a cell (see section 3.1.1.1. for details). The isometric figures representing each cell are placed below the corresponding cell boxes at the cell level for horizontal compactness. Typically, the architectural component boxes containing the constituent architectural components at one level (e.g., cell level) are placed below the architectural component box that contains the corresponding higher-level constitutive architectural component at the level above (e.g., ensemble level). However, in the case of only a portion of an entire decomposition is shown for the sake of compactness and brevity, the correspondence between the above and below levels can be traced using the labelling convention, and functional compositional connectors and lines. There are often repeating architectural components (e.g., cell) used to form a higher-level architectural component in the hierarchy. Instead of showing these identical architectural component boxes as a part of the decomposition, the *repeat sign* (⊟) is used as a visual indicator in the cell-label area of these architectural component boxes to indicate that they are being employed multiple times (Figure 74, I.A.1.b. Mid).

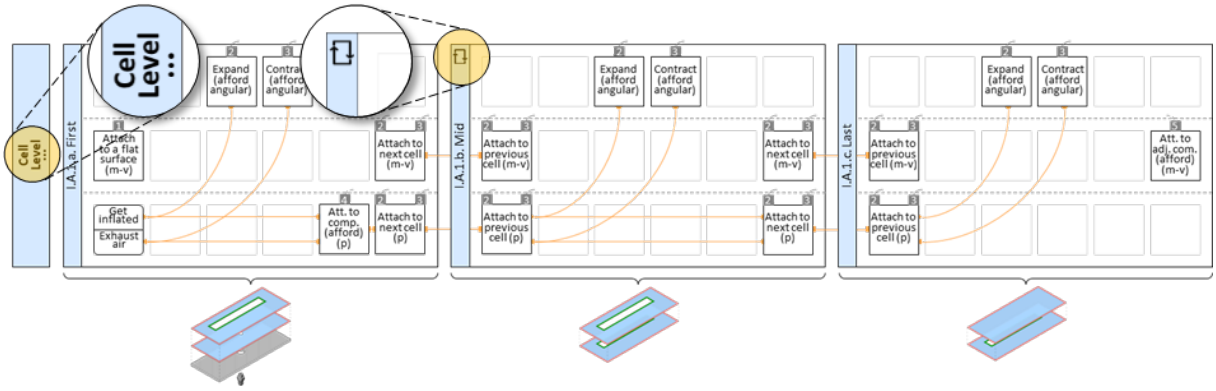

Figure 74. The representation of architectural components as part of the decomposition. The horizontal band representing the cell level contains a set of architectural component boxes that are labelled in outline form (e.g., I.A.1.a., I.A.1.b., and I.A.1.c.), where the label corresponds to a particular architectural component. Each of these architectural component boxes contains a figure that illustrates the corresponding architectural. There are often repeating architectural components (e.g., cell) used to form a higher-level architectural component in the hierarchy, which is indicated by the repeat sign (↻) used in the cell-label area of these architectural component boxes. There can be many unique architectural components that need to be represented to describe a decomposition to its full extent. In such cases, the continuation symbol *(...)* is used in the level-labelling area of the corresponding band to indicate that there are more architectural, therefore functional, components that are not being shown.

Depending on the complexity of the product system, there can be a large number of unique architectural components that need to be represented if the goal is to describe a decomposition to its full extent. In the case of visualizing only a relevant portion of a decomposition, it is important to visually indicate that there are more architectural, therefore functional, components that are not being shown. This is addressed by using a *continuation symbol (...)* in the level-labelling-area of the corresponding band as highlighted in Figure 74 (left). There are external constraints such as enclosures, brackets, fabric, and sliders that act as auxiliary architectural components to which the architectural components forming a constrained layer pneumatic system are attached. Although these auxiliary architectural components are not visualized as a part of the architectural hierarchy for brevity, their effects on generating higher-level functionalities manifest themselves especially at the assembly levels by modifying the assembly functions.

The functional components associated with a specific architectural component are represented within the corresponding architectural component box and are visualized by following the diagramming conventions described as a part of functional grammar (detailed in Section 3.1.2.). The organizational relationship among the functional components is visually indicated using compositional lines and connectors, and connectivity lines and connectors linking their boxes. The compositional lines link a set of constituent functional components to a set of constitutive functional components using their respective connectors that display target constitutive function

identification numbers, describing the relationship between adjacent levels (e.g., cell level and ensemble level) in the hierarchy. Some constitutive functional components are being contributed by a large number of constituent functional components. In such cases, instead of having many constituent connectors attached to the bottom edge of the constitutive functional component box, the *continuation symbol (...)* is used for compactness (Figure 75).

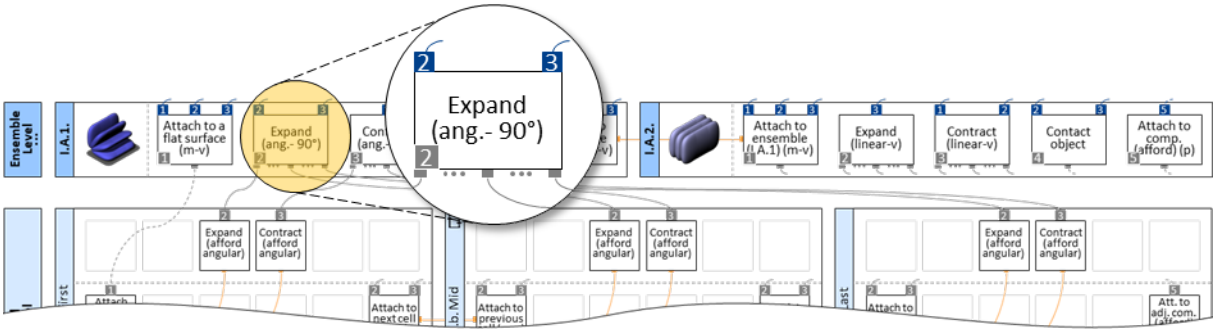

Figure 75. The representation of functional components as part of the decomposition. The functional components associated with a specific architectural component are represented within the corresponding architectural component box. The highlighted functional component, *expand (angular-90°)*, is associated with the vertical ensemble (I.A.1.), therefore is represented within its architectural component box.

The connectivity lines link two compatible functional components, which are placed in different architectural component boxes within the same level, using their respective connectivity connectors (Figure 76, left), indicating that there is a mechanical or pneumatic connection between these two functional components. The directionality related details of the mechanical connection between functional components (i.e., being attached horizontally or vertically) are textually described in the corresponding functional component boxes using abbreviations (i.e., (m-h), (m-v), or (m-h,v)). The directionality of the pneumatic connection between functional components (e.g., horizontally between skin layers or vertically through pneumatic attachments and tubing) has no effect on the resulting functional behavior of the cell, and therefore is not detailed.

Some constitutive functional components provide an affordance of a functionality (e.g., *contact external component (afford)*) instead of directly providing a functionality at a particular level in the hierarchy (e.g., cell level). This is indicated textually using *(afford)* in the corresponding functional component boxes. In such cases, the afforded functionality propagates to and being actualized at the higher levels in the hierarchy (e.g., ensemble level) (e.g., *contact object*) (Figure 76, right).

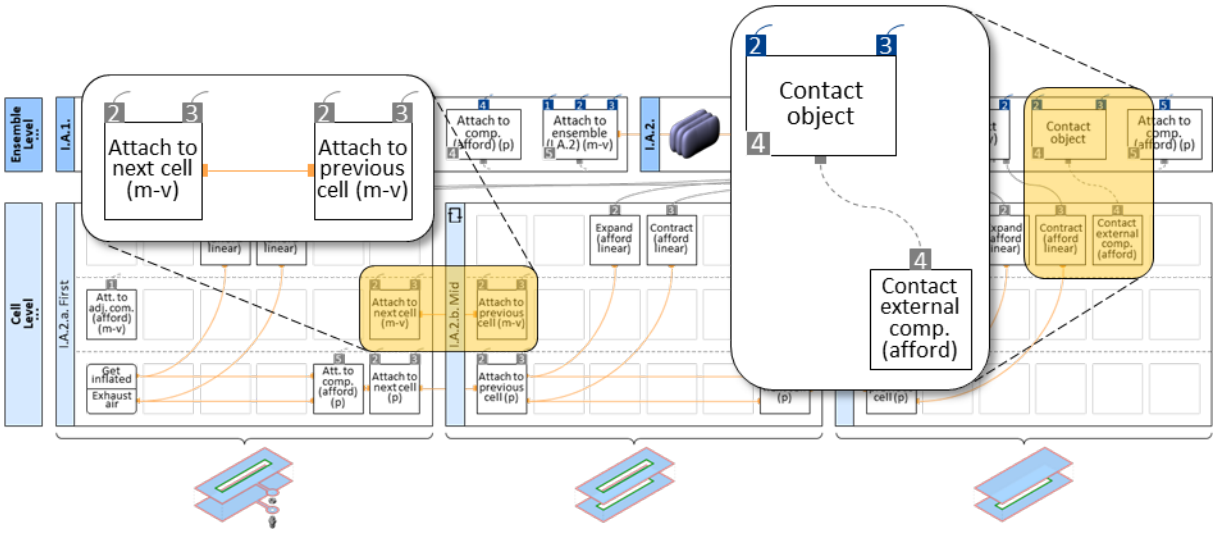

Figure 76. The use of connectivity connectors and lines, and actualization of affordance of a functionality. The connectivity lines (orange) mechanically or pneumatically link two compatible functional components, which are placed in different architectural component boxes within the same level, using their respective connectivity connectors (shown on the left). The afforded functionalities propagate to and are actualized at the higher levels in the hierarchy (shown on the right)

The functional component boxes representing the constituent basic functions (i.e., cell functions) are grouped and laid out in a three-row (top, middle, and bottom) format in their corresponding architectural component boxes at the cell level. The cell functions, which emerge from the sub-cellular construction and are primarily related to the physical behaviors a cell exhibits, are located and detailed on the top row at the cell level. The functional components that enable the organization among different types of adjacent cells or cell variations are located and detailed on the bottom (pneumatic, e.g., *attach to next cell pneumatically (p)*) and middle (mechanical, e.g., *attach to next cell mechanically (m)*) rows, detailing the connectivity among adjacent cells. A special pneumatic affordance component that provides two or more pneumatic affordance operations such as *get inflated, let air in, exhaust air,* and *vacuum* is located on the left-most portion of the bottom row and is differentiated from the functional component boxes by having rounded corners and divided into sections for each operation. The sections of this special component are linked to the relevant primary cell functions, which need pneumatic activation to perform their functionalities, and to the cell functions that are responsible for organizing the pneumatic connections among the functional components within and across levels throughout the hierarchy. This enables the traceability to and from the technology sub-capabilities throughout the functional hierarchy, providing direct view into the operational aspects of the product system.

By adhering to the functional grammar and diagramming conventions described, the constituent and constitutive functional components form the functional hierarchy. The functional hierarchy is displayed within the corresponding architectural hierarchy as a part of the hierarchical functional architectural decomposition approach, providing a direct view into the system hierarchy enabling the analysis of the existing systems and re-synthesis of alternative ones.

3.1.2. Functional Architectural Decomposition Example

The hierarchical functional architectural decomposition approach is demonstrated using the mobile phone restraint mat as an illustrative example, which provides context for the description of the approach throughout the system levels. The most basic architectural component, the cell, is constructed from its sub-cellular features. The functional and architectural components are then combined at each level from the cell level up to the system level, providing a direct view into the system hierarchy and producing a product system (i.e., device) that provides a set of technology capabilities at the highest level. Since the physical structures of constrained layer pneumatic product systems in general, and the mobile phone restraint mat in particular, are fundamentally hierarchical, the various architectural components are labelled in outline form according to this hierarchy (I., I.A., I.A.1. etc.) as shown in Figure 77.

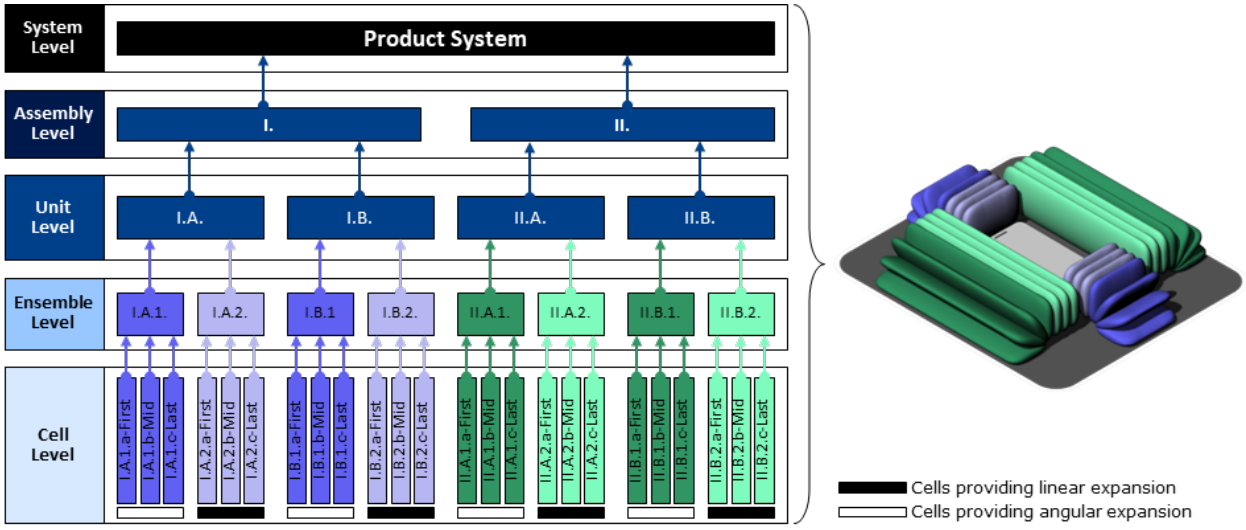

Figure 77. The decomposition of mobile phone restraint mat as an illustrative example. The mobile phone restraint mat is used to demonstrate the functional architectural decomposition approach. The architectural components composing the mobile phone restraint mat are labelled in outline form according to this hierarchy (I., I.A., I.A.1. etc.).

3.1.2.1. Cell Level

The cell level catalogues the types of cells, cell variations, the pneumatic affordances (e.g., get inflated, exhaust air), and the constituent basic functions (i.e., cell functions) in a three-row format, enabling the embodiment of a constrained layer pneumatic system. Any cell can be architecturally modified in many ways, generating a cell variation, which either replicates or modifies the existing cell function or introduces a new one. The nature or the number of cell functions emerging from the sub-cellular construction shows similarities or differences depending on the characteristics (e.g., perimeter shape or skin layer characteristics) of the sub-cellular features of the cells.

The sub-cellular features of one of the particular cells (I.A.1.a.) that make up the mobile phone restraint mat are compactly represented using the sub-cellular grammar template in categorical tabular form as an example in Figure 78. Skin characteristics are shared between the top and bottom layups that constitute this particular cell, whereas the constraints and some of the connection features vary between top and bottom layup. Accordingly, this cell (I.A.1.a.) is composed of highly flexible and extensible TPU layers that are of same thickness (0.2 mm) and transversally uniform. The top and bottom skin layers are mechanically connected to each other around their perimeter, forming a rectangular inflatable pouch, affording functions, *expand (afford angular)* and *contract (afford angular)*, later at the cell level. The perimeter of a cutout, which is located off-center on the inner region of the top skin layer, affords the mechanical connection to the bottom skin layer of the next cell with an identically located cutout (I.A.1.b.) to allow the formation of an ensemble at the ensemble level. Such off-centeredness affords *expand (angular-90°)* ensemble function. The bottom skin layer is permanently attached to a flat rigid base surface as an external constraint. A low-pressure barbed pneumatic fitting is attached to the bottom cell skin with a rubber washer and a hex nut through a 1/8-inch punched hole through the skin and through the flat rigid base surface, enabling control over pressure inside the cell. The off-centered cutout also affords a pneumatic connection between this (I.A.1.a.) and the adjacent cell (I.A.1.b.). These specified features provide a basis for cell and ensemble formation at the higher levels of the functional architectural decomposition. The mechanical and pneumatic connectivity among the adjacent cells is represented using connectivity connectors and lines, which are connecting compatible functional components (e.g., *attach to next cell (m-v)* or *(p)*).

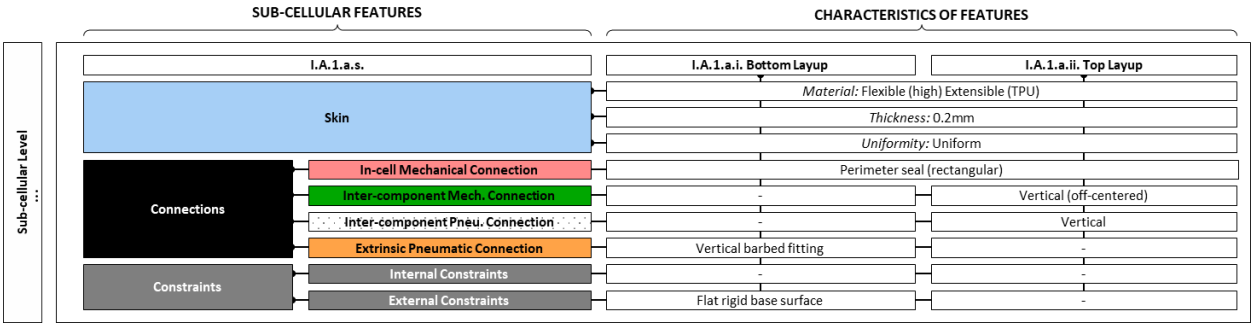

Figure 78. The sub-cellular feature characteristics of a cell. The characteristics of the sub-cellular features - skin, connections, and constraints - of one of the cell variations (I.A.1.a.s.) that constructs the mobile phone restraint mat are compactly represented using the sub-cellular grammar template in categorical tabular form as an example.

In the mobile phone restraint mat example, there are three cell variations within the particular vertical ensemble (I.A.1.): first (I.A.1.a.), mid (I.A.1.b.), and last (I.A.1.c.) cells (Figure 79). Each variation has slightly different sub-cellular feature characteristics, providing slightly different sets of constituent basic functions (e.g., *attach to a flat surface (m-v)*, *attach to adjacent component (m-v)*). For example, only the first cell is designed to be connected to an external air source, which is represented by a specific functional component with filleted corners providing pneumatic affordances such as *get inflated* and *exhaust air*, and gets vertically (v) mechanically (m) attached to a flat surface, whereas only the last cell can afford vertically (v) mechanically (m) getting attached to the adjacent architectural component (which is actualized at the ensemble level as *attach to ensemble (I.A.2.) (mechanical-vertical)*). The constituent basic functions enabling mechanical and pneumatic attachment to the adjacent cells, as well as providing *expand (afford angular)* and *contract (afford angular)* are shared among all cell variations. In the case of the cells within this example ensemble (I.A.1.), the expansion and the contraction are the primary functions and are qualified with the term (*afford angular*) denoting that how they are capable of aggregating to an *expand (angular-90°)* aggregate constitutive compound function at the ensemble level due to their off-centered inter-component mechanical connections.

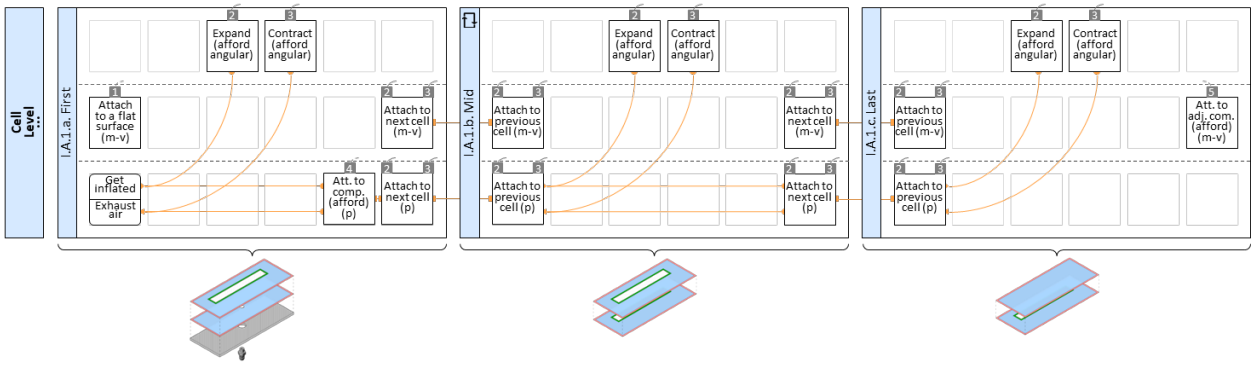

Figure 79. The cell level constituent architectural components (cells) and corresponding constituent basic functions. A set of cell variations (I.A.1.a., I.A.1.b., and I.A.1.c.) that form a particular ensemble (I.A.1.) of the mobile phone restraint mat system is represented at the cell level. Each variation has slightly different sub-cellular feature characteristics, providing slightly different sets of constituent basic functions as demonstrated.

It is useful to identify the relationship between the sub-cellular feature characteristics and the constituent basic functions of the cell, particularly in the presence of multiple cell variations. The inception of each one of these constituent basic functions provided by each cell variation can be traced back from the functional components of each cell via the function identification number of which background is color-coded to the sub-cellular feature categories (i.e., skin, connections, constraints) to the sub-cellular feature characteristics which give rise to the constituent basic functions (Figure 80). For example, *expand (afford angular)* functional component provided by the cell (I.A.1.a.) is assigned with number "*2*" as a function identification number with blue and black background. The rectangular boxes that are assigned with the same number with blue, pink, and green backgrounds represent the sub-cellular feature characteristics (e.g., *skin uniformity: uniform, in-cell mechanical connection: perimeter seal (rectangular)*, *inter-component mechanical connection: vertical (off-centered)*) that affect the emergence of the *expand (afford angular)* cell function. By changing the characteristics of sub-cellular features, the constituent basic functions of a cell can be adjusted or substituted with new functions.

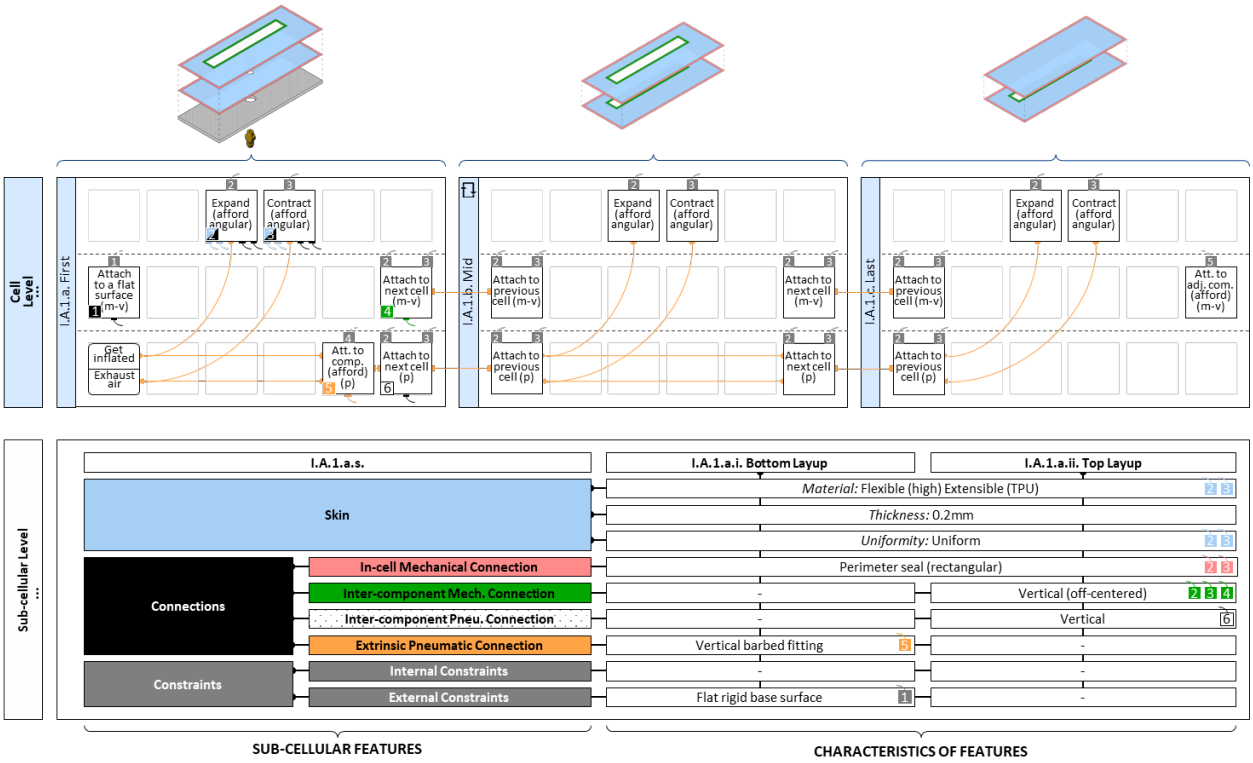

Figure 80. The relationship between the sub-cellular feature characteristics and the constituent basic functions of a cell. The inception of each one of the constituent basic functions provided by each cell variation can be traced back from the functional components of each cell via the function identification number of which background is color-coded to the sub-cellular feature categories (i.e., skin, connections, constraints) to the sub-cellular feature characteristics which give rise to the constituent basic functions.

3.1.2.2. Ensemble Level

The ensemble level describes the collection of cells that are assembled together to provide ensemble level constitutive architectural components and corresponding constitutive compound functions. Assembling multiple cells in a stacked fashion generates a vertical ensemble, and assembling multiple cells side by side on a plane generates a horizontal ensemble. The ability to assemble multiple cells in different ways to generate vertical or horizontal ensembles resides in the characteristics of sub-cellular features of those cells.

The architectural decomposition of the particular ensemble (I.A.1.) constituting the mobile phone restraint mat is shown in Figure 77. In this particular example, three cell variations (I.A.1.a., I.A.1.b., and I.A.1.c.), each has the sub-cellular feature of off-centered vertical inter-component mechanical (and pneumatic) connections, and thus are stacked on top of each other to form a constitutive architectural component, a vertical ensemble (I.A.1.). The corresponding functional decomposition at the ensemble level illustrates the combination of the constituent basic functions that each cell provides, producing constitutive compound functions such as *expand (angular-90°)*, effectively summing up the individual *expand (afford angular)* constituent basic functions of each cell. This accumulation of functions is synchronized both mechanically and pneumatically through the mutual mechanical and pneumatic attachments between adjacent cells (i.e., *attach to next/previous cell (mechanical-vertical)* and *attach to next/previous cell (pneumatic)*). While some constituent basic functions accumulate in the ensemble, others simply propagate to become functional components of the ensemble, such as the bottom cell's *attach to a flat surface (mechanical-vertical)*. Additionally, some functions, which provided affordances at the cell level (e.g., *attach to adjacent component (afford) (mechanical-vertical)*), are actualized at the ensemble level (e.g., *attach to ensemble (I.A.2.) (mechanical-vertical)*) since the two ensembles attach to each other to compound the unit (I.A.) (Figure 81).

In addition to the vertical ensemble (I.A.1.) providing the *expand (angular-90°)* ensemble function, a modified set of cells form a vertical ensemble (I.A.2.) providing an *expand (linear-vertical)* ensemble function. The difference in the sub-cellular features of the cells which make up this linear expansion ensemble relative to the cells which make up the angular expansion example

is that the vertical inter-component mechanical (and pneumatic) connections are centered rather than off-centered.

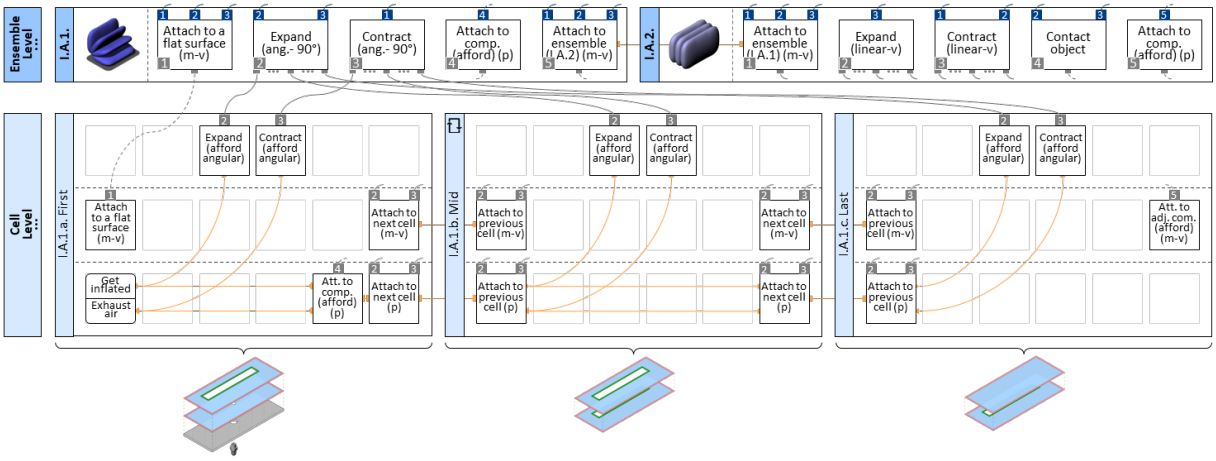

Figure 81. The ensemble level constitutive architectural components and corresponding constitutive compound functions. Three cell variations (I.A.1.a., I.A.1.b., and I.A.1.c.) are stacked on top of each other to form a constitutive architectural component, a vertical ensemble (I.A.1.). The functional aggregation of cell variations (I.A.1.a., I.A.1.b., and I.A.1.c.) creates a set of ensemble (I.A.1.) functions.

3.1.2.3. Unit Level

The unit level specifies the details of how multiple ensembles are combined together to produce a unit. In parallel with the architectural component combination, the constituent compound functions provided by the ensembles are combined into constitutive compound functions at the unit level.

In the mobile phone restraint mat example (Figure 82), the two ensembles shown (I.A.1. and I.A.2.) combine to form one of two identical units (I.A. and I.B.) which are oriented 180° apart within the assembly, combining and converting the various ensemble level constituent compound functions into unit level constitutive compound functions. For example, *attach to flat surface (mechanical-vertical), contract (angular-90°), attach to ensemble (I.A.1. & I.A.2.) (mechanical-vertical),* and *contract (linear-vertical)* ensemble level constituent compound functions combine to produce the heterogeneously emergent constitutive compound function, *stow,* at the unit level. Similarly, *attach to flat surface (mechanical-vertical), expand (angular-90°), attach to ensemble (I.A.1. & I.A.2.) (mechanical-vertical), expand (linear-vertical),* and *contact object* ensemble level constituent compound functions combine to produce another heterogeneously emergent constitutive compound function, *push (linear-horizontal)*, at the unit level (Figure 82). Similar to the ensemble level, *attach to cell ensemble (I.A.2.) (mechanical-vertical)* and *attach to cell ensemble (I.A.1.) (mechanical-vertical)* functional components cancel out in the formation of the

unit (I.A.). Architectural components such as unit (II.A.) and unit (II.B.) as well as the ensembles that are combined to produce these units provide functional components, which are architecturally identical to (although geometrically longer than) the ones provided by unit (I.A.) and unit (I.B.), therefore are not shown here for brevity.

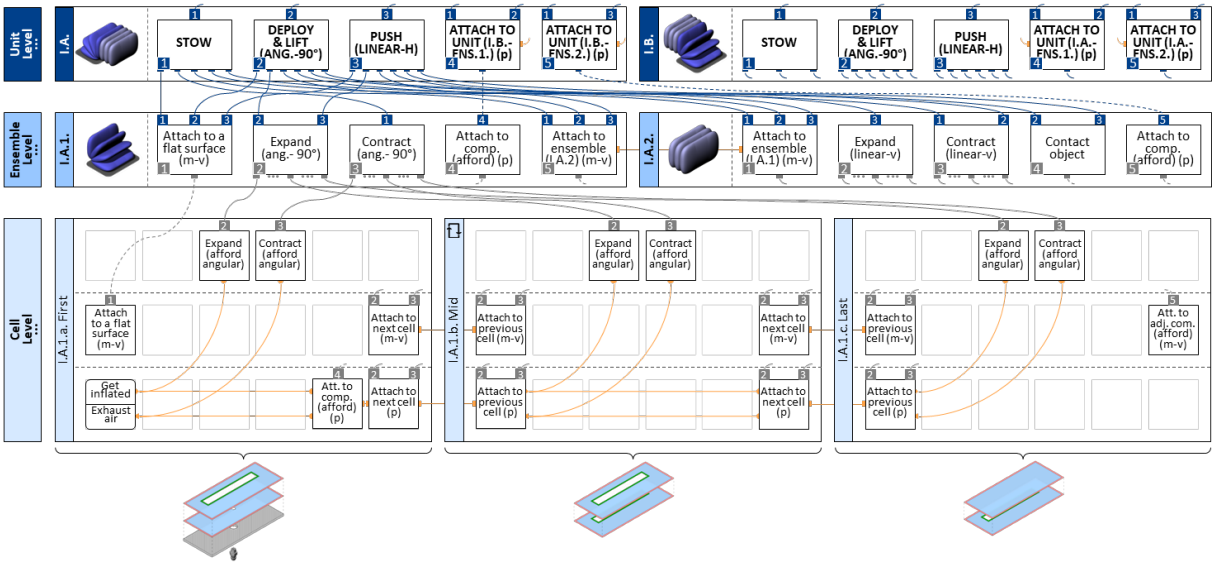

Figure 82. The unit level constitutive architectural components and corresponding constitutive compound functions. Two vertical ensembles (I.A.1. and I.A.2.) are stacked on top of each other to form a constitutive architectural component, a unit (I.A.). The functional aggregation of these vertical ensembles (I.A.1. and I.A.2.) creates a set of unit (I.A.) functions.

3.1.2.4. Assembly and System Level

The assembly level describes the details of how multiple units are architecturally and functionally combined together to produce a set of (sub)assemblies providing a set of assembly level constitutive compound functions. Assembling multiple units into a (sub)assembly may require the use of external components (e.g., brackets, enclosure). The combination of a set of (sub)assemblies produces the product system at the highest level in the architectural hierarchy, concurrently producing a set of technology (sub)capabilities at the highest level in the functional hierarchy. In general, the difference between the system level technology sub-capabilities and the assembly level functionalities highlights the difference between the device being acted upon by the user in the device's relevant operation state (at the assembly level) and the user's experience with the device in the user-device system's relevant interaction mode (at the system level).

In the mobile phone restraint mat example (Figure 83), the two assemblies shown (I. and II.) are formed as a result of the combination of two sets of two identical units (I.A. & I.B. and II.A. & II.B.) which are oriented 90° apart within the product system, aggregating, combining, and

converting the various unit level constituent compound functions into assembly level constitutive compound functions. For example, multiple instances of unit level constituent compound functions, *stow* and *deploy & lift (angular-90°),* are separately contributing to their constitutive compound function versions at the assembly level, fundamentally amplifying the same set of functionalities. However, two opposing instances of a particular unit level constituent compound function, *push (linear-horizontal)*, combine to produce the assembly level heterogeneously emergent constitutive compound function, *squeeze*. Further combination of the assembly level constituent compound functions at the system level produces three technology sub-capabilities as the assembly level architectural components combine to produce the product system at the highest level. These technology sub-capabilities are *stow, orient phone in X,* and *orient phone in Y* the further combination of which produce the overall technology capability: *orient phone automatically*.

The overall technology capability, *orient phone automatically,* is the primary user-facing purpose of the device while the three sub-capabilities directly map to the three user-device interaction modes (i.e., *stowing, orienting phone in X, and orienting phone in Y*). Each interaction mode requires the activation of a set functional components through their respective pneumatic affordance operations, denoted with operating sequence identification letter (e.g., a, b, c, d). Note that the three technology sub-capabilities and the emergent technology capability all reside within the system level in the functional hierarchy.

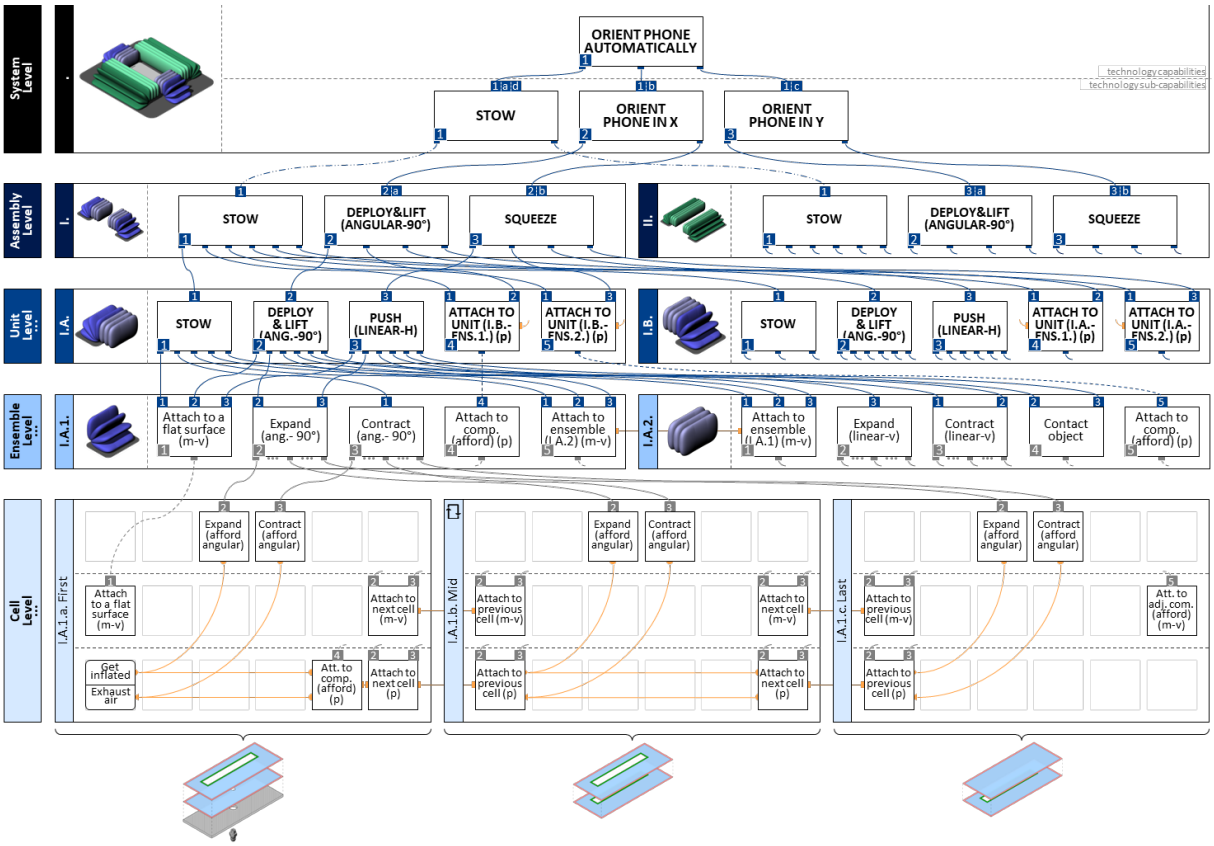

Figure 83. The (partial) functional architectural decomposition of mobile phone restraint mat. Two assemblies (I. and II.) are formed as a result of the combination of two sets of two identical units (I.A. & I.B. and II.A. & II.B.) within the product system, aggregating, combining, and converting the various unit level constituent compound functions into assembly level constitutive compound functions. Further combination of the assembly level constituent compound functions at the system level produces three technology sub-capabilities as the assembly level architectural components combine to produce the product system at the highest level. These technology sub-capabilities are *stow, orient phone in X,* and *orient phone in Y* the further combination of which produce the overall technology capability: *orient phone automatically*.

3.1.2.5. Pneumatic Operating States and Sequences

The hierarchical functional architectural decomposition of the mobile phone restraint mat describes three system-level interaction modes each of which needs to be operated using their respective pneumatic affordance operations (Figure 84). The cyclic sequence of the operation of these interaction modes is denoted with the system-level operating sequence identification letters (a, b, c, and d), which are assigned to the corresponding technology sub-capabilities provided at the system level: *a)* the initial stowed mode, sequentially orienting the mobile phone in the *b)* x and *c)* y directions, and *d)* returning to the stowed mode upon accomplishing the intended task, completing the cycle as *a* and *d* both label the same interaction mode. Each one of the sequential orienting operation steps (*b* and *c*) relies on the sequential deployment of two sets of ensembles for each direction (i.e., x and y) separately (Figure 84, assembly level). Each of these two-step

operations is denoted with assembly-level operating sequence identification letters (*a, b*). For the x direction, within assembly I., the first two ensembles (I.A.1. and I.B.1., which are constituent architectural components of their respective opposing units I.A. and I.B.) that are attached to the base mat, angularly deploy and inwardly lift the mobile phone. Then, the second two ensembles (I.A.2. and I.B.2., which are the remaining constituent architectural components of the same opposing units I.A. and I.B.) that are vertically attached to the angularly deploying ensembles, linearly push the mobile phone to the center of the charging mat before finally squeezing it to ensure the ideal orientation in the x direction. The same sequence is repeated for the y direction within assembly II. by using the remaining two sets of ensembles (II.A.1. and II.B.1, II.A.2. and II.B.2.). This results in positioning the mobile phone on the charging mat in the ideal orientation for maximizing the charging efficiency.

The cyclic operation sequence can be traced from the system level down to the cell level using compositional and connectivity lines. In this manner, the modes forming the operation sequence are mapped to the corresponding pneumatic affordance operations, providing an understanding of how the system operates. For example, to orient the mobile phone in the x direction (system-level operation sequence *b*), assembly I. needs to angularly deploy and lift the phone first, and then center it on the mat by squeezing it (the operational tracing is shown in Figure 84 using red and blue highlights). This is enabled by two separate assembly functions, *deploy & lift (angular-90°)* and *squeeze,* both requiring separate pneumatic affordance operations. To activate the *deploy & lift (angular-90°)* assembly function, each cell composing the pneumatically connected ensembles (I.A.1.) and (I.B.1.) needs to be inflated, whereas the air in each cell composing the pneumatically connected ensembles (I.A.2.) and (I.B.2.) needs to be exhausted. This is accomplished by simultaneously activating two separate pneumatic affordance operations: 1) *get inflated* in cell I.A.1.a., which simultaneously inflates the remaining cells composing ensemble I.A.1. through the pneumatic connectivity cell functions, *attach to next/previous cell (pneumatic),* as well as simultaneously inflating the opposing ensemble I.B.1. through the relevant pneumatic connectivity unit functions, and 2) *exhaust air* in cell I.A.2.a., which similarly simultaneously deflates the remaining cells composing ensemble I.A.2. and all of ensemble I.B.2.. To activate the *squeeze* assembly function, each cell composing the pneumatically connected ensembles (I.A.1.) and (I.B.1.) needs to maintain their inflated state, and each cell composing the pneumatically connected

ensembles (I.A.2.) and (I.B.2.) needs to be inflated, requiring two separate identical pneumatic affordance operations: *get inflated* in cell I.A.1.a., and *get inflated* in cell I.A.2.a..

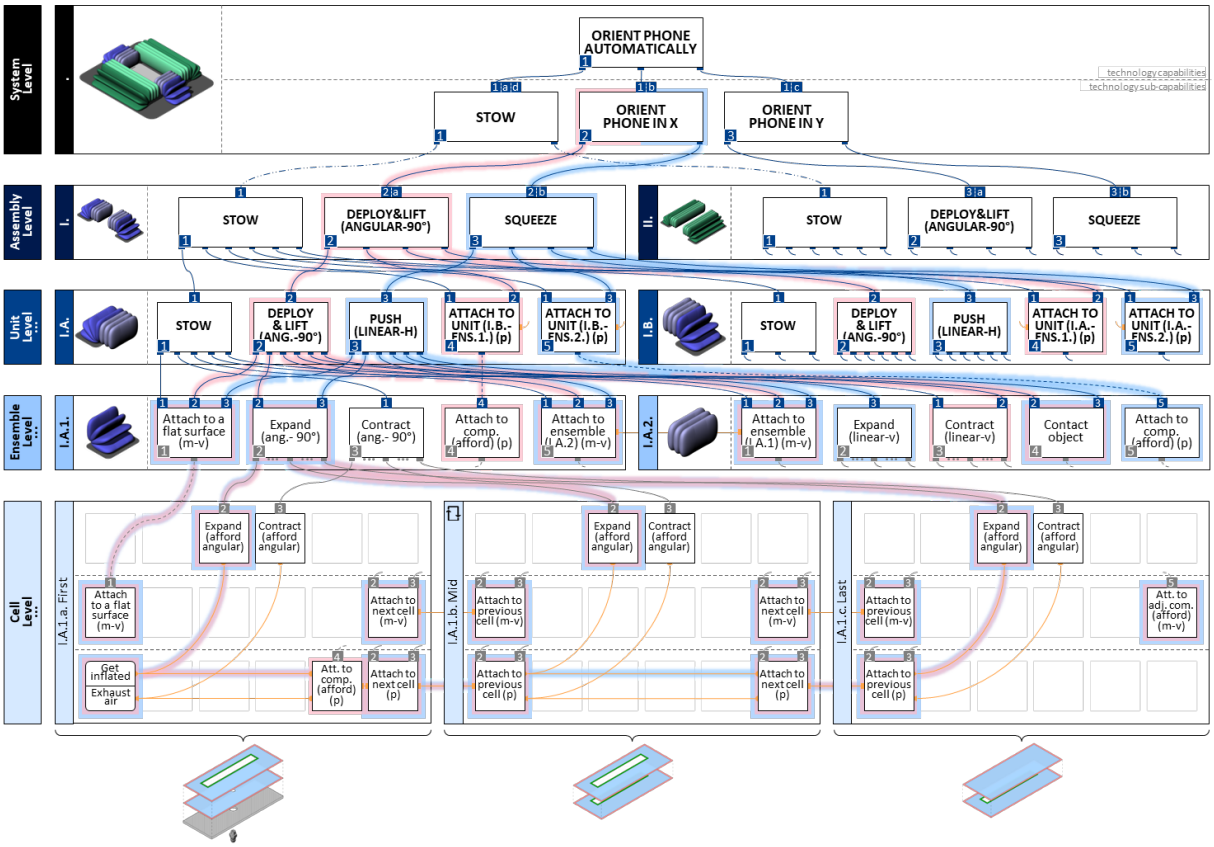

Figure 84. The pneumatic operating states and sequences of the mobile phone restraint mat. The cyclic operation sequence (indicated by letters *a,b,c,* and *d*) of technology sub-capabilities can be traced from the system level down to the cell level using compositional and connectivity lines. In this manner, the modes forming the operation sequence are mapped to the corresponding pneumatic affordance operations, providing an understanding of how the system operates.

Note that this sequence (system-level operation sequence *b*), defining the *orient phone in x* sub-capability, represents one possible sequencing of pneumatic affordance operations *get inflated* and *exhaust air* in cells I.A.1.a. and I.A.2.a.. The exact same sequencing of pneumatic affordance operations is used in cells II.A.1.a. and II.A.2.a. to activate the *orient phone in y* sub-capability. Differently from these two sub-capabilities, the remaining sub-capability, *stow*, is achieved through a simultaneous activation of *exhaust air* pneumatic affordance operation in cells I.A.1.a., I.A.2.a., II.A.1.a., and II.A.2.a.. Not all combinations or sequences of the relevant pneumatic affordance operations are employed in this product system. In general, different combinations and sequences of pneumatic affordance operations can be used to produce different functionalities depending on the design context.

The traceability of the cyclic sequence of operation modes by using hierarchical functional architectural decomposition provides insights regarding the multi-faceted relationship among the technology (sub)capabilities, the functional components, the architectural components, and the selective activation of combinations/sequences of pneumatic affordance operations, enabling an integrated understanding of how the system works.

3.1.3. Structural Features

To ensure a consistent and transferable iterative analysis and synthesis of constrained layer pneumatic product systems as well as the re-synthesis of alternative systems using existing systems as a basis, the hierarchical functional architectural decomposition of constrained layer pneumatic product systems must incorporate a set of structural features regarding the functional and architectural hierarchies. In the functional hierarchy, other than the highest-level functional components (e.g., technology capabilities), all functional components must have a constituent role (i.e., a function should serve a higher-level role to appear in the hierarchy). Similarly, other than the lowest-level functional components that act as constituent basic functions (e.g., cell functions), all functional components must be constituted from lower-level functional components. Thus, new functional components cannot be created or destroyed, tracing up or down respectively through the hierarchy. As a result, the system level functional components can be traced back to their lowest-level constituent functional components and to the corresponding characteristics of the sub-cellular features that give rise to these functional components. This enables the identification of the relevant design variables and the causes of potential performance couplings and the potential ways to mitigate such couplings by making aggregational or component-wise modifications in the system which affects architectural and functional hierarchies simultaneously.

The resulting structures that emerge from functional and architectural hierarchies are the result of the grammars used to form them. The architectural hierarchy can be represented as a tree structure unlike the functional hierarchy, which often contains a lower-level functional component (e.g., an ensemble function) composing multiple higher-level functional components (e.g., unit functions) simultaneously. These higher-level multiple functional components (e.g., unit functions) themselves often compose a single higher-level functional component (e.g., an assembly function), therefore generating functional loops in the functional hierarchy. Because each

functional component resides within a specific architectural component, such functional loops reside within and must respect the tree graph structure of the architectural hierarchy.

The structure of the functional architectural hierarchies exposes an understanding of design relationships and couplings from the sub-cellular feature characteristics up to the system level technology (sub)capabilities. In some cases, a product system has a relatively flat architectural hierarchy at a lower level of which (e.g., ensemble level) the product system is fully architecturally composed (e.g., ensemble = product system). The fully composed product system at the lower level of the architectural hierarchy (e.g., ensemble level) must be represented as an architectural component of that respective level (e.g., ensemble) and must directly propagate upwards through multiple levels in the architectural hierarchy until the system level. The functional hierarchy, however, does not mirror the architectural propagation since it potentially incorporates aggregate and emergent constitutive functional components at each level alongside with the propagated constitutive functional components due to the changing context up through the system hierarchy levels. In such cases containing direct propagation (i.e., a flat hierarchy) of architectural components from lower levels to higher levels in the architectural hierarchy, there generally exist trade-offs among performance levels of various technology sub-capabilities. Conversely, the more hierarchical a system's architecture is, the less performance levels of various sub-technology capabilities tend to be coupled. Thus, the hierarchical functional architectural decomposition approach provides not only a tool for conceptual design of constrained layer pneumatic product systems but also a tool for aiding parametric design (note: this is done explicitly in Chapter 4).

3.2. Design Strategies for Re-Synthesizing Existing Constrained Layer Pneumatic Systems

The hierarchical functional architectural decomposition approach provides a direct and holistic analysis of a constrained layer pneumatic product system's architecture, functionality, and performance aspects, affording a re-synthesis of an existing already-synthesized system. In this context, a constrained layer pneumatic product system architecture comprises a set of architectural components and governs the hierarchical relationships among these architectural components. A constrained layer pneumatic product system embodies a range of high-level functionalities (e.g., technology sub-capabilities) attainable by employing the lower-level functionalities of its architectural components. The quality of performance of these capabilities is measured by using a

relevant set of performance metrics through each operation state required to accomplish the tasks targeted by the constrained layer pneumatic product system.

Because the hierarchical functional architectural decomposition approach simultaneously relates the architectural hierarchy and functional hierarchy through the system hierarchy, it enables the tailoring and adaptation of the existing systems' architecture, functionality, and performance aspects, generating alternative and novel designs. These existing systems' architecture, functionality, and performance aspects are often coupled to one another. Changing one of them affects the remaining aspects, which introduces potential tradeoffs. For example, simplifying the architectural components of an existing system to reduce the manufacturing costs might potentially make a negative impact on the resulting re-synthesized system's performance, or changing the architectural components to expand the existing system's functionality might potentially require more complicated architecture. Therefore, the use of the hierarchical functional architectural decomposition approach for the iterative analysis and re-synthesis of an already existing constrained layer pneumatic system requires a systemization, a set of design strategies, which would aid the identification of potential re-synthesis opportunities and the consequent tradeoffs among the system aspects before making any design modification at a conceptual design stage.

The design strategies systematize the re-synthesis of an existing constrained layer pneumatic product system by enabling the identification of the design goals that motivate the re-synthesis, the design objectives that are to be achieved while implementing the defined goals, the design modifications that actualize these design goals, and the potential design tradeoffs that emerge as a result of the design modifications. The implementation of these strategies is demonstrated through a set of re-synthesis examples of the constrained layer pneumatic product systems that were previously introduced in Chapter 2. A qualitative evaluation of the potential performance parametric and architectural couplings, providing design guidelines for the future re-syntheses of the existing constrained layer pneumatic product systems.

3.2.1. Design Strategy Elements for Re-synthesis

The proposed design strategies are defined by the way they address four main strategic elements that drive the re-synthesis process: 1) *design goals*, which are determined to make a desirable improvement targeting the system's architecture, performance, and/or functionality, i.e., *why* the design change is being made, 2) *design objectives*, which identify the primary impact of

the design change, i.e., *what* design change is being made, 3) *design modifications*, which encompass the specific actions that are going to be taken to update the system's current state, i.e., *how* the design change is being made, and 4) *design trade-offs*, which are the potential adverse effects on the system's architecture, performance, and/or functionality that are coupled to the desirable improvements determined by the design goals, i.e., *why-not* make the design change.

Design strategies can be categorized into three main types: *re-design*, *incremental innovation,* and *radical innovation*. Although a design objective (i.e., re-implementing, adjusting, or changing functionality) is the primary impact that the re-synthesis is striving for, initiating a re-synthesis process would be abstract and difficult without having a design goal and associated potential tradeoffs already defined. Having a design goal provides a purpose for the re-synthesis, such as simplifying architecture or expanding technology capability, while motivating the design modifications. The design modifications govern the structural changes in the system affecting the physical design of the components or the aggregation of the components. As a result of these changes, tradeoffs related to system aspects often emerge. For example, changing components to simplify architecture may only be achievable if a decreased performance is allowed in many design cases.

The design goals (*WHYs*) and tradeoffs (*WHY-NOTs*) are detailed in relation to each other since there is usually a reciprocal interdependence between them as outcomes of the design strategy. Similarly, the objectives (*WHATs*) and modifications (*HOWs*) together describe the nature of a design change and are also detailed in relation to each other as the approach taken by the design strategy. Ten design strategies emerge from various combinations of these elements, aiming to facilitate the re-synthesis of existing constrained layer pneumatic product systems using the hierarchical functional architectural decomposition approach.

3.2.1.1. Design Goals and Trade-offs

A design goal provides a desirable purpose for which a set of modifications in an existing architecture is meant to achieve. However, modifying the architecture for achieving the desired purpose that is set by the design goal often generates an undesired outcome, i.e., a tradeoff, which may negatively affect at least one of the remaining system aspects.

As a part of the design strategies for re-synthesizing existing constrained layer pneumatic product systems using the hierarchical functional architectural decomposition approach, four relevant design goals and three design tradeoffs are identified. These are: *simplification of the*

architecture, *enhancement of the performance*, *expansion of the technology capability*, and *discovery of new technology capability* for the design goals, and *complexification of the architecture, decrease in the performance,* and *reduction of the technology capability* for the design tradeoffs.

Figure 85 tabulates four design goal and tradeoff couplings in relation to which system aspect they affect. The first three design goals together interact with all the design tradeoffs as indicated by the number-coded boxes under each goal and tradeoff, whereas the fourth design goal, the discovery of new technology capability, is independent of any design tradeoffs.

	ARCHITECTURE	PERFORMANCE	FUNCTIONALITY	
GOAL (WHYs)	Simplify 1 2	Enhance 3	Expand 4	Discover 5
TRADE-OFF (WHY-NOTs)	Complexify 3 4	Decrease 1	Reduce 2	-

Figure 85. Design goal and tradeoff couplings in relation to the system aspects they affect. Each one of the first three design goals, *simplification of the architecture, enhancement of the performance,* and *expansion of the technology capability*, interact with the design tradeoffs as indicated by the number-coded boxes under each goal and tradeoff. The fourth design goal, *discovery of new technology capability*, is independent of any design tradeoffs.

The five cases (four couplings plus discovery) have various potential effects from implementing the design goals with their respective tradeoffs imposed on the resulting system's architecture, performance, and/or functionality, and are detailed as follows:

1. ***Simplification of the architecture vs decrease in the performance:*** Simplifying the physical components that make up the architecture of a system is desirable and potentially serves many purposes such as potentially reducing the manufacturing costs, enabling easier operation, or ease of maintenance. However, such simplifications often introduce reduction in performance quality. In some design cases, the achievable performance quality with an existing system might be more than required to successfully perform a set of targeted design tasks. In redesign contexts, a decrease in the performance quality of such systems through re-synthesis in the conceptual stage which results from the simplification of a set of architectural components may be permissible, lending itself to systems with less complicated architecture that provides just the right amount of usefulness to its user.

2. ***Simplification of the architecture vs reduction of the technology capability:*** One (or more) of multiple functionalities that construct the overall technology capability can be removed if it is not crucial for completing the targeted task. This reduction of technology capability introduces an opportunity to simplify the architecture of the existing system since there is an interdependence between the functional and architectural hierarchies in the context of constrained layered pneumatic product system design. Since the technology capabilities offered by the re-synthesized system are reduced and therefore fundamentally different than those of the existing system, the performance qualities of the existing and re-synthesized systems become incomparable.
3. ***Enhancement of the performance vs complexification of the architecture:*** Enhancing the performance of a technology capability (e.g., accomplishing the targeted task faster or more precisely) generally improves the usefulness of a system, and potentially provides a more satisfactory user experience. However, a given design concept may have a limit to the performance attainable through parametric design, necessitating a change in design concept which can be achieved through changing its architecture. Such an architectural change may increase the complexity of the existing system but may be justifiable to achieve the enhanced performance.
4. ***Expansion of the technology capability vs complexification of the architecture:*** Technology capabilities are the highest-level functionalities that are provided by a constrained layer pneumatic product system to a user in a particular design context. Expanding these capabilities (e.g., expanding "provide rollability" to "provide shapability") through a re-synthesis is one way of generating an incremental or radical innovation, which targets different design contexts requiring different design tasks. Since there is an interdependent coexistence of the functional and architectural hierarchies in any constrained layer pneumatic product system, an attempt to expand the highest-level functionalities (technology capabilities) in a system will require a set of changes regarding its architectural components, often resulting in a more complicated architecture. Since the technology capabilities offered by the re-synthesized system are expanded and therefore fundamentally different than those of the existing system, the performance qualities of the existing and re-synthesized systems become incomparable as well.

5. ***Discovery of new technology capability:*** Technology capabilities can be repurposed as a result of a change in the architectural hierarchy in an existing system, enabling a discovery of new technology capabilities. Since the resulting re-synthesized system's overall functionality, architecture, and performance aspects differ from the existing one, no trade-offs are associated with the discovery of new technology capabilities as a design goal. Rather, a completely new system emerges.

3.2.1.2. Objectives and Modifications

A design objective identifies the primary impact of carrying out a re-synthesis. An objective can be either *re-implementing the existing functionalities, adjusting the existing functionalities,* or *changing the existing functionalities* provided by a constrained layer pneumatic product system. The ability to re-implement the existing functionalities provided by a product system enables the design of alternative product systems with alternative architectural hierarchies while providing the same set of highest-level functionalities, while meeting a design goal related to improving some aspect of architectural complexity or quality of performance. The same set of existing functionalities can be adjusted to be expanded or reduced by modifying the existing architectural hierarchy, which enables the generation of alternative product systems with altered architectural hierarchies affording incremental change in the provided set of functionalities trading off with some aspect of architectural complexity. The existing functionalities can also be changed completely by modifying the existing architectural hierarchy, which enables the design of alternative product systems with different architectural hierarchies affording radical change (i.e., discovery) of the provided set of functionalities.

Re-implementing, adjusting, or changing functionalities can be achieved at any hierarchical level by modifying the relevant architectural components of a system, serving the purpose of tailoring the system's architectural, functional, and performance aspects to achieve desired design goals. Design modifications can be categorized into two groups: *changing components* or *changing aggregation*. The six combinations of design objectives and modifications that can be employed as a part of the re-synthesis process are detailed as follows:

1. ***Re-implementing functionalities by changing components:*** One way of re-implementing the functionalities provided by an existing constrained layer pneumatic product system is to make component-level modifications, which often affects the overall architecture of a system. These component-level modifications (e.g., replacing an ensemble with a simpler

ensemble that provides the same function) might take place at any level of the architectural hierarchy, producing architectural components with alternative designs that contribute to the existing highest-level functionality. The ability of providing same highest-level functionality using modified components facilitates tailoring the system's performance and/or the complexity of its architecture.

2. ***Re-implementing functionalities by changing aggregation:*** Another way of re-implementing the functionalities provided by an existing constrained layer pneumatic product system is to make aggregational modifications. These aggregational changes (e.g., repeating a unit in parallel to amplify performance of its existing function) affect the overall architecture of the existing system without affecting the lower-level architectural components composing the system, producing alternative design which preserves both the higher and lower-level functional components, and the constituent architectural components. The quality of the system performance and/or the complexity of the architecture can be tailored by making such aggregational modifications.
3. ***Adjusting functionalities by changing components:*** Functionalities provided by an existing product system can be adjusted by making component-level modifications (e.g., increasing the complexity of an existing cell to expand the existing cell function) that can be initiated at any hierarchical level, producing architectural components with alternative designs that alter the existing higher-level functionality. Such adjustments can produce incremental innovations providing expanded or reduced technology capabilities. Since there is a fundamental change in capability, performance before and after re-synthesis is no longer comparable.
4. ***Adjusting functionalities by changing aggregation:*** An alternative way of adjusting functionalities provided by an existing constrained layer pneumatic product system is to make aggregational modifications (e.g., duplicating an ensemble oppositionally in parallel to introduce an extension of its existing function) that influence the overall architectural hierarchy of the system without affecting the lower-level architectural components. This enables incremental innovations, providing expanded or reduced technology capabilities. The performance of the system before and after re-synthesis is no longer comparable due to the fundamental change in capabilities.

5. ***Changing functionalities by changing components:*** Functionalities provided by an existing system can be changed by making component-level modifications (e.g., replacing a cell with a different cell that provides a new, different cell function or an expansion of the current cell function) that can be initiated at any hierarchical level, producing architectural components with alternative designs that change the existing higher-level functionality. These changes can produce radical innovations providing completely new capabilities due to which performance before and after re-synthesis is not comparable.
6. ***Changing functionalities by changing aggregation:*** An alternative way of changing functionalities is making aggregational modifications (e.g., repurposing a cell ensemble which currently provides a particular functionality in its current architectural context by placing it in a different architectural context where it affords a different functionality), which does not impose any modification on the lower-level architectural components and can be initiated at any hierarchical level above the cell level. This aggregational change enables a re-synthesis process resulting in a radical innovation, creating a new product with a new set of capabilities. The performance before and after re-synthesis is not comparable due to the newly discovered capability.

3.2.1.3. Design Strategy Directions

Each re-synthesis design strategy comprises a design objective, a design goal, a design modification, and an associated tradeoff (if applicable). A design objective is achievable by actualizing a design modification to attain a design goal while allowing a design tradeoff. Based on this, ten distinct design strategies encompassing different combinations of design strategy elements for the re-synthesis of an existing constrained layer pneumatic product system are formulated. These proposed design strategies enable designers to generate variations of existing systems during the early-stage product design process, guiding them to three overall design strategy directions: *re-design, incremental innovation,* and *radical innovation*. These strategies are laid out schematically in Figure 86 in tabular form where the three columns correspond to three design objectives, re-implement functionalities, adjust functionalities, and change functionalities, and the two major rows correspond to two design modifications, change component and change aggregation. Each cell in the first two columns of the table is split horizontally into two sub cells corresponding to reciprocal directions of the corresponding design goal and trade-off. The goals

and trade-offs referred to in the table are listed below the table. Each sub cell contains a statement of the design strategy in terms of the design objective that is achieved by the modification that is made to obtain the particular design goal while allowing the particular trade-off. The table is partitioned by shading into sections corresponding to the three design strategy directions, which map one-to-one to the three design objective columns:

1. ***Re-design:*** The purpose of re-design is to revise an existing constrained layer pneumatic product system, targeting a better fit to a design context regarding their complexity of architecture and quality of performance. There are four design strategies that drive re-synthesis toward the re-design direction. Each of these strategies focuses on re-implementing existing functionalities while tailoring trade-offs between the complexity of architecture and the quality of performance by changing the existing architectural components or by changing the aggregational aspects of the existing architectural hierarchy. This direction corresponds to the left (gray) column of the table in Figure 86.
2. ***Incremental innovation:*** The purpose of incremental innovation is to provide an improvement of an existing constrained layer pneumatic product system induced by changes in its architecture, performance, and/or functionality. There are four design strategies that drive re-synthesis toward the incremental innovation direction. Each of these strategies focuses on adjusting the existing functionalities while tailoring trade-offs between the extent of the resulting functionalities and the complexity of the architecture by changing the existing architectural components or by changing the aggregational aspects of the existing architectural hierarchy. This direction corresponds to the middle (light red) column of the table Figure 86.
3. ***Radical innovation:*** The purpose of radical innovation is to provide the ability to develop new systems that use an existing constrained layer pneumatic product system as a starting point. There are two design strategies that drive re-synthesis toward the radical innovation direction. Both strategies are geared towards changing existing functionalities to provide new technology capabilities to users. While all the previously mentioned strategies require tailoring the tradeoff between the complexity of architecture and the quality of performance (left column in Figure 86) or the tradeoff between the complexity of architecture and the extent of functionality (middle column in Figure 86), the remaining two design strategies

enabling radical innovation (right column in Figure 86) adopts the discovery of new functionalities and is independent of any trade-offs.

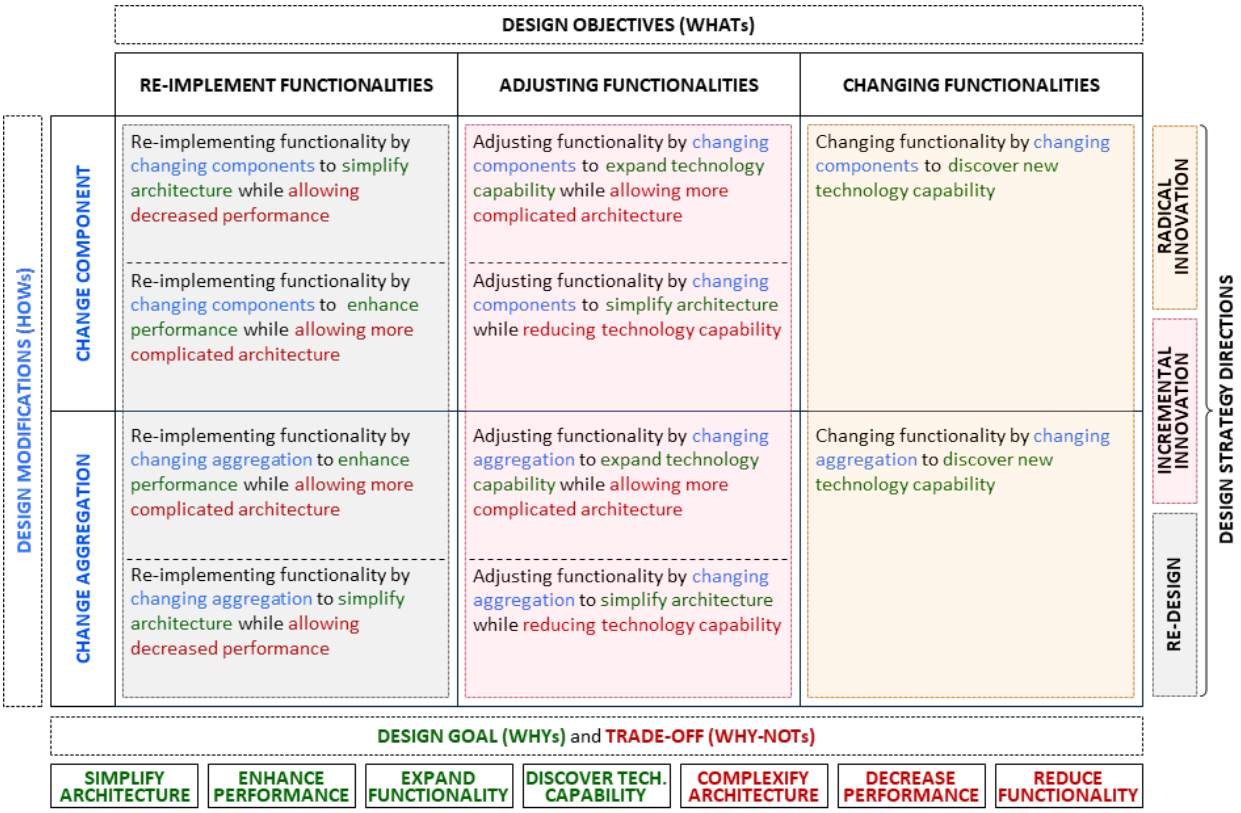

Figure 86. Re-synthesis design strategies. Each design strategy comprises a design objective (WHAT), a design goal (WHY), a design modification (HOW), and an associated tradeoff (WHY-NOT) (if applicable). A design objective is achievable by actualizing a design modification to attain a design goal while allowing a design tradeoff. Based on this, ten distinct design strategies encompassing different combinations of design strategy elements for the re-synthesis of an existing constrained layer pneumatic product system are formulated. These proposed design strategies enable designers to generate variations of existing systems during the early-stage product design process, guiding them to three overall design strategy directions: *re-design, incremental innovation,* and *radical innovation*.

These ten design strategies for the re-synthesis of existing constrained layer pneumatic product systems using the hierarchical functional architectural decomposition approach empowers designers to generate design alternatives of any constrained layer pneumatic product systems at a conceptual level as a part of the early-stage product design process. Each one of these design strategies will be demonstrated using the previously introduced constrained layer pneumatic product system examples as starting points to develop alternative designs.

3.2.2. Re-synthesized Design Examples

The ten proposed design strategies that can guide the re-synthesis process in the direction of re-design, incremental innovation, and radical innovation are demonstrated using a set of already-

synthesized constrained layer pneumatic product systems as starting points, lending themselves to the generation of early-stage conceptual design alternatives. The generation of these conceptual design alternatives highlights the adaptability of the hierarchical functional architectural design approach as a design tool capitalizing on the systematic formulation of design objectives, modifications, goals, and tradeoffs as a set of design strategies that can be adopted for the re-synthesis process. The first two design strategy directions, re-design and incremental innovation, are demonstrated using two re-synthesis examples each, whereas the last design strategy direction, radical innovation, is demonstrated using four re-synthesis examples.

3.2.2.1. Re-design

For the re-design of already existing constrained layer pneumatic product systems, four design strategies containing two pairs with reciprocal design goals of tradeoffs are proposed:

- RD-1) Re-implementing functionality by changing components to simplify architecture while allowing decreased performance,
- RD-2) Re-implementing functionality by changing components to enhance performance while allowing more complicated architecture,
- RD-3) Re-implementing functionality by changing aggregation to enhance performance while allowing more complicated architecture, and
- RD-4) Re-implementing functionality by changing aggregation to simplify architecture while allowing decreased performance.

The mobile phone restraint mat is re-synthesized as an example to demonstrate the application of the first and second (reciprocal) re-design strategies (RD-1, RD-2). The active rear seat pocket is re-synthesized as an example to demonstrate the application of the third and fourth (reciprocal) re-design strategies (RD-3, RD-4).

3.2.2.1.1. Re-design Example #1: Mobile Phone Restraint Mat V1 to V2 (RD-1 & RD-2)

The hierarchical functional architectural decomposition of the mobile phone restraint mat, which automatically positions and orients a mobile phone over an inductive charger, was detailed in previous sections (e.g., section 3.2.). Its architecture consists of two assemblies, which are architecturally identical (although parametrically of different lengths) and are made of two pneumatically connected opposing units (Figure 87). Each of these units is made of two

pneumatically separate vertical ensembles that are stacked on top of each other. The first ensemble attaches to the base mat and produces aggregate angular expansion and contraction. The second ensemble attaches to the first and provides aggregate linear expansion and contraction. The resulting unit functions, *deploy & lift (angular-90°)* and *push (linear-horizontal)*, contribute to the assembly functions, *deploy & lift (angular-90°)* and *squeeze*, which are operated in a particular sequence to produce the technology sub-capability, *orient phone in x*. A cyclic operation sequence of *orient phone in x* with the remaining sub-capabilities, *stow* and *orient phone in y*, each requiring their own operation combination/sequence of assembly functions, produces the overall technology capability, *orient phone automatically*, at the system level.

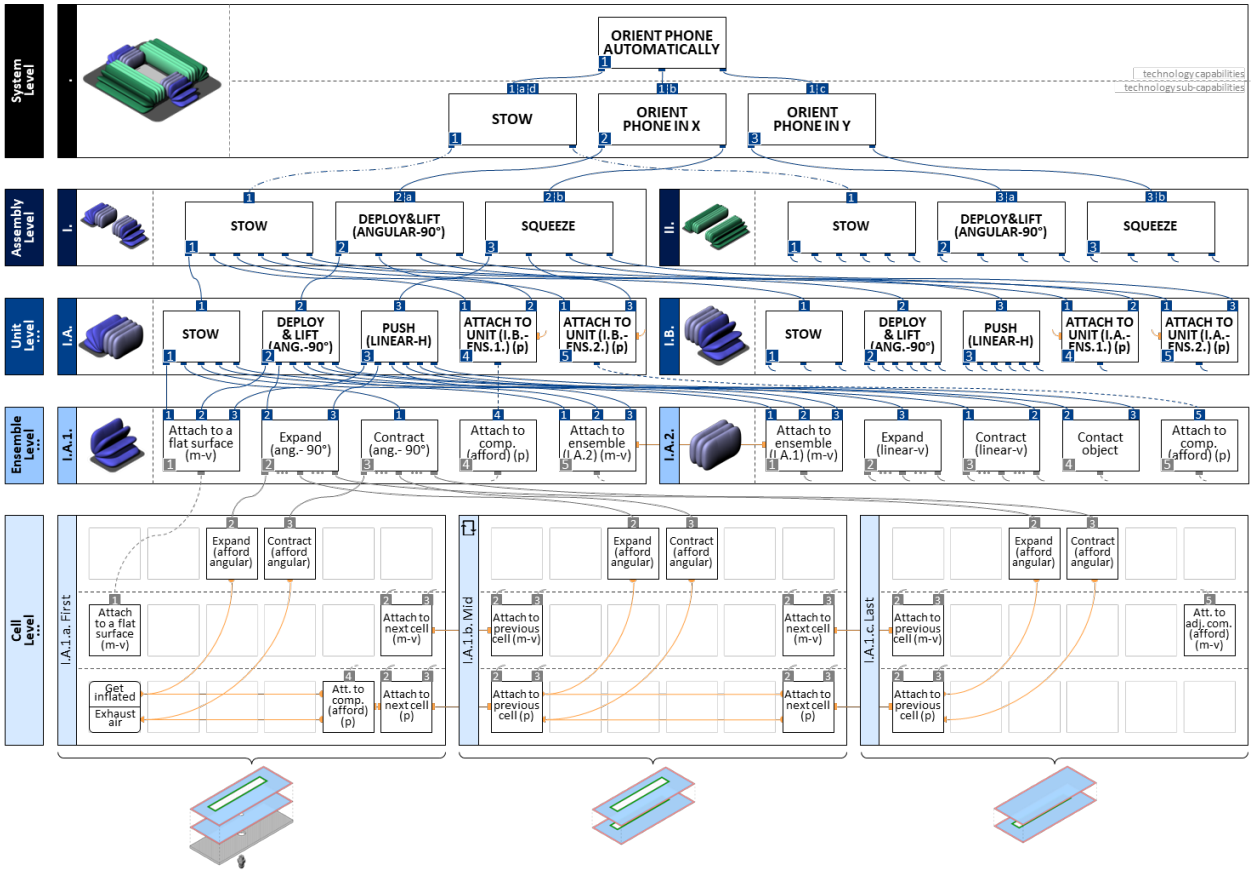

Figure 87. The hierarchical functional architectural decomposition of the mobile phone restraint mat V1. The architecture of the mobile phone restraint mat consists of two assemblies (I., II.), which are architecturally identical and are made of two pneumatically connected opposing units (I.A., I.B.). Each of these units is made of two pneumatically separate vertical ensembles that are stacked on top of each other. The ensembles (e.g., I.A.1., I.A.2.) composing a unit are architecturally different and providing different primary ensemble functions (e.g., *expand (angular-90°), expand (linear-v)*). Combinations of different sets of ensemble functions enables unit functions, which enable the assembly functions. The propagation and sequential operation of the assembly functions affords the technology sub-capabilities, *stow, orient phone in x,* and *orient phone in y*, enabling *orient phone automatically* technology capability at the system level.

The current system represents a conceptual design, which accomplishes the targeted task, however the need for multiple unique architectural components and nested operational sequences to produce the product system may introduce design challenges (e.g., increased manufacturing costs, errors due to complex sequential operation, etc.) at the later stages of the product design process (e.g., embodiment). To simplify the system, the overall functionality can be re-implemented using a re-design strategy (RD-1) by making component level-changes to the architectural hierarchy. Although this would potentially induce a decrease in its performance quality as a tradeoff, providing an alternative design with a simplified architectural complexity can be more advantageous later in the embodiment stage. An alternative simpler approach to orient the mobile phone is to provide a surface that can bend on demand to make the mobile phone passively slide to the center of the charging mat in two system-level single-step operations (rather than two two-step operations nested down to the assembly level) by employing gravitational force (Figure 88).

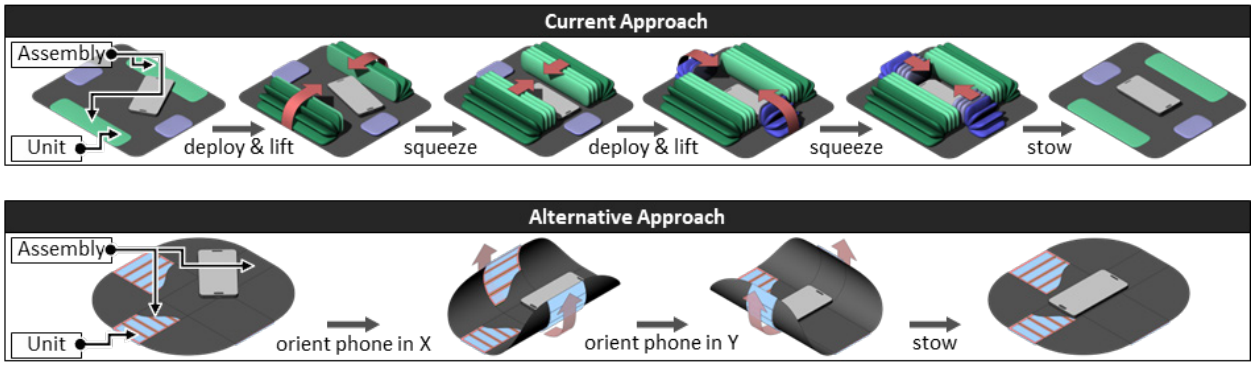

Figure 88. Comparison of the current (V1) and alternative (V2) approaches for orienting a mobile phone on a charging mat. The current approach to orient a mobile phone on a charging mat requires multiple unique architectural components and nested operational sequences (deploy & lift, squeeze, deploy & lift, squeeze, and stow) which may introduce design challenges (e.g., increased manufacturing costs, errors due to complex sequential operation, etc.) at the later stages of the product design process. An alternative simpler approach to orient the mobile phone is to provide a surface that can bend on demand to make the mobile phone passively slide to the center of the charging mat in two system-level single-step operations by employing gravitational force.

This alternative system is generated by simplifying the architecture by changing components at the unit level to produce bending surfaces. This affects the resulting system's overall architecture and the sub-cellular features that induce the generation of alternative cells. Each cell forming the re-synthesized system consists of a thin top skin layer and a thick bottom skin layer both of which are made of inextensible and flexible plastic sheet material. These two skin layers with asymmetrical cross sections are permanently sealed around the cell perimeter, enclosing an elongated inflatable cavity. Once activated through pneumatic affordance operation, *get inflated*,

the thin top skin layer expands out of plane and pulls laterally in-plane, which forces the thick bottom skin layer to *bend* to counterbalance the moment generated. These cells (I.A.1.a. First, I.A.1.a. Mid, I.A.1.c. Last) which are arranged to form a horizontal ensemble (I.A.1.), provide constitutive basic functions, which compose an emergent constitutive compound function at the ensemble level, *bend,* once inflated, and another emergent constitutive compound function, *flatten,* using the elastic recovery force passively generated by the thick bottom skin layer once activated by the pneumatic affordance operation, *let air out*. The sequential activation of assembly (I.) comprising orthogonally oriented units (I.A. and I.B.) that are formed by opposing cell ensembles (I.A.1. & I.A.2. and I.B.1. & I.B.2. respectively) makes the mobile phone slide and center on the charging mat, first in the x direction, then in the y direction. The cyclic operating sequence can be traced from the system level to the cell level using the operating sequence identification letters that are assigned to each technology sub-capability provided by this re-synthesized system, which directly map to the operation states: *a)* stow, *b)* orient phone in x, *c)* orient phone in y, and *d)* stow again, mapping each state to the corresponding pneumatic affordance operation. Unlike the sub-capabilities provided by the initial version of the mobile phone restraint mat, none of the sub-capabilities provided by the re-synthesized system requires their own operation combinations/sequences of assembly functions, which simplifies the overall product operation.

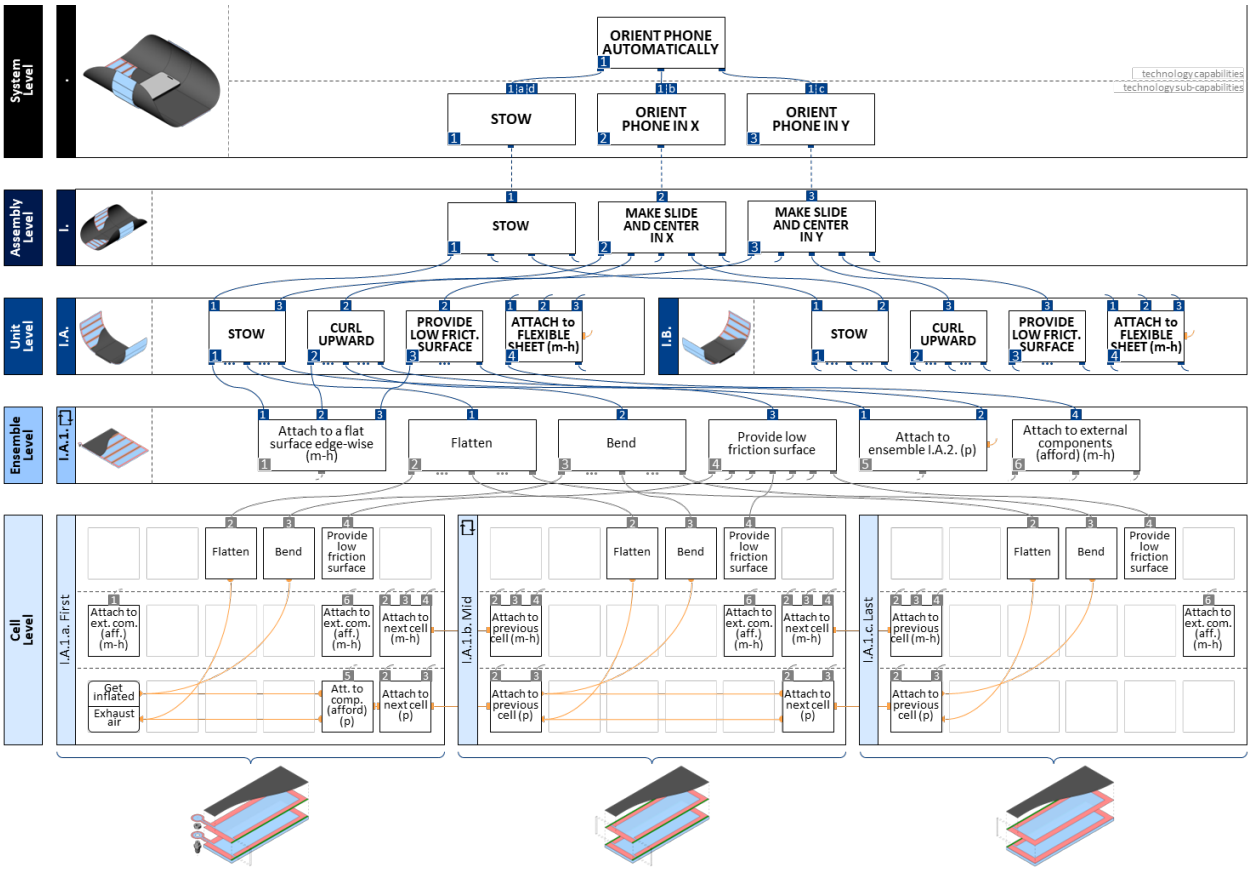

Figure 89. The hierarchical functional architectural decomposition of the mobile phone restraint mat V2. The alternative mobile phone restraint mat system (V2) re-implements the overall functionality using a re-design strategy (RD-1) by simplifying the architecture of the initial system (V1) by changing components at the unit level, therefore is affecting the design of all the lower-level architectural components to produce bending surfaces. The architecture of this alternative system consists of one assembly (I.), which is made of two architecturally identical units (I.A. and I.B.). The sequential activation of assembly (I.) comprising orthogonally oriented units (I.A. and I.B.), which are formed by identical but opposing cell ensembles (I.A.1. & I.A.2. and I.B.1. & I.B.2. respectively), makes the mobile phone slide and center on the charging mat, first in the x direction, then in the y direction, providing the same highest-level functionality, *orient phone automatically*.

As illustrated in Figure 90, this re-synthesis process simplifies the architecture by reducing the number of unique cell ensembles that are required to form a unit as a part of the initial system. A set of two of these alternative cell ensembles (I.A.1., I.A.2.), which can bend and flatten on demand, form a unit (I.A.), two of which form an assembly (I.) at the higher level in the re-synthesized system's architectural hierarchy. Thus, this re-synthesis involves substituting the initial unit with a simpler one made of two identical ensembles rather than two unique ensembles, potentially reducing the complexity regarding manufacturing and providing simpler product operation by reducing the number of operating sequences.

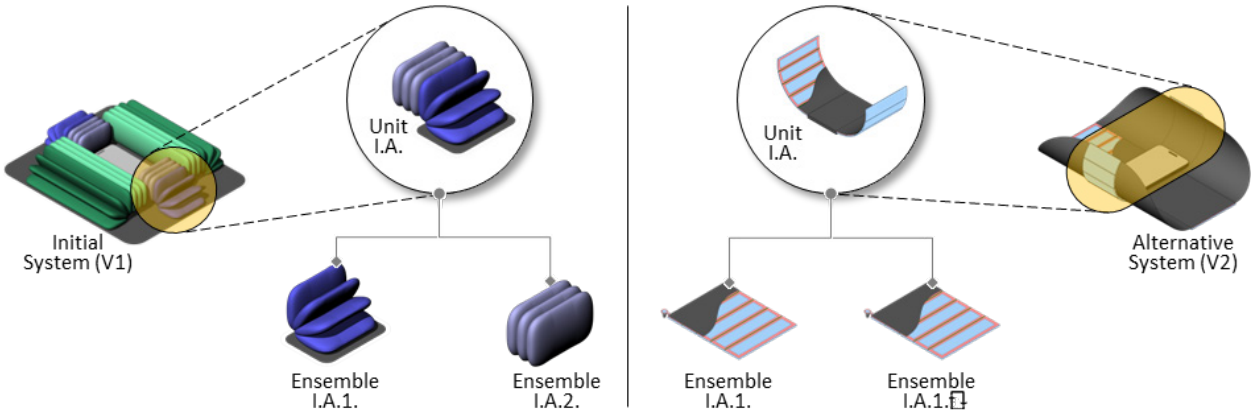

Figure 90. Simplifying the architecture while potentially allowing decreased performance. The re-synthesis process involves substituting the initial unit (shown on the left) with a simpler one (shown on the right), which is made of a single ensemble rather than two unique ensembles. This potentially reduces the complexity regarding manufacturing and provides simpler product operation by reducing the number of operating sequences.

The quantification of the performance comparison between these two alternative systems requires experimental characterization. However, at a conceptual level, one can argue that the initial version of the mobile phone charging mat might perform relatively better since it is relying on active use of actuation to push the phone into the proper location and orientation rather than the passive use of gravitational force on a shaped surface. Such active use of actuation may provide more precise control over the task of orienting the mobile phone. The relative value and appropriateness of simplifying the architecture in the expense of potentially decreasing the performance through re-synthesis process needs to be assessed based on the design context, which is affected by myriad factors such as manufacturability, targeted manufacturing costs, meeting quantified performance goals, and setting and meeting user needs and expectations.

3.2.2.1.2. Re-design Example #2: Active Rear Seat Pocket V1 to V2 (RD-3 & RD-4)

The second example for the re-design process adopts the third proposed design strategy (RD-3), which employs the hierarchical functional architectural decomposition of the active rear seat pocket that can morph into a pre-defined shape, providing easy one-handed access to the storage compartment by opening and closing the pocket on demand during transportation. The active rear seat pocket's architecture consists of one ensemble that is attached in the assembly to a set of sliders and stretchable fabric constrained by a plastic enclosure attached to a vehicle seat (Figure 91).

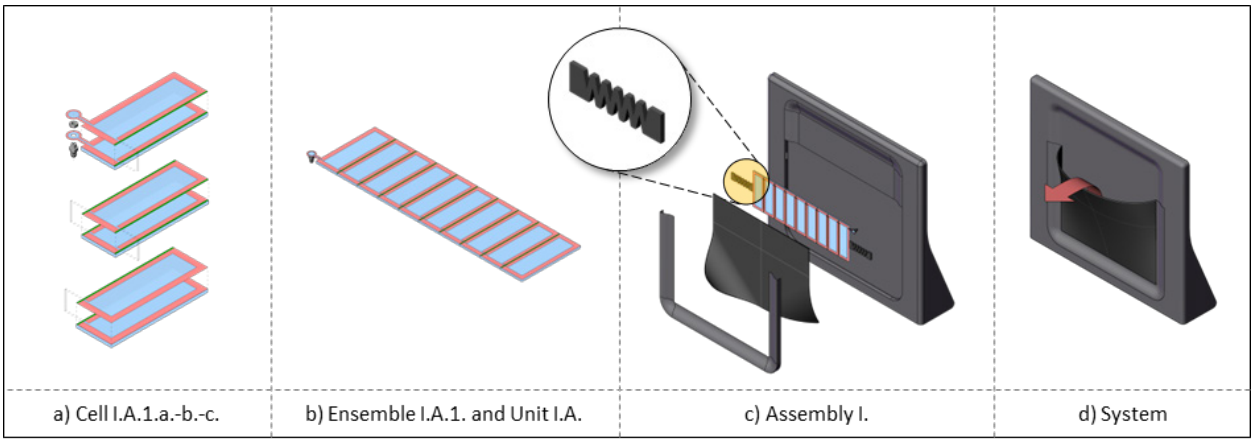

Figure 91. The active rear seat pocket product system. The active rear seat pocket can morph into a pre-defined shape, providing easy one-handed access to the storage compartment by opening and closing the pocket on demand during transportation (d). The active rear seat pocket's architecture is made of a set of cells (a), composing a horizontal ensemble (b), which is attached in the assembly to a set of sliders and stretchable fabric constrained by a plastic enclosure attached to a vehicle seat (c).

This ensemble is identical in structure to the ensemble introduced in the previous re-synthesis employing RD-1 (Figure 89) but without the inclusion of a low friction surface and with only the affordance of *attach to external components (mechanical-horizontal, vertical)*. At the ensemble level, different sets of constituent basic functions produce constitutive compound functions, *flatten* and *bend*, both of which are directly propagated to unit level. Also at the unit level, the ensemble's attachment affordances become actualized attachments to specific auxiliary architectural components: *attach to sliders (mechanical-horizontal)* and *attach to stretchable fabric (mechanical-vertical)*, enabling its incorporation in the assembly. In the assembly, *flatten* and *bend* of the unit combined with the auxiliary architectural attachments produce the assembly functions, *flatten pocket lip* and *bend pocket lip outward*, contributing to the technology sub-capabilities at the system level, *open* and *close pocket* on demand. These sub-capabilities enable the overall technology capability of enabling the opening of the rear seat pocket selectively, which provides users easy access to the storage compartment when needed (Figure 92).

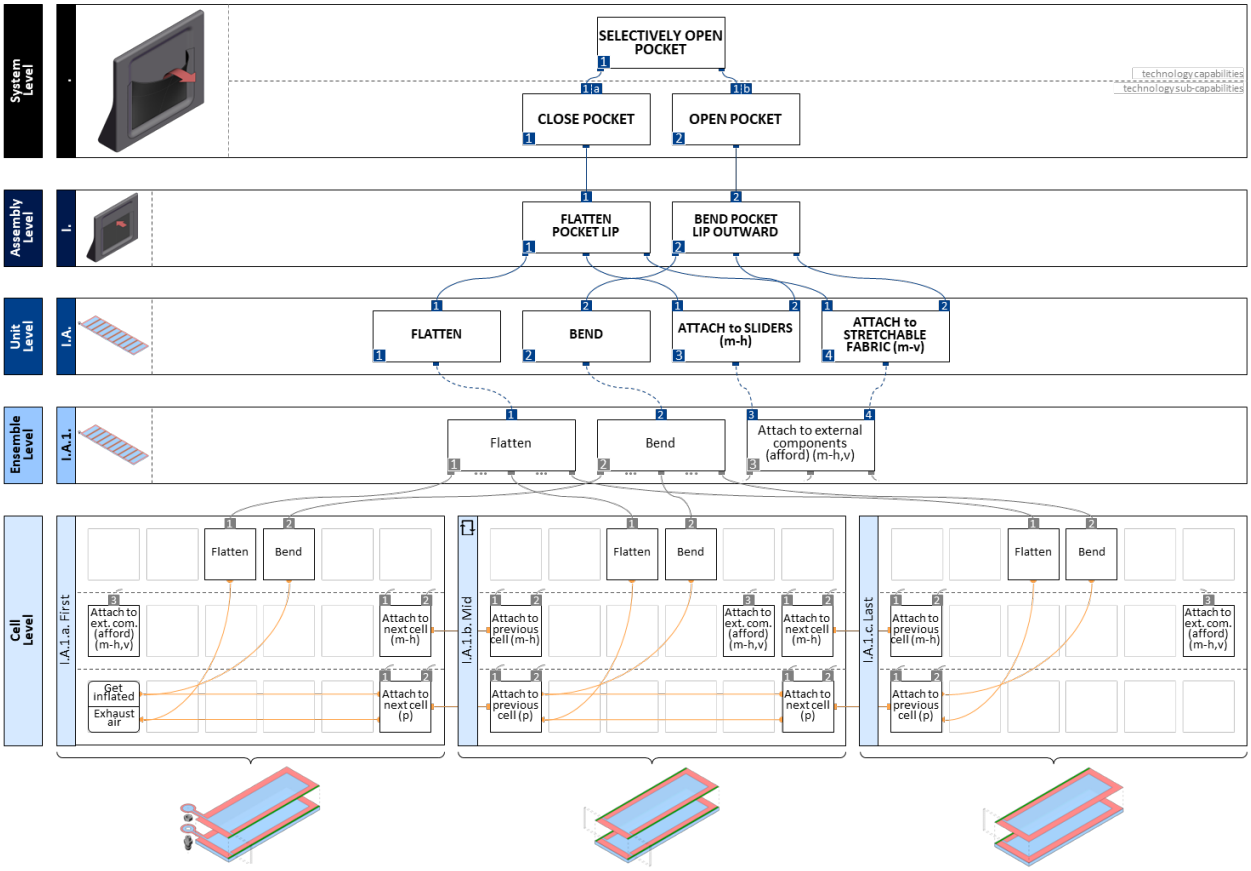

Figure 92. The hierarchical functional architectural decomposition of the active rear seat pocket V1. The active rear seat pocket's architecture consists of one ensemble that is attached in the assembly to a set of sliders and stretchable fabric constrained by a plastic enclosure attached to a vehicle seat. This ensemble provides *flatten* and *bend* ensemble functions, which enable the generation of *flatten pocket lip and bend pocket lip outward* assembly functions at the assembly level. Each of these assembly functions enables the technology sub-capabilities, *close pocket* and *open pocket*, which provide the overall technology capability of enabling the opening of the rear seat pocket selectively, providing users easy access to the storage compartment when needed.

The overall performance of this version of the active rear seat pocket is driven by its ensemble level architectural and functional components. The activation of the *bend* functional component provided by horizontal ensemble (I.A.1.) only induces bending outward of the upper lip of the pocket, which may not be considered sufficient to provide adequate access to the full pocket down to its bottom, thus motivating a re-design to enhance the overall performance. The overall functionality of the initial system can be re-implemented by changing its aggregation to enhance its performance through a re-synthesis process using a re-design strategy (RD-3). Duplicating the ensemble (I.A.1) in the initial system and re-orienting it to form a "T" shaped unit (I.A.) would provide more uniformly distributed actuation affecting both the top and bottom portions of the re-designed active rear seat pocket, increasing the quality of the interaction by improving the user's accessibility to the items stored (Figure 93).

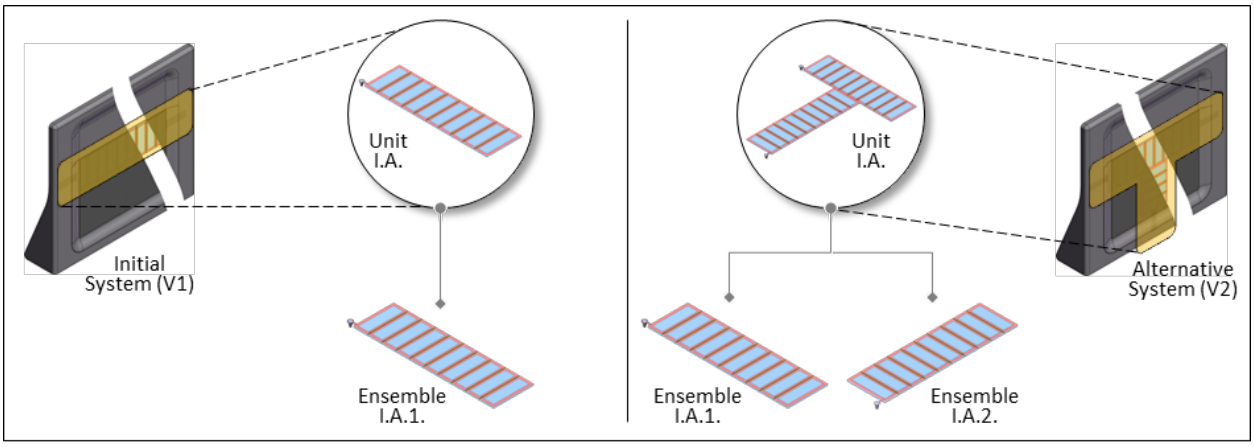

Figure 93. Enhancing performance while allowing more complicated architecture. The re-synthesis process involves substituting the initial unit (shown on the left) with a more complex one (shown on the right), which is made of two identical ensembles forming a "T" shape, providing more uniformly distributed actuation affecting both the top and bottom portions of the re-designed active rear seat pocket (V2), increasing the quality of the interaction by improving the user's accessibility to the items stored.

This alternative system is generated by changing the aggregation at the unit level, yielding enhanced performance by allowing more complicated architecture that contains a unit that is made of two identical ensembles instead of one (Figure 94). Although this affects the resulting system's overall architecture, it has no major effect on the design of the architectural components at the ensemble and cell levels, including the sub-cellular feature characteristics. Each cell forming the re-synthesized system is almost identical to their initial versions and provides same set of primary cell functions such as *flatten* and *bend*. In addition, the re-synthesized cells provide two additional cell functions, *attach to adjacent component (afford) (pneumatic)*, and *attach to adjacent component (afford) (mechanical-horizontal)*, affording pneumatic and mechanical connections between the horizontal ensembles at the ensemble level, enabling them to operate concurrently within the "T" shaped unit. As illustrated in Figure 94, as a result of changing the existing architectural aggregation at the unit level without introducing any new unique architectural components, this re-synthesis potentially enhances the resulting overall performance by making the larger pocket surface area bend outward as opposed to the isolated actuation only affecting the pocket lip.

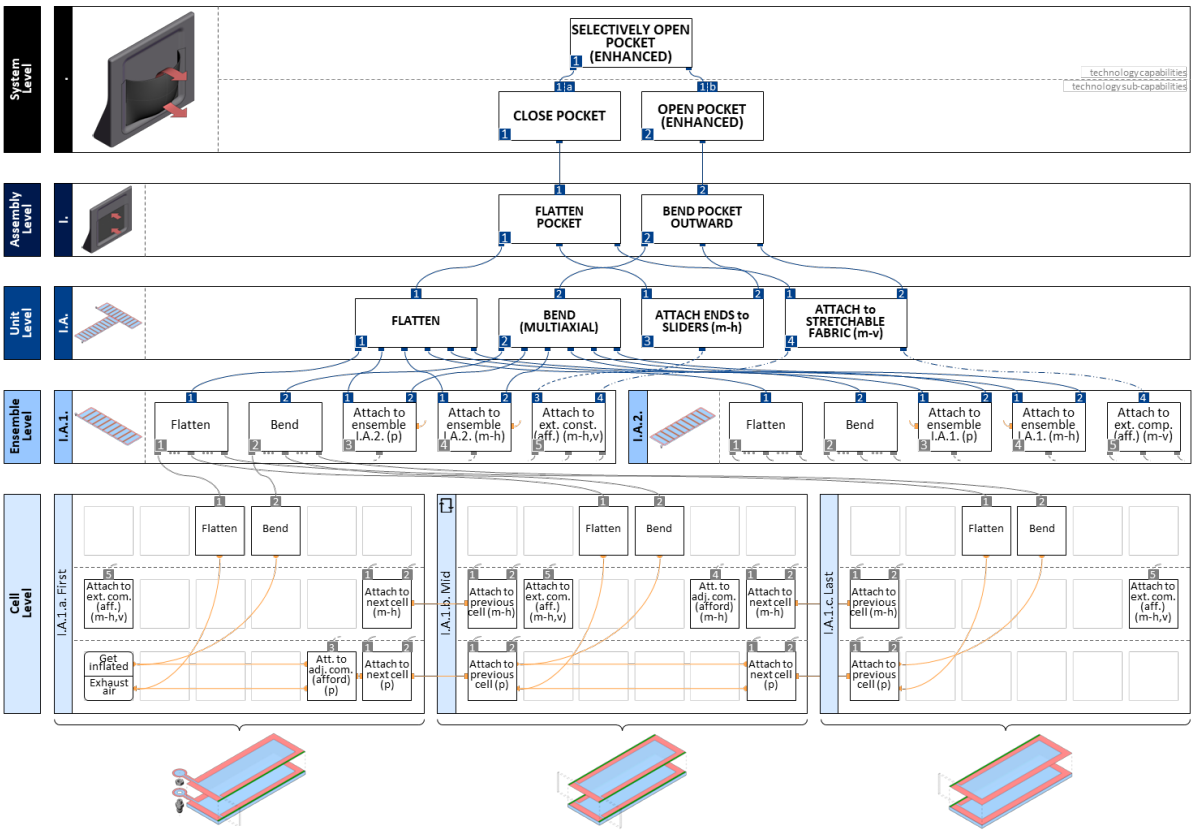

Figure 94. The hierarchical functional architectural decomposition of the active rear seat pocket V2. The alternative active rear seat pocket (V2) re-implements the overall functionality using a re-design strategy (RD-3) by changing the aggregation of the initial system (V1) at the unit level to enhance performance while allowing more complicated architecture. The architecture of this alternative system consists of one assembly (I.), which is made of a "T" shaped unit (I.A.) composed of two identical horizontal ensembles (I.A.1., I.A.2.). Since this "T" shaped unit can bend outward multiaxially, it enhances the performance of the technology sub-capability, *open pocket (enhanced)*.

The relative value of enhancing the performance at the expense of allowing a more complicated architecture through this re-synthesis process needs to be assessed. The evaluation of the appropriateness of these two design alternatives (V1 vs. V2) for a particular design context (e.g., in-vehicle experience or in-flight experience) would require further studies including an analysis of a quantified performance comparison and a user experience assessment as a part of the later stages of product design process. The reversal of this process is an example for the re-synthesis process by adopting the fourth re-design strategy (RD-4), which would have produced the initial design of the active rear seat pocket (V1) with a relatively simpler architecture while allowing decreased performance.

The purpose of re-design is to re-implement the existing functionalities provided by existing constrained layer pneumatic product systems to provide a better fit to targeted design contexts. The hierarchical functional architectural decomposition approach provides a basis for the

application of four associated design strategies (RD-1, RD-2, RD-3, and RD-4) that facilitate the re-design process. Two separate re-design processes are demonstrated through re-synthesizing the mobile phone restraint mat and the active rear seat pocket product systems, where the trade-offs between the complexity of architecture and the quality of performance are tailored by changing the existing architectural components or by changing the aggregational aspects of the existing architectural hierarchies. These result in the generation of alternative design concepts that re-implement the existing functionalities, which aids the enrichment of early-stage conceptual design process in a systematic way.

3.2.2.2. Incremental Innovation

For the incremental innovation of already existing constrained layer pneumatic product systems, four design strategies containing two pairs with reciprocal design goals of tradeoffs are proposed:

- II-1) Adjusting functionality by changing components to expand technology capability while allowing more complicated architecture,
- II-2) Adjusting functionality by changing components to simplify architecture while reducing technology capability,
- II-3) Adjusting functionality by changing aggregation to expand technology capability while allowing more complicated architecture, and
- II-4) Adjusting functionality by changing aggregation to simplify architecture while reducing technology capability.

The application of the first two proposed design strategies for incremental innovation (II-1, II-2) are demonstrated through the re-synthesis of the stiffness changing reconfigurable office space divider. The last two proposed design strategies (II-3, II-4) are demonstrated through further re-synthesis of the active rear seat pocket, which was previously used as an example to showcase the application of re-design strategies RD-3 and RD-4.

3.2.2.2.1. Incremental Innovation Example #1: Reconfigurable Office Space Divider to Moldable Active Cargo Blanket (II-1 & II-2)

The first and second design strategies (II-1, II-2) that facilitate incremental innovation through re-synthesis focus on adjusting the functionality provided by an existing system by changing the

sub-cellular features of its existing architectural components. A reconfigurable office space divider, which can be manually posed into different rigidized configurations as a thin, lightweight, and flat divider in open office spaces and home office contexts, and can be compactly rolled and stowed away, is used as an example to initiate the re-synthesis (II-1).

The reconfigurable office space divider product system consists of one ensemble that propagates upwards as a part of its relatively flat architectural hierarchy (Figure 95). However, its functional hierarchy unfolds from the system level to the cell level, describing the relationship between its *one-degree-of-freedom (1-dof) reconfigurability* technology capability and the constituent basic functions. Each cell (I.A.1.a. First, I.A.1.b. Mid, I.A.1.c. Last) contributing to the formation of the horizontal ensemble (I.A.1.) is made of opposing rigid rectangular tiles that are sandwiched between airtight skins, allowing *1-dof hinge-like motion*. These tiles jam against each other when a vacuum is applied, freezing the relative positions of the tiles. Each cell is customized to provide a set of constituent basic functions (e.g., *attach to next cell (m-h)*) that are required to form a horizontal ensemble, which provides constitutive compound functions at the ensemble level (e.g., *retain shape*). The mechanical attachments between adjacent cells are achieved by sharing each of the tiles, which are permanently attached to the bottom skin layer of a cell, with the corresponding bottom tile of an adjacent cell in addition to sharing the skin layers. Such sharing is indicated by gray tiles in the corresponding three-dimensional (isometric) illustration. Various sets of these ensemble functions compose the unit functions. For example, while two ensemble functions, *move 1-dof hinge-like* and *stiffen*, separately afford two emergent unit functions, *free bendability (1-dof)* and *rigidize*, a set of three ensemble functions, *retain shape, spring back, and stiffen*, all simultaneously contribute to the generation of one unit function, *set target shape*. Other than the *free bendability (1-dof)* unit function, which affords the generation of the *bend manually (1-dof)* assembly function that requires user intervention in the context of the assembly, all the resulting unit functions directly propagate to the assembly level. At the assembly level, the combination of *bend manually (1-dof)* and *set target shape* enables the first two of the technology sub-capabilities, *roll-and-stowability* and *(re)posability (1-dof).* The third and the last technology sub-capability, *rigidizability*, is afforded by the assembly function, *rigidize*.

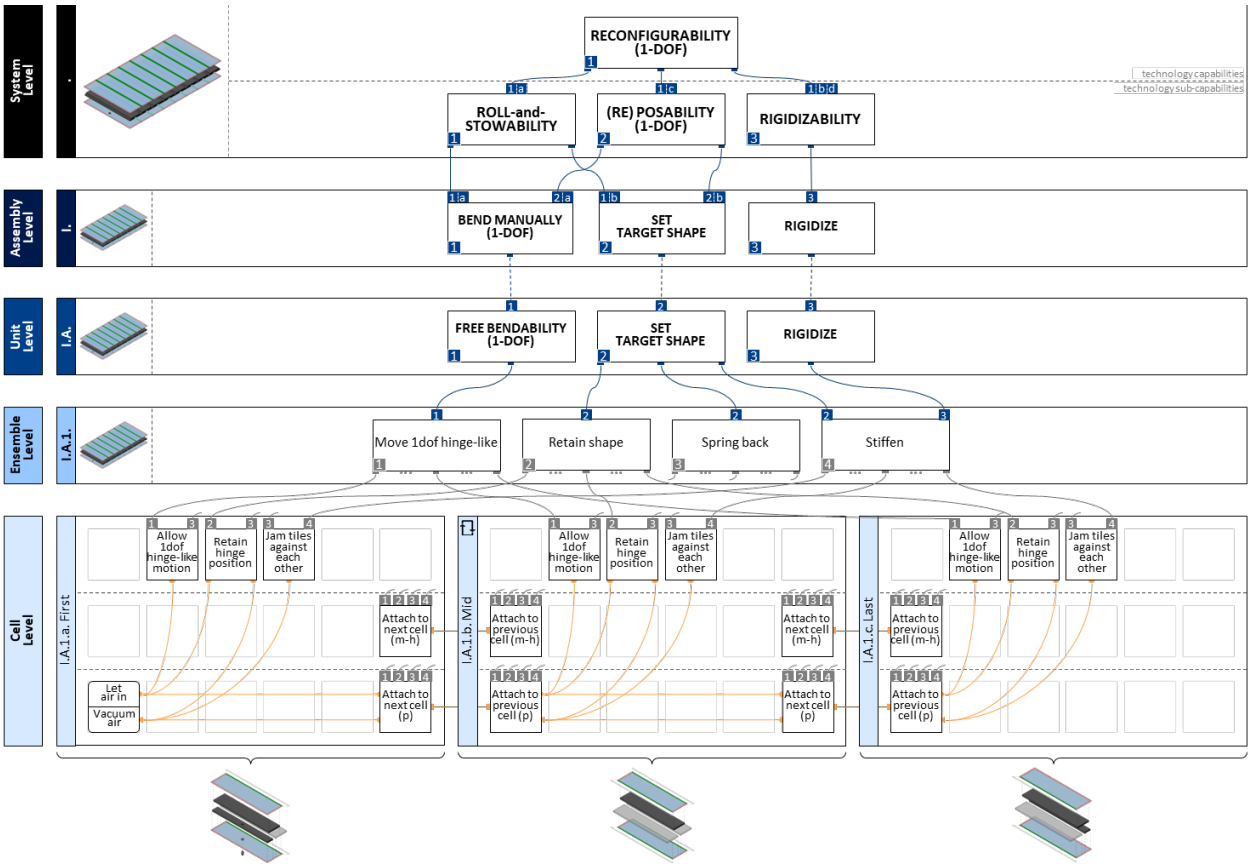

Figure 95. The hierarchical functional architectural decomposition of the reconfigurable office space divider. The architecture of the reconfigurable office space divider consists of one ensemble (I.A.1.) that propagates upwards as a part of its relatively flat architectural hierarchy. Its functional hierarchy unfolds from the system level to the cell level, describing the relationship between *reconfigurability (1-dof)* technology capability and the constituent basic functions (e.g., *allow 1dof hinge-like motion, jam tiles against each other*) provided by a set of customized cells equipped with internal constraints.

The difference between the system level technology sub-capabilities and the assembly level functionalities highlights the difference between the device being acted upon by the user in the device's relevant operation state (at the assembly level) and the user's experience with the device in the user-device system's relevant interaction mode (at the system level). These technology sub-capabilities align with the interaction modes of the reconfigurable office space divider, affording *reconfigurability (1-dof)* as the highest-level functionality. Each interaction mode is enabled through the activation of the corresponding operation states through the corresponding pneumatic affordance operations. The sequential order of the interaction modes are denoted with the operating sequence identification letters (i.e., a, b, c, and d): *a)* the initially rolling and stowing the divider, which requires manually bending it into a rolled form and setting this rolled shape by gradually vacuuming the air out from the system, *b)* rigidizing the rolled shape by maximizing the vacuum applied, *c)* re-posing the divider by manually bending it into a shape after letting air into the system

and then setting this re-posed shape by gradually vacuuming air out from the system again, and *d)* rigidizing the re-posed shape by maximizing the vacuum applied to the system once more as a final step.

The current system represents a conceptual design providing the reconfigurability technology capability with one bending degree of freedom, creating a curved surface. Increasing the bending degrees of freedom from one to two expands the current reconfigurability technology capability, providing a ground for the design of new applications such as moldable active cargo blanket that can be draped over arbitrary objects, shaped into complex geometries, and rigidized to keep the target form as a curved surface. One way of actualizing such expansion can be accomplished by using an incremental innovation strategy (II-1) to make component-level changes at the sub-cellular level affecting the constituent basic functions provided by each cell in the current system. The limitation related to the rotational degree of freedom in the current system is imposed by a particular cell function, *allow 1-dof hinge-like motion*, which is a consequence of using slender rectangular tiles as internal constraints as a part of the sub-cellular features. These overlapping rectangular tiles in each cell only afford linear folding lines in one direction. Changing the geometry from rectangles to triangles and overlapping the opposing tiles as shown in Figure 96 enable the emergence of multiple linear folding lines in three different directions in the alternative cell formation, which would *allow multi-hinge-like motion* as a result at the cell level.

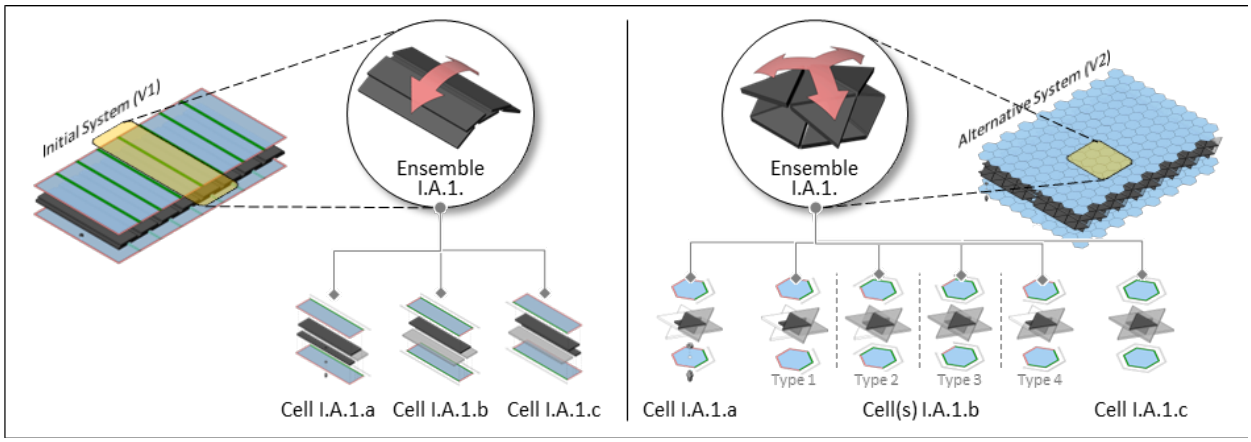

Figure 96. Expanding technology capability while allowing more complicated architecture. The initial highest-level functionality provided by the reconfigurable office space divider is adjusted and expanded by making component-level changes through the re-synthesis geared towards incrementally innovating using the first design strategy (II-1). Changing the geometry from rectangles (left) to triangles (right) and overlapping the opposing tiles enable the emergence of multiple linear folding lines in three different directions in the alternative cell formation, which would allow multi-hinge-like motion as a result at the cell level, eventually enabling *moldability* technology capability. Unlike the initial system, the re-synthesized one requires six cell variations (I.A.1.a., I.A.1.b. (Type 1-2-3-4), I.A.1.c.), therefore its architecture is inherently more complicated.

This alternative system is generated by equipping each cell with more sophisticated internal constraints: opposing equilateral triangular tiles (Figure 97). The initial system equipped with rectangular tiles only required three cell variations (I.A.1.a. First, I.A.1.b. Mid, I.A.1.c. Last) to ensure the mechanical and pneumatic connectivity among the adjacent cells forming a horizontal ensemble. However, the alternative system requires six cell variations (I.A.1.a. First, I.A.1.b. Boundary (Type 1-2-3-4), I.A.1.c. Inner) to ensure the mechanical and pneumatic connections among adjacent cells to form a horizontal ensemble that extends in both directions on a plane. The mechanical attachments among adjacent cells are achieved in a similar manner as in the reconfigurable office space divider: through sharing skins and tiles with neighboring cells (up to six). The overall functional and architectural hierarchies of these two systems, the initial one and the re-synthesized one, are similar at cell, ensemble, and unit levels. The architectural propagation from ensemble to system level is identical in both hierarchies. Functionally, the re-synthesized system expands the extent of an existing cell function, *allow 1-dof hinge-like motion*, in addition to providing a new cell function, *contact external object (afford) (mechanical-vertical),* which is propagated to unit level after being actualized at the ensemble level. This *contact external objects* affordance at the cell level is created through a sub-cellular feature characteristic of one or both skin layers to be sufficiently robust to endure contact with external objects. The *contact external objects* unit function in combination with another unit function, *free bendability*, give rise to two new assembly functions, *drape under gravity* and *conform manually into shape*, which are both crucial in terms of adjusting the overall functionality of the initial system by contributing to the generation of expanded technology sub-capabilities, *drapability* and *shapability,* respectively. These two new sub-capabilities, when combined with the initially existing sub-capability, *rigidizability*, and sequentially activated through their respective pneumatic affordance operations, generate the overall technology capability, *moldability*.

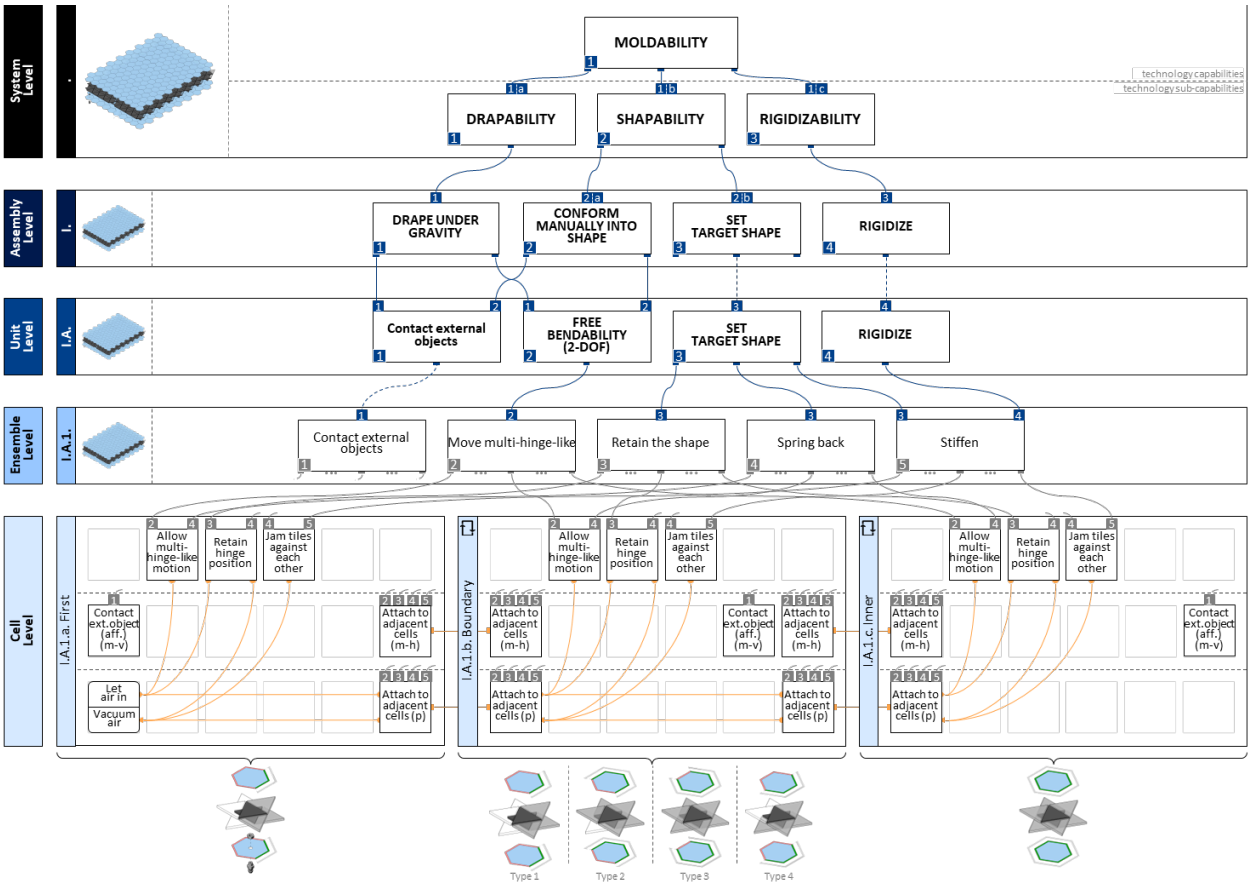

Figure 97. The hierarchical functional architectural decomposition of the moldable active cargo blanket. The architectural decomposition of the moldable active cargo blanket is identical to the initial system's architectural decomposition since ensemble (I.A.1.) propagates upwards as a part of the relatively flat architectural hierarchy. Functionally, the re-synthesized system expands the extent of an existing cell function, allow 1-dof hinge-like motion, in addition to providing a new cell function, contact external object (afford) (mechanical-vertical). These additional lower-level functionalities give rise to two new assembly functions, *drape under gravity* and *conform manually into shape*, which are both crucial in terms of adjusting the overall functionality of the initial system by contributing to the generation of expanded technology sub-capabilities, *drapability and shapability*, respectively. These two new sub-capabilities, when combined with the initially existing sub-capability, *rigidizability*, generate the overall technology capability, *moldability*.

Unlike the previous re-synthesis examples using re-design strategies (RD-1-2-3-4) focusing on the re-implementation of the existing highest-level functionality, the existing highest-level functionality provided by the reconfigurable office space divider is adjusted and expanded by making component-level changes through the re-synthesis geared towards incrementally innovating using the first design strategy (II-1). Although the technology capabilities of these two systems are related (*reconfigurability (1-dof)* vs. *moldability*), a direct comparison between their performances is not possible. The reciprocal of this re-synthesis (II-1) is an example for the application of the second design strategy (II-2) that targets incrementally innovating by

capitalizing on adjusting functionality by changing components to simplify architecture while reducing technology capability.

3.2.2.2.2. Incremental Innovation Example #2: Active Rear Seat Pocket V1 to V3 (II-3 & II-4)

The third and fourth design strategies (II-3, II-4) that facilitate incremental innovation through re-synthesis focus on adjusting functionality provided by an existing system by changing the way its architectural components aggregate to produce higher level architectural components without inducing any significant change in the lower-level architectural components beyond those changes required to enable the aggregation. The initial version of the active rear seat pocket (V1), which was previously used to demonstrate the application of the re-design strategy (RD-3) resulting in an active rear seat pocket with an enhanced performance (V2), is used as a starting point to initiate another re-synthesis that targets incremental innovation (II-3). Adopting this strategy (II-3) expands the existing technology capability of the initial version of the active rear seat pocket (V1), generating an alternative version (V3).

As previously detailed, the architecture of the initial version of the active rear seat pocket (V1) comprises one horizontal ensemble that is attached to a set of sliders, stretchable fabric, and a plastic enclosure attached to a vehicle seat. The seat pocket lip bends and morphs outward through the activation of the pneumatic affordance operation, *get inflated* (Figure 92).

The initial system enables one-handed easy access to the stored items by actively bending the rear seat pocket lip outward, opening it on demand. However, it does nothing to secure the stored items beyond allowing the pocket lip to close using the *flatten* cell function, which is afforded by the elastic recovery force generated by the thick bottom skin layer. One of the technology sub-capabilities, *close pocket*, provided by the initial system (V1), can be expanded using an incremental innovation strategy (II-3) by making aggregational changes to the architectural hierarchy.

By duplicating the existing horizontal ensemble and stacking it vertically face-to-face on the existing ensemble that bends outwards, it is possible to generate an additional functionality to the top portion of the active rear seat pocket's inner surface (Figure 98). This process forms a unit (I.A.) that is made of two vertically aggregated identical horizontal ensembles (I.A.1., I.A.2.), each of which can independently *bend* and *flatten*, the first of which causes the unit *bend outward,* and the second of which causes the unit *bend inward* once activated though their respective pneumatic affordance operations, *get inflated*, providing an active rear seat pocket with expanded

functionality of actively securing the stored items in various transportation contexts; ensemble (I.A.1.) bends the pocket lip outward to provide the same level of accessibility for the personal item storage as the initial version (V1) does, while the additional ensemble (I.A.2.) bends inward, generating a distributed force on the top portion, and therefore secures the seat pocket lip, preventing the stored items from slipping out or being scattered under unpredictable transportation conditions (e.g., in offroad driving or flight turbulence contexts).

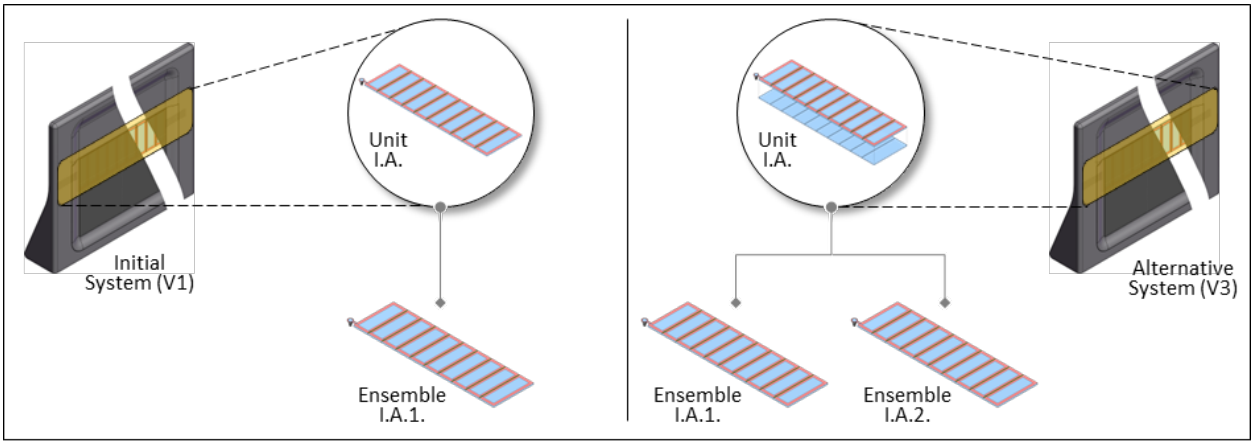

Figure 98. Expanding technology capability while allowing more complicated architecture. By duplicating the existing horizontal ensemble and stacking it vertically face-to-face on the existing ensemble that bends outwards, it is possible to generate an additional functionality to the top portion of the active rear seat pocket's inner surface. This process forms a unit (I.A.) that is made of two vertically aggregated identical horizontal ensembles (I.A.1., I.A.2.), each of which can independently bend and flatten, enabling the expansion of the initial set of technology sub-capabilities by introducing *secure pocket* sub-capability to the system.

This alternative system is generated by changing the aggregation at the unit level, producing an expanded technology sub-capability by allowing a more complicated architecture. Although this affects the resulting system's overall architecture above the ensemble level, it has no direct impact on the levels below in the architectural hierarchy (Figure 99). Each cell forming the horizontal ensemble in the re-synthesized system is physically identical to their initial counterparts except for providing an additional cell function, *attach to adjacent component (afford) (mechanical-vertical)*, which is actualized at the ensemble level as *attach to ensemble I.A.1 & I.A.2 (mechanical-vertical)*, enabling the mechanical connection between vertically aligned horizontal ensembles at the ensemble level. This affords the alternative technology sub-capability, *secure pocket*, to users at the system level, which contributes to the overall technology capability, *selectively open/secure pocket*. Since these two horizontal ensembles are not pneumatically connected, the operations corresponding to technology sub-capabilities, *close pocket, open pocket,* and *secure pocket*, can be controlled separately on demand as indicated by the operating sequence

identification letter *x* that is assigned to each sub-capability, each of which is associated with the user-device interaction modes (i.e., closing pocket, opening pocket, securing pocket).

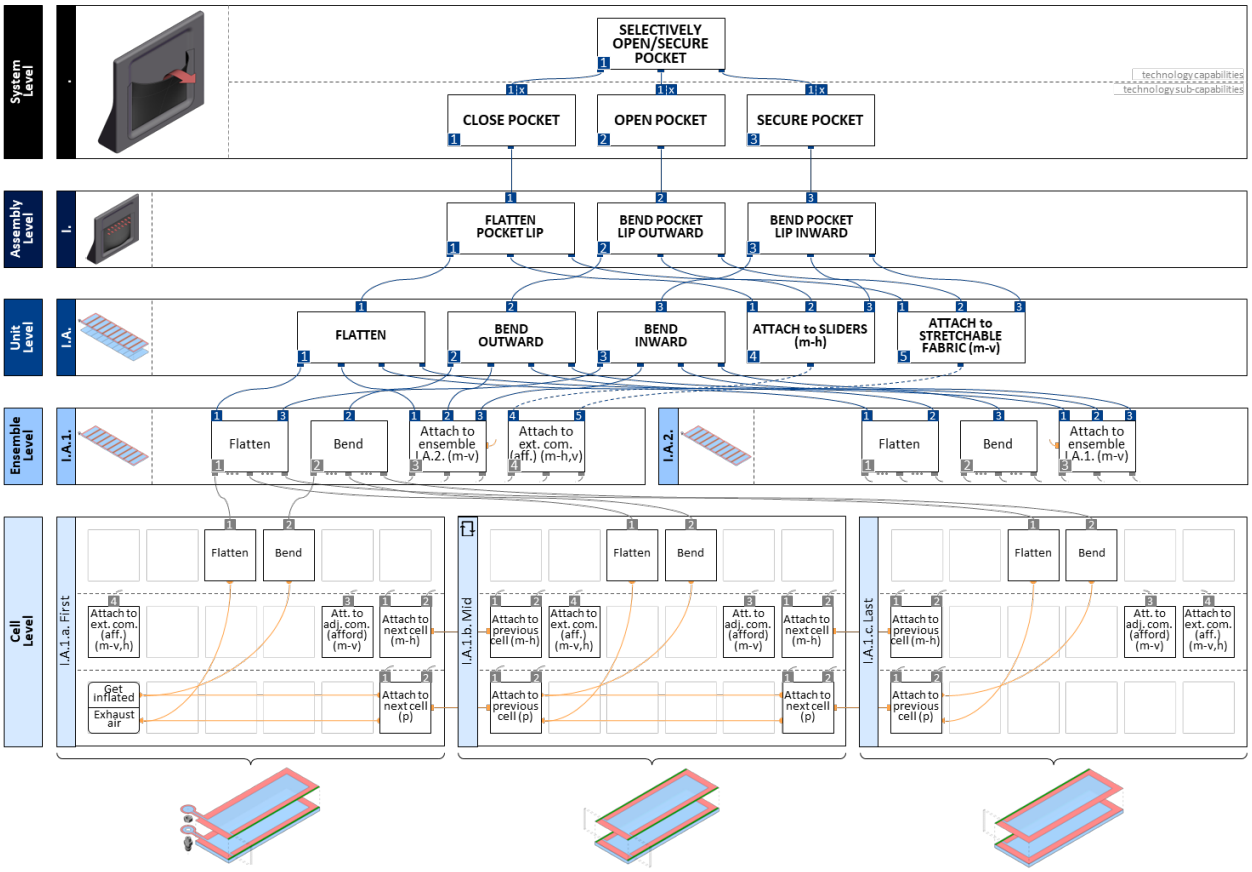

Figure 99. The hierarchical functional architectural decomposition of the active rear seat pocket V3. The alternative system (V3) is generated by changing the aggregation at the unit level, producing an expanded technology sub-capability by allowing a more complicated architecture. Although this affects the resulting system's overall architecture above the ensemble level, it has no direct impact on the levels below in the architectural hierarchy. The aggregational change at the unit level expanded the system's highest-level functionality by enabling *secure pocket* technology sub-capability.

The relative value of expanding the technology capability at the expense of allowing more complicated architecture through this re-synthesis (II-3) can be assessed by evaluating the appropriateness of these two design alternatives (V1 vs V3) in a particular design context (e.g., in offroad driving or flight turbulence contexts). This can be achieved by conducting further studies encompassing an analysis of a quantified performance comparison and a user experience assessment. The reciprocal of this re-synthesis is an example for the application of the fourth and last incremental innovation strategy (II-4), which produces the single-ensemble-unit design of the active rear seat pocket (V1) with a relatively simpler architecture affording reduced technology capability relative to the double-ensemble-unit design (V3).

The purpose of employing incremental innovation design strategies is to adjust the existing functionalities provided by existing constrained layer pneumatic product systems to provide a better fit to targeted design contexts. The hierarchical functional architectural decomposition approach provides a basis for the application of four associated design strategies (II-1, II-2, II-3, and II-4) that facilitate the incremental innovation process. Two separate incremental innovation design processes are demonstrated through re-synthesizing the reconfigurable office space divider and the active rear seat pocket product systems, where the trade-offs between the extent of the technology capability and the complexity of architecture are tailored by changing the existing architectural components or by changing the aggregational aspects of the existing architectural hierarchies. These result in the generation of alternative design concepts providing adjusted functionalities, adding to the systematic enrichment of early-stage conceptual design process.

3.2.2.3. Radical Innovation

For the radical innovation of already existing constrained layer pneumatic product systems, two design strategies both of which are independent of any trade-offs are proposed:

- RI-1) Changing functionality by changing components to discover new technology capability, and
- RI-2) Changing functionality by changing aggregation to discover new technology capability.

The application of the first proposed design strategy facilitating radical innovation (RI-1) is demonstrated through the re-synthessis of the reconfigurable office space divider which results in generating a morphing windshield cowling product system. For the application of the second radical innovation design strategy (RI-2), the decompositions of two separate product systems are re-synthesized: the mobile phone restraint mat and variable friction cargo mat. The first one results in generating a deployable storage bin, and the second one results in generating two radical innovations, a variable stiffness/detent control knob and an easy-release ice cube tray.

3.2.2.3.1. Radical Innovation Example #1: Reconfigurable Office Space Divider to Morphing Windshield Cowling (RI-1)

The first design strategy (RI-1) that facilitates radical innovation through a re-synthesis process employs changing functionality by changing components of an existing system. A newly conceived system, a morphing windshield cowling, is a pneumatically activated structure that can

curl on demand to open up a gap for wipers to function and can flatten to secure the gap between the car hood and windshield when the wipers are no longer in use to protect against debris such as leaves and snow. The previously described reconfigurable office space divider provides a natural starting point for the design of the morphing windshield cowling; it can be manually curled or flattened and rigidly holds its shape. To create the morphing windshield cowling, radical changes to this functionality are required both in terms of removing and introducing sets of functionalities, operating in a completely different context. While the morphing windshield cowling does not need to be posable into arbitrary shapes, it must attach to the hood and actively curl, rigidly holding a single curled shape as well as actively flatten, pressing against the windshield to secure the gap on demand without physical interaction from a user.

The reconfigurable office space divider product system, as initially detailed in Figure 95, is made of cells each of which contains internal constraints composed of two opposing tile layers that are permanently attached to the top and bottom skins. The gap between each tile allows a hinge-like motion in the absence of vacuum, enabling users to manually bend the divider into a target shape before the gradual introduction of vacuum into the system, which initiates jamming of the opposing tile layers against each other, eventually making the divider rigidly hold its targeted shape.

This targeted shape can take numerous forms in the use context of the manually reconfigurable office space divider; however, the morphing windshield cowling needs to afford only two target shapes, curled and flattened, both of which are required to be achieved on demand without the user's active intervention. Since there is no need to retain arbitrary hinge positions in the use context of the morphing windshield cowling, adopting only one layer of the initial array of tiles that are used to form the reconfigurable office space divider is sufficient to provide the required hinge-like motion, which forms a basis for generating an active bending motion. One way of generating such active bending motion is to change the shape of the tiles forming the adopted tile layer, which is initially made of thin, flat, and slender rigid rectangular tiles. These tiles are replaced by a set of upside-down T-shaped tiles of which top and bottom surfaces are mechanically attached to the top and bottom skin layers, forming a hinge and a vacuumable cavity as a part of a new basic cell (I.A.1.a.BC1) as shown in Figure 100. Each basic cell contains two adjacent T-shaped tiles of which interfacing surfaces along the hinge are angled, which *limit the bending motion* of the hinge. Once activated through the pneumatic affordance operation, *vacuum*, the thin

top skin layer gets pushed inward due to external atmospheric pressure and pulls transversally on the hinge, producing the constituent basic function, *bend hinge*. As the pneumatic affordance operation, *let air in*, is activated (rather than *vacuum*), the *relax hinge* constituent basic function is activated at the basic cell level.

Changing the shape of the tile layer enables the higher-level *curling* functionality in the decomposition hierarchy; however, to expand the functionalities at the higher levels even further for enabling an actively controllable *flattening* functionality, a separate basic cell (I.A.1.a.BC2) with pneumatic affordance operations activated independently of the other basic cell (I.A.1.a.BC1), is introduced to the system being re-synthesized. This basic cell is made of two skin layers that are mechanically attached to each other to form an inflatable cavity. Two flat and thin rigid tiles with a gap between are permanently attached to the outer surface of the top skin layer as an external constraint, forming a hinge line. Once activated through the pneumatic affordance operation, *get inflated*, the thin bottom skin layer expands out of plane and pulls laterally in-plane, which causes the top skin layer that is constrained by the rigid tiles to *bend the hinge*. Similarly, As the pneumatic affordance operation, *exhaust air*, is activated (rather than *get inflated*), the *relax hinge* constituent basic function is activated at the basic cell level.

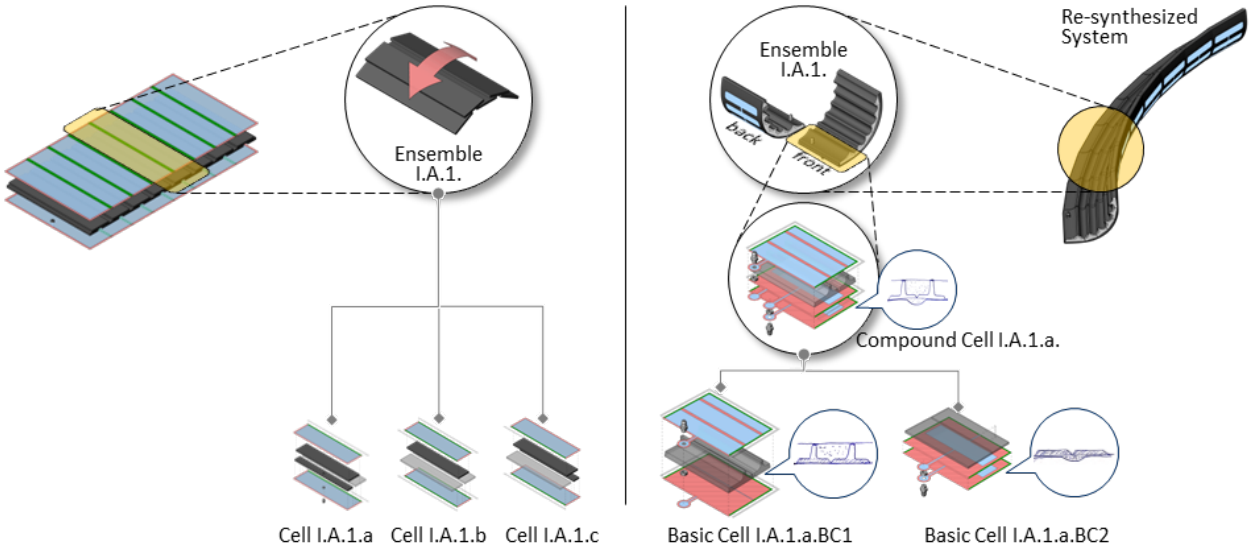

Figure 100. Changing components to discover new technology capability. The initially used thin, flat, and slender rigid rectangular tiles (left) are replaced by a set of upside-down T-shaped tiles (right) of which top and bottom surfaces are mechanically attached to the top and bottom skin layers, forming a hinge and a vacuumable cavity as a part of a new basic cell (I.A.1.a.BC1). This enables the generation of an active bending functionality once the re-synthesized system is activated through the pneumatic affordance operation, vacuum. An additional basic cell (I.A.1.a.BC1) is introduced to the system being re-synthesized, enabling flattening functionality at the higher-levels in the hierarchy once activated through a separate pneumatic affordance operation, get inflated. These functionalities together at the system level enable the technology capability: *selectively cover wiper gap*.

The two basic cells (I.A.1.a.BC1 and I.A.1.a.BC2) are vertically aggregated on top of each other and mechanically attached to form a compound cell that can produce a set of compound functions using the basic constituent functions each basic cell provides through two sets of simultaneous pneumatic affordance operation combinations (*vacuum & exhaust air* and *let air in & get inflated*) (Figure 101). The mechanical connection between these two basic cells is achieved by integrating the two basic cells such that the bottom skin layer of the upper basic cell (I.A.1.a.BC1) is shared with the top skin layer of the lower basic cell (I.A.1.a.BC2), thus merging the lower flat portion of the T-shaped tiles of the upper basic cell with the flat tiles of the lower basic cell, merging the hinge. This compound cell (I.A.1.a. First) can *bend upward* and *engage hard stops* by activating the simultaneous pneumatic affordance operation combination, *vacuum* and *exhaust air,* which activates the corresponding constituent basic functions, *bend hinge* (provided by I.A.1.a.BC1) and *relax hinge* (provided by I.A.1.a.BC2). The second simultaneous pneumatic affordance operation combination, *let air in* and *get inflated*, activates the corresponding constituent basic functions, *relax hinge* (provided by I.A.1.a.BC1) and *bend hinge* (provided by I.A.1.a.BC2), which produces the compound cell function, *bend downward*.

A set of variations of this compound cell forms a horizontal ensemble (I.A.1.) by employing the relevant compound cell function, *attach to next compound cell (mechanical-horizontal) (pneumatic),* which also contributes to three primary functionalities composed at the ensemble level. The compound cell functions, *bend downward* and *bend upward*, contribute to the emergent constitutive compound functions, *straighten* and *curl*, at the ensemble level, respectively. Similarly, the combination of *bend upward* and *engage hard stops* contributes to the generation of *rigidly hold curled shape*. This is different than *curl* in the sense that *curling* occurs throughout the entire motion whereas *rigidly hold curled shape* only occurs after the full motion is achieved and additional vacuum is applied. As a set of variations of this ensemble (I.A.1.) is horizontally arrayed to form a unit (I.A.), the ensemble functions, *straighten, curl,* and *rigidly hold curled shape*, are combined with *attach to next ensemble (mechanical-horizontal) (pneumatic)*, producing the unit functions, *flatten, curl,* and *rigidly hold curled shape,* which are all propagated to the assembly level. The ensemble functions that afford contacting and getting mechanically attached to external components are propagated to the unit level to be later actualized at the assembly level as *attach to car hood (mechanical-horizontal)* and *contact windshield (mechanical-vertical)*.

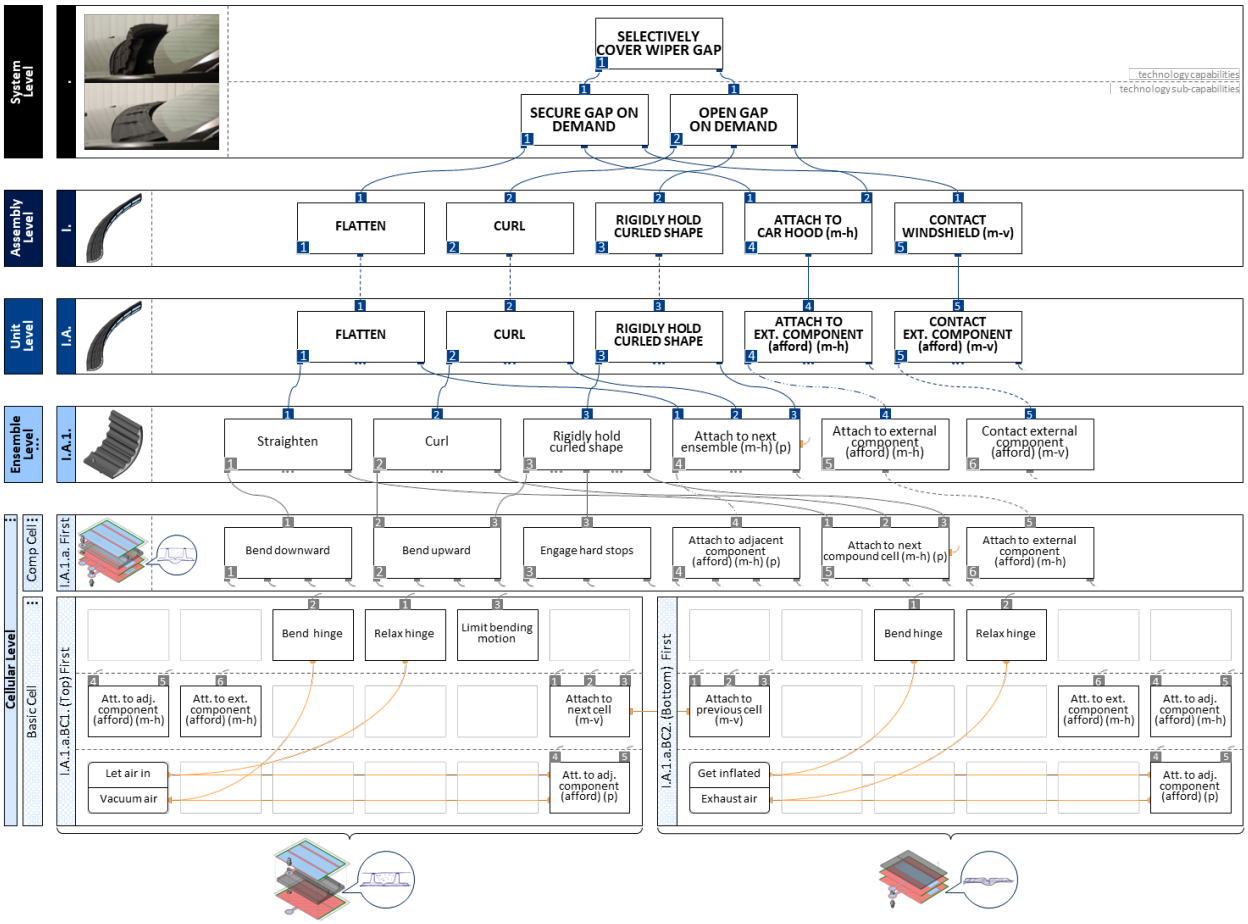

Figure 101. The hierarchical functional architectural decomposition of the morphing windshield cowling. The architecture of the morphing windshield cowling consists of a unit (I.A.) that is made of an array of horizontal ensembles (e.g., I.A.1.). Each horizontal ensemble consists of a set of compound cells (e.g., I.A.1.a.) each of which is made of two separate basic cells (e.g., I.A.1.a.BC1., I.A.1.a.BC2.) that are vertically combined and sharing a skin layer. Through their independent pneumatic operations, these basic cells provide a set of basic cell functions such as *bend hinge, relax hinge,* and *limit bending motion* alongside several mechanical and pneumatic attachment functions. The various combinations of these basic cell functions enable compound cell functions (e.g., *bend downward, bend upward, engage hard stops*), which contribute to the primary ensemble functions: *straighten, curl,* and *rigidly hold curled shape*. These assembly functions enable the technology sub-capabilities, *secure gap on demand* and *open gap on demand*, providing the users the ability of selectively cover the wiper gap of their cars.

It is important to note that the unit (I.A.) and assembly (I.) levels are architecturally identical. However, the actualization of the unit functions that provide the affordance of interacting with the external components at the assembly level functionally anchors the generic unit in the specific design context of the assembly, producing the more specific assembly functions. This grants the emergence of the use context-specific technology (sub)capabilities at the system level. Therefore, it is possible to make use of the exact or modified versions of this unit (I.A.) in different use contexts to facilitate radical innovations geared towards producing new technology (sub)capabilities addressing different needs (e.g., designing a morphing aircraft wing to save fuel

and/or reduce noise pollution, or designing automotive air dams and spoilers that can morph into different configurations on demand to adjust the drag).

In the current use context addressing the windshield wiper use, the simultaneous combination of the assembly functions, *flatten*, *attach to car hood (mechanical-horizontal),* and *contact windshield (mechanical-vertical)*, enables the first technology sub-capability, *cover gap on demand*. This eliminates the debris accumulating under the hood by securing the gap between the hood and the windshield in addition to potentially enhancing the aerodynamic performance of the car by providing a continuous surface from the hood to the windshield. The simultaneous combination of the assembly functions, *curl, rigidly hold curled shape*, and *attach to car hood (mechanical-horizontal),* enables the second technology sub-capability, *open gap on demand*. This provides the ability to operate the wipers as needed. These two higher level functionalities at the system level together produce the highest-level functionality, the overall technology capability, *morph*.

As illustrated in Figure 100, this re-synthesis employing the modification of the sub-cellular feature characteristics of the existing cells (e.g., Figure 100 (left), Cell I.A.1.a.) enabled a radical innovation by facilitating the discovery of a new technology capability.

3.2.2.3.2. Radical Innovation Example #2: Mobile Phone Restraint Mat to Deployable Storage Bin (RI-2)

The second design strategy (RI-2) facilitating the radical innovation through a re-synthesis process employs changing functionality by changing the aggregation of the architectural components in an existing system. A new system, a deployable storage bin, is a pneumatically activated structure that can be stowed away flat when not in use and can be deployed to manage and restrain cargo in a moving vehicle. The previously described mobile phone restraint mat provides a natural starting point for the design of the deployable storage bin; it can stow flat and deploy to orient a mobile phone on a charging mat automatically. To create the deployable storage bin, one of the existing vertical ensembles that composes the mobile phone restraint mat architecture is adopted but the way it aggregates to produce a unit is changed, which provides a basis for re-purposing a set of existing functionalities as well as introducing a set of new ones, operating in a completely different context. While the deployable storage bin does not need to orient any external objects, it must provide a load-bearing rigid structure to accommodate a wide array of cargo items.

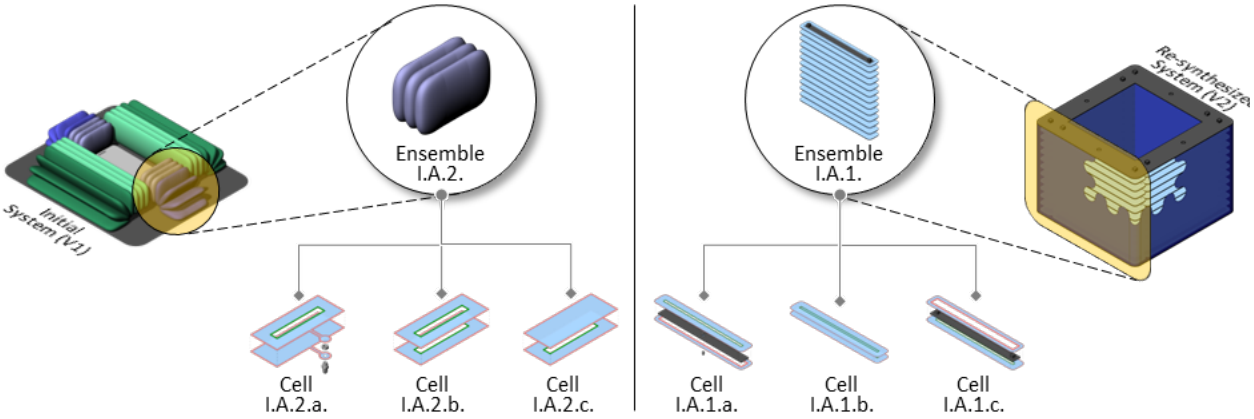

Figure 102. Changing aggregation to discover new technology capability. The deployable storage bin is generated by adopting one of the existing vertical ensembles (I.A.2.) that composes the mobile phone restraint mat architecture and by changing the way it aggregates to produce a unit. This provides a basis for re-purposing a set of existing functionalities as well as introducing a set of new ones, operating in a completely different context. While the deployable storage bin does not need to orient any external objects, it must provide a load-bearing rigid structure to accommodate a wide array of cargo items.

The mobile phone restraint mat product system, as initially detailed in Figure 87, is made of two assemblies (I. and II.) that are formed as a result of the combination of two pairs of two identical units (I.A. & I.B. and II.A. & II.B.) which are oriented 90° apart within the product system. Each of these units is made of two vertically aggregated unique vertical ensembles (e.g., I.A.1. and I.A.2.). One of these ensembles, vertical ensemble I.A.2., provides *expand (linear-vertical)*, *contract (linear- vertical)*, and *contact object* ensemble functions as a part of the mobile phone restraint mat decomposition, which is detailed in Figure 103 (cell level). This vertical ensemble (I.A.2.) and the functionalities it provides can be adapted and re-purposed as a part of the re-synthesis generating the deployable storage bin product system.

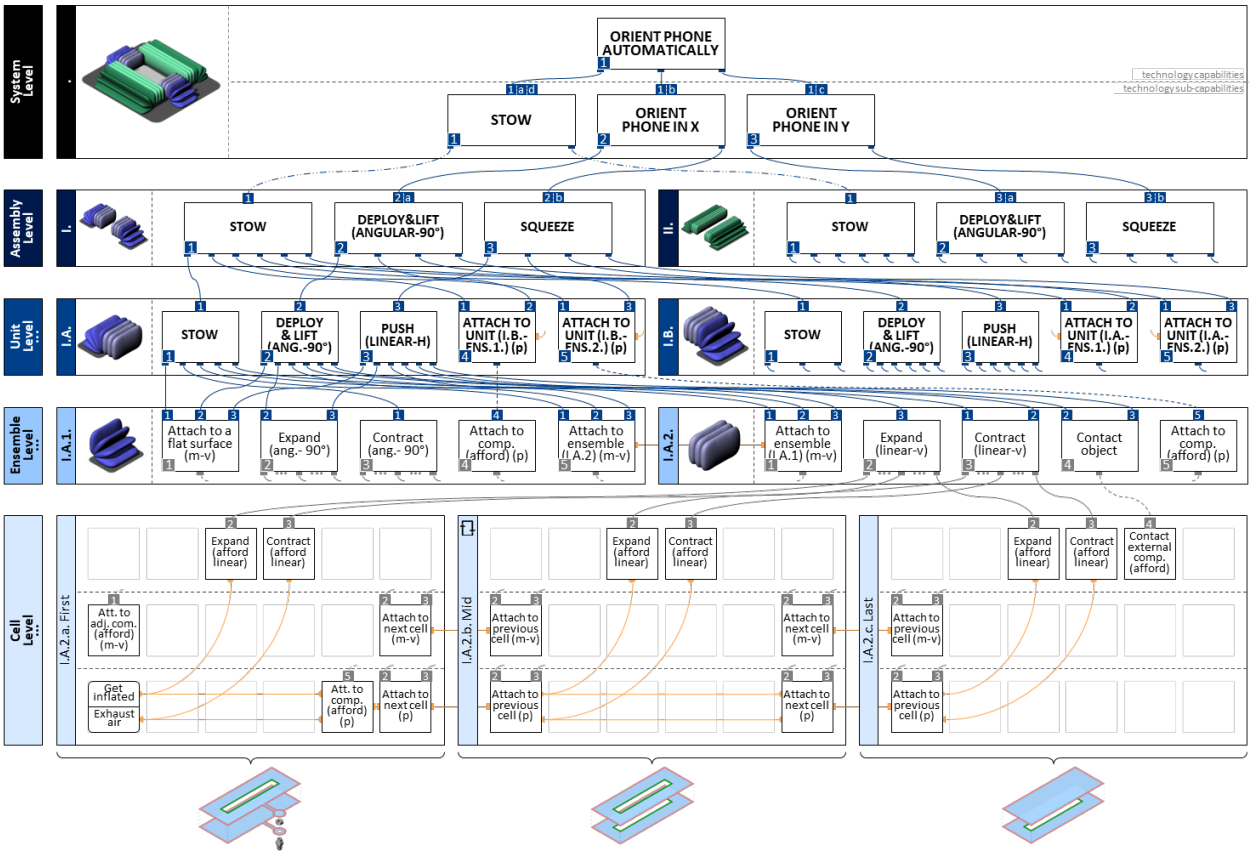

Figure 103. The hierarchical functional architectural decomposition of the mobile phone restraint mat V1 (showing the cells composing ensemble I.A.2.). The previously described mobile phone restraint mat (V1) consists of two assemblies (I., II.), which are architecturally identical and are made of two pneumatically connected opposing units (I.A., I.B.). Each of these units is made of two pneumatically separate vertical ensembles that are stacked on top of each other. The ensembles (e.g., I.A.1., I.A.2.) composing a unit are architecturally different and providing different primary ensemble functions (e.g., *expand (angular-90°), expand (linear-v)*). Combinations of different sets of ensemble functions enables unit functions, which enable the assembly functions and technology (sub)capabilities at the higher levels in the system hierarchy. One of the constituents of the mobile phone restraint mat, ensemble I.A.2., provides a natural starting point for the design of the deployable storage bin; it can stow flat and expand linearly on demand.

In the context of the deployable storage bin (Figure 104), the adapted vertical ensemble (I.A.1.) is architecturally almost identical to ensemble (I.A.2.) from the mobile phone restraint mat, providing *expand (linear)* and *contract (linear)* ensemble functions. However, its constituent first (I.A.1.a.) and last cells (I.A.1.c.) contain attachment plates as internal constraints, which provide affordances for its use in the deployable storage bin system context. Each cell in the ensemble also has the additional affordance to *attach to external constraint (mechanical-horizontal)*, which enables the ensemble to *attach to inextensible fabric constraint (mechanical-horizontal).* When combined with fabric to form a unit (I.A.), the *expand (linear)* ensemble function converts to the *expand (linear-limited)* unit function, serving to *enhance stiffness*. Mechanical attachment of the

unit to the top and bottom assembly plates and pneumatic attachment to the adjacent units that form the assembly (I.) are actualized at the unit level, allowing the assembly structure to *enhance structural rigidity*. Both attachment related unit functions are separately combined with the remaining unit functions, *contract (linear)* and *expand (linear-limited)*, generating the remaining assembly functions: *stow* and *deploy container*, respectively. While the assembly functions, *stow* and *deploy container*, are propagated directly to the system level as technology sub-capabilities, the combination of *deploy container* and *enhance structural rigidity* assembly functions generates the third and last technology sub-capability, *contain cargo* in the use context of the system. These three technology sub-capabilities contribute to the overall technology capability at the system level of the deployable storage bin application that enables users to selectively deploy and stow the container to accommodate their cargo on demand.

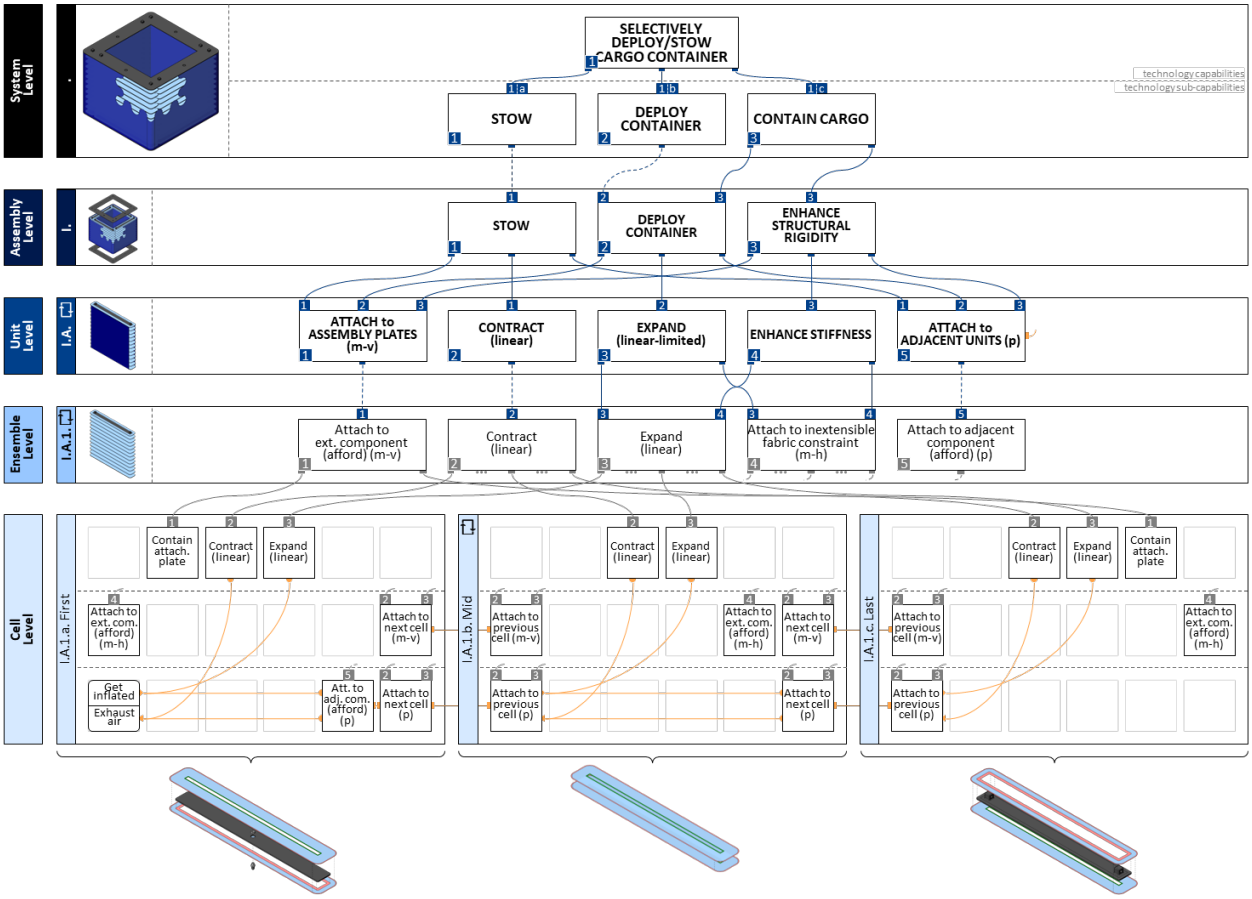

Figure 104. The hierarchical functional architectural decomposition of the deployable storage bin. The architecture of the deployable storage bin consists of an assembly (I.) containing four identical units (I.A.) each of which is based on the same vertical ensemble (I.A.1.), which is architecturally almost identical to ensemble (I.A.2.) from the mobile phone restraint mat, providing expand (linear) and contract (linear) ensemble functions. This ensemble's constituent first (I.A.1.a.) and last cells (I.A.1.c.) contain attachment plates as internal constraints that provide affordances for its use in the deployable storage bin system context. Attachment related affordances are actualized at the higher levels in the system, enabling the assembly functions: *stow, deploy container,* and *enhance*

structural rigidity. While the assembly functions, stow and deploy container, are propagated directly to the system level as technology sub-capabilities, the combination of deploy container and enhance structural rigidity assembly functions generates the third and last technology sub-capability, contain cargo in the use context of the system.

This re-synthesis facilitated the discovery of a new technology capability as a result of modifying the way a multiplicity of an existing architectural component (the mobile phone restraint mat system, ensemble I.A.2.) aggregates at the unit level without imposing any significant change on the sub-cellular feature characteristics of that architectural component as illustrated in Figure 102.

3.2.2.3.3. Radical Innovation Example #3: Variable Friction Cargo Mat to Variable Friction / Detent Control Knob and to Easy-release Ice Cube Tray (RI-2)

Two additional re-syntheses demonstrate the versatility of the second design strategy (RI-2) employing changing functionality by changing aggregation of the existing systems. Both of these processes accomplish the design goal of discovering new technology capabilities by re-purposing subsets of architectural components that form one of the previously introduced systems, the variable friction cargo mat (Figure 63), which can change its surface properties between high and low friction states by selectively activating its two interdigitated units, enabling easy cargo loading or restraint. These two re-syntheses generate two new product systems: a *variable friction/detent control knob* and an *easy-release ice cube tray*. The variable friction/detent control knob is a pneumatically activated system that can provide tailorable haptic feedback to its users by selectively changing the knob friction and/or detent spacing. The easy-release ice cube tray facilitates the removal of otherwise-often-stuck large ice cubes from their plastic tray by using a pneumatically activated simple linear actuation system, aiming to improve the overall user experience. To create these radically different product systems, the functionalities provided by one of the ensembles and cells forming the variable friction cargo mat, *expand (linear)* and *contact (linear)*, can be adapted to operate in different contexts without introducing any major changes to the existing subcellular feature characteristics of the adopted architectural components (Figure 105).

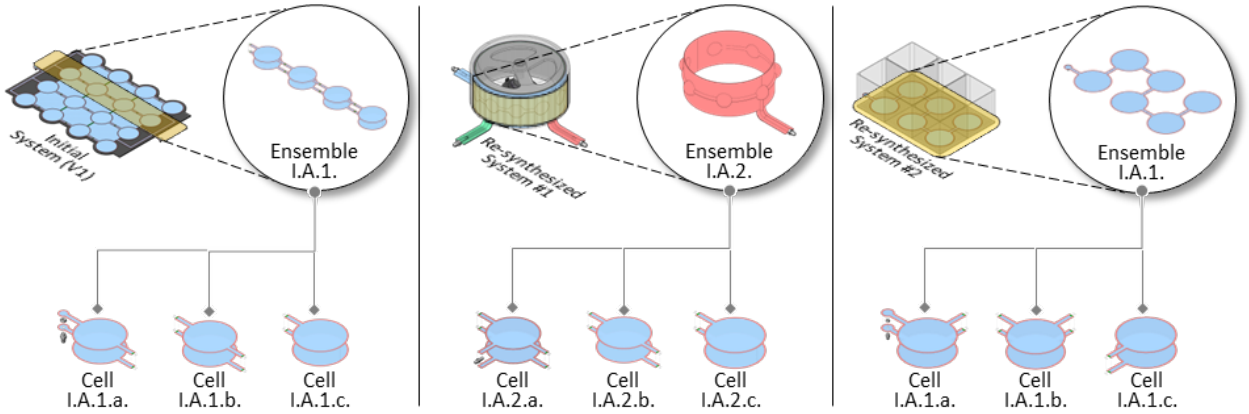

Figure 105. Changing aggregation to discover new technology capabilities. Two new product systems, a variable friction/detent control knob and an easy-release ice cube tray, are generated, demonstrating the versatility of the second design strategy (RI-2) employing changing functionality by changing aggregation through a re-synthesis of an initial system, the variable friction cargo mat. To create these radically different product systems, the functionalities provided by one of the ensembles and cells forming the variable friction cargo mat, *expand (linear)* and *contact (linear)*, are adapted to operate in different contexts without introducing any major changes to the existing subcellular feature characteristics of the adopted architectural components.

A relevant portion of the hierarchical functional architectural decomposition of the variable friction cargo mat is shown in Figure 106. In the context, a horizontal ensemble (I.A.1.), which is made of a set of slightly varying cells (e.g., I.A.1.a. First), provides the *expand (linear)*, *contract (linear)*, and *provide low friction* ensemble functions in addition to functions that afford pneumatic and mechanical attachments and contacting external components. All these ensemble functions are compounded by the combination of their relevant cell level constituent basic functions (Figure 106, cell level). An array of this horizontal ensemble (I.A.1.) forms a horizontal unit (I.A.) that provides the primary unit functions, *lift, flatten,* and *provide low friction fixed surface*. In combination with this horizontal unit (I.A.), another horizontal unit (I.B), which differently provides the *provide high friction fixed surface* unit function, composes the assembly when attached in an interdigitated manner to the first unit. Two sets of combinations of unit functions enable the assembly functions*, allow slide in XY* and *resist slide in XY*, each of which enables the technology sub-capabilities, *ease cargo loading* and *restrain cargo*, respectively.

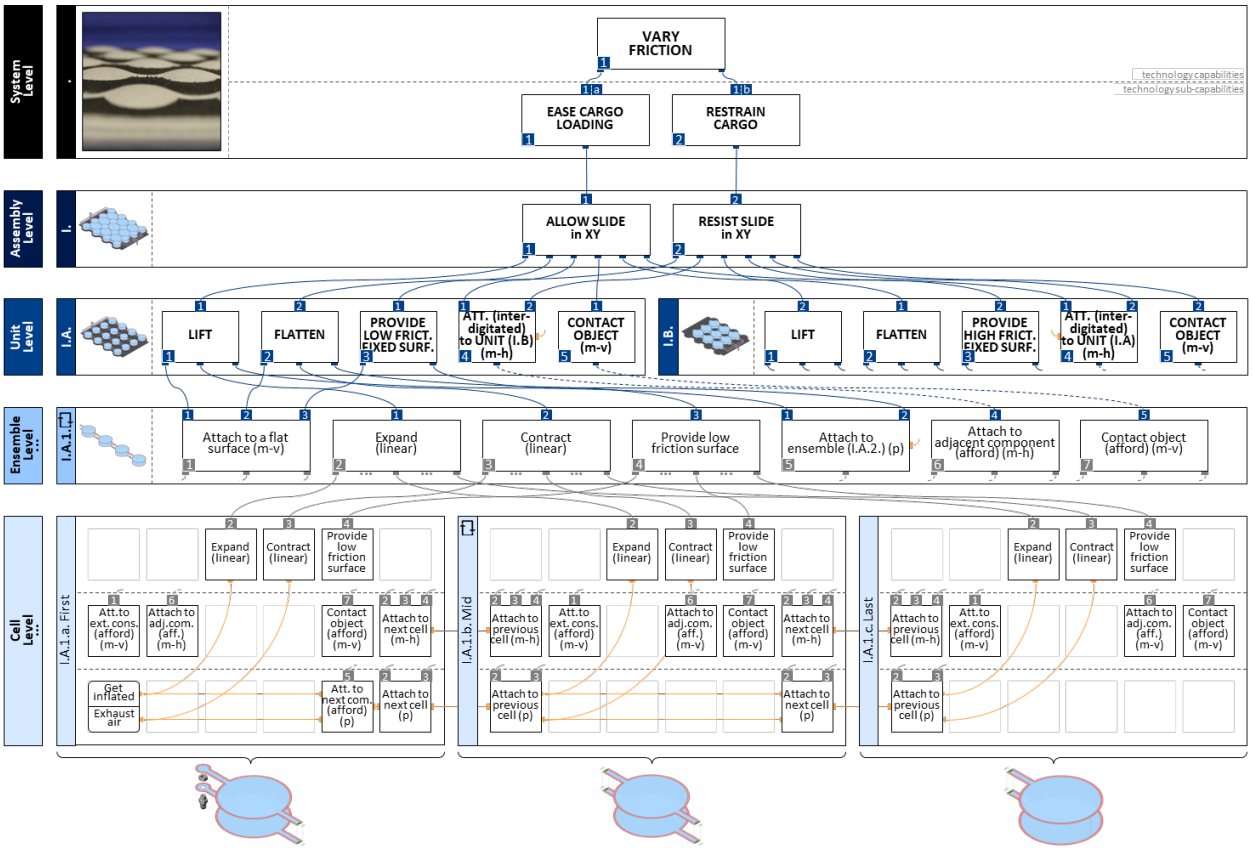

Figure 106. The hierarchical functional architectural decomposition of the variable friction cargo mat. The architecture of the variable friction cargo mat consists of an assembly (I.) containing two different units (I.A., I.B.) each of which is separately based on a set of identical horizontal ensembles (e.g., I.A.1.) that are made of variations of a cell (e.g., I.A.1.a.). Combination of these cells provide the *expand (linear), contract (linear),* and *provide low friction* ensemble functions in addition to functions that afford pneumatic and mechanical attachments and contacting external components. An array of this horizontal ensemble (I.A.1.) provides the primary unit functions, *lift, flatten,* and *provide low friction fixed surface*. Combination of this unit with the other unit (I.B.), which differently provides *low friction fixed surface,* generates *allow slide in XY* and *resist slide in XY* assembly functions. These functions enable the system level technology sub-capabilities, *ease cargo loading* and *restrain cargo,* through varying cargo mat's surface friction on demand.

One of the ensembles forming the variable friction cargo mat product system, the horizontal ensemble (I.A.1.), which is made of an array of circular cells, creates a protruded surface when activated through the pneumatic affordance operation, *get inflated*, providing a natural starting point for the design of the variable friction/detent control knob, and is adopted and re-purposed (Figure 107, e.g., ensemble I.A.2.).

As a part of this system being re-synthesized, there are three variations of this horizontal ensemble the constituents of which can be controlled through separate pneumatic affordance operations (Figure 107, cell level). Two of these ensembles (I.A.2. and I.A.3.) contain different numbers of circular cells (seven and eleven), generating differently spaced patterns of spherical domes once inflated and are vertically aggregated on top of each other. A third similar ensemble

(I.A.1.) is modified such that the circular cells replaced with a single oblong one covering the entire ensemble area. This third ensemble is mechanically attached to a curved rigid surface, providing a base over which other two ensembles are vertically aggregated, forming a complete unit. These three ensembles (I.A.1., I.A.2., and I.A.3.) provide variations of functions that enable mechanical and pneumatic attachment to adjacent components and the same set of primary ensemble functions: *expand outward (linear)* and *become muted*, which are functionally almost identical to the primary functions (*expand (linear)* and *contact (linear)*) provided by the original ensemble used to compose the variable friction cargo mat (Figure 106, I.A.1.). However, at the unit level, the constitutive compound functions that are provided in this new system significantly diverge. Instead of providing the unit functions, *lift, flatten,* and *provide low friction fixed surface*, the re-synthesized unit provides *become fully muted (mode 0), continuously bulge (mode 1),* and two instances of *generate sets of protrusions (mode 2 and mode 3)* in addition to the unit function enabling attachment to and contacting a perforated control knob enclosure. At the assembly level, the perforated knob enclosure is attached to the remaining components, enabling the combination of unit functions to provide assembly functions: *freely allow rotation (mode 0), continuously constrain rotation (mode 1),* and two instances of *intermittently constrain rotation (mode 2 and mode 3)*. The first two and last two of these assembly functions are separately combined to enable the technology sub-capabilities, *vary knob friction on demand* and *vary knob detent spacing on demand*, which can be effectively used to tailor the required physical effort to operate the knob, generating varying tactile feedback, and potentially providing a tailored haptic interaction at the highest level.

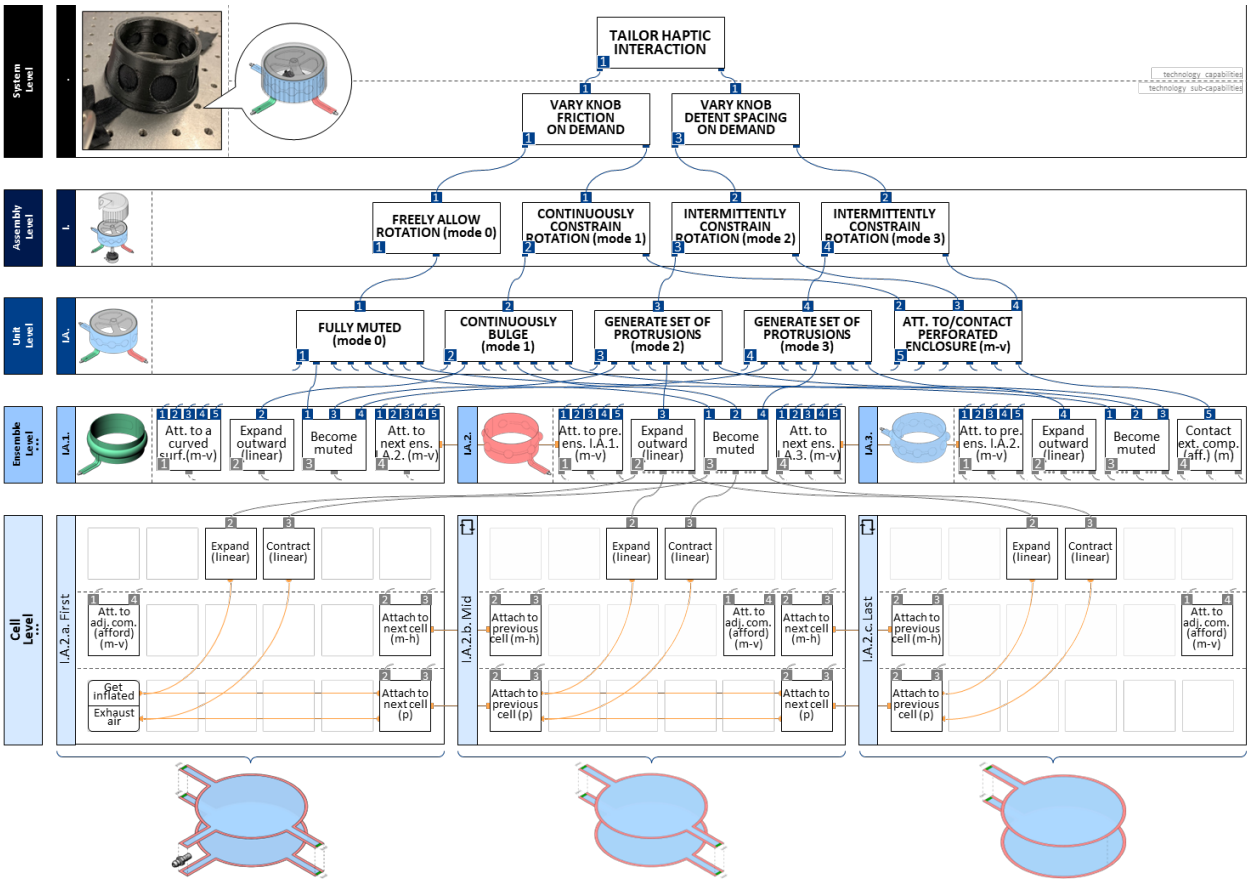

Figure 107. The hierarchical functional architectural decomposition of the variable friction/detent control knob. The architecture of the variable friction/detent control knob consists of an assembly (I.) containing a unit (I.A.) made of variations of a vertical ensemble (I.A.2.), which is architecturally almost identical to the ensemble (I.A.1.) from the variable friction cargo mat, providing *expand outward (linear)* and *become muted* ensemble functions. At the unit level, the generated unit functions that are provided in this new system significantly diverge. The re-synthesized unit provides *become fully muted (mode 0), continuously bulge (mode 1),* and two instances of *generate sets of protrusions (mode 3 and mode 4)* in addition to the unit function enabling attachment to and contacting a perforated control knob enclosure. Different combinations of these unit functions enable assembly functions, *freely allow rotation (mode 0), continuously constrain rotation (mode 1),* and two instances of *intermittently constrain rotation (mode 2 and mode 3),* affording the technology sub-capabilities: *vary knob friction on demand* and *vary knob detent spacing on demand*, which allows tailoring the haptic interaction at the highest level.

The horizontal ensemble (I.A.1.) forming the variable friction cargo mat is made of circular cells each of which can act as an actuator that can lift an external object in contact vertically when activated through the pneumatic affordance operation, *get inflated*, providing a natural starting point for the design of the easy-release ice cube tray. This tray provides an alternative way of releasing large ice cubes (2x2 in.) for the making of craft cocktails requiring less dilution. Such large ice cubes often stick in the tray, frustrating users when the existing ice cube trays are used (e.g., requiring twisting, peeling each ice cube separately).

For the design of the easy-release ice cube tray, one of the cells (Figure 106, I.A.1.a.) that is used to compose the variable friction cargo mat system is adopted and re-purposed, providing same

set of primary cell functions, *expand (linear)* and *contract (linear)*. As a part of this system being re-synthesized, a set of architecturally and functionally almost identical variations of this adopted cell is generated, in a snake-like array pattern forming a horizontal ensemble (Figure 108, I.A.1.) that provides primary ensemble functions that are identical to the ones provided by the ensemble forming the variable friction cargo mat: *expand (linear)* and *contract (linear)* in addition to providing *attach to a flat base plate (mechanical-vertical)* and *contact object (afford) (mechanical-vertical)*. These ensemble functions compound the unit functions, *expand upward (linear), contract downward (linear), attach to ice cube tray wall (mechanical-vertical),* and *contact ice cube (mechanical-vertical)*, the first of which enables pushing of the large ice cubes when activated through the pneumatic affordance operation, *get inflated*, and the second of which enables the flattening of the bottom surface of the ice cube tray when activated through the pneumatic affordance operation, *exhaust air*, at the assembly level. These assembly functions enable the sequentially operated technology sub-capabilities, *release ice cubes* and *reset ice cube tray*, providing the overall effortless ice cube making and releasing experience to users.

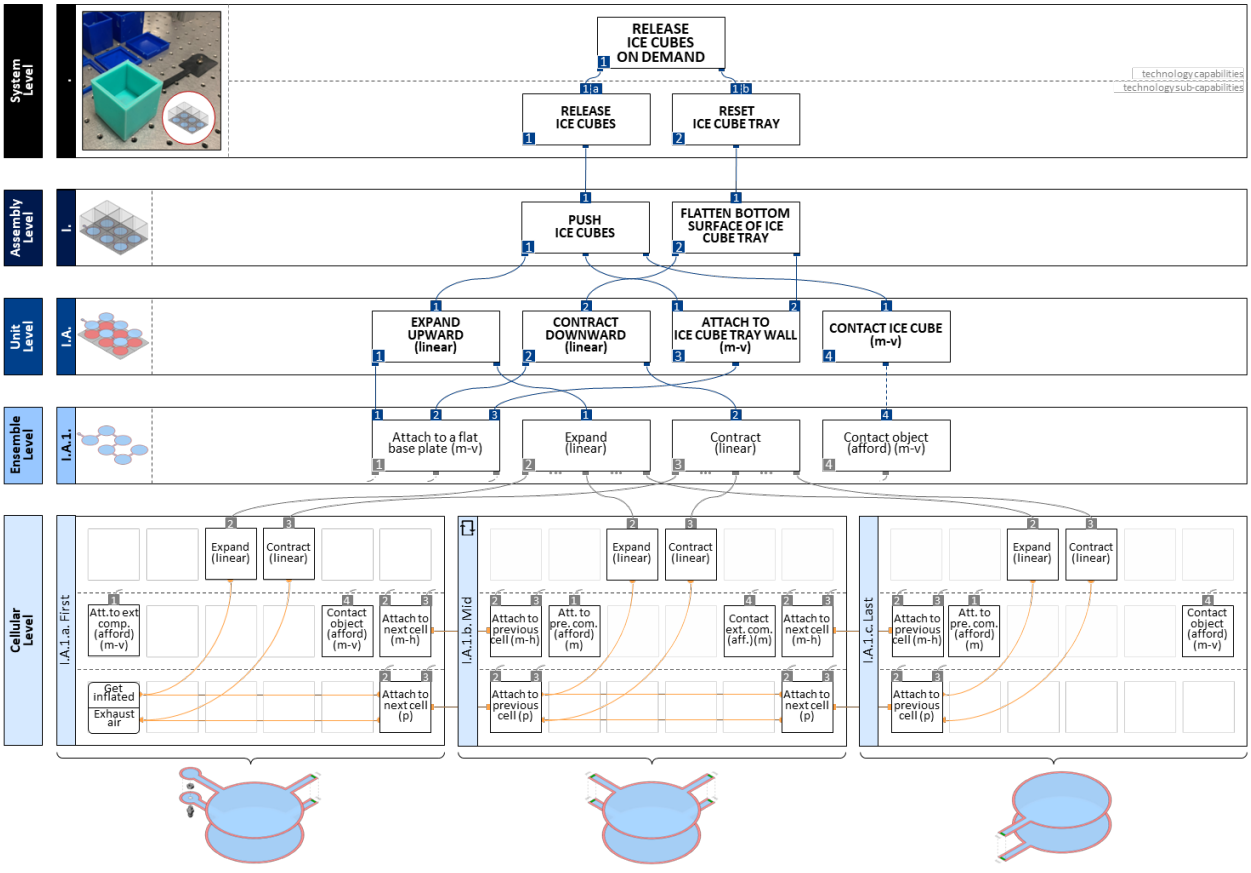

Figure 108. The hierarchical functional architectural decomposition of the easy-release ice cube tray. For the design of the easy-release ice cube tray, one of the cells that is used to compose the variable friction cargo mat system

is adopted and re-purposed, providing same set of primary cell functions, *expand (linear)* and *contract (linear)*. As a part of this system being re-synthesized, a set of architecturally and functionally almost identical variations of this adopted cell is generated, in a snake-like array pattern forming a horizontal ensemble, providing higher-level versions of the same cell functions. As the ensemble gets attached to a base plate at the ensemble level and to an ice cube tray walls at the unit level, *push ice cubes* and *flatten bottom surface of the ice cube tray* assembly functions are enabled. Each of these assembly functions enable *release ice cubes* and *reset ice cube tray* technology sub-capabilities at the system level in the hierarchy.

By changing the way a particular architectural component aggregates to form higher level architectural components in the architectural hierarchy, new system functionalities are discovered, facilitating radical innovation through the re-synthesis process. The resulting technology capabilities (i.e., release ice cubes and tailor haptic interaction) are categorically different than the ones provided by the starting example (i.e., vary friction). Unlike the previously exemplified design strategies (RD-1-2-3-4, II-1-2-3-4), the radical innovation design strategies (RI-1, RI-2) present no trade-offs because of this discovery of new technology capabilities as the design goal.

3.2.3. Performance Coupling Evaluations

A constrained layer pneumatic product system provides a single technology capability (e.g., moldability, in the case of moldable active cargo blanket system), which itself is made of a set of technology sub-capabilities (i.e., drapability, shapability, and rigidizability) enabling users to accomplish certain tasks.

The execution of an action afforded by each of a set of technology sub-capabilities (e.g., rigidizability) through its respective interaction mode (e.g., rigidizing) can be quantified as an aspect (e.g., rigidizability performance) of overall system performance (i.e., moldability) by using a set of quantifiable performance metrics (e.g., flexural rigidity, post yield elasticity). However, the aspects of a system's performance are often interrelated since technology capabilities are the highest-level constitutive functional components which emerge from an overlapping set of lower-level constituent functional components. Such overlap may introduce couplings among performance aspects, making it difficult to improve the overall performance of the system when these couplings manifest themselves as tradeoffs (i.e., negatively correlated couplings). Modifying an architectural component or the way that a set of architectural components aggregates during a re-synthesis process affects the architectural hierarchy, which also affects the functional hierarchy of a system simultaneously. Since these design changes affect the couplings in the system, it is important to understand how the architectural and functional hierarchies generate or break such couplings through the re-synthesis process.

There are two primary sources of performance couplings: 1) *parametric performance coupling*, where a particular sub-cellular feature characteristic contributes upwards through the functional hierarchy to more than one technology sub-capability, and 2*) architectural performance coupling*, where interactions between two higher-level architectural components (e.g., adjacent ensembles forming a unit) either limit their ability to be independently parametrized or impact the performances of each other's functions.

3.2.3.1. Parametric Performance Coupling (cell level)

A constrained layer pneumatic product system comprises a set of physical components (i.e., parameterized architectural components) each of which possesses a set of physical properties (e.g., a design variable such as the area of the inflatable cavity enclosed by permanently sealed cell skins) the values of which determine the extent of the physical behavior exhibited by that specific physical component (e.g., the extent of expanding). In some cases, a design variable, which is closely related to the sub-cellular feature characteristics, affects the performances of multiple functionalities upwards through the functional hierarchy, contributing to the performances of more than one technology sub-capability at the system level. In such cases, changing the value of such a design variable simultaneously affects the performances of the technology sub-capabilities, introducing parametric performance coupling at the system level. For example, in the case of tailoring the performance of the moldable active cargo blanket, the impacts of changing the design variables are highly coupled. In this product system, the same set of internally tiled variations of cells combine at the system level to provide the overall moldability technology capability as a combination of the drapability, shapability, and rigidizability sub-capabilities. Thus, the sub-capability performances all arise from the sub-cellular feature characteristics of the same set of individual cells. This coupling can be traced through the functional hierarchy where the lower-level (e.g., cell level) constituent functional components simultaneously contribute to multiple higher-level (e.g., ensemble level) constitutive functional components. Therefore, modifying any design variables (e.g., tile size, tile thickness, or inter-tile gap) associated with the performance of a function provided by cells at the cell level profoundly affects the performances of a set of higher-level functional components simultaneously, and renders the individual tailoring of each sub-capability performance separately impossible.

3.2.3.2. Architectural Performance Coupling

A set of physical components (i.e., parameterized architectural components) forming a constrained layer pneumatic product system is represented by the product's architectural hierarchy detailing the relationship among all of its constitutive architectural components composing the product system at the system level. The way these architectural components are physically brought together may couple their performance in one of two ways: 1) through *parametric design couplings*, for example, to ensure compatibility of size, the parametrization of a particular horizontal ensemble composing a vertical unit, which is made up of multiple unique horizontal ensembles, may be limited by the parametric values used for the embodiment of the other ensembles, and 2) through *physical interactions*, for example, vertically layered ensembles may attenuate each other's performance when performing functions such as expand out of plane, such that the changes in sub-cellular feature characteristics (e.g., skin thickness) may exaggerate or mitigate this performance coupling.

The variable friction cargo mat can be given as an example for the architectural performance coupling that is generated through parametric design couplings. This product system contains two interdigitated units (I.A. and I.B.) each made of a set of horizontal ensembles separately providing low and high friction surfaces through activation by their respective pneumatic affordance operations as they contact and lift the target objects, enabling them to be easily slid into place (technology sub-capability: *allow slide*) or to stay stationary (technology sub-capability: *resist slide*) on demand. Since the two units are mechanically attached to each other in an interdigitated manner, any change made in the sub-cellular feature characteristics of a cell or multiplicity of cells composing any of these units influence the embodiment of the adjacent unit, therefore making the design of these units parametrically coupled due to the system's architectural design. For instance, doubling the value of the diameter of the circular cells (e.g., I.A.1.a.), which produce the low friction surface and linear expansion functionalities, results in doubling the distance it extends once the cell is inflated at the same pressure level and increasing the lifting force it affords at the higher levels in the functional hierarchy. Since the range of target objects that can be used as a cargo can vary, tailoring the extent of the actuation stroke and the load bearing capacity generated is necessary for different use contexts (e.g., commuter hatchback vs utility pickup truck). However, the fixed size of the overall area that is covered by these two interdigitated units makes it is impossible to change the design variables (e.g., diameter of cells) of one of the units without

limiting the embodiment of the other unit, since increasing the size of one necessitates reducing the size of the other. Such architectural coupling between design variables stemming from the way the architectural components aggregate (in this case horizontal interdigitation of the units) to compose the product system couples the range of performance that can be produced by those components.

The variable friction/detent control knob can be given as an example for the architectural performance coupling that is generated due to physical interactions between architectural components. There are three unique horizontal ensembles (I.A.1., I.A.2, and I.A.3.) composing a vertical unit (I.A.) as a part of this product system. These ensembles, which are made up of different numbers of different cells, are permanently stacked on top of each other. Therefore, a modification on the sub-cellular feature characteristics of the cells forming any of these vertically aggregated horizontal ensembles potentially affects the performances of the functions provided by the remaining two ensembles. For example, replacing the flexible and soft bottom skin layer of the cells forming ensemble (I.A.3.) with an inextensible and stiffer material would not affect the performance of one of the unit functions, *generate set of protrusions (mode 3)*. However, it would have a negative effect on the performance of the unit functions generated by the remaining two ensembles (I.A.1. and I.A.2), which are layered below, the activation of which would be somewhat blocked by the inextensible and stiffer bottom skin layer of the cells forming ensemble (I.A.3.). The mitigation of such an architectural performance coupling can be achieved by re-synthesizing the unit horizontally instead of vertically by using the same set of horizontal ensembles. However, this requires larger product packaging, which introduces another trade-off to be considered through the design process.

3.2.3.3. Evaluating Couplings During Re-synthesis

While performance aspects are not the primary concern during the conceptual design stage, the identification and qualitative evaluation of potential couplings, which will impact the embodiment design stage, is useful and important. Re-synthesizing an existing product system during the conceptual design stage may introduce performance couplings since a design modification affects the architectural aggregation in the hierarchy and/or changes the sub-cellular feature characteristics as a part of the re-synthesis.

For example, the initial version of the active rear seat pocket's (V1) architecture is made of one ensemble (I.A.1.) that provides the *bend* ensemble function once activated through its

respective pneumatic affordance operation, *get inflated*, and the *flatten* ensemble function afforded by the elastic recovery force generated by each cell's relatively thicker bottom skin layer once the air inside the bladders is exhausted from the system. These ensemble functions are propagated to the unit level as unit functions. Unlike the initial version (V1), the re-synthesized active rear seat pocket's (V3) architecture is made of a unit (I.A.) that is composed of two horizontal ensembles (I.A.1. and I.A.2.) that are stacked vertically face-to-face, providing the *bend outward, bend inward,* and *flatten* unit functions. Stacking these two ensembles on top of each other results in stacking the relatively thicker bottom skins of each cell separately forming these ensembles as well, generating an increased amount of elastic recovery force affecting the overall system performance. This introduces an architectural performance coupling that is generated due to physical interactions between architectural components (ensemble I.A.1. and ensemble I.A.2. in this case). The increased amount of elastic recovery force improves the performance of the *flatten* unit function; however, it adversely affects the performances of both unit functions, *bend outward* and *bend inward*. The relative importance of the performances of these functions depends on the product use context and iteratively impact the conceptual and embodiment design stages.

Similarly, as a part of the initial version of the mobile phone restraint mat's (V1) architecture, two different vertical ensembles (I.A.1. and I.A.2.) are vertically combined to create a unit (I.A.), which provides the *deploy & lift (angular-90°)*, and *push (linear)* unit functions. An assembly (I.), which is made of two pneumatically connected opposing identical units (I.A. and I.B.), provides the *deploy & lift (angular-90°)* and *squeeze* assembly functions, which are sequentially activated through their pneumatic affordance operations. Since these assembly functions are afforded by two identical units containing two different ensembles, their performances are primarily decoupled and it is possible to tailor the performances of these functions separately. However, unlike the initial version (V1), two identical horizontal ensembles (I.A.1. and I.A.2.) are horizontally combined to create a unit (I.A.) as a part of the re-synthesized mobile phone restraint mat's (V2) architecture. This unit provides the *curl upward* and *provide low friction surface* unit functions that conceptually replace the d*eploy & lift (angular-90°)* and *push (linear)* unit functions provided by the initial version (V1), simplifying the overall architectural hierarchy. Thus, instead of a two-step sequential operation, the task of orienting the mobile phone on the charging mat in one axis (e.g., orienting phone in x) in the re-synthesized system is accomplished by a one-step operation through which the architectural components curl upward to slide the phone on the low friction

surface to the center of the mat using gravity. This, although simplifying the architecture and operational complexity of the system, introduces a potential performance coupling since the *curl upward* and *provide low friction surface* unit functions are both primarily contributed to by the *bend* and *provide low friction surface* cell functions, respectively. The fact that these two cell functions are contained as a part of the same basic architectural component (e.g., I.A.1.a.), the changes in the sub-cellular feature characteristics (e.g. changing skin type to modify surface friction properties) to tailor the performance of the one will affect the performance of the other (e.g., increasing stiffness of the low friction skin, reducing bending performance).

In both of these contexts, the hierarchical functional architectural decomposition approach provides a direct view into the system hierarchy at the conceptual design stage, enabling the identification of the potential performance couplings as a result of making aggregational and/or component-wise (i.e., modifying sub-cellular features characteristics) design modifications. This enhances the systematic re-synthesis process afforded by the hierarchical functional architectural decomposition approach to enable re-design, incremental innovation, and radical innovation of constrained layer pneumatic product systems.

3.3. Conclusion

This chapter presents a formal hierarchical analytical design description, *the hierarchical functional and architectural decomposition*, which provides a direct view into the hierarchical structure of a system's coupled form and functionality. By breaking down the hierarchy into five primary levels—cell, ensemble, unit, assembly, and system—this approach effectively demonstrates how architectural and functional components at each level are composed of components from the levels below. This comprehensive representation facilitates a deeper understanding of the system's organization and interdependencies among system architectural, functional, operational, and performance aspects. This decomposition approach supports early-stage goal-oriented synthesis, analysis, and re-synthesis of user-interacting structurally adaptable multi-mode product concepts employing constrained layer pneumatic systems at a conceptual level.

Formal grammars and diagramming methods are established to effectively describe and consistently connect the constituents of the hierarchical functional and architectural decomposition across each level of the hierarchy. The hierarchical functional architectural decomposition

approach is demonstrated as a useful tool for gaining understanding and providing insights into the architecture, functionality, and operation of user-interacting structurally adaptable multi-mode product concepts. By facilitating a consistent foundation for describing and communicating the system's interrelated architectural, functional, and operational aspects, this approach paves the way for exploring alternative system interrelationships during the early stages of the design process.

Through the use of a case study of a mobile phone restraint mat, the terminology describing each level of the hierarchical functional architectural decomposition is contextualized and communicated. Diagramming conventions, as well as the different pneumatic operating states and sequences involved, are concretized, building on the pneumatic affordance operations introduced in Chapter 2.

The interrelated architectural and functional breakdown facilitates iterative synthesis at the higher levels, where the basic architectural components (i.e., cells) are combined to produce compound ones (i.e., ensembles, units, assemblies, system), corresponding to the generation of compound functions (i.e., ensemble functions, unit functions, assembly functions, technology capabilities) from the combination of basic ones (i.e., cell functions). This approach empowers designers to generate design alternatives for multi-mode product concepts using constrained layer pneumatic systems through re-synthesis, which involves modifying or substituting architectural components without impacting the existing higher-level functionalities. It also enables the synthesis of new systems, given a library of existing functional assemblies, units, ensembles, and cells.

Ten design strategies aimed at systematizing the re-synthesis process of a structurally adaptable multi-mode product concept employing constrained layer pneumatic systems are formulated using the hierarchical functional architectural decomposition approach as a basis. This formulation encompasses defining a combination of design objectives (*what*), design goals (*why*), design modifications (*how*), and associated tradeoffs (*why-not*). Each strategy's design objective is achievable by actualizing a design modification to attain a design goal while allowing a design trade-off for the re-synthesis of an existing multi-mode product using a constrained layer pneumatic product system.

The formulated design strategies empower designers to explore various design alternatives for product concepts utilizing constrained layer pneumatic systems during the initial stages of product design, promoting re-design, incremental innovation, and radical innovation. The implementation

of the proposed design strategies for re-synthesizing multi-mode products that use constrained layer pneumatic systems for structural adaptability is showcased through five existing design concept examples from Chapter 2 (section 5), which serve as starting points for goal-oriented development of alternative designs. Consequently, eight alternative designs are generated, with two aimed at re-design, two focused on incremental innovation, and the remaining four targeting radical innovation, validating the usefulness of the hierarchical functional architectural decomposition approach.

While the hierarchical functional architectural decomposition approach is presented in the context of designing structurally adaptable multi-mode product concepts using constrained layer pneumatic systems, it can be further applicable for the analysis, synthesis, and re-synthesis of system designs for many other highly structured architectural classes of systems relying on architectural and functional hierarchies.

Chapter 4. Architectural and Parametric Design for Multi-modal Performance

Adaptive moldable surfaces are emerging active technologies for which constrained layer pneumatic systems have the potential to provide a technological basis. They have the repeatable ability to passively conform to varying shapes, activate to rigidly hold the shape or object, and then reset back to a passive condition. These adaptive capabilities enable the design of a new generation of multi-mode products of high value in many fields: 1) medical applications such as a moldable orthopedic cast that can be tailored to different users and can be reused [88], a wheelchair positioning device to correct the posture of stroke patients [89], and wearable variable stiffness structures in a rehabilitation context [90], 2) human-computer interaction and consumer products such as flexible displays with controllable stiffness capabilities [184] and furniture and footwear with reconfigurable jamming parts [85], 3) the entertainment industry such as adaptive moldable surfaces which can be used as wearables with haptic feedback for more immersive gaming experience [185], and 4) the transportation industry for constraining cargo for secure transportation from one location to another [186]. For these applications, there are three primary functionalities provided by adaptive moldable surfaces: drapability, shapability, and rigidizability. *Drapability* requires a surface that can passively arrange itself over the shape of a target object under its own weight in a fabric-like manner. *Shapability* requires a surface that can be manually conformed to the curvature and shape of a desired configuration. *Rigidizability* requires a surface that can change its stiffness on demand after being shaped to securely hold its shape against potential external forces. In most applications, the transition between operation states activating each of these functionalities needs to be fast and reversible. The technological design of adaptive moldable surfaces with all three functionalities present is interesting due to the inherent tradeoffs among them as the same design features impact the performances of all three functionalities. In the high-payoff application space of user-interacting products, the priority of these capabilities can significantly vary depending on the application. This is further complicated by constraints to

ensure safety and package (compactness and weight) viability. Thus, it is important to have a good understanding of the coupled relationship between the design features and all three functionalities simultaneously to drive the design of effective products.

Extensive research has been conducted in various fields focusing on the use of traditional materials, smart materials, and pneumatically activated systems for the design of adaptive moldable surfaces. Traditional materials such as gallium-silicone composite [187], woven polyester with integrated PLA [188], and 3D printed PLA [189] with embedded heating elements can change temperature through the glass transition temperature of the material to induce stiffness change. This approach has been used to enable applications such as a transformable table clock/wearable biometric sensor [187], a wearable active finger brace [188], and a tailorable custom-fitting musculoskeletal support system [189]. However, the temperature for activating material glass transitioning (30-48C) and the time required for switching from one state to another limit this approach. Smart materials such as nickel-titanium shape memory alloys [190], polyurethane based shape memory polymers [191], and SMA wires coupled with buckling springs [192] can enable the design of surfaces of which stiffness can be controlled on demand. This approach has been used to develop self-fitting wearables for spaceflight applications [190], a morphing airfoil that can both change stiffness and enable bending and axial strains [191], and a multi-layered beam that can switch between compliant and stiff states [192]. However, the operating temperatures required to activate shape memory alloys (~20-120°C) and polymers (~20-55°C) limits the design freedom in the context of physically safe and viable user-product interactions.

A promising approach for user-facing applications is pneumatically activated composites consisting of an airtight bladder containing a regular or irregular array of components in one of three categories: granular, fibrous, or layered material. When the air is vacuumed from the bladder, friction force between the encapsulated components increases, causing the transition from soft to rigid states. Granular jamming has been comprehensively studied by researchers to identify the relative contributions of the granule shape, granule size [193], and material type [194], [195] on the change in stiffness in different operation states. Applications range from universal robot grippers [194], [196], [197] to transformable and temporary spaces [198], and from malleable and organic user interfaces [6], [199] to reusable molds for free-form concrete constructions [200]. However, such applications occupy large volumes due to the architecture of the system, lacking

compactness both in soft and rigid states. Research in fiber jamming has focused on the effects of using various fiber materials and surface finishing on the resulting stiffness change to enable applications such as soft robots [201] and variable stiffness surgical manipulators [202], [203]. However, most of the demonstrated applications are in tubular form and require elaborate fabrication process with complex drive mechanisms, which limit their applicability. Layer jamming replaces the granular or fibrous materials with layers of sheets, resulting in a compact cross-section. Researchers have explored the effects of using multiple layers of woven, interleaved, creased, perforated, and overlapping fish-scale-like layers [85], [204], using commercially available affordable sheet materials such as copy paper, sandpaper, various types of fabric, PET foil [204], mylar [205], Kapton, polyester, PTFE, and PTFE-coated fiberglass [206]. Examples range from medical applications such as a reusable moldable medical cast [88], a wheelchair posture positioning device [89], and wearable rehabilitation structures [90], [207] to applications in the human-computer interaction field and consumer products such as flexible displays [184] and reconfigurable furniture and footwear [85]. This can be extended to the transportation industry for a seat belt damper using layer jamming to quickly switch from soft to rigid states to maximize comfort and safety [206]. However, traditional layer jamming structures composed of inextensible sheets lack the capability of bending in transverse and longitudinal axes simultaneously without creasing which limits their conformability to arbitrary configurations. Researchers addressed this issue by using multiple layers of extensible woven fabric sheets [208]. However, the maximum achievable stiffness is limited by the stiffness of the individual fabric sheets. Increasing the number of fabric sheet layers in an airtight bladder may enhance the overall achievable stiffness, yet the resulting structure would occupy a large volume similar to granular or fiber jamming structures.

More recently, a tile-based rigidization [90], [209], [210] approach has emerged as a sub-category of constrained layer pneumatic systems, which can alleviate the disadvantages of granular, fiber, and traditional layer jamming, capitalizing on opposing arrays of rigid tiles encapsulated in an airtight bladder enabling continuous control over overall stiffness. Because of the ability of adjacent tiles to move relative to each other, the tile-based rigidization approach provides a thin profile surface that affords bending in two directions simultaneously, rendering surfaces more drapable and shapable. Research to date has mainly concentrated on the enhancement of rigidization capabilities activated by vacuum pressure. This chapter more broadly explores internally tiled pneumatic textiles and the coupled relationship of the design features with

all three high-level functionalities (i.e., sub-capabilities) simultaneously to drive the design of effective products. The variety of the different types of architectures, which make up internally tiled pneumatic textiles, can be organized hierarchically into a set of broad classes, some of which have more specific sub-classes, each allowing a specific set of possible architectural feature variations (Note: the hierarchical organization of the types of pneumatic textile architectures is entirely separate from the hierarchical decomposition of one particular constrained layer pneumatic system architecture as discussed in Chapter 3). The overall textile architecture is introduced with three key example tile architectural classes: bladder-attached, internal sheet-attached, and mutually interlocking. The operational state of the textile varies as a function of vacuum pressure, providing the core technology sub-capabilities: drapability, shapability, and rigidizability. To enable a rigorous study of the impact of tile architectural design relative to the technology sub-capability performances, measurable engineering performance metrics are defined and experimentally characterized: draping angle for drapability, conformability and setability for shapability, and flexural rigidity and post yield elasticity for rigidizability. The broad hierarchical architectural design space of internally tiled pneumatic textiles is systematically explored by conducting three consecutive studies, each exploring a different level of the architectural hierarchy: 1) a tile architectural study, analyzing the effects of using different tile architectural classes, 2) a design coupling study, analyzing tradeoffs among performance metric pairs within tile architectural subclasses, and 3) an architectural feature variations study, analyzing the effects of shifting the tile array layers and including an intermediate friction layer. These studies enable an efficient method for addressing a broad design space of internally tiled pneumatic textiles, uncovering the wide range of interrelated (sub)capabilities catering to the design of user-interacting adaptive moldability applications.

To demonstrate the application of internally tiled pneumatic textiles in the design process of structurally adaptable multi-mode products, a design case study, *moldable active cargo blanket*, which targets providing a solution for securing and transporting loose cargo of varying items in a moving vehicle, is conducted. By employing an architectural design representing a particular architectural class and sub-class (i.e., bladder-attached non-connected tiles) and a particular set of architectural feature variations that are available in that sub-class, the tile geometry design variables are identified. To develop an understanding of the relationship between the identified tile geometry design variables and resulting performance of each technology sub-capability, a

predictive empirical model is built and validated based on a half factorial design of experiments. This model relates tile geometry design variable variations to the resulting quantifiable engineering performance metric values, capturing the mechanically complex behavior of the moldable active cargo blanket. This model enables an algebraic method for selecting a specific set of tile geometry design variables to obtain intended design outcomes in terms of quantified engineering performance metrics. This method is demonstrated by tailoring the moldability performance of three different active cargo blankets each suited to different target use contexts, the performances of the resulting designs are experimentally validated against their intended design goals. The work in this chapter provides the enabling basis for the structurally adaptable multi-mode moldable active cargo blanket application as well as a more general technology basis.

4.1. Internally Tiled Pneumatic Textiles

Internally tiled pneumatic textiles exhibit shifts from providing one technological sub-capability to another as vacuum pressure is introduced to the system as shown in Figure 109. They exhibit fabric-like physical behavior in terms of being drapable over arbitrary forms at atmospheric pressure. However, the same pneumatic textiles can be shaped manually by external forces and be posed into intended forms by applying a vacuum. As the vacuum pressure reaches a maximum, the pneumatic textiles hold their shape with enhanced stiffness. In the enhanced stiffness state, the pneumatic textiles perform as load-bearing rigid structures, resisting external forces that otherwise disturb the intended target form. An in-depth understanding of the relation between the technology sub-capabilities obtained at the different vacuum pressure levels and the design features of the pneumatic textiles is crucial for the implementation of these layered structures in user-interacting multi-mode products. To achieve such understanding, a generic architecture captures the basic constituents of the internally tiled pneumatic textiles. This provides a basis to categorize the multiple types of tile architectural classes. The operation states (draping, shaping, rigidizing), which are induced by the changes in vacuum pressure inside an airtight pneumatic textile, relate to the type of these architectural classes, enabling technology sub-capabilities (*drapability, shapability, rigidizability*), which are combined to provide the overall capability, *moldability*.

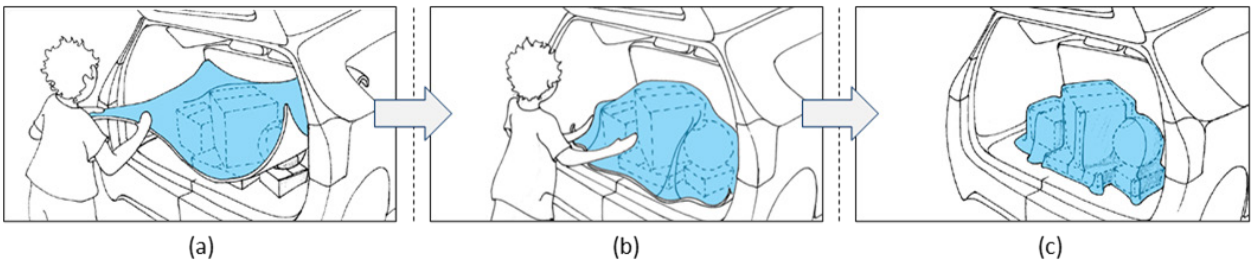

Figure 109. An example use of the key functionalities of internally tiled pneumatic textiles as a moldable cargo blanket. (a) A pneumatic textile can be draped over arbitrary objects at atmospheric pressure. (b) It can be manually shaped into various configurations to accommodate target forms as the vacuum pressure is introduced to the airtight bladder. (c) It can be fully rigidized as the vacuum pressure reaches a maximum, providing a secure transportation of a cargo.

4.1.1. Architecture

The architecture of internally tiled pneumatic textiles is composed of one or multiple layups which are based on layers of rigid tiles arrayed in regular patterns within an airtight bladder. Each one of these layups contains an exterior fabric layer and an inner airtight layer which form the bladder skin when combined, and a layer (or layers) composed of an array of tiles. A pneumatic fitting attached to one of these layups allows control over pressure inside the layered structure in relation to atmospheric pressure. Based on variations in the pressure level, an internally tiled pneumatic textile can transition from soft to rigid states as tiles are pushed against each other due to the force generated by the external atmospheric pressure. The various adaptive moldability sub-capabilities are functions of pressure. In Figure 110, the architectural layup of a specific class of internally tiled pneumatic textile is shown as an example on the left, with a detail of the tile array on the right. An individual tile is designed with its shape (e.g., extruded triangle, hexagon, or complicated 3d form), size, height or thickness, and features such as protrusions on the tile surface. The array pattern and layup are designed in the way these individual tiles are brought together, the number of tile array patterns encapsulated in the airtight bladder, and their relative position to each other.

The tile, array, and layup design affect the resulting performance of a pneumatic textile and can be hierarchically categorized into various tile architectural classes each composed of one or more subclasses for which particular feature variations exist. A comprehensive understanding of the inherent characteristics of these architectural classes is important considering the fact that variables regarding to the design of individual tiles, the selection of material, and the fabrication techniques vary based on the architectural class to which a pneumatic textile belongs.

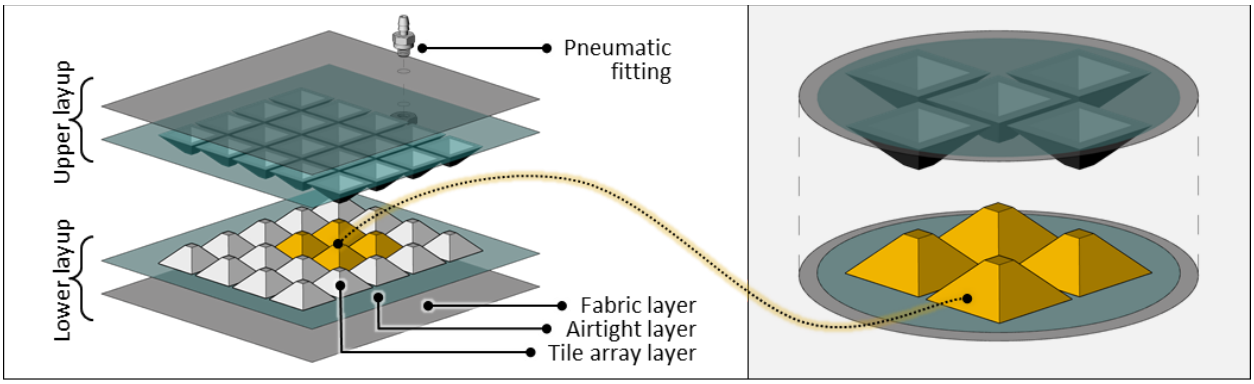

Figure 110. An example generic architecture of the internally tiled pneumatic textiles. The architecture of the internally tiled pneumatic textiles is composed of airtight fabric forming an airtight bladder, a pneumatic fitting, and tile array layers. Each tile array layer is made of rigid tiles that are arrayed in regular patterns. The approaches for creating such spatial order among the adjacent tiles inside the enclosing bladder is facilitated by the type of tile architectural class a pneumatic textile belongs to.

4.1.2. Tile Architectural Classes

Internally tiled pneumatic textiles can be categorized into three main architectural classes based on the approaches that provide a defined spatial order among the adjacent tiles inside a bladder, hence facilitating the formation of the tile array patterns. These architectural classes are *bladder-attached tiles*, *internal sheet-attached tiles*, and *mutually interlocking tiles*. Each architectural class shows differences regarding to the formation of the tile array layers, the strategies for the layup of these layers, and the relationship between the tile array layers and the bladder skin. Based on these differences, the pneumatic textiles provide varying levels of technology (sub)capability performance.

4.1.2.1. Bladder-Attached Tiles

The bladder-attached tiles class contains tiles that are permanently attached on the bladder's interior skin, which ensures a regular array pattern among adjacent tiles. One subclass of this basic architecture, *bladder-attached non-connected tiles*, where the only connection between adjacent tiles is the bladder skin itself, is shown in Figure 111 on the left. In this case, the bladder skin provides flexibility between individual tiles in a hinge-like manner. A variation of this architecture that accommodates tile design features to connect the adjacent tiles to each other is the *bladder-attached connected tiles* subclass, illustrated in Figure 111 on the right. These additional tile design features enhance the overall stiffness of such a layered structure; however, it reduces the hinge-like ability of the non-connected tiles, negatively affecting the draping performance.

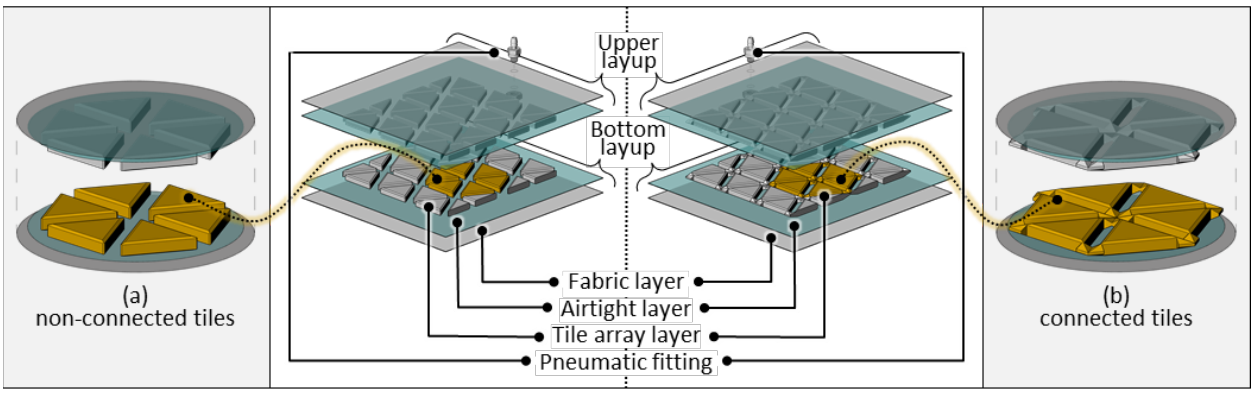

Figure 111. Example architectures of the bladder-attached tile class. (a) The bladder-attached non-connected tile subclass features an array of tiles that are not physically connected to each other and are permanently attached to the bladder's interior skin. (b) The bladder-attached connected tile subclass features an array of tiles where each tile is also physically connected to the adjacent tiles via additional design features. Any pneumatic textile categorized under bladder-attached tiles class contains two opposing tile array layers.

The design variables such as the tile shape, the features connecting adjacent tiles to each other, and the gap between each tile affect the resulting performance of a pneumatic textile made of the bladder-attached tiles. For example, as the size of the gap between adjacent tiles decreases, the range of hinge-like motion will reduce. This presents an overall performance tradeoff between technology sub-capabilities such as reducing gap size to make a less drapable but more rigid pneumatic textile. The tile material is another factor that has an effect on the resulting performance. For example, a pneumatic textile in which tiles are made of stiffer material would provide relatively better rigidizability performance in comparison to another one accommodating relatively less stiff tiles where all the remaining design variables remain unchanged. For the bladder-attached tiles class, the type of material needs to be compatible with the material of the bladder's interior skin to enable permanent bonding by either heat sealing or the use of adhesives.

4.1.2.2. Internal Sheet-Attached Tiles

The internal sheet-attached tiles architectural class, unlike the bladder-attached tiles class, has no dependency on the bladder to maintain the tile array pattern. Instead of using permanent bonding to the bladder skin to create a defined tile array pattern, it makes use of an extra layer in sheet form to which the individual tiles are attached to maintain their spatial locations within the airtight bladder. In Figure 112, an example configuration of the internal sheet-attached tiles is shown, which consists of two opposing layups of hexagonal tiles facing one another. Each tile contains two parts: a bottom part with grooved pegs and a top part with through-holes. The bottom part with pegs snaps into the top part through the sheet layer, which is precisely perforated,

defining the gap between adjacent tiles, keeping the tile array pattern together, yet enabling individual tiles to have the capability of hinge-like motion.

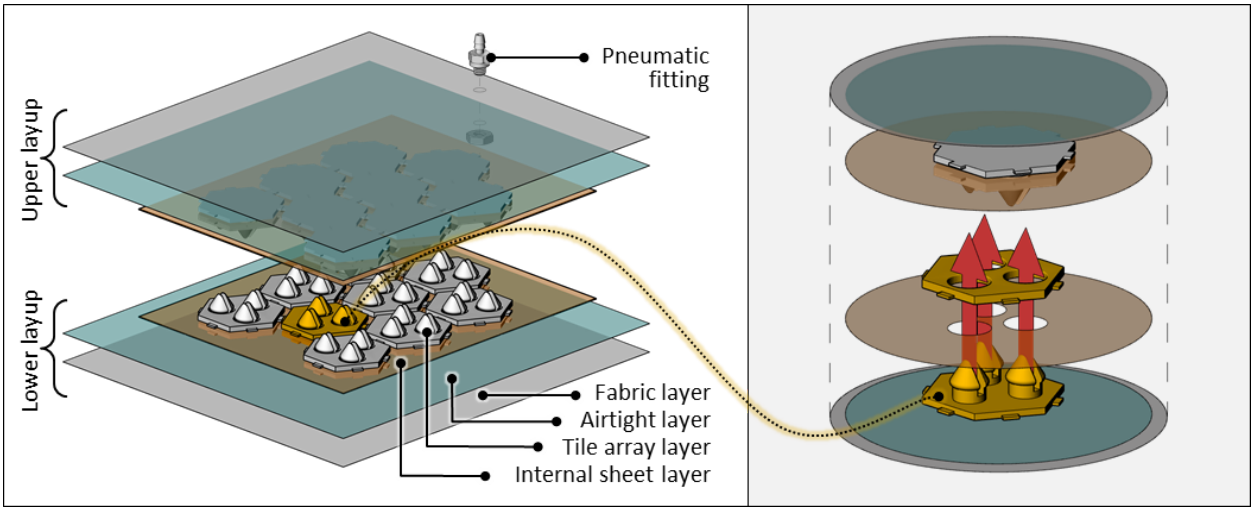

Figure 112. An example architecture of the internal sheet-attached tile class. Each tile in this example internal sheet-attached tile class contains two parts: bottom and top, featuring grooved pegs and through holes respectively. These two parts snap into each other through a pattern-perforated internal sheet layer, which governs the resulting tile array layer spatial formation. Any pneumatic textile categorized under internal sheet-attached tiles class contains two opposing tile array layers.

The performance of a pneumatic textile containing internal sheet-attached tiles is influenced by factors such as the material used to fabricate tiles, the design of each tile (shape, size, height, and number of pegs), the size of the gap between tiles, and the material properties of the internal sheet layer. For example, a pneumatic textile containing relatively small steel tiles with only one peg and a hole attached through a perforated silk layer with large amount of gap between adjacent tiles would provide far better drapability performance in comparison to another one accommodating relatively large polypropylene tiles with three pegs and holes attached through a perforated dense polyester layer with small amount of gap between bordering tiles. The separation of bladder skin and the tile array layer provides advantages in terms of the material selection and ease of scalable fabrication, which enables employing alternative fabrication techniques such as additive manufacturing, molding, or adhesive bonding of the tiles directly on the internal sheet layer. However, there is a potential risk of having misaligned tile array layers since they are free to move inside the airtight bladder, which would have an adverse effect on the load-bearing and rigidizability performance.

4.1.2.3. Mutually Interlocking Tiles

The mutually interlocking tiles architectural class, similar to the internal sheet-attached class, has no bladder dependency for tile arrangement. However, it makes use of complementary tile features to connect adjacent tiles together to maintain a regular tile array pattern instead of using an extra sheet layer. A pneumatic textile made of the mutually interlocking tiles can function by containing only one tile array layer unlike the pneumatic textiles made of tiles categorized under the other architectural classes, which necessitate at least two layers of tile arrays. Each individual tile that forms the array pattern has equal numbers of complementary features; one instance of this is shown in Figure 113, a tile making use of loops and legs. These complimentary design features enable any tile to be interlocked to its neighboring tiles. This provides flexibility since the legs can slide and rotate within their corresponding loops. Such flexibility allows these layered structures to be drapable under atmospheric pressure and shapable as vacuum is being introduced to the system. The size of the gap between adjacent tiles becomes minimum as the legs slide all the way back in the loops when the air is fully vacuumed out of the bladder, resulting in an enhanced overall stiffness of the pneumatic textile. Concurrently, the asymmetrical nature of the individual tiles induces a cinching motion because of the moment generated by the shrinkage of the bladder skin around the legs.

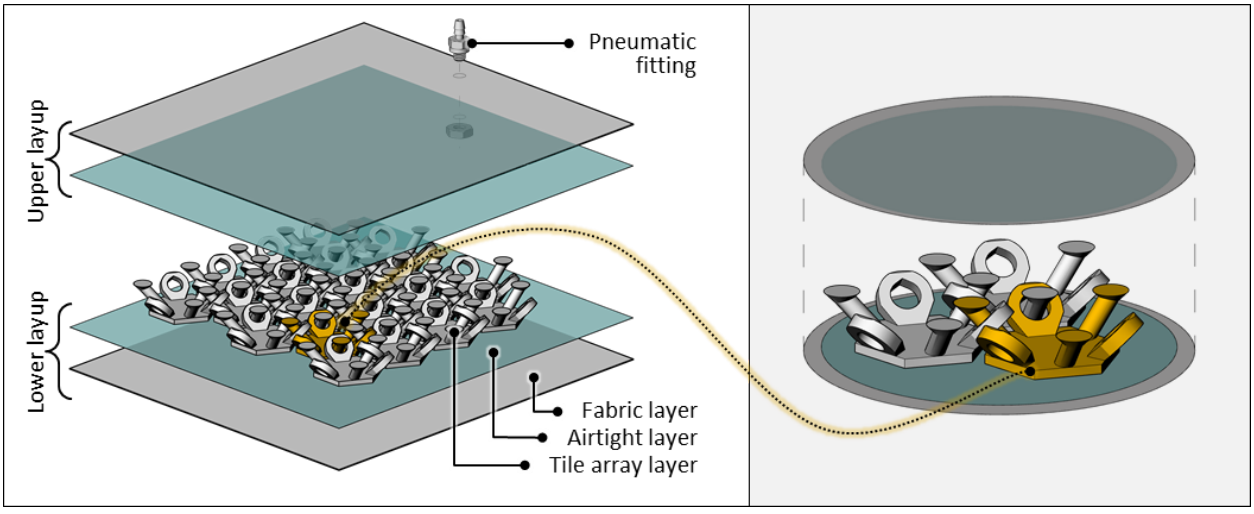

Figure 113. An example architecture of the mutually interlocking tile class. Each tile in this mutually interlocking tile class has complementary design features such as rigid loops and legs. Adjacent tiles are held together using these features, resulting in the formation of a regular tile array pattern. Pneumatic textiles categorized under mutually interlocking tiles class contains only one tile array layers unlike the other tile architectural classes.

The material and the shape of the tiles affect the performance of the pneumatic textiles that are made of the mutually interlocking tiles. The details of the complementary features such as the

height and the angle of legs and loops influence cinching, hence have an effect on the shapability performance. For example, a pneumatic textile made of tiles featuring relatively longer and shallow angled (<45°) legs and loops would outperform its counterpart that is made of tiles featuring relatively shorter and 45° angled legs and loops in terms of shapability performance. As for the internal sheet-attached tiles, the separation of the tile array layer and the bladder skin facilitates more freedom regarding to the selection of material, scalable fabrication, and the design of mutually interlocking tiles through which distinct functionalities such as cinching can be achievable in comparison with the bladder-attached tiles.

4.1.3. Operation

The overall technology capability, *moldability,* is the primary user-facing purpose of the moldable multi-mode products equipped with internally tiled pneumatic textiles while the three sub-capabilities directly map to the three user-product interaction modes: *drapability, shapability, and rigidizability*. Each interaction mode requires the activation of a set of lower-level functionalities through their respective pneumatic affordance operations. Therefore, the internally tiled pneumatic textiles operate between three states using different sets of pneumatic affordance operations.

The hierarchical functional architectural decomposition of the moldable active cargo blanket concept was introduced in Chapter 3, demonstrating the inherent interrelation among architectural and functional components composing the product system providing the *moldability* technology capability at the system level while providing an insight about the operation and performance of the entire system. Since the moldable active cargo blanket is a particular application of the broader internally tiled pneumatic textiles technology, the decomposition shown in Figure 114 can be used as a starting point to help indicate the operations and functionalities that are relevant to its use in the context of the particular design application.

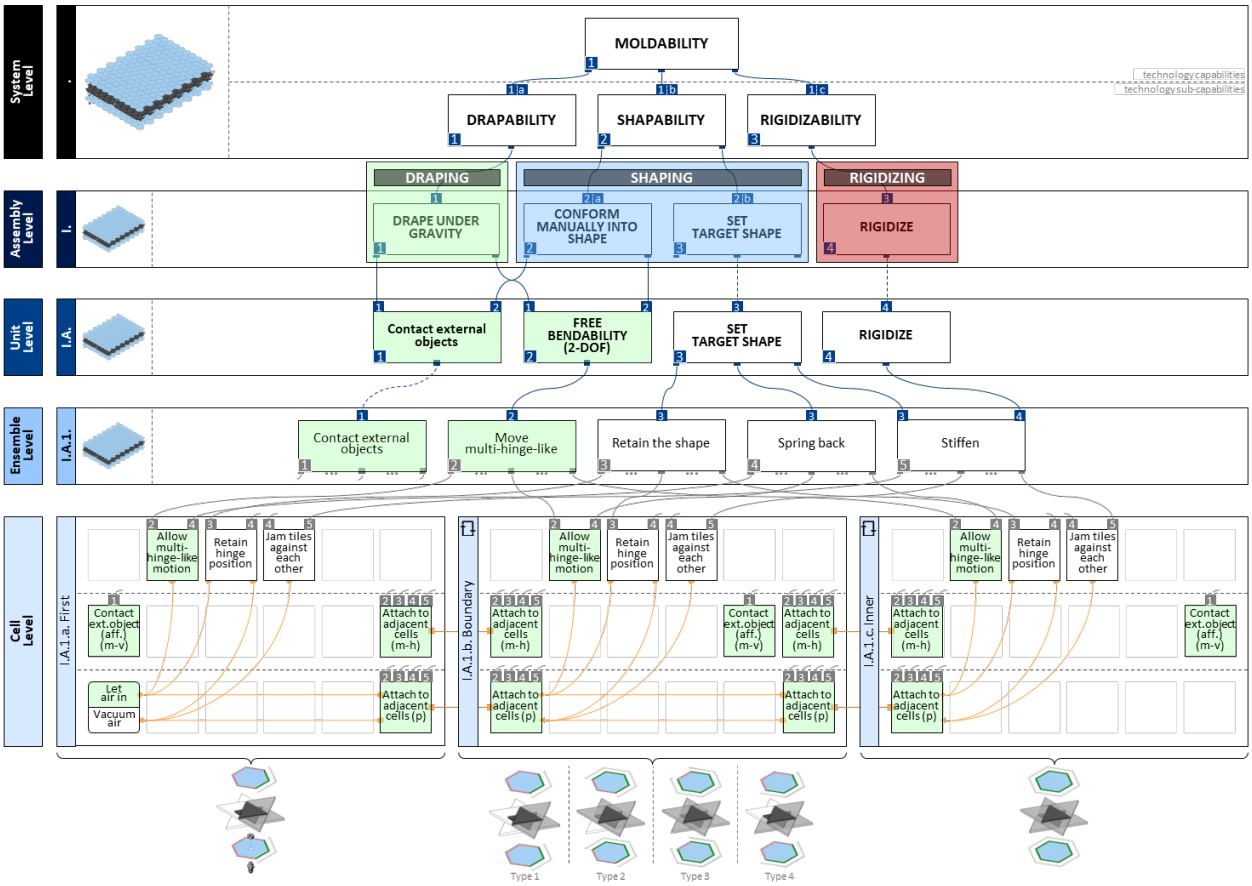

Figure 114. The hierarchical functional architectural decomposition of the moldable active cargo blanket used as a starting point for performance metric identification. The architectural decomposition of the moldable active cargo blanket is identical to the initial system's architectural decomposition since ensemble (I.A.1.) propagates upwards as a part of the relatively flat architectural hierarchy. Functionally, the re-synthesized system expands the extent of an existing cell function, allow 1-dof hinge-like motion, in addition to providing a new cell function, contact external object (afford) (mechanical-vertical). These additional lower-level functionalities give rise to two new assembly functions, *drape under gravity* and *conform manually into shape*, which are both crucial in terms of adjusting the overall functionality of the initial system by contributing to the generation of expanded technology sub-capabilities, *drapability and shapability*, respectively. These two new sub-capabilities, when combined with the initially existing sub-capability, *rigidizability*, generate the overall technology capability, *moldability*.

As highlighted in Figure 114, three operation states are identified as *draping, shaping,* and *rigidizing* (highlighted in green, blue, and red, respectively), where each of the operation states corresponds to a set of assembly functions producing the relevant technology sub-capabilities at the system level. The operation state in which a set of assembly functions is activated through the use of pneumatic affordance operations (e.g., *let air in*) can be traced from the system level down to the cell level using compositional and connectivity lines. The operating sequence of the assembly functions producing a particular technology sub-capability can be denoted with operating sequence identification letters (e.g., a, b, c, d). For example, *drapability* technology sub-capability is activated in drapability interaction mode, which requires the activation of *drape under gravity*

assembly function in draping operation state (note: no operating sequence identification letter is used since there is only one assembly function to be activated). Tracing down the constituents of this assembly function (highlighted in green in Figure 114) using compositional and connectivity lines results in indicating which pneumatic affordance operation (*let air in* in this case) is required for the activation of the relevant technology sub-capability at the system level.

Such interconnectivity can be further traced back to the roots of the constrained layer pneumatic systems using operation state diagrams that are introduced in Chapter 2. As highlighted in the decomposition (Figure 114), the *drapability* technology sub-capability requires the use of two cell-level functions at the cell level: *contact external object (afford) (mechanical-vertical)* and *allow multi-hinge-like motion,* only the second of which requires *let air in* operation. An identical relationship exists between the functionality (*allow multi-hinge-like motion*) and the operation of that specific functionality (*let air in*) within the context of generating cells as building blocks in isolation, without being part of a multi-mode product system. The operation state diagram of the isolated cell that provide *allow multi-hinge-like motion, retain hinge position,* and *jam tiles against each other* emergent cell functions through the use of combinations of pneumatic affordance operations demonstrates this parity (Figure 115). The full set of possible state transitions described in this operation state diagram affords the full array of possible operational sequences suitable for a wide variety of applications. However, any particular application may only require a subset of the possible transitions to activate the required sets of functionalities. On the other hand, the functional architectural decomposition only describes and employs the necessary operations specific to the application in context (e.g., the moldable active cargo blanket shown in Figure 109). Thus, having access to both complimentary descriptions is useful for the design process of structurally adaptable multi-mode products.

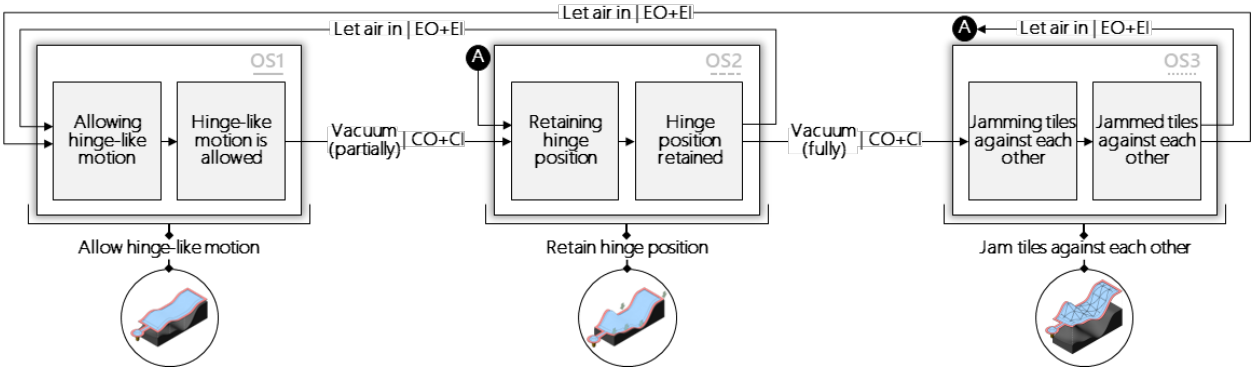

Figure 115. Allow hinge-like motion/retain hinge position/jam operation state transition diagram. The operation state diagram of the isolated cell that provide *allow multi-hinge-like motion, retain hinge position, and jam tiles against*

each other emergent cell functions through the use of combinations of pneumatic affordance operations provides a basis for the activation of the relevant technology sub-capabilities at the system level..

In the context of developing structurally adaptable multi-mode products such as moldable active cargo blanket by using internally tiled pneumatic textiles, the three operation states are described as follows: 1) the *Draping* state, where the pneumatic textile behaves like a fabric in the absence of a vacuum pressure, 2) the *Shaping* state, which is induced by the external forces that enable the conformation of the pneumatic textile into an intended form while the air is being vacuumed out from the bladder, and 3) the *Rigidizing* state, where the pneumatic textile becomes as stiff as possible due to the practically maximum vacuum pressure inside the bladder. Although the operation states are shared among all the tile architectural classes, the resulting physical behaviors and the performance quality of a pneumatic textile differ from one tile architectural class to another.

4.1.3.1. Draping

The internally tiled pneumatic textiles exhibit fabric-like behavior in the draping operation state. The gap between adjacent tiles enables the individual tiles to shift, allowing them to have a hinge-like motion relative to each other. As shown in Figure 116, this makes the pneumatic textile drapable, which facilitates the accommodation of any target object topography to a degree by bending to the target form under its own weight. The tile architectural class affects the nature of the draping behavior of a pneumatic textile. The bladder-attached tiles have fixated locations on their corresponding bladder skins; thus, they are not free to move in translation and rotation relative to these skins. However, each tile array layer can move independently of one another, and each individual tile can have a hinge-like motion relative to its adjacent tiles. For the internal sheet-attached tiles, the bladder skin does not restrict the draping behavior, but the perforated internal layer that keeps individual tiles together as an array pattern does. The mutually interlocking tiles drape independent of the bladder skin restriction as well. However, the tile features such as legs and loops that interlock neighboring tiles to each other affects the draping behavior by limiting the maximum obtainable gap and angle between tiles. In addition, the asymmetrical design of these tiles produces hard-stops that constrain the draping behavior differently for convex and concave bending directions.

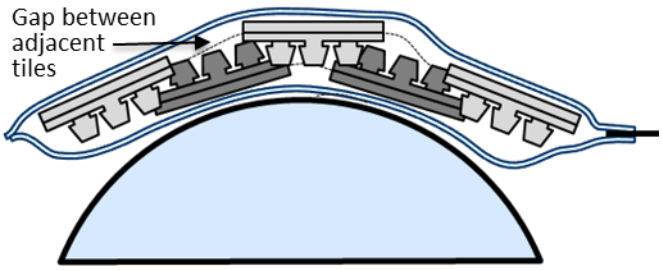

Figure 116. The draping operation state. A pneumatic textile operates in draping state in the absence of vacuum, where the textile deforms in a fabric-like manner due to gravity. The gap between adjacent tiles enables relative shifting and angular deflection, resulting in the passive accommodation of a target form to a degree.

The quality of drapability performance of a pneumatic textile is influenced by the geometry of an individual tile, additional tile features and variations such as the way tile layers overlap with each other. For example, a pneumatic textile made of a tile array pattern with a large gap between adjacent tiles provides better drapability performance in comparison to one with a smaller gap. Accommodating relatively smaller and heavier tiles improves the drapability performance of a pneumatic textile as well.

4.1.3.2. Shaping

Manually conforming a pneumatic textile into a shape of a target object initializes the shaping state. The position of the individual tiles inside the bladder can be arranged relative to their adjacent tiles by applying an external force, for example by using hands. In this way, the pneumatic textile can be conformed into varying shapes. However, without the presence of an external force, the individual tiles shift back from their conformed positions to their neutral draped positions. For this reason, the shaping state necessitates the transitional application of vacuum that generates permanent and distributed external force over the pneumatic textile. During the transition of relative pressure level inside the bladder, the opposing tiles and the adjacent tiles begin jamming against each other, restricting relative motion of the tile array layers, setting the pneumatic textile into the conformed shape. The shaping behavior, composed of conforming and setting behaviors, shows differences among the tile architectural classes. The asymmetrical nature of the mutually interlocking tiles biases the structure to cinch towards a particular direction when the vacuum pressure is applied. Thus, it is relatively more difficult to conform and set the pneumatic textile made of the mutually interlocking tiles to an arbitrary target shape. For the pneumatic textiles belonging to other tile architectural classes, such bias does not exist since their layup is symmetrical with the accommodation of two opposing tile array layers inside the bladder.

Changing the design of the tiles affects the quality of the shapability performance. For example, a pneumatic textile made of relatively larger tiles provides worse shapability performance in comparison to one that is made of smaller tiles. Depending on the tile design, as the relative vacuum pressure level increases, the pneumatic textiles may spring back as shown in Figure 117. The springing back motion occurs due to the rotational force generated by the tiles as they are compressed on each other and by the bladder skin as it is being shrunk against the gap between each tile. In general, as tile size gets larger, the springing back force increases, reducing the shapability performance of a pneumatic textile.

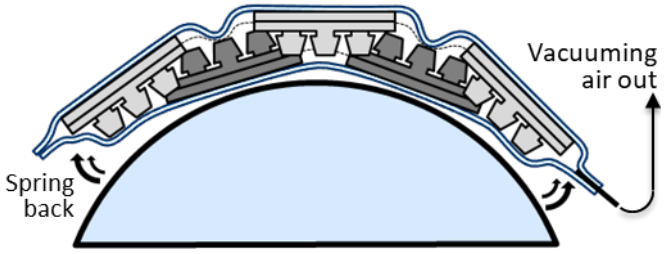

Figure 117. The shaping operation state. Conforming an already draped pneumatic textile into a shape of a target object initializes the shaping operation state. Without the presence of an external force, the individual tiles in pneumatic textiles tend to shift back to their neutral draped positions. Vacuum pressure introduced to the airtight bladder decreases the effect of such shifting by providing a permanent and distributed force over the pneumatic textile, setting it to a shape. Increase in vacuum pressure may induce spring-back due to the rotational force generated by the opposing tiles.

4.1.3.3. Rigidizing

The rigidizing operation state is accomplished by vacuuming most of the air out from the airtight bladder. In this state, the opposing tiles jam against each other, restricting the tile array layers from shifting relative to each other due to friction and/or interference, and minimizing folding or bending along the gap lines as shown in Figure 118. The level of restriction in the rigidized state can be adjusted as a function of the vacuum pressure level inside the airtight bladder. A rigidized pneumatic textile, by nature of its flexural rigidity, can resist deformation under external loads to a degree. The permanent deformation of a rigidized shape occurs when the external forces are so large that the individual tiles can no longer maintain their relatively fixed positions inside the bladder. This results in yielding, where opposing tiles begin sliding over each other and the tile array layers potentially get disengaged, although some of this post yield deformation is recovered through residual elasticity. The level of deformation is related to the flexural rigidity of the pneumatic textile, which is influenced by the bending stiffness properties of the tile material and the bladder skin composite. For pneumatic textiles that are made of either internal sheet-attached tiles or mutually interlocking tiles, the contact force between the tile array

layers and the bladder skin increases when vacuum is applied, increasing friction. As a result, it is relatively more difficult for any tile to shift its relative position inside the bladder as opposed to the case in the draping state. In addition, the bladder skin forces adjacent tiles laterally together by pulling into the gap lines. This improves the overall stiffness of the final configuration of the pneumatic textiles. However, for pneumatic textiles that are made of bladder-attached tiles, improved rigidity is achieved only by jamming opposing tile array layers and pulling into gap lines since each individual tile is already permanently bonded to the bladder skin.

As for the other operation states, the rigidizability performance can be tailored by changing the specifications of an individual tile geometry design. In general, having wider gaps among the adjacent tiles or eliminating features such as protrusions on individual tile surfaces affects the rigidizability performance negatively. The pneumatic textiles made of stiffer and larger tiles provide better rigidizability performance. However, changing the tile geometry design variables simultaneously affects the drapability and shapability performances as well.

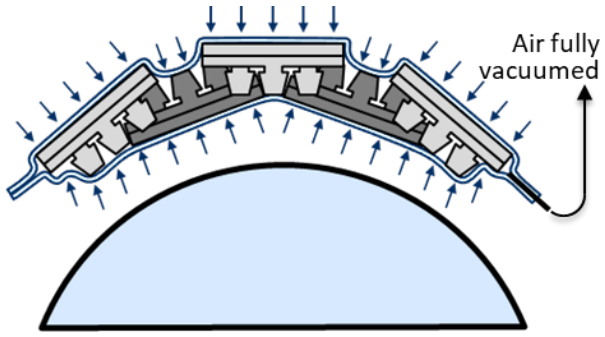

Figure 118. The rigidizing operation state. Rigidizing a pneumatic textile is accomplished by vacuuming all the air out from the bladder, which jams the opposing tiles against each other. This increases the friction and/or interference between the tile array layers, resulting in minimizing folding or bending along the gap lines and restricting the relative tile movement, hence enhancing the stiffness of a pneumatic textile.

4.1.4. Moldability Performance Across Different Architectural Approaches

Internally tiled pneumatic textiles technology affords a plethora of architectures. The selection of a tile architectural class/subclass, the architectural feature variations corresponding to each class/subclass, and the tile design variable values such as the individual tile geometry values and the amount of gap between adjacent tiles forming the tile array layers all simultaneously affect the performances of three key technology sub-capabilities provided by these pneumatic textiles. This creates a useful and broad design space in which the performances of the sub-capabilities are inherently interrelated.

There is a need for a rigorous study enabling the quantified understanding of the relative contribution of using different architectural approaches to render this emerging moldability technology capability useful in the design of various structurally adaptable user-interacting multi-mode applications for different contexts. For example, while shapability and rigidizability performances would be of higher priority for a moldable medical cast application that needs to be operated by a medical expert, drapability performance would be of a higher priority for the design of a moldable active cargo blanket that needs to be draped over arbitrary objects by an end-user. Since the overall moldability performance of any internally tiled pneumatic textile is a set of combined performances obtained at the different operation states, the effects of the tile architectural classes/subclasses and architectural feature variations on the pneumatic textile's performance at each operation state need to be quantified.

The hierarchical functional architectural decomposition of the moldable active cargo blanket concept, which facilitates the embodiment of the operation states, can also be employed to better comprehend the interrelation among the functionalities, their performance in each operation state, and the design of the architectural components that affect both. From these functionalities and operations, a set of quantifiable performance metrics relevant to each technology sub-capability can be extracted, which then can be used to characterize the relationship between the highest-level functionality, moldability, and the design variables that are relevant to the lowest-level architectural components ranging from the variations of architectural class to individual tile shape. Furthermore, the functional decomposition of each technology sub-capability informs the design of experimental procedures required for the characterization of the sub-capability performance. For example, the *shapability* sub-capability is decomposed into *conform manually into shape* and *set target shape* assembly functions (highlighted in blue in Figure 119). *Conform manually into shape* is demonstrated as a constitutive of *contact external objects* and *free bendability (2-dof)* unit functions, the second of which is produced by *move multi-hinge-like* ensemble function. Therefore, to characterize the shapability performance, a prototype of an internally tiled pneumatic textile as an embodiment of a particular architectural design needs to *contact external objects* to perform a *multi-hinge-like motion* over that object. The characterization of the range of multi-hinge-like motion allows objective comparison among differently designed pneumatic textile prototypes, enabling a quantified understanding of the system level technology sub-capability, *shapability*, performance. The remaining sets of quantifiable performance metrics is extracted for

characterizing the performances of the drapability and rigidizability sub-capabilities by using the same approach through employing the decomposition.

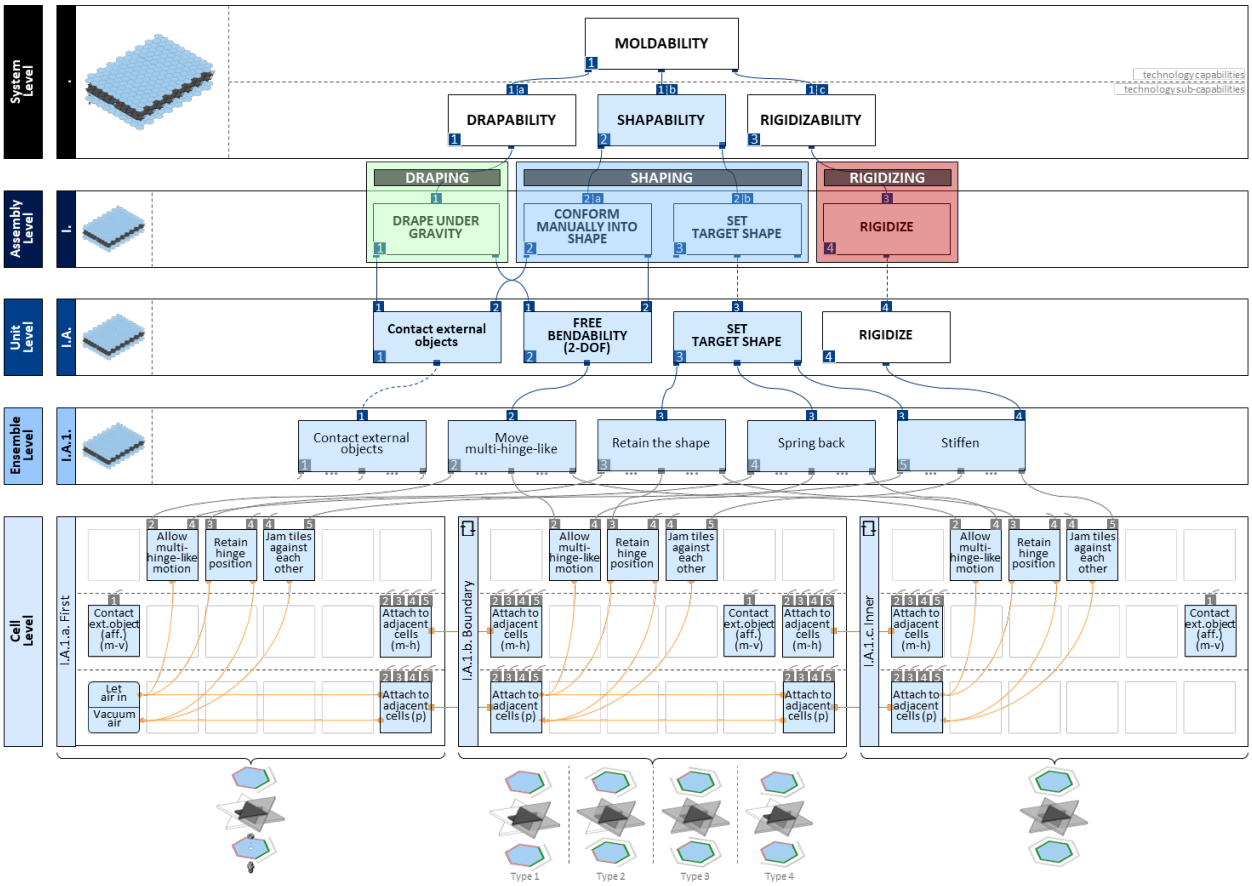

Figure 119. The hierarchical functional architectural decomposition of the moldable active cargo blanket used as a starting point for performance metric identification. The architectural decomposition of the moldable active cargo blanket is identical to the initial system's architectural decomposition since ensemble (I.A.1.) propagates upwards as a part of the relatively flat architectural hierarchy. Functionally, the re-synthesized system expands the extent of an existing cell function, allow 1-dof hinge-like motion, in addition to providing a new cell function, contact external object (afford) (mechanical-vertical). These additional lower-level functionalities give rise to two new assembly functions, *drape under gravity* and *conform manually into shape*, which are both crucial in terms of adjusting the overall functionality of the initial system by contributing to the generation of expanded technology sub-capabilities, *drapability and shapability*, respectively. These two new sub-capabilities, when combined with the initially existing sub-capability, *rigidizability*, generate the overall technology capability, *moldability*.

Using the hierarchical functional architectural decomposition approach enables decomposing the system level technology capability and sub-capabilities into sets of quantifiable engineering performance metrics, which are simultaneously affected by the architectural design of the system. While the ultimate goal of quantifying performance is to capture the ability of the technology to provide the intended technology capabilities and sub-capabilities in the context of the product use, this use-base performance is fundamentally subjective. Therefore, as a surrogate, objective engineering metrics to capture the performance of the technological functionalities (that

correspond to the assembly and lower-level functionalities) which produce those capabilities are developed by making use of hierarchical functional architecture decomposition. Since the hierarchical functional architectural decomposition shown in Figure 119 comprehensively gathers information about all the system aspects (architecture, functionality, operation, and performance), a distilled version of the decomposition is produced (Figure 120) to concisely demonstrate the overall moldability performance of an internally tiled pneumatic textile as a combination of the interrelated performances of technology sub-capabilities and their corresponding quantifiable engineering performance metrics, which are simultaneously affected by the architectural design details such as the architectural class, sub-class, and features.

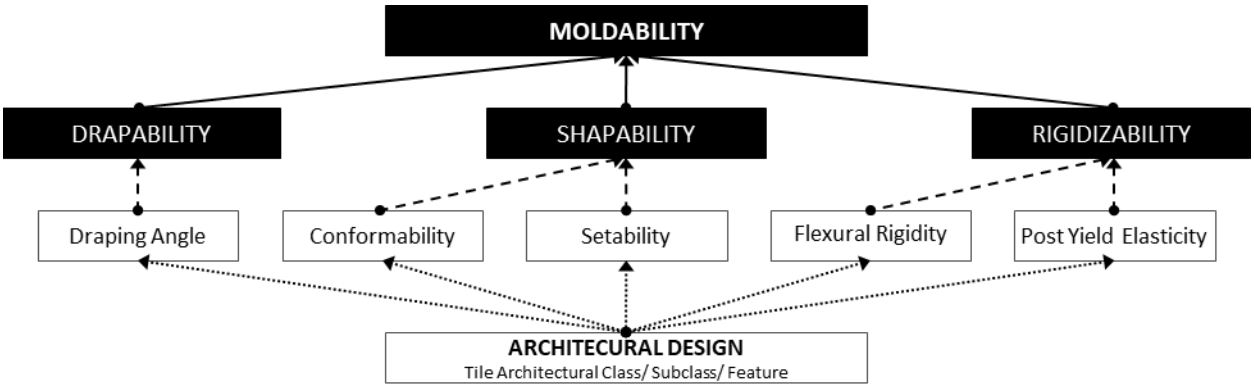

Figure 120. The engineering performance metrics for three key technology sub-capabilities. Moldability is an emergent technology capability comprising drapability, shapability, and rigidizability technology sub-capabilities. The performance of each one of these technology sub-capabilities can be objectively measured by using a respective set of quantifiable engineering performance metrics, where the draping angle metric characterizes the drapability performance, the conformability and setability metrics characterize the shapability performance, and the flexural rigidity and post yield elasticity metrics characterize the rigidizability performance. Architectural design details such as tile architectural class, subclass, and features affect the resulting performances of technology sub-capabilities.

As shown in Figure 120, the characterization of the drapability performance requires one performance metric, which is identified as draping angle. The draping angle performance metric is an embodiment of *drape under gravity* assembly function (shown in Figure 119), which requires contacting an external object and bending freely under the external influence of gravity. The characterization of the shapability performance requires two separate performance metrics since shapability has two contributing assembly functions: *conform manually into shape* and *set target shape* (shown in Figure 119). The performance metric identified for these two aspects of shapability performance are conformability and setability. While conformability performance metric is an embodiment of *conform manually into shape* assembly function and is similar to draping angle since it requires contacting an external object and bending freely, it uses manually

generated external forces instead of using the sole influence of gravity. The setability performance metric is an embodiment of *set target shape* assembly function, which requires retaining the conformed shape of a pneumatic textile and potentially springing back during transitioning to stiffened physical state as a result of introducing gradual vacuum to the system. The characterization of the rigidizability performance requires two separate performance metrics as well. Although the rigidizability sub-capability has one primary contributing assembly function, *rigidize*, its embodiment can be described as a combination of two different aspects of the performance of that functionality. The performance metrics identified for characterizing the rigidizability performance are flexural rigidity, which quantifies to what degree a pneumatic textile stiffens in the elastic behavior region before yield occurs, and post yield elasticity, which quantifies to what degree a pneumatic textile keep its targeted shape after permanent deformation occurs due to the application of excessive external forces (shown in Figure 119).

A set of experimental procedures is devised to collect data for quantifying each engineering performance metric to enable the comparison between the performances of the internally tiled pneumatic textile prototypes that vary in terms of the tile architectural class/subclass and architectural feature variations. This guides the architectural design of structurally adaptable multi-mode applications using the pneumatic textiles technology to meet the targeted performance requirements driven by the design context.

4.2. Prototype fabrication

To provide a quantified understanding of the pneumatic textile performance across different architectural approaches, experimental characterization of representative prototypes is required. Fabricating these representative prototypes for experimental characterization requires two main sets of steps: the fabrication of tiles and the fabrication of bladders. While the fabrication steps for tiles show variations depending on the type of the tile architectural class to which particular prototype belongs, the fabrication steps for bladders are global and applicable to any prototype that are categorized under any architectural class.

4.2.1. Fabrication of Tiles

Each prototype of the internally tiled pneumatic textiles contains at least one tile array layer. Regardless of which architectural class a pneumatic textile belongs to, each tile was fabricated

using an FDM (fused deposition modeling) 3D printing process. Four types of thermoplastic filaments (ABS, NinjaFlex®, SemiFlex®, and Armadillo®) with diameters of 2.9mm, and three models of 3D printing machines (Lulzbot TAZ5 with Flexystruder toolhead, Lulzbot TAZ5 with Aerostruder toolhead, and Lulzbot TAZ6 with Standard toolhead) were used for the fabrication of the tiles. The type of each prototype's tile architectural class informed the selection of the type of filament material for the fabrication. The tile array patterns were modelled in the computer aided design software Rhinoceros 3D and Solidworks. The corresponding stereolithography files of these 3D models were generated and imported into CURA Lulzbot Edition, which is an open-source 3D slicer application that converts stereolithography files into layers, generating printer-specific g-code. Then, depending on the type of tile architectural class, the tile array layers were 3D printed either on thermoplastic polyurethane (TPU) coated bladder skin or on a bare 3D printing surface.

4.2.1.1. Fabrication of Bladder-Attached Tiles

The fabrication of the bladder-attached tiles requires permanent bonding between each tile and the bladder's TPU coated inner surface. Instead of bonding tiles by using adhesives as an extra step, TPU based filaments with various shore hardness properties (NinjaFlex® 85A, SemiFlex® 98A, and Armadillo® 75D) were selected since they provide sufficient thermal bonding during the 3D printing process. As shown in Figure 121, the entire Lulzbot TAZ5 3D printer's printing bed (290mm x 290mm) was covered with TPU coated nylon fabric (Seattle Fabric Inc., 200 denier oxford fabric) by using double sided tape. The edges of the fabric were clamped with binder clips to eliminate any deformation over the fabric's surface during printing. Then, the filament was deposited by using an Aerostruder or Flexystruder toolhead over the fabric at temperature levels spanning from 220°C to 230°C, which are within the suitable range for the thermal bonding of the resulting tile array pattern with the TPU coated nylon bladder skin.

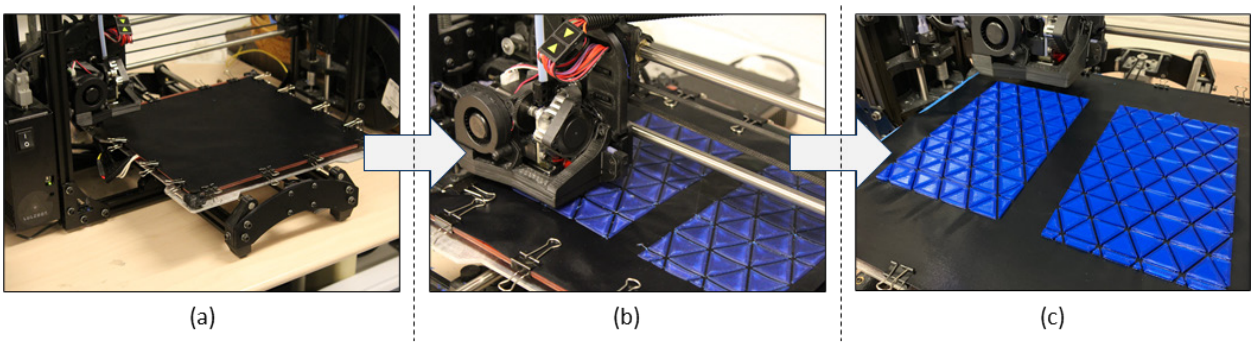

Figure 121. Fabrication process of the bladder-attached tiles. (a) TPU coated 200 denier oxford nylon fabric is fixed over a Lulzbot TAZ5 3D printer's printing surface by using double sided tape and binder clips. (b) The Armadillo® TPU filament is deposited over the fabric at temperature levels spanning from 220°C to 230°C, resulting with a permanent bonding between the initial tile layers and the bladder skin. (c) The side-by-side fabrication of two layers of bladder-attached tiles is finalized.

4.2.1.2. Fabrication of Internal Sheet-Attached Tiles

The tiles forming the prototypes that represent the internal sheet-attached tiles class were 3D printed in batches using a Lulzbot TAZ 6 with the standard toolhead using ABS filament at 235°C. The internal sheet layer was created by perforating plain nylon fabric (Seattle Fabric Inc., 30 denier ripstop) on a Cricut Maker desktop CNC die-cutting machine. The tiles with the grooved pegs were snapped into the corresponding tiles with holes through the perforated nylon fabric in between as shown in Figure 122. The fabrication of the tile array layers requires manual assembly unlike the prototypes made of the bladder-attached tiles. Hence, the size of a prototype is not restricted by the 3D printing area and it is more easily scalable.

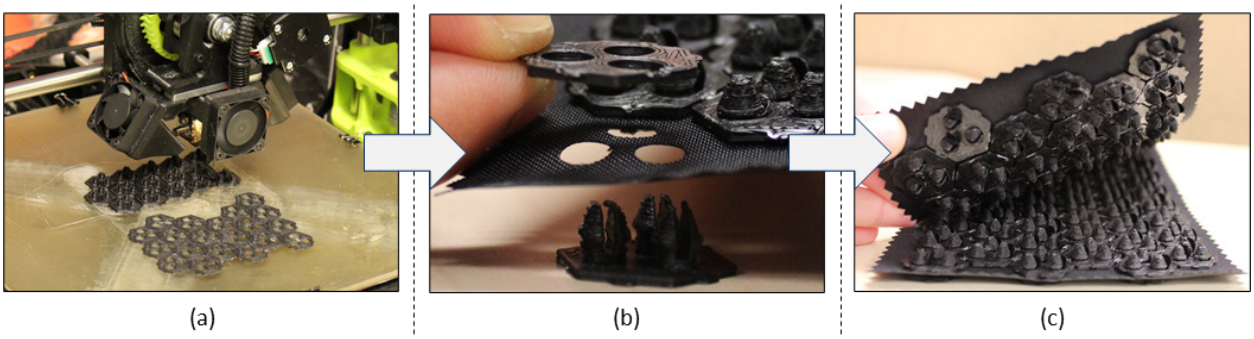

Figure 122. Fabrication process of the internal sheet-attached tiles. (a) The bottom and top tile parts featuring grooved pegs and through holes are 3D printed in batch quantities using a Lulzbot TAZ 6 with the standard toolhead using ABS filament at 235°C. (b) These two tile parts snapped into each other through a nylon fabric layer which is perforated using Cricut Maker desktop CNC machine. (c) The assembly of two opposing layers of internal sheet-attached tiles are finalized.

4.2.1.3. Fabrication of Mutually Interlocking Tiles

The fabrication of the mutually interlocking tiles requires manual assembly as well, which also removes the limitation of size arising from the 3D printing process. Pre-interlocked patches of these tiles were fabricated using a Lulzbot TAZ6 3D printer with the standard toolhead using ABS filament at 235°C. Upon 3D printing, these separate patches were interlocked manually by inserting the corresponding legs and hooks of adjacent tiles together as shown in Figure 123.

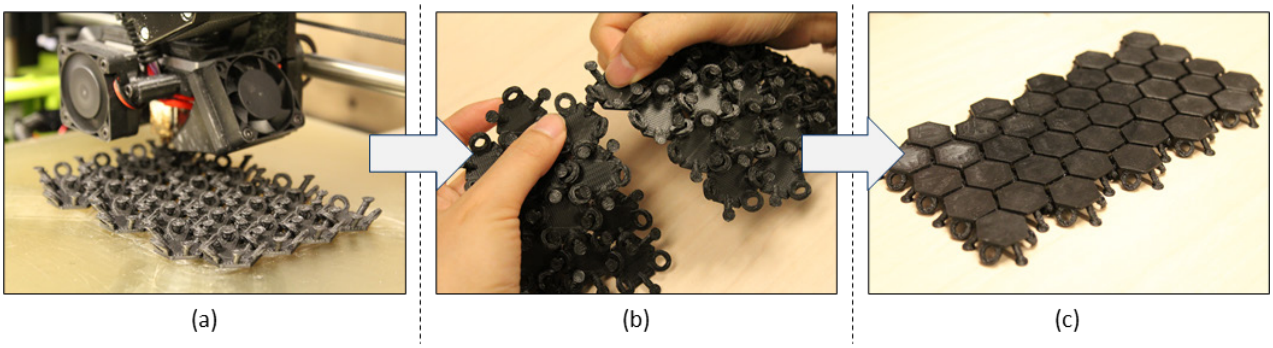

Figure 123. Fabrication process of mutually interlocking tiles. (a) Pre-interlocked patches of mutually interlocking tiles are 3D printed using a Lulzbot TAZ 6 with the standard toolhead using ABS filament at 235°C. (b) The separate patches are manually interlocked to each other. (c) A layer of mutually interlocking tiles is finalized.

4.2.2. Fabrication of Bladders

The steps for fabricating the airtight bladders are shared among each tile architectural class as shown in Figure 124. The bladders are fabricated in four steps. First, the three edges of two layers of TPU coated nylon fabric facing each other were heat sealed by using a linear impulse sealer (Uline 12" Model H-190) to form a pouch with an opening (Figure 124(a)). For the prototypes made of the internal sheet-attached tiles and the mutually interlocking tiles, the tile array layer or layers were placed inside this pouch (Figure 124(b)). Since each individual tile in the bladder-attached tiles class had been printed on TPU coated nylon fabric, the fabric already containing the tiles was used to form the pouch. A low-pressure barbed pneumatic fitting (McMaster #2844K13) was attached to one of the bladder surfaces near the opening of the pouch with a rubber washer and a hex nut through a 1/8-inch punched hole (Figure 124(c)). The remaining unsealed edge of the bladder was heat sealed by using the linear impulse sealer as a final step, forming an airtight pneumatic textile prototype (Figure 124(d)).

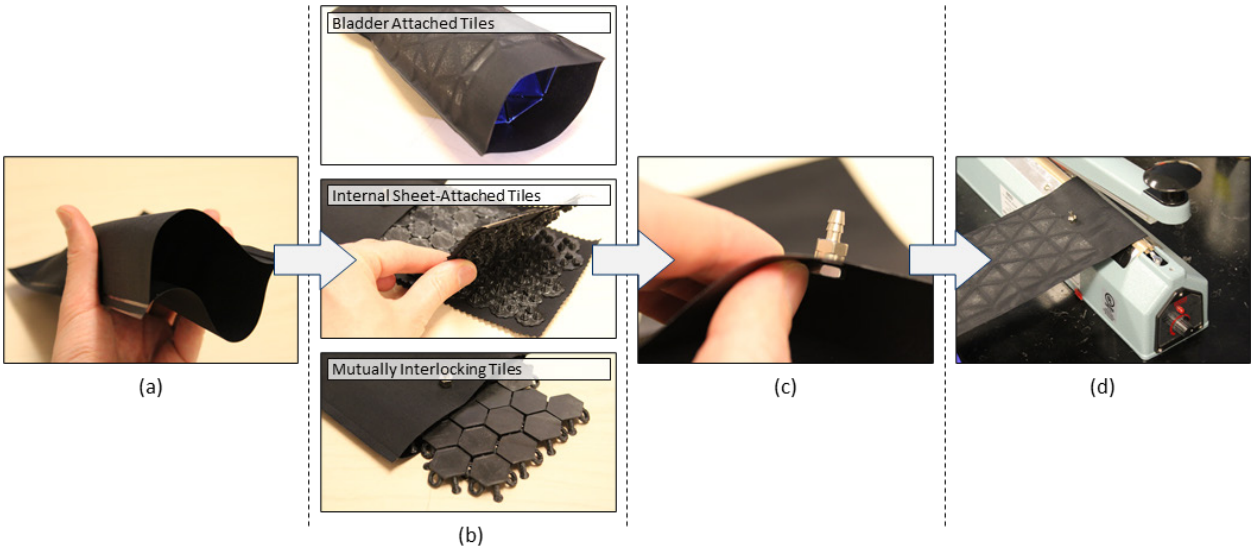

Figure 124. Bladder fabrication process. (a) Three edges of two layers of TPU coated nylon fabric facing each other are heat sealed using a linear impulse sealer, forming a pouch. (b) While two opposing layers of internal sheet-attached tiles and a layer of mutually interlocking tiles are placed inside these pouches, the fabric permanently accommodating bladder-attached tiles is used to form a pouch. (c) A low-pressure barbed pneumatic fitting is attached to one of the bladder surfaces near the opening of the pouch with a rubber washer and a hex nut through a 1/8-inch punched hole. (d) The remaining open edge of the bladder is heat sealed using the linear impulse heat sealer, forming an airtight pneumatic textile prototype.

A set of pneumatic textile prototypes representing each tile architectural class is shown in Figure 125 demonstrating their unvacuumed and vacuumed states. While the prototypes seem almost identical in the absence of vacuum, the differences across their tile array layer details become visible when vacuum applied.

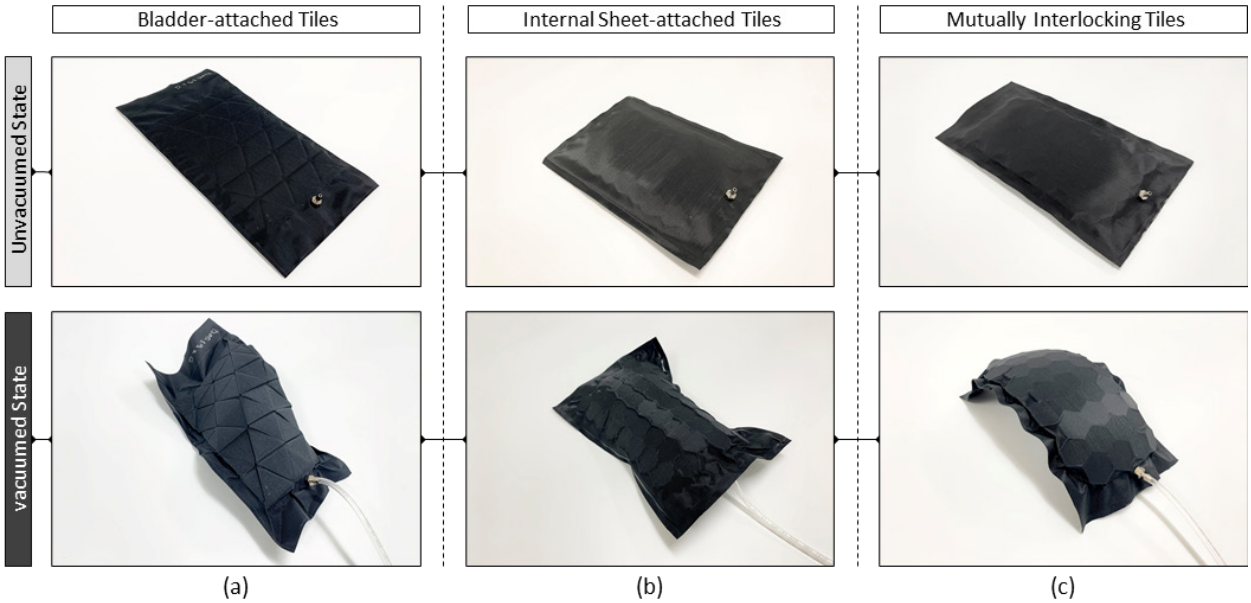

Figure 125. A set of pneumatic textile prototypes representing each tile architectural class. Once the bladder fabrication is completed, the prototypes representing different tile architectural classes/subclasses almost seem identical in unvacuumed state. (a) A set of prototypes representing (a) bladder-attached tile class, (b) internally sheet-attached tile class, and (c) mutually interlocking tile class are shown in unvacuumed and vacuumed states.

4.3. Experimental Characterization of Performance Metrics

An internally tiled pneumatic textile's moldability performance is a combination of performances of its technology sub-capabilities: drapability, shapability, and rigidizability. The performance of each sub-capability is characterized by a set of quantifiable engineering performance metrics: the drapability performance is quantified by one metric, draping angle, and the shapability and rigidizability performances are quantified by sets of two metrics each. The shapability performance can be divided into conformability and setability metrics, and the rigidizability performance can be broken down into flexural rigidity and post yield elasticity metrics. For the quantification of each one of these engineering performance metrics, an experimental procedure that enables testing and data collection was developed. The units and ranges of the underlying measurements vary from one performance metric to another, making the direct understanding of the significance of a score on any particular metric difficult, as well as making the direct comparison among metrics complicated. To convey a direct understanding of the merit of a score and enable direct comparison, the raw measurements were transformed into a natural functional scale in which the score naturally ranges from zero to one and units become dimensionless. In this scale, zero represents the theoretical worst case where no functionality towards the performance metric is observed (i.e. not draping at all, not rigid at all), and one represents the theoretical best case where the functionality towards the performance metric is ideal (i.e. unrestricted draping, solidly rigid). This enables the direct comparison of the engineering performance metric scores of pneumatic textiles representing different architectural approaches.

4.3.1. Drapability

The technology sub-capability, drapability, has only one engineering performance metric, which is draping angle. It is defined as the amount of two-dimensional deformation (i.e. one degree of freedom) an internally tiled pneumatic textile prototype experiences due to its own weight in a cantilevered condition. The purpose of the drapability test is to characterize and quantify the ability of the pneumatic textile to accommodate the shape of an object it is simply placed over.

Researchers have previously developed various methods to quantify fabric drape. The Flexometer, which was devised to measure the bending length of a thin piece of fabric (6in.x1in) draping to a predefined angle, enables the comparison of the draping quality of different types of textiles in two dimensions [211]. To quantify the fabric drape in three-dimensions, Chu et al. developed the Drapemeter, which is an optical instrument capturing the trace of a draped pattern of a circular fabric sample clamped between two circular flat plates with smaller radii [212]. The relationship between the traced area of the draped fabric sample and the area in flat condition provides a normalized metric, the drape coefficient. The British standard for the measurement of the fabric drape (BS5058) by using a Drapemeter requires a fabric sample size 24 cm, 30 cm, or 36 cm in diameter. In contrast to these out-of-plane gravity tests, an in-plane gravity test developed by Mei et al. proposed unidirectional fabric drape testing method by using a large piece of fabric (50 cm by 87 cm), where the effect of gravity is parallel to the fabric plane, enabling the quantification of a free hanging fabric drape by 3D scanning and analyzing the shape of the fabric edge [213].

These methods are applicable to a wide range of traditional textiles. However, the internally tiled pneumatic textiles are made of multiple layers (textile layer, TPU layer, and the tile array layer), which make them thicker, stiffer, and more difficult to fabricate than woven or knitted textiles. Due to the relatively high stiffness of internally tiled pneumatic textiles, three-dimensional fabric drape was not observable when standard fabric sample sizes required by existing methods were used. Fabricating larger prototypes and test apparatus to accommodate them was not pragmatic for this study. Thus, a variation of the flexometer testing procedure was used to quantify the draping angle of relatively small sized (10 cm by 12 cm) pneumatic textile prototypes. One end of a pneumatic textile prototype was clamped parallel to the ground without any vacuum pressure applied while the other end of the prototype was held horizontally (Figure 126(a)). The other end was released and allowed to freely hang downward as shown in Figure 126 (b), and a photo of the draped prototype was taken from the side view. The resulting draping angle (θ) in relation to the ground plane was measured from the photo (Figure 126(c)). To provide a natural functional scale of this metric, the draping angle metric score, D, 0° and 90° are defined as the theoretical worst and best cases. This range is linearly mapped to the zero to one scale, where one represents ideal performance,

$$\boldsymbol{D} = \frac{(\theta)}{(90)}. \quad (1)$$

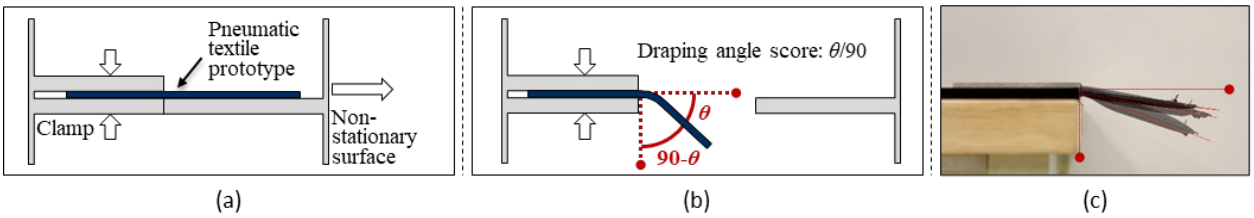

Figure 126. The drapability testing procedure. (a) A portion of each pneumatic textile is clamped between two stationary surfaces first, while the remaining portion (of equal length across the prototypes) is resting on a non-stationary surface that can be laterally translated for the drapability test. (b) The non-stationary surface is being laterally translated, making the pneumatic textile drape under its own weight before the photo of the draped prototype is captured from the side view. (c) Photos of three pneumatic textile prototypes are overlaid, demonstrating the difference between their drapability performances.

4.3.2. Shapability

The technology sub-capability, shapability, has two engineering performance metrics, conformability and setability. Separate experimental procedures were developed to quantify each of these metrics. The purpose of the shapability tests is to capture the ability of the pneumatic textile to be shaped to and hold the shape of objects with varying degrees of curvature.

4.3.2.1. Conformability

The conformability engineering performance metric is the first aspect of shapability and is defined as the pneumatic textile's ability to be manually conformed to a variety of complex shapes without vacuum pressure applied. It was measured by placing a pneumatic textile prototype over each of a set of cylinders with different radii and recording the minimum radius to which each prototype could conform without applying excessive force (Figure 127(a-b)). This measurement, while somewhat subjective, can be performed repeatably by identifying the point at which the force required to bend the prototype starts to increase significantly. Examples of cylinder radii that were considered as conformable (Figure 127(c)) and unconformable (Figure 127(d)) are shown. In total, seven cylinders based on the stock pipe availability with radii ranging from 6.35 mm to 55.5 mm were used throughout the conformability tests, listed in Table 3.

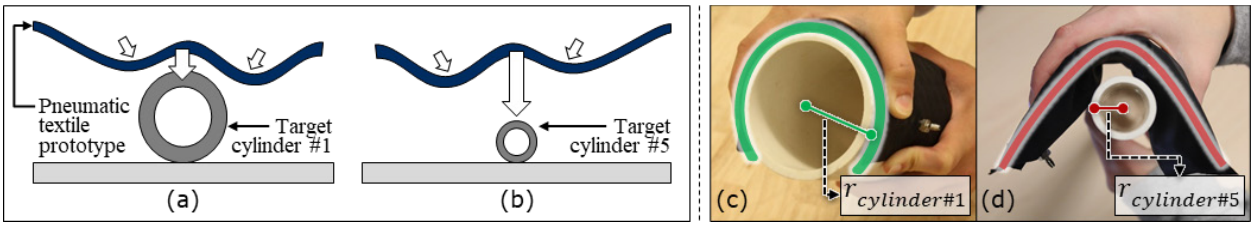

Figure 127. The shapability testing procedure for quantifying conformability. (a, c) While a pneumatic textile prototype successfully conforms to target cylinder #1 (r=55.5mm), (b, d) it fails to conform to the target cylinder #5 (r=19mm).

Table 3. Radii of seven cylinders used in conformability and setability tests

#Cylinder	#1	#2	#3	#4	#5	#6	#7
Radius (mm)	55.5	44.5	28.6	22.5	19	13.35	6.35

To provide a natural functional scale of this metric, the conformability metric score,

$$\boldsymbol{C} = \frac{\left(r_{cylinder\#1} - r_{minimumconformed}\right)}{\left(r_{cylinder\#1} - r_{cylinder\#7}\right)}, \quad (2)$$

is defined as the range of the cylinders' radii to which a pneumatic textile prototype successfully conformed divided by the range of the cylinders' radii used throughout the testing. This ratio represents the conformable fraction of the tested cylinder range. This results in a natural functional scale ranging from zero to one, where zero indicates the prototype can conform to none of the cylinders, and one indicates the prototype can conform to all of the cylinders. Establishing a standard set of cylinders that covers a wide enough range of radii is important since the naturally scaled metric depends on the range of the set of cylinders used.

4.3.2.2. Setability

The setability engineering performance metric is the second aspect of shapability, and is defined as the ability of a pneumatic textile to hold its conformed configuration once shaped to a given geometry when vacuum is applied. It was measured by first conforming a prototype to the cylinder with the largest radius from the conformability test cylinder set without vacuum applied. While manually holding the prototype in this shape around the cylinder, a vacuum of -25inHg (i.e., -12.28 psi) was gradually applied (Figure 128(a-c)). The rigidized prototype was then released, generally allowing it to spring back somewhat from its conformed shape as illustrated in Figure 128(b-d). The resulting final curvature of each prototype was traced on paper, scanned, digitally traced and converted into a Bezier curve in a vector graphics capable software package (e.g., Rhinoceros). Each Bezier curve was simplified to fit an arc, the radius of which enabled the

calculation of the discrepancy between the target cylinder radius and the radius of the sprung-back prototype.

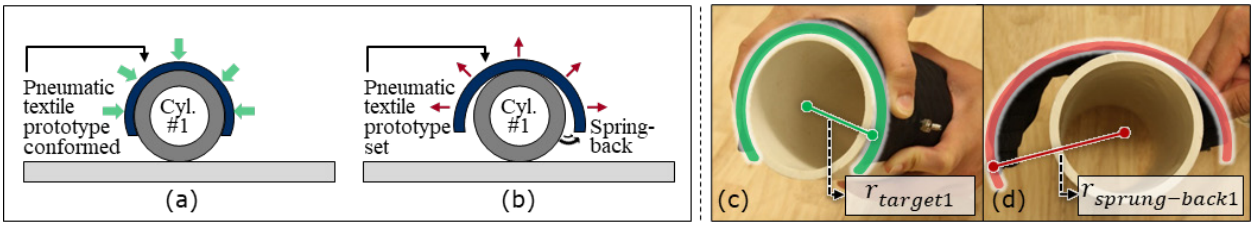

Figure 128. The shapability testing procedure for quantifying setability. (a, c) As a second part of the shapability test, each pneumatic textile prototype is conformed to each of a set of cylinders using hands and vacuumed. (b, d) Once the rigidized prototype is released, it generally springs back. The discrepancy between the target and sprung-back curvatures informs the setability performance metrics score calculation.

To provide a natural functional scale of this metric for each target cylinder i, the setability metric score, S_i, is calculated from the two corresponding curvatures as

$$\boldsymbol{S} = \frac{1}{n}\sum_{i=1}^{n} S_i = \frac{1}{n}\sum_{i=1}^{n}\left[1 - \frac{\frac{1}{r_{target_i}} - \frac{1}{r_{sprung-back_i}}}{\frac{1}{r_{target_i}}}\right], \tag{3}$$

where curvature is defined as the reciprocal of radius. The difference between the target curvature and the sprung-back curvature divided by the target curvature represents the relative loss of curvature due to springback. Subtracting this relative loss from one provides the fraction of curvature maintained, i.e. the naturally functional setability metric, which ranges from zero (no curvature is maintained: unsettable) to one (all curvature is maintained: perfectly settable). In a case where a prototype failed to conform to a particular cylinder, the setability was computed using the target cylinder curvature and the sprung-back curvature value obtained from the smallest cylinder to which the prototype successfully conformed. A series of setability tests for a single prototype over the set of cylinders is shown in Figure 129. In this case, the prototype successfully conformed to cylinders radii 19mm and above, springing back by roughly a constant amount. To compute an overall setability score, the average of the scores from all the cylinders was taken.

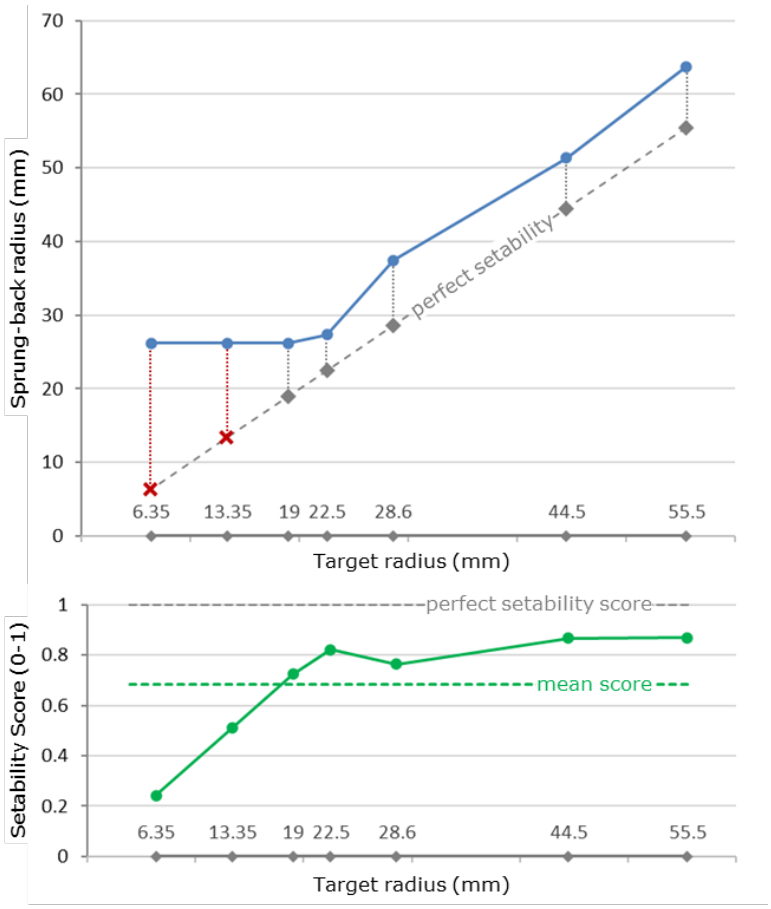

Figure 129. Calculation method for the setability metric score. For each target cylinder (#1 to #7) with different radii (6.35 mm to 55.5 mm), the setability metric score, $\boldsymbol{S_i}$, is calculated by using the difference between the target curvature, $\boldsymbol{1/r_{target_i}}$, (dashed line, top), and the sprung-back curvature, $\boldsymbol{1/r_{sprung-back_i}}$, (blue solid line, top) divided by the target curvature ($\boldsymbol{1/r_{target_i}}$), which represents the relative loss of curvature due to springback of a prototype. By subtracting this relative loss from 1, the fraction of curvature maintained is obtained for a given cylinder (green solid line, bottom). Taking the average of the fractions of curvatures maintained for all the cylinders provides the setability performance metric score for each pneumatic textile prototype.

4.3.3. Rigidizability

The technology sub-capability, rigidizability, has two engineering performance metrics. These are flexural rigidity and post yield elasticity. Under the influence of bending moments with relatively small magnitudes, an internally tiled pneumatic textile prototype maintains its original shape in the rigidized state by springing back elastically after the moment is released. The flexural rigidity metric quantifies to what degree a pneumatic textile stiffens in the elastic behavior region before yield occurs. The yield moment is the maximum bending moment that can be applied to the pneumatic textile prototype without permanently deforming its original configuration in the rigidized state. The post yield elasticity metric measures the portion of curvature recovered once the influence of large bending moment exceeding the yield moment is removed (the remainder is

lost to permanent deformation). An experimental procedure and a testing device were developed to quantify both of these engineering performance metrics. The purpose of the rigidizability test is to characterize the ability of a pneumatic textile to maintain its shape under the influence of external forces.

An experimental setup was built to hold each pneumatic textile prototype between two metal clamps that are each free to rotate around their respective axes (Figure 130(a)). The linear force generated by a set of weights, which were incrementally added to and removed from the setup, is transformed to a bending moment by a pulley system. The inclusion of a linear bearing at one of the clamps ensures that a pure moment is applied between the two clamps, essentially replicating a four-point bending test [214]. The resulting moment makes the clamps rotate, causing the pneumatic textile prototype to bend outwards (Figure 130(b)). The amount of angular deflection at the stationary clamp is measured with an optical incremental rotary encoder (US Digital E5) attached to the clamp's shaft. A pressure gauge is monitored to keep the vacuum pressure level constant throughout the testing of each prototype.

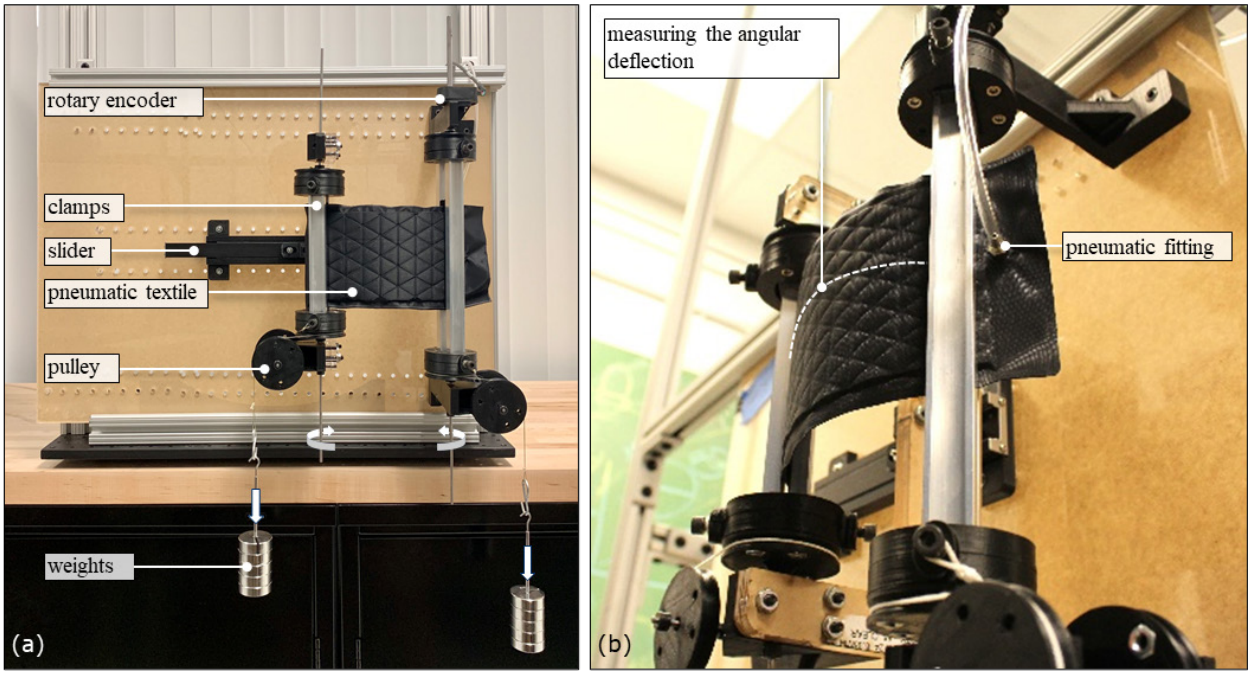

Figure 130. The experimental setup for measuring rigidizability performance metrics. (a) The rigidizability test experimental setup consists of clamps to secure the pneumatic textile prototypes, a set of pulleys to transform the linear force to a moment, a linear bearing attached to one of the clamps to ensure a pure moment applied to the prototype, and a rotary encoder to measure the angular deflection as a function of the moment applied. (b) In the rigidizing state, the pneumatic textile prototype is fully vacuumed and deflecting as a function of the moment applied. The amount of deflection is captured using an optical incremental rotary encoder.

The rigidizability test procedure contains three steps that need to be executed for each weight increment. The first step is resetting the potential effect of the test apparatus friction and the tile slippage that a prototype might be subjected to due to its architectural configuration after being clamped and vacuumed in the experimental setup. Thus, deflecting the prototype inward by manually applying external force on its center until the rotary encoder measures 17.5° is required (Figure 131(a)). The prototype settles into a near equilibrium position after waiting for 30 seconds, and then the angular deflection is recorded representing the prototype's baseline flat condition, A_i, before application of the i^{th} weight increment. The second step consists of adding the i^{th} weight increment to the experimental setup, waiting for another 30 seconds to make the prototype reach a near-equilibrium position, and recording the angular deflection, B_i (Figure 131(b)). The third and the last step is to record the deflection angle, C_i, after removing the i^{th} weight increment and waiting for another 30 seconds to let the prototype elastically recover some of its deformation (Figure 131(c)). This deflection angle value contains the embedded effects of the test apparatus friction and the tile slippage, which is reset by executing the first step of the rigidizability test for the next weight increment. This cycle is repeated with incrementally increasing weights until the prototype deforms to a degree that the sliding clamp is in contact with the stationary clamp.

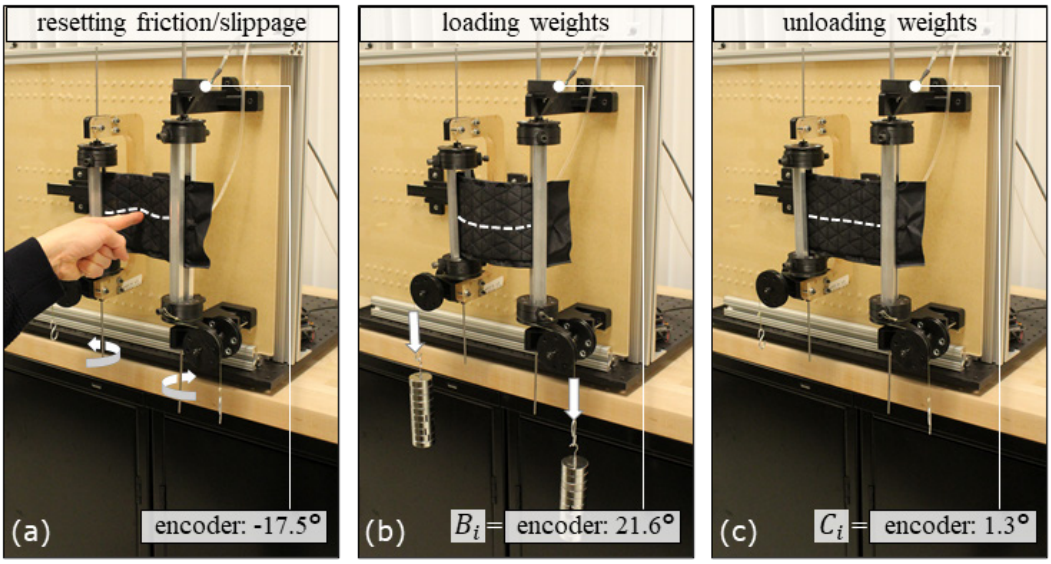

Figure 131. The rigidizability testing procedure for quantifying flexural rigidity and post yield elasticity. This procedure contains three steps that need to be executed for each weight increment for each pneumatic textile prototype. (a) The first step is to reset any potential test apparatus friction and tile slippage effects, which is achieved by deflecting the prototype inward by manually applying external force on its center until the rotary encoder measures 17.5° after which it is released. The angular deflection, after waiting for 30 seconds, represents the prototype's baseline flat condition, $\boldsymbol{A_i}$, before application of the $\boldsymbol{i^{th}}$ weight increment. (b) The second step is to add the $\boldsymbol{i^{th}}$ weight increment to the experimental setup, wait another 30 seconds to allow the prototype to reach a near-equilibrium position, and

record the angular deflection, $\boldsymbol{B_i}$. (c) The third step is to remove the $\boldsymbol{i^{th}}$ weight increment, wait another 30 seconds to let the prototype elastically recover some of its deformation, and record the deflection angle, $\boldsymbol{C_i}$.

Each cycle produces a hysteresis curve as shown in Figure 132, with one curve corresponding to each weight increment. Each hysteresis curve i contains the three recorded data points, A_i, B_i, and C_i, where A_i is the initial measured angular deflection before application of the i^{th} weight increment, B_i is the angular deflection corresponding to the moment generated by the i^{th} weight increment, and C_i is the angular deflection after unloading the i^{th} weight increment.

By definition, in Figure 132, A_1 is 0°, representing the initial angular deflection of the prototype before application of the 1^{st} weight increment. B_1 is the angular deflection corresponding to the moment generated by the 1^{st} weight increment, and C_1 is the angular deflection after unloading the 1^{st} weight increment. A_2 is equal to A_1in this case, since the prototype only deformed elastically by the moment generated by the 1^{st} weight increment, and there was no residual angular deflection after unloading this weight increment from the experimental setup. As the weight increment increases (i.e. 2^{nd} and later sets of weights), the hysteresis curves typically become larger and shift to the right on the x axis, indicating that the prototype begins to deform plastically as it accumulates residual angular deflection (after the second cycle in this case). The flexural rigidity and post yield elasticity metrics are computed by analyzing the angular deflection (B_i), and the residual angular deflection (A_{i+1}) values, respectively.

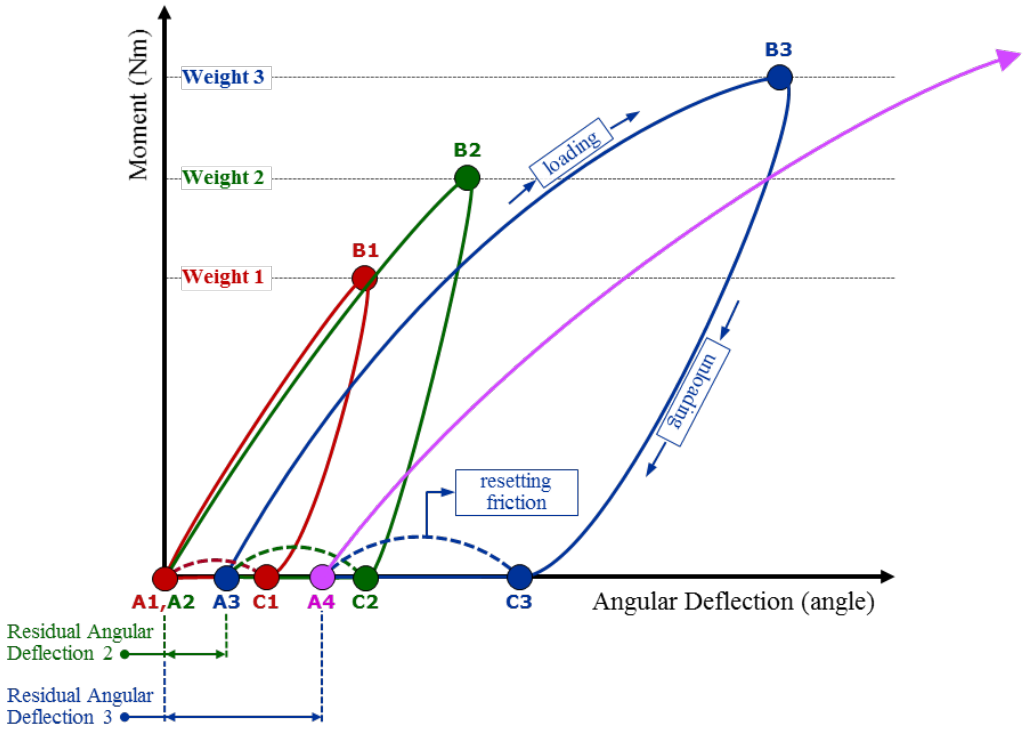

Figure 132. A set of example moment-angular deflection hysteresis curves for calculating rigidizability engineering performance metric scores. Each hysteresis curve $\boldsymbol{i}$ contains three recorded data points, $\boldsymbol{A_i}$, $\boldsymbol{B_i}$, and $\boldsymbol{C_i}$, where $\boldsymbol{A_i}$ is the initial measured angular deflection before application of the $\boldsymbol{i^{th}}$ weight increment, $\boldsymbol{B_i}$ is the angular deflection corresponding to the moment generated by the $\boldsymbol{i^{th}}$ weight increment, and $\boldsymbol{C_i}$ is the angular deflection after unloading the $\boldsymbol{i^{th}}$ weight increment. The flexural rigidity and post yield elasticity metrics were computed by analyzing the angular deflection ($\boldsymbol{B_i}$), and the residual angular deflection values ($\boldsymbol{A_{i+1}}$), respectively.

4.3.3.1. Flexural Rigidity

The flexural rigidity engineering performance metric is the first aspect of rigidizability and is defined as the resistance offered by a layered structure while undergoing bending by a pure moment. To measure the flexural rigidity metric, the yield moment is identified as a first step. To provide a repeatable and more objective method to identify the yield moment, the residual angular deflection values (A_{i+1}) are plotted against the i^{th} moment (computed from the i^{th} weight increment) to visualize the moment where the prototype begins to accumulate plastic deformation as shown by example data in Figure 133(a). The pre-yield region where the prototype deformed elastically is highlighted with a green color, and the post-yield linear region where the prototype no longer returned to its baseline flat shape is highlighted with red. By plotting the angular deflection values (B_i) versus moment applied (Figure 133(b)), the slope of the resulting moment-angle curve in the pre-yield region provides the structural bending stiffness of the entire pneumatic textile prototype.

Since the experimental procedure was performed with a pure bending loading condition, the effect of prototype length can be removed to provide a measure of the flexural rigidity, which was a bending property of a beam. A uniform beam of length l deforms in pure bending by an angle θ under a moment $M = \theta(EI)/l$ where E is the material modulus of elasticity and I is the second moment of area of the beam's cross section. The slope of the moment-angle curve represents the structural bending stiffness, $(EI)/l$, and the product (EI) is referred to as the (absolute) flexural rigidity of the beam. Since each prototype may have a slightly different clamped length, the slope of the moment-angle curve is multiplied by the prototype length to produce the absolute flexural rigidity of the prototype with physical units.

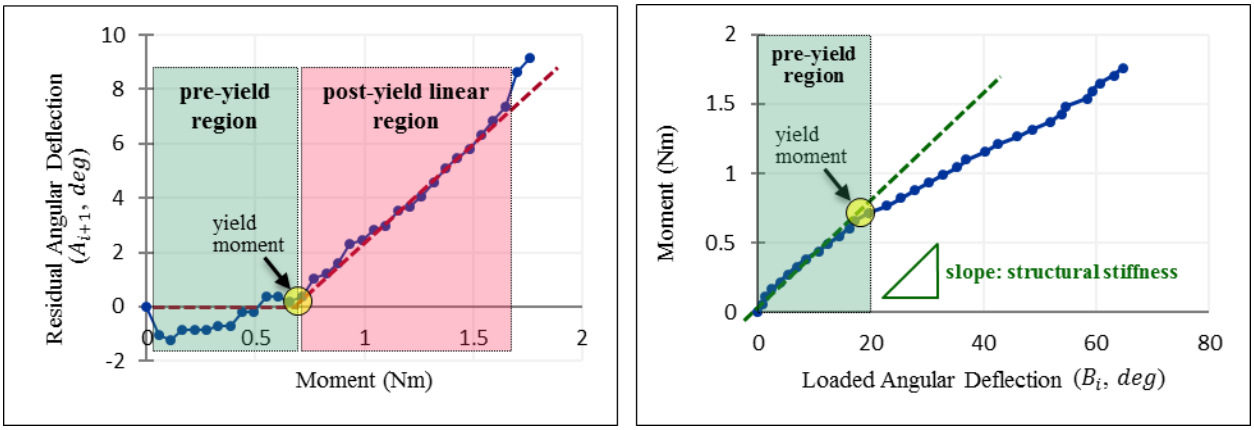

Figure 133. An example set of plots for the calculation of flexural rigidity score. (a) The residual angular deflection values (A_{i+1}) for each prototype are plotted against the i^{th} moment (computed from the i^{th} weight increment) to visualize the moment where the prototype begins accumulating plastic deformation, enabling the identification of the yield moment, pre-yield region, and post-yield linear region. (b) By plotting the angular deflection values (B_i) versus moment applied, the slope of the resulting moment-angle curve in the pre-yield region provides the structural bending stiffness of the entire pneumatic textile prototype, enabling the calculation of the flexural rigidity metric score on a natural functional scale.

To provide a natural functional flexural rigidity metric score, R, the absolute flexural rigidity values, which naturally vary from 0 (completely un-rigid) to infinity (perfectly rigid) are normalized and transformed to a 0 to 1 scale using a standard logistic function,

$$\boldsymbol{R} = \left[\frac{2}{1 + e^{-\frac{(EI)_j}{(EI)_0}}}\right] - 1, \tag{4}$$

where $(EI)_j$ is the absolute flexural rigidity of the j^{th} pneumatic textile prototype independent of its length, and $(EI)_0$ is a normalizing reference flexural rigidity of a solid beam of the cross section of a representative prototype (102.5x4mm cross section) made of a representative tile material, Armadillo (modulus of elasticity: 350 MPa). This results in a natural functional scale ranging from

zero to one, where zero indicates the prototype is not rigid at all, deforming under the influence of any external force, and one indicates the prototype is perfectly rigid, resisting all the external forces it is subjected to. Since the mid-point of the logistic function (0.46) corresponds to the rigidity of a representative solid plate, some prototypes can score higher than 0.46 due to the material, architecture, and dimensions of prototype.

4.3.3.2. Post Yield Elasticity

The post yield elasticity engineering performance metric is the second aspect of rigidizability. Beyond the yield moment, the accumulation of the residual angular deflection (A_{i+1}) values become observable in the post-yield linear region (Figure 134(a)) and increase as the loaded angular deflection B_i increases. The slope of the plot of the residual angular deflection versus the loaded angular deflection represents the portion of angular deflection lost to yield (Figure 134(b)). This slope naturally varies from zero (perfectly elastic, no yield) to one (perfectly plastic, no elastic recovery). Since elastic behavior is desirable for maintaining shape under load, this metric is subtracted from one to convert to a natural functional metric scale representing the post-yield elasticity, E, where

$$\boldsymbol{E} = 1 - \left(\frac{\Delta Residual\ Angular\ Deflection}{\Delta Loaded\ Angular\ Deflection}\right). \quad (5)$$

This metric represents the fraction of deformation that is elastically recovered after yield, where zero indicates the prototype remains fully deformed after bending, and one indicates the prototype fully recovers its shape after bending.

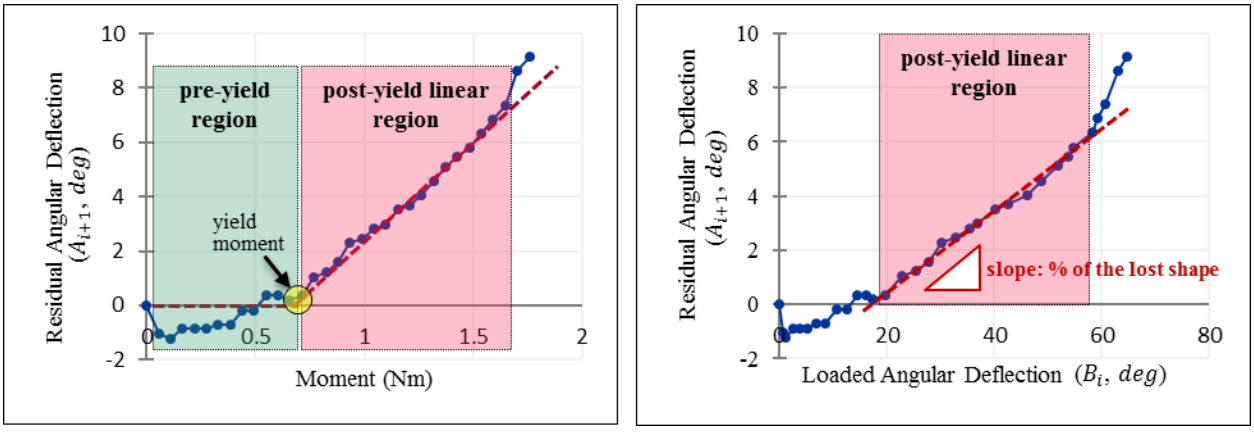

Figure 134. An example set of plots for the calculation of post yield elasticity score. (a) In post-yield linear region, the accumulation of the residual angular deflection ($\boldsymbol{A_{i+1}}$) values for each pneumatic textile prototype become observable and increase as the moment increases. (b) The slope of the plot of the residual angular deflection versus

the loaded angular deflection in this region represents the portion of angular deflection lost to yield. Since elastic behavior is desirable for maintaining shape under load, this metric is subtracted from one, providing the post-yield elasticity metric score on a natural functional metric scale.

4.4. Systematic Exploration of Hierarchical Architectural Design Space

To design structurally adaptable multi-mode products by employing internally tiled pneumatic textiles, an in-depth understanding of the effects of tile architectural class/subclass and the architectural feature variations corresponding to each class/subclass on the internally tiled pneumatic textile's performance needs to be established in the first place. To build such in-depth understanding, running a series of controlled experiments is required. However, the design space of the internally tiled pneumatic textiles is broad and open ended. Conducting a full design of experiments over the entire design space by incorporating all possible combinations of the tile architectural classes and subclasses with their corresponding feature variations is not feasible. Thus, three experimental studies are conducted in a hierarchical manner, each exploring one layer of the architectural hierarchy: the analysis of performances across tile architectural classes, the analysis of design couplings within a tile architectural subclass, and the analysis of the effects of architectural feature variations.

The hierarchy is structured such that the layer with the largest impact is studied first; the choice of tile architectural class determines the available options for an architectural subclass selection, and the choice of subclass determines what architectural feature variations are available for that particular subclass. Therefore, a comparative performance study across tile architectural classes is executed first. Representative examples from each class and subclass are generated, enabling a performance comparison across pneumatic textile prototypes. The quantifiable engineering performance metrics capturing the drapability, shapability, and rigidizability performances are measured in their respective operation states. The effects of different tile architectural classes on the pneumatic textile's overall performance are analyzed based on the comparison of the performance metric scores of the individual representatives from each class. A study from which correlation matrices are generated from a set of representatives within a subclass showing the dependencies between the pairs of performance metrics evaluates the differences in design couplings across two different architectural subclasses. A final study evaluates the effects of architectural feature variations of one representative architecture on the resulting overall performance.

The results of hierarchical architectural design space studies lay the foundation for creating versatile, structurally adaptable multi-mode products that employ internally tiled pneumatic textiles to deliver moldability technology capability, which combines the technology sub-capabilities: drapability, shapability, and rigidizability. A potential use for these three technology sub-capabilities is in the design of a flexible, active cargo blanket that aims to securely hold and transport items with a wide range of shapes and sizes within a moving vehicle.

4.4.1. Comparative Performance Evaluation Across Tile Architectural Classes

Tile architectural class has a major influence on the form of pneumatic textiles, hence on its drapability, shapability, and rigidizability performances. Understanding the effects of the different tile architectural classes on the pneumatic textile's overall moldability performance is an essential first step that provides a basis to make a design decision, selecting a particular tile architectural class.

Eight prototypes that contain various tile array layers representing three different tile architectural classes were designed and fabricated. Table 4 summarizes the specifications of the prototypes used throughout the performance comparison study of the tile architectural classes. Six prototypes represent the bladder-attached tiles class, half of which are from the non-connected tiles subclass while the other half are from the connected tiles subclass. One prototype each represents the internal sheet-attached tiles and the mutually interlocking tiles classes. In Figure 135, the shapes of the individual tiles, their size relative to each other, and how each tile is brought together to form a patch of a tile array layer are illustrated. The dimensions of the resulting tile array layers vary somewhat since the shape and size of each individual tile forming their respective tile array layers are not identical, but a discrete number of tiles must be used.

Table 4. Study of comparing different tile architectural classes

#Prototype	Tile architectural class	Tile architectural sub-class	Tile height (mm)	Tile base area (mm^2)	Tile array layer size (mm)	Tile material
BN1 (truncated square pyramid)	Bladder-attached tiles	Bladder-attached non-connected tiles	4	100	186 x 98	Semiflex TPU
BN2 (truncated cone)			5	78.5	180 x 100	
BN3 (extruded equilateral triangle)			2	52.9	176 x 102,5	Armadillo TPU
BC1 (truncated octagon pyramid)		Bladder-attached connected tiles	4	186.4	180 x 105	Semiflex TPU
BC2 (truncated hexagon pyramid)			4	65	180 x 95	
BC3 (extruded equilateral triangle)			2	52.9	180 x 104	
IS1 (snap fit hexagon)	Internal sheet-attached tiles	X	5	295	180 x 110	ABS
MI1 (interlocked hexagon)	Mutually interlocking tiles	X	8.4	346.4	180 x 100	ABS

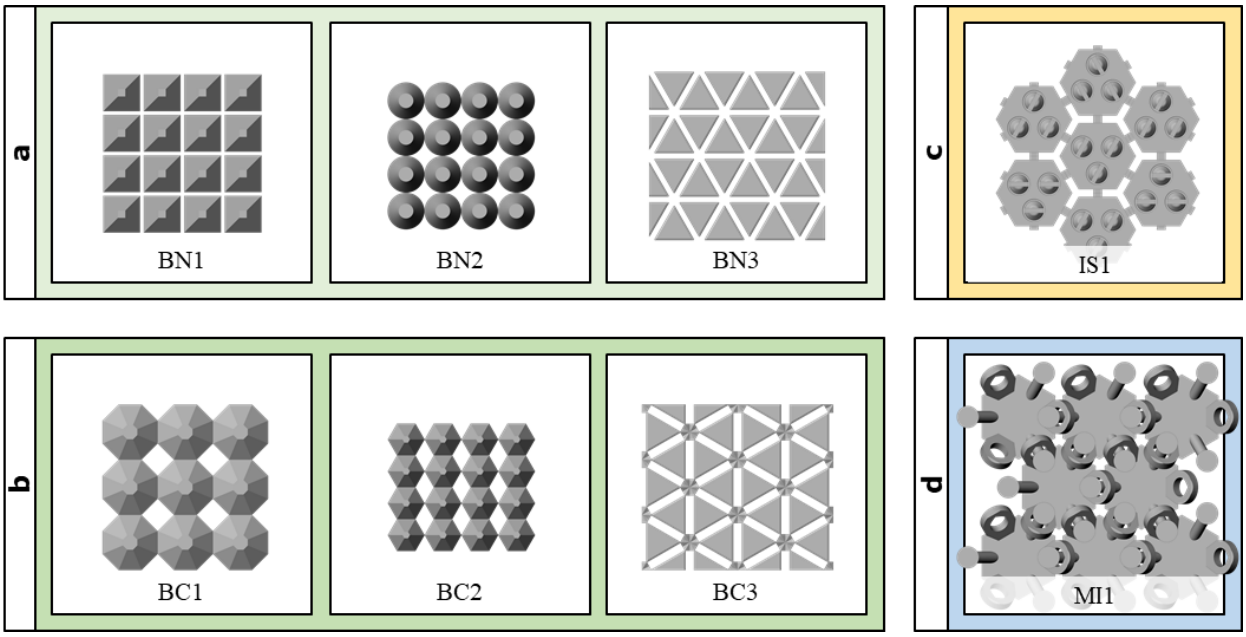

Figure 135. Tile array patches representing three tile architectural classes. (a) Three pneumatic textile prototypes are made of bladder-attached non-connected tile array patches labelled BN1 (truncated square pyramid), BN2 (truncated cone), and BN3 (extruded equilateral triangle). (b) Three pneumatic textile prototypes are made of bladder-attached connected tile array patches labelled BC1 (truncated octagon pyramid), BC2 (truncated hexagon pyramid), and BC3 (extruded equilateral triangle). (c) One pneumatic textile prototype is made of internal sheet-attached tile patch labelled IS1 (snap fit hexagon), and (d) one pneumatic textile prototype is made of mutually interlocking tile patch labelled MI1 (interlocked hexagon).

The performance in all five metrics was tested for each prototype and the relevant engineering performance metric scores were quantified by processing and transforming the raw data into the corresponding natural functional scale, between zero and one. In Figure 136, the performance metric scores of eight different prototypes representing three different tile architectural classes are compared on the natural functional scale, where the dashed black line shows the corresponding group average for each metric.

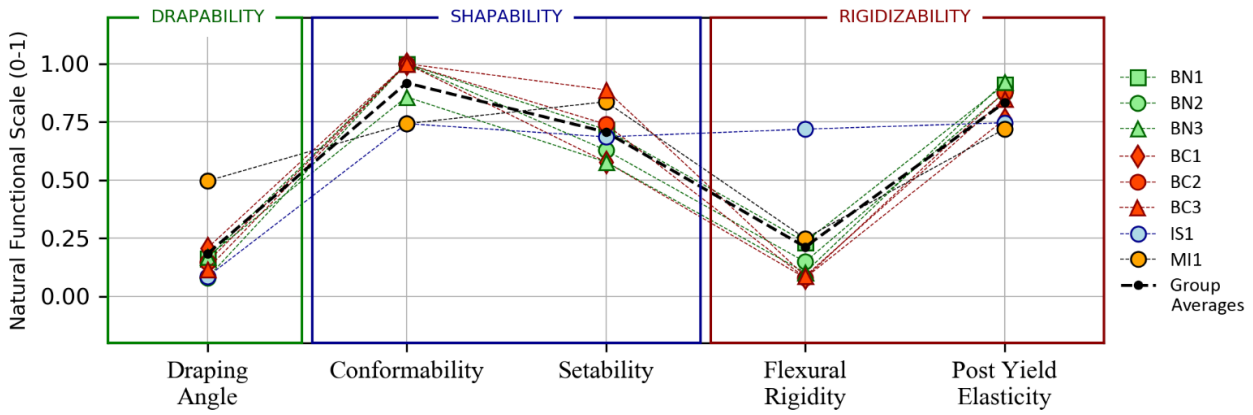

Figure 136. Tile architectural class study comparative results. The range of performance metric for each engineering performance metric on the natural functional scale (0-1) varies across prototypes. While the mean

conformability, setability, and post yield elasticity scores of all eight prototypes are above 0.5 on the natural functional scale with a similar range, draping angle and flexural rigidity scores are below 0.25 on average with relatively larger range. Six prototypes representing two subclasses of the bladder-attached tiles class (BN1-2-3 and BC1-2-3) show minimal spread regarding draping angle, conformability, and post yield elasticity performance metric scores. The prototype representing mutually interlocking tiles class (MI1) performs significantly better than any other prototypes in draping angle; however, it has the lowest conformability and post yield elasticity scores. Similarly, the prototype representing internal sheet-attached tiles provides the best flexural rigidity performance while providing the worst draping angle and conformability scores across all prototypes.

Across all the architectural classes, the range of performance of the different performance metrics varied. The mean scores for the conformability, setability, and post yield elasticity performance metrics are all located at the upper portion on the natural functional scale, indicating all the prototypes performed well regarding these metrics on average. Most of the prototypes representing the bladder-attached tiles class displayed perfect conformability whereas the prototypes representing the other tile architectural classes, scored lower in conformability. All the prototypes performed well in setability with no obvious difference across the prototypes representing different tile architectural classes. The performance metric scores showed minimal spread in post yield elasticity, where all the prototypes representing the bladder-attached tiles class recovered their deformation after bending in the post yield linear region more successfully than the rest of the prototypes.

The mean scores for the draping angle and flexural rigidity performance metrics are located at the bottom portion on the same scale, indicating the prototypes performed unsatisfactorily on average. Both the draping angle and flexural rigidity scores differ in wider ranges in comparison to the first group. All the prototypes that contain two layers of tile array layers show low variability around the mean in the draping angle performance metric except one prototype with a positively outlying score. This prototype (MI1) represents the mutually interlocking tiles class, which contains only one tile array layer, facilitating the interconnected tiles to be draped in a less restricted way, thus providing relatively higher draping angle score. Similarly, all the prototypes show low variability in the flexural rigidity performance metric except one prototype with a positively outlying score. This prototype (IS1) represents the internal sheet-attached tiles class. It contains two opposing tile array layers, where the individual tiles are larger than the average tile size across prototypes and made of stiffer material (ABS). In addition to these, the hexagonal tiles form a honeycomb pattern with non-linear folding lines, which enhance the stiffening capability of this particular prototype when vacuum is applied.

While different prototypes perform better in some metrics than others, direct comparison between prototypes over all the metrics is difficult because the means and ranges for each quantified performance metric scores are dissimilar. Normalizing the natural functional metric scores relative to the mean of each metric is helpful for making relative comparisons over all metrics across architectural classes. To achieve this, each performance metric score is calculated as a percentage of their respective group average, where the group average is the mean score of the entire set of prototypes of all classes. This percentage is then shifted to be centered at zero such that it represents a percent variation relative to the group average. While comparing normalized scores can provide a clearer view of the relative performance, the absolute merit contained in the natural functional metrics is lost in the normalization. Plotting the normalized performance metric scores of prototypes in each tile architectural class in isolation facilitates the inspection of the relative strength and weaknesses of the tile architectural classes. The set of normalized performance metric scores is compared to the corresponding group averages, which are highlighted with a black dashed line at the zero level (by definition) on each plot.

The normalized performance metric scores of the six prototypes, which represent the bladder-attached tiles class, are shown in Figure 137. Two subclasses, employing non-connected and connected tiles, are color coded with green and red, respectively. In this tile architectural class, the ranges of the deviations from the corresponding group averages for conformability and post yield elasticity metrics are minimal in the positive direction since the means are elevated by one of the other tile architectural classes. The setability metric shows a moderate range of deviation, whereas the draping angle and flexural rigidity metrics both show relatively larger spread in the negative direction.

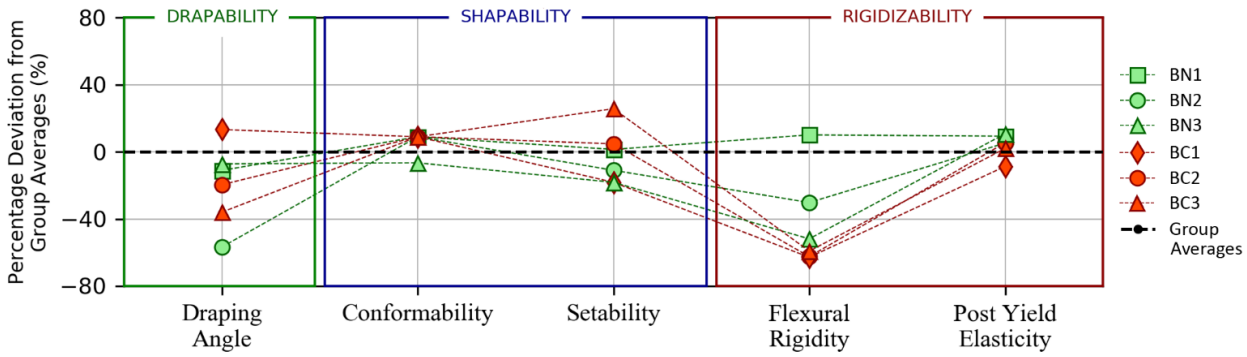

Figure 137. Normalized performance metric scores of prototypes representing bladder-attached tile class. The natural functional metric scores are normalized relative to the group averages (indicated by 0%) of each respective metric enabling making relative comparisons over all metrics across architectural classes and subclasses. While the range of conformability and post yield elasticity performance metrics on the normalized scale are smaller relative to

the other metrics and centered around the group averages, the range of draping angle and flexural rigidity metrics are larger, and their average scores are below 0%. The prototypes in bladder-attached connected tile class (BC1-2-3) perform better in draping angle, conformability, and setability, whereas the remaining prototypes (BN1-2-3) produce better results in flexural rigidity and post yield elasticity performance metrics.

The prototype (BC2) that performs the best in the draping angle performance metric employs connected truncated hexagon pyramid tiles, which have smaller tile base area and average tile height across the prototypes representing the bladder-attached tile architectural class. In line with this, the prototype (BN1) that employs non-connected truncated cone pyramid tiles, which have average tile base area but the tallest tile height, presents the worst draping angle performance. Almost all of the prototypes regardless of employing non-connected or connected tiles have the same conformability performance metric scores. However, the prototypes (BN1-2-3) employing non-connected tiles perform worse in the setability metric on average. This is due to having a gap between their non-connected tiles, which induces deformation of the conformed shape once the vacuum pressure applied to the pneumatic textile prototype. All the prototypes employing non-connected tiles perform better in the flexural rigidity performance metric. Although the post yield elasticity performance metric scores do not vary much, the prototypes employing non-connected tiles perform slightly better. In general, the graph indicates that changing the tile architectural subclass and tile geometry design causes a shift in the resulting performances of the prototypes in this class.

The prototype (IS1) representing the internal sheet-attached tile class achieves the best flexural rigidity score (239% above the mean) across all prototypes; however, all the remaining normalized performance metric scores are below the corresponding group averages as illustrated in Figure 138. The individual tiles forming the two opposing layups of the prototype representing the internal sheet-attached tiles class are made of stiffer material and have larger tile base area when compared to the ones in the bladder-attached tiles class. In addition to the difference in the tile base area, this prototype employs the largest overall thickness for the combination of its tile array layers, where each tile employs protrusions on their surface, increasing the friction between two opposing tile array layers. All these factors contribute to the flexural rigidity performance, explaining the highest score across all prototypes. The honeycomb pattern forming each tile array layer creates non-linear folding lines, which hinders the draping and conforming capabilities, resulting with the relatively lower draping angle and conformability performance metric scores.

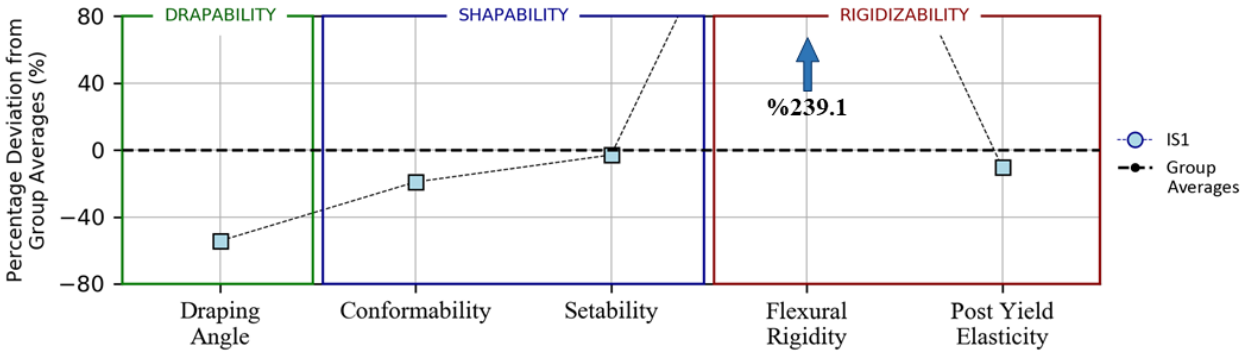

Figure 138. Normalized performance metric scores of the prototype representing internal sheet-attached tile class. IS1 achieves the best flexural rigidity metric score (239.1%), however all the remaining normalized performance metric scores for this prototype are below the corresponding group averages.

The prototype (MI1) representing the mutually interlocking tile class performs the best regarding draping angle as shown in Figure 139. The normalized scores for the setability and flexural rigidity metrics are slightly above the corresponding group averages, whereas the ones for conformability and post yield elasticity metrics are the worst among all prototypes. The mutually interlocking tiles have complementary design features that provide flexibility as the legs can slide and rotate within their corresponding loops in unvacuumed state, improving the draping angle score. However, the same features limit the conformability score of the pneumatic textile since there is a hard stop where each individual tile collide with the adjacent ones. The asymmetrical nature of the tile array layer induces the cinching behavior when vacuum is applied, which improves the setability score as it minimizes the springing back from the target cylinders that are used in the setability test.

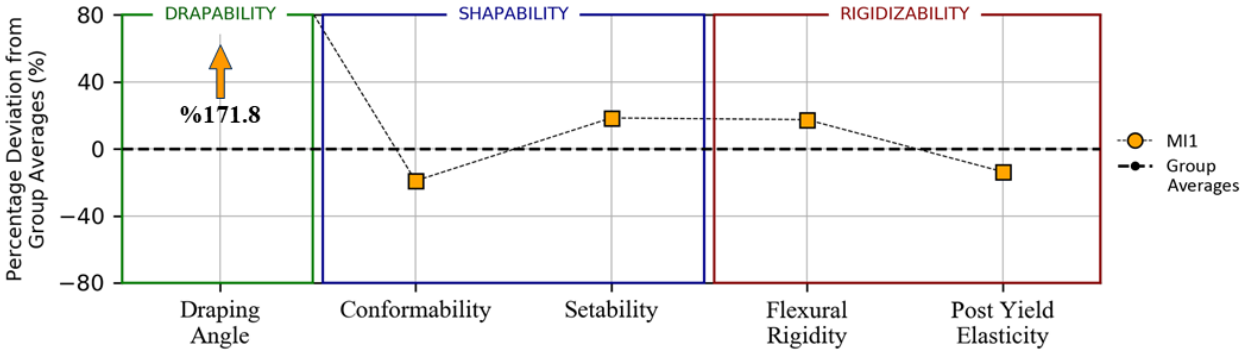

Figure 139. Normalized performance metric scores of the prototype representing mutually interlocking tile class. MI1 achieves the best draping angle performance metric score (171.8%). The prototype's normalized scores for the setability and flexural rigidity metrics are slightly above the corresponding group averages, whereas the ones for conformability and post yield elasticity metrics are the worst among all prototypes used in the study.

While each architectural class has various strengths and weaknesses according to the normalized scores, there is no single class/subclass that performs the best across all the

performance metrics. Thus, each pneumatic textile prototype, regardless of the tile architectural class they represent, produces performance metric scores that trade off with one another. For example, while the prototype representing the internal sheet-attached tiles provides outstanding flexural rigidity score due to the use of relatively larger and taller tiles, it performs the poorest with respect to the draping angle and conformability performance metrics. Similarly, the prototype representing the mutually interlocking tiles, containing only one tile array layer, provides the best draping angle score; however, the conformability and post yield elasticity performance metric scores are the worst across all prototypes in return. The bladder-attached tiles class lacks a representative prototype of which normalized performance metric scores simultaneously exceeds the group averages as well; yet, the ranges of the normalized scores vary both above and below the corresponding group averages. The tile heights and tile base areas are both relatively shorter and smaller in this class when compared to the ones in the remaining classes, explaining the lower flexural rigidity performance metric scores. This suggests the potential of developing better performing pneumatic textiles in the bladder-attached tiles class by changing the tile geometry design variables.

Choosing a particular prototype representing a particular tile architectural class can be more favorable than choosing another one depending on the design context. For example, a certain design application might require an excellent rigidizability performance for which the drapability and shapability performances are of secondary importance. In such case, choosing an internal sheet-attached tiles class and further exploring the architectural feature variations in that class would likely yield better performance results matching the desired moldability criteria. If above-average level drapability, shapability, and rigidizability performances are required for another design application, choosing a bladder-attached tiles class would provide a better ground for the further layers of the hierarchical architectural design space exploration process.

To demonstrate the next study corresponding to the tile architectural subclass layer of the architectural hierarchy, the bladder-attached tiles class is selected. However, the comparative analysis between the tile architectural subclasses in this tile class is not straightforward due to the absence of a single prototype that simultaneously performs well across all performance metrics. Another useful technique that can provide insights for understanding the effects of the tile architectural classes/sub-classes on the resulting performances is to analyze the relationships

between the pairs of performance metric scores of the prototypes to evaluate important design couplings.

4.4.2. Design Coupling Evaluation Within Tile Architectural Subclasses

Generally, design tradeoffs exist between competing factors. It is possible to improve a set of performance metrics of a pneumatic textile by changing its architectural features and tile geometry design variables; however, there will be simultaneous negative effects on the remaining ones. Understanding such dependencies between the pairs of performance metrics is the first step to enable tailoring the overall performance of a pneumatic textile. The assessment of the direction and strength of the correlations between pairs of performance metric scores provides a rationale to identify which tile architectural subclass under the bladder-attached tiles class presents the least amount of negative dependency between its performance metric pairs. The absence of negative dependency (and more so the presence of positive dependency) implies that through proper design, any metric performance can be independently improved with minimal tradeoffs.

The design freedom regarding the architectural features and tile geometry will be increased by choosing the tile architectural subclass with the lower amount of negative correlation between its performance metrics. Making an assessment is required regarding how the direction and strength of the correlations between the pairs of performance metrics change as the grouping of prototypes is sequentially narrowed down. Thus, the correlation matrices are generated for the prototypes representing the bladder-attached tiles class (n=6) first, and separately for each of the subclasses representing attached (n=3) and non-attached (n=3) tiles, second. In the following tables, matrices of Pearson product-moment correlation coefficients for the pairs of performance metric scores are shown. The strengths of the correlations are categorized based on the guide that Evans [215] suggests where the shades of orange and green colors highlight the varying magnitude of negative and positive associations. A value of one or negative one represents the strongest linear association, and a value of zero represents no linear association between the pair of metrics.

The correlation matrix for the prototypes representing the bladder-attached tiles class is shown in Table 5, where the strength of the resulting correlations is mostly moderate or weak, and the direction is mostly negative. The draping angle shows weak negative correlations with conformability and post yield elasticity, and moderate negative correlation with setability. While conformability moderately correlates with setability in positive direction, it moderately correlates

with post yield elasticity in negative direction. There is a moderate positive association between flexural rigidity and post yield elasticity. In general, there is no strong or very strong negative dependencies between the performance metrics in the bladder-attached tiles class, but the quantity of the moderate negative dependencies are larger than the positive ones. However, analyzing correlations for both subclasses taken together obfuscates differences between the two classes and does not provide information to aid understanding the effects of each subclass on the resulting performances. Analyzing correlation matrices for the pairs of performance metrics by separating the prototypes into two groups based on the type of subclasses they represent enables a systematic way of analyzing, where the quantity and strength of the dependencies can be compared across these groups.

Table 5. Pearson correlation matrix for prototypes representing bladder-attached tiles class (n=6)

	Draping angle	Conformability	Setability	Flexural rigidity	Post yield elasticity
Draping angle	1.00	-0.25	-0.40	-0.15	-0.36
Conformability		1.00	0.45	0.16	-0.48
Setability			1.00	-0.02	0.10
Flexural rigidity				1.00	0.49
Post yield elasticity					1.00
Strength of correlations	very weak	weak	Moderate	strong	very strong
	(.00)-(-.19)	(-.20)-(-.39)	(-.40)-(-.59)	(-.60)-(-.79)	**(-.80)-(-1.0)**
	(.00)-(.19)	(.20)-(.39)	(.40)-(.59)	(.60)-(.79)	**(.80)-(1.0)**

In the bladder-attached connected tiles subclass, all the prototypes have same conformability metric score, preventing the calculation of correlation coefficients for the pairs of metrics including conformability. Thus, conformability is excluded from this analysis. There are very strong negative correlations between the draping angle and the rest of the performance metrics, while setability shows very strong positive association with flexural rigidity, and strong positive association with post yield elasticity. There is a weak positive correlation between flexural rigidity and post yield elasticity as shown in Table 6.

Table 6. Pearson correlation matrix for prototypes representing bladder-attached connected tiles (n=3)

	Draping angle	Conformability	Setability	Flexural rigidity	Post yield elasticity
Draping angle	1.00	NA	**-0.99**	**-0.81**	**-0.84**
Conformability		1.00	NA	NA	NA
Setability			1.00	**0.89**	0.74
Flexural rigidity				1.00	0.37
Post yield elasticity					1.00
Strength of correlations	very weak	weak	Moderate	strong	very strong
	(.00)-(-.19)	(-.20)-(-.39)	(-.40)-(-.59)	(-.60)-(-.79)	**(-.80)-(-1.0)**
	(.00)-(.19)	(.20)-(.39)	(.40)-(.59)	(.60)-(.79)	**(.80)-(1.0)**

In the bladder-attached non-connected tiles subclass, not only are the quantity and the strength of the negative correlations between the pairs of performance metrics relatively lower, but also the positive correlations are stronger and larger in quantity as shown in Table 7. There is a moderate negative correlation between the draping angle and conformability, while a very strong positive correlation between draping angle and post yield elasticity is observed. Conformability shows strong positive correlations with setability and flexural rigidity, while showing strong negative correlation with post yield elasticity. There is a one-to-one positive linear association between setability and flexural rigidity.

Table 7. Pearson correlation matrix for prototypes representing bladder-attached non-connected tiles (n=3)

	Draping angle	Conformability	Setability	Flexural rigidity	Post yield elasticity
Draping angle	1.00	-0.56	0.08	0.10	**0.98**
Conformability		1.00	0.78	0.77	-0.70
Setability			1.00	**1.00**	-0.10
Flexural rigidity				1.00	-0.09
Post yield elasticity					1.00
Strength of correlations	very weak	weak	Moderate	strong	very strong
	(.00)-(-.19)	(-.20)-(-.39)	(-.40)-(-.59)	(-.60)-(-.79)	**(-.80)-(-1.0)**
	(.00)-(.19)	(.20)-(.39)	(.40)-(.59)	(.60)-(.79)	**(.80)-(1.0)**

In Table 8, the quantities of the correlation coefficients that exist in each grouping of prototypes is shown, where red colored ones highlighting negative and green colored ones highlighting positive directions. While the combined prototype grouping mostly consists of weak to moderate correlations, the two separate subclass groupings contain moderate to very strong correlations. The ratio of the number of positive to negative correlations becomes greater by separating the subclasses, and the non-connected tiles subclass shows the largest ratio of positive to negative correlations. Based on the comparison between the sum of correlations regarding quantity and strength, the pneumatic textile prototypes representing the bladder-attached non-connected tiles subclass is found to be more flexible in terms of providing design freedom. The quantity and strength of the negative dependencies between its performance metric pairs in the non-connected tiles subclass is relatively minimized, indicating minimal design tradeoffs, while the quantity and strength of the positive correlations is relatively maximized indicating that multiple metrics can be improved simultaneously.

Table 8. Quantified comparison of the correlation direction and strength across prototype groupings

	Strength of the Correlation (Evans, 1996)	Bladder-attached Tiles (n=6)		Bladder-attached Connected Tiles (n=3)		Bladder-attached Non-connected Tiles (n=3)	
# of Negative vs Positive Correlations Across Tile Architectural Class Categories	weak (.20-.39)	2	0	0	1	0	0
	moderate (.40-.59)	2	2	0	0	2	0
	strong (.60-.79)	0	0	0	1	0	2
	very strong (.81-1.0)	0	0	3	1	0	2
Sum of Correlations (quantity)		4	2	3	3	2	4
Sum of Correlations (magnitude)		-0.53		-0.63		2.26	

In this subclass, the prototype made of equilateral triangle tiles is selected to demonstrate the next study corresponding to the architectural feature variations. It supports more architectural features regarding the tile layer and architectural layup, and lends itself to varying tile geometry design to improve and tailor pneumatic textile performance.

4.4.3. Comparative Performance Evaluation Across Architectural Feature Variations

Two main variations of the architectural features are explored in this experimental study by using the equilateral triangle tiles representing the bladder-attached non-connected tiles subclass. The effects of alternating the way the tile array layers overlap with each other and introducing a layer of thin (0.3mm) soft TPU sheet between the tile array layers on the pneumatic textile performance were measured from which the most favorable combination of architectural feature variations is identified.

4.4.3.1. Tile Layer Overlap

The selected pneumatic textile prototype (BN3) is made of two tile array layers, where all the individual non-connected tiles perfectly overlap with their opposing ones. Such perfect alignment, in combination with the effect of the gap between adjacent tiles, provides a folding pattern on the pneumatic textile prototype, enhancing the hinge-like ability of the individual tiles and enabling relative rotational motion. This is expected to have an observable negative effect on the resulting flexural rigidity performance metric score.

To improve the flexural rigidity performance of the downselected architectural variation (a) that contains perfectly overlapping tile array layers, an alternative version (b) containing a shifted formation of the tile array layers, where the center of mass of every other overlapping tile pairs is in alignment, was fabricated without changing any other design variable Figure 140.

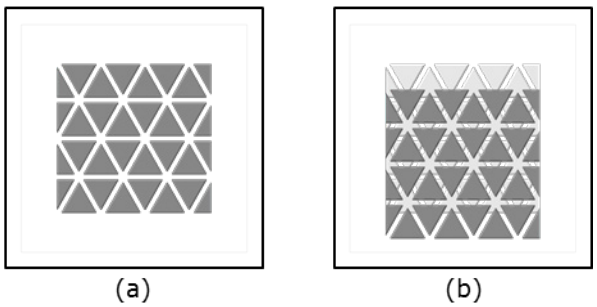

Figure 140. Tile overlap variations for the selected pneumatic textile prototype (BN3). (a) The original prototype (BN3) made of perfectly overlapping tile array layers (b) and an alternative version (BN3.1) made of shifted tile array layers are shown in top view.

After testing and measuring the relevant performance metric scores in the natural functional scale for the alternative prototype, each performance metric score was normalized as a percentage of the respective group average, where the group average is the mean score of the entire set of prototypes used in the comparative performance evaluation study across tile architectural classes. To make an assessment regarding the effect of shifting the tile array layer overlap, the set of normalized performance metric scores for the two prototypes is shown relative to the corresponding average scores of all previous prototypes (n=8), which are highlighted with a black dashed line at the zero level on the plot in Figure 141. Accordingly, shifting the tile array layers had a major positive influence on the flexural rigidity metric score, which was increased by 43%. However, it negatively affected the draping angle and setability metrics by reducing the scores by 40% and 20%, respectively. Conformability and post yield elasticity metric scores showed no variation. The overall performance was decreased by only 3% on average.

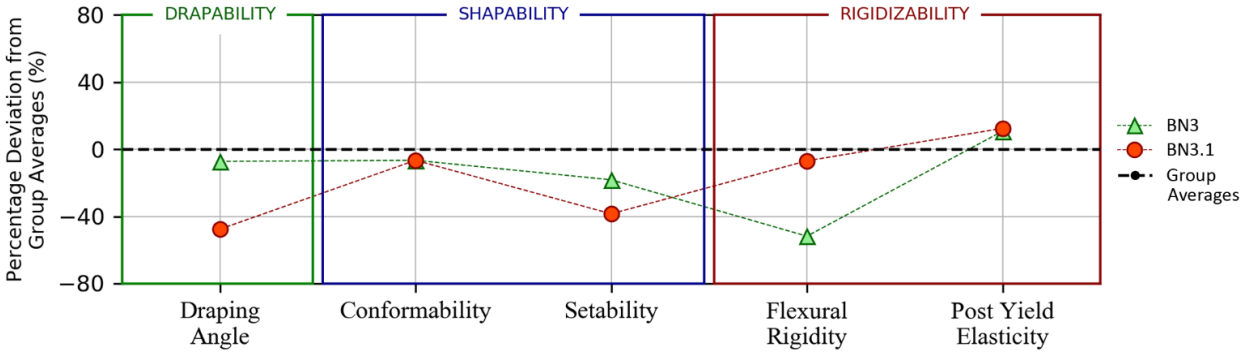

Figure 141. Tile overlap study comparative results. The prototype (BN3.1) with the shifted tile array layers performs 43% better than the one (BN3) with perfectly overlapping tile array layers. While there is no effect on the conformability and post yield elasticity performance metric scores, the draping angle (-40%) and setability (-20%) performance metric scores are negatively affected as a result of using shifted tile overlap architectural feature variation.

The increase in the resulting flexural rigidity performance metric score, and the decrease in the draping angle and setability scores were expected because the hinge-like ability of the individual tiles is reduced by shifting the way the tile array layers overlap with each other. Since there is no significant negative effect on the overall pneumatic textile performance, accommodating shifted opposing tile array layers as an architectural feature is selected for the next step in the pneumatic textile design process.

4.4.3.2. Intermediate Layer Layup

To improve the level of drapability lost by introducing shifted opposing tile layers, an additional architectural feature variation is introduced: an intermediate layer layup. The selected pneumatic textile prototype's operation is affected by the gap between the neighboring tiles forming the tile array layers. In the course of draping or shaping the pneumatic textile over arbitrary objects, it is likely for an individual tile to be blocked by the edges of tiles that form the opposing tile layer, resulting in a reduced range of translational and rotational motion. One way of addressing this drawback is to introduce a continuous soft surface between the tile array layers to lubricate this sliding for better drapability (Figure 142).

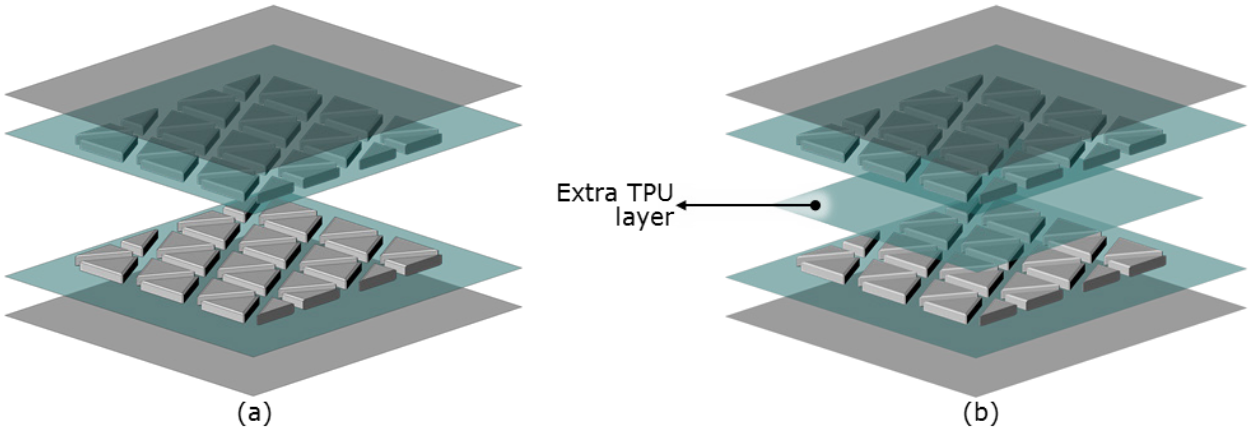

Figure 142. Intermediate layer layup variations for the selected pneumatic textile prototype (BN3.1). (a) The prototype (BN3.1) made of shifted tile array layers with no intermediate layer in-between, (b) and an alternative version (BN3.2) made of shifted tile array layers with an intermediate layer in-between are shown in isometric view.

The effects of inserting a thin sheet of soft TPU layer with a thickness of 0.3mm in between the tile array layers were measured. A pneumatic textile prototype (BN3.2) identical to the shifted tile prototype but containing a thin soft TPU layer was fabricated and tested. The difference between performance metrics for the two different versions, having one sheet of TPU layer in-between the tile array layers and having none, is shown in Figure 143.

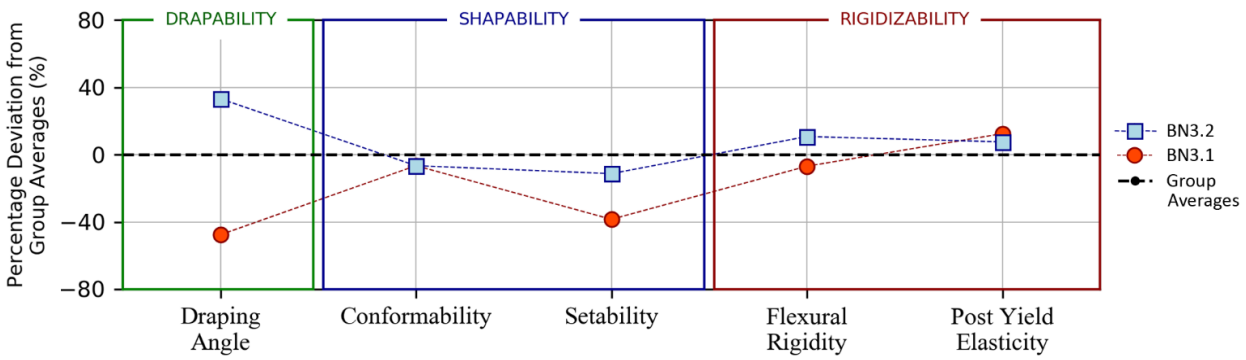

Figure 143. Intermediate layer layup study comparative results. Introducing an intermediate layer between the tile array layers results with 81%, 27%, and 17% increases in draping angle, setability, and flexural rigidity performance metric scores, respectively, without almost making no negative effect on the remaining performance metric scores.

As expected, inserting a TPU layer in between the tile array layers as a part of the pneumatic textile layup had a large positive effect on the draping angle by providing a lubricating surface between the opposing tiles, increasing the normalized score by 81%. In addition, the soft TPU layer becomes compressed between the tile array layers when vacuum is applied. This increases the friction between overlapping tiles, resulting in better setability and flexural rigidity performances. As shown in Figure 143, the setability and flexural rigidity performance metric scores were increased by 27%, and 17%, respectively, while conformability and post yield elasticity were left almost unchanged.

The overall pneumatic textile performance was improved by 24% on average when compared to the performance of the pneumatic textile that does not contain any TPU layer in between its tile array layers. Introducing an intermediate layer layup as an architectural variation overcame the losses introduced by shifting the tiles. As a result of this study, having a TPU layer in between the tile array layers and shifting the layers relative to each other are identified as the final combination of architectural feature variations.

4.5. Parametric Design Case Study: Moldable Active Cargo Blanket Using Internally Tiled Pneumatic Textiles

Systematically and efficiently exploring the architectural design space of internally tiled pneumatic textiles through a hierarchical series of three experimental studies enabled developing an understanding of how variations in tile architectural class/subclass and corresponding architectural features impact the moldability performance of internally tiled pneumatic textiles. The findings of these studies provide a basis for the development of structurally adaptable multi-

mode products that use internally tiled pneumatic textiles to provide moldability technology capability as a combination of drapability, shapability, and rigidizability technology sub-capabilities. One potential application of these three sub-capabilities is in the design of a moldable active cargo blanket, which targets securing and transporting loose cargo of vastly varying shape and size in a moving vehicle.

Restraining loose cargo is an ongoing challenge in the transportation industry. The use of cargo nets and dividers is a convenient method of restraint, but they limit the size of cargo that can be restrained and are not reliable when used for many small items, often resulting in these items spilling and scattering during transport. Using multiple elastic cords with hooks can provide flexibility for restraining larger items in a trunk, however using these devices is relatively more difficult and time consuming for the users, and the availability of anchor points for attaching the hooks in the trunk vary from one vehicle to another. Another widely adopted approach is using rigid storage bins to store relatively small sized cargo items, but such storage bins themselves need to be secured and take up space when they are not in use.

To address the shortcomings of the currently available cargo transportation approaches, a promising alternative approach is to design a blanket-like lightweight and thin surface that can be draped over, manually conformed and set to various shapes, and easily stiffen on demand for securely enveloping and constraining a random collection of cargo items in various forms and sizes (Figure 144). This would be able to effectively constrain much wider range of item sizes and shapes, would be relatively user friendly (i.e. quick and simple to use), and would not require specific vehicle adaptation and/or attachment points as compared to exiting approaches. The design of such an adaptive moldable surface must strike a balance between the performance of its three key technology sub-capabilities: *drapability*, *shapability*, and *rigidizability*. Each of these capabilities needs to be activated on demand in a fast and reversible manner through their respective operation states. Developing a technological basis that enables the transition between these states is challenging due to the inherent tradeoffs among the technology sub-capability performances since the same design features have simultaneous impact on each of them. Moreover, the balance among the technology sub-capability performances needs to be tailored based on the vehicle segment, style, and/or customer expectations. An off-road vehicle which is designed to travel over rough terrain hauling heavy-duty equipment would require a higher priority on the rigidizability performance, whereas prioritizing the drapability and/or shapability performances

would be more appropriate for a fuel-efficient commuter vehicle which is often used for transporting grocery bags.

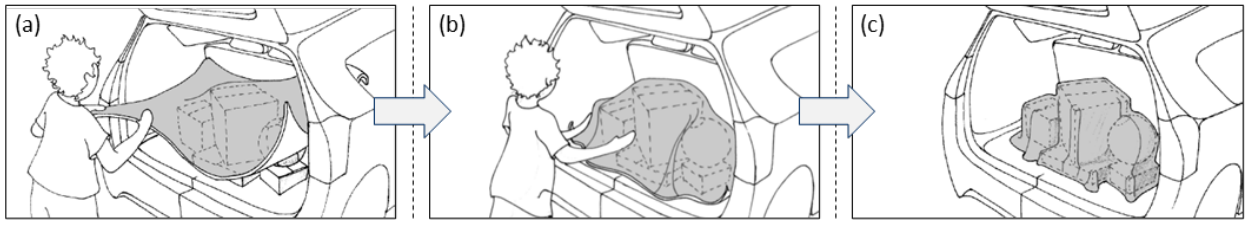

Figure 144. An example use case of a moldable active cargo blanket. (a) The active cargo blanket can be draped over arbitrary objects at atmospheric pressure. (a) It can be manually shaped into various configurations to match target forms as the vacuum pressure is introduced to the airtight bladder. (c) It can be fully rigidized as the vacuum pressure reaches a maximum.

The architecture of moldable active cargo blanket is based on the equilateral triangle tiles of which tile array layers are shifted relative to each other and containing an intermediate TPU layer representing the bladder-attached non-connected tiles subclass as shown in Figure 145 on the left. To be able to tailor the balance among the technology sub-capability performances, the shape of each individual tile composing a tile layer needs to be parametrized. This allows developing an understanding of the relationship between the tile geometry design variables and resulting performance of each capability.

The tile geometry design variables characterizing the overall form of the selected tile array layer are: 1) the *tile size* described by one of the edge lengths, 2) the *gap* described by the distance between adjacent tiles, and 3) the *tile height* described by the extent of the extrusion. These design variables correspond to the characteristics of a specific subcellular feature sub-category, internal constraints listed under the constraint category (see section 2.1.2. in Chapter 2). The top and bottom tile array layers are shifted relative to each other to ensure that no folding pattern emerges when the tile array layers are overlapped (Figure 145, right). The resulting overall moldability performance of the active cargo blanket is directly affected by the tile geometry design variables. For instance, employing larger and thicker tiles with minimized gap between the adjacent tiles has an adverse effect on the way the resulting draping behavior, but it simultaneously improves its rigidizability performance. This introduces a tradeoff among the technology sub-capability performances. A comprehensive understanding of the relationship between tile geometry design variables and the performance of each technology sub-capability is crucial for the systematic design of the active cargo blanket with a tailored moldability performance.

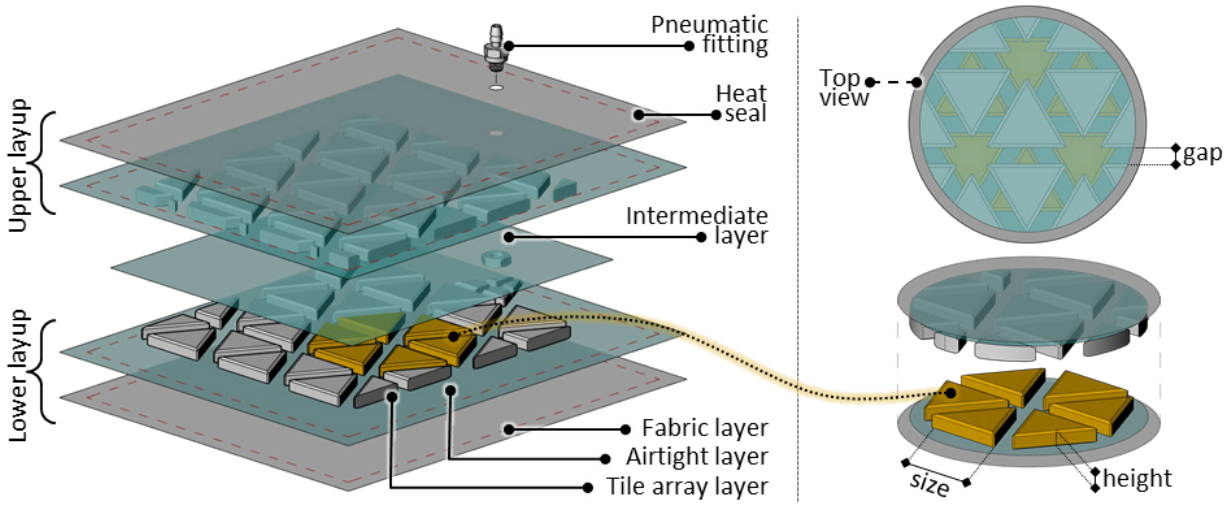

Figure 145. The architecture of a moldable active cargo blanket. (a) A moldable active cargo blanket comprises two layups, a soft and flexible intermediate layer between these layups, and a pneumatic fitting. Each layup contains a nylon fabric layer, TPU layer, and a tile array layer, which is made up of bladder-attached non-connected tiles. (b) The top and bottom tile array layers are shifted relative to each other to ensure that no folding pattern emerges when the tile array layers are overlapped.

The moldable active cargo blanket operates between same set of three states as the generic internally tiled pneumatic textiles do (Figure 146). In the draping state, under atmospheric pressure, the active cargo blanket behaves like a piece of fabric, which can be thrown on and draped over a set of randomly arranged objects. In the shaping state, it can be manually conformed to a target form by using external motive forces while the vacuum is being introduced, helping it to keep its conformed shape. In the rigidizing state, the active cargo blanket reaches its peak stiffness level due to the vacuum pressure applied, holding its shape against external loads.

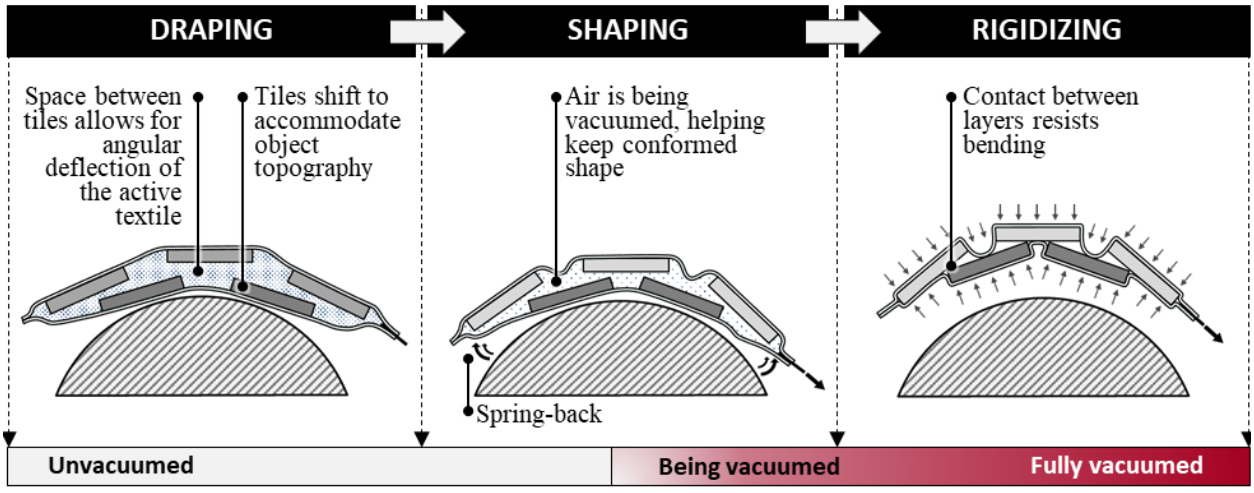

Figure 146. The operation states of an active cargo blanket. (a) An active cargo blanket operates in draping state in the absence of vacuum, where it deforms in a fabric-like manner due to gravity. The space between adjacent tiles

enables relative shifting and angular deflection, aiding the passive accommodation of a target form. (b) The shaping operation state is initialized by actively conforming (i.e., using hands) an active cargo blanket into a shape of a target configuration, which requires a gradual vacuum pressure as a next step to generate a permanent and distributed force for maintaining the target shape. (c) Rigidizing an active cargo blanket is accomplished by vacuuming almost all the air out from the bladder, which jams the opposing tiles against each other, resulting with enhancing its overall stiffness.

To design the moldability performance of the active cargo blanket, the overall performance needs to be decomposed into a set of interrelated performances, which then can be quantified as a function of the tile geometry design variables. A quantified relationship between the tile geometry design variables and the resulting interrelated performances will enable the systematic design of an active cargo blanket that can provide a tailored moldability performance as demonstrated in (Figure 147).

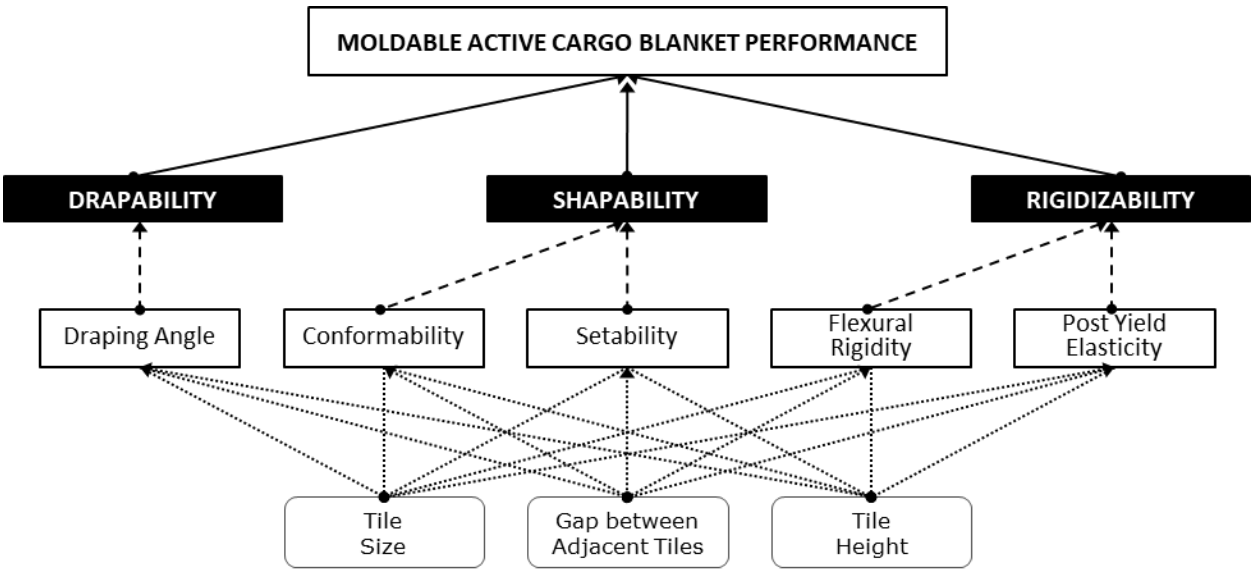

Figure 147. Quantification of a moldable active cargo blanket performance. Moldability is an emergent technology capability comprising drapability, shapability, and rigidizability technology capabilities. A set of objectively quantifiable engineering performance metrics is identified for each one these technology capabilities, where the drapability performance is characterized by the draping angle metric, the shapability performance is characterized by the conformability and setability metrics, and the rigidizability performance is characterized by the flexural rigidity and post yield elasticity metrics. The tile geometry design variables (the tile size, gap between adjacent tiles, and tile height) simultaneously affect the resulting metric scores and technology capability performances.

4.5.1. Tile Geometry Design Variable Selection

The shape of the individual tiles that form the moldable active cargo blanket's tile array layers affects the drapability, shapability, and rigidizability performances simultaneously. Exploring the relation between the tile shapes and the resulting active cargo blanket's performance requires conducting a controlled experimental parametric study. Representative examples employing bladder-attached non-connected equilateral triangle tiles of which tile array layers are shifted relative to each other and containing an intermediate TPU layer are generated and their technology

capability performances are experimentally measured. A set of multiple linear regression models are used to understand the effects of changing the tile geometry design variables on the resulting engineering performance metric scores. A model-based approach facilitating the design of active cargo blanket prototypes with tailored technology capabilities using an algebraic tailoring method is developed and experimentally validated.

4.5.1.1. Parametric Study Representative Sample Set

For the moldable active cargo blanket architecture made of equilateral triangle tiles, the design variables that describe an individual tile are the tile size (s), gap between adjacent tiles (g), and tile height (h) (Figure 148(a)). To understand how different tile geometry design variable values influence the active cargo blanket's performance, a representative set of prototypes was systematically designed and fabricated based on: the tile size variable with two levels (20mm and 30mm), the tile gap variable with three levels (1.5mm, 2.25mm, and 3mm), and the tile height variable with four levels (1mm, 2mm, 3mm, and 4mm). A full factorial design of experiments using the three design variables with different levels requires fabricating and testing twenty-four (2x3x4) active cargo blanket prototypes, which was not pragmatic. Instead, a nearly balanced half fraction of the full factorial design was generated using the Federov exchange algorithm implemented in the *AlgDesign* library in the R statistical computing environment. This provides a design of experiments with minimal correlation between its factors in cases where there is an imbalance between variable levels. Figure 148(b) displays the tile geometry design variable values for each prototype that was fabricated and tested (indicated in green) for the study in relation to the full set of possible prototypes. The values of design variables of the selected prototypes are also tabulated in Table 1.

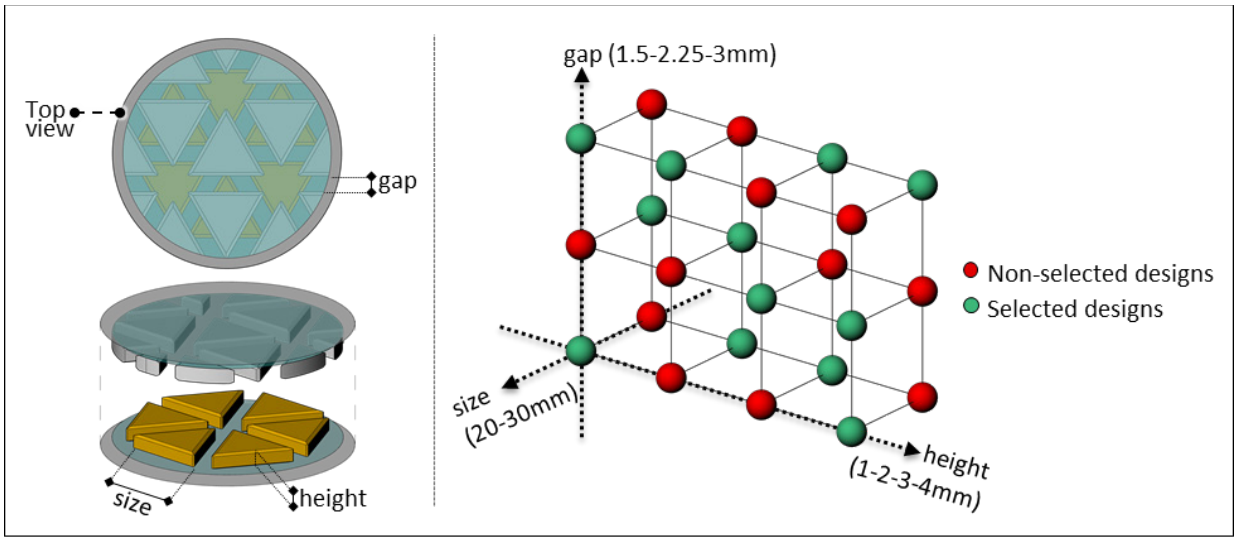

Figure 148. Tile geometry design variables parametric study. (a) Tile size, tile height, and the gap between adjacent tiles are the tile geometry design variables used to design the parametric study exploring the relationship between these variables and the resulting technology capability performances. (b) A nearly balanced half fraction of the full factorial design was generated using the Federov exchange algorithm implemented in the AlgDesign library in the R statistical computing environment.

Table 9. List of moldable active cargo blanket prototypes used in tile geometry design variable study

Cargo blanket prototype #	tile size (*s*)	gap between tiles (*g*)	tile height (*h*)
405	30 mm	1.5 mm	2 mm
406	30 mm	1.5 mm	3 mm
407	20 mm	1.5 mm	1 mm
408	20 mm	1.5 mm	4 mm
409	20 mm	3 mm	2 mm
412	20 mm	3 mm	1 mm
413	20 mm	2.25 mm	3 mm
414	30 mm	2.25 mm	2 mm
415	30 mm	2.25 mm	1 mm
416	20 mm	2.25 mm	4 mm
417	30 mm	3 mm	3 mm
418	30 mm	3 mm	4 mm

4.5.1.2. Model of Relationship Between Tile Geometry Design Variables and Engineering Performance Metrics

Each of the prototypes in the design of experiments was experimentally tested for all five performance metrics as described in Section 4. A set of five multiple linear regression analyses was used to develop a predictive model of the effects of the tile geometry design variables on each of the performance metrics. This modeling approach is illustrated in Figure 149.

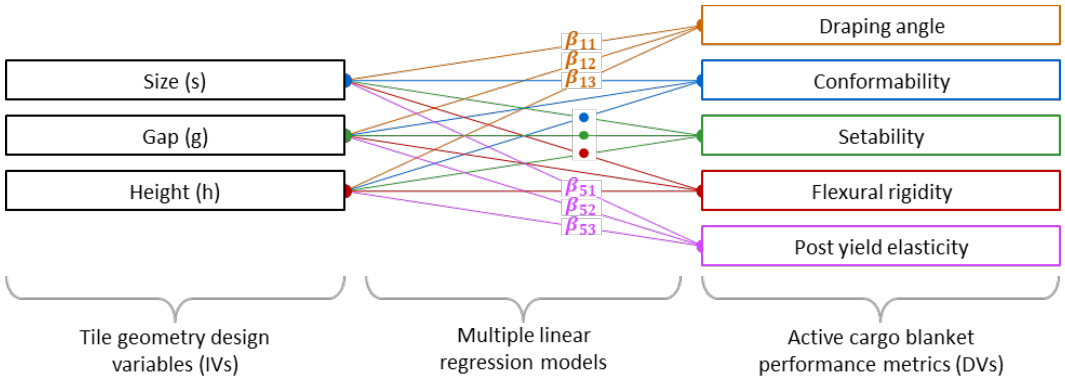

Figure 149. Modelling the relationship between tile geometry design variables and engineering performance metrics. A set of multiple linear regression models are used to develop a predictive model of the effects of the tile size, gap, and height on the resulting performance metric scores.

Table 10 summarizes the results of the regression models, where each performance metric is impacted differently and with different statistical significance by each of the tile geometry design variables. In this model, each performance metric m_i is a linear function of the three geometry design variables s, g, and h, with coefficient β_{ij} corresponding to the contribution of the j^{th} design variable on the i^{th} performance metric plus an intercept coefficient β_{i0}:

$$m_i = \beta_{i0} + \beta_{i1}s + \beta_{i2}g + \beta_{i3}h. \quad (6)$$

Table 10. Summary of the set of multiple linear regressions predicting each performance metric as a function of tile geometry design variables

	Draping angle	**Conformability**	**Setability**	**Flexural Rigidity**	**Post Yield Elasticity**
	β_{1j}(SE)	β_{2j}(SE)	β_{3j}(SE)	β_{4j}(SE)	β_{5j}(SE)
Size	-.0032 (.0028)	-.015*** (.0014)	-.0062 (.0050)	.012* (.0044)	-.0014 (.0031)
Gap	.0509# (.0225)	-.01187 (.0116)	-.0610 (.0410)	-.09245* (.0362)	.0418 (.0252)
Height	-.0290* (.0123)	-.01187# (.0064)	.0435# (.0224)	.10554*** (.0198)	.0003 (.0138)
Intercept	.1905# (.0919)	1.2152*** (.0475)	.6894** (.1673)	-.10179 (.1478)	.7471*** (.1029)
***R*-squared**	.6002	.9358	.4841	.8408	.2703
$F_{3,8}$	4.004	38.85	2.502	14.08	0.988
p-value	.0518	4.08e-05	.1333	.0015	.4458

Note. β_{ij} is the unstandardized regression coefficient, showing the effect of one unit increase or decrease in each predictor variable on each engineering performance metric. (SE) is the standard error of a coefficient, which is the standard deviation of that sampling distribution. R-squared represents the proportion of the variance for each engineering performance metric explained by the predictor variables. The statistical significance level of the predictors is shown by ***p < .001, **p <.01, *p < .05, #p < .1.

Table 10 lists the statistical significance levels for each linear regression model that predicts the corresponding performance metric as a function of tile geometry design variables, where a $p<0.05$ is considered statistically significant. Accordingly, the three design variables acting as predictors in the regression models explained 94% of the variance in conformability scores among the measured prototypes ($F(3,8)=38.9$, $p<0.001$), and 84% of the variance in flexural rigidity

scores ($F(3,8)= 14.1$, $p<0.05$). In addition to computing the coefficients β_{ij} themselves, the regression produces a p-value indicating the statistical significance level of each coefficient ($p<0.05$ is significant). It was found that the tile size (β_{21}=-0.015, $p<0.001$) significantly predicted the active cargo blanket prototypes' conformability performance metric scores, while the tile size (β_{41}=0.012, $p<0.05$) and tile height (β_{43}=0.106, $p<0.01$) were both significant predictors for the flexural rigidity performance metric scores. 60% of the variance in the draping angle performance metric scores was explained by the predictors ($F(3,8)=4.00$, $p=0.052$) only slightly above at the significance level cut off. No significant relation between the predictors and the setability or post yield elasticity performance metric scores was found. Assuming that such relationships do exist, this can be possibly improved either by expanding the set of experiments to reduce the unexplained variance in the setability and post yield elasticity performance metric scores, or to change the structure of the linear model to include higher order terms. Although the linear regression models predicting the setability and post yield elasticity performance metrics are not considered statistically significant, these portions of the set of regression models remain incorporated to demonstrate the design approach. The measured performance metric scores of the active cargo blanket prototypes that were used to construct the predictive model itself were compared to the predictions provided by the set of regression models (*i.e.* regression model residuals). The discrepancies between the predicted and measured scores for each performance metric are calculated as a fraction of the corresponding measured scores to determine the model error percentage. Overall, the model error was 18% on average for these twelve prototypes.

To provide further validation of the predictive model, two arbitrarily designed additional active cargo blanket prototypes were fabricated and tested which were not in the original design of experiments. The tile geometry design variable values for these prototypes are listed in Table 11.

Table 11. List of moldable active cargo blanket prototypes used for validating the predictive model performance

Cargo blanket prototype #	tile size (s)	gap between tiles (g)	tile height (h)
411	30 mm	3 mm	2 mm
402(TPU)	20 mm	1.5 mm	2 mm

After measuring and extracting the relevant engineering performance metric scores for the additional set of active cargo blanket prototypes, the predicted and measured performance metric scores were compared to each other, shown in Figure 150. While the gray bars represent the predicted scores, blue bars show the measured scores for each active cargo blanket prototype. 60%

of the predicted performance metric scores are within the range of the error bars, which indicate the estimated 95% confidence intervals from the model.

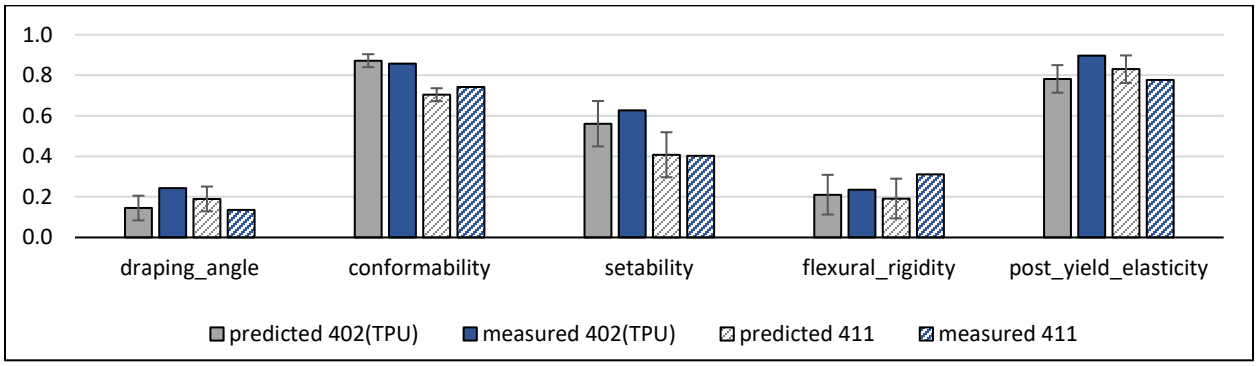

Figure 150. The discrepancy between predicted and measured performance metric scores for the additional prototypes (#402(TPU) and #411). 60% of the predicted performance metric scores are within the range of the error bars, which indicate the estimated 95% confidence intervals from the model. The prediction error is 17% on average across all the performance metric scores for these two additional prototypes.

The model predicted the performance metric scores for these additional active cargo blanket prototypes with 17% error on average. This aligns with the earlier stated average error rate (18%), where the model predicting the active cargo blanket prototypes that were used to construct the predictive model itself. Table 12 breaks down this 17% error as average error per prototype and average error per performance metric. Accordingly, the draping angle and flexural rigidity were the least predictable performance metrics with 40% and 24% error rates on average. The conformability, setability, and post yield elasticity were the most predictable with 3%, 6%, and 10% error rates, respectively.

Table 12. Deviation of the predicted scores from measured scores as a fraction of the measured scores.

	Draping angle Error (%)	Conformability Error (%)	Setability Error (%)	Flexural rigidity Error (%)	Post yield elasticity Error (%)	Avg error per prototype
402 (TPU)	0.40	0.05	0.01	0.38	0.07	0.18
411	0.40	0.02	0.10	0.10	0.13	0.15
Avg error per perf. metric	0.40	0.03	0.06	0.24	0.10	**0.17**

4.5.1.3. Model-Based Performance Tailoring

Predictive models are useful if the goal is to forecast the resulting moldability performance of an active cargo blanket with a certain tile geometry. However, often in a design process, the goal is not just to predict the overall performance as an outcome, but to tailor the design, balancing the relative importance of each performance metric. For example, while one application may require a moldable active cargo blanket with a greater draping capability, another application may demand

better rigidizability performance (e.g., an off-road vehicle would require a higher priority on the rigidizability performance, whereas prioritizing the drapability and/or shapability performances would be more appropriate for a fuel-efficient commuter vehicle which is often used for transporting grocery bag). Identifying the values for the tile geometry design variables by trial and error to provide such tailored performance outcomes requires many iterations, impeding the design process. To address this drawback, in Figure 151, a modelling approach for designing an active cargo blanket with a tailored moldability performance is developed. An intended set of relative weights (w_n) is assigned to the engineering performance metrics. An algebraic tailoring method enables identifying the tile geometry design variables that provides the tailored moldability performance according to the weights as an outcome.

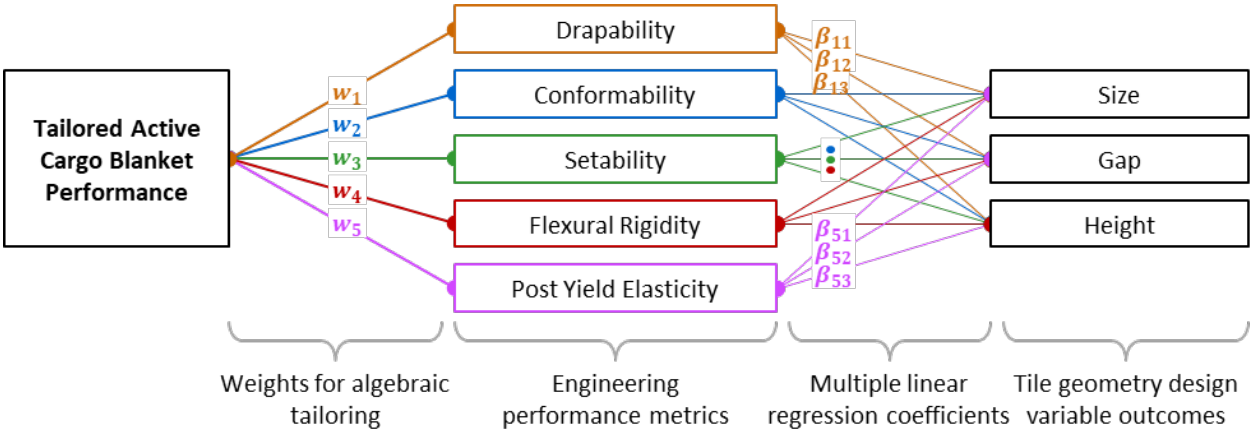

Figure 151. Algebraic tailoring method for designing active cargo blankets with tailored moldability performance. The algebraic tailoring method uses the maximization of the weighted sum of the engineering performance metrics to enable the identification of the tile geometry design variable values that provide the intended moldability performance as an outcome.

The algebraic tailoring method relies on the maximization of the weighted sum of the engineering performance metrics, with bounds placed on each of the tile geometry design variables at the limits used in the design of experiments to avoid predictive extrapolation. The weighted sum of metrics (P_T) is

$$P_T = \underbrace{[W_1 \quad \cdots \quad W_5]\begin{bmatrix}\beta_{11} & \cdots & \beta_{13}\\ \vdots & \ddots & \vdots\\ \beta_{51} & \cdots & \beta_{53}\end{bmatrix}}_{B_W}\begin{bmatrix}s\\ g\\ h\end{bmatrix} + [W_1 \quad \cdots \quad W_5]\begin{bmatrix}\beta_{10}\\ \vdots\\ \beta_{50}\end{bmatrix}, \tag{7}$$

where W_i is a relative weight for each performance metric, β_{ij} is the unstandardized coefficient defining the relation between the i^{th} tile geometry design variable and the j^{th} performance metric, s is the tile size, g is the gap between adjacent tiles, and h is the tile height. The signs of each

element of the resulting 1x3 matrix B_W, which is a product of the 1x5 relative weight matrix W and the 5x3 β coefficient matrix, provide the information required to make design decisions regarding tile geometry. Given independent bounds on each tile geometry design variable, optimization over such a linear model drives the variables towards the corners of the design space over which the predictive model is constructed. Thus, by examining the signs of the elements of B_W, the optimal tailored design can be determined.

For example, the tile geometry design variables that would provide a balanced performance across all the engineering performance metrics can be identified by using equally distributed weights as follows,

$$= \underbrace{[0.2 \quad 0.2 \quad 0.2 \quad 0.2 \quad 0.2]\begin{bmatrix} -0.0032 & \cdots & -0.0290 \\ \vdots & \ddots & \vdots \\ -0.0014 & \cdots & 0.0003 \end{bmatrix}}_{B_W}\begin{bmatrix} s \\ g \\ h \end{bmatrix} + [0.2 \quad 0.2 \quad 0.2 \quad 0.2 \quad 0.2]\begin{bmatrix} 0.1905 \\ \vdots \\ 0.7471 \end{bmatrix} \tag{8}$$

$$= \underbrace{[-0.0028 \quad -0.0145 \quad +0.0217]}_{B_W}\begin{bmatrix} s \\ g \\ h \end{bmatrix} + [0.548082]. \tag{9}$$

Depending on the signs (-, -, +) of each element in the resulting B_W matrix (1x3) shown in Equation 9, size, gap, and height values for the tile geometry design variables that maximize the balanced active cargo blanket performance in the intended direction are identified. The first and second elements in the B_W matrix corresponding to the tile size and gap between adjacent tiles are negative. Thus, the lower bounds used in the design of experiment for these geometry variables are selected; 20mm for tile size and 1.5mm for the gap between adjacent tiles. The last element in the B_W matrix corresponding to the tile height is positive, resulting in the selection of the upper bound, 4mm, which was used in the design of experiments. To demonstrate this ability further, two additional active cargo blanket designs are exemplified in Table 13 with differently weighted performance metrics: a blanket-like active cargo blanket heavily favoring the draping angle and a rigid active cargo blanket weighting flexural rigidity the most.

Table 13. Assigning weights to performance metrics for the intended design outcomes

	Draping angle	Conformability	Setability	Flexural rigidity	Post yield elasticity
Blanket-like active cargo blanket	0.8	0.2	0	0	0
Rigid active cargo blanket	0	0	0.1	0.8	0.1
Balanced active cargo blanket	0.2	0.2	0.2	0.2	0.2

Distinctive weighting of the performance metrics generates different B_W matrices (1x3) and sets of tile geometry design variable values for each active cargo blanket design as tabulated in

Table 14. The resulting tile geometry design variable values are highlighted in relation with the design space (Figure 152). The prototypes for the blanket-like and balanced active cargo blankets already exist as a part of the original half-fraction design of experiments. Thus, an additional active cargo blanket prototype only for the rigid active cargo blanket was fabricated and tested for the validation of the algebraic design tailoring approach. In all three cases, the algebraic tailoring approach drives the design into one of the corners of the design space.

Table 14. Elements of Bw matrices and resulting tile geometry design variable values for each active cargo blanket design examples

	B_{W1}	B_{W2}	B_{W3}	s (mm)	g (mm)	h (mm)
Blanket-like active cargo blanket	-0.0056	+0.0383	-0.0256	20	3	1
Rigid active cargo blanket	+0.0088	-0.0759	+0.0888	30	1.5	4
Balanced active cargo blanket	-0.0028	-0.0145	+0.0217	20	1.5	4

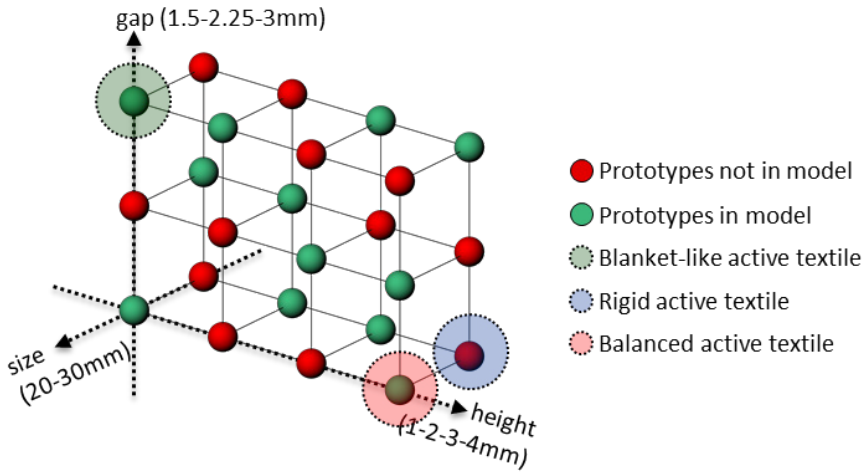

Figure 152. Tile geometry design variable values for the tailored active cargo blanket prototype examples. The algebraic tailoring method is used to generate blanket-like, rigid, and balanced active cargo blanket prototypes with differently weighted performance metrics. The resulting tile geometry design variable values for these additional prototypes are highlighted in relation with the already existing design space.

In Figure 153, the measured scores are compared to the predicted performance metric scores of the blanket-like, rigid, and balanced active cargo blanket prototypes. The predicted values are shown with gray bars, where the measured scores are illustrated with the green, blue, and red colored bars, respectively. The dotted rectangles behind each pair of bars indicate the range of performance metric scores used to construct the predictive model enabling the visualization of the tailored performance relative to the entire experimental set, providing a ground for the validation of the algebraic design tailoring approach.

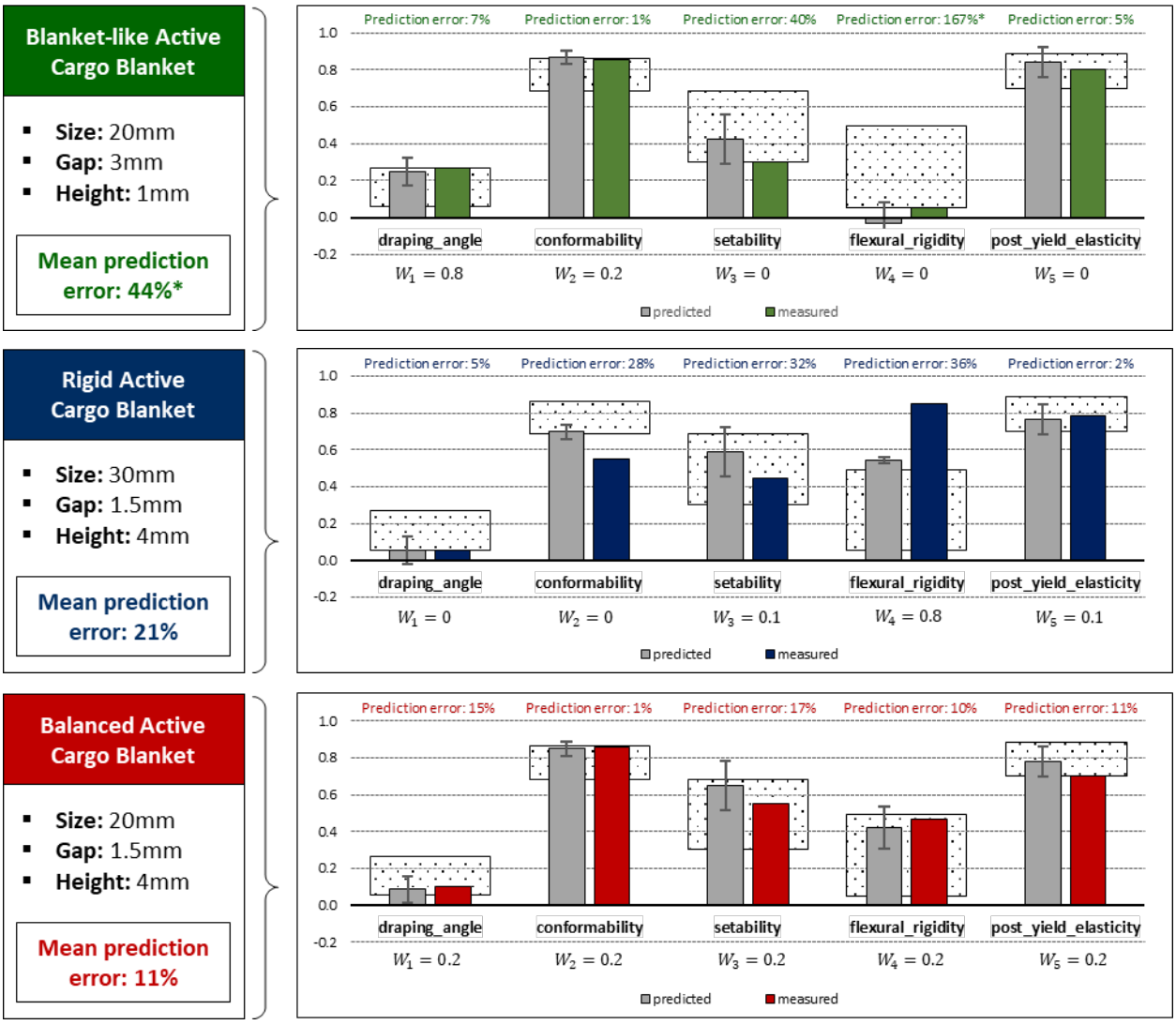

Figure 153. The discrepancy between predicted and measured performance metric scores for the active cargo blanket prototypes with tailored performances. The predicted performance metric scores are shown with gray bars, where the measured scores are illustrated with the green, blue, and red colored bars for the blanket-like, rigid, and balanced active cargo blanket prototypes respectively. The dotted rectangles behind each pair of bars indicate the range of performance metric scores used to construct the predictive model. The mean prediction error for the blanket-like active cargo blanket prototypes is 44% due to the large prediction error (167%) for the flexural rigidity performance metric score, which is the result of the fact that predicted and measured scores for this metric were both small numbers, inflating the error rate. The mean prediction errors for rigid and balanced active cargo blanket prototypes are 21% and 11% respectively.

For the design of blanket-like active cargo blanket prototype, the draping angle performance metric was given the highest weight (w_1=0.8) among all the performance metrics. The predicted and the measured scores for the draping angle illustrate that the blanket-like active cargo blanket prototype provided the best-intended performance among the sample population. In addition to the having the highest score for the draping angle, the conformability score, which was given the second highest weight (w_2=0.2) is also maximized in relation to the sample population as

predicted. The rest of the performance metric scores, because their weightings were zero, are not minimized, but rather lie arbitrarily within the sample population range. The large prediction error (167%) for the flexural rigidity performance metric score is the result of the fact that the predicted (-0.034) and the measured (0.051) scores are both small numbers which inflate the error rate since the predicted score is used as a denominator. The average prediction error rate for predicting the performance metric scores of the blanket-like active cargo blanket is 13.5% when the flexural rigidity performance metric is not taken into account.

For the design of the rigid active cargo blanket prototype, the flexural rigidity performance metric was assigned with the highest weight (w_4=0.8) and resulted with the measured score that far surpassed the sample population's range of flexural rigidity metric. The lower weighted metrics (setability and post yield elasticity, $W_3 = W_5 = 0.1$) resulted in values in the middle of the range of the sample population, since the low weightings drive the design partially to improve these metrics as much as possible without sacrificing the flexural rigidity. As predicted, the draping angle and conformability performance metrics, which were given the lowest weights ($w_1 = w_2 = 0$), resulted in scores that are lower than the sample population's corresponding metric ranges. The average prediction error rate for predicting the performance metric scores of the rigid active cargo blanket prototype is 21%.

For the design of the balanced active cargo blanket prototype, all the performance metrics were equally weighted, where all the resulting predicted and measures metric scores are within the predictive model's range as intended. Tailoring each one of the five performance metrics independently by only using three tile geometry design variables is not achievable. However, sequentially identifying an active cargo blanket design with a tile architecture subclass, where the quantity and strength of the positive correlations among its performance metric pairs are relatively larger and stronger compared to alternative active cargo blanket designs, enabled tailoring the five performance metrics simultaneously by using three design variables, enabling a balance to be stricken between all five metrics [x: reference to the 1st paper]. The average prediction error rate for predicting the performance metric scores of the balanced active cargo blanket prototype is 11%.

To further illustrate the design success in terms of tailoring the technology capabilities of active cargo blankets, the resulting performance metric scores of the blanket-like, rigid, and balanced prototypes are compared to the average scores of the prototypes that were used in the parametric study for the tile geometry design variable selection (in Section 5). As shown in Figure 154, the

blanket-like cargo blanket prototype is 76% more drapable relative to the average performance represented by the dashed black line. Likewise, the rigid cargo blanket prototype outperforms the average flexural rigidity performance by 234%. The performance metric scores of the balanced cargo blanket prototype are closer to the average scores, which aligned with the design intent of producing balanced performance among all the metrics.

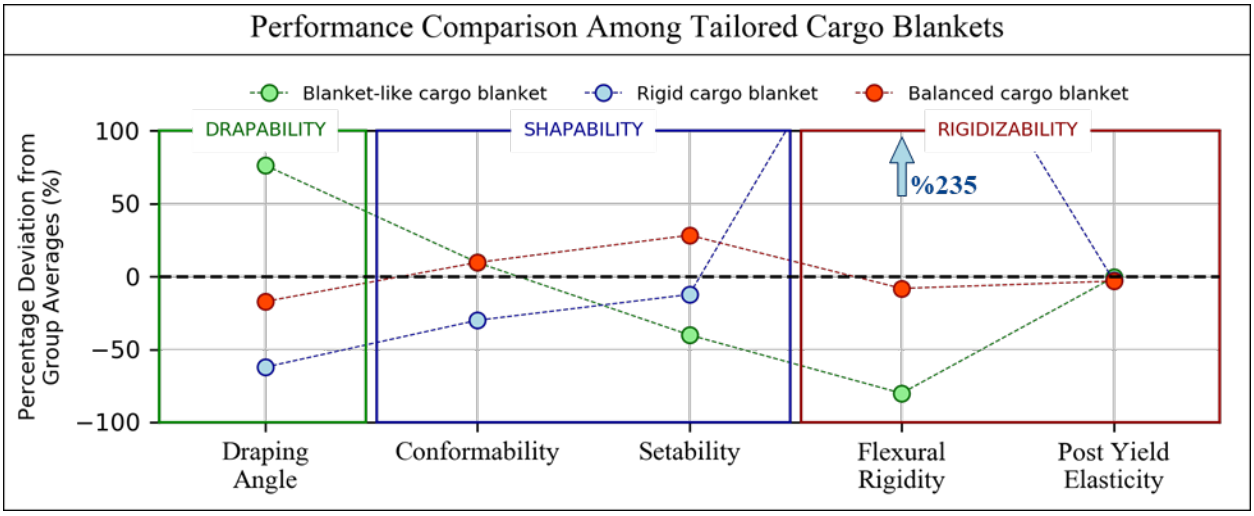

Figure 154. Performance comparison between the tailored active cargo blanket prototypes and the prototypes (n=12) used to generate the predictive model. The performance metric scores of the blanket-like, rigid, and balanced active cargo blanket prototypes are compared to the average scores of the prototypes that were used to generate the predictive model, which is shown with the black dashed line (0%). The blanket-like active cargo blanket prototype performs the best in draping angle performance metric (76% higher score than the average) and the rigid active cargo blanket prototype performs the best in flexural rigidity performance metric (235% higher score than the average). The balanced active cargo blanket prototype provides performance metric scores that are closer to the average matching the design intent.

The algebraic design tailoring approach enables the design of the active cargo blankets with tailored moldability performances, reducing the amount of the design iteration by providing the optimized values for the tile geometry design variables. By using these values, the prototypes were fabricated, achieving the intended design goals.

4.6. Conclusion

In this chapter, a series of architectural and parametric design studies is presented, focusing on designing a structurally adaptable multi-mode product concept, *moldable active cargo blanket*, using internally tiled pneumatic textiles. These studies provide an understanding of the hierarchical architectural structure, functionality and operation, and the interdependent relationship between architectural and parametric design, as well as the performance of drapability, shapability, and rigidizability technology sub-capabilities.

Internally tiled pneumatic textiles are built on the tile-based rigidization technique, which enables the technology capability of moldability into complex geometries with a thin, flat, and lightweight structure, addressing the drawbacks of pneumatic structures built on granular, fibrous, and layer jamming approaches. Composed of layers of rigid tiles arranged in regular patterns within an airtight bladder, internally tiled pneumatic textiles offer adjustable stiffness depending on the vacuum pressure applied. The architectural class/subclass of a pneumatic textile along with the specific architectural feature variations and tile geometry design variable values have a great influence on the pneumatic textile's moldability performance.

Three main tile architectural classes, bladder-attached tiles, internal sheet-attached tiles, and mutually interlocking tiles are based on the formation of the tile array patterns encapsulated in airtight bladder systems. Examining the cell level operation states and emergent cell functions as described in Chapter 2 coupled with the hierarchical functional architectural decomposition approach described in Chapter 3, which relates those cell-level operation states to technology (sub)capabilities, highlights the emergence of the operation states, draping, shaping, and rigidizing. Through these operation states, pneumatic textiles can change their structural configurations and functionalities based on the interaction that takes place between the layers of rigid tile arrays enable the emergence of three key technology sub-capabilities: drapability, shapability, and rigidizability, which together, create the moldability technology capability. The overall moldability performance of an internally tiled pneumatic textile is broken down as a combination of the performances of its constituent technology sub-capabilities.

A set of engineering performance metrics is defined by making use of the hierarchical functional architectural decomposition approach, one for each technology sub-capability performance to quantitatively capture all aspects of the overall pneumatic textile performance. This exploits the relationship between technical performance from a technological point of view to the context-specific product use performance from a user-interaction point of view to enable direct empirical measurements that have implications on the product use. Experimental procedures to collect data enable quantification of the sets of engineering performance metrics constituting the performances of technology sub-capabilities, where the draping angle quantifies drapability, conformability and setability quantify shapability, and flexural rigidity and post yield elasticity quantify rigidizability performance. Since the units of the underlying measurements differ from one performance metric to another, the direct comparison among performance metrics is enabled

by transforming the raw data into a dimensionless natural functional scale. In this scale, the scores range from the theoretical worst case (zero), where no functionality towards the performance metric is observed, to the theoretical best case (one), where the ideal functionality towards the performance metric is observed.

A systematic approach is adopted for the exploration of the hierarchical architectural design space of internally tiled pneumatic textiles. This approach aids the understanding of the design space by performing comparative analyses of the effects on the performance metric scores of tile architectural classes first, design couplings among performance metric pairs in the context of tile architectural subclasses second, and architectural feature variations third. The assessment of the relative strengths and weaknesses of each tile architectural class, bladder-attached, internal sheet-attached, and mutually interlocking, on moldability performance is achieved by analyzing the plots of normalized performance metric scores of the prototypes, aided by the natural functional scale rendering all the metrics directly comparable. While none of the three tile architectural classes studied clearly outperforms the others in all metrics simultaneously, each one presents tradeoffs which can be advantageously leveraged depending on the design context. For example, the internally sheet-attached tile class exhibits relatively high rigidizability performance (239% above the group average), whereas the bladder-attached tile class exhibits relatively balanced performance across all metrics.

The bladder-attached tile class, which contains two subclasses, connected and non-connected tiles, with three tile geometry designs in each, is used to demonstrate a correlation-based tile architectural subclass comparison technique. This technique enables a complete view of the strengths of the pairwise design tradeoffs and synergies among a particular tile architectural class across all the metrics. Pairwise correlation matrix analyses show that the bladder-attached non-connected tiles subclass provided the minimized quantity and strength of negative dependencies between its performance metric pairs, reducing design tradeoffs.

In the bladder-attached non-connected subclass, which contains three pneumatic textile designs with varying tile geometries, the pneumatic textile that is made of equilateral triangles was used to study the effects of architectural feature variations due to its simple tile geometry, which provides effective packaging, ease of manufacturability, and affordance for more architectural feature variations. This study uses a direct comparison approach to measure the effects of alternating the way the tile array layers overlap with each other and inserting a layer of thin and

soft elastomeric sheet between the tile array layers on the performance of this particular pneumatic textile in the bladder-attached non-connected tile subclass. Shifting the opposing tile array layers relative to each other provides a positive impact on the flexural rigidity metric score (43% relative increase), while negatively affecting the draping angle and setability metric scores (40% and 20% relative decrease, respectively). Introducing a layer of thin and soft elastomeric sheet overcomes not only these negative effects on draping angle and setability metric scores (81% and 27% relative increase, respectively), but also further improves the flexural rigidity metric score (17% relative increase) without causing any decline in the performance of the remaining metrics.

For the application of internally tiled pneumatic textiles in the context of designing structurally adaptable multi-mode products, a design case study focusing on the design of moldable active cargo blanket, which targets securing and transporting loose cargo of vastly varying shape and size in a moving vehicle, is demonstrated. The architecture of the moldable active cargo blanket is based on the findings of the hierarchical architectural design space studies, resulting in downselecting the equilateral triangle tiles of which tile array layers are shifted relative to each other and containing an intermediate TPU layer representing the bladder-attached non-connected tiles subclass. Three tile design geometry variables are identified for this downselected architecture: tile size, the gap between adjacent tiles, and the tile height, enabling conducting a tile geometry design variable value selection study. This study empirically constructs a predictive model of the effects of the values of tile size, the gap between adjacent tiles, and the tile height on the performance metric scores of the active cargo blanket prototypes. Using an optimally balanced partial factorial experimental design with twelve active cargo blanket prototypes with variations in each of these variables, the performance metric scores were measured. A set of multiple linear regression models captures the relationship between the tile geometry design variable values and the engineering performance metric scores, enabling the prediction of the performance metric scores for given values of the tile size, gap between adjacent tiles, and tile height. The validation of the predictive model was assessed with 17% error on average by predicting the performance metric scores of two arbitrarily designed additional prototypes.

This model forms the basis of an algebraic design tailoring approach, enabling the design of active cargo blankets with tailored moldability performances by facilitating the balance among engineering performance metrics. This approach was used to identify the optimized values for the tile geometry design variables for the design of prototypes providing tailored performances based

on a set of relative weights assigned to their engineering performance metrics. The resulting ability to tailor the technology sub-capabilities of an active cargo blanket prototype was demonstrated by designing and fabricating three additional prototypes: blanket-like, rigid, and balanced cargo blankets, with distinctly tailored technology sub-capability performances. The resulting performance metric scores of these tailored prototypes were compared to the average performance metric scores of the prototypes that were used in the parametric study for the tile geometry design variable selection, validating that the algebraic design tailoring approach successfully aids the meeting of intended design goals. This enables the adaptation of the technology to specific vehicle segments, styles, and/or customer needs and expectations.

The experimental systematic architectural analysis approach presented in this chapter relates the multiple operating states of the structurally adaptable internally tiled pneumatic textile technology to relevant performance metrics which drive the design. The experimental studies corresponding to different layers of architectural hierarchy drive the exploration of the broad design space by first addressing the most significant categorical design decisions and eventually focusing down to more specific variations of the features to meet potential performance goals. This allows a much larger portion of design space to be addressed efficiently at a higher level of abstraction before approaching the detailed design level including the identification of the values for the tile geometry design variables. This is especially important for the development of new structurally adaptable multi-mode product concepts such as moldable active cargo blanket employing internally tiled pneumatic textiles which present a huge variety of architectural forms and multiple customer-facing interaction modes. While the empirical construction of a predictive model and the algebraic design tailoring approach are demonstrated in the context of moldable active cargo blanket application design, the general methodology apply well to any other design case in which there is an inherent trade-off between the design variables and resulting quantifiable performance metrics.

Chapter 5. Conclusions

The goal of this research was to develop the design science foundation enabling a systematic early-stage design space exploration for emerging constrained layer pneumatic system technologies that provides a basis for the design of structurally adaptable multi-mode products providing multiple functionalities affording physical interaction with users. Three research objectives were accomplished to realize this goal:

- **Technological Foundation for Emerging Constrained Layer Pneumatic Systems.** Developed a systematic basis for capturing the breadth of structurally adaptable basic architectural and corresponding functional components that provide elemental building blocks for exploring, designing, and implementing multi-mode product concepts enabling users to access a variety of technology capabilities across different operation states and interaction modes.
- **Design Supported by Hierarchical Functional Architectural Decomposition.** Established a formal hierarchical analytical design description that provides a direct view into the hierarchical structure of a system's interrelated form and function, which supports goal-oriented re-synthesis of user-interacting structurally adaptable multi-mode products employing constrained layer pneumatic systems at a conceptual level.
- **Architectural and Parametric Design for Multi-modal Performance.** Built an understanding of how to explore and relate conceptual architectural variations and parametric design variations within a particular category of constrained layer pneumatic systems, internally tiled pneumatic textiles, to the quantifiable performance of a structurally adaptable multi-mode product, enabling negotiation between performance metrics to obtain intended design outcomes.

It was necessary to address all these objectives to systematically describe and explore constrained layer pneumatic systems and to comprehensively relate the architectural, functional, operational, and performance related systems aspects to one another. This enables the systematic

design of numerous user-interacting structurally adaptable multi-mode products that are based on the constrained layer pneumatic system technological approach, providing different technology capabilities to users in different operational states.

5.1. Research Overview and Contributions

The application of constrained layer pneumatic systems presents significant potential for the design of multi-mode products that can adapt to users' needs by providing multiple functionalities in different modes. In Chapter 1, a review of the current state-of-the-art revealed that the lack of an established foundation for the systematic development of such products poses a significant challenge in achieving a balanced design across all system aspects, including architecture, functionality, operation, and performance. This makes it difficult to implement a holistic early-stage design approach that enables such balance. To overcome this challenge and make this new technological design approach operationally useful in the early-stage design process, a systematic description of the system aspect components was needed, facilitating a better understanding of the relationship among these components, leading to a more insightful exploration of this emerging design space.

To meet the goal of this research and establish the design science base for designing structurally adaptable multi-mode products using constrained layer pneumatic systems, the research objectives are addressed through three primary tasks: 1) defining and detailing constrained layer pneumatic systems architecture, operation, behavior, and fabrication, 2) developing a hierarchical functional architectural decomposition approach for supporting the synthesis, analysis, and re-synthesis of structurally adaptable multi-mode product concepts, and 3) demonstrating an approach for the exploration and architectural and parametric design for tailored multi-modal performance.

5.1.1. Technological Foundation for Constrained Layer Pneumatic Systems

For centuries, multi-mode products have provided users with multiple sets of functionalities across different interaction modes, achieved through various non-reconfigurable, modular, or structurally adaptable configurations dictated by their architecture. Traditionally, most of these products required manual operation by users due to their non-reconfigurable or modular configurations. However, recent advances in pneumatically activated systems have introduced

embedded solutions for on-demand structural transformations, allowing for seamless transitions between modes in structurally adaptable configurations, presenting a potential for designing new genre of innovative products in transportation, aerospace, architecture, robotics, biomedical, and consumer devices. This dissertation developed the technological foundation for employing constrained layer pneumatic systems as a new technological approach that has the potential to enable numerous structurally adaptable multi-mode product applications. By facilitating complex three-dimensional actuation motions distributed throughout a product's structure in a highly customizable, lightweight, space-saving, and cost-effective manner, this approach caters to users' changing needs by offering tailored functionalities through multiple operation states for diverse situations.

To address the range of research issues related to the systematic description of constrained layer pneumatic systems and the comprehensive exploration of the attainable technology capabilities using these systems, a hierarchically organized architecture was developed. This architecture consists of multiple airtight skin layers that form interconnected inflatable or vacuumable air cavities, pneumatic ports to control the relative pressure within the system, and internal and/or external constraints that shape the form and functionalities of the system when pneumatically activated.

To describe and communicate the emergent complexity of the constrained layer pneumatic system's structural organization, a five-level architectural hierarchy was introduced. This hierarchy spans from the cell level, which outlined the arrangement among the most fundamental architectural components, to the system level, encompassing the entirety of the product at its highest level of organization. The cell, considered as the most basic component in the architectural hierarchy, provides not only the lowest-level functionalities but also comprises a complex arrangement of sub-cellular features. To fully describe the architecture of a cell, its sub-cellular features were logically organized into three main sub-cellular feature categories. These categories were identified as *skin*, which described the characteristics of skin layers, *connectivity*, which described the cell construction and arrangement, and *constraints*, which described the physical restrictions influencing the fundamental behaviors exhibited by the cell. Pneumatic affordances, responsible for the activation of the cell's functionality through its imposed structure when operated, were classified into four groups depending on their capacity to actively or passively raise or lower the system's internal pressure. The operation of the pneumatic affordances activates

fundamental cell behaviors, which were also divided into four categories based on their ability to expand or contract the air cavity within the cell's structure, either in-plane or out-of-plane. The fundamental behaviors activated by pneumatic affordance operations give rise to the emergent cell functions, which are heavily affected by the characteristics of subcellular features of a cell. To explore and understand the breadth of attainable emergent cell functions, a catalog showcasing cell architectural variations and relating them to the resulting set of functionalities was created.

The discussion of the architectural influence on the associated emergent cell functions was facilitated by a comprehensive grammar and a visual language developed for consistently describing, communicating, and comprehending the architecture, operation, and functionality of the cells that make up constrained layer pneumatic systems. To enable the embodiment of architecturally diverse cells, potential fabrication techniques and material systems were explored and classified into three main categories. Within each category, alternative methods for fabricating a proto-cell (i.e., the simplest possible cell) were enumerated to provide a practical basis for design prototyping. This enabled the experimental survey of emergent cell functions exhibited across various operation states. By categorically introducing various subcellular feature characteristic variations, a range of architecturally diverse, operationally adaptable, and functionally useful cell alternatives was generated as building blocks, relating architecture to functionality, offering a selection of emergent cell function pairings, such as *extend/pull, straighten/hinge, flatten/bend, become non-porous/become porous, flatten/buckle bi-stably, mute/texturize, roll/unroll, grow in-plane/shrink in-plane, flatten/cinch,* and *allow hinge-like motion/retain hinge position/jam*. To demonstrate the usefulness and applicability of these building blocks in the context of early-stage design of structurally adaptable multi-mode products, five distinct design concepts were introduced. Each concept provided unique technology capabilities for user interaction in context-specific settings, showcasing how cell-level components could be combined hierarchically in different ways to create an overall system.

5.1.2. Design Supported by Hierarchical Functional Architectural Decomposition

To provide a systematic foundation for the design of structurally adaptable multi-mode product concepts employing constrained layer pneumatic systems, an integrated hierarchical characterization scheme was established. This scheme enabled capturing the relationships among architectural, functional, operational, and performance aspects, facilitating iterative synthesis and

analysis during the early-stage design process. To offer insights into the system's coupled form and functionality, a hierarchical functional and architectural decomposition approach was introduced. The overall system hierarchy was divided into five primary levels, cell, ensemble, unit, assembly, and system, to demonstrate the composition of architectural and functional components at each level in the hierarchy from the levels below. The analysis and visualization of coupled functional and architectural relationships within hierarchical levels were enabled by a block diagrammatic technique. The comprehensive representation of the system aspects was facilitated by using this technique, offering insights into the system's multi-mode operation while classifying architectural and functional components based on their constituent or constitutive roles in composing the overall product system. To contextualize formal grammars, terminology, and diagramming conventions describing the decomposition approach, a decomposition of a specific case study, mobile phone restraint mat, was showcased, proving the approach useful for understanding and communicating interrelated architectural, functional, and operational aspects during early design stages. This comprehensive representation enabled an in-depth understanding of the system's organization and interdependencies, which promoted iterative synthesis, aiding designers to generate design alternatives by re-synthesizing the existing concepts without impacting their higher-level functionalities or by synthesizing new systems, given a library of existing architectural components and associated functionalities.

To systematize the re-synthesis process for structurally adaptable multi-mode product concepts employing constrained layer pneumatic systems, ten design strategies were developed and categorized under three design strategy directions: re-design, incremental innovation, and radical innovation. Each strategy was formulated based on a combination of design objectives (*what*), design goals (*why*), design modifications (*how*), and associated trade-offs (*why-not*). To demonstrate the implementation of these goal-oriented design strategies in re-synthesizing multi-mode products with structural adaptability, five existing design concept examples from Chapter 2 served as starting points for goal-oriented alternative design development. Each strategy's design objective was achieved by implementing design modifications to meet specific goals, while accommodating trade-offs during the re-synthesis. As a result, eight alternative designs were generated: two exemplifying re-design, two illustrating incremental innovation, and four demonstrating radical innovation, validating the usefulness of and the flexibility provided by the hierarchical functional architectural decomposition approach.

This approach promotes collaboration across different disciplines by facilitating a consistent and transferable iterative analysis, synthesis, and re-synthesis of structurally adaptable multi-mode products using constrained layer pneumatic product systems. While presented in the context of designing structurally adaptable multi-mode product concepts using constrained layer pneumatic systems, the hierarchical functional architectural decomposition approach can also be applied to the analysis, synthesis, and re-synthesis of system designs for other highly structured architectural classes of systems relying on architectural and functional hierarchies.

5.1.3. Architectural and Parametric Design for Multi-modal Performance

Constrained layer pneumatic systems offer unique technology capabilities, including tailorable distributed complex actuation motions, changes in structural properties, and various means of sensing. To showcase their potential in structurally adaptable multi-mode product applications, a systematic design approach focused on a specific architectural variation: internally tiled pneumatic textiles. These pneumatic textiles can transform from soft to rigid states, enabling moldability on demand.

Internally tiled pneumatic textiles consist of rigid tiles arrayed in regular patterns within an airtight bladder, with overall stiffness controlled by vacuum pressure. Their architecture was categorized into three tile architectural classes based on the approaches providing a defined spatial order among the adjacent tiles inside a bladder: bladder-attached tiles, internal sheet-attached tiles, and mutually interlocked tiles. These textiles provide a thin profile surface that can be molded into complex geometries, providing a specific technology capability, moldability. They have multiple operation states (draping, shaping, and rigidizing) that align with user interaction modes, supported by the cell level operation states and emergent cell functions as described in Chapter 2. Moldability was decomposed into three sub-capabilities, drapability, shapability, and rigidizability, the performance of each was characterized through a set of engineering performance metrics that were identified using hierarchical functional architectural decomposition approach which was described in detail in Chapter 3. This exploited the relationship between technical performance from a technological point of view to the context-specific product use performance from a user-interaction point of view to enable direct empirical measurements that have implications on the product use.

To quantify the overall moldability performance in relation to the functional, operational, and architectural aspects, a set of procedures corresponding to each technology sub-capability was

developed, enabling the characterization of five dimensionless performance metrics (i.e., draping angle, conformability, setability, flexural rigidity, post yield elasticity) on a natural scale of zero to one to quantify the performance of the lower-level functionalities contributing to the performance of the higher-level ones (i.e., drapability, shapability, and rigidizability). This natural scaling enables the comparison of conceptually distinct metrics which commonly are necessary to characterize the multi-mode products' operations.

To understand the effects of tile architectural class/subclass and corresponding architectural feature variations on internally tiled pneumatic textiles' performance, a hierarchical series of three experimental studies was conducted, including analyzing comparative performances across three tile architectural classes, analyzing design couplings within the bladder-attached tiles architectural class using correlation matrices, which is crucial because, structurally adaptable multi-mode products fundamentally rely on such couplings, and evaluating comparative performances among different pneumatic textiles based on tile layer overlap and intermediate layer layup architectural feature variations. To allow the design of structurally adaptable multi-mode products with tailored technology sub-capability performance, a predictive algebraic design approach was developed and validated. This approach enabled an empirical fit to describe the relationship between sub-cellular feature characteristics (i.e., tile size, gap, and height) of a particular type of internally tiled pneumatic textiles and the metrics which quantify the performance of higher-level functionalities (i.e., drapability, shapability, rigidizability performances). This approach to navigate the inherent multi-modal performance coupling was used to design moldable active cargo blankets with tailored moldability performance, and their performances were experimentally validated against design goals.

Though the results focus on internally tiled pneumatic textiles and their specific design application (i.e., moldable active cargo blanket), the design techniques and analysis can be applied to other constrained layer pneumatic system architectures that provide multiple sets of trading-off functionalities through multiple operation states enabling the design of other structurally adaptable multi-mode product systems.

5.2. Future Research

The established design science foundation offers a versatile, scalable platform to support various future research efforts in the field of structurally adaptable multi-mode product design

using constrained layer pneumatic systems and other technological approaches. Several potential research directions are identified to facilitate the successful expansion of this foundation.

5.2.1. Expanding the Design Science Foundation: Exploring Alternative Technologies, Methods, and Research Avenues

The application of the developed design science foundation enabling the early-stage design of structurally adaptable multi-mode products was demonstrated by using emerging constrained layer pneumatic systems as a technological basis within the scope of this dissertation. The general applicability of this foundation can be further demonstrated by using other hierarchically organized technological approaches, such as active knits the architecture of which is based on the hierarchical use of shape memory alloy wires [216] where the properties of the wire create he functionality of a loop (i.e., cell) which produces emergent functionalities when used to compose a knit pattern (i.e., ensemble) which affords the creation of more complex behaviors in a grid pattern (i.e., unit/assembly) which then to compose the full structure of the device as a restructured grid (i.e., system) [65]. This foundation also can be extended to metamaterials-based systems like heterogenous mechanical metamaterials [217] or reconfigurable prismatic architected materials [218]. Researchers have shown the potential of these material-/smart-material-based technological approaches by designing a range of architectural and functional building blocks that demonstrate structural adaptations in different operation states (e.g., a flat unit of active knit patch transforms into an arched structural formation when heated). The variations and extensions of these building blocks can be employed to design structurally adaptable multi-mode systems and the hierarchical functional architectural decomposition approach can be used to re-synthesize alternative systems based on existing ones to make incremental improvements or to generate novel systems.

Chapter 3 described a qualitative method that could guide the identification of parametric and architectural performance relationships in the context of re-synthesizing alternative multi-mode product systems. The analysis of performance relationships and comparative assessments of the complexities of emerging alternative systems resulting from re-synthesis can be further systematized. One way to achieve this systematization is by incorporating Design Structure Matrix (DSM) methods, which aid in managing complexity by concentrating on the components of complex systems and their interconnections, into the hierarchical architectural functional decomposition approach [219], [220]. The objective quantification of dependencies among the

components of system aspects (i.e., architectural, functional, operational, performance) would offer a more robust foundation, thus enabling designers and engineers to select appropriate design solutions without relying somewhat on their intuition and experience, potentially reducing the risk of numerous iterations during the early-stage design process.

The emerging constrained layer pneumatic system capabilities, a sample of which was demonstrated in Chapter 2, can be expanded through further exploration of each subcellular feature category, as their associated characteristics are inherently open-ended. For instance, in Chapter 4, an in-depth investigation of the layered internal constraints subcategory was conducted. Similar comprehensive examinations can be performed for other subcellular feature categories, such as skin uniformity, in-cell mechanical connection typologies, and internal/external tendon constraints, highlighting the vast research potential within constrained layer pneumatic systems. The subcellular feature characteristics of architectural components and their associated functionalities can be used for synthesizing, analyzing, and re-synthesizing new multi-mode product systems. Numerous architectural and parametric design studies can be designed to quantitatively model the relationship between parametric design variables and multi-modal performance of these new systems. Developing analytical models explaining the relationship between architectural components and subcellular feature characteristics and the associated functionalities, in addition to the empirical modelling effort, would significantly improve the ability to predict the resulting performances of the functionalities. In addition to providing a growing library of physical building-blocks (demonstrated in Chapter 2), software packages and add-ons can be developed based on the future analytical models for enabling designers to integrate constrained layer pneumatic system building blocks into their digital design process (e.g., an add-on similar to Grasshopper, which is a graphical algorithm editor, for Rhinoceros 3D design software). The improved predictive capabilities combined with the digital integration enabling the simulation of constrained layer pneumatic systems' structural transformations can further facilitate the early-stage design of structurally adaptable multi-mode products.

5.2.2. User Experience Integration for Structurally Adaptable Multi-Mode Product Design

The established design science foundation illustrates the operational usefulness of emerging constrained layer pneumatic system technologies for the technology-driven design of structurally adaptable multi-mode products, which deliver multiple functionalities for physical user

interactions. However, the suitability of employing constrained layer pneumatic systems within user-interacting multi-mode product systems to cater to targeted user experiences is yet to be demonstrated. To achieve this objective, future research could focus on creating a framework that connects the objective technological system aspects (i.e., architectural, functional, operational, performance) of structurally adaptable multi-mode products to the subjective aspects of user experience (e.g., perceived performance of the functionalities provided by a multi-mode product).

In Chapter 4, an empirical quantification of the objective technological system aspects was exemplified by identifying a set of engineering performance metrics (i.e., draping angle, conformability, setability, flexural rigidity, post-yield elasticity) using the hierarchical functional architectural decomposition approach detailed in Chapter 3. Experimental procedures for data collection facilitated the quantification of engineering performance metric sets, which then quantify the performances of technology sub-capabilities. Draping angle quantifies drapability, while conformability and setability quantify shapability, and flexural rigidity and post-yield elasticity quantify rigidizability performance. Since the overall system-level technology capability, moldability, was decomposed into three system-level technology sub-capabilities (drapability, shapability, and rigidizability), these experimental procedures enable the capture of the overall moldability performance provided by a pneumatic textile featuring a specific architectural design. As validated in Chapter 4, the architectural and parametric design approach enabled tailoring the multi-modal performance of multi-mode products by systematically relating each technology sub-capability performance to a specific set of sub-cellular feature characteristics of the multi-mode product systems (Figure 155). In the context of designing a moldable active cargo blanket, this specific set of sub-cellular feature characteristics was downselected as *tile size, the gap between adjacent tiles,* and *tile height*, describing the design variables associated with a specific sub-cellular feature category, *constraints.*

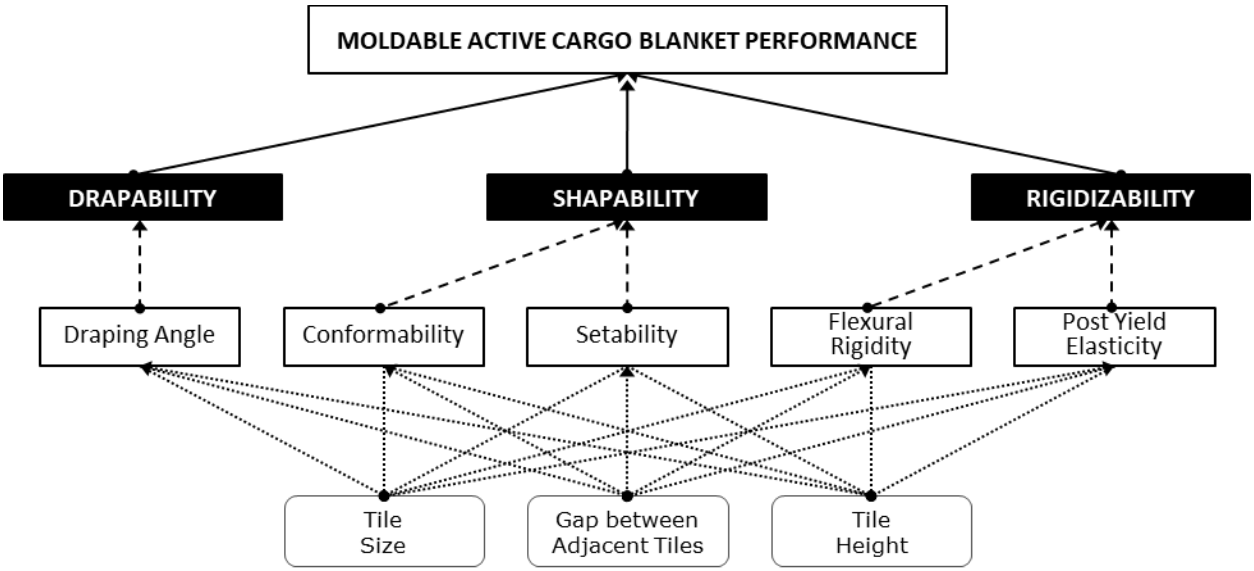

Figure 155. Quantification of a moldable active cargo blanket performance. Moldability is an emergent technology capability comprising drapability, shapability, and rigidizability technology capabilities. A set of objectively quantifiable engineering performance metrics is identified for each one these technology capabilities, where the drapability performance is characterized by the draping angle metric, the shapability performance is characterized by the conformability and setability metrics, and the rigidizability performance is characterized by the flexural rigidity and post yield elasticity metrics. The tile geometry design variables (the tile size, gap between adjacent tiles, and tile height) simultaneously affect the resulting metric scores and technology capability performances.

By assigning an intended set of relative weights (w_n) to the engineering performance, the algebraic tailoring method enabled the identification of the tile geometry design variables that provides the tailored moldability performance according to the weights as an outcome as illustrated in Figure 156 and detailed in Equation 10.

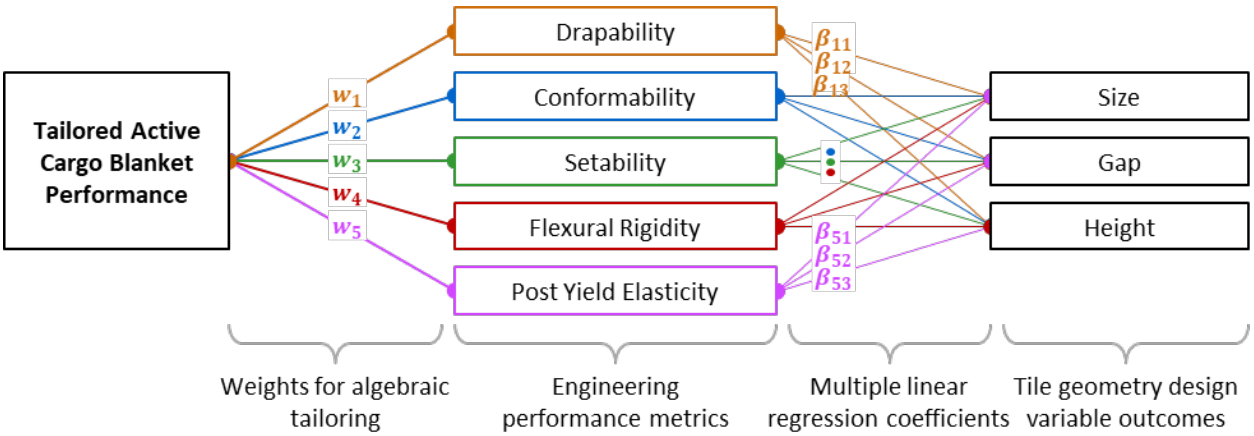

Figure 156. Algebraic tailoring method for designing active cargo blankets with tailored moldability performance. The algebraic tailoring method uses the maximization of the weighted sum of the engineering performance metrics to enable the identification of the tile geometry design variable values that provide the intended moldability performance as an outcome.

$$P_T = \underbrace{[W_1 \quad \cdots \quad W_5]\begin{bmatrix}\beta_{11} & \cdots & \beta_{13}\\ \vdots & \ddots & \vdots\\ \beta_{51} & \cdots & \beta_{53}\end{bmatrix}}_{B_W}\begin{bmatrix}s\\ g\\ h\end{bmatrix} + [W_1 \quad \cdots \quad W_5]\begin{bmatrix}\beta_{10}\\ \vdots\\ \beta_{50}\end{bmatrix}, \tag{10}$$

In the context of this dissertation, the set of multiple linear regression coefficients (β_{ij}) was determined using empirical modeling, achieved by carrying out a parametric design study. The relative weights (w_n) were determined arbitrarily to test and verify the algebraic tailoring method's effectiveness in terms of technical performance from a technological point of view. However, successfully designing for user experience requires understanding users' collective perception of the moldability performance, which in turn demands an understanding of the perceived technology sub-capability performances. To achieve this, an expanded version of the algebraic tailoring method, which decomposes the perceived moldability performance into perceived drapability, shapability, and rigidizability performances, each of which then can be related to their respective set of engineering performance metrics, is proposed (Figure 157).

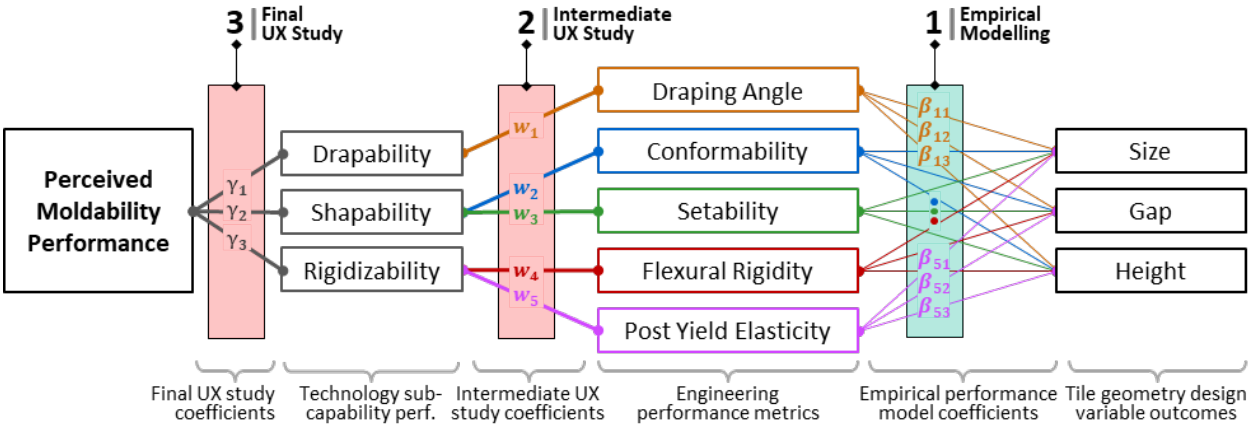

Figure 157. Expanded algebraic tailoring method for capturing perceived moldability performance. The expanded algebraic tailoring method uses the maximization of the weighted sum of the engineering performance metrics to enable the identification of the tile geometry design variable values that provide the intended perceived moldability performance as an outcome.

This expansion requires conducting two separate sets of human subject studies: 1) *intermediate UX study* targeting to model the perceived technology sub-capability performances as a function of the subcellular feature characteristics (i.e., size, gap, height) and 2) *final UX study* targeting to model the overall perceived moldability performance as a function of perceived technology sub-capability performances. As a part of intermediate UX study, subjective perceptual metrics per technology sub-capability (drapability, shapability, and rigidizability) need to be identified and empirically related to the objective set of engineering performance metrics corresponding to

technology sub-capability. A set of human subject studies needs to be conducted using systematically differentiated small-scale active cargo blanket prototypes to discover users' perception of the engineering performance metrics. Data could be collected for each technology sub-capability performance by having users compare systematically randomized pairs of small-scale prototypes with different levels of engineering performances to evaluate which prototype within each pair is perceived as providing relatively better performance. Figure 158 illustrates a potential intermediate UX study plan and setting containing three consecutive sub-studies focusing on each technology sub-capability performance: perceived drapability performance study, perceived shapability performance study, and perceived rigidizability performance study.

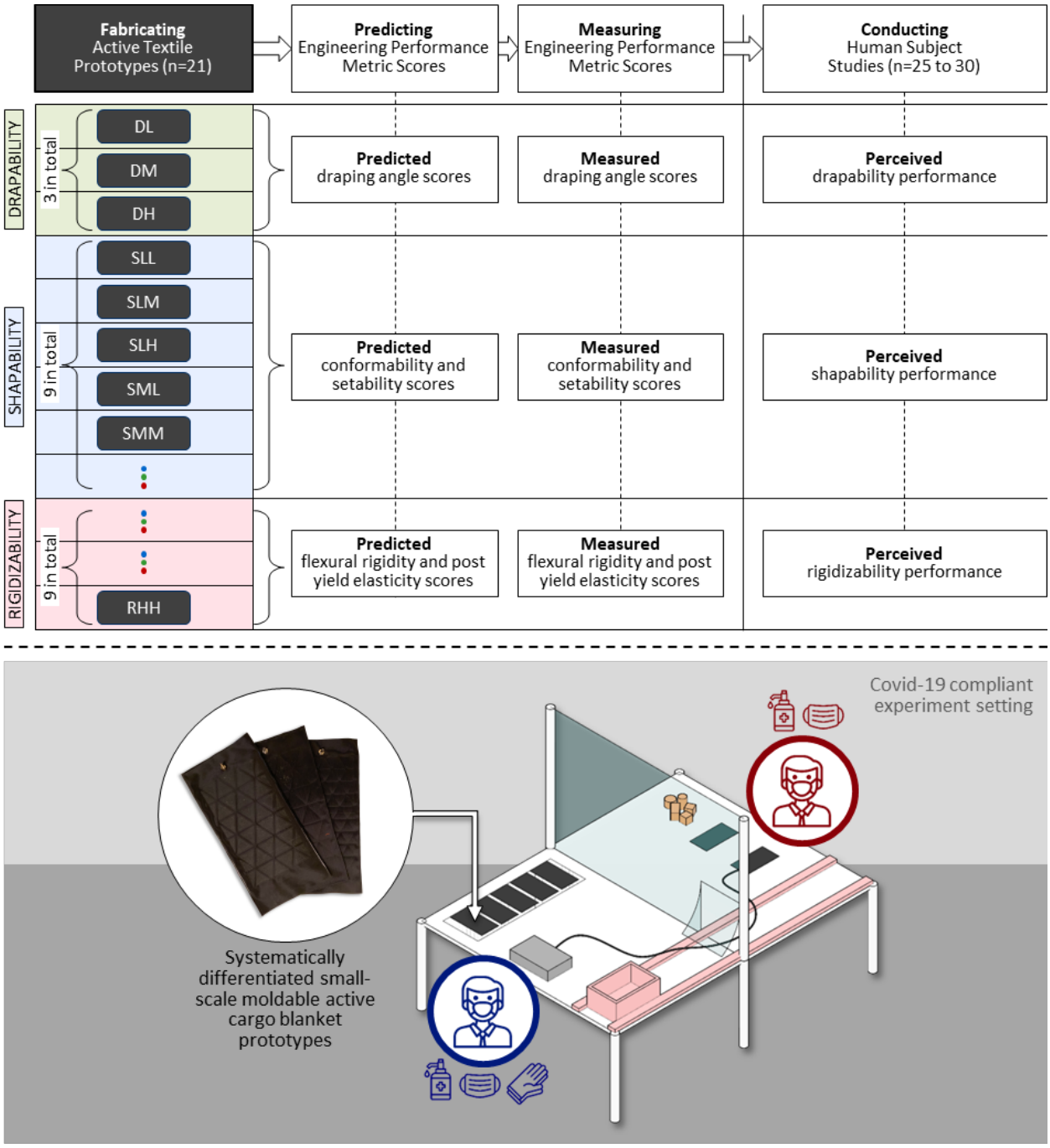

Figure 158. A potential intermediate UX study plan. The intermediate UX study comprises three sequential sub-studies, each corresponding to a specific technology sub-capability performance: perceived drapability performance study, perceived shapability performance study, and perceived rigidizability performance study (shown in top portion). A COVID-19 compliant potential experimental setup is visualized (shown in bottom portion).

A combination of quantified statistical methods based on Bradley-Terry (BT) model can be used to produce a model showing the relationship between the subjective data that rank the perceived performance of the small-scale active cargo blanket prototypes for each technology sub-

capability and the objective technical performance quantified by using the engineering performance metrics. For example, from an engineering standpoint, the performance of a specific technology sub-capability, such as shapability, is quantified using conformability and setability performance metrics. It was assumed that both metrics contribute equally to shapability performance. The findings of the intermediate UX study may help determine the relative importance of each objective engineering performance metric (e.g., the relative significance of conformability vs. setability) in terms of producing their respective subjectively perceived technology sub-capability performance (e.g., shapability performance).

The final UX study aims to model the relative importance of each technology sub-capability performance in terms of producing the overall moldability performance. To achieve this, a set of systematically differentiated full-scale moldable active cargo blanket prototypes, which represents different levels of drapability, shapability, and rigidizability performances, needs to be fabricated. These full-scale prototypes then can be used in various task completion studies in the context of molding an active cargo blanket over a particular cargo configuration (e.g., a collection of different sized cardboard boxes, grocery bags, and arbitrary objects that are commonly transported) to capture the user's comparative experience of interacting with each systematically differentiated prototypes. This can be done by measuring the effectiveness of each prototype in completing targeted tasks (e.g., the time it takes to mold prototype A vs prototype B), by recording the video of users interacting with each prototype and analyzing for example the ease of use based on a set of pre-defined metrics, by employing biometric sensors that can be used to quantify the physical effort exerted during user-prototype interaction, or by administering survey during and/or after user-prototype interaction takes place. The data collected can be analyzed using a combination of quantified statistical methods analogous to the one proposed for the analysis of the data collected in intermediate UX study. The findings of the final UX study unveil the relative importance of each technology sub-capability performance (e.g., the relative significance of drapability vs shapability vs rigidizability) in terms of producing the overall technology capability performance, moldability. By splitting the user studies in two phases, a detailed understanding of the perceived technical performance is enabled without requiring conducting full-scale in-application-context user-studies which require significantly more prototyping efforts and resources, which is only required in the smaller final UX study.

The combination of the intermediate and final UX studies will enable an aggregated user experience model. Furthermore, the aggregated user experience model can be combined with the engineering model. Since the engineering model relates the sub-cellular feature characteristics (i.e., tile geometry design variables) to engineering performance metric outcomes and the user experience model relates these engineering performance metric outcomes to subjective perceptual metrics, these two models are linked. This combination provides the ability to predict user's perception of moldable active textile performance directly from the tile geometry design variables, and thus enables a holistic design of the structurally adaptable multi-mode product including both technological and quantified user experience aspects. This exploits the relationship between technical performance from a technological point of view to the context-specific product use performance from a user-interaction point of view to enable direct empirical measurements that have implications on the product use. The general approach described in the context of moldable active cargo banket design equally applies to the design of any user-interacting multi-mode products with multiple states of operation by providing a systematic link between technology development and user experience aspects of its implementation as a product.

1.1. Closing

Research on *constrained layer pneumatic systems* began with growing interest to explore unprecedented ways of providing pneumatically activated three dimensionally distributed complex actuation motions, on demand changes in structural properties, and various means of sensing capabilities that can be easily tailored to be integrated to the structure of the products.

This provided a technological basis for an emerging design space of a new genre of products, *structurally adaptable multi-mode products*, offering multiple sets of functionalities that can be activated on demand to adapt to the changing user or environmental needs over time. However, designing such products with enhanced capabilities introduces an increase in technology and design complexity as well as design and performance coupling when compared to the design of conventional products. The well-established design methodologies often do not address these trade-offs as a part of design process; therefore, the need for a systematic design approach in the context of designing structurally adaptable multi-mode products using constrained layer pneumatic systems was identified.

To address this, the goal of this research was formulated to develop the design science foundation to enable a systematic early-stage design space exploration for emerging constrained layer pneumatic system technologies that provides a basis for the design of structurally adaptable multi-mode products providing multiple functionalities affording physical interaction with users. The resulting knowledge base from this work enables the development of innovative architectural components with unique functionalities when pneumatically operated, tailored to specific design application needs. Furthermore, it lays a solid foundation for comprehensively describing, exploring, and relating architectural, functional, operational, and performance-related system aspects to design a new generation of multi-modal products. These products feature adaptive structures that offer functional adaptability, aiming to deliver more while consuming less. By addressing users' diverse needs, they promote inclusive and equitable user-product interaction opportunities.

Bibliography

[1] N. F. Roozenburg and J. Eekels, Product design: fundamentals and methods. Wiley, 1995.

[2] K. Ulrich, “The role of product architecture in the manufacturing firm,” Research policy, vol. 24, no. 3, pp. 419–440, 1995.

[3] “Definition of MODE,” Mar. 26, 2023. https://www.merriam-webster.com/dictionary/mode (accessed Mar. 28, 2023).

[4] H. Lyness and D. Apostolopoulos, “Validation of two reconfigurable wheel-track testbeds for military vehicles,” Journal of Terramechanics, vol. 98, pp. 34–41, Dec. 2021, doi: 10.1016/j.jterra.2021.03.004.

[5] D. J. Hartl, D. C. Lagoudas, F. T. Calkins, and J. H. Mabe, “Use of a Ni60Ti shape memory alloy for active jet engine chevron application: I. Thermomechanical characterization,” Smart Materials and Structures, vol. 19, no. 1, p. 015020, 2009.

[6] S. Follmer, D. Leithinger, A. Olwal, N. Cheng, and H. Ishii, “Jamming user interfaces: programmable particle stiffness and sensing for malleable and shape-changing devices,” in Proceedings of the 25th annual ACM symposium on User interface software and technology - UIST ’12, Cambridge, Massachusetts, USA: ACM Press, 2012, p. 519. doi: 10.1145/2380116.2380181.

[7] K. T. Ulrich and W. P. Seering, “Function sharing in mechanical design.,” in AAAI, 1988, p. 342.

[8] M. Myrup Andreasen, C. T. Hansen, and P. Cash, “Conceptual Design-Interpretations, Mindset and Models, Conceptual Design.” Springer International Publishing. http://doi. org/10.1007/978-3-319-19839-2_1, 2015.

[9] W. Beitz, G. Pahl, and K. Grote, “Engineering design: a systematic approach,” Mrs Bulletin, vol. 71, 1996.

[10] P. Rodgers and A. Milton, Product design. Laurence King, 2011.

[11] L. T. Blessing and A. Chakrabarti, DRM: A design reseach methodology. Springer, 2009.

[12] K. T. Ulrich, “Product design and development: TataMcGraw-Hill Education New York,” 2003.

[13] G. S. Al′tshuller, The innovation algorithm: TRIZ, systematic innovation and technical creativity. Technical innovation center, Inc., 1999.

[14] N. P. Suh, “Axiomatic design theory for systems.,” Research in engineering design, vol. 10, no. 4, 1998.

[15] E. Kroll, S. S. Condoor, and D. G. Jansson, Innovative conceptual design: theory and application of parameter analysis. Cambridge University Press, 2001.

[16] J. Fahl, T. Hirschter, S. Haag, T. Staiger, and A. Albers, “Functions in the early phase of product development: A systematic literature review,” in 2020 IEEE International Symposium on Systems Engineering (ISSE), IEEE, 2020, pp. 1–9.

[17] C. Eckert, “That which is not form: the practical challenges in using functional concepts in design,” AI EDAM, vol. 27, no. 3, pp. 217–231, 2013.

[18] P. E. Vermaas, “The coexistence of engineering meanings of function: four responses and their methodological implications,” AI EDAM, vol. 27, no. 3, pp. 191–202, 2013.

[19] C. F. Kirschman and G. M. Fadel, “Classifying functions for mechanical design,” 1998.

[20] R. B. Stone and K. L. Wood, “Development of a functional basis for design,” in International Design Engineering Technical Conferences and Computers and Information in Engineering Conference, American Society of Mechanical Engineers, 1999, pp. 261–275.

[21] A. Chakrabarti and L. Blessing, “Representing functionality in design,” AI EDAM, vol. 10, no. 4, pp. 251–253, 1996.

[22] C. Liu, “Multimodal Product Design: a Development of Engineering Design Models in Systematic Approach,” 2016.

[23] P. Gu, M. Hashemian, S. Sosale, and E. Rivin, “An integrated modular design methodology for life-cycle engineering,” CIRP Annals, vol. 46, no. 1, pp. 71–74, 1997.

[24] K. T. Ulrich, S. D. Eppinger, and M. C. Yang, Product design and development, vol. 4. McGraw-Hill higher education Boston, 2008.

[25] J. K. Gershenson, G. J. Prasad, and Y. Zhang, “Product modularity: definitions and benefits,” Journal of Engineering design, vol. 14, no. 3, pp. 295–313, 2003.

[26] A. P. Lehnerd and M. H. Meyer, The power of product platforms. Simon and Schuster, 2011.

[27] T. W. Simpson, Z. Siddique, and R. J. Jiao, Product platform and product family design: methods and applications. Springer Science & Business Media, 2006.

[28] H. Ishii and B. Ullmer, “Tangible bits: towards seamless interfaces between people, bits and atoms,” in Proceedings of the ACM SIGCHI Conference on Human factors in computing systems, 1997, pp. 234–241.

[29] M. Sturdee, A. Everitt, J. Lindley, P. Coulton, and J. Alexander, “Visual methods for the design of shape-changing interfaces,” in Human-Computer Interaction–INTERACT 2019: 17th IFIP TC 13 International Conference, Paphos, Cyprus, September 2–6, 2019, Proceedings, Part III 17, Springer, 2019, pp. 337–358.

[30] I. Poupyrev, T. Nashida, and M. Okabe, “Actuation and tangible user interfaces: the Vaucanson duck, robots, and shape displays,” in Proceedings of the 1st international conference on Tangible and embedded interaction, 2007, pp. 205–212.

[31] M. K. Rasmussen, E. W. Pedersen, M. G. Petersen, and K. Hornbæk, “Shape-changing interfaces: a review of the design space and open research questions,” in Proceedings of the SIGCHI Conference on Human Factors in Computing Systems, 2012, pp. 735–744.

[32] J. Alexander et al., “Grand challenges in shape-changing interface research,” in Proceedings of the 2018 CHI conference on human factors in computing systems, 2018, pp. 1–14.

[33] M. Coelho and J. Zigelbaum, “Shape-changing interfaces,” Personal and Ubiquitous Computing, vol. 15, pp. 161–173, 2011.

[34] O. Bau, U. Petrevski, and W. Mackay, “BubbleWrap: a textile-based electromagnetic haptic display,” in CHI’09 Extended Abstracts on Human Factors in Computing Systems, 2009, pp. 3607–3612.

[35] T. Rewiri-Chrastecky, “Sentience: 3D printed living products,” 2014.

[36] D. Leithinger and H. Ishii, “Relief: a scalable actuated shape display,” in Proceedings of the fourth international conference on Tangible, embedded, and embodied interaction, 2010, pp. 221–222.

[37] S. Jang, L. H. Kim, K. Tanner, H. Ishii, and S. Follmer, “Haptic edge display for mobile tactile interaction,” in Proceedings of the 2016 CHI conference on human factors in computing systems, 2016, pp. 3706–3716.

[38] M. Vázquez, E. Brockmeyer, R. Desai, C. Harrison, and S. E. Hudson, “3d printing pneumatic device controls with variable activation force capabilities,” in Proceedings of the 33rd Annual ACM Conference on Human Factors in Computing Systems, 2015, pp. 1295–1304.

[39] C. Harrison and S. E. Hudson, “Providing dynamically changeable physical buttons on a visual display,” in Proceedings of the SIGCHI Conference on Human Factors in Computing Systems, Boston MA USA: ACM, Apr. 2009, pp. 299–308. doi: 10.1145/1518701.1518749.

[40] Y. Li, D. Xue, and P. Gu, “Design for product adaptability,” Concurrent Engineering, vol. 16, no. 3, pp. 221–232, 2008.

[41] P. Gu, M. Hashemian, and A. Y. Nee, “Adaptable design,” CIRP annals, vol. 53, no. 2, pp. 539–557, 2004.

[42] P. Gu, D. Xue, and Y. Chen, “General adaptable product design,” in Global Product Development: Proceedings of the 20th CIRP Design Conference, Ecole Centrale de Nantes, Nantes, France, 19th-21st April 2010, Springer, 2011, pp. 27–40.

[43] N. D, “2003 Ford Freestyle FX Concept,” Supercars.net, Apr. 20, 2016. https://www.supercars.net/blog/2003-ford-freestyle-fx-concept/ (accessed Mar. 23, 2023).

[44] “Benders Adaptable Utensils - Green/Blue (Boon),” www.usbabycity.com. https://www.usbabycity.com/product-p/117271.htm (accessed Mar. 23, 2023).

[45] “Liftware Steady | Liftware.” https://www.liftware.com/steady/ (accessed Mar. 21, 2023).

[46] A. Chakrabarti, “Sharing in design-categories, importance, and issues,” in International Conference on Engineering Design (ICED), 2001, pp. 21–23.

[47] C. Liu, H. P. Hildre, H. Zhang, and T. Rølvåg, “Conceptual design of multi-modal products,” Research in Engineering Design, vol. 26, pp. 219–234, 2015.

[48] C. Liu, H. P. Hildre, H. Zhang, and T. Rølvåg, “Product architecture design of multi-modal products,” Research in Engineering Design, vol. 27, pp. 331–346, 2016.

[49] Garmin and G. L. or its subsidiaries, “Forerunner 920XT,” Garmin. https://www.garmin.com/en-US/p/137024 (accessed Apr. 05, 2023).

[50] “2023 Hyundai Elantra Hybrid | Compact Sedan | Hyundai USA.” https://www.hyundaiusa.com/us/en/vehicles/elantra-hybrid (accessed Apr. 05, 2023).

[51] B. Hannaford and J. Winters, “Actuator properties and movement control: biological and technological models,” Multiple Muscle Systems: Biomechanics and Movement Organization, pp. 101–120, 1990.

[52] C. Greco, P. Kotak, L. Pagnotta, and C. Lamuta, “The evolution of mechanical actuation: from conventional actuators to artificial muscles,” International Materials Reviews, vol. 67, no. 6, pp. 575–619, 2022.

[53] H. Kim, C. Coutrix, and A. Roudaut, “KnobSlider: design of a shape-changing UI for parameter control,” in Proceedings of the 2018 CHI Conference on Human Factors in Computing Systems, 2018, pp. 1–13.

[54] J. Gertler, “V-22 osprey Tilt-rotor aircraft: background and issues for congress,” Library of Congress Washington DC Congressional Research Service, 2009.

[55] M. Thota and K. W. Wang, “Reconfigurable origami sonic barriers with tunable bandgaps for traffic noise mitigation,” Journal of Applied Physics, vol. 122, no. 15, p. 154901, 2017.

[56] W. B. S. Jr, J. S. Sirkis, and P. T. Gardiner, “Smart materials and structures: what are they?,” Smart Mater. Struct., vol. 5, no. 3, p. 247, Jun. 1996, doi: 10.1088/0964-1726/5/3/002.

[57] R. Bogue, “Smart materials: a review of capabilities and applications,” Assembly Automation, vol. 34, no. 1, pp. 16–22, Jan. 2014, doi: 10.1108/AA-10-2013-094.

[58] L. E. M. Lignarolo, C. Lelieveld, and P. Teuffel, “Shape morphing wind-responsive facade systems realized with smart materials,” in Adaptive Architecture: An International Conference, London, UK, March 3-5, 2011, Citeseer, 2011.

[59] D. K. Patel et al., “Highly Dynamic Bistable Soft Actuator for Reconfigurable Multimodal Soft Robots,” Adv Materials Technologies, vol. 8, no. 2, p. 2201259, Jan. 2023, doi: 10.1002/admt.202201259.

[60] “Project Overview ‹ HelioZZZ: a smart (material) sleep mask,” MIT Media Lab. https://www.media.mit.edu/projects/heliozzz/overview/ (accessed Mar. 22, 2023).

[61] I. W. Hunter, J. M. Hollerbach, and J. Ballantyne, “A comparative analysis of actuator technologies for robotics,” Robotics Review, vol. 2, pp. 299–342, 1991.

[62] W. Kim, “Model-based Design Framework for Shape Memory Alloy Wire Actuation Devices.,” PhD Thesis, 2016.

[63] J. A. Redmond, D. Brei, J. Luntz, A. L. Browne, and N. L. Johnson, “Spool-packaging of shape memory alloy actuators: Performance model and experimental validation,” Journal of intelligent material systems and structures, vol. 23, no. 2, pp. 201–219, 2012.

[64] W. Kim, B. Utter, J. Luntz, D. Brei, H. Muhammad, and P. Alexander, “Model-Based Shape Memory Alloy Wire Ratchet Actuator Design,” presented at the ASME 2013 Conference on Smart Materials, Adaptive Structures and Intelligent Systems, American Society of Mechanical Engineers Digital Collection, Feb. 2014. doi: 10.1115/SMASIS2013-3333.

[65] J. Abel, J. Luntz, and D. Brei, “Hierarchical architecture of active knits,” Smart materials and Structures, vol. 22, no. 12, p. 125001, 2013.

[66] M. S. Verma, A. Ainla, D. Yang, D. Harburg, and G. M. Whitesides, “A Soft Tube-Climbing Robot,” Soft Robotics, vol. 5, no. 2, pp. 133–137, Apr. 2018, doi: 10.1089/soro.2016.0078.

[67] A. M. Kübler, S. U. Rivera, F. B. Raphael, J. Förster, R. Siegwart, and A. M. Okamura, “A Multi-Segment, Soft Growing Robot with Selective Steering.” arXiv, Dec. 07, 2022. Accessed: Feb. 25, 2023. [Online]. Available: http://arxiv.org/abs/2212.03951

[68] H. Sareen et al., “Printflatables: Printing Human-Scale, Functional and Dynamic Inflatable Objects,” in Proceedings of the 2017 CHI Conference on Human Factors in Computing Systems, Denver Colorado USA: ACM, May 2017, pp. 3669–3680. doi: 10.1145/3025453.3025898.

[69] D. Melancon, B. Gorissen, C. J. García-Mora, C. Hoberman, and K. Bertoldi, “Multistable inflatable origami structures at the metre scale,” Nature, vol. 592, no. 7855, pp. 545–550, Apr. 2021, doi: 10.1038/s41586-021-03407-4.

[70] S. Häuplik-Meusburger, B. Sommer, and M. Aguzzi, “Inflatable technologies: adaptability from dream to reality,” Acta Astronautica, vol. 65, no. 5–6, pp. 841–852, 2009.

[71] E. Siéfert, E. Reyssat, J. Bico, and B. Roman, “Programming stiff inflatable shells from planar patterned fabrics,” Soft Matter, vol. 16, no. 34, pp. 7898–7903, 2020.

[72] “Hövding 3 | Airbag for urban cyclists,” Hövding. https://hovding.com/hovding3/ (accessed Apr. 05, 2023).

[73] J. Ou et al., “aeroMorph - Heat-sealing Inflatable Shape-change Materials for Interaction Design,” in Proceedings of the 29th Annual Symposium on User Interface Software and Technology, Tokyo Japan: ACM, Oct. 2016, pp. 121–132. doi: 10.1145/2984511.2984520.

[74] H. D. Yang, “Design, Manufacturing, and Control of Soft and Soft/Rigid Hybrid Pneumatic Robotic Systems,” PhD Thesis, Virginia Tech, 2019.

[75] A. Wihardja et al., “Posable Tensegrity-Constrained Inflatable Kinematic Graphical Analysis,” presented at the ASME 2020 Conference on Smart Materials, Adaptive Structures and Intelligent Systems, American Society of Mechanical Engineers Digital Collection, Nov. 2020. doi: 10.1115/SMASIS2020-2385.

[76] E. Kim, J. Luntz, D. Brei, W. Kim, P. Alexander, and N. Johnson, “Tendon constrained inflatable architecture: rigid axial load bearing design case,” Smart Mater. Struct., vol. 30, no. 5, p. 055004, Mar. 2021, doi: 10.1088/1361-665X/abe610.

[77] T. Li, J. Luntz, D. Brei, W. Kim, and P. Alexander, “Hinged Tile-Based Air Surface for Morphing Windshield Cowling,” in Smart Materials, Adaptive Structures and Intelligent Systems, American Society of Mechanical Engineers, 2022, p. V001T04A017.

[78] K. Benli, J. Luntz, D. Brei, W. Kim, P. Alexander, and N. Johnson, “Towards functional architectural decomposition of constrained layer inflatable systems,” Proceedings of the Design Society, vol. 1, pp. 3219–3228, 2021.

[79] L. Yao, R. Niiyama, J. Ou, S. Follmer, C. Della Silva, and H. Ishii, “PneUI: pneumatically actuated soft composite materials for shape changing interfaces,” in Proceedings of the 26th annual ACM symposium on User interface software and Technology, 2013, pp. 13–22.

[80] Y.-T. Lin and P.-H. Hsu, “Dynamic Inflatable Structures and Digital Fabrication Process,” in 40th Conference on Education and Research in Computer Aided Architectural Design in Europe, eCAADe 2022, Education and research in Computer Aided Architectural Design in Europe, 2022, pp. 311–320.

[81] H. J. Youn and A. Shtarbanov, “PneuBots: Modular Inflatables for Playful Exploration of Soft Robotics,” in Extended Abstracts of the 2022 CHI Conference on Human Factors in Computing Systems, 2022, pp. 1–6.

[82] H. Kim, A. Everitt, C. Tejada, M. Zhong, and D. Ashbrook, “Morpheesplug: A toolkit for prototyping shape-changing interfaces,” in Proceedings of the 2021 CHI Conference on Human Factors in Computing Systems, 2021, pp. 1–13.

[83] P. Webb, V. Sumini, A. Golan, and H. Ishii, “Auto-inflatables: Chemical inflation for pop-up fabrication,” in Extended Abstracts of the 2019 CHI Conference on Human Factors in Computing Systems, 2019, pp. 1–6.

[84] C. Han, R. Takahashi, Y. Yahagi, and T. Naemura, “PneuModule: Using Inflatable Pin Arrays for Reconfigurable Physical Controls on Pressure-Sensitive Touch Surfaces,” in Proceedings of the 2020 CHI Conference on Human Factors in Computing Systems, Honolulu HI USA: ACM, Apr. 2020, pp. 1–14. doi: 10.1145/3313831.3376838.

[85] J. Ou, L. Yao, D. Tauber, J. Steimle, R. Niiyama, and H. Ishii, “jamSheets: thin interfaces with tunable stiffness enabled by layer jamming,” in Proceedings of the 8th International Conference on Tangible, Embedded and Embodied Interaction - TEI ’14, Munich, Germany: ACM Press, 2013, pp. 65–72. doi: 10.1145/2540930.2540971.

[86] A. Russomanno, Z. Xu, S. O’Modhrain, and B. Gillespie, “A pneu shape display: Physical buttons with programmable touch response,” in 2017 IEEE World Haptics Conference (WHC), Munich, Germany: IEEE, Jun. 2017, pp. 641–646. doi: 10.1109/WHC.2017.7989976.

[87] Y. Matoba, T. Sato, N. Takahashi, and H. Koike, “ClaytricSurface: an interactive surface with dynamic softness control capability,” in ACM SIGGRAPH 2012 Emerging Technologies on - SIGGRAPH ’12, Los Angeles, California: ACM Press, 2012, pp. 1–1. doi: 10.1145/2343456.2343462.

[88] T. Mitsuda and N. Matsuo, “SHAPE STABILIZER USING AN ARTICULATION-TYPE PASSIVE ELEMENT,” Proceedings of the JFPS International Symposium on Fluid Power, vol. 2005, no. 6, pp. 722–727, 2005, doi: 10.5739/isfp.2005.722.

[89] J. F. Veneman, I. Manterola, M. Bureau, and J. H. Jung, “Varstiff, an innovative variable stiffness material, applied in a Wheelchair Positioning Device.,” p. 4.

[90] A. Sadeghi, A. Mondini, and B. Mazzolai, “Preliminary Experimental Study on Variable Stiffness Structures Based on Textile Jamming for Wearable Robotics,” in Wearable Robotics: Challenges and Trends, M. C. Carrozza, S. Micera, and J. L. Pons, Eds., in Biosystems & Biorobotics, vol. 22. Cham: Springer International Publishing, 2019, pp. 49–52. doi: 10.1007/978-3-030-01887-0_10.

[91] P. Polygerinos, Z. Wang, K. C. Galloway, R. J. Wood, and C. J. Walsh, “Soft robotic glove for combined assistance and at-home rehabilitation,” Robotics and Autonomous Systems, vol. 73, pp. 135–143, Nov. 2015, doi: 10.1016/j.robot.2014.08.014.

[92] A. Chandra, J. C. Lopez Tonazzi, D. Stetson, T. Pat, and C. K. Walker, “Inflatable membrane antennas for small satellites,” in 2020 IEEE Aerospace Conference, Big Sky, MT, USA: IEEE, Mar. 2020, pp. 1–8. doi: 10.1109/AERO47225.2020.9172737.

[93] R. E. Freeland, G. D. Bilyeu, G. R. Veal, M. D. Steiner, and D. E. Carson, “Large inflatable deployable antenna flight experiment results,” Acta Astronautica, vol. 41, no. 4–10, pp. 267–277, Aug. 1997, doi: 10.1016/S0094-5765(98)00057-5.

[94] E. Seedhouse, “Bigelow Expandable Activity Module,” in Bigelow Aerospace: Colonizing Space One Module at a Time, E. Seedhouse, Ed., Cham: Springer International Publishing, 2015, pp. 87–98. doi: 10.1007/978-3-319-05197-0_5.

[95] R. Gurt, “Design and analysis of reinforced rubber membranes for inflatable dams,” in Textiles composites and inflatable structures VII: proceedings of the VII International Conference on Textile Composites and Inflatable Structures, Barcelona, Spain. 19-21 October, 2015, CIMNE, 2015, pp. 306–317.

[96] A. L. Bloxom, S. C. Yim, A. J. Medellin, and C. S. Vince, “Testing of Inflatable Structures of Rapidly Deployable Port Infrastructures,” in Volume 6: Ocean Engineering, Rotterdam, The Netherlands: ASMEDC, Jan. 2011, pp. 55–68. doi: 10.1115/OMAE2011-49101.

[97] A. Rodríguez, E. Oñate, and J. Marcipar (presenter), “Design of an inflatable, modular and portable footbridge,” Monograph CIMNE, Jan. 2017, Accessed: Feb. 25, 2023. [Online]. Available: https://www.scipedia.com/public/Rodríguez_et_al_2017a

[98] P. Beccarelli and J. Chilton, “Advantages of lightweight tensioned coated fabrics and foils façades for the building sector,” in Textiles composites and inflatable structures VI: proceedings of the VI International Conference on Textile Composites and Inflatable Structures, Barcelona, Spain. 9-11 October, 2013, CIMNE, 2013, pp. 200–211.

[99] D. Terwagne, M. Brojan, and P. M. Reis, “Smart Morphable Surfaces for Aerodynamic Drag Control,” Adv. Mater., p. 4, 2014.

[100] B. Tome, “Pneumatically Augmenting Inelastic Materials for Texture Changing Interfaces,” Doctoral dissertation, Massachusetts Institute of Technology, 2015.

[101] R. Niiyama et al., “poimo: Portable and Inflatable Mobility Devices Customizable for Personal Physical Characteristics,” in Proceedings of the 33rd Annual ACM Symposium on User Interface Software and Technology, Virtual Event USA: ACM, Oct. 2020, pp. 912–923. doi: 10.1145/3379337.3415894.

[102] S. W. Kwok et al., “Magnetic Assembly of Soft Robots with Hard Components,” Adv. Funct. Mater., vol. 24, no. 15, pp. 2180–2187, Apr. 2014, doi: 10.1002/adfm.201303047.

[103] G. Singh, S. Patiballa, X. Zhang, and G. Krishnan, “A Pipe-Climbing Soft Robot,” in 2019 International Conference on Robotics and Automation (ICRA), Montreal, QC, Canada: IEEE, May 2019, pp. 8450–8456. doi: 10.1109/ICRA.2019.8793815.

[104] H. K. Yap et al., “A Fully Fabric-Based Bidirectional Soft Robotic Glove for Assistance and Rehabilitation of Hand Impaired Patients,” IEEE Robot. Autom. Lett., vol. 2, no. 3, pp. 1383–1390, Jul. 2017, doi: 10.1109/LRA.2017.2669366.

[105] X. Zhang et al., “Bubble: Wearable Assistive Grasping Augmentation Based on Soft Inflatables,” in Extended Abstracts of the 2019 CHI Conference on Human Factors in Computing Systems, Glasgow Scotland Uk: ACM, May 2019, pp. 1–6. doi: 10.1145/3290607.3312868.

[106] M. M. Coad et al., “Vine Robots,” IEEE Robot. Automat. Mag., vol. 27, no. 3, pp. 120–132, Sep. 2020, doi: 10.1109/MRA.2019.2947538.

[107] P. A. der Maur et al., “RoBoa: Construction and Evaluation of a Steerable Vine Robot for Search and Rescue Applications,” in 2021 IEEE 4th International Conference on Soft Robotics (RoboSoft), New Haven, CT, USA: IEEE, Apr. 2021, pp. 15–20. doi: 10.1109/RoboSoft51838.2021.9479192.

[108] F. Ilievski, A. D. Mazzeo, R. F. Shepherd, X. Chen, and G. M. Whitesides, “Soft Robotics for Chemists,” Angew. Chem., vol. 123, no. 8, pp. 1930–1935, Feb. 2011, doi: 10.1002/ange.201006464.

[109] K. C. Galloway et al., “Soft Robotic Grippers for Biological Sampling on Deep Reefs,” Soft Robotics, vol. 3, no. 1, pp. 23–33, Mar. 2016, doi: 10.1089/soro.2015.0019.

[110] S. Li, D. M. Vogt, D. Rus, and R. J. Wood, “Fluid-driven origami-inspired artificial muscles,” Proc. Natl. Acad. Sci. U.S.A., vol. 114, no. 50, pp. 13132–13137, Dec. 2017, doi: 10.1073/pnas.1713450114.

[111] M. Zhu, Y. Mori, T. Wakayama, A. Wada, and S. Kawamura, “A Fully Multi-Material Three-Dimensional Printed Soft Gripper with Variable Stiffness for Robust Grasping,” Soft Robotics, vol. 6, no. 4, pp. 507–519, Aug. 2019, doi: 10.1089/soro.2018.0112.

[112] P. E. Webb, “Chemical inflation for assisted assembly,” PhD Thesis, Massachusetts Institute of Technology, 2017.

[113] B. Gorissen, W. Vincentie, F. Al-Bender, D. Reynaerts, and M. D. Volder, “Modeling and bonding-free fabrication of flexible fluidic microactuators with a bending motion,” J. Micromech. Microeng., vol. 23, no. 4, p. 045012, Feb. 2013, doi: 10.1088/0960-1317/23/4/045012.

[114] X. Yang and S. Druga, “Legoons: Inflatable Construction Kit for Children,” in Extended Abstracts of the Annual Symposium on Computer-Human Interaction in Play Companion Extended Abstracts, in CHI PLAY ’19 Extended Abstracts. New York, NY, USA: Association for Computing Machinery, Oct. 2019, pp. 139–146. doi: 10.1145/3341215.3356980.

[115] E. T. Roche et al., “A Bioinspired Soft Actuated Material,” Advanced Materials, vol. 26, no. 8, pp. 1200–1206, 2014, doi: 10.1002/adma.201304018.

[116] K. S. Lachenmeier and K. Murai, “Development of three-dimensional reinforced membrane technology for high performance balloon and inflatable applications,” Advances in Space Research, vol. 33, no. 10, pp. 1732–1735, 2004.

[117] Y. Nishioka et al., “Development of a pneumatic soft actuator with pleated inflatable structures,” Advanced Robotics, vol. 31, no. 14, pp. 753–762, 2017.

[118] L. G. Munoz, J. Luntz, D. Brei, and W. Kim, “Tile-based rigidization surface parametric design study,” in Smart Structures and NDE for Industry 4.0, SPIE, 2018, pp. 73–87.

[119] J. C. Jung and H. Rodrigue, “Film-based anisotropic balloon inflatable bending actuator,” Journal of Mechanical Science and Technology, vol. 33, pp. 4469–4476, 2019.

[120] L. Perovich, P. Mothersill, and J. B. Farah, “Awakened Apparel: Embedded Soft Actuators for Expressive Fashion and Functional Garments,” p. 4.

[121] P. M. Khin, H. K. Yap, M. H. Ang, and C.-H. Yeow, “Fabric-based actuator modules for building soft pneumatic structures with high payload-to-weight ratio,” in 2017 IEEE/RSJ International Conference on Intelligent Robots and Systems (IROS), IEEE, 2017, pp. 2744–2750.

[122] R. Niiyama, X. Sun, C. Sung, B. An, D. Rus, and S. Kim, “Pouch motors: Printable soft actuators integrated with computational design,” Soft Robotics, vol. 2, no. 2, pp. 59–70, 2015.

[123] I. Jones, “Transmission laser welding strategies for medical plastics,” in Joining and Assembly of Medical Materials and Devices, Elsevier, 2013, pp. 344–371e.

[124] P. W. Alexander and O. Stoneman, “Motion sickness mitigation device,” Dec. 31, 2019

[125] F. Schmitt, O. Piccin, L. Barbé, and B. Bayle, “Soft robots manufacturing: A review,” Frontiers in Robotics and AI, vol. 5, p. 84, 2018.

[126] R. J. Good, “On the definition of adhesion,” The Journal of Adhesion, vol. 8, no. 1, pp. 1–9, 1976.

[127] H. K. Yap, J. H. Lim, F. Nasrallah, J. C. Goh, and R. C. Yeow, “A soft exoskeleton for hand assistive and rehabilitation application using pneumatic actuators with variable stiffness,” in 2015 IEEE international conference on robotics and automation (ICRA), IEEE, 2015, pp. 4967–4972.

[128] X. Gong et al., “Rotary actuators based on pneumatically driven elastomeric structures,” Advanced Materials, vol. 28, no. 34, pp. 7533–7538, 2016.

[129] S. Konishi, F. Kawai, and P. Cusin, “Thin flexible end-effector using pneumatic balloon actuator,” Sensors and Actuators A: Physical, vol. 89, no. 1–2, pp. 28–35, 2001.

[130] A. J. Kinloch and A. J. Kinloch, Adhesion and adhesives: science and technology. Springer Science & Business Media, 1987.

[131] H. Onusseit, “The influence of adhesives on recycling,” Resources, Conservation and Recycling, vol. 46, no. 2, pp. 168–181, 2006.

[132] K. L. Yam, The Wiley encyclopedia of packaging technology. John Wiley & Sons, 2010.

[133] P. Ohta et al., “Design of a lightweight soft robotic arm using pneumatic artificial muscles and inflatable sleeves,” Soft robotics, vol. 5, no. 2, pp. 204–215, 2018.

[134] N. Oh and H. Rodrigue, “Toward the development of large-scale inflatable robotic arms using hot air welding,” Soft Robotics, vol. 10, no. 1, pp. 88–96, 2023.

[135] S.-H. Park, J. Yi, D. Kim, Y. Lee, H. S. Koo, and Y.-L. Park, “A lightweight, soft wearable sleeve for rehabilitation of forearm pronation and supination,” in 2019 2nd IEEE International Conference on Soft Robotics (RoboSoft), IEEE, 2019, pp. 636–641.

[136] R. L. Baines, S. K. Patiballa, and R. Kramer-Bottiglio, “Rapidly Reconfigurable Inextensible Inflatables,” in 2021 IEEE 4th International Conference on Soft Robotics (RoboSoft), IEEE, 2021, pp. 29–34.

[137] H. J. Silvers Jr and S. Wachtell, “Perforating, welding and cutting plastic films with a continuous CO2 laser’. PA State University, Eng,” in Proc, 1970, pp. 88–97.

[138] ralph124c, “Laserweld Your Own Inflatables,” Instructables. https://www.instructables.com/Laserweld-Your-Own-Inflatables/ (accessed Mar. 20, 2023).

[139] “Fabacademy Barcelona 2018.” https://fabacademy.org/2018/labs/barcelona/students/javier-alboguijarro/week16.html (accessed Mar. 20, 2023).

[140] M. J. Troughton, Handbook of plastics joining: a practical guide. William Andrew, 2008.

[141] H. D. Yang and A. T. Asbeck, “A layered manufacturing approach for soft and soft-rigid hybrid robots,” Soft Robotics, vol. 7, no. 2, pp. 218–232, 2020.

[142] A. A. Amiri Moghadam et al., “Toward Development of Inflatable Stents with Application in Endovascular Treatments,” Advanced Functional Materials, vol. 28, no. 51, p. 1804147, 2018, doi: 10.1002/adfm.201804147.

[143] P. W. Alexander et al., “Pneumatic shade,” US20210170837A1, Jun. 10, 2021 Accessed: Mar. 20, 2023. [Online]. Available: https://patents.google.com/patent/US20210170837A1/en

[144] W. M. Kim et al., “Low profile pressure regulator,” US11119515B2, Sep. 14, 2021 Accessed: Mar. 20, 2023. [Online]. Available: https://patents.google.com/patent/US11119515B2/en

[145] A. Sadeghi, A. Mondini, and B. Mazzolai, “A Vacuum Powered Soft Textile-Based Clutch,” Actuators, vol. 8, no. 2, Art. no. 2, Jun. 2019, doi: 10.3390/act8020047.

[146] J. Chen et al., “Superelastic, Sensitive, and Low Hysteresis Flexible Strain Sensor Based on Wave-Patterned Liquid Metal for Human Activity Monitoring,” ACS Appl. Mater. Interfaces, vol. 12, no. 19, pp. 22200–22211, May 2020, doi: 10.1021/acsami.0c04709.

[147] N. Correll, Ç. D. Önal, H. Liang, E. Schoenfeld, and D. Rus, “Soft Autonomous Materials—Using Active Elasticity and Embedded Distributed Computation,” in Experimental Robotics: The 12th International Symposium on Experimental Robotics, O. Khatib, V. Kumar, and G. Sukhatme, Eds.,

in Springer Tracts in Advanced Robotics. Berlin, Heidelberg: Springer, 2014, pp. 227–240. doi: 10.1007/978-3-642-28572-1_16.

[148] J. Shintake, H. Sonar, E. Piskarev, J. Paik, and D. Floreano, "Soft pneumatic gelatin actuator for edible robotics," in 2017 IEEE/RSJ International Conference on Intelligent Robots and Systems (IROS), Sep. 2017, pp. 6221–6226. doi: 10.1109/IROS.2017.8206525.

[149] C. M. Schumacher, M. Loepfe, R. Fuhrer, R. N. Grass, and W. J. Stark, "3D printed lost-wax casted soft silicone monoblocks enable heart-inspired pumping by internal combustion," RSC Advances, vol. 4, no. 31, pp. 16039–16042, 2014, doi: 10.1039/C4RA01497A.

[150] A. D. Marchese, R. K. Katzschmann, and D. Rus, "A Recipe for Soft Fluidic Elastomer Robots," Soft Robotics, vol. 2, no. 1, pp. 7–25, Mar. 2015, doi: 10.1089/soro.2014.0022.

[151] J. W. Kow, P. Culmer, and A. Alazmani, "Thin soft layered actuator based on a novel fabrication technique," in 2018 IEEE International Conference on Soft Robotics (RoboSoft), Apr. 2018, pp. 176–181. doi: 10.1109/ROBOSOFT.2018.8404916.

[152] J. W. Kow, "Development of a Fabrication Technique for Soft Planar Inflatable Composites," phd, University of Leeds, 2020. Accessed: Mar. 20, 2023. [Online]. Available: https://etheses.whiterose.ac.uk/27674/

[153] B. Goveia da Rocha, O. Tomico, P. Markopoulos, and D. Tetteroo, Inflatable actuators based on machine embroidery. 2019. doi: 10.17028/RD.LBORO.9724688.V1.

[154] V. Mecnika, M. Hoerr, I. Krievins, S. Jockenhoevel, and T. Gries, "Technical Embroidery for Smart Textiles: Review," Materials Science. Textile and Clothing Technology, vol. 9, no. 0, Art. no. 0, 2014, doi: 10.7250/mstct.2014.009.

[155] D.-G. Ahn, "Directed Energy Deposition (DED) Process: State of the Art," Int. J. of Precis. Eng. and Manuf.-Green Tech., vol. 8, no. 2, pp. 703–742, Mar. 2021, doi: 10.1007/s40684-020-00302-7.

[156] A. Standard, "Standard terminology for additive manufacturing technologies," ASTM International F2792-12a, pp. 1–9, 2012.

[157] M. K. Thompson et al., "Design for Additive Manufacturing: Trends, opportunities, considerations, and constraints," CIRP annals, vol. 65, no. 2, pp. 737–760, 2016.

[158] W. Gao et al., "The status, challenges, and future of additive manufacturing in engineering," Computer-Aided Design, vol. 69, pp. 65–89, 2015.

[159] A. Davoudinejad et al., "Additive manufacturing with vat polymerization method for precision polymer micro components production," Procedia CIRP, vol. 75, pp. 98–102, 2018.

[160] B. N. Peele, T. J. Wallin, H. Zhao, and R. F. Shepherd, "3D printing antagonistic systems of artificial muscle using projection stereolithography," Bioinspiration & biomimetics, vol. 10, no. 5, p. 055003, 2015.

[161] D. K. Patel, A. H. Sakhaei, M. Layani, B. Zhang, Q. Ge, and S. Magdassi, "Highly stretchable and UV curable elastomers for digital light processing based 3D printing," Advanced Materials, vol. 29, no. 15, p. 1606000, 2017.

[162] Z. Yan and H. Peng, "FabHydro: Printing Interactive Hydraulic Devices with an Affordable SLA 3D Printer," in The 34th Annual ACM Symposium on User Interface Software and Technology, 2021, pp. 298–311.

[163] O. Gülcan, K. Günaydın, and A. Tamer, “The state of the art of material jetting—a critical review,” Polymers, vol. 13, no. 16, p. 2829, 2021.

[164] G. Dämmer, S. Gablenz, A. Hildebrandt, and Z. Major, “PolyJet-printed bellows actuators: design, structural optimization, and experimental investigation,” Frontiers in Robotics and AI, vol. 6, p. 34, 2019.

[165] G. Dämmer, M. Lackner, S. Laicher, R. Neumann, and Z. Major, “Design of an inkjet-printed rotary bellows actuator and simulation of its time-dependent deformation behavior,” Frontiers in Robotics and AI, vol. 8, p. 663158, 2021.

[166] G. Dämmer, S. Gablenz, A. Hildebrandt, and Z. Major, “Design of an Additively Manufacturable Multi-Material Light-Weight Gripper with integrated Bellows Actuators,” Adv. sci. technol. eng. syst. j, vol. 4, no. 2, pp. 23–33, 2019.

[167] H. Husker, “Inflatable Acoustic Meta-Material,” PhD Thesis, University of Maryland, College Park, 2021.

[168] M. Matsuura et al., “Blow-up Print: Rapidly 3D Printing Inflatable Objects in the Compressed State,” in ACM SIGGRAPH 2022 Posters, 2022, pp. 1–2.

[169] S. Schlatter, G. Grasso, S. Rosset, and H. Shea, “Inkjet Printing of Complex Soft Machines with Densely Integrated Electrostatic Actuators,” Advanced Intelligent Systems, vol. 2, no. 11, p. 2000136, 2020, doi: 10.1002/aisy.202000136.

[170] S. S. Crump, “Apparatus and method for creating three-dimensional objects,” Jun. 09, 1992

[171] J. J. Beaman, D. L. Bourell, C. C. Seepersad, and D. Kovar, “Additive manufacturing review: Early past to current practice,” Journal of Manufacturing Science and Engineering, vol. 142, no. 11, 2020.

[172] H. K. Yap, H. Y. Ng, and C.-H. Yeow, “High-force soft printable pneumatics for soft robotic applications,” Soft Robotics, vol. 3, no. 3, pp. 144–158, 2016.

[173] C. Tawk, Y. Gao, R. Mutlu, and G. Alici, “Fully 3D printed monolithic soft gripper with high conformal grasping capability,” in 2019 IEEE/ASME International Conference on Advanced Intelligent Mechatronics (AIM), IEEE, 2019, pp. 1139–1144.

[174] C. Han, R. Takahashi, Y. Yahagi, and T. Naemura, “3D Printing Firm Inflatables with Internal Tethers,” in Extended Abstracts of the 2021 CHI Conference on Human Factors in Computing Systems, 2021, pp. 1–7.

[175] B. Sparrman et al., “Printed silicone pneumatic actuators for soft robotics,” Additive Manufacturing, vol. 40, p. 101860, 2021.

[176] O. D. Yirmibesoglu et al., “Direct 3D printing of silicone elastomer soft robots and their performance comparison with molded counterparts,” in 2018 IEEE International Conference on Soft Robotics (RoboSoft), IEEE, 2018, pp. 295–302.

[177] K. Hajash, B. Sparrman, C. Guberan, J. Laucks, and S. Tibbits, “Large-scale rapid liquid printing,” 3D Printing and Additive Manufacturing, vol. 4, no. 3, pp. 123–132, 2017.

[178] B. Sparrman, S. Kernizan, J. Laucks, S. Tibbits, and C. Guberan, “Liquid printed pneumatics,” in ACM SIGGRAPH 2019 Emerging Technologies, 2019, pp. 1–2.

[179] L. Zhou et al., “Multimaterial 3D printing of highly stretchable silicone elastomers,” ACS applied materials & interfaces, vol. 11, no. 26, pp. 23573–23583, 2019.

[180] J. T. Muth et al., “Embedded 3D printing of strain sensors within highly stretchable elastomers,” Advanced materials, vol. 26, no. 36, pp. 6307–6312, 2014.

[181] P. W. Alexander et al., “Masked fabrication inflatable devices,” Jun. 07, 2022

[182] R. Suzuki, R. Nakayama, D. Liu, Y. Kakehi, M. D. Gross, and D. Leithinger, “Lifttiles: Modular and reconfigurable room-scale shape displays through retractable inflatable actuators,” in Adjunct Proceedings of the 32nd Annual ACM Symposium on User Interface Software and Technology, 2019, pp. 30–32.

[183] R. Suzuki, R. Nakayama, D. Liu, Y. Kakehi, M. D. Gross, and D. Leithinger, “LiftTiles: constructive building blocks for prototyping room-scale shape-changing interfaces,” in Proceedings of the fourteenth international conference on tangible, embedded, and embodied interaction, 2020, pp. 143–151.

[184] Y. Matoba, T. Sato, N. Takahashi, and H. Koike, “ClaytricSurface: an interactive surface with dynamic softness control capability,” in ACM SIGGRAPH 2012 Emerging Technologies on - SIGGRAPH ’12, Los Angeles, California: ACM Press, 2012, pp. 1–1. doi: 10.1145/2343456.2343462.

[185] T. Mitsuda, S. Kuge, M. Wakabayashi, and S. Kawamura, “Wearable Force Display Using a Particle Mechanical Constraint,” Presence: Teleoperators & Virtual Environments, vol. 11, no. 6, pp. 569–577, Dec. 2002, doi: 10.1162/105474602321050703.

[186] P. W. Alexander et al., Selectively rigidizable membrane. Google Patents, 2021.

[187] S.-H. Byun et al., “Mechanically transformative electronics, sensors, and implantable devices,” Sci. Adv., vol. 5, no. 11, p. eaay0418, Nov. 2019, doi: 10.1126/sciadv.aay0418.

[188] T. P. Chenal, J. C. Case, J. Paik, and R. K. Kramer, “Variable stiffness fabrics with embedded shape memory materials for wearable applications,” in 2014 IEEE/RSJ International Conference on Intelligent Robots and Systems, Chicago, IL, USA: IEEE, Sep. 2014, pp. 2827–2831. doi: 10.1109/IROS.2014.6942950.

[189] F. Qin et al., “ExoForm: Shape Memory and Self-Fusing Semi-Rigid Wearables,” in Extended Abstracts of the 2021 CHI Conference on Human Factors in Computing Systems, Yokohama Japan: ACM, May 2021, pp. 1–8. doi: 10.1145/3411763.3451818.

[190] R. M. Granberry, K. P. Eschen, A. J. Ross, J. M. Abel, and B. T. Holschuh, “Dynamic Countermeasure Fabrics for Post-Spaceflight Orthostatic Intolerance,” aerosp med hum perform, vol. 91, no. 6, pp. 525–531, Jun. 2020, doi: 10.3357/AMHP.5560.2020.

[191] G. McKnight and C. Henry, “Variable stiffness materials for reconfigurable surface applications,” presented at the Smart Structures and Materials, San Diego, CA, W. D. Armstrong, Ed., San Diego, CA, May 2005, p. 119. doi: 10.1117/12.601495.

[192] M. Henke and G. Gerlach, “A multi-layered variable stiffness device based on smart form closure actuators,” Journal of Intelligent Material Systems and Structures, vol. 27, no. 3, pp. 375–383, Feb. 2016, doi: 10.1177/1045389X15577645.

[193] A. Jiang, G. Xynogalas, P. Dasgupta, K. Althoefer, and T. Nanayakkara, “Design of a variable stiffness flexible manipulator with composite granular jamming and membrane coupling,” in 2012 IEEE/RSJ International Conference on Intelligent Robots and Systems, Vilamoura-Algarve, Portugal: IEEE, Oct. 2012, pp. 2922–2927. doi: 10.1109/IROS.2012.6385696.

[194] F. Putzu, J. Konstantinova, and K. Althoefer, “Soft Particles for Granular Jamming,” in Towards Autonomous Robotic Systems, K. Althoefer, J. Konstantinova, and K. Zhang, Eds., in Lecture

Notes in Computer Science, vol. 11650. Cham: Springer International Publishing, 2019, pp. 65–74. doi: 10.1007/978-3-030-25332-5_6.

[195] S. M. Zeyb Sayyadan and M. M. Moniri, “Mechanical behaviors of jammable robotic structures; prediction and computation,” Int J Intell Robot Appl, vol. 3, no. 1, pp. 71–86, Mar. 2019, doi: 10.1007/s41315-018-0067-5.

[196] M. Fujita et al., “Jamming layered membrane gripper mechanism for grasping differently shaped-objects without excessive pushing force for search and rescue missions,” Advanced Robotics, vol. 32, no. 11, pp. 590–604, Jun. 2018, doi: 10.1080/01691864.2018.1451368.

[197] N. G. Cheng et al., “Design and Analysis of a Robust, Low-cost, Highly Articulated manipulator enabled by jamming of granular media,” in 2012 IEEE International Conference on Robotics and Automation, St Paul, MN, USA: IEEE, May 2012, pp. 4328–4333. doi: 10.1109/ICRA.2012.6225373.

[198] T. Tachi, M. Masubuchi, and M. Iwamoto, “Rigid Origami Structures with Vacuumatics: Geometric Considerations,” p. 8.

[199] A. A. Stanley and A. M. Okamura, “Controllable Surface Haptics via Particle Jamming and Pneumatics,” IEEE Trans. Haptics, vol. 8, no. 1, pp. 20–30, Jan. 2015, doi: 10.1109/TOH.2015.2391093.

[200] F. F. Huijben, “Vacuumatics: 3D formwork systems : Investigations of the structural and morphological nature of vacuumatic structures so as to be used as semi-rigid formwork systems for producing ‘free forms’ and customised surface textures in concrete for architectural applications,” 2014, doi: 10.6100/IR775509.

[201] M. Brancadoro, M. Manti, S. Tognarelli, and M. Cianchetti, “Preliminary experimental study on variable stiffness structures based on fiber jamming for soft robots,” in 2018 IEEE International Conference on Soft Robotics (RoboSoft), Livorno: IEEE, Apr. 2018, pp. 258–263. doi: 10.1109/ROBOSOFT.2018.8404929.

[202] M. S. Moses, M. D. M. Kutzer, Hans Ma, and M. Armand, “A continuum manipulator made of interlocking fibers,” in 2013 IEEE International Conference on Robotics and Automation, Karlsruhe, Germany: IEEE, May 2013, pp. 4008–4015. doi: 10.1109/ICRA.2013.6631142.

[203] M. Brancadoro, M. Manti, F. Grani, S. Tognarelli, A. Menciassi, and M. Cianchetti, “Toward a Variable Stiffness Surgical Manipulator Based on Fiber Jamming Transition,” Front. Robot. AI, vol. 6, p. 12, Mar. 2019, doi: 10.3389/frobt.2019.00012.

[204] V. Wall, R. Deimel, and O. Brock, “Selective stiffening of soft actuators based on jamming,” in 2015 IEEE International Conference on Robotics and Automation (ICRA), Seattle, WA, USA: IEEE, May 2015, pp. 252–257. doi: 10.1109/ICRA.2015.7139008.

[205] J. L. C. Santiago, I. D. Walker, and I. S. Godage, “Continuum robots for space applications based on layer-jamming scales with stiffening capability,” in 2015 IEEE Aerospace Conference, Big Sky, MT: IEEE, Mar. 2015, pp. 1–13. doi: 10.1109/AERO.2015.7118897.

[206] I. Choi, N. Corson, L. Peiros, E. W. Hawkes, S. Keller, and S. Follmer, “A Soft, Controllable, High Force Density Linear Brake Utilizing Layer Jamming,” IEEE Robot. Autom. Lett., vol. 3, no. 1, pp. 450–457, Jan. 2018, doi: 10.1109/LRA.2017.2761938.

[207] Y. S. Narang, B. Aktaş, S. Ornellas, J. J. Vlassak, and R. D. Howe, “Lightweight Highly Tunable Jamming-Based Composites,” Soft Robotics, vol. 7, no. 6, pp. 724–735, Dec. 2020, doi: 10.1089/soro.2019.0053.

[208] T. Mitsuda, “Variable-stiffness Sheets Obtained using Fabric Jamming and their applications in force displays,” in 2017 IEEE World Haptics Conference (WHC), Munich, Germany: IEEE, Jun. 2017, pp. 364–369. doi: 10.1109/WHC.2017.7989929.

[209] G. Mcknight, R. Doty, A. Keefe, G. Herrera, and C. Henry, “Segmented Reinforcement Variable Stiffness Materials for Reconfigurable Surfaces,” Journal of Intelligent Material Systems and Structures, vol. 21, no. 17, pp. 1783–1793, Nov. 2010, doi: 10.1177/1045389X10386399.

[210] J. E. Luntz, L. Giner Munoz, D. E. Brei, and W. Kim, “Tile-based rigidization surface parametric design study,” in Smart Structures and NDE for Industry 4.0, N. G. Meyendorf, Ed., Denver, United States: SPIE, Mar. 2018, p. 21. doi: 10.1117/12.2300912.

[211] F. T. Peirce, “26—THE ‘HANDLE’ OF CLOTH AS A MEASURABLE QUANTITY,” Journal of the Textile Institute Transactions, vol. 21, no. 9, pp. T377–T416, Jan. 1930, doi: 10.1080/19447023008661529.

[212] C. C. Chu, C. L. Cummings, and N. A. Teixeira, “Mechanics of Elastic Performance of Textile Materials,” p. 10.

[213] Z. Mei, W. Shen, Y. Wang, J. Yang, T. Zhou, and H. Zhou, “Unidirectional Fabric Drape Testing Method,” PLoS ONE, vol. 10, no. 11, p. e0143648, Nov. 2015, doi: 10.1371/journal.pone.0143648.

[214] J. R. Davis, Tensile testing. ASM international, 2004.

[215] J. D. Evans, Straightforward statistics for the behavioral sciences. Thomson Brooks/Cole Publishing Co, 1996.

[216] J. M. Abel, “Active Knit Actuation Architectures.,” PhD Thesis, 2014.

[217] A. Ion, D. Lindlbauer, P. Herholz, M. Alexa, and P. Baudisch, “Understanding metamaterial mechanisms,” in Proceedings of the 2019 CHI Conference on Human Factors in Computing Systems, 2019, pp. 1–14.

[218] J. T. Overvelde, J. C. Weaver, C. Hoberman, and K. Bertoldi, “Rational design of reconfigurable prismatic architected materials,” Nature, vol. 541, no. 7637, pp. 347–352, 2017.

[219] S. D. Eppinger and T. R. Browning, Design structure matrix methods and applications. MIT press, 2012.

[220] “The Design Structure Matrix (DSM),” The Design Structure Matrix (DSM). https://dsmweb.org/ (accessed Apr. 02, 2023).